A Simulated Annealing Global Maximum Power Point Tracking Method for Photovoltaic Systems Experiencing Non-Uniform Environmental Conditions

Sarah Louise Lyden

B.Sc-B.E (Hons), University of Tasmania, 2011

Submitted in fulfilment of the requirements for the Degree of
Doctor of Philosophy

University of Tasmania

June 2015

ABSTRACT

Photovoltaic (PV) systems have immense potential due to the abundance of available solar energy and the capability of these systems to be implemented in a distributed manner. This clean, renewable and sustainable energy source can provide a solution to concerns about the shortage of fossil fuels, global warming, greenhouse gas emissions and pollution in general. Residential PV systems enable consumers to take control of generating electricity to satisfy their own load requirements and potentially export any excess energy to the distribution grid. Investing in a PV system requires significant initial capital and PV cells have a very limited efficiency. Residential customers who invest in a PV system expect to be able to have the best return on their investment by utilising the power available in the sunlight to the greatest extent possible. The potential power available from such systems can be dramatically reduced due to shading of the modules and ineffective control strategies to overcome the influence of shading. PV cells exhibit a non-linear Power-Voltage (P-V) characteristic leading to a unique point corresponding to optimal operation. This point is referred to as the Maximum Power Point (MPP), and varies depending on the environmental conditions. Typical conditions in a residential environment involve obstacles such as trees, houses and power poles which may cause shading across all or part of the PV system throughout the day. Shading from these obstacles leads to increased non-linearity in the P-V characteristic as multiple maxima can be exhibited. Traditionally, Maximum Power Point Tracking (MPPT) techniques have been developed to track a single maximum on the P-V characteristic based on simple techniques such as hill climbing. These techniques inherently fail when multiple maxima are exhibited under Partial Shading Conditions (PSC).

The work documented in this thesis consists of two main parts. In the first part, a study of modelling PV cells and an extensive shading study for an eight-module PV system is conducted. This analysis has led to the classification of partial shading phenomena based on the time scale as either *constant*, *static* or *transient* partial shading, and exploring the effect that each aspect of partial shading has on the relative location of the Global Maximum Power Point (GMPP).

The second part comprehensively explores the concept of MPPT and presents a review of techniques proposed in the literature with consideration of their performance under non-uniform environmental conditions. A Global MPPT (GMPPT) method is proposed based on the global optimisation technique of Simulated Annealing (SA) and its performance is verified through simulations and experimental application.

The key contributions of this thesis include proposing a shading classification based on the time of influence of the shading and studying how this affects the relative location of the GMPP, development and optimisation of a SA based GMPPT method, and the merging of these results to develop a comprehensive and enhanced GMPPT strategy.

The main concerns associated with modelling PV cells and modules are introduced and a model of the BP380 PV module is developed based on the commonly used Single Diode Model (SDM) for PV modules. The SDM provides a good balance between accuracy and simplicity and is shown to model the experimentally measured P-V and Current-Voltage (I-V) characteristics of the BP380 modules with acceptable accuracy. A model is also developed and experimentally validated based on combining two series-connected modules modelled using the SDM to explore PSC.

A PV system comprised of eight series-connected PV modules, modelled based on the BP380 PV modules, is developed to explore the influence of PSC. A methodology for calculating the position of the shadow tip and determining which cells are shaded by an object is proposed and used to perform five case studies exploring the effects of constant, static and transient partial shading. Constant partial shading is defined as a mismatch in the potential of the modules in a system based on factors such as manufacturing tolerance, cell degradation and damage over time. This type of shading should remain roughly the same for all time. Static partial shading is considered as shading that moves much slower than the movement of clouds across the sky and represents the shading that occurs on the modules due to the presence of obstacles in the environment. Finally, transient shading is the quickest shading phenomena and is represented by the changing irradiance due to the movement of clouds across the sky.

An extensive review of maximum power extraction strategies is presented. Each technique is assessed against key criteria identified as being essential for a universally applicable GMPPT strategy. In particular, the methods are assessed on whether they can locate a global maximum reliably, the method complexity and its ease of application to other PV systems. The analysis suggests that a global maximum power extraction strategy with moderate complexity and limited dependence on system specific parameters is needed.

The proposed SA based GMPPT method is introduced in the form of simple studies showing the effectiveness of the method in converging to a GMPP based on a two module PV system, eight module PV system, basic grid connected system and through experimental verification on the two series-connected BP380 PV modules. The key parameters of the SA method are explored in more detail to assess their influence on the effectiveness of the proposed method.

The main advantages of the proposed methodology for GMPPT is that it is not significantly more complex than the common perturb and observe (P&O) MPPT technique, yet has far superior performance in converging to the GMPP. Additionally, when compared to the Particle Swarm Optimisation (PSO) method which is commonly used for GMPPT, the SA based method has less complexity yet similar performance in converging to the GMPP. By incorporating understanding of the relative location of the GMPP under different PSC, the technique is enhanced to improve accuracy and convergence time. In residential environments one of the key factors is minimising cost and ensuring maximum efficiency. For this reason, a low cost and low complexity MPPT method that can achieve GMPP identification is essential, to enable systems implemented in residential environments to be utilised to the greatest extent possible.

DECLARATION

This thesis contains no material which has been accepted for a degree or diploma by the University or any other institution, except by way of background information and duly acknowledged in the thesis, and to the best of the my knowledge and belief no material previously published or written by another person except where due acknowledgement is made in the text of the thesis, nor does the thesis contain any material that infringes copyright.

This thesis may be made available for loan and limited copying and communication in accordance with the Copyright Act 1968.

Sarah Louise Lyden

ACKNOWLEDGEMENTS

I am incredibly grateful for the support, encouragement and guidance extended to me by my supervisors Dr. Md. Enamul Haque, Prof. Michael Negnevitksy and Dr. Ameen Gargoom. Thanks to their dedication, understanding and direction, undertaking my PhD has been a challenging, yet thoroughly rewarding and enjoyable experience.

I wish to thank the technical staff in the electrical workshop for their valuable guidance in developing the experimental prototypes described in this thesis. In particular, I would like to thank Mr. James Lamont for his guidance in developing the experimental work and for his willingness to help me setup the experiment at very short notice whenever the sun came out, and Mr. Bernard Chenery for his assistance with Labview.

Finally, I would like to thank my family and friends who were so accommodating and generous with their time in reading and reviewing chapters and for their patience and ongoing interest in my studies even during times of difficulty.

Contents

List of Figures

List of Tables

LIST OF ABBREVIATIONS

3PI-P&O ... 3-Points Incremental Perturb and Observe

ADC ..... Analog to Digital Converter

AESC ..... Adaptive Extremum Seeking Control

AIST ..... National Institute of Advanced Industrial Science and Technology

ANN ..... Artificial Neural Network

BL ..... Bridge-Linked

BST ..... Bisection Search Theorem

CPDC ..... Compensation Power-Dedicated DC-DC Converter

CVT ..... Constant Voltage Tracking

DAQ ..... Data Acquisition Device

DDM ..... Double Diode Model

DIRECT ... Dividing Rectangles

DMPPT .... Distributed MPPT

DPP ..... Differential Power Processing

EMTP ..... Electro-magnetic Transient Program

ESC ..... Extremum Seeking Control

FLC ..... Fuzzy Logic Control

FPGA ..... Field Programmable Gate Array

FulCurvE ... Full Curve Estimation

GMPP ..... Global Maximum Power Point

GMPPT .... Global Maximum Power Point Tracking

GPO ..... Generalised Perturb and Observe

HC ..... Hill Climbing

HCPSO ..... Hybrid Chaotic Particle Swarm Optimisation

HCPV ..... High Concentration Photovoltaic

IncCond .... Incremental Conductance

INR ..... Incremental Resistance

ISDM ..... Ideal Single Diode Model

I-V ..... Current-Voltage

LMPP ..... Local MPP

MIC ..... Module Integrated Converters

MPP ..... Maximum Power Point

MPPE ..... Maximum Power Point Estimation

MPPT ..... Maximum Power Point Tracking

NA ..... Nested Annealing

NI ..... National Instruments

NREL ..... National Renewable Energy Laboratory

P&O ..... Perturb and Observe

PE ..... Power Electronics

PIP ..... Power Independence Principle

POT ..... Power Operating Triangle

PSC ..... Partial Shading Conditions

PSO ..... Particle Swarm Optimisation

PV ..... Photovoltaic

P-V ..... Power-Voltage

RCC ..... Ripple Correlation Control

SA ..... Simulated Annealing

SDM ..... Single Diode Model

SEPIC ..... Single-ended Primary-inductor Converter

SMC ..... Sliding Mode Control

SP ..... Series-Parallel

SQ ..... Simulated Quenching

SSDM ..... Simplified Single Diode Model

STC ..... Standard Test Conditions

SVR ..... Support Vector Regression

TCT ..... Total-Cross-Tied

TEODI ..... Technique based on the Equalisation of the Output operating points in correspondence of the forced Displacement of the Input operating points of two identical PV systems

TTZ ..... Threshold Tracking Zone

VM ..... Voltage Window

VSC ..... Voltage Source Converter

VWS ..... Voltage Window Search

LIST OF SYMBOLS

a ..... Vector normal to module surface

A ..... Diode ideality factor

α ..... Elevation angle (°)

α_1 ..... Power curve trap ratio

α_2 ..... Cooling constant

$Azimuth$ ... Azimuth angle

β ..... Variable for β-method

β_{max} ..... Maximum value for β-method

β_{min} ..... Minimum value for β-method

β_t ..... Tilt angle of panel (°)

β_l ..... Lundy cooling constant

c ..... Logarithmic cooling constant

c_1, c_2 ..... Acceleration coefficients

c_l ..... Linear cooling constant

c_q ..... Simulated quenching cooling constant

d^* ..... Maximum depth of all states that are local but not global maxima

δ ..... Declination angle (°)

$dP_{0.5}$ ..... Change in power in half step (W)

dP_1 ..... Change in power in full step (W)

E_g ..... Bandgap energy

$E(k)$ ..... Energy at sample k

EoT ..... Equation of time

η ..... Efficiency

FF ..... Fill factor

G ..... Irradiance (W/m^2)

G_{best} ..... Best position of all particles

$G_{horizontal}$ ... Irradiance component in horizontal plane (W/m^2)

$G_{incident}$ ..... Incident irradiance (W/m^2)

G_{module} ..... Irradiance on module at tilt angle β_t (W/m^2)

G_n ..... Nominal irradiance (W/m^2)

H ..... Object height (m)

HRA ..... Hour angle

ΔI ..... Incremental current (A)

I_0 ..... Diode saturation current (A)

$I_{0,n}$ ..... Nominal diode saturation current (A)

I_{mpp} ..... Current at MPP (A)

I_{ph} ..... Light generated current (A)

$I_{ph,n}$ ..... Nominal light generated current (A)

I_{pv} ..... Current at operating point (A)

I_{sc} ..... Short-circuit current (A)

$I_{sc,n}$ ..... Nominal short-circuit current (A)

k ..... Iteration/sample

k_1 ..... Fractional short-circuit current constant

k_2 ..... Fractional open-circuit voltage constant

k_i ..... Current constant

k_v ..... Voltage constant

K ..... Boltzmann constant (1.38×10^{-23} J/K)

K_I ..... Temperature coefficient of current (%/°C)

L ..... Shadow length (m)

LST ..... Local solar time

$LSTM$ ..... Local standard time meridian

N ..... Day of the year

N_p ..... Number of cells/modules in parallel

N_s ..... Number of cells/modules in series

ω ..... Longitude angle (°)

ω_i ..... Inertia weight

ΔP ..... Power change threshold

P_0 ..... Object coordinates (x, y, z)

$P_1 ... P_4$ ..... Coordinates of PV cell corners (x, y, z)

$P_{best,i}$ ..... Best position of particle i

$P_{max,e}$ ..... Experimental maximum power at MPP (W)

$P_{max,m}$ ..... Calculated maximum power at MPP (W)

$P_{pv,new}$ ..... New PV power at steady-state operating point

$P_{pv,last}$ ..... PV power when first reaches steady state

P_s ..... Shadow point (x, y, z)

$P(i)$ ..... Power at previous best sample (W)

$P(k)$ ..... Power at sample k (W)

$P(\lambda)$ ..... Solar power density at wavelength λ

ϕ ..... Latitude (°)

Φ_i^k ..... Particle velocity

Φ_i^{k+1} ..... Particle new velocity

Pr ..... Probability of acceptance

q ..... Electron charge (1.6×10^{-19} C)

r_1, r_2 ..... Random variables

R_s ..... Series resistance (Ω)

R_{sh} ..... Shunt resistance (Ω)

s ..... Sun vector

sf ..... Shading factor

$\Delta T = T - T_n$ Temperature difference (K)

ΔT_{GMT} ..... Difference in local time from GMT in hours

T ..... Temperature on absolute scale (K)

T_n ..... Nominal temperature (K)

$T(0)$ ..... Initial temperature (°C)

$T(k)$ ..... Temperature at sample k (°C)

TC ..... Time correction

ΔV ..... Incremental voltage (V)

V_{mpp} ..... Voltage at mpp (V)

V_{oc} ..... Open-circuit voltage (V)

$V_{oc,n}$ ..... Nominal open-circuit voltage (V)

V_{pv} ..... Voltage at operating point (V)

V_t ..... Junction thermal voltage

$V_{t,n}$ ..... Nominal junction thermal voltage

x ..... Shadow tip x coordinate (m)

x_i^k ..... Particle position

x_i^{k+1} ..... Particle new position

y ..... Shadow tip y coordinate (m)

Chapter 1

Introduction

1.1 Background

As the world becomes more concerned about the ongoing availability of existing energy resources, increased attention is being placed on the potential of using renewable energy resources to combat the energy crisis, rising fuel and electricity costs and concerns about sustainability. These renewable sources of energy are continually replenished and will not run out during our lifetime. Additionally, the use of renewable resources has an environmental implication as it ensures that resources can be utilised in a sustainable manner, unlike the dwindling available supply of coal and other fossil fuels.

The integration of renewable energy sources in electricity networks around the world has been steadily increasing for several years. Key contributors to this increase in renewable resources include hydro, wind and solar. These three renewable energy resources play an important role in the energy supply in Tasmania, Australia. The backbone of the network is the presence of Hydro dams which were first established 100 years ago (in 1914) [1]. There are 30 hydro power stations in Tasmania with a capacity of over 2600 MW. Since 2002, Tasmania has also commissioned two key wind farms that are now operational. The Woolnorth wind farm has a capacity of 140 MW, and the newly commissioned Mussleroe wind farm has a capacity of 168 MW [2]. Wind farms in Tasmania are connected into the network at a single connection point in a similar way to how conventional power generators are connected to the network. The penetration of solar energy in Tasmania is far more distributed, as these sources are mainly connected as small scale residential systems, with a direct connection at the distribution level of the grid. At the end of 2014, small scale Photovoltaic (PV) in Tasmania had the capability to contribute over 80

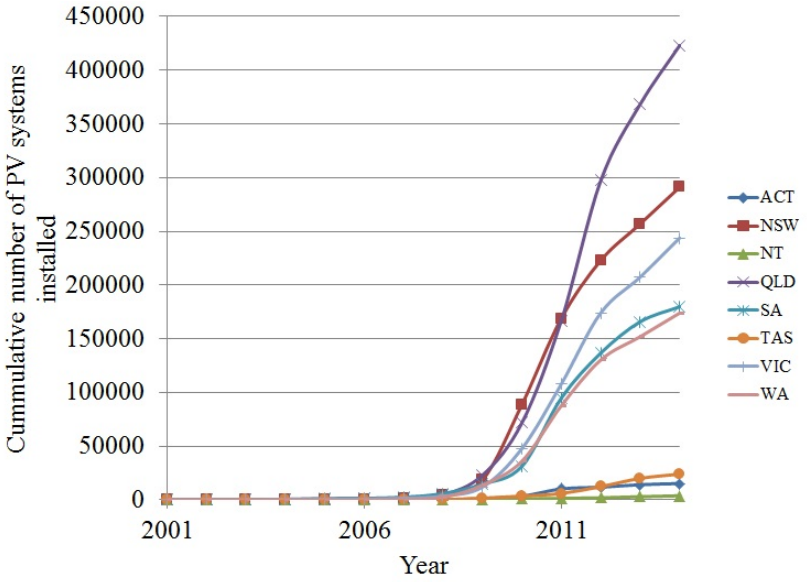

Figure 1.1: Cumulative number of PV installations in each state of Australia (2001-2014).

MW of electricity [3].

While distributed PV contributes a smaller amount of power to the network than the existing hydro power infrastructure and the established wind farms, it is becoming a more widely utilised source of energy as consumers start to take control of generating their own electrical power. In particular, this leads to the model where a household becomes a *prosumer*, a portmanteau of *producer* and *consumer*, rather than a consumer, as the residence can both produce and consume electricity [4].

In 2013, renewable sources of electricity supplied 14.76% of Australia's total electricity demand. Of this 11% was contributed by solar PV (approximately 1.6% of Australia's total demand) [5]. While this is significantly smaller than the contribution from other renewable sources such as wind and hydro, the number of installed PV installations around Australia is increasing significantly each year. Fig. 1.1 shows the cumulative number of solar PV installations in each state of Australia since 2001 [3].

There are two key areas that small scale PV integration research can be categorised as. The first relates to the consumer side, and the second to the electricity grid side. Consumers who purchase PV systems are making an

investment which they expect will perform and produce the maximum energy possible for their use, and potential economic gain, by exporting this power to the distribution grid. Power networks were originally designed to deliver electricity from large power stations to small loads distributed throughout the network [6]. By integrating PV systems into the network, the flow of power on the distribution network becomes bidirectional as the PV system exports energy to the grid when the energy produced exceeds the energy use of the household at that point in time. This is a key issue during the middle of the day when sunlight is typically abundant, but household loads are typically lower. Introducing bidirectional power flow into the network can lead to problems in the operation of protection equipment, voltage rise at certain nodes in the network and can affect the lifetime of existing grid infrastructure [7–13].

This thesis considers the first area of small scale PV integration mentioned above, with respect to improving the available power yield from a PV system to satisfy the customer when the system is installed in a typical residential environment. A typical residential environment is one in which there could be shading on the panels at various times throughout the day due to obstacles in the environment such as a neighbour's tree, and where the system is sufficiently small on a geographical basis such that the potential irradiance on each panel is identical (i.e. shading from clouds affects all panels simultaneously).

1.2 Global Maximum Power Point Tracking Under Non-Uniform Environmental Conditions

PV systems exhibit non-linear current-voltage (I-V) and power-voltage (P-V) characteristics leading to a unique operating point which needs to be tracked to enable successful system operation. Under non-uniform environmental conditions, the I-V and P-V characteristics become more complex and may exhibit multiple local maxima. For three series-connected modules, where each module is comprised of 36 cells, the I-V and P-V characteristics under uniform environmental conditions are shown in Figs. 1.2 and 1.3, respectively. For three series-connected modules experiencing Partial Shading Conditions (PSC),

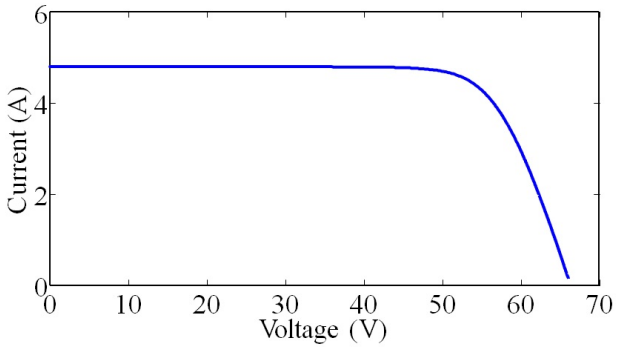

Figure 1.2: Uniform I-V characteristics for a three series-connected PV modules.

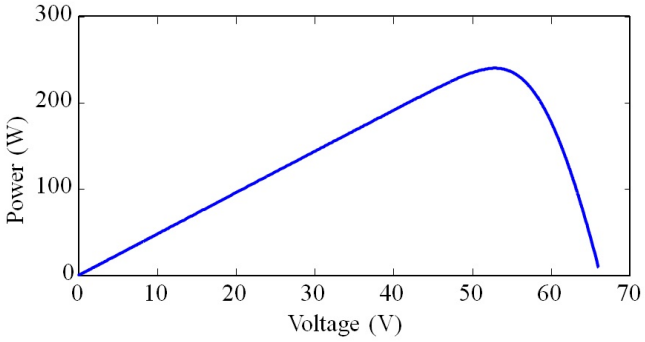

Figure 1.3: Uniform P-V characteristics for a three series-connected PV modules.

the corresponding I-V and P-V characteristics are shown in Figs. 1.4 and 1.5, respectively. PV systems are integrated with DC-DC converters to boost the voltage level, and then may be connected via an inverter to the distribution grid. A typical PV system is shown in Fig. 1.6.

Maximum power point tracking (MPPT) acts to output a PWM signal to control a DC-DC converter to control the amount of power extracted from the PV system. Traditionally, approaches to track the MPP have relied on a Perturb and Observe (P&O) or Hill Climbing (HC) approach to seek the maxima. A HC approach will only search until it locates a maxima, and cannot determine if it has found the global maxima. Many newer MPPT methods have been proposed to improve the power extraction from PV systems under PSC [14–18]. In general, these techniques lead to an increase in the cost or complexity of implementation, require knowledge of the PV system parameters and cannot easily be applied to other systems or are unable to guarantee GMPPT in all environmental conditions. MPPT for systems operating under PSC is an important consideration and most PV systems installed in residential environments will be subject to PSC to varying degrees.

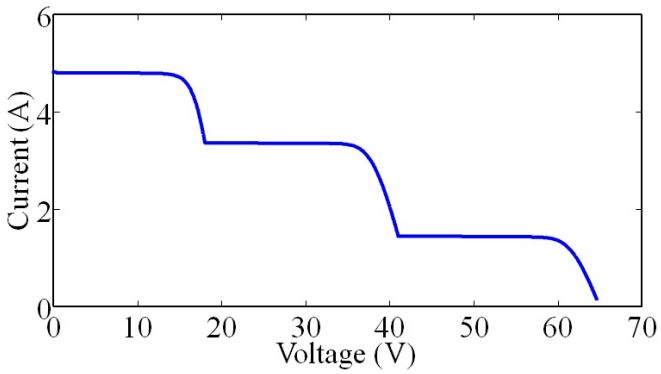

Figure 1.4: I-V characteristics for three series-connected modules experiencing non-uniform conditions, with irradiances 1000 W/m^2, 700 W/m^2, 300 W/m^2, temperature 25°C.

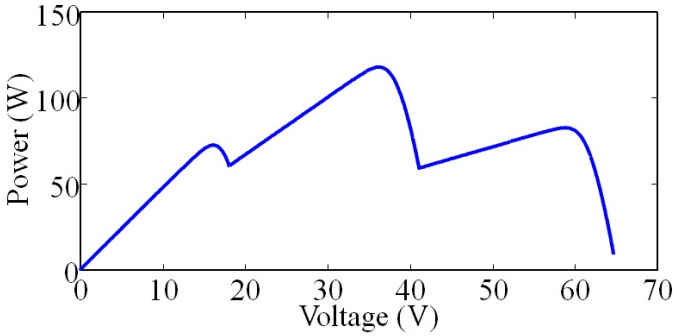

Figure 1.5: P-V characteristics for three series-connected modules experiencing non-uniform conditions, with irradiances 1000 W/m^2, 700 W/m^2, 300 W/m^2, temperature 25°C.

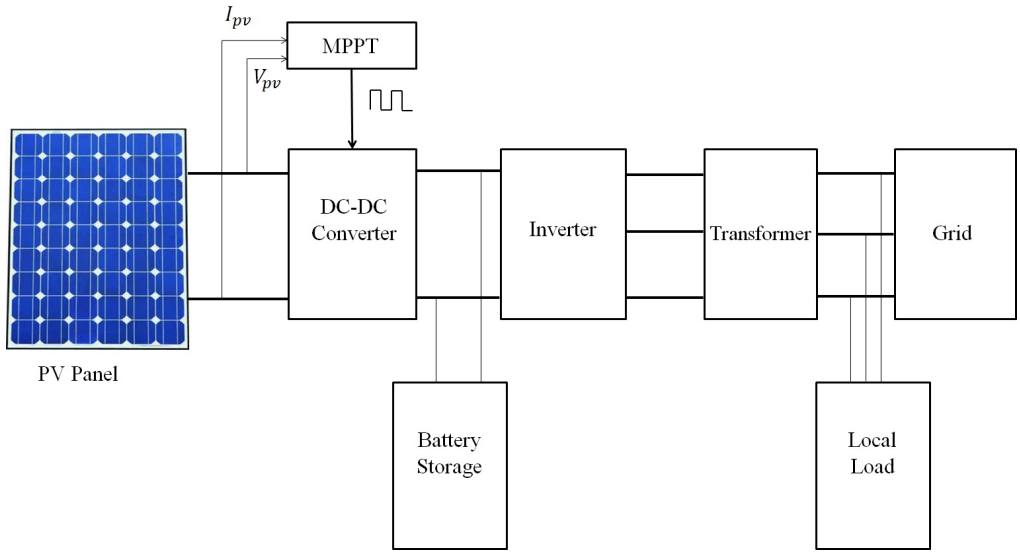

Figure 1.6: Typical block diagram of PV system with local battery storage, local load and grid connection.

1.3 Research Motivation

PV systems operating in residential environments invariably experience PSC due to a variety of factors including shade from objects in the immediate environment, internal cell mismatch and physical damage to the cells. These PSC can dramatically affect the amount of power available from a PV system, as finding the optimum operating point turns into a problem where the global maxima of the highly non-linear P-V characteristic needs to be quickly and accurately found. Most conventional techniques designed for tracking to this unique operating point are designed on the basis of uniform operating conditions which produce a singular maxima in the P-V characteristic and frequently fail to track the global optima under non-uniform conditions. While some techniques have been developed to achieve Global Maximum Power Point Tracking (GMPPT), these techniques either add to the cost or complexity of the implementation, cannot be easily applied to other systems due to their dependence on initial or system specific parameters, and may only work effectively under anticipated shading conditions [19–21].

An improved MPPT method is needed to enable PV systems to be operated at their greatest capacity at all times. PV systems have a high cost of energy [22]. It is therefore important, from an economic point of view, to maximise the power extracted from such systems. Due to the distributed nature of PV systems in residential environments, factors such as PSC become significant so tracking the GMPP is crucial to ensure effective utilisation of these systems.

The work presented in this thesis firstly considers and characterises the types of partial shading effects that a PV system would experience in the residential environment and considers the effect that these shading effects would have on the relative location (with respect to the voltage) of the GMPP. This analysis utilises real irradiance data obtained from the Bureau of Meteorology in Australia and the results feed into the proposed GMPPT technique.

1.4 Research Objectives and Contributions

The main objective of this thesis is to develop a reliable GMPPT technique that can extract maximum power from PV system under non-uniform conditions. The PSC studies conducted in the thesis, provide useful observations to improve the performance of GMPPT techniques. The proposed technique is developed on the basis of the optimisation technique of Simulation Annealing (SA) and has complexity similar to the commonly implemented P&O technique. The proposed SA GMPPT technique is demonstrated to have superior performance to other techniques including the common P&O technique and the more recent Particle Swarm Optimisation (PSO) technique specifically designed to operate under PSC. Finally, the SA GMPPT technique is improved based on studies of the key parameters of the method and observations of the location of the GMPP voltage as PSC are experienced.

The contributions of this thesis are:

- Development and experimental validation of a MATLAB/Simulink based model of the BP380 PV modules under uniform and non-uniform environmental conditions.
- Development of a MATLAB/Simulink model of a PV system, composed of eight series-connected modules, experiencing PSC.
- Extensive study of PSC in residential environments and the characterisation of the type of shadow and how this effects the relative location of the GMPP.
- A comprehensive review and comparison of PV MPPT methods for both uniform and non-uniform environmental conditions.
- Development and implementation of a suitable low complexity yet effective SA based GMPPT method.
- Comprehensive study of the effects of the key parameters of the SA method for MPPT implementation.
- Extension of the SA GMPPT technique to improve performance.

1.5 Thesis Outline

The current first chapter describes the energy situation in Tasmania, Australia and outlines a breakdown of the key issues that needs to be considered in the design and application of PV systems in the distribution network.

Chapter 2 presents a literature review of the standard modelling approaches utilised to demonstrate the behaviour of PV cells under different environmental conditions. This chapter applies one of the most common, yet sufficiently accurate methods, to model the BP380 [23] PV modules using a variety of different techniques to estimate the model parameters. The modelling performance is validated with experimental measurements for a single module and for two series-connected modules under non-uniform conditions. Models produced in this chapter are used throughout the thesis.

In Chapter 3 the PSC PV model is introduced and used to study the effect that partial shading has on the location of the Global Maximum Power Point (GMPP), particularly with respect to the voltage at the GMPP. This is performed on a simulation model of a PV system, comprised of eight series-connected PV modules based on the model developed in Chapter 2. *Constant*, *static* and *transient* PSC are defined and case studies are presented to isolate the effect that each type of PSC has on the GMPP voltage. A method to determine the shading factor of modules which are in the path of an object shadow is also presented in this chapter.

Chapter 4 reviews the extensive area of PV Maximum Power Point Tracking (MPPT) characterising those techniques designed for both uniform and non-uniform operating conditions. This review leads to the conclusion that there is still a need for a GMPPT technique with low complexity which can be easily adapted to other PV systems.

The need for an improved MPPT technique is addressed in Chapter 5 through the description and development of a GMPPT technique based on the optimisation method of Simulated Annealing. The SA GMPPT technique is introduced in this chapter and is explored in a two module and eight module implementation.

Experimental validation of the method using the two BP380 PV modules is also presented in this chapter.

Chapter 6 explores the key parameters of the SA based GMPPT method and makes suggestions on the most promising parameters to tune to improve the performance both with respect to convergence time and accuracy. Simulations presented in this chapter perform multiple iterations for each parameter and each environmental condition to average the performance. Thirty P-V characteristics developed throughout the analysis in Chapter 3 are utilised in this study.

Chapter 7 combines results from the previous chapters of the thesis to enhance the SA based GMPPT method. In particular, a suitable searching range can be determined based on the observations from Chapter 3. The results from Chapter 6 in exploring the influence of parameters prove valuable in this chapter.

Finally, conclusions and future research directions are given in Chapter 8.

1.6 Supporting Publications

1.6.1 Published

This research has produced the following refereed conference publications.

S. Lyden, M. E. Haque, A. Gargoom, M. Negnevitsky, P. I. Muoka, "Modelling and parameter estimation of photovoltaic cell", *22nd Australasian Universities Power Engineering Conference (AUPEC)*, pp. 1-6, 26-29 Sept. 2012

S. Lyden, M. E. Haque, A. Gargoom, M. Negnevitsky, "Modelling Photovoltaic Cell: Issues and operational constraints", *IEEE International Conference on Power System Technology (POWERCON)*, pp. 1-6, Oct. 30 - Nov. 2, 2012

S. Lyden, M. E. Haque, A. Gargoom, M. Negnevitsky, "Review of Maximum

Power Point Tracking Approaches Suitable for PV Systems under Partial Shading Conditions", *23rd Australasian Universities Power Engineering Conference (AUPEC)*, pp. 1-6, 29 Sept. - 2 Oct. 2013

S. Lyden and M. E. Haque, "Comparison of the Perturb and Observe Simulated Annealing Approaches for Maximum Power Point Tracking in a Photovoltaic System under Partial Shading Conditions", *IEEE Energy Conversion Congress and Exposition (ECCE)*, pp. 2517-2523, 14-18 Sept. 2014

S. Lyden, M. E. Haque and D. Xiao, "Application of a Simulated Annealing Technique for Global Maximum Power Point Tracking of PV Modules Experiencing Partial Shading", *IEEE Industrial Electronics Society (IECON)*, pp. 1977-1983, 29 Oct. - 1 Nov. 2014

1.6.2 Under review

The following journal papers have been submitted and are currently undergoing review.

S. Lyden and M. E. Haque, "Maximum Power Point Tracking Techniques for Photovoltaic Systems: A Comprehensive Review and Comparative Analysis" (submitted to *Renewable and Sustainable Energy Reviews* on 27 January 2015, revised 27 May 2015 (minor correction), manuscript ID RSER-D-15-00206).

S. Lyden and M. E. Haque, "A Simulated Annealing Global Maximum Power Point Tracking Approach for PV Modules under Partial Shading Conditions" (submitted to *IEEE Transactions on Power Electronics* on 1 February 2015, revised 23 April 2015 (minor correction), manuscript ID TPEL-Reg-2015-01-0175).

S. Lyden and M. E. Haque, "Modelling, Parameter Estimation and Assessment of Partial Shading Conditions of Photovoltaic Modules" (under preparation to submit to *Solar Energy*).

S. Lyden and M. E. Haque, "A Generalised Simulated Annealing based Global Maximum Power Point Tracking technique", (under preparation to submit to *IEEE Transaction on Industrial Informatics*).

S. Lyden and M. E. Haque, "A Hybrid Simulated Annealing and Perturb and Observe Maximum Power Point Tracking Technique" (under preparation to submit to *IEEE Journal of Photovoltaics*).

Chapter 2

Modelling of Photovoltaic Cells

2.1 Introduction

Photovoltaic (PV) cells demonstrate a non-linear Current-Voltage (I-V) and Power-Voltage (P-V) characteristic which needs to be carefully considered when modelling PV cells. In order to effectively design systems utilising PV cells, accurate tools are needed which can predict these characteristics and model them under changing environmental conditions [24, 25]. Traditionally, PV cells have been used for low-power, low-voltage applications, however they are now increasingly being integrated into the electricity grid [26] as a viable source of renewable energy. Effective PV cell models can be used to analyse the performance of converters and develop advanced control strategies including Maximum Power Point Tracking (MPPT) in a less material-intensive and costly manner [27, 28].

This chapter describes the principle of operation for PV cells and the main ways in which these cells are modelled. In particular, methods proposed to extract the parameters of the Single Diode Model (SDM), one of the more commonly used PV cell models, are described. The key factors that affect the power available from PV cells are explored including irradiance and temperature effects, cell degradation and the presence of partial shading conditions (PSC). The chapter ends by validating the use of the SDM for modelling BP380 PV modules [23] under both uniform and non-uniform environmental conditions.

The purpose of this chapter is to explore the key factors that limit the effective operation of PV cells and to develop a model with sufficient accuracy for use in the studies conducted in subsequent chapters. These studies include

a detailed study of the impacts of PSC in Chapter 3, and in developing the Simulated Annealing based GMPPT method presented in Chapters 5, 6 and 7. Despite the range of modelling methods available, the SDM is chosen as it provides a balance between accuracy and simplicity that other models cannot match.

2.2 PV Cells Principle of Operation

A PV cell is a device that converts the energy in sunlight into DC electrical power [26, 28–37]. This is achieved by utilising the properties of semiconductor materials, from which PV cells are constructed, in particular the photovoltaic effect. The key feature of a PV cell is a p-n junction which is formed when a p-type and n-type semiconductor are brought together [32]. A current is generated when this junction is illuminated with photons of sunlight, as the energy from the photons is used to create charge carriers in the p-n junction [28, 30]. These charge carriers create a current which can flow through an external circuit and are only formed when the incident photon has sufficient energy to detach covalent electrons from the semiconductor [28, 38]. The construction of the PV cell is shown in Fig. 2.1.

Sunlight contains photons of varying wavelengths and corresponding energies which are either used by Earth-bound processes such as the heat-cycle, weather-cycle and photosynthesis, or emitted back into space [32]. Depending on the

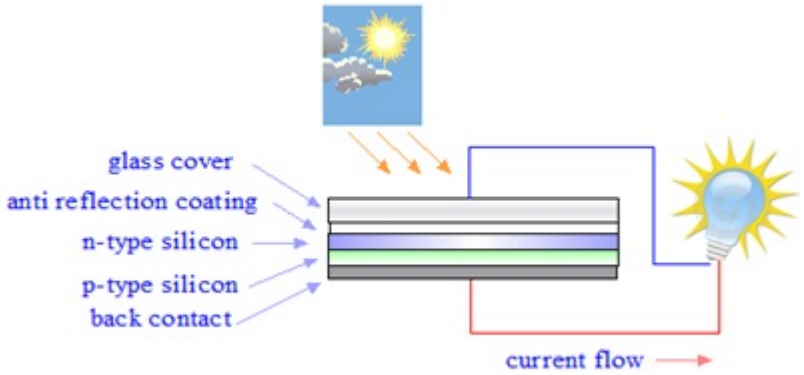

Figure 2.1: PV cell construction.

energy of photons incident on a PV cell p-n junction, electricity may or may not be generated. The quantifying factor is known as the bandgap of the semiconductor material, which is the energy level at which the cell operates. As such, any photons with insufficient energy will not create useful electricity and any photons with energy exceeding the bandgap will only generate electricity at the bandgap energy level of the PV cell. The remaining energy of these photons is then dissipated to the environment as heat. Using a semiconductor with a lower bandgap creates an opportunity for a wider range of the radiation spectrum to be used, but limits the voltage at which electricity can be generated [28,29,33]. To improve the utilisation of the solar spectrum multilayer or multijunction PV cells can be utilised [39]. In these PV cells, different layers of PV cell material with different bandgap energies can be combined in a vertical or lateral configuration [39]. Typically, for a vertical multibandgap configuration, the cells are layered such that the largest bandgap is at the top and the smallest is at the bottom [40].

The efficiencies of PV cells have been steadily increasing over a number of years. In 2005, typically PV cells were constructed from crystalline silicon materials and had efficiencies 14-17% [41]. Now, ten years later, cell efficiencies have increased substantially. A six-monthly published record of the maximum efficiencies of different types of PV cells, most recently published in January 2015, has indicated that the maximum efficiencies achieved with Silicon single bandgap PV cells is 25.6 ± 0.5 % [42]. The five junction PV cells, manufactured by Spectrolab with testing conducted by National Renewable Energy Laboratory (NREL) in August 2013, were shown to have the highest efficiencies of all considered cells with an efficiency of 38.8 ± 1.9 % [43]. A multijunction GaInP/GaAs; GaInAsP/GaInAs cell manufactured by Soitec was shown to have an efficiency of 46.0 ± 2.2 % in testing conducted by the National Institute of Advanced Industrial Science and Technology (AIST) in October 2014 [42]. Clearly, this highlights the enhanced potential of PV cells that are constructed from multibandgap materials.

The output characteristics of a PV cell are highly non-linear due to the p-n junction, and subsequently are usually modelled using a diode as an equivalent circuit element [37, 44]. The PV cell characteristic I-V curve is dependent on the irradiance energy and the temperature, which means that model parameters at Standard Test Conditions (STC) deviate when compared to actual variable

operating conditions [32, 37, 45]. This variability creates a need for accurate modelling mechanisms to demonstrate PV cell operation under changing environmental conditions. The non-linear I-V and P-V characteristics for the BP380 PV module, with 36 cells connected in series, under uniform environmental conditions are shown in Fig. 2.2.

To create a p-n junction, a semiconductor material must be doped with intentional impurities [29, 31]. These impurities are included in the material substitutionally with atoms of the host crystal. The type of doping atom

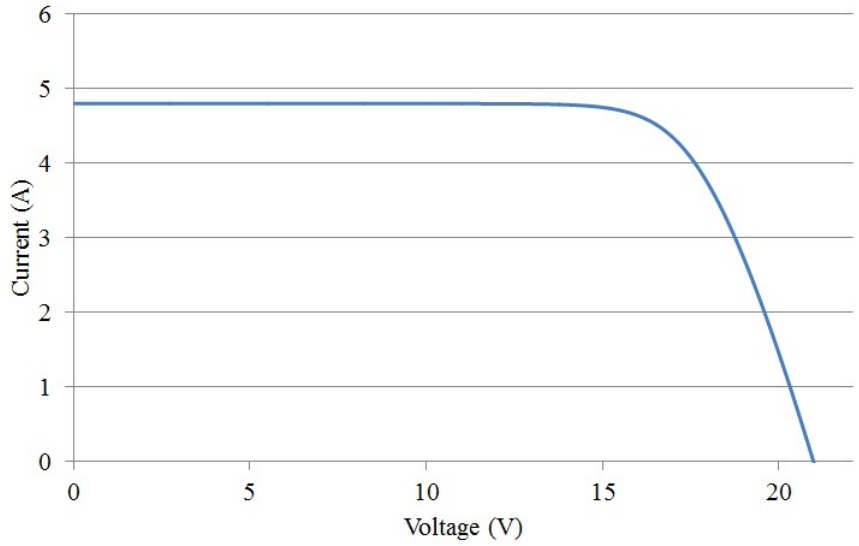

(a) I-V characteristic.

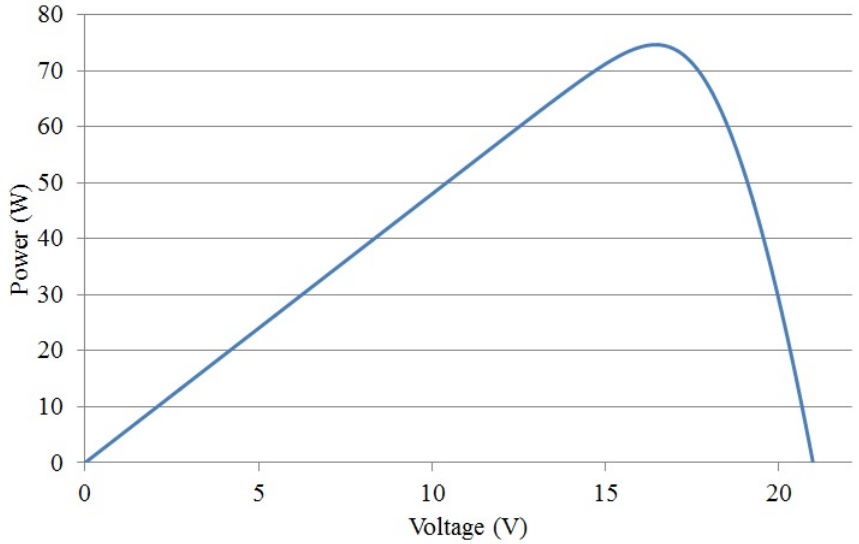

(b) P-V characteristic.

Figure 2.2: I-V and P-V characteristics for single BP380 PV module under uniform conditions, 1000 W/m^2, 25°C.

determines what properties this gives to the semiconductor. A dopant such as a group III atom (i.e. Boron) will create holes in the lattice structure which can be released with a lower energy level than those released from the silicon atoms in the same structure. Additionally, a group V atom (i.e. Phosphorus) allows free electrons to be established in the material, as a lower energy level is required to release the extra electron from each group V atom [31]. Typical dopants are Boron and Phosphorus due to their high solid solubilities and the ease with which highly-doped layers can be produced [29].

2.3 Types of PV Cells

A variety of different PV cell technologies are available including crystalline and thin film technologies. Crystalline PV materials involve a regular, periodic arrangement of atoms forming a crystal structure, while thin film materials are constructed using lamination techniques to produce a material thickness of only a few micrometres [32].

Crystalline PV cells can be classified based upon the type of crystalline structure. As such, single crystalline silicon, polycrystalline and semicrystalline silicon comprise three common PV cell categories. Single crystalline silicon is the most commonly used material to manufacture PV cells in a process which can be slow and energy intensive [30]. The polycrystalline and semicrystalline materials are less expensive to manufacture and can be produced much more rapidly, however frequently have a lower energy conversion efficiency [30].

Thin film PV technology relies upon layers of PV material that are only micrometres in thickness being applied to a substrate [30]. These materials include Copper Indium diselenide ($CuInSe_2$), Cadmium Telluride (CdTe), Gallium Arsenide (GaAs) or amorphous silicon vapour. Amorphous silicon technologies use about 1% of the equivalent material used in crystalline silicon PV cells [30].

Most PV cells are constructed using some form of silicon material. This is due to silicon having properties which make it well suited to generating electricity.

These factors include high electrical resistivity, low saturation current density and the solar radiation adsorption capabilities of the material [29]. Other materials mentioned above are often capable of higher efficiencies than silicon materials, but generally have higher costs and other limitations which reduce their use [29]. Silicon, while not being the most efficient semiconductor material for PV applications, is the most commonly used due to it being the most economically viable semiconductor to manufacture [28].

Newer technologies include 3D solar cells, where light is collected through a wide angle light collection and is able to bounce around the solar cell structure to improve the interactions of the photons with the solar cell materials [46]. Printable organic PV cells have been developed by the CSIRO and can produce between 10 and 15 W per square meter utilising a different part of the spectrum to traditional silicon based cells [47, 48].

2.4 Modelling of PV Cells

Many models can be utilised to emulate the characteristics of a PV cell. These models vary in complexity, accuracy and adaptability to modelling varying environmental conditions. The output characteristics of a PV cell are highly non-linear due to the p-n junction, and subsequently are usually modelled using a diode as an equivalent circuit element to model diffusion and recombination currents [37, 44, 49].

A variety of modelling techniques have been proposed in the literature [25, 28, 33, 35, 37, 50–53]. The most commonly used include the Single Diode Model (SDM), its simplified (SSDM) and ideal (ISDM) forms, and the Double Diode Model (DDM). Other techniques rely on curve fitting to the solar cell characteristics [53], using artificial intelligence to 'learn' the characteristic behaviour [51, 52], or linearisation and the formation of Thevenin equivalent circuits [35]. In some cases the I-V and P-V characteristics are modelled by using an approximate form composed of polynomials [54]. Some models even consider thermodynamic modelling to enable even more accurate investigation and prediction of module temperature and the corresponding effects on the

electricity generated [52]. Additionally, simulation and modelling of equivalent circuits can occur using electronics-based simulation [25, 55] or hybrid simulation techniques which merge mathematical models with electronics-based models [33].

Analytical circuit based models of PV cells use common circuit elements including current sources, resistors and diodes to model the PV cell I-V and P-V characteristics. The key models in this category include the SDM, ISDM, SSDM and DDM. The SDM, SSDM, ISDM and DDM are shown in Fig. 2.3. Despite the number and diversity of PV cell modelling techniques proposed, of the analytical methods for modelling of PV characteristics, the SDM is generally accepted to have the best balance between accuracy and simplicity [28,35,44,45,56].

All the analytical circuit-based models involve panel-specific parameters which must be estimated for accurate modelling. This data is not directly available and needs to be estimated based on manufacturers datasheets [28, 45, 50]. Additionally, these parameters are functions of environmental conditions including temperature and irradiance and vary depending on manufacturing tolerances [35, 49].

Despite the wide diversity of techniques for modelling PV cells in the literature, the SDM is often accepted to have the best balance between accuracy and simplicity [28, 45]. In particular, the SDM requires only five parameters to be

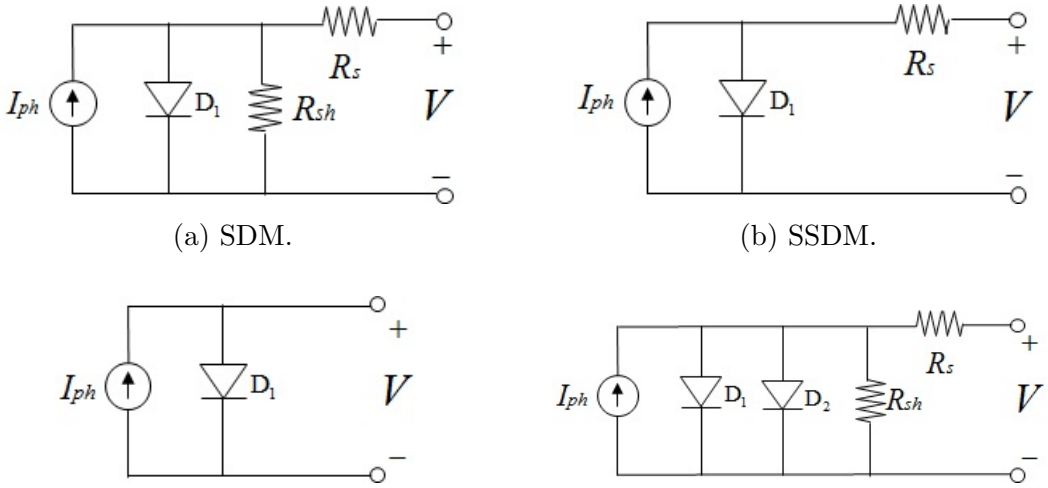

(a) SDM. (b) SSDM.

(c) ISDM. (d) DDM.

Figure 2.3: Analytical circuit based models, (a) SDM, (b) SSDM, (c) ISDM, (d) DDM.

estimated for accurate modelling, while the DDM requires seven parameters. Despite the popularity and use of the SDM, it does possess some limitations in modelling the more complex processes of two-dimensional current flow, surface recombination and light confinement which more comprehensive models can provide [52]. The SDM is discussed in more detail in Section 2.5.

2.5 Single Diode Model

The SDM exhibits a balance between accuracy and simplicity and is now considered in more detail. By adopting the SDM, I-V and P-V characteristics of moderate accuracy model PV cells with a smaller computational burden when compared to more complex models such as the DDM.

Equation (2.1) gives the I-V characteristic as indicated by the SDM shown in Fig. 2.3.

$$I = I_{ph} - I_0 \left[\exp \frac{q(V + IR_s)}{AKT} - 1 \right] - \frac{V + IR_s}{R_{sh}} \tag{2.1}$$

where I_{ph} is the light-generated current of the cell, I_0 is the diode saturation current, q is the electron charge (1.6×10^{-19}C), K is the Boltzmann constant (1.38×10^{-23}J/K), T is the temperature on absolute scale (K) and A is the diode ideality factor.

The load current (2.1) is a transcendental non-linear equation which increases the complexity of modelling a PV system [50]. Equation (2.1) features five parameters I_{ph}, I_0, R_s, A and R_{sh} which are functions of environmental conditions and manufacturing tolerance and need to be accurately estimated for modelling purposes [28, 45, 50]. However, this information is not directly provided on manufacturer datasheets. Rather, information is provided highlighting the voltage and current at what are termed the *remarkable* points [28] and the temperature coefficients of the open-circuit voltage and short-circuit current [28, 49]. These *remarkable* points include the short-circuit, open-circuit and peak power points given by $(0, I_{sc})$, $(V_{oc}, 0)$ and (V_{mpp}, I_{mpp}), respectively.

On the datasheet these *remarkable* points are only described under STC, that is, 25°C, 1000W/m^2. Subsequently, the temperature and irradiance dependence of the parameters needs to be generalised to enable comprehensive modelling of the cell performance.

Often manufacturer's datasheets will also provide graphs describing the electrical characteristics of the panel under changing temperature and irradiance [57] to verify experimental and simulation models.

2.5.1 PV module model using the SDM

Each PV cell can only produce a limited voltage and current. In order to boost the voltage and current to suit applications such as residential scale PV system implementation, series and parallel combinations of individual cells are required. A string consists of several PV cells connected in series such that the voltage of the string becomes the cumulative voltage of the individual cells. To boost the current, several strings are connected in parallel to create a module [32]. Multiple modules can then be connected in series and parallel to form larger PV systems. The I-V characteristics for a module experiencing uniform environmental conditions replicate those for an individual cell by scaling by N_s and N_p representing the number of cells in series and parallel, respectively. The I-V characteristic for a module composed of $N_s \times N_p$ cells is given in (2.2).

$$I = N_p\left(I_{ph} - I_0\left(\exp\frac{q\left(\frac{V}{N_s} + \frac{I}{N_p}R_s\right)}{AKT} - 1\right) - \frac{\left(\frac{V}{N_s} + \frac{I}{N_p}R_s\right)}{R_{sh}}\right) \tag{2.2}$$

2.6 Parameter Estimation for the SDM

As shown, the SDM has five parameters I_{ph}, I_0, R_s, A and R_{sh} which need to be estimated from the data provided in the manufacturer's datasheet or from experimental measurements. A variety of approaches are proposed in the literature to achieve this goal [37, 45, 56, 58, 59]. These techniques rely on analytical equations, iterative techniques, experimental measurements, least-squares or single-variable

optimisation approaches and artificial intelligence techniques [37, 45, 56, 58, 59].

The key parameters can be estimated at STC by considering the data available in the manufacturer's datasheet or data from experimental testing. After determining these values, the temperature and irradiance dependencies, further discussed in Section 2.7, can be applied to the STC quantities.

In this section two key analytical methods for obtaining the parameters of the SDM will be described. Following this, a simple analytical technique to obtain the parameters of the ISDM will be discussed and then finally, a few other methods for parameter estimation described. These techniques rely on analytical equations and iterative techniques to converge to an appropriate set of parameters to model PV cell characteristics.

2.6.1 Analytical method one

In [45], a system of five equations is formed by considering the three remarkable points provided on the datasheet and two other key properties of the I-V and P-V characteristics. The three equations based on the remarkable points listed on the datasheet are given by (2.3) to (2.5).

$$I_{sc} = I_{ph} - I_0\Big[\exp\frac{I_{sc}R_s}{V_t} - 1\Big] - \frac{I_{sc}R_s}{R_{sh}} \tag{2.3}$$

$$0 = I_{ph} - I_0\Big[\exp\frac{V_{oc}}{V_t} - 1\Big] - \frac{V_{oc}}{R_{sh}} \tag{2.4}$$

$$I_{mpp} = I_{ph} - I_0\Big[\exp\frac{V_{mpp} + I_{mpp}R_s}{V_t} - 1\Big] - \frac{V_{mpp} + I_{mpp}R_s}{R_{sh}} \tag{2.5}$$

where, $V_t = \frac{AN_sKT}{q}$ is the junction thermal voltage.

The additional conditions include the MPP condition and the current slope condition at short-circuit and are given in (2.6) and (2.7), respectively.

$$\frac{\mathrm{d}P}{\mathrm{d}V}_{atMPP} = 0 \tag{2.6}$$

$$\frac{\mathrm{d}I}{\mathrm{d}V}_{atI_{sc}} \approx -\frac{1}{R_{sh}} \tag{2.7}$$

To reduce the complexity of the algebraic manipulations required by this technique, several simplifications are made in the analysis. These simplifications include neglecting the '-1' term from the original SDM characteristic in (2.1), producing (2.8) and various other small simplifications throughout the process. The simplifications are generally justified by identifying that the component neglected is much smaller in value than what is retained in the equation and subsequently has a smaller effect on the results.

$$I = I_{ph} - I_0 \exp \frac{q(V + IR_s)}{AKT} - \frac{V + IR_s}{R_s h} \tag{2.8}$$

A simplification process is outlined which reduces the system of equations to three implicit and two explicit equations. The Gauss-Seidel iterative technique can be applied to the implicit equations to solve within a certain tolerance and then the explicit equations can be solved to obtain the remaining parameters.

2.6.2 Analytical method two

A second analytical method [28] firstly assumes a diode ideality factor of 1 and defines equations for the light-generated and diode saturation currents. A relationship is then developed linking the resistances to consideration of the key properties of the MPP. In general, there should only be one unique pair of resistances (R_s, R_{sh}) which will result in the maximum calculated power matching the maximum power at the actual MPP location. That is, a pair of resistances which leads to the condition

$$P_{max,m} = P_{max,e} = V_{mpp} I_{mpp} \tag{2.9}$$

where, $P_{max,m}$ is the measured power calculated from the characteristic and $P_{max,e}$ is the experimentally measured maximum power or that indicated on the datasheet.

A relationship is defined which expresses the shunt resistance in terms of the series resistance and is given in (2.10). The resistances are solved by iteratively

incrementing the series resistance (as it should be small) until an appropriate shunt resistance is calculated.

$$R_{sh} = \frac{V_{mpp}(V_{mpp} + I_{mpp}R_s)}{I_{ph}V_{mpp} - I_0 V_{mpp}\left[\exp\left(\frac{\frac{q}{kT}(V_{mpp} + I_{mpp}R_s}{AN_s}\right) - 1\right] - P_{max,e}} \tag{2.10}$$

The light-generated current is approximated by the short-circuit current and the diode saturation current is given by (2.11) in this technique.

$$I_0 = \frac{I_{sc}}{\exp\left(\frac{qV_{oc}}{AN_s kT}\right) - 1} \tag{2.11}$$

The basic parameters, that is I_{ph}, I_0 and A are determined in the algorithm using the approximations and equations provided and then an iterative process is commenced to determine the most suitable resistance values. This process works by starting with a small series resistance (usually $R_s = 0$), evaluating what the shunt resistance should be, and then determining the resulting characteristic. The characteristic provides a MPP voltage, current and power which can be compared with the anticipated values. If the maximum power does not match with the expected value, or the maximum power does not occur at the expected MPP location, the process is repeated for a small increment of R_s. The iterative process continues until a suitable (R_s, R_{sh}) pair is determined which enables the MPP to match the experimental MPP (or that from the datasheet) at the appropriate MPP location.

2.6.3 Analytical method three

The analytical method for the ISDM contains fewer parameters which need estimating [50]. The I-V characteristic of the ISDM is given in (2.12).

$$I = I_{ph} - I_0 \exp\left(\frac{V}{AKT}\right) \tag{2.12}$$

The approximation $I_{ph} = I_{sc}$ is used in this method to reduce the number of parameters requiring evaluation. The technique relies on an analytical process

to determine the parameters by substituting the remarkable points in (2.12). As the ISDM characteristic is only a function of voltage, iterative techniques are not required to determine the parameters.

2.6.4 Other methods of parameter estimation

Other methods to enable parameter estimation of the SDM or the other analytical circuit-based models include least-squares, and single-variable optimisation approaches. These methods are described below.

2.6.4.1 Least-squares

A non-linear least-squares optimisation approach based on a trust-region algorithm to determine the five parameters of the SDM is described in [60]. The process involves writing five functions similar to the approach in [45] based on the datasheet information, and then combining these functions to form a single function which can be minimised to determine the parameters simultaneously. Upper and lower bounds are specified for each parameter in this implementation. The process requires fewer iterations and computational time compared with other parameter estimation techniques.

2.6.4.2 Single-Variable Optimisation

A Single-Variable optimisation approach is described in [58] which reduces the optimisation process to only require the optimisation of a single parameter. This single parameter is the series resistance R_s. The process involves maximising the coefficient of determination R^2 between the experimental and model data. This method has been tested on monocrystalline, polycrystalline and amorphous PV modules and demonstrates good robustness against noise.

2.7 Factors Affecting Solar Power Generation

2.7.1 Environmental dependence of parameters

The literature suggests that the I-V characteristics are dependent on internal characteristics such as the series and shunt resistances (which have a low temperature dependence [44]), and external influences including irradiation level and temperature [28, 55, 61]. The variations in the I-V and P-V characteristics under different irradiance and temperature are shown in Figs. 2.4 and 2.5, respectively. As the irradiance decreases the maximum power available decreases and as the temperature increase the maximum power available decreases [25, 28].

The temperature of the cell depends on a number of factors including packing box material, thermal dissipation, absorption, ambient temperature and wind speed [44]. As the temperature of the cell rises, due to internal characteristics and environmental factors, some parameters of the solar cell model vary. In particular, the open-circuit voltage decreases rapidly while a very minor increase occurs in the short-circuit current [31]. This is observed as a reduction in efficiency when the cell temperature rises [29, 31]. The cell temperature can be observed to also have an effect on the light-generated current and diode saturation current [28, 44, 45].

The irradiance level that an individual cell is exposed to directly affects the light-generated current and the short-circuit current [28, 45]. The key factors which determine baseline radiation received by a given location include the geographical location in relation to the equator, the season, air mass and hour of the day [35, 45]. Those factors which govern the transient radiation received by the location include temperature, humidity, reflectivity of the area, angle of tilt of the PV modules, wind speed and shading [45]. Solar irradiation incident on the cell largely affects the light-generated current which in turn affects the short-circuit current (as this is directly proportional to the light-generated current) [28, 45].

The relationships for the light generated current and diode saturation current

taking into account temperature and irradiance dependence are given in (2.13) and (2.14), respectively.

$$I_{ph} = (I_{ph,n} + K_I \Delta T)\frac{G}{G_n} \tag{2.13}$$

where, $I_{ph,n}$ is the light-generated current at nominal conditions, ΔT is the

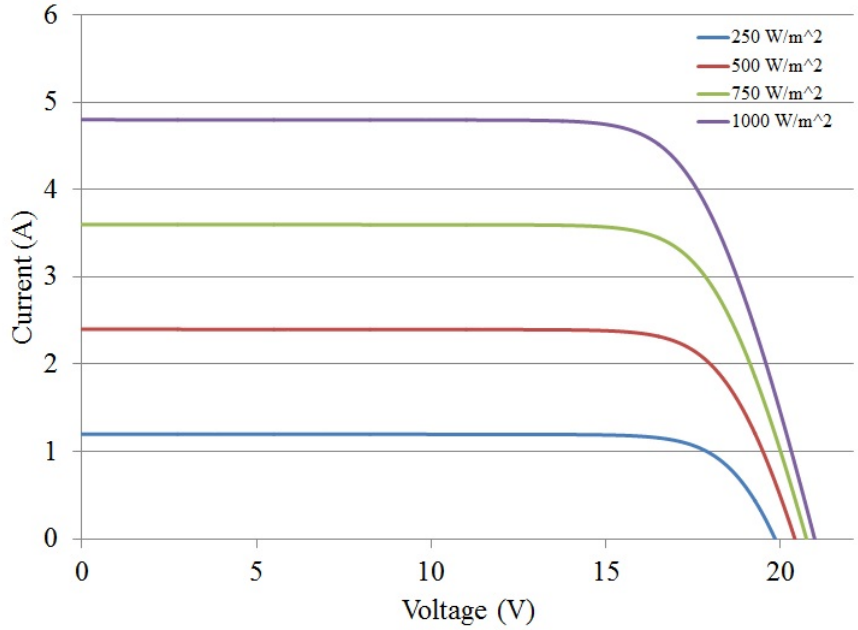

(a) I-V dependence on irradiance.

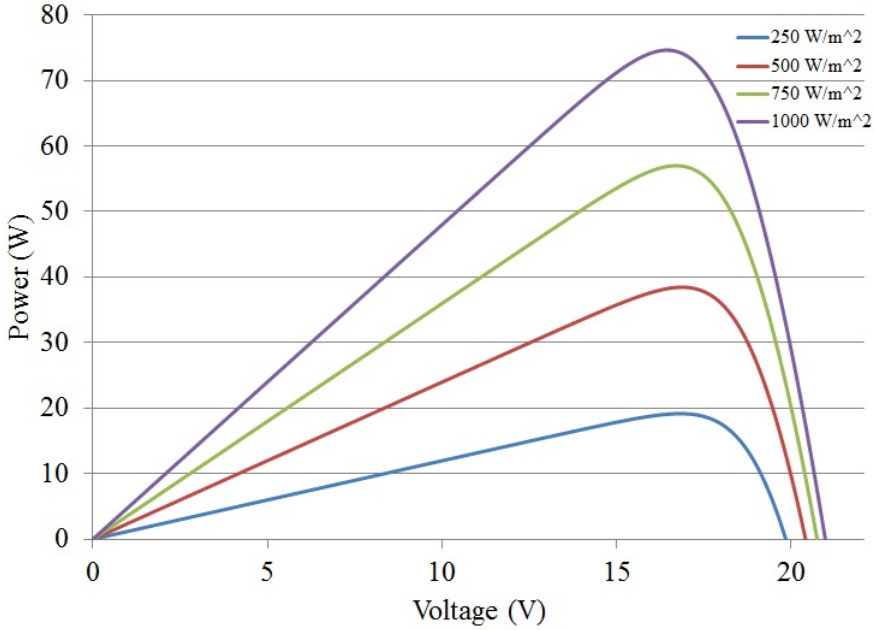

(b) P-V dependence on irradiance.

Figure 2.4: Variation of characteristics with irradiance.

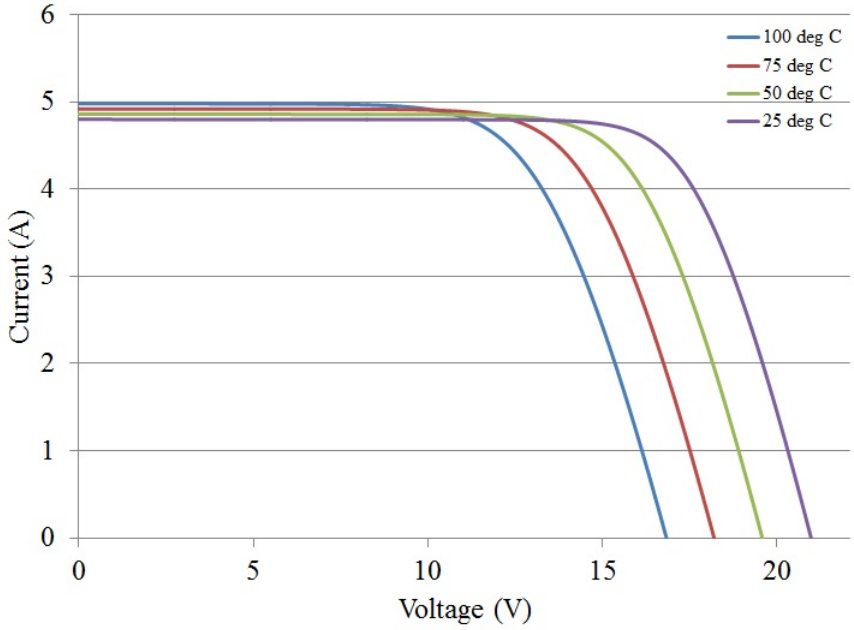

(a) I-V dependence on temperature.

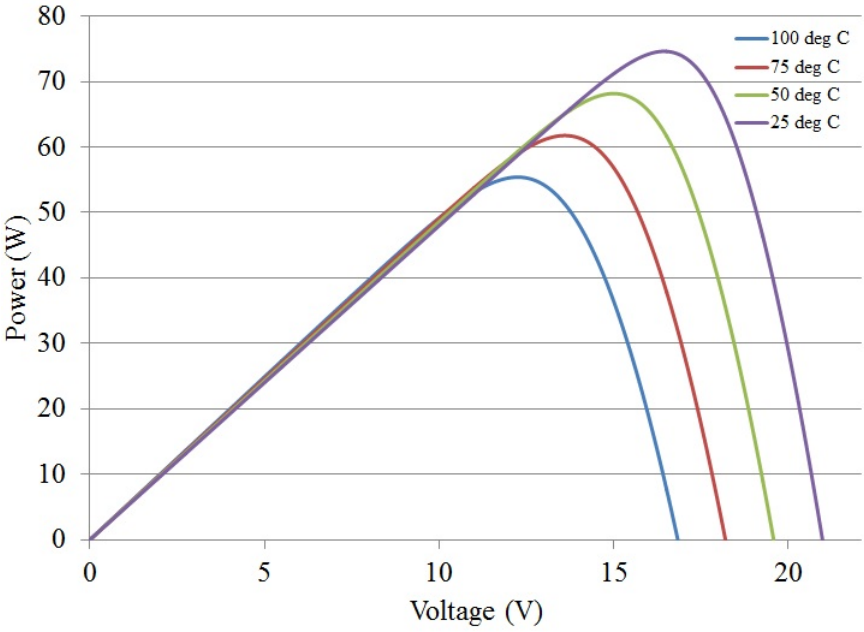

(b) P-V dependence on temperature.

Figure 2.5: Variation of characteristics with temperature.

difference between the current cell temperature and the nominal temperature ($\Delta T = T - T_n$), G is the irradiance on the device surface in W/m^2, K_I is the temperature coefficient of the current and G_n is the nominal irradiance ($1000W/m^2$).

$$I_0 = I_{0,n}\left(\frac{T_n}{T}\right)^3 \exp\left[\frac{qE_g}{AK}\left(\frac{1}{T_n} - \frac{1}{T}\right)\right] \tag{2.14}$$

where, $I_{0,n}$ is the nominal saturation current given in (2.15) and E_g is the bandgap energy of the cell (typically 1.12eV for polycrystalline silicon at $25°C$ [28]).

$$I_{0,n} = \frac{I_{sc,n}}{\exp \frac{V_{oc,n}}{AV_{t,n}} - 1} \tag{2.15}$$

where, $I_{sc,n}$ is the nominal short-circuit current, $V_{oc,n}$ is the nominal open-circuit voltage and $V_{t,n}$ is the nominal junction thermal voltage.

Some authors have attempted to develop equations for the temperature and irradiance dependence of the series and shunt resistances, however, they usually conclude that the temperature and irradiance dependencies are insignificant when compared to the parameters already outlined above [44, 49]. In [59], relationships for the series and shunt resistances are described for the DDM indicating that at low light intensities the shunt resistance is inversely proportional to the irradiance, but is constant beyond $100W/m^2$. The literature suggests that the series and shunt resistance dependence on temperature is quite low and proposed relationships are shown not to be validated experimentally [44, 49]. As with irradiance, the temperature dependence of the resistances are usually neglected in modelling, indicating that they have a very low dependence on environmental conditions.

Other environmental factors which could affect the performance of a PV module are outlined in [52]. These additional factors include irregular dust patterns on the cells, electrical and thermal component mismatch, water vapour intrusion and corrosion, damage from hail, wind, installation, generation of hot spots and electrical failures.

Component mismatch arises because the cells in a string are never identical in terms of their equivalent parameters and the resistances of the connective wires [55]. Photocurrent mismatch can occur when cells are connected in series, as the individual cells in a string produce different currents due to the internal cell properties and environmental conditions. As each cell is producing a different current, the smallest of these currents constrains the current of the remaining cells in the string [29]. To minimise the effect that a damaged or limiting cell

may have on other cells in the string, bypass diodes are frequently connected in anti-parallel with a cell or group of cells [24, 32, 49, 62]. Bypass diodes enable cells producing at a lower current to be bypassed, however will lead to increased non-linearity in the I-V and P-V characteristics.

In general, the faults that arise during PV module operation result from component mismatch, partial shading or from electrical faults [27]. These faults affect the performance and operation of the PV module. In particular, faults affect MPPT operation and the connection to the grid [27].

2.7.2 Cell degradation

The PV cell models frequently considered (including those considered in this thesis), demonstrate modelling under relatively static operating conditions with constant temperature and irradiance. Some factors that could result in performance disparities between models and actual PV cells under the same operating conditions relate to cell degradation. Cell degradation refers to how the internal properties and capabilities of the cells vary after time, sun exposure and physical damage [63, 64]. The amount of cell degradation varies depending on the type of PV cell considered and the conditions that it operates in [64]. As cell degradation occurs, the output capability and efficiency of the cells will be reduced resulting in a lower MPP for operation.

A detailed analysis of the degradation modes that a solar cell undergoes when it is utilised in an outdoor environment is provided in [63]. Several degradation modes are identified including those relating to the cleanliness and condition of the PV module surface, internal changes in the properties of the PV cell caused by light exposure and time, mismatching between cells and variations across the lifetime due to temperature exposure [63]. In [64], these degradation modes are all considered in the context of time and temperature based degradation to develop parameters for the DDM.

For accurate and efficient modelling of long-term operation and reliablity of PV modules, it is essential that these degradation modes can be modelled.

2.8 Peak Power Operation

To generate the maximum power for a given irradiance and temperature it is essential that the PV array is operated at the MPP, P_{max}, defined by the module voltage at the MPP, V_{mpp}, and the module current at the MPP, I_{mpp}. The PV maximum power is defined by [38]:

$$P_{max} = V_{mpp} I_{mpp} \tag{2.16}$$

Other defining factors of the MPP relate to the slope of the P-V curve at this point. As the peak power operation point refers to the MPP, this corresponds to the point where,

$$\frac{\mathrm{d}P}{\mathrm{d}V} = 0 \tag{2.17}$$

The voltage of the MPP is largely affected by changes in temperature, while the current is mainly affected by irradiance level [44]. To control the operating point to coincide with the MPP under changing conditions MPPT algorithms need to be utilised to provide control signals to a converter to extract the maximum power [24, 32, 56].

When exposed to uniform solar irradiation the non-linear I-V characteristics will have one ideal operating point which will provide the maximum power [33].

To operate a PV module effectively and efficiently, it is essential that environmental factors which directly affect the maximum power operating point of the module are identified and acted upon. The efficiency of a PV module relates to the actual useful power output when compared to the power available from the sunlight incident on the cells [30]. As such, the module efficiency is given by (2.18) [32].

$$\eta = \frac{V_{mpp} I_{mpp}}{P_s} = FF \frac{V_{oc} I_{sc}}{\int_0^\infty P(\lambda).\mathrm{d}\lambda} \tag{2.18}$$

where, the fill factor (FF) is a measure of how much solar energy is captured by

a given module and is given by

$$FF = \frac{V_{mpp} I_{mpp}}{V_{oc} I_{sc}} \tag{2.19}$$

Also, $P(\lambda)$ is the solar power density at a particular wavelength λ.

2.9 Modelling of PV Systems Under Non-Uniform Conditions

One of the most significant reasons for a reduction in power from a PV module arises due to partial shading [49]. When cells do not receive uniform radiation, the electrical characteristics across the module vary creating a more complex P-V relationship. The configuration of these connected and partially shaded cells, as well as the number of connected cells has a large influence on the power produced under these conditions [24, 34]. As such, configurations could be designed to be able to operate optimally under PSC. The main sources of partial shading are passing clouds and shadow from nearby buildings, trees and telephone poles [24]. Due to the fluctuations in power that could arise as a result of partial shading, there is a financial implication for utilities [24]. As such, predictive models that can quantify the likely power to be available could be invaluable when accompanied by economic analysis to determine feasibility of a PV system before its implementation.

Some models are proposed in the literature to demonstrate the partial shading case [24, 49, 65–70]. Due to the complexity of modelling an individual cell these models are often formed by combining the characteristics of individual cells under different conditions according to how they are connected together. Being able to accurately model the performance and operation of PV systems under PSC is essential for developing and evaluating MPPT techniques under such conditions. As the size of installed PV systems increases and high efficiency operation becomes highly desirable, knowing how the PV system characteristics vary with a change in conditions and under non-uniform conditions is important.

A PSpice model has been developed to evaluate PSC and provide equations for the dual-peak case to predict the voltage and power of each peak [68]. Despite only providing equations to calculate the power and voltage at the MPPs in the case of two peaks on the P-V characteristic, the authors suggest that with some modifications the equations could be extended to deal with multiple MPPs. The DDM is used with parameters determined by curve-fitting to I-V characteristics at three different irradiance levels in this implementation. Validation of the equations for the dual-peak case is provided based on simulation and experimental results.

In [34], a Labview tool is introduced to analyse the I-V and P-V characteristics under PSC. This paper uses terminology introduced in [24] to divide the system into sub-assemblies, series assemblies, groups and an array based on the shading characteristics. Two case studies are presented to demonstrate the performance [34]. The SDM is used to model each cell in a MATLAB model to study the PSC characteristics in [24].

A model in LTSpice is proposed in [65]. In this model, the effects of the bypass diode configuration and number of bypass diodes is explored. Additionally, the impact of a moving shadow across the PV system is investigated. Each cell has its own light generated current which is related to the area of the cell that is shaded and the transmittance of the shadow. The results support that under certain PSC, the configuration of the bypass diodes has a more significant impact on the performance than the number of bypass diodes.

An analytical model based on the SDM is presented in [71] to demonstrate how the characteristics appear when the modules have different orientations. This refers to the case where modules may be located on different surfaces of the same building and subsequently experience different irradiances.

MATLAB is used to model three series-connected cells using the SDM [66]. In this implementation a variety of shading conditions are applied to the system and the results are experimentally validated using Solkar 3712/0507 PV modules. Mäki et. al. also propose a PSC model developed in MATLAB using the SDM and use their model to assess how system shading and shading strength affect the system operation [72]. The model is validated through experimental testing

with a Raloss SR30-36 PV module in an indoor test environment.

Bishops PV cell model is presented as a MATLAB implementation in [69]. Bishops model incorporates an extra term in the SDM to model avalanche breakdown as it affects the shunt resistance term. In this model, cell temperature is determined by using a thermal energy balance that considers the amount of solar power absorbed by the module, that lost by convection and radiation and the electrical power output of the module. Bishops model is also used in [70] to develop a PSC modelling strategy based on describing a system as being composed of strings, blocks and units. Each unit is defined by a series of flags indicating its electrical position and configuration and its physical position and properties. Each string is solved with the damped Newton method by considering the non-linear system of equations and Jacobian matrix. In the paper, the method is implemented using MATLAB, however, it could also be applied on other platforms. Solving for each string provides a solution for the string current, and these currents are combined to obtain the overall system current.

The SSDM is used in a C-language implementation with PSIM to model PSC in [67]. The interface is developed using C++ and allows the user to indicate the shading of the cells, in the module. The PSIM simulator models the module characteristics using a current source which is controlled by the output current of the series connected PV cells.

A MATLAB-based model which considers PSC and electrical mismatch at the cell level is presented in [62]. The Wisconsin 7-parameter SDM is applied in the analysis and 3D shading models are used to map shadows onto the array plane. The method is validated through comparison with the PV*SOL Expert system.

Piecewise linear branches are used to approximate the PV equivalent circuit in [73] and is implemented in Electro-magnetic Transient Program (EMTP). These simulation studies consider the shading percentage, number of shaded cells, bypass cell configuration and overall module configuration.

2.10 Modelling the BP380 PV Module in MATLAB/Simulink

In this section the model of the BP380 PV module developed in MATLAB/Simulink is presented and validated using experimental data obtained from testing an actual PV module. Firstly, the model will be described and the results of using the parameter estimation techniques already presented using the datasheet information will be detailed. Following this the experimental setup and data collection will be reported. Finally, the model is statistically validated using the experimental data.

2.10.1 Parameter estimation results

The key parameters on the manufacturer datasheet for the BP 380 PV module are given in Table 2.1. Using the three key parameter estimation techniques, identified in Section 2.6, programs have been developed in MATLAB to provide a baseline to use as model parameters for the SDM to model the BP 380 PV module. These estimated parameters are firstly used to validate the simulation model with the experimental data and then the parameters are refined manually to improve the curve-fitting of the model particularly around the key point of interest, the MPP.

The results for the three applied parameter estimation techniques are given Table 2.2.

Table 2.1: BP380 datasheet parameters.

Parameter	**Value**
V_{oc}	22.1 V
I_{sc}	4.8 A
V_{mpp}	17.6 V
I_{mpp}	4.55 A
P_{mpp}	80 W
Temperature coefficient of I_{sc}	$(0.065 \pm 0.015)\%/°C$
Temperature coefficient of V_{oc}	$-(80 \pm 10)mV/°C$

Table 2.2: Parameters estimated.

	Method One	**Method Two**	**Method Three**
V_t	0.8568	0.8328	-
R_s	0.4318 Ω	0.4380 Ω	-
R_{sh}	3.554 kΩ	1.083 kΩ	-
I_0	0.0307 nA	14.3 pA	2.48 μA
I_{ph}	4.8001 A	4.80 A	4.80 A
A	0.9260	0.9	1.65

When the parameters from method one and method two are applied in the simulation model for STC (1000 W/m^2, 25 $°C$) and the equation for the ISDM case (method three) are applied on these conditions, the I-V and P-V characteristics given in Figs. 2.6 and 2.7 are obtained. Visually, the I-V and P-V characteristics produced using method one and method two are identical despite the difference in parameter values. The characteristics produced using method three are very different to those for method one and method two particularly around the MPP. Method three predicts a higher MPP power at a higher voltage. It can be seen from looking at the characteristic that method three is a poor fit, as it predicts that the MPP voltage will be about 0.8 V higher than that given in the datasheet. In all subsequent analysis, only method one and method two will be considered.

To assess how well the characteristics produced using method one and method two match, for each voltage the difference in the current and power in the characteristics produced using each method are calculated and graphed against the voltage. This is shown in Figs. 2.8 and 2.9, for the current and power difference, respectively.

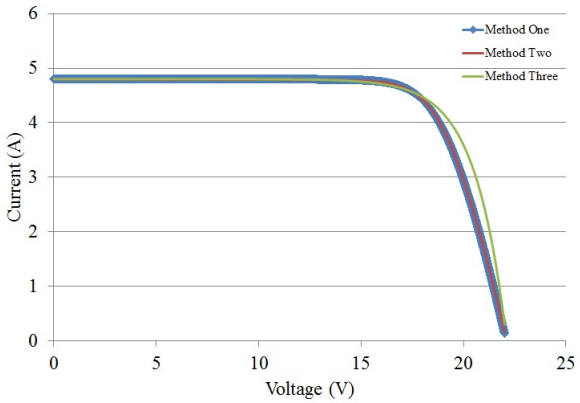

Figure 2.6: I-V characteristics produced using method one, two and three parameter estimation techniques.

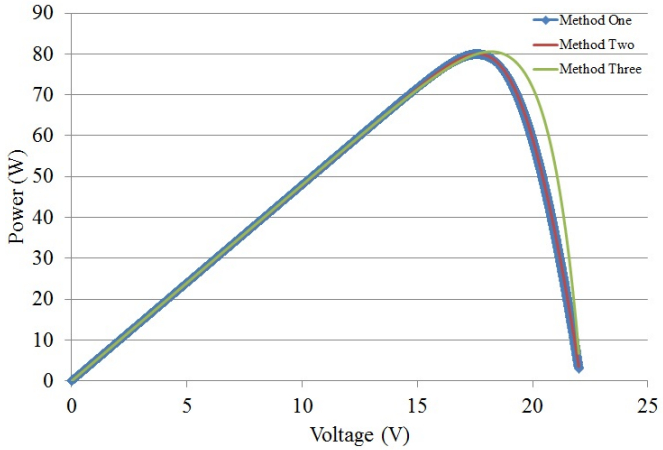

Figure 2.7: P-V characteristics produced using method one, two and three parameter estimation techniques.

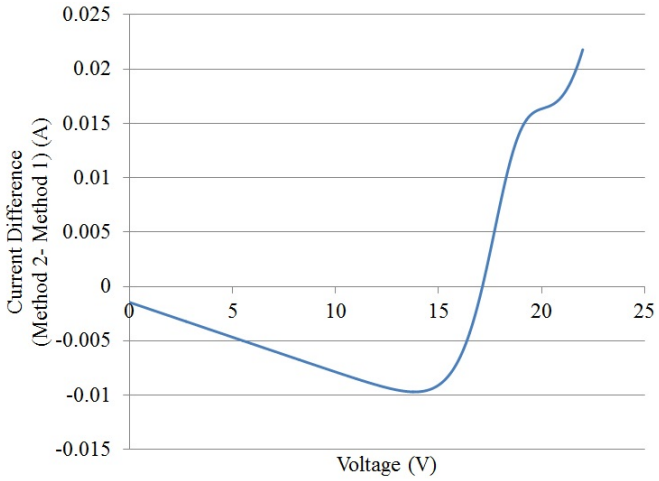

Figure 2.8: Error in current between method one and method two characteristics.

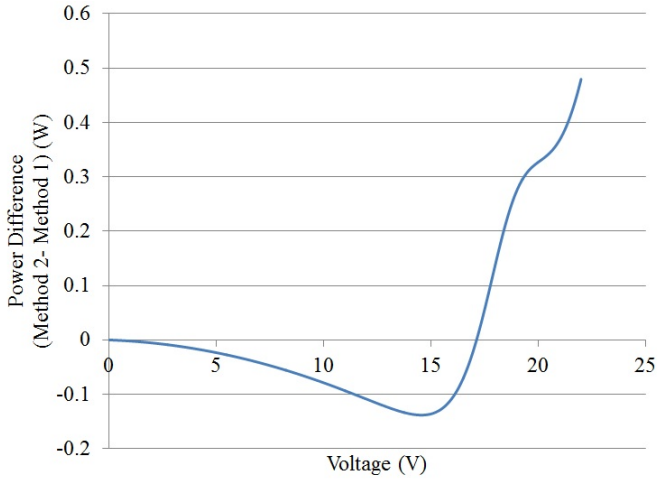

Figure 2.9: Error in power between method one and method two characteristics.

To assess the sensitivity of the I-V and P-V characteristics to variations in the parameters, a ± 5% and ±10% variation is applied to each parameter from method one in isolation to illustrate the effects.

The effect of varying the diode ideality factor is shown in Fig. 2.10. It can be seen that decreasing the diode ideality factor moves the MPP to a lower voltage and lower power. Increasing the diode ideality factor increase the power at the MPP and moves the MPP to a higher voltage. The diode ideality factor is also seen to affect the open-circuit voltage.

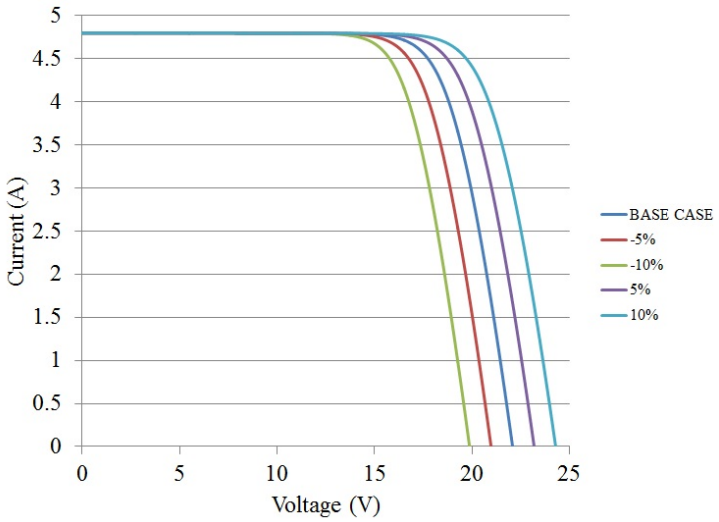

(a) I-V.

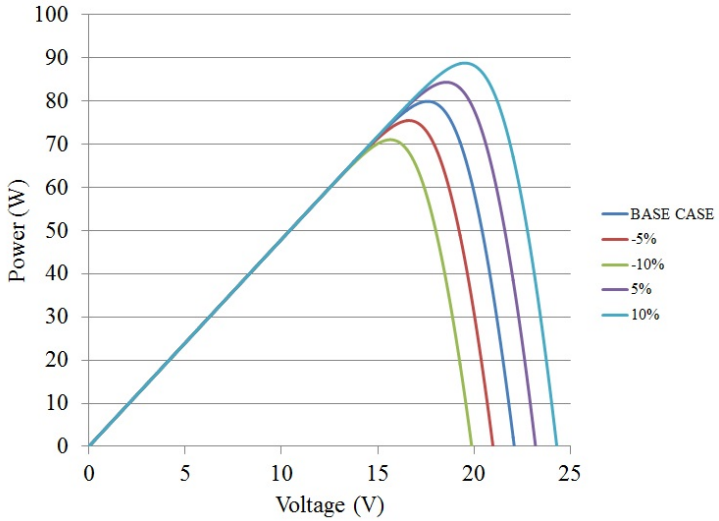

(b) P-V.

Figure 2.10: I-V and P-V characteristic variations for varying diode ideality factor.

The variation of the I-V and P-V characteristics with changing shunt resistance are shown in Fig. 2.11. The characteristics appear identical in all cases indicating that tuning the shunt resistance will not assist in improving the fitting of the model to experimental characteristics.

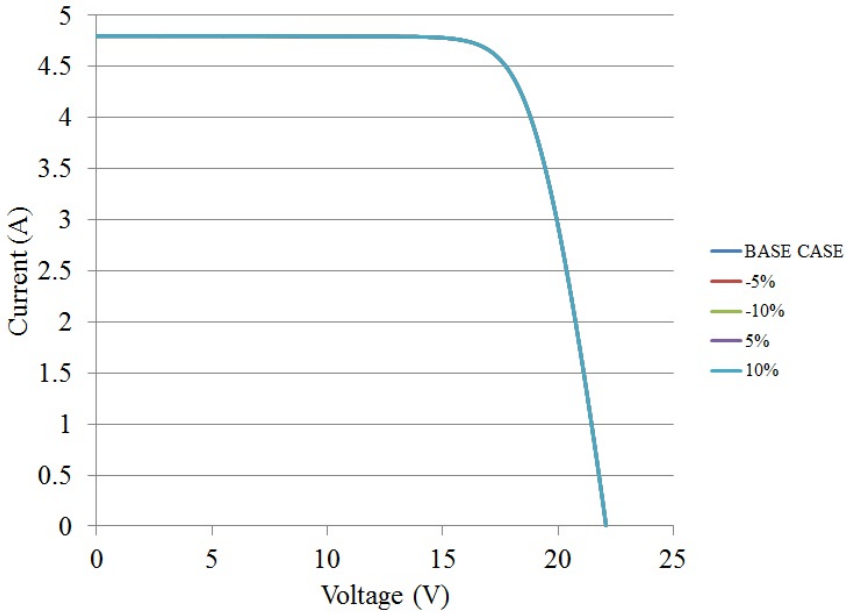

(a) I-V.

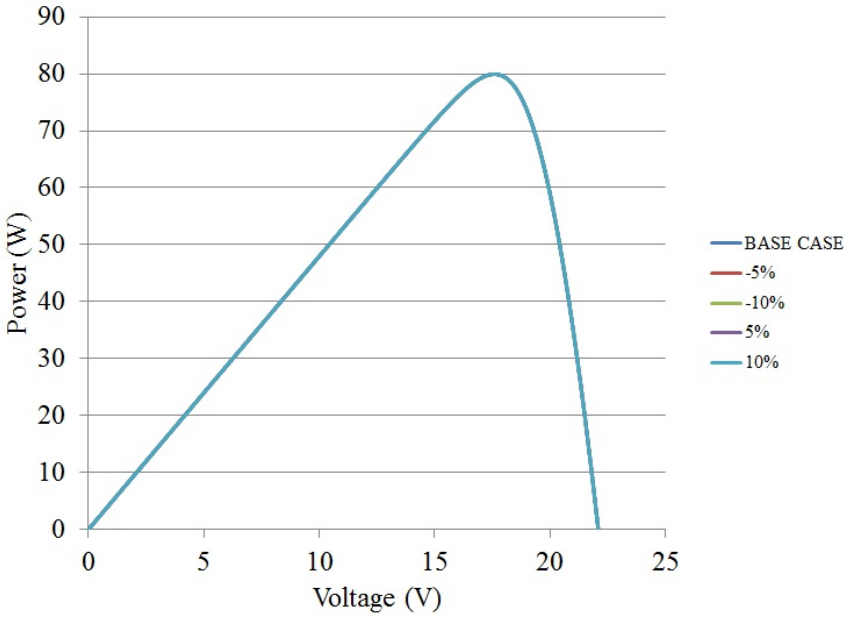

(b) P-V.

Figure 2.11: I-V and P-V characteristic variations for varying shunt resistance.

Figure 2.12 shows the variation in the I-V and P-V characteristics for varying light generated current. As is expected, because the light generated current is related to the short-circuit current, a change is observed in the short circuit current and the behaviour in the current source region. Additionally, a decrease in the light generated current results in a decrease in the power at the MPP.

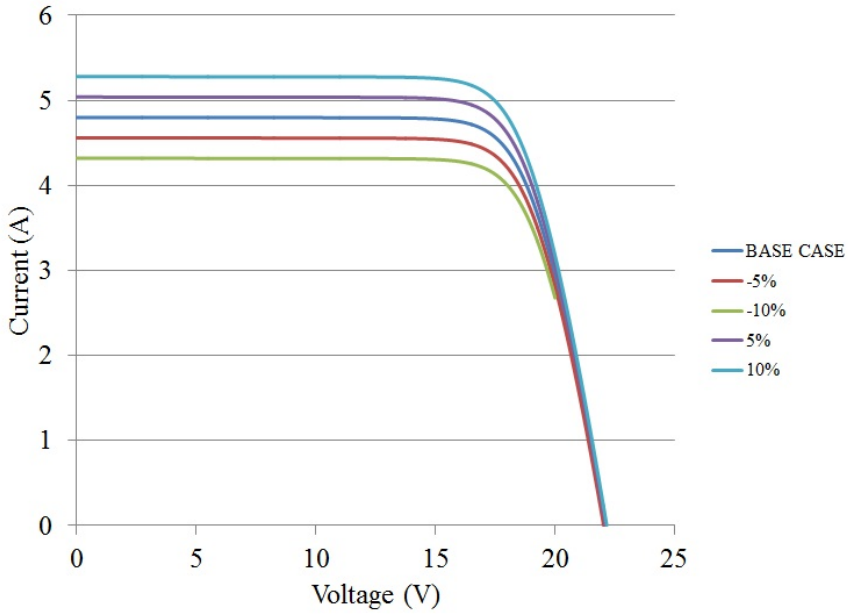

(a) I-V.

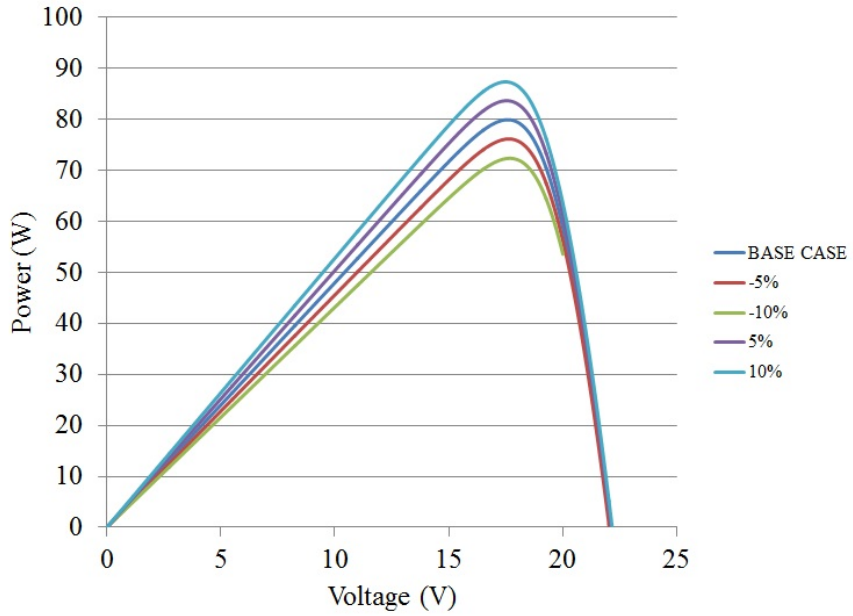

(b) P-V.

Figure 2.12: I-V and P-V characteristic variations for varying light generated current.

In Fig. 2.13, the effect of varying the diode saturation current is explored. The results show that the diode saturation current has a very limited effect on the I-V and P-V characteristics.

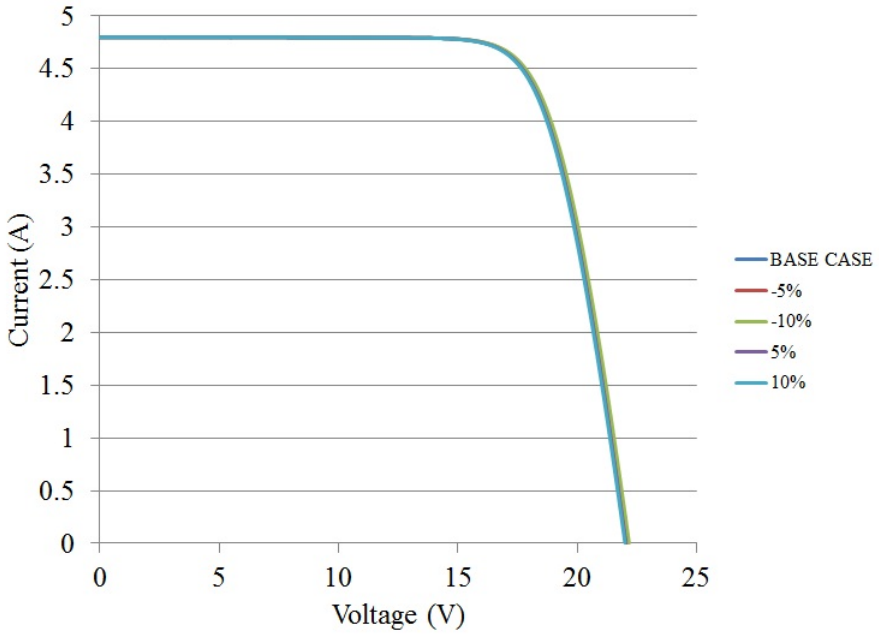

(a) I-V.

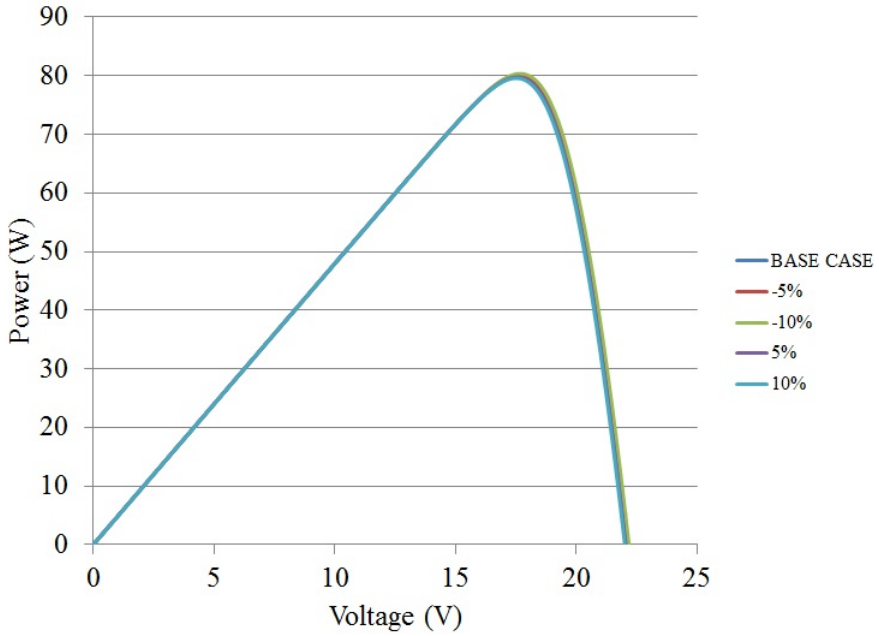

(b) P-V.

Figure 2.13: I-V and P-V characteristic variations for diode saturation current.

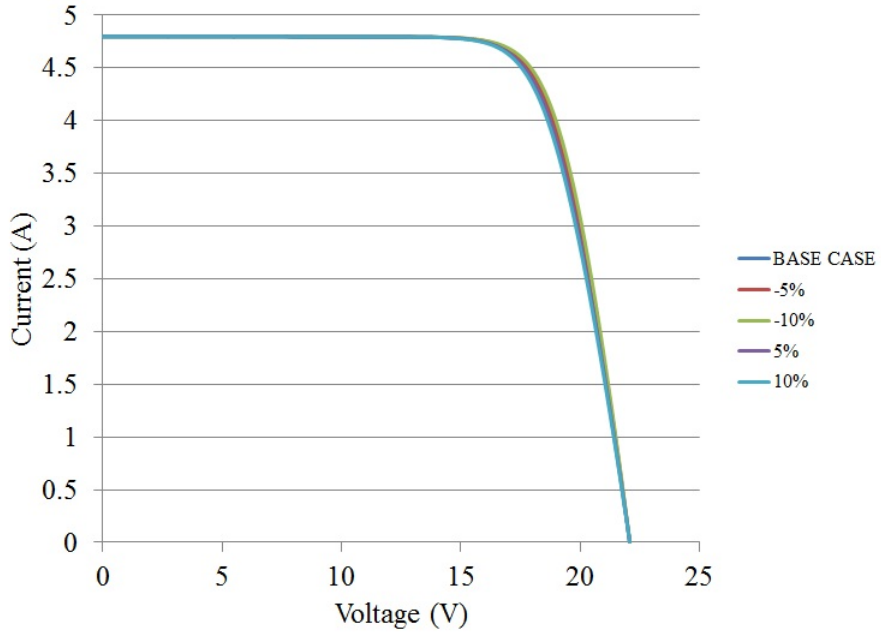

(a) I-V.

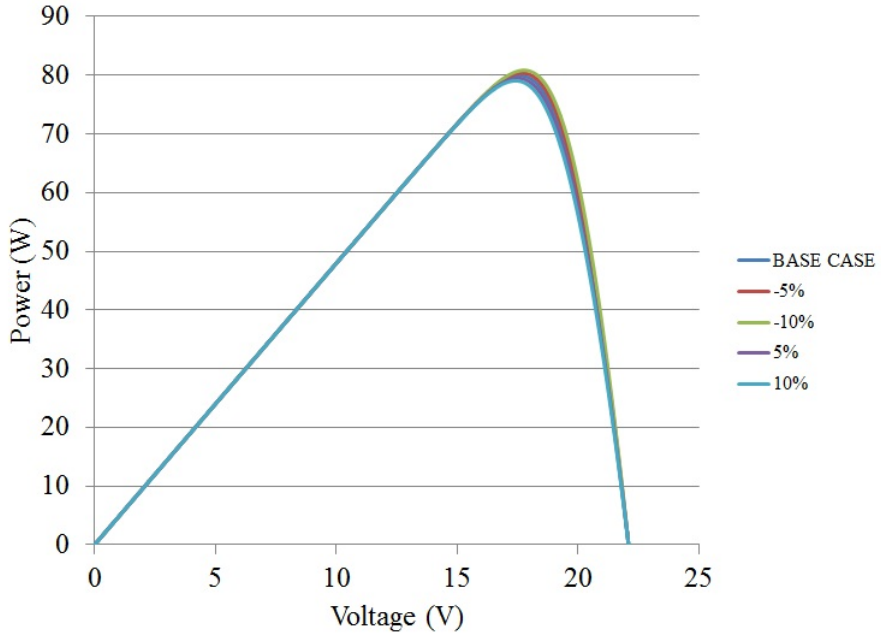

(b) P-V.

Figure 2.14: I-V and P-V characteristic variations for varying series resistance.

Figure 2.14 shows the effect of varying the series resistance. It can be seen that increasing the series resistance will decrease the power at the MPP slightly. This agrees with the literature, because as a result of cell degradation, the maximum power will decrease with time and the series resistance will increase [74]. The series resistance may increase due to a number of factors including corrosion of the modules and the internal connectors, degradation of the silicon and breaking of the internal connections between the cells [75, 76]. A study conducted at the

NREL assessing the degradation of different types of modules has shown that a degradation of around 0.5%/year occurs, with this resulting in a decrease in short-circuit current and with a clear increase in the series resistance [77].

These results suggest that the diode ideality factor, A, and the series resistance, R_s are the most suitable parameters to modify to improve the model fit to the experimental data. The light generated current I_{ph} is also shown to have a considerable effect on the characteristics, however will be held constant at 4.8001 A throughout the analysis. This enables a correction factor for the irradiance to be defined as the sensor module and test modules may not be exactly aligned during testing.

2.10.2 Experimental setup

To measure the I-V and P-V characteristics the BP380 module was placed on the roof of the Engineering building and connected to rheostats which enabled most of the voltage range to be swept. The irradiance was measured using a Kimo SL200 solar irradiance sensor [78]. The voltage, current and power at each time are measured using a PM1000+ power analyser and data is recorded using a purpose built Labview program run in Labview 2011. The experimental setup is shown in Figs. 2.15 and 2.16.

Data is recorded via a custom Labview interface as shown in Fig. 2.17.

2.10.3 Simulation model in MATLAB/Simulink

The simulation model is developed on the basis of the SDM and initially uses parameters calculated from parameter estimation method one [45]. The MATLAB/Simulink based model is shown in Fig. 2.18 to Fig. 2.20. As is supported from the results in Fig. 2.10 to Fig. 2.13, the most significant parameters which can be tuned to improve the model fit are the diode ideality factor (A), and the series resistance (R_s). In improving the model, the variation

Figure 2.15: Experimental setup.

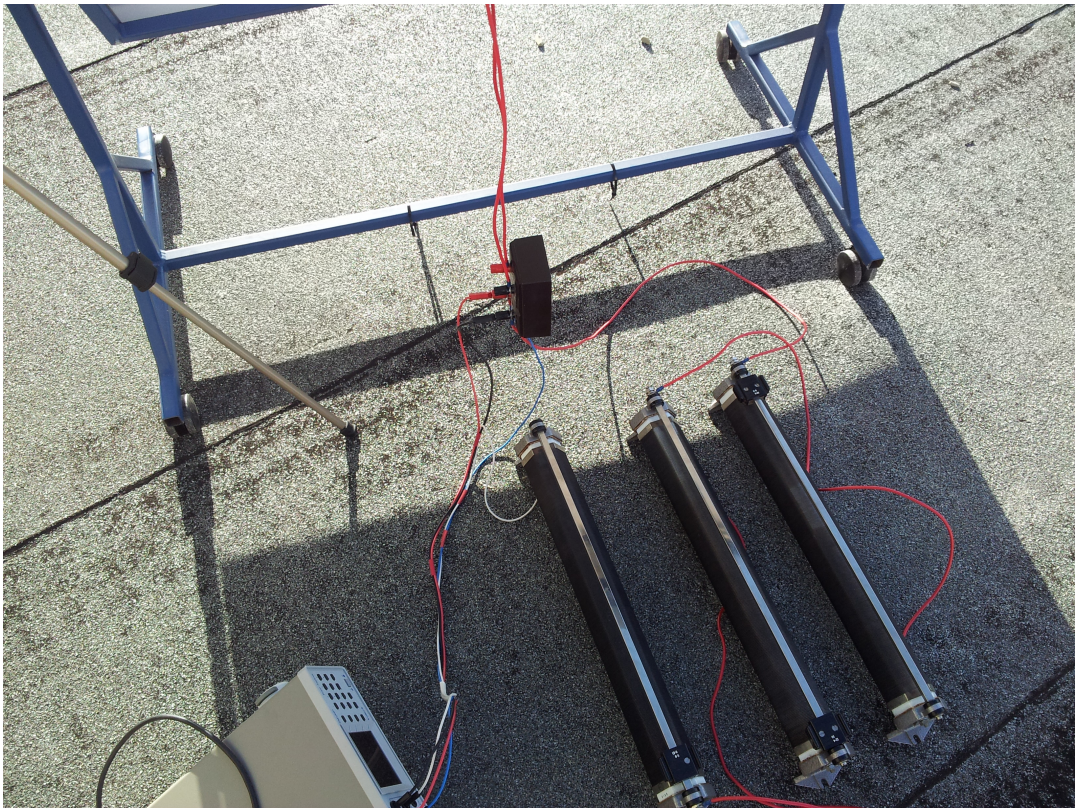

Figure 2.16: Experimental setup.

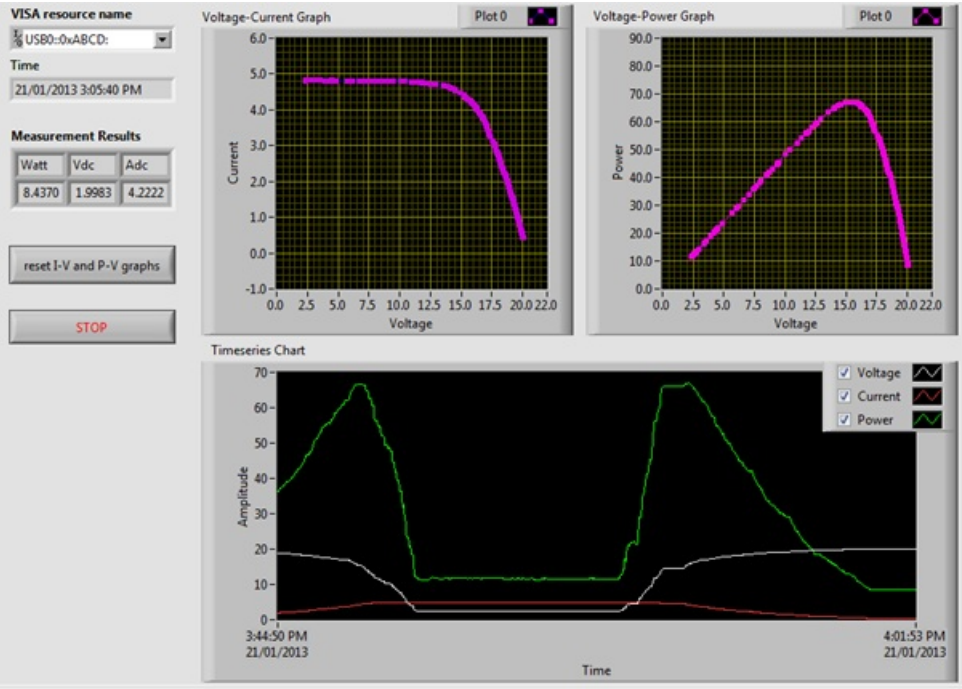

Figure 2.17: Labview interface.

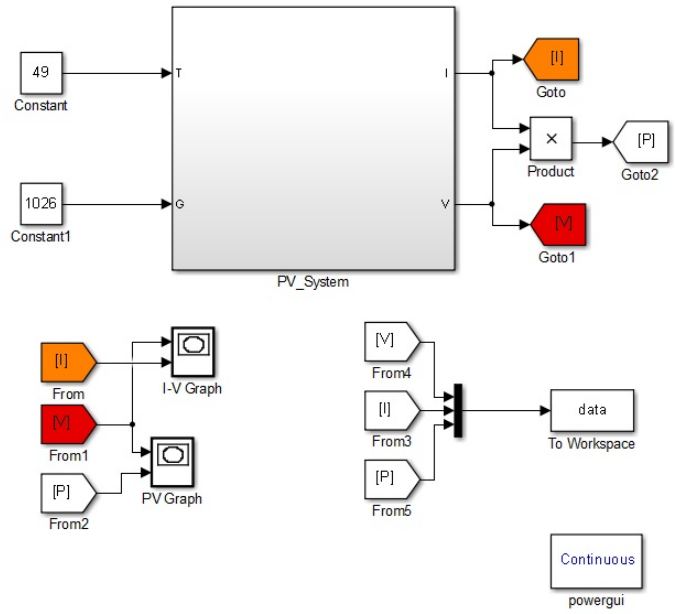

Figure 2.18: MATLAB model of single PV modules.

in these parameters is constrained to be no more than 10%.

The calculation of the light generated current, diode current and shunt current in the MATLAB/Simulink model are all given in Appendix A.

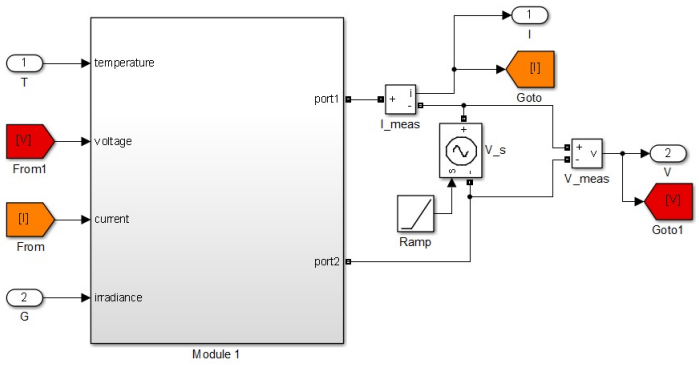

Figure 2.19: MATLAB model of single PV modules.

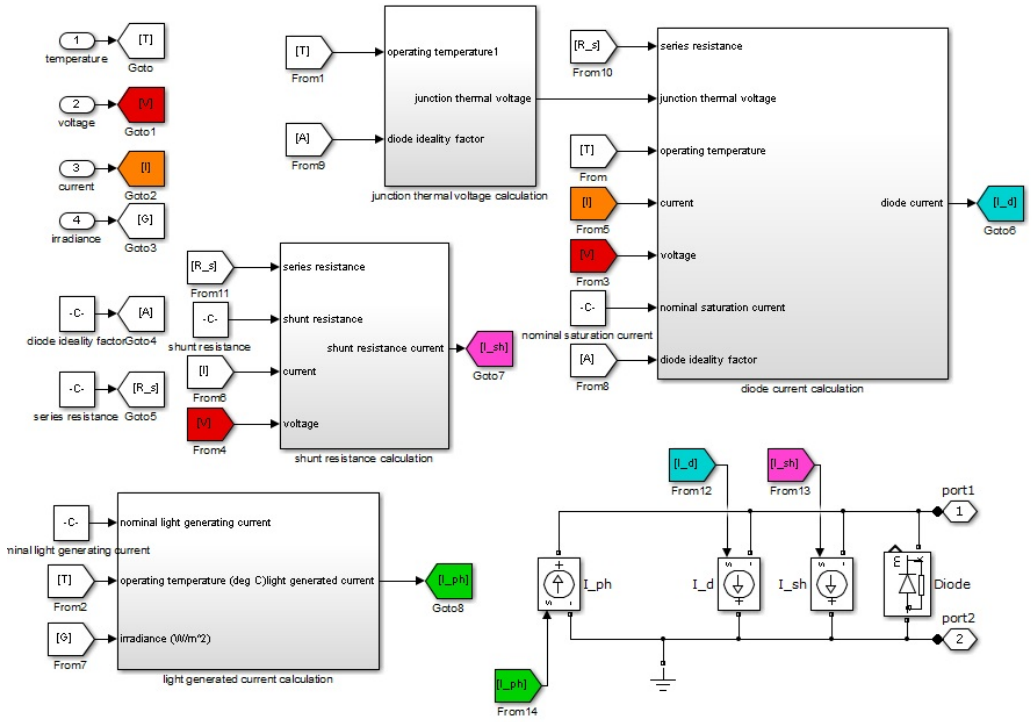

Figure 2.20: MATLAB model of single PV modules.

2.10.4 Model validation

For each of the two BP380 PV modules several I-V curve traces are performed to obtain the I-V and P-V characteristics for model validation. The base parameters used in the model are those from method one [45]. These parameters are allowed to vary within ±10% to improve the model fit. For module one, 14

samples of the I-V and P-V characteristics are used to validate the model and for module two, nine characteristics are used. In each case, the experimental data is compared with the simulation model to determine where the model is least well matched and to see if modifying the parameters can improve the fit of the model at these points. For both module one and module two, the most significant point on the P-V characteristics where the experimental and simulation characteristics are not well matched is at the MPP. After improving the fitting by modifying the diode ideality factor and the series resistance, the maximum error in the power for module one is on average 5.16% around the MPP, and for module two the maximum error in the power is on average 4.03% around the MPP. A sample I-V and P-V characteristic for module two is shown in Figs. 2.21 and 2.22, respectively. This shows very good matching of the characteristics at the lower voltages, a deviation of about 5% around the MPP and a slight difference in the open-circuit voltage. In general, the characteristics produced using the simulation model with the modified parmeters follow the overall shape of the I-V and P-V characteristics produced experimentally. The model has sufficient accuracy in modelling the I-V and P-V characteristics with only a 5% error in the power at the key point of interest the MPP. A 5% error is acceptable as it enables characteristics to be produced with a lower computational burden than with using a more complex model like the DDM. Due to the nature of studies completed in this thesis, a PV module model that can reasonably represent the I-V and P-V characteristics with minimal complexity is preferred. Due to the approximately 5% error in the power at the MPP, all results produced by the simulation model will slightly overestimate the power available.

The final parameters used for each module to achieve the improved model fit are given in Table 2.3.

Table 2.3: Parameters for module one and module two models.

	Module One	**Module Two**
V_t	0.8140	0.8225
R_s	0.47498 Ω	0.47498 Ω
R_{sh}	3.554 kΩ	3.554 kΩ
I_0	0.0307 nA	0.0307 pA
I_{ph}	4.8001 A	4.80001 A
A	0.8797	0.0.88896

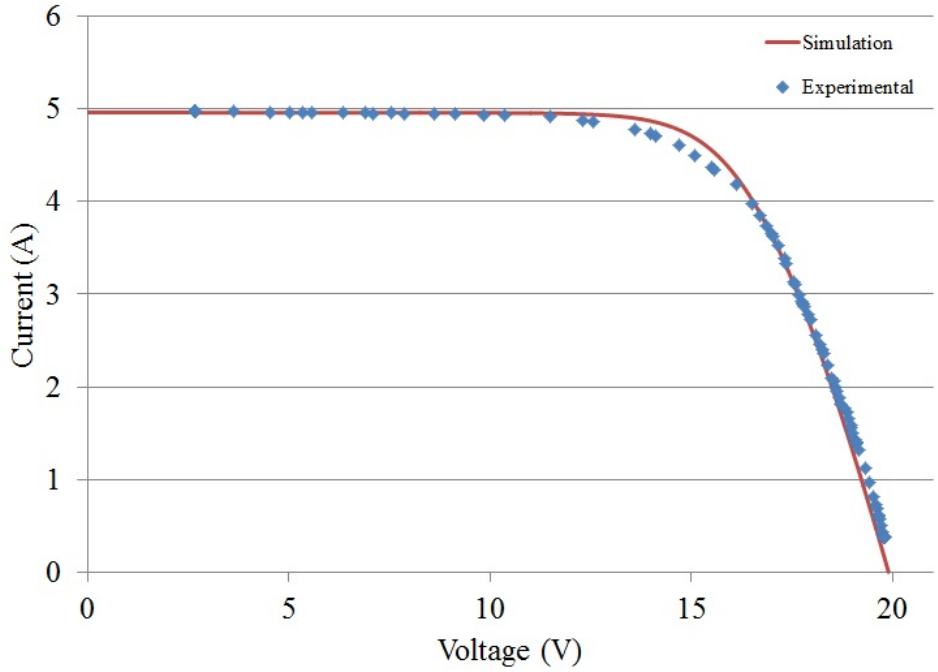

Figure 2.21: Simulation and experimental I-V characteristics for module two with irradiance $1021W/m^2$, temperature 49°C.

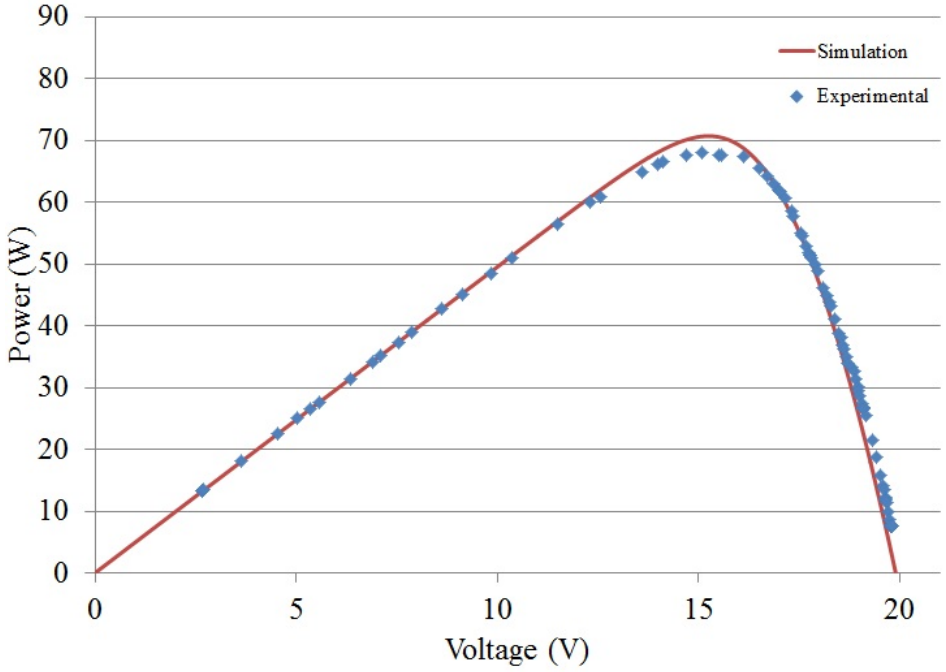

Figure 2.22: Simulation and experimental P-V characteristics for module two with irradiance $1021W/m^2$, temperature 49°C.

2.10.5 Extending the model to Partial Shading Conditions

Two modules are connected in series in the simulation model in MATLAB/Simulink to validate the performance of the model in modelling PSC as

shown in Figs. 2.23 and 2.24. Two Powertech Monocrystalline ZM-9091 5W PV modules are exposed to the same environmental conditions as each of the BP380 modules to provide a real-time indication of the irradiance. The short circuit current of these 5W modules is continually monitored as it is proportional to the irradiance on the module. PSC are the result of covering one panel with fabric to reduce the irradiance to approximately 50-60% of the environmental irradiance using one layer of white cotton fabric. This is a similar technique to that used by [79] for developing PSC. Fig. 2.25 shows the experimental setup for the partial shading studies.

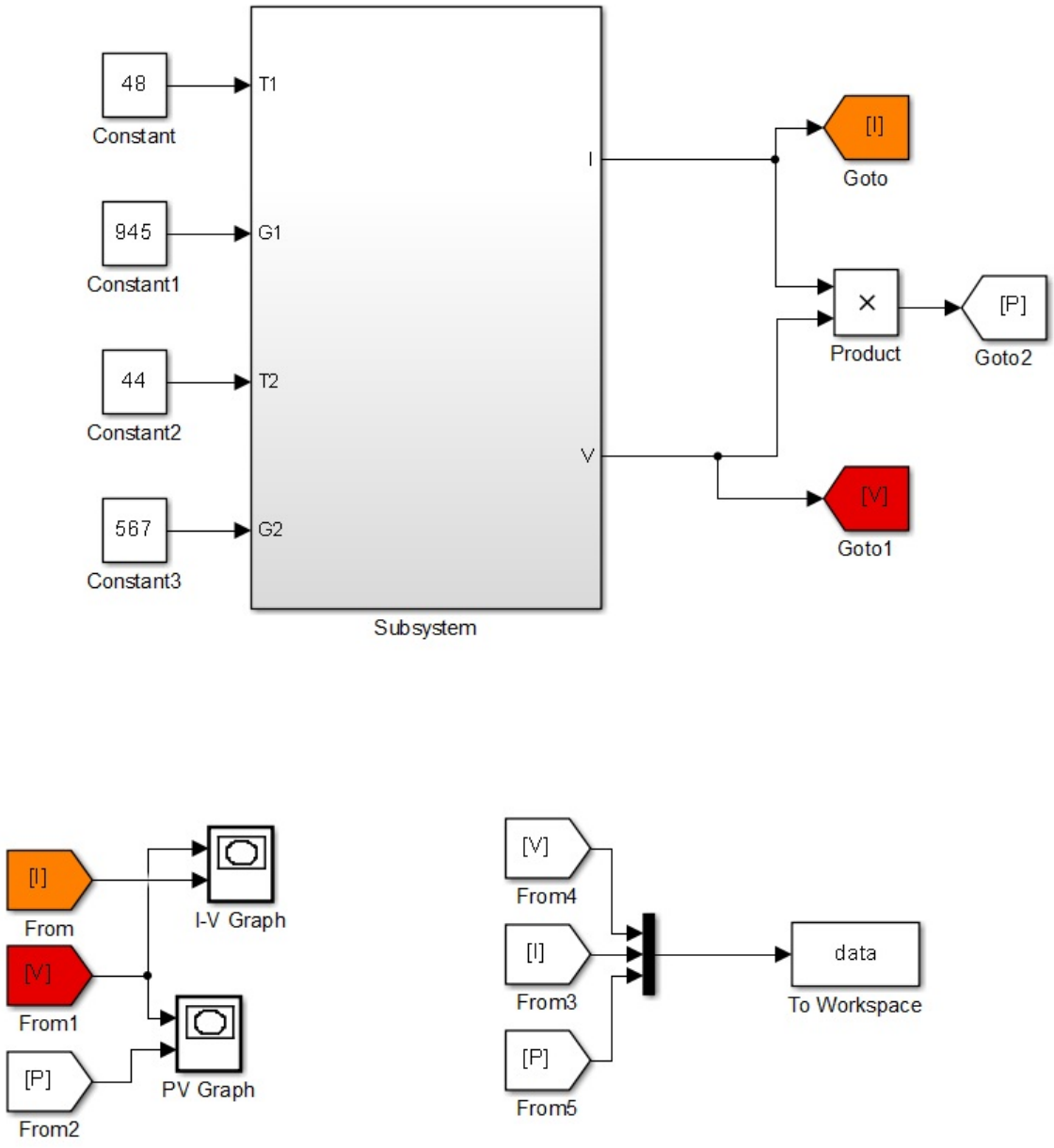

Figure 2.23: Model of two series-connected PV modules.

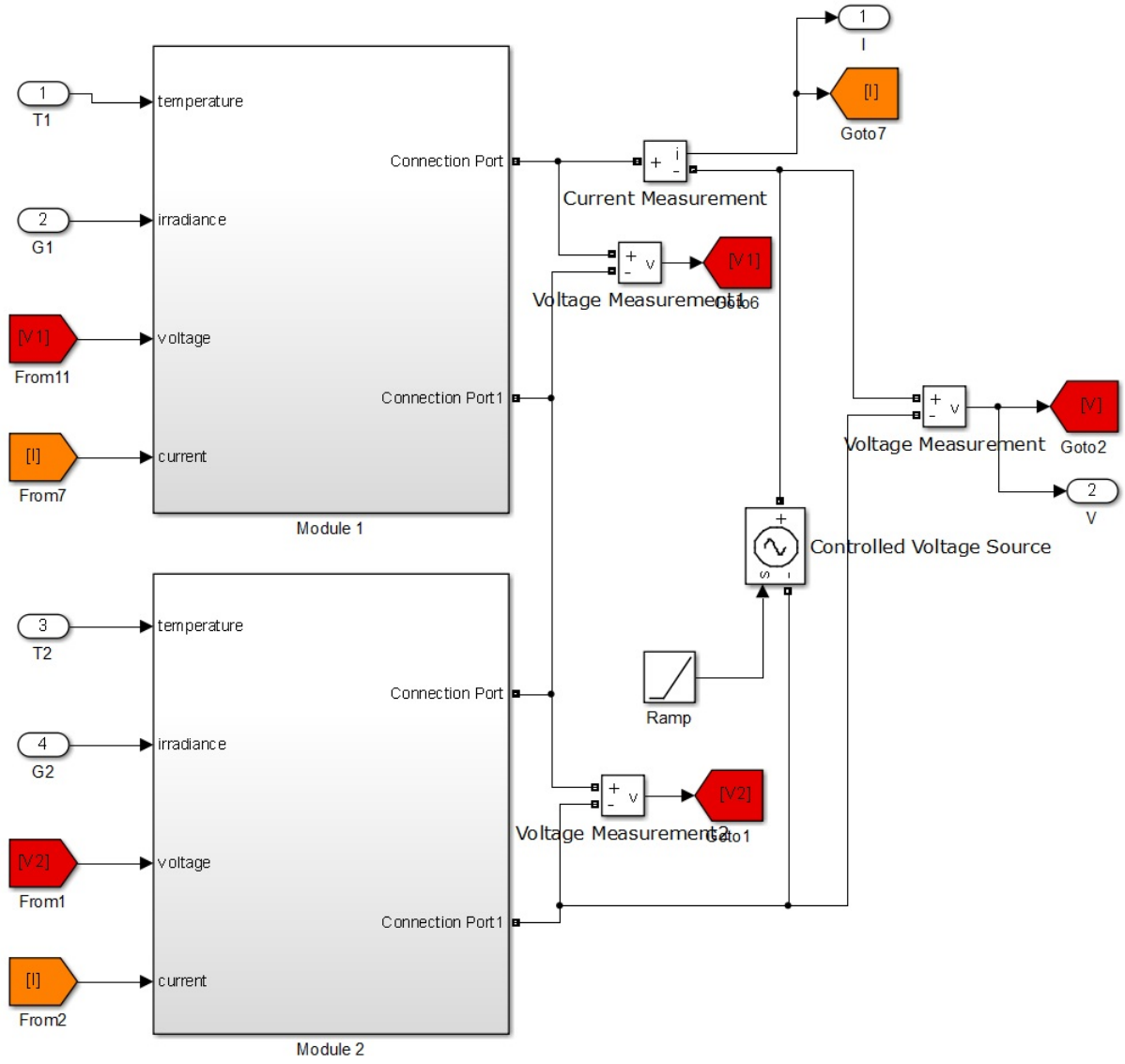

Figure 2.24: Model of two series-connected PV modules.

The model parameters determined for each module as shown in Table 2.3 are used for the two modules in simulation. In a similar method to the single module validation, the experimental and simulation characteristics are compared to see how well they match and to identify any sections where the model has reduced accuracy. Twenty partial shading I-V curve traces are considered in this study. Each case is a combination of fabric covering one module to reduce the irradiance and the variable irradiance due to cloud cover.

Three sample cases for the partial shading study are shown in Fig. 2.26 to 2.28. For Fig. 2.26, module two is covered with one layer of the white fabric. Ten I-V curve traces are performed with this single layer of fabric, with varying ambient

Figure 2.25: Partial Shading Conditions experimental setup.

irradiances and exhibit similar results to that shown in Fig. 2.26. Two layers of the white fabric are placed over module two to develop the results shown in Fig. 2.27. Eight I-V curve traces are performed under these conditions. Finally, in Fig. 2.28, all fabric is removed and the two panels are connected in series to produce I-V and P-V characteristics that demonstrate the slight mismatch between the two modules. Two I-V curve traces are performed under these conditions. In all cases, the module temperature for both modules is approximately 47°C.

The characteristics shown do not match exactly, however, they show that the SDM is capable of replicating the I-V and P-V characteristics under PSC

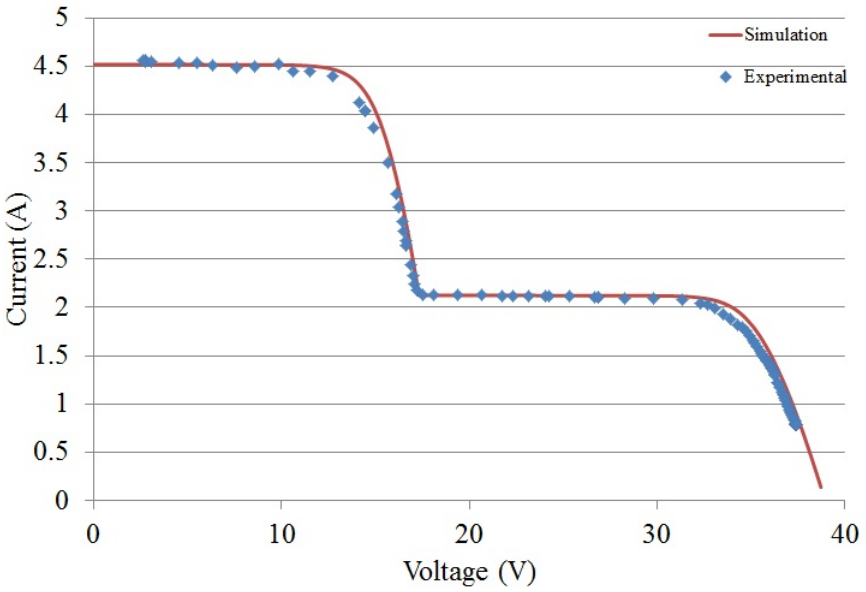

(a) I-V.

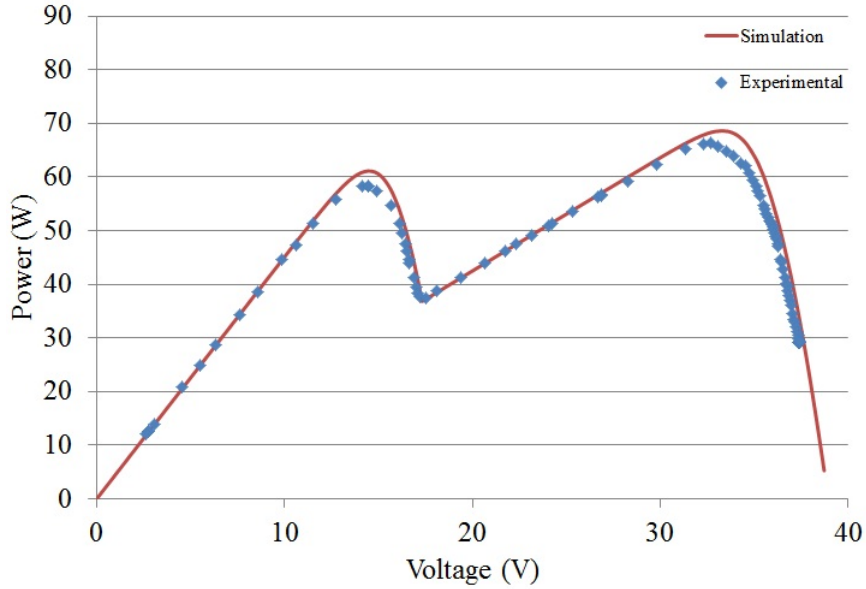

(b) P-V.

Figure 2.26: Simulation and experimental I-V and P-V characteristic variations for sample PSC, with module one irradiance 931 W/m^2, module two irradiance 439 W/m^2.

with a reasonable level of accuracy. The key area of mismatch, as occurred with the single module validation, is around the MPP. In general, the model overestimates the amount of power available at the MPP by about 5%. Keeping this in mind, the models are sufficient to perform MPPT simulations and will generally estimate a MPP location that is slightly different from that experienced experimentally. Additionally, in testing there are some slight errors

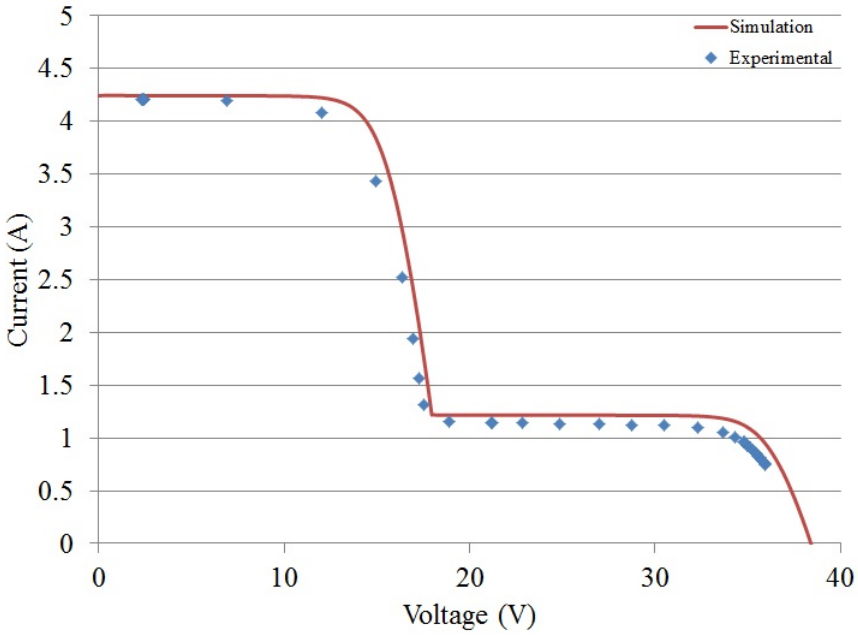

(a) I-V.

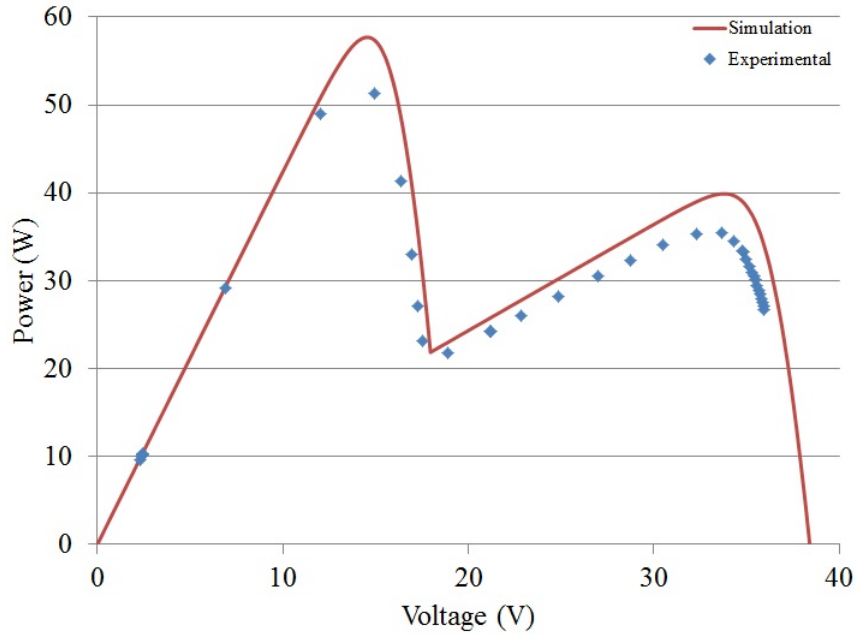

(b) P-V.

Figure 2.27: Simulation and experimental I-V and P-V characteristic variations for sample PSC, with module one irradiance 875 W/m^2, module two irradiance 251 W/m^2.

in the irradiance and temperature measurement due to the ambient conditions not remaining constant during the test period, which are manifested as slight differences between the simulation and experimental characteristics.

The results observed are similar to those in [80], however with slightly lower

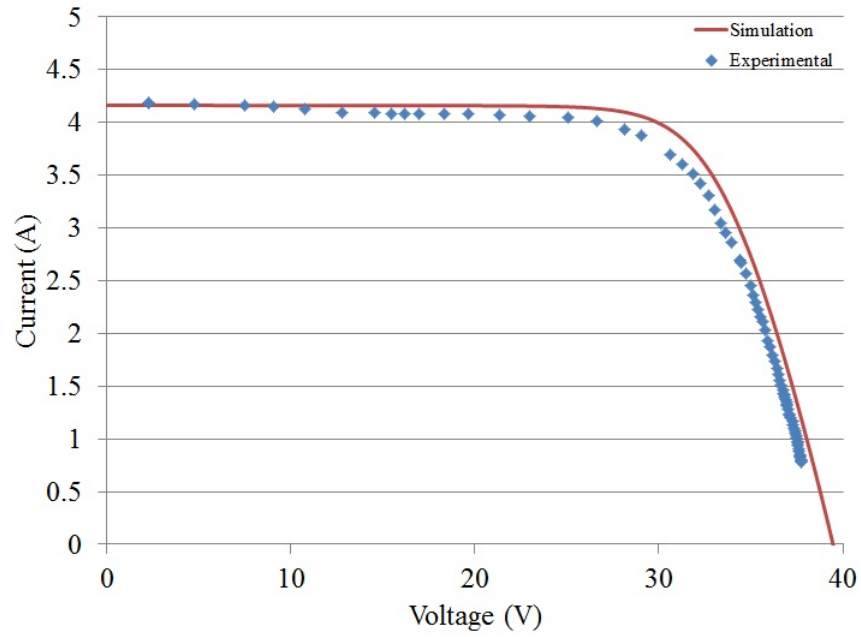

(a) I-V.

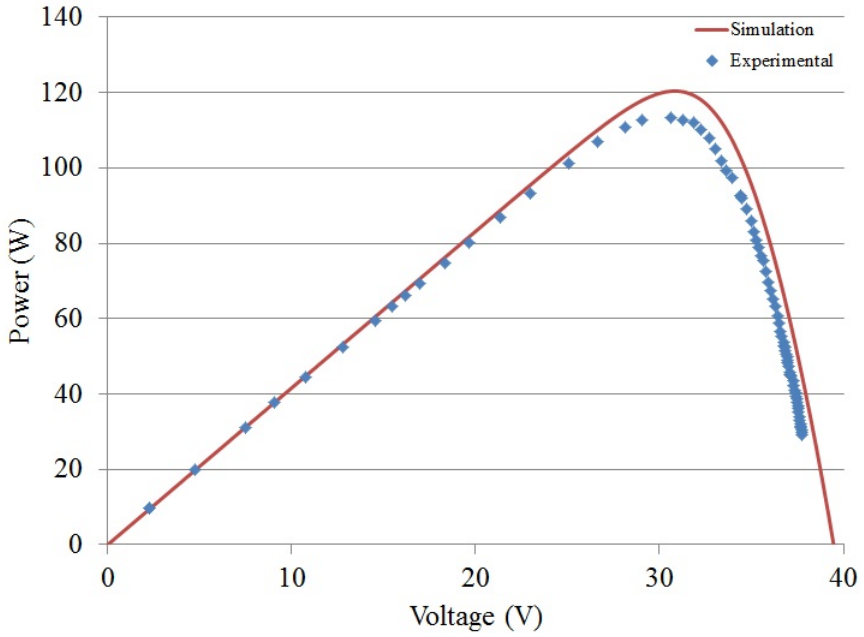

(b) P-V.

Figure 2.28: Simulation and experimental I-V and P-V characteristic variations for sample PSC, with module one and module two irradiance 858 W/m^2.

accuracy around the MPPs. As has already been discussed, this may be due to the fact that the cells, due to their age, have degraded further than anticipated in the 10% variation in parameters considered in the single module validation, or due to the limited accuracy of measuring the irradiance and temperature due to changes in the environment occurring during the test period.

2.11 Conclusion

In this chapter, the common modelling methods for emulating the I-V and P-V characteristics of PV cells have been described. The SDM, due to its simplicity, yet relative accuracy in modelling PV cells has been explored in more detail. Different parameter estimation techniques have been compared, and show that very similar characteristics are produced regardless of the parameter estimation method applied. Experimental validation of the SDM is performed to confirm that the developed model is suitable for modelling the BP380 PV module. Model validation under uniform and non-uniform irradiance conditions has been presented to show that multiple SDM modules can be connected in series in the Matlab model to represent a larger system.

Chapter 3

Modelling and Assessment of Partial Shading Conditions for PV Systems

3.1 Introduction

Photovoltaic systems can experience a multitude of factors in the environment which can lead to effects considered as partial shading conditions (PSC). In this chapter, the main sources of partial shading are described and a process is established to assess the effect of different types of partial shading on the GMPP to better inform GMPPT techniques. Firstly, this chapter defines three PSC classification types which are then explored to assess how each type will affect the relative location of the GMPP. Modelling of an eight module PV system is presented with authentic shading conditions determined from calculations of the proportion of the PV module covered by shadow at any point in time. Five case studies are considered which show the effects that each type of PSC may have on the P-V characteristic of the PV system. This study enables some key conclusions to be reached about the movement of the GMPP voltage under different types of PSC. In particular, if an eight module system experiences a difference in irradiance on each module due to shading, the system will potentially exhibit eight different maxima on the P-V characteristic. How is it possible to identify which maxima is most likely the GMPP? When the conditions change will the GMPP voltage remain around the same MPP or will it move to another MPP location? These questions are addressed in this chapter based on simulation studies and provide useful guidelines for the development of MPPT techniques to enable intelligent searching under changes in the environmental conditions. While the studies presented in this chapter focus on an eight module PV system, the methodology can be extended to any number of modules and any number of

obstacles in the environment.

In general, partial shading, or changing irradiance and temperature across a PV panel, can be separated into different effects based on the time scale. In this chapter these will be referred to as *constant*, *static* and *transient* partial shading. Constant partial shading effects arise from internal mismatch between the modules and is present regardless of the environmental conditions. This constant partial shading acts to reduce the irradiance seen by the panel and is represented in this analysis by reducing the fraction of the real environmental irradiance seen by the module. Static partial shading changes slowly with time. This includes the shadow created by objects like trees, power poles and other structures in the environment. Unlike constant PSC, the static partial shading will change with time and is based on the position of the sun in the sky and how objects in the environment cast shadows on the modules. The static partial shading will result in a significant reduction in the irradiance experienced by the module. Finally, transient PSC is the fastest changing PSC considered and arises due to the environmental conditions, in particular the passage of clouds over the system reducing the irradiance. For large-scale systems which may experience non-uniform transient PSC, the effect on the GMPP will become more significant, as it is not possible to assume that all modules receive the same environmental irradiance when they are geographically dispersed.

The scale of system considered in this analysis is a residential scale system consisting of eight series-connected PV modules. Due to the size of the system, the transient partial shading is assumed to be constant across all the modules in the system. Transient PSC is represented in this model by using real one-minute solar irradiance data available from the Australian Bureau of Meteorology [81]. Constant partial shading occurs due to module mismatch and is represented by applying a scaling factor to each panel based on its relative measure of mismatch. For instance, if module one has a mismatch factor of 1 and module two has a mismatch factor of 0.95 and the one minute solar data indicates an irradiance of 350 W/m^2, then module one would experience 350 W/m^2 and module two would experience 332.5 W/m^2. The static partial shading is considered by including an obstacle in the environment and tracking the position of the sun and when the shadow covers parts of the PV system. Where a module is partially covered, its irradiance is reduced based on a scaling factor related to the number of shaded

and unshaded cells in the module. Where a module is completely shaded by the object in the environment, its irradiance will be 0 W/m^2 regardless of the actual irradiance experienced by the other modules in the system.

The intention of this analysis is to indicate which partial shading component is most significant in causing the location of the GMPP, with respect to the voltage, to move and how often this occurs. These results can be used to separate the effects of constant, static and transient partial shading to improve the performance of GMPPT techniques, by only performing a GMPPT searching process at an appropriate time scale. While the system considered is a simple representation, the approach can be extended to more complex PV systems featuring more obstacles in the environment.

One-minute solar data is used for each day of the year, to ensure that seasonal variation is accounted for in this analysis. This data is available in Tasmania at the Cape Grim weather monitoring station located at (-40.6817,144.6892) [82]. One second data is also considered from the National Renewable Energy Laboratory at the Oahu Measurement Site (in Hawaii) located at (21.31533, -158.087) [83].

In this chapter, the equations to define the shadow position are defined. A comparison on how the GMPP voltage varies with time is considered using one minute and one second irradiance data to validate the use of one minute data in these studies. The one minute irradiance data is used in five cases studies with a variety of obstacle placements in the environment to evaluate the movement of the GMPP voltage under different obstacle conditions. Finally, the result from each section are summarised to demonstrate the effects that transient, static and constant partial shading phenomena have on the relative location of the GMPP and local MPPs.

3.2 Related Research

A variety of different approaches have been recommended for studying PSC in PV systems. These approaches range from authentic shading analyses where the shadow from objects are considered based on the position of the PV modules and the sun at the time of interest [62, 84–87], to approaches where artificial shading conditions are used to explore how PSC affect the PV characteristics [65, 72, 73].

PSC on PV modules where there are obstacles present in the environment is considered in [84]. The effects of direct and diffuse irradiance are considered separately in this analysis. Objects in the environment are defined by polygon surfaces such that different shapes can be constructed. A direct irradiance reduction factor is defined which relates the shaded area to the total cell area, similar to the approach of the shading factor described in this chapter. Surface integrals are used to determine the diffuse irradiance reduction on the surface of the PV modules based on the sun's position and the global irradiance [84].

The solar angle of incidence and the sun's position in the sky for a PV module placed anywhere in the world is calculated in a MATLAB/Simulink model in [85]. The purpose of this study is to be able to track the position of the sun in the sky to provide an indication of the amount of irradiance available to a PV module at any point in time.

In [86] the outline of relevant obstacles in the environment are approximated using a set of linear functions and the irradiance in the plane of the PV module is determined using the Perez model to incorporate the effects of the direct and diffuse components of the irradiance. The authors use a teodolite to make measurements of the topographic coordinates of objects in the environment so that the boundaries of these objects can be described by linear functions. In this paper, the shading factor is defined as the ratio of the irradiance lost due to shading to the total irradiance received by the shaded PV module. For objects that are not solid, a transmission factor is incorporated to reduce the diffuse irradiance and develop a more comprehensive shading factor. The simulation results are compared with experimental measurements to validate the proposed approach.

3D shading analysis is presented for mapping the shadows from objects on the PV modules to enable partial shading and electrical mismatch to be modelled at the cell level in [62]. Shadows are mapped onto the surface of the PV module by using knowledge of the sun's position and a simplified ray tracing methodology. The irradiance available to a cell is the averaged shaded and unshaded state of the cell. Diffuse and reflected components of the irradiance are still received by any cell which is completely shaded by an opaque object. The authors are interested determining the annual losses occurring due to partial shading.

A PV systems installers guide [87], identifies shading as being either temporary (such as dirt or snow on the module surface), due to the location (including shade from objects such as trees and other buildings in the environment), from the building (such as direct shade from a chimney) or as a result of self-shading. The guide suggests that close objects provide a direct shading which causes a more significant reduction in irradiance than objects that are far away. The use of specialised software to perform shading analysis is also recommended in this guide.

In [65] a circuit based model to assess PSC of PV system is presented, where the light-generated current of the module is given by an equation that considers the shaded area, photo-current density and the shadow transmittance. Shading studies presented in this paper explore a vertically and horizontally moving shadow across the PV system representing artificial shading conditions.

P-V characteristics produced under PSC are explored in [72], where the shading on individual cells is broken into thirds. In addition to exploring the changes that happen to the power under PSC, the voltage at the MPP is also considered. In particular, it is noted that while under uniform conditions the MPP will be about 80% of the open-circuit voltage of the system, however this will not be observed when PSC are present. Shading is considered in terms of a shading strength and a percentage of the system that is shaded. Shading is represented as a percentage in [73] and the influence of the number of connected shaded cells is explored. Bypass diode configuration is explored as a way to maximise the power available under PSC.

The analysis presented in this chapter is unique as it focuses on exploring how

the relative location of the GMPP voltage varies with changes in the shading conditions. A simplified shading analysis is used where the PV system is assumed to be in the horizontal plane, the global horizontal irradiance is used as a single irradiance, and the shadow from objects is mapped onto the module position based on the position of the sun at the time of interest. The key benefits of performing this study include identifying regions of the P-V curve where the GMPP is most likely to be located, and to show that under changing environmental conditions, this GMPP voltage is unlikely to vary significantly. In fact, the transitions of the GMPP voltage under different conditions are explored to show that it is very unlikely that between two successive environmental conditions caused by constant, static and transient PSC, that the GMPP voltage will transition further than to an adjacent MPP.

3.3 Calculating the Position of the Sun and the Shadow Length and Position

The shadow tip location in Cartesian coordinates can be calculated using the following series of equations [85,88,89]. The following definitions can be made

- ϕ = latitude
- δ = declination angle
- α = elevation angle
- ω = longitude angle
- HRA = hour angle
- N = day of the year
- ΔT_{GMT} = difference of local time from GMT in hours (10 hours in Tasmania)

Firstly, the hour angle (HRA) can be calculated by considering the local time and correcting to obtain the local solar time. Consider that the local standard time meridian (LSTM) is

$$LSTM = 15^{\circ}\Delta T_{GMT} \tag{3.1}$$

additionally, let B be defined by

$$B = \frac{360}{365}(N - 81) \tag{3.2}$$

The equation of time (EoT) is

$$EoT = 9.87 \sin 2B - 7.53 \cos B - 1.5 \sin B \tag{3.3}$$

The time correction (TC) is

$$TC = 4(\omega - LSTM) + EoT \tag{3.4}$$

This provides a local solar time (LST) of

$$LST = LT + \frac{TC}{60} \tag{3.5}$$

Now the hour angle (HRA) is

$$HRA = 15^{\circ}(LST - 12) \tag{3.6}$$

The elevation angle can be calculated as

$$\alpha = \arcsin[\sin \delta \sin \phi + \cos \delta \cos \phi \cos HRA] \tag{3.7}$$

The azimuth can be calculated as

$$Azi = \arccos\left[\frac{\sin \delta \cos \phi - \cos \delta \sin \phi \cos HRA}{\cos \alpha}\right] \tag{3.8}$$

$$Azimuth = \begin{cases} Azi, & \text{if } HRA < 0. \\ 360^{\circ} - Azi, & \text{if } HRA > 0 \end{cases} \tag{3.9}$$

The shadow length can be calculated using

$$L = \frac{H}{\tan \alpha} \tag{3.10}$$

where, H is the height of the object in the environment.

Given the calculated azimuth and elevation angle for each minute at the location, the x and y positions corresponding to the tip of the shadow can be evaluated using 3.11 and 3.12.

$$x = L[\frac{\sin(Azimuth - 180°)}{\tan\alpha}] \tag{3.11}$$

$$y = L[\frac{\cos(Azimuth - 180°)}{\tan\alpha}] \tag{3.12}$$

This provides an approximate representation of the shadow from an object in the (x,y) coordinate system. Other factors including the angle and height of the PV modules could also be factored into the analysis. Additionally, more complex shapes could be implemented in the environment. The approximate model is used in this study to minimise the computational burden associated with using the full detailed model which is described later in this chapter.

3.4 Simulation Model to Validate the Effects of Partial Shading

BP380 PV modules [23] form the basis for the simulation model used in this chapter. Eight modules are connected in series and experience non-uniform environmental conditions due to moving shadows from obstacles in the environment representing static PSC and cell degradation modelled as constant PSC. Real irradiance data is used to model transient PSC which is assumed to affect all modules simultaneously due to the size of the system. Each obstacle in the environment is defined based on its own coordinate system where the PV modules are located to the South-East of the obstacle. The obstacle is located at the origin of its coordinate system. The obstacle data file also contains the height and width of the obstacle. The system is simulated to be located in Tasmania at the site of the Cape Grim weather monitoring station at latitude -40.6817 and longitude 144.6892. At this site, one minute solar irradiance data is recorded throughout the year. The analysis is focussed on the performance under PSC, so only the minutes of data throughout the year when the modules experience shading due to the obstacles, are considered. The global irradiance is used to provide a simplified analysis of the shading conditions to reduce the

computational burden associated with executing a more detailed shading model based on suggestions given later in this chapter.

Each module has a shading factor which is assessed by considering the number of cells in the module that may be shaded. A cell is considered to be shaded if its mid-point is within half of the shadow width from the central shadow projection. The shadow projection is calculated using the shadow geometry based on the position of the object and the position of the sun at the time of interest. The end point of the shadow is evaluated using the equations for the shadow geometry and the central shadow projection is considered to be a straight line joining the object's origin to the shadow tip. The width of the shadow is assumed to be equal to the object width and uniform at all distances away from the object origin. The shading factor represents the percentage of cells shaded in the module and how this limits the irradiance available to that module. For instance, if no cells are shaded, the shading factor is 1 as all cells receive the global horizontal irradiance. However, if all the cells are shaded in the module, the shading factor becomes 0. The shading factor is defined in (3.13).

$$sf = 1 - (\text{shaded cells}/36) \tag{3.13}$$

The irradiance on each module is determined by multiplying the shading factor by the one-minute irradiance data obtained from the Australian Bureau of Meteorology [81]. This irradiance is then also multiplied by the constant PSC shading factor representing the effect of cell degradation on the irradiance received by the module. The combination of the object shading and cell degradation modelled by shading factors and the real irradiance data creates an authentic indication of the irradiance experienced by the modules when shading occurs in the environment.

An object in the environment is oriented at position (0,0) where the y-axis points in the direction of north, and the x-axis points east. The PV system considered in case 1 is located 10 meters south of the obstacle and 5 meters east. This is shown in Fig. 3.1. The dimensions of each PV module are 0.537 m x 1.209 m. The width of the shadow is assumed equal to the width of the obstacle and the (x,y) co-ordinates of the tip of the shadow are assumed to lie along the centre of the width.

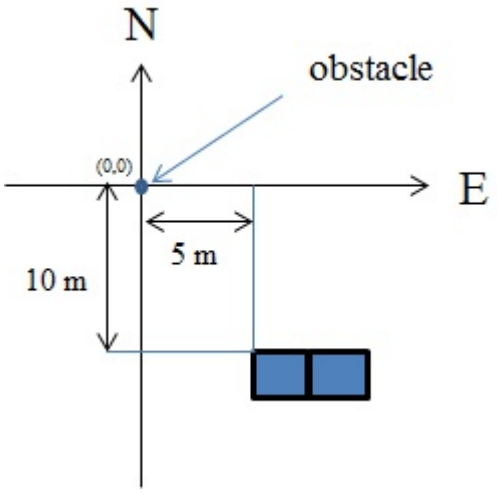

Figure 3.1: XY representation of the obstacle and PV modules in the environment for case 1.

The execution process in the model involves using the real irradiance data as the base amount of irradiance that each module experiences. The time of day data is combined with the obstacle location and the equations presented in Section 3.3. This gives a shadow vector in terms of an x and y coordinate corresponding to the tip of the shadow. Each module then considers this shadow vector and whether or not it will pass through any of the cells in the module. This is determined by looking at the angle and length of the vector. Each module has an angle range defined for each obstacle which indicates when shading might occur. If the shadow vector is within this range, it is evaluated if the shadow vector will cause shading on any of the cells in the module. Cells may be shaded by multiple obstacles at any one time. The shadow vector gives the centrepoint of the shadow and the width is incorporated to see if the centrepoint of each cell is within the tolerance/width of the centreline of the obstacle's shadow. Once the shaded cells for each module have been determined, the factor of the 36 cells which are shaded gives the shading factor for the module. This process is completed for each module and gives the relative irradiance on each module.

At each minute the shading factors are determined and the real irradiance from the Bureau of Meteorology one-minute data is applied in the system. Using this data the I-V and P-V characteristics are obtained by sweeping the voltage across the range 0 to 157 V. This is repeated for each minute of data in the irradiance file.

The process outputs a number of data files which are detailed below. Sample output files are given in Appendix B.

- *year_month_day_x.xlsx* - This file contains information on the I-V and P-V curves obtained for the particular day of study. The data columns correspond to reference time, time, voltage, current, power.
- *year_month_mpps.xlsx* - This file contains information on the GMPP locations for each test irradiance. The data columns correspond to reference time, irradiance, MPP power, MPP voltage, MPP current.
- *year_month_shaded_patterns_1.xlsx* - This file contains information on which cells in the module experience shading at each point in time. If a cell is shaded it is indicated as 1, if it is unshaded it is 0. There is a corresponding file for each module. The data columns correspond to reference time, irradiance, cell1....cell36.
- *year_month_shadow_location.xlsx* - This file records the (x,y) coordinates of the shadow tip for each object considered for each sample irradiance. The data columns correspond to reference time, x and y coordinates of each obstacle.
- *year_month_irradiance_on_all_modules.xlsx* - This data file gives the shading factors and irradiance on each module and combines the information from the shading patterns file for each module. The data columns correspond to reference time, module1...module8 irradiance.

Of these files, the *year_month_mpps.xlsx* file is used in the analysis in this chapter to show how the MPP location varies with changing irradiance and the movement of shadow in the environment. The MPP power will continually jump due to the changing irradiance in the environment which is unavoidable. The MPP voltage however should undergo a much smaller jump as the irradiance changes. The analysis is interested in how far the MPP voltage moves under PSC and how frequently it moves between successive MPPs. In particular in [90], it is identified that the MPPs lie with separation of approximately $0.8V_{oc}$, so this analysis looks to see how frequently the GMPP jumps to another peak under real irradiance conditions and with a variety of obstacles in the environment. The purpose of this analysis is to identify how frequently GMPPT should be initiated and to determine whether an intelligently tuned conventional MPPT technique could provide superior performance by remaining around the location of the most likely GMPP.

The inputs to the simulation are an irradiance file and an obstacles file. A sample few lines from an irradiance file is shown in Fig. 3.2, where the columns are:

- A - year
- B - month
- C - day
- D - hour
- E - minute
- F - simulation time
- G - input for lookup table for voltage sweep, alternates between 0 and 157 so that the simulation model varies the voltage across this range
- H - irradiance

A sample obstacles file for two obstacles in the environment is shown in Fig. 3.3, where the columns are:

- A - height
- B - width
- C - obstacle x coordinate relative to PV system
- D - obstacle y coordinate relative to PV system

The proposed flowchart of this PSC assessment is shown in Fig. 3.4 for a PV system consisting of eight modules. It is possible to change the number of modules by changing the constant in the decision block *If module_ref* <= 8 of Fig. 3.4. The eight module simulation model is shown in Fig. 3.5 to Fig. 3.8.

	A	B	C	D	E	F	G	H
1	2010	4	16	6	42	0	0	100
2	2010	4	16	7	38	0.1	157	105.41
3	2010	4	16	7	39	0.2	0	116.47
4	2010	4	16	7	40	0.3	157	127.71
5	2010	4	16	7	41	0.4	0	134.89
6	2010	4	16	7	42	0.5	157	133.64
7	2010	4	16	7	43	0.6	0	132.9
8	2010	4	16	7	44	0.7	157	124.33

Figure 3.2: Irradiance input file sample.

	A	B	C	D
1	20	0.25	-5	10
2	1	0.25	-0.1	0.1

Figure 3.3: Obstacles input file sample for two obstacles.

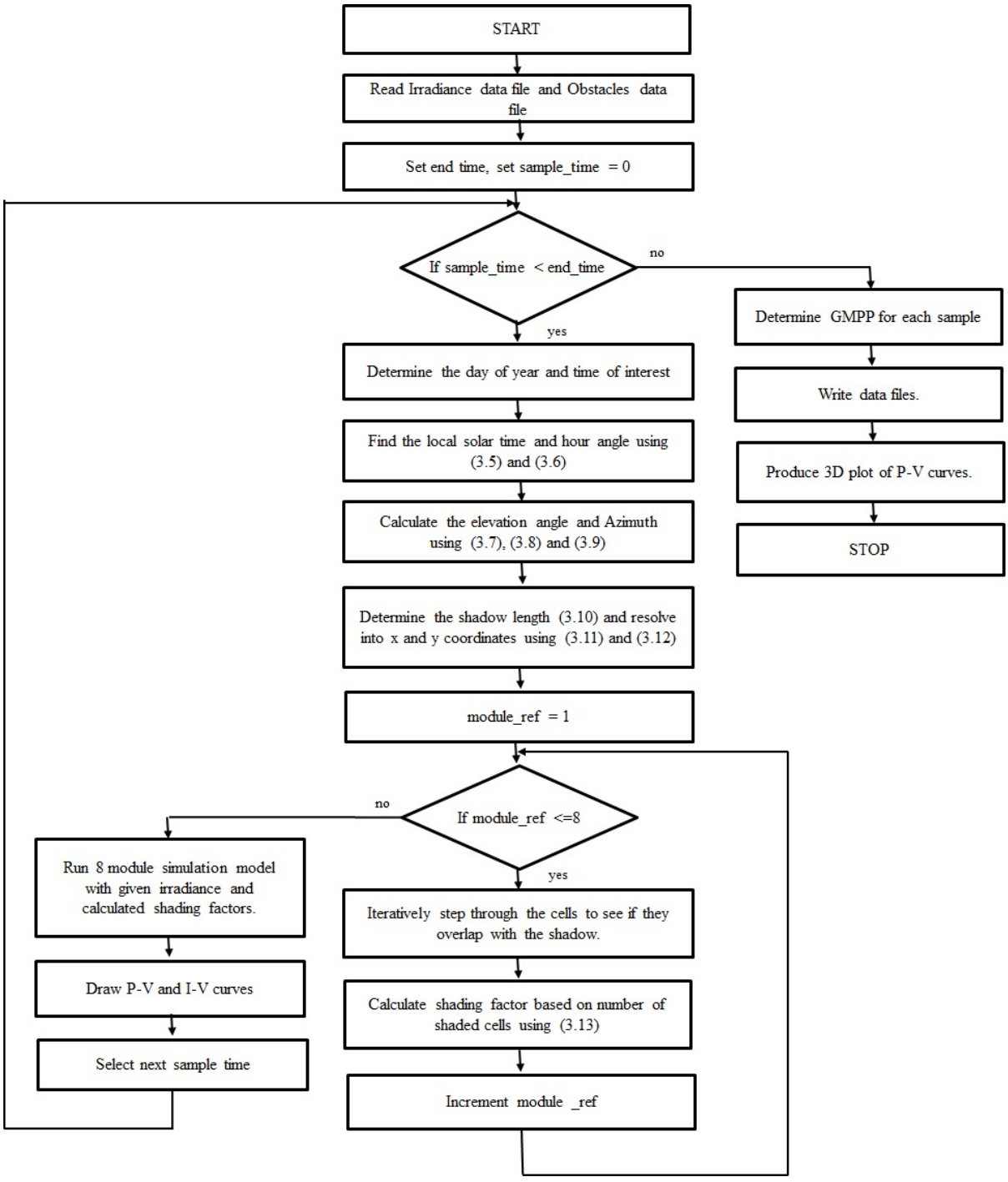

Figure 3.4: Proposed partial shading study flowchart for PV system with eight modules and any number of obstacles.

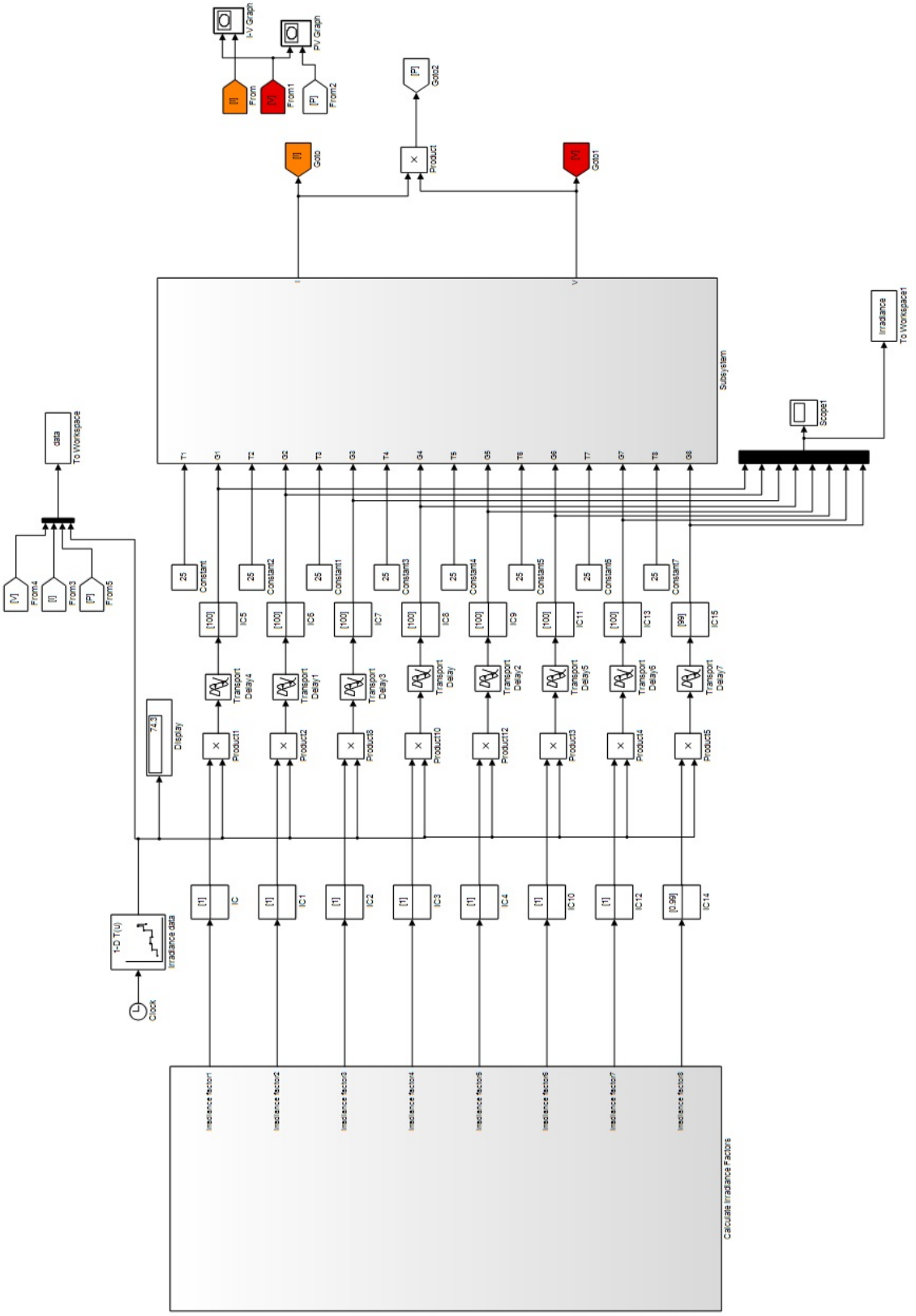

Figure 3.5: Overall eight PV module simulation model.

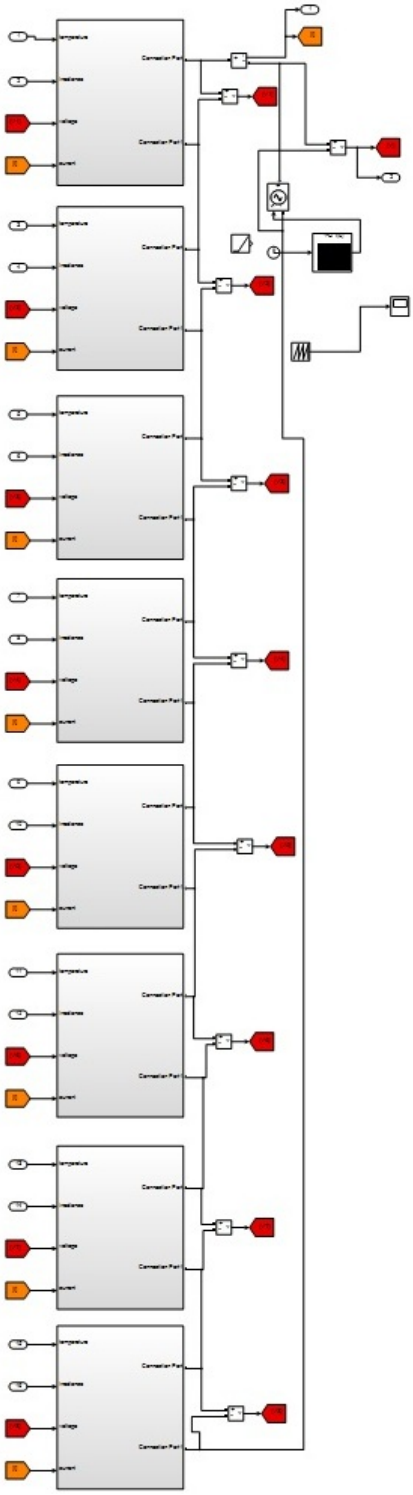

Figure 3.6: Eight PV module simulation model inside subsystem of Fig. 3.5.

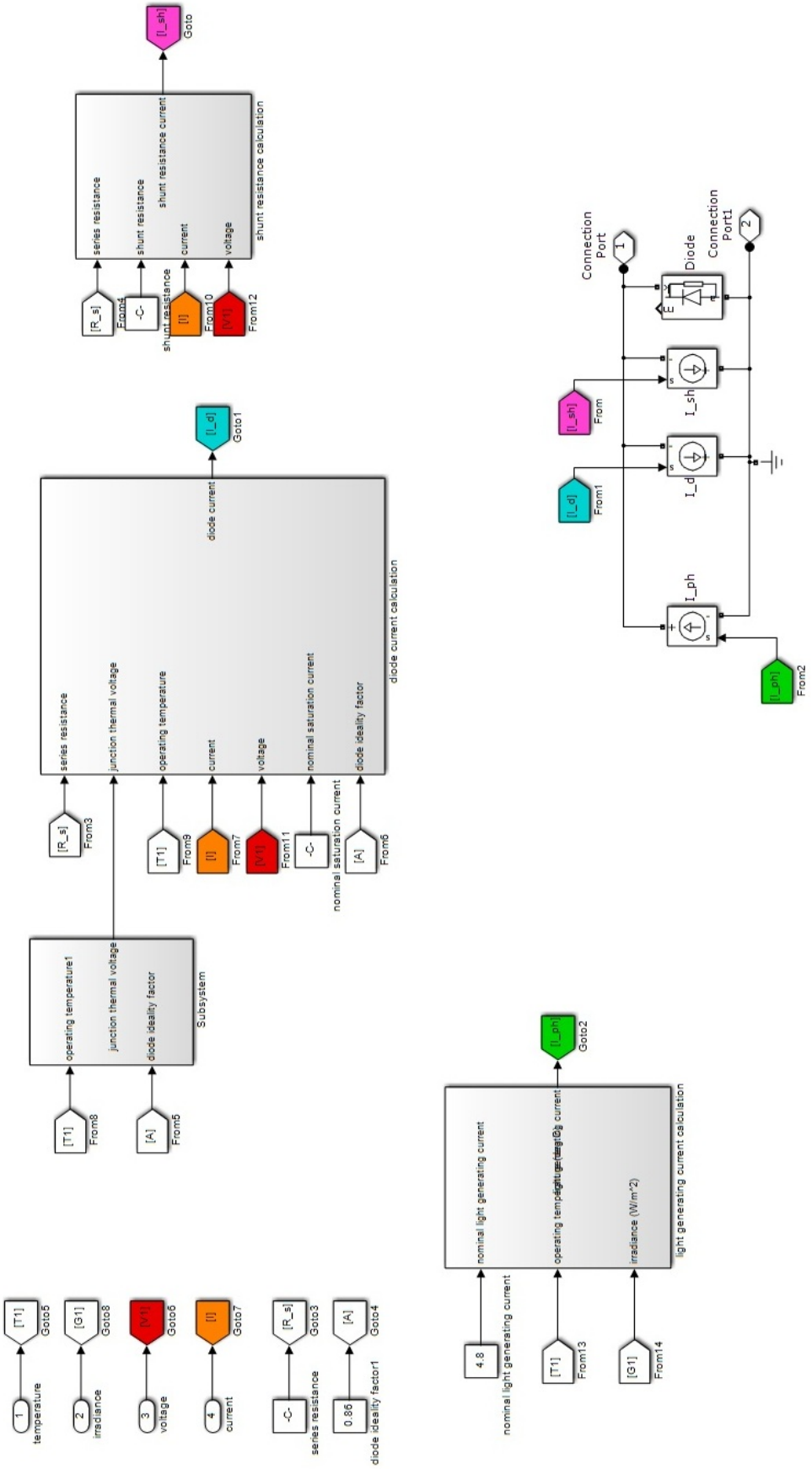

Figure 3.7: Model of each PV module.

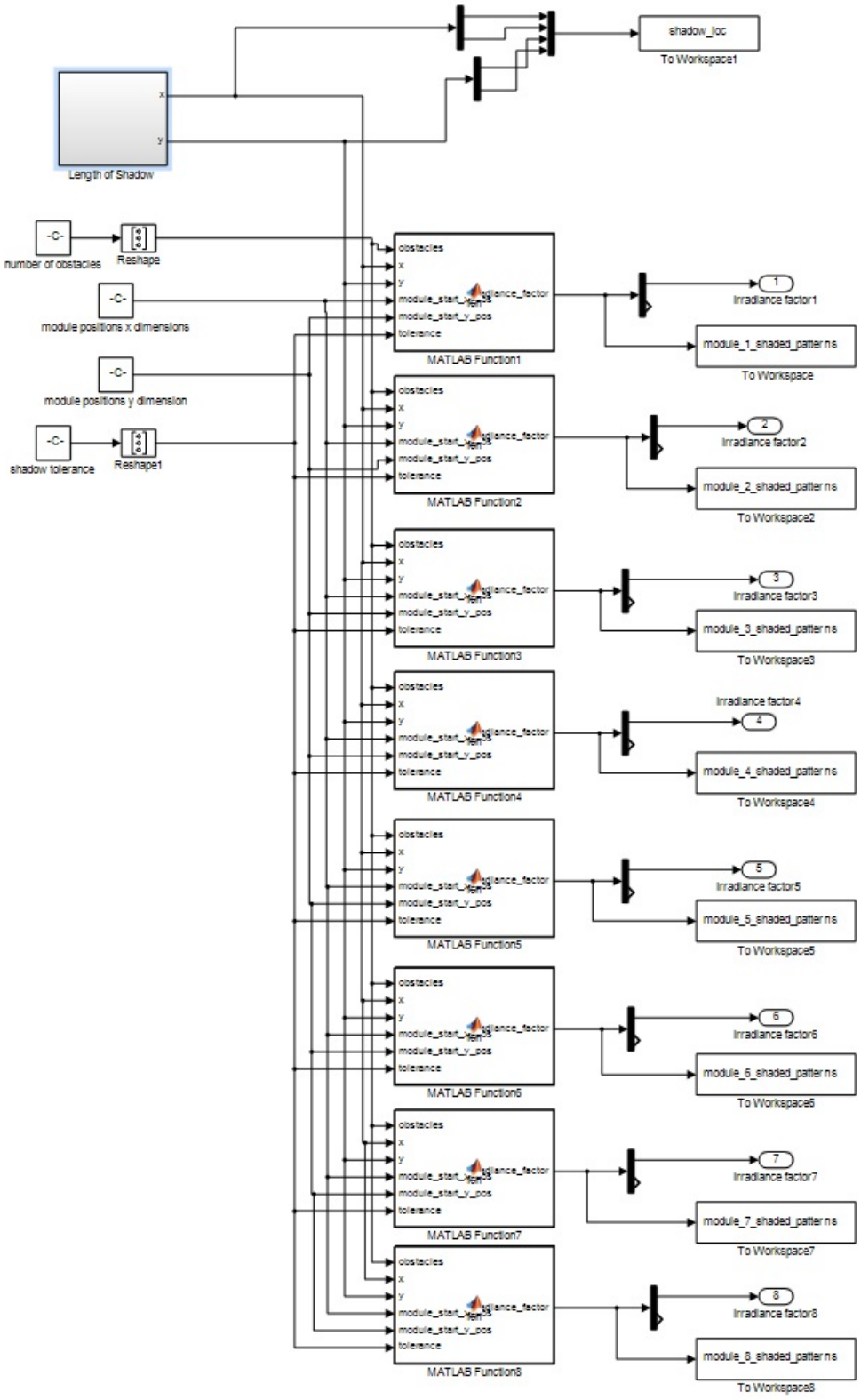

Figure 3.8: Irradiance factors calculation.

3.5 Comparing One Minute and One Second Irradiance Data

The main data available in Tasmania, for assessing how the irradiance changes, is averaged on a one minute basis. To verify that this data is sufficient to demonstrate PSC experienced within Tasmania, albeit on a different time scale, a similarly placed obstacle was explored using one second data from the National Renewable Energy Laboratory (NREL) [91] for a single day of interest at a location in the USA. 19 March 2010 is used for this study with an obstacle placed at 5 m south and 2 m east of the PV system location. The obstacle has a height of 20 m and width of 0.25 m, which is the same as the obstacle considered in case 1 of the one minute irradiance simulation for comparison. The reason for the slightly different obstacle position for the two cases is due to the physical location of the sensor in either the Southern or Northern hemisphere. The obstacle is placed to enable shading of the PV system to occur during the time of interest. Figure 3.9 shows the irradiance and movement of the GMPP voltage for 3000 seconds over the time of interest. Figure 3.10 shows the irradiance and movement of the GMPP voltage for the 70 minutes over the time of interest. The day of interest for the one minute data is 16 April 2010.

From inspection in Figs. 3.9 and 3.10, the trends of moving between relative MPPs for the GMPP exhibited with the one second data is similar, although maybe slightly less frequent than with the one minute data. This suggests that using the one minute data with the modelling of obstacles in this thesis perhaps represents a worst case scenario of the transition of the GMPP as the irradiance changes. It can also be seen that the one second transitions are a step of either one MPP or two MPP while the one minute transitions shown are only for one MPP steps with one obstacle in the environment. This phenomena of transitions between relative MPP locations for the GMPP is explored in more detail later in this chapter. It can be seen that the more substantial factor on the location of the GMPP voltage is the movement of the shadow across the panels rather than the instantaneous irradiance, such that the one minute timescale of the irradiance transitions is appropriate for this study. The one minute data is preferable to use in the simulation as it originated in Tasmania where this study is conducted, and ensures that a wide selection of data can be obtained without the computational burden of using one second data.

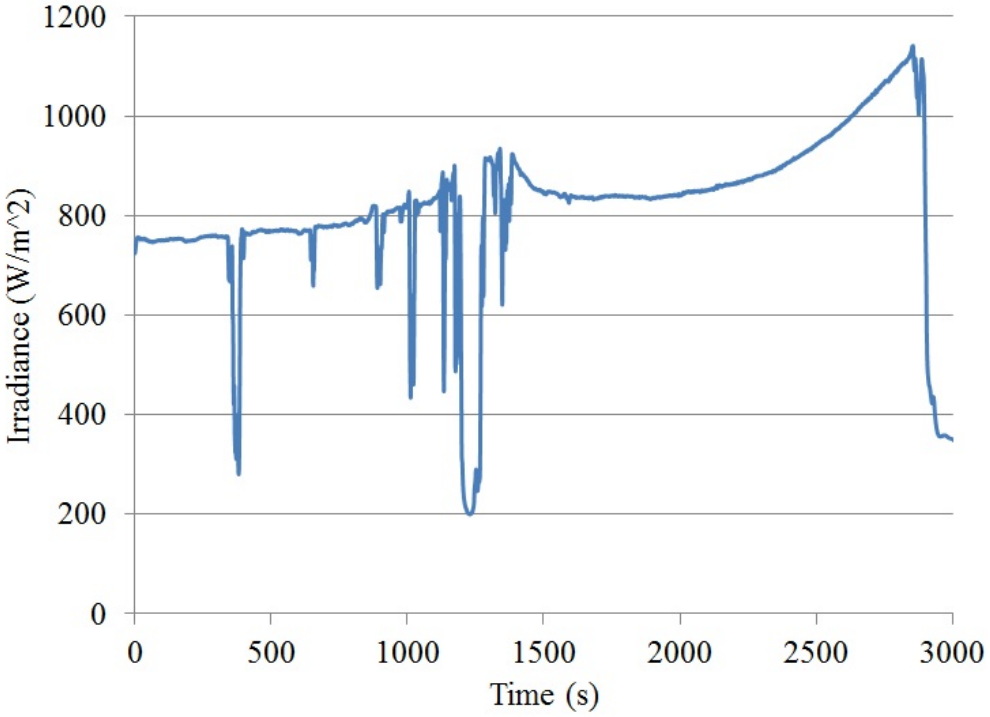

(a) One second irradiance for 19 March 2010 between 9:51:07 and 10:41:06.

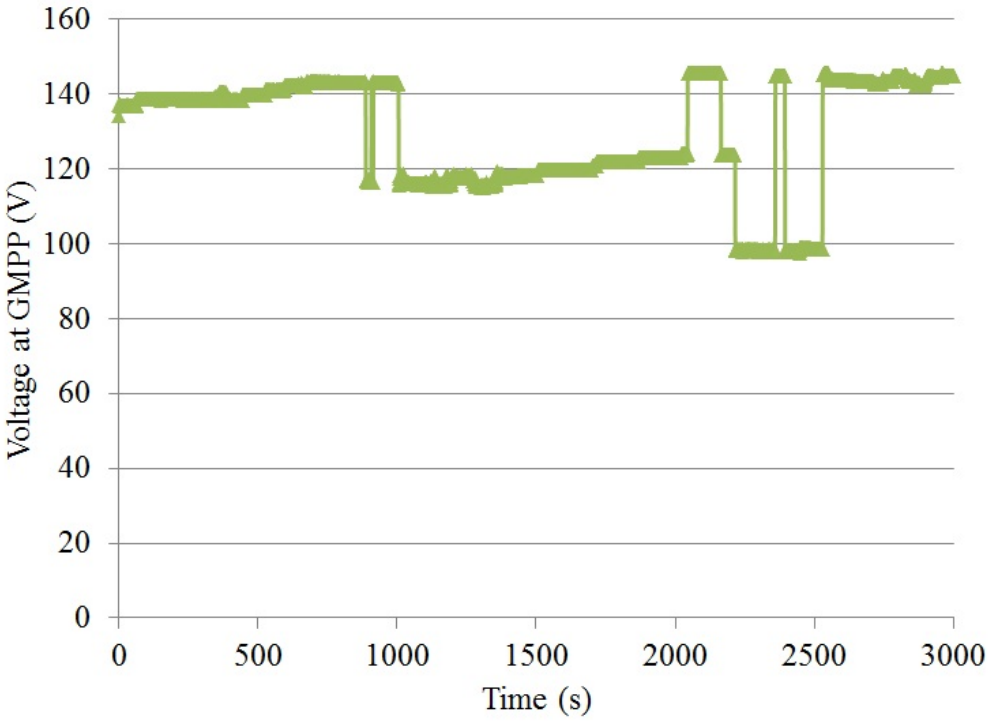

(b) Voltage at GMPP for one second irradiance for 19 March 2010 between 9:51:07 and 10:41:06.

Figure 3.9: GMPP voltage variation for one second irradiance data sample.

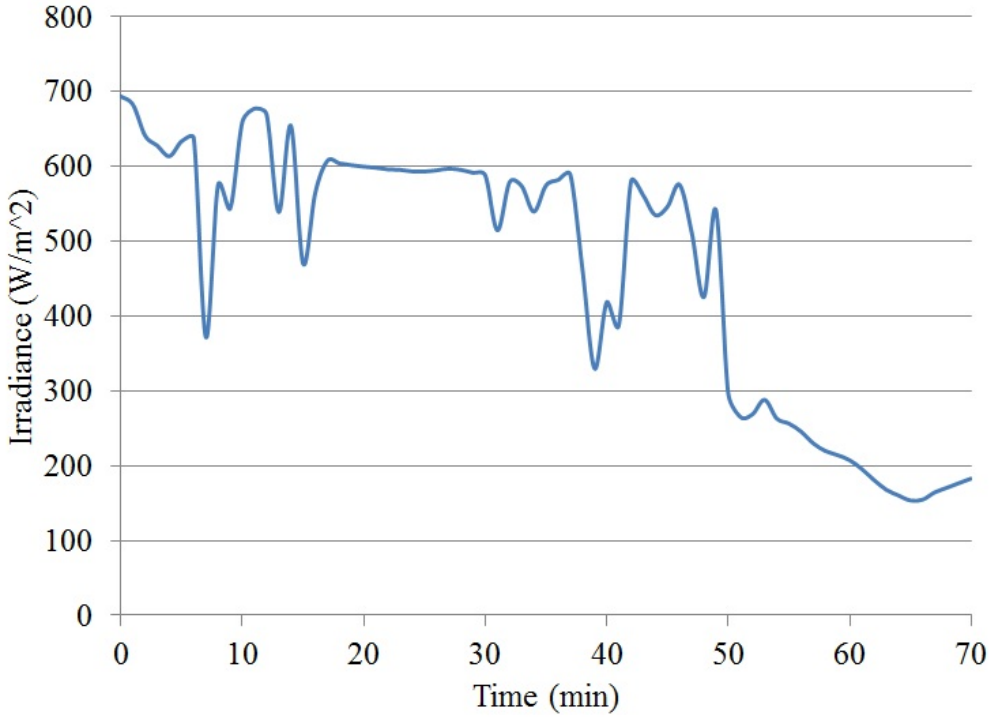

(a) One minute irradiance for 16 April 2010 between 13:39:00 and 14:48:00.

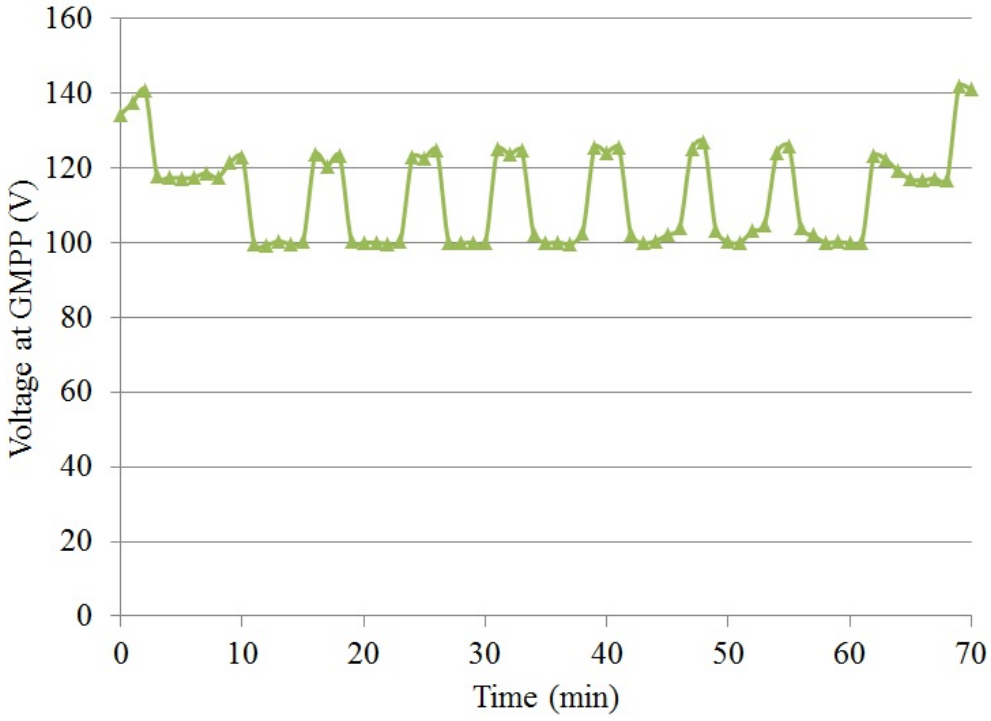

(b) Voltage at GMPP for one minute irradiance for 16 April 2010 between 13:39:00 and 14:48:00.

Figure 3.10: GMPP voltage variation for one minute irradiance data sample.

3.6 Partial Shading Case Studies

Several different cases are simulated to determine the effects that constant, static and transient PSC have on the location of the GMPP. In this section, one minute irradiance data is used from 2010 at the Cape Grim weather monitoring station, in Northern Tasmania, Australia. Only the minutes where the obstacles cause shade on the system, according to the simulation model outlined earlier in this chapter, are considered. Note that due to incomplete one minute solar data sets, there are some days that should be included as shaded days in this analysis, but have been omitted.

3.6.1 Case 1

Case 1 considers a single obstacle in the environment as shown in Fig. 3.1. This object has a height of 20 m and width of 0.25 m and could represent a power pole or thin tree in the nearby environment. The object causes shading on the PV system between 28 February 2010 and 11 October 2011. This provides 222 days of data and 15655 minutes where the PV system experiences some shading.

For each minute of irradiance data corresponding to the modules experiencing shading, the I-V and P-V characteristics are determined to provide information on the movement of the GMPP. In each day, the P-V characteristics are combined to create a 3D figure showing how the characteristics change with time. A sample 3D representation of the changing characteristics is given in Fig. 3.11. This shows the P-V curve obtained under each sample condition. By representing as a 3D surface it is possible to see the variations in the GMPP power across the time of interest and to also quite clearly see that the voltage that corresponds to the GMPP moves between the different MPPs depending on the conditions.

The shading across each module can be visualised by indicating the shaded cells by a darker cell as is shown in Fig. 3.12 for the first 14 minutes where shading occurs on the modules on 20 March 2010.

The power, voltage and current at the GMPP for each characteristic is also

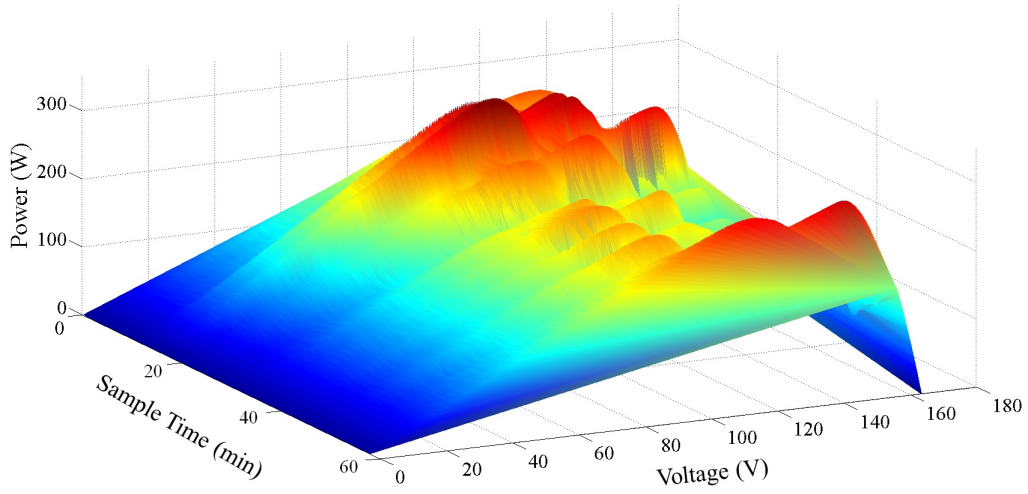

Figure 3.11: Sample 3D representation of P-V characteristics for 20 March 2010 during the 58 minutes of shading.

determined to enable the movement of the GMPP to be analysed. The two key points of interest are how the GMPP power and voltage change across the different minutes of the simulation. In each minute, the irradiance on each module is influenced by the effects of the static shading from the obstacle in the environment and the change environmental irradiance. Figure 3.13, shows the movement of the GMPP power across the 58 test cases for 20 March 2010. Figure 3.14 shows the movement of the GMPP voltage, otherwise known as the optimal operating point, for each of the 58 test cases for 20 March 2010.

From Fig. 3.13, it can be seen that the power at the GMPP is very variable. When this is graphed with the changing environmental irradiance against time, as shown in Fig. 3.15, it can be seen that the variable power at the GMPP is closely related to the variable environmental irradiance.

Figure 3.16 shows the GMPP voltage variation for the first day of the month of the eight months when shading occurs. This shows that the voltage at the GMPP varies in a consistent pattern across the year. From this it can be inferred that the voltage at which the GMPP occurs is more affected by the shading from obstacles in the environment than the transient irradiance.

From [90] it is known that the MPPs are spaced by about 80% of the open-circuit voltage. Using this idea, regions of the voltage can be defined that correspond

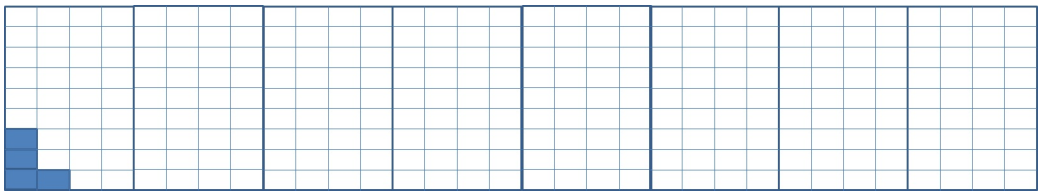

(a) Shading at time 13:35.

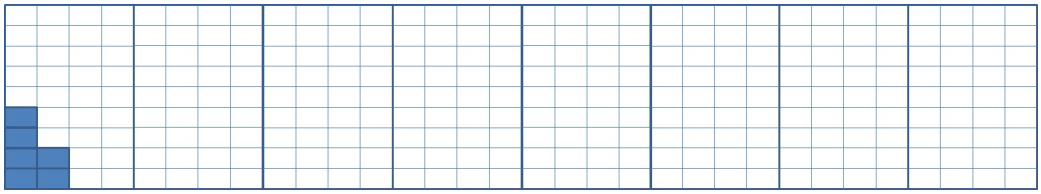

(b) Shading at time 13:36.

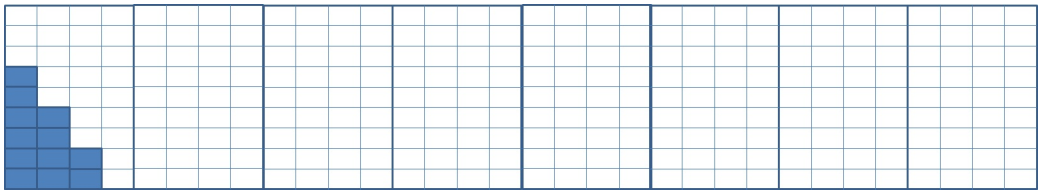

(c) Shading at time 13:37.

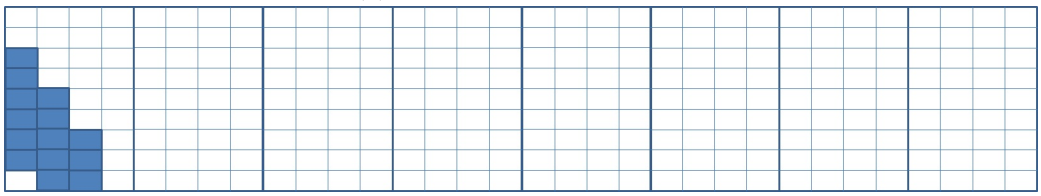

(d) Shading at time 13:38.

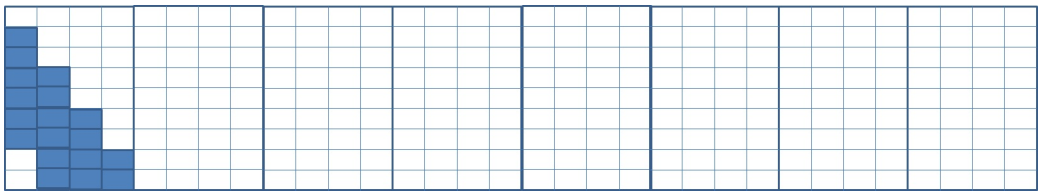

(e) Shading at time 13:39.

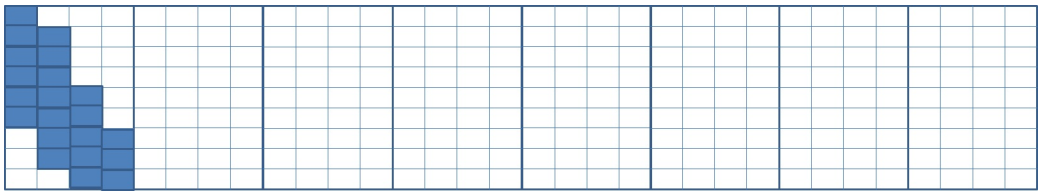

(f) Shading at time 13:40.

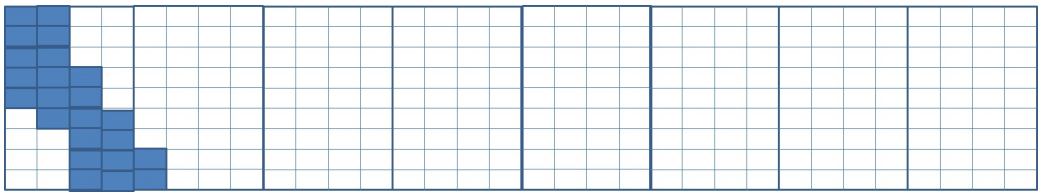

(g) Shading at time 13:41.

Figure 3.12: Sample shading for 20 March 2010 during the first 14 minutes of shading.

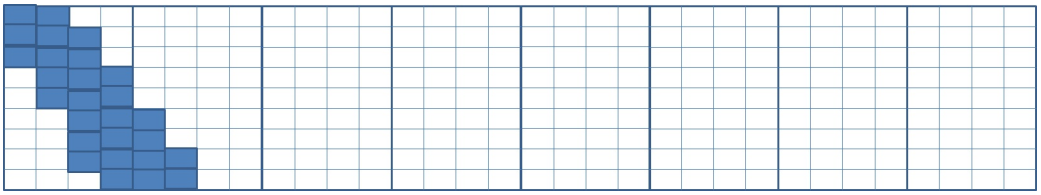

(h) Shading at time 13:42.

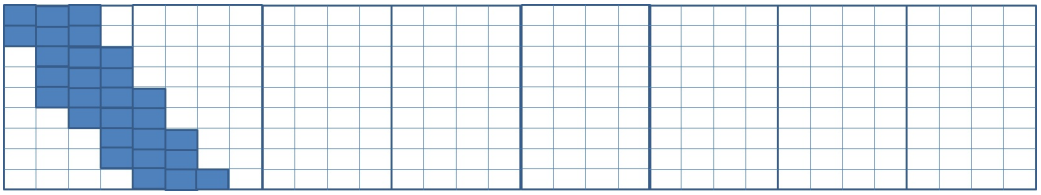

(i) Shading at time 13:43.

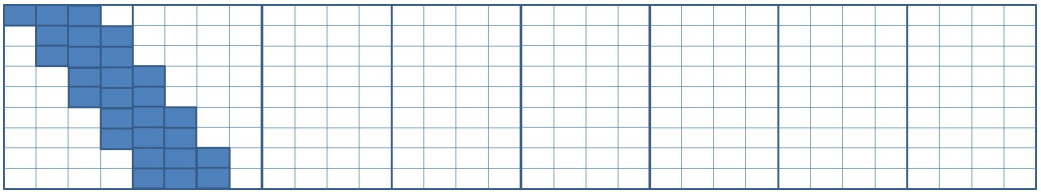

(j) Shading at time 13:44.

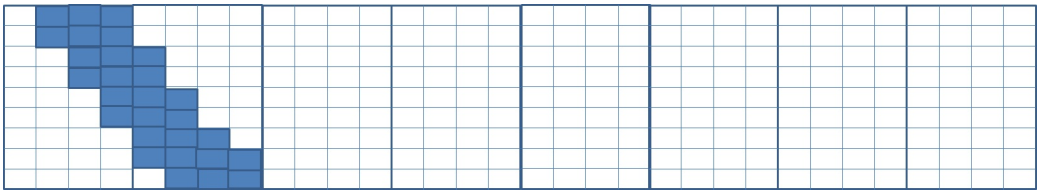

(k) Shading at time 13:45.

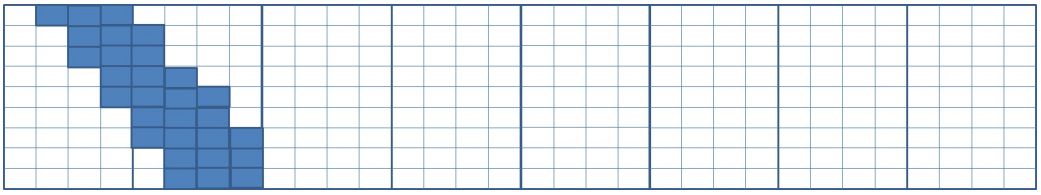

(l) Shading at time 13:46.

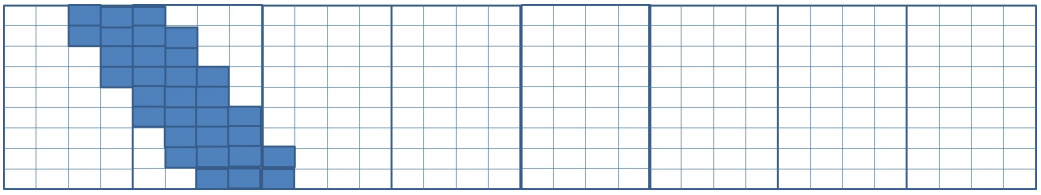

(m) Shading at time 13:47.

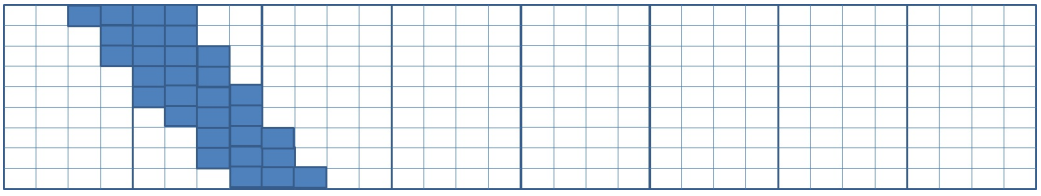

(n) Shading at time 13:48.

Figure 3.12 : Sample shading for 20 March 2010 during the first 14 minutes of shading (continued).

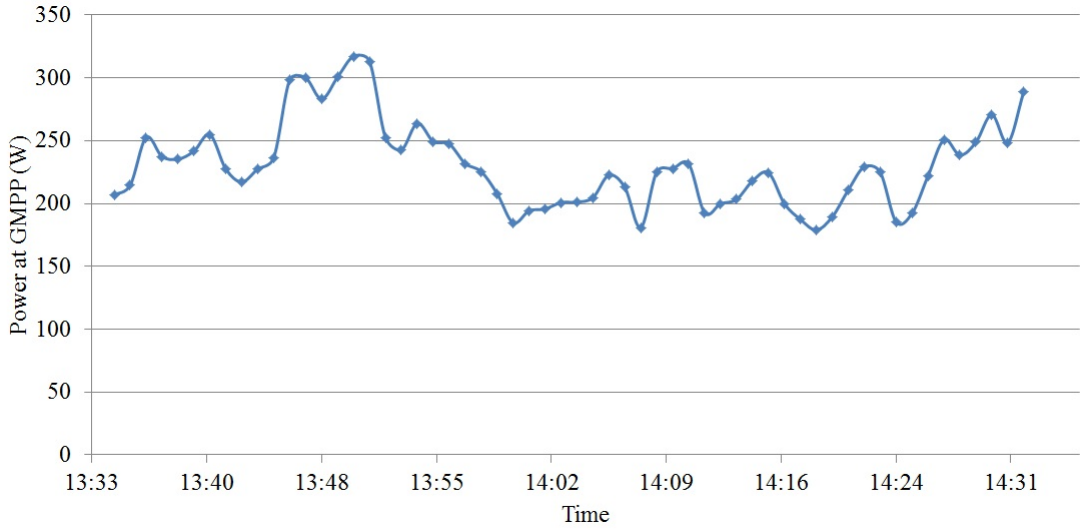

Figure 3.13: Sample of the power at the GMPP for 20 March 2010 during the 58 minutes of shading.

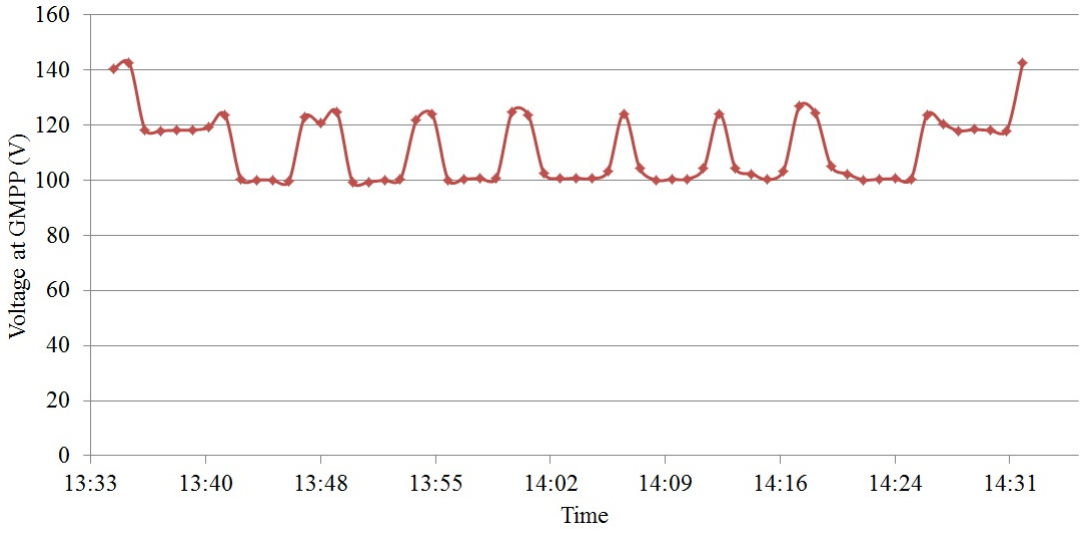

Figure 3.14: Sample of the voltage at the GMPP for 20 March 2010 during the 58 minutes of shading.

to each MPP. From the characteristics and the transitions between the different MPPs, Table 3.1 has been produced. This table characterises the number of transitions that occur between MPPs that are adjacent or are separated by a larger voltage, and indicates the number of minutes that the GMPP lies in each respective MPP location. For each case, the average, minimum, maximum and standard deviation are given. The MPP locations are defined in Fig. 3.17. Each solid line indicates approximately $0.8V_{oc}$ spacing. Each MPP will be within a small band around each solid line. For the sample case of 20 March 2010, it can be seen that the GMPP is at either MPP6, MPP7 or MPP8 for case 1.

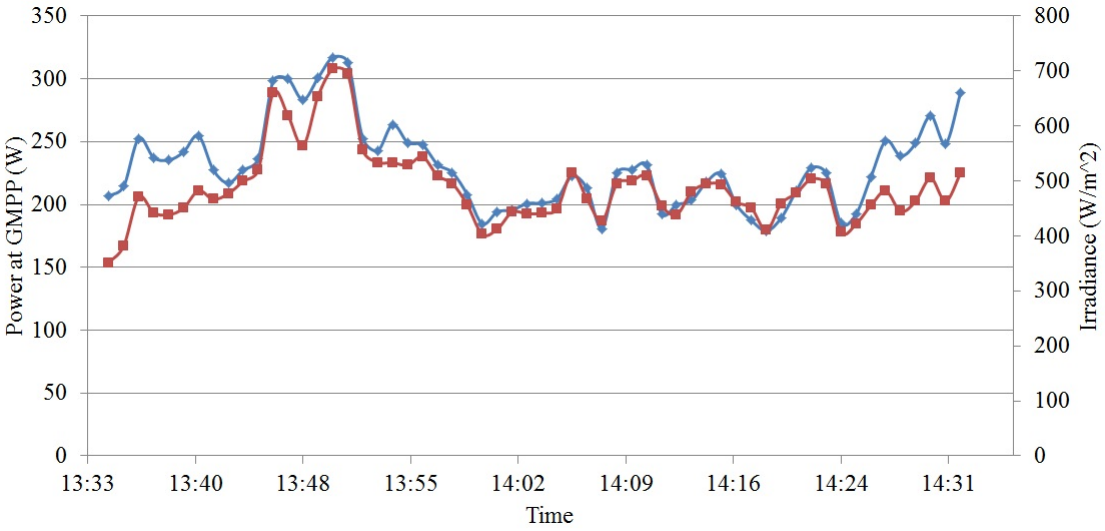

Figure 3.15: Sample of the power (blue) at the GMPP with the irradiance (red) for 20 March 2010 during the 58 minutes of shading.

Table 3.1: Transitions and MPP locations for case 1.

	One MPP transitions	**Two MPP transitions**	**MPP6**	**MPP7**	**MPP8**
Average	15.55	0.07	36.40	29.64	4.47
Minimum	0	0	0	0	2
Maximum	18	5	60	41	16
Standard Deviation	2.12	0.41	10.50	6.62	1.97
Count	3453	15	8083	6580	992

From Table 3.1 it can be seen that the GMPP voltage will most likely remain at the same level (77.85%) or undergo a one MPP transition (22.06%) between each minute of irradiance. In 0.1% of cases, a two MPP transition was observed. It can also be seen that during the shading time, the GMPP is most likely to be at MPP6 (51.63%), followed by MPP7 (42.03%), then MPP8 (6.34%).

Conclusions that can be drawn from this first test case are:

- The power output at the GMPP is mostly influenced by the transient irradiance.
- The operating voltage corresponding to the GMPP is mostly affected by the movement of the shading across the system.
- A regular pattern in the movement of the GMPP voltage is observed throughout the year.
- With one obstacle in the environment, the GMPP operating voltage is unlikely to move outside of a one MPP transition.

This suggests that a smaller searching range could be used when trying to locate

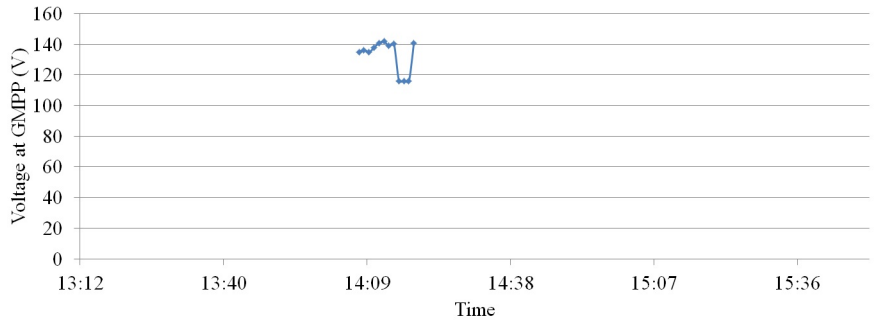

(a) 1 March 2010 GMPP voltage.

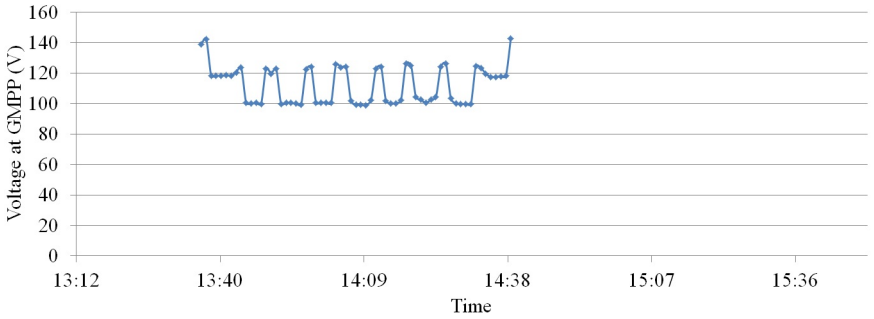

(b) 1 April 2010 GMPP voltage.

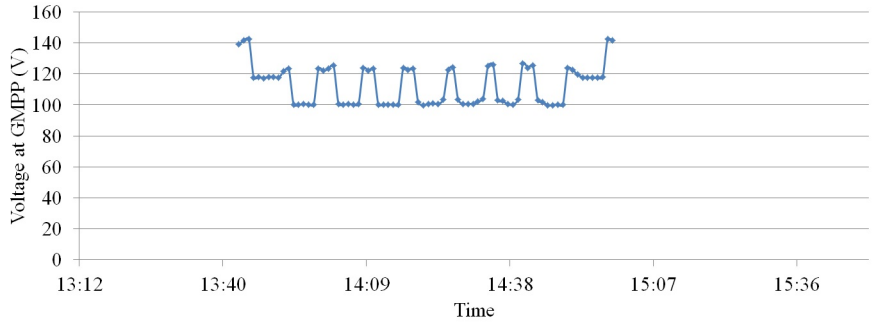

(c) 1 May 2010 GMPP voltage.

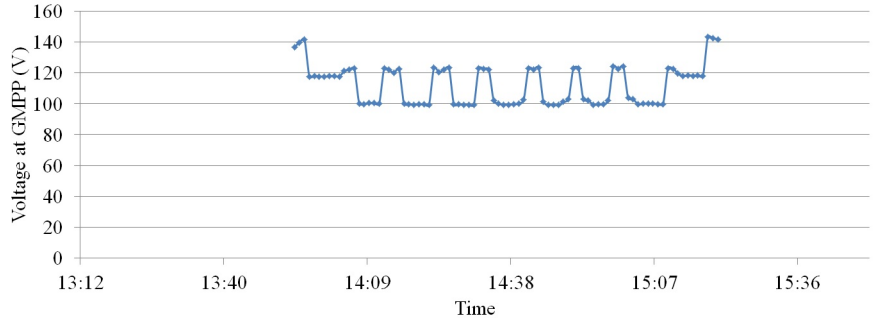

(d) 1 June 2010 GMPP voltage.

Figure 3.16: Variation in the GMPP voltage on the first day of the month for the time of testing.

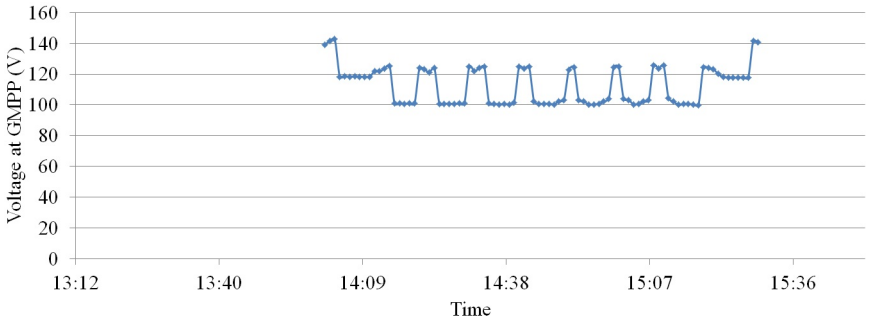

(e) 1 July 2010 GMPP voltage.

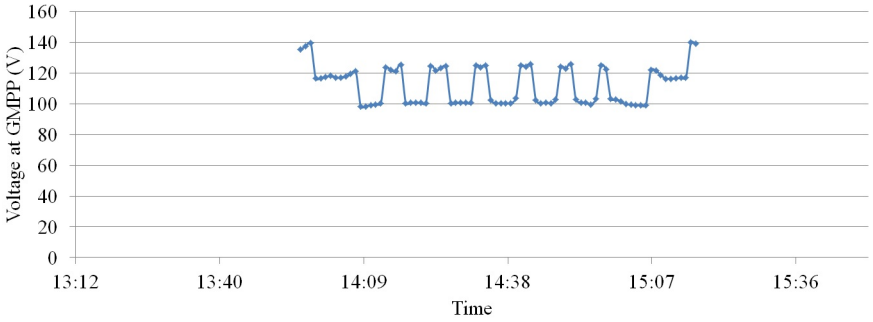

(f) 1 August 2010 GMPP voltage.

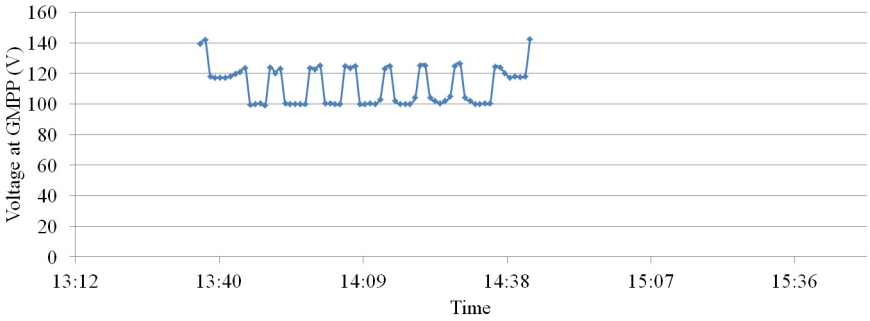

(g) 1 September 2010 GMPP voltage.

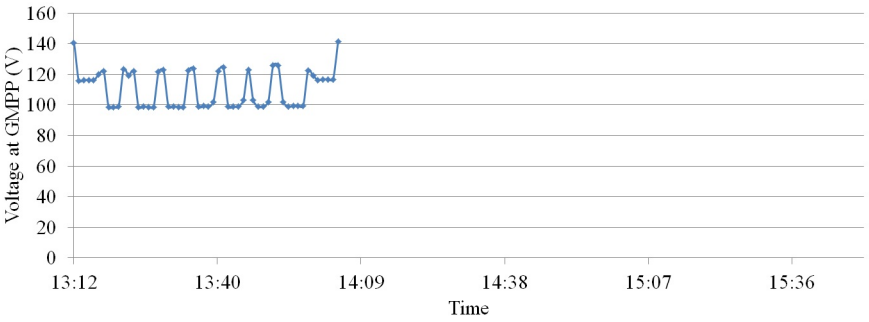

(h) 1 October 2010 GMPP voltage.

Figure 3.16 : Variation in the GMPP voltage on the first day of the month for the time of testing (continued).

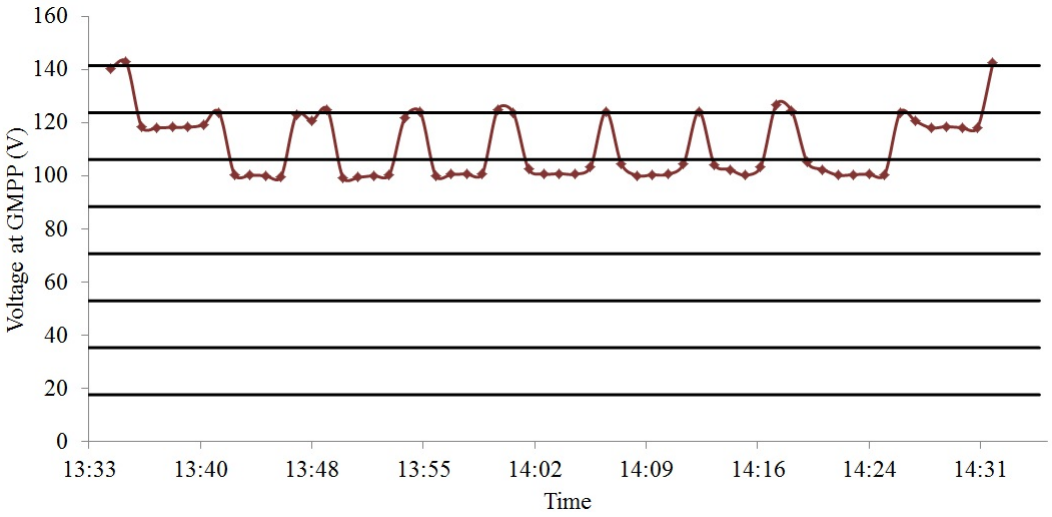

Figure 3.17: MPP locations defined on 20 March 2010 GMPP voltage locations.

the GMPP for a system experiencing similar shading conditions to this case study. Additionally, as the GMPP is most likely to undertake a transition of only one MPP (or approximately 17.7 V), it would be simple to check the power at the MPP on either side of a located maxima to ensure that it is in fact the GMPP. Due to the regular pattern of the movement of the GMPP voltage throughout the year, it would be possible to study fewer days of data and achieve the same observations.

3.6.2 Case 2

In case 2, there are two obstacles in the environment as shown in Fig. 3.18. The same obstacle as in case 1 is used in the environment with an additional object placed closer to the PV system. This new object has height 1 m and width 0.25 m and could represent a chimney on the roof of the structure where the PV system is located. The objects cause shading on the PV system between 4 February 2010 and 31 October 2010. This provides 263 days of data and 68513 minutes where the PV system experiences some shading.

As in case 1, the I-V and P-V characteristics are produced for each shading condition and the transient irradiance to determine the movement of the GMPP. For 20 March 2010, a 3D representation of the P-V characteristics is given in Fig. 3.19. This shows the P-V curve obtained under each sample condition.

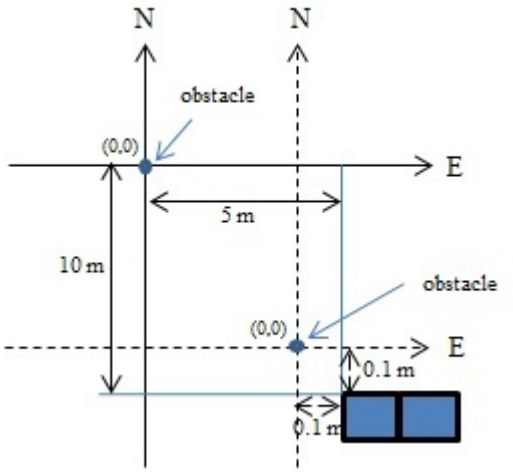

Figure 3.18: XY representation of the obstacles and PV modules in the environment for case 2.

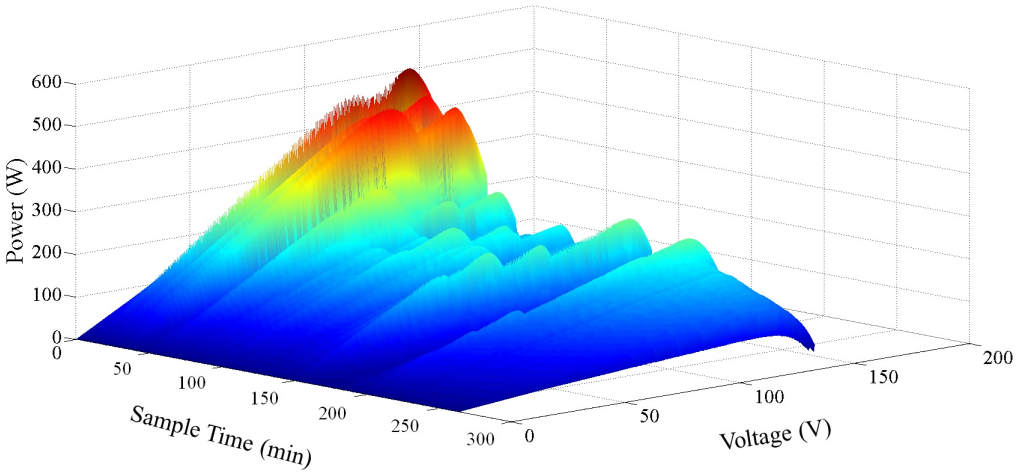

Figure 3.19: Sample 3D representation of P-V characteristics for 20 March 2010 during the 265 minutes of shading with the two obstacles.

It is quite clear that with two obstacles in the environment, the voltage that corresponds to the GMPP moves between the different MPPs depending on the conditions.

Figure 3.20 shows the movement of the GMPP power across the 256 test cases for 20 March 2010. Figure 3.21 shows the movement of the GMPP voltage, otherwise known as the optimal operating point, for each of the 256 test cases for 20 March 2010.

From Fig. 3.20, it can be seen that the power at the GMPP is very variable. When this is graphed with the changing environmental irradiance against time,

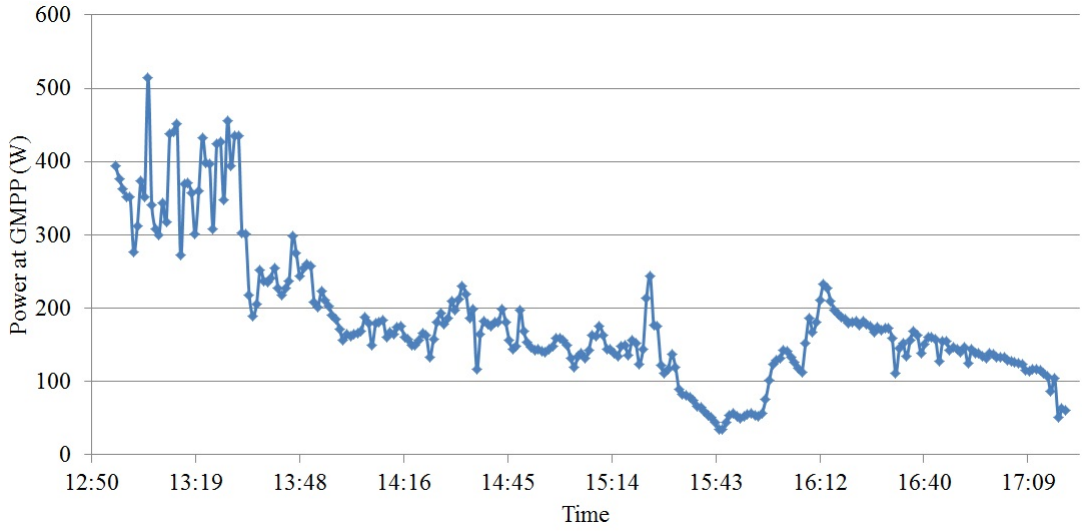

Figure 3.20: Sample of the power at the GMPP for 20 March 2010 during the 256 minutes of shading.

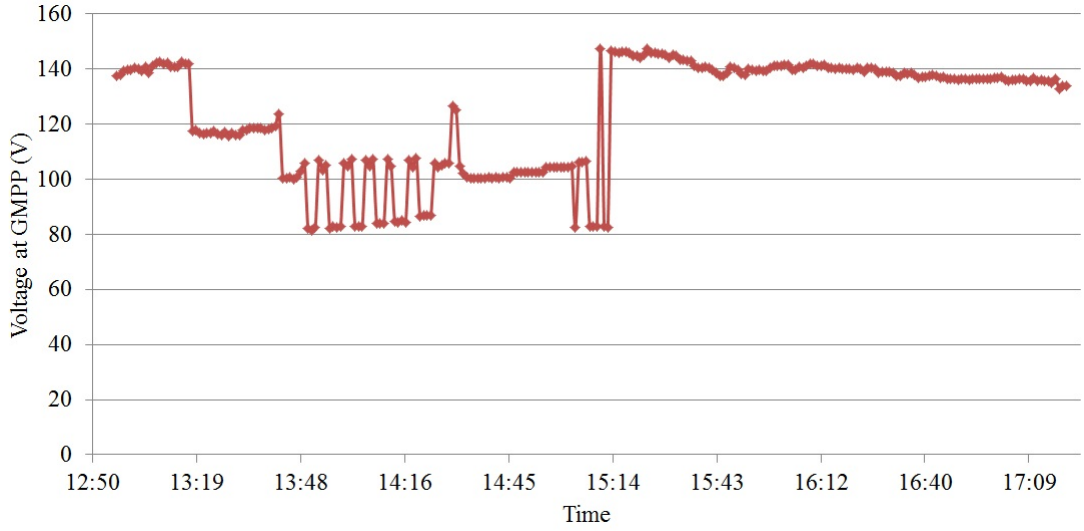

Figure 3.21: Sample of the voltage at the GMPP for 20 March 2010 during the 256 minutes of shading.

as shown in Fig. 3.22, it can be seen that the variable power at the GMPP is closely related to the variable environmental irradiance. It can be seen from Fig. 3.21 that the MPPs where the GMPP may exist are MPP5, MPP6, MPP7 and MPP8. This indicates that case 2 exhibits more possible locations for the GMPP than case 1. Additionally, with the presence of a second obstacle three MPP transients and four MPP transitions can be observed, although these are still far less frequent than the one MPP transients. In one sample case a transition of five MPPs was also observed.

Figure 3.23 shows the GMPP voltage variation for the first day of the month of

the eight months of the year when shading occurs on the first day of the month (February is excluded as the shading study starts from 4 February 2010). As in case 1, this shows a consistent pattern in the movement of the GMPP voltage across the year. This supports that the voltage at which the GMPP occurs is more affected by the shading from obstacles in the environment than by the transient irradiance.

The transitions and the MPP locations for case 2 are given in Table 3.2 and Table 3.3, respectively.

From the results it can be seen that the GMPP will most likely remain at

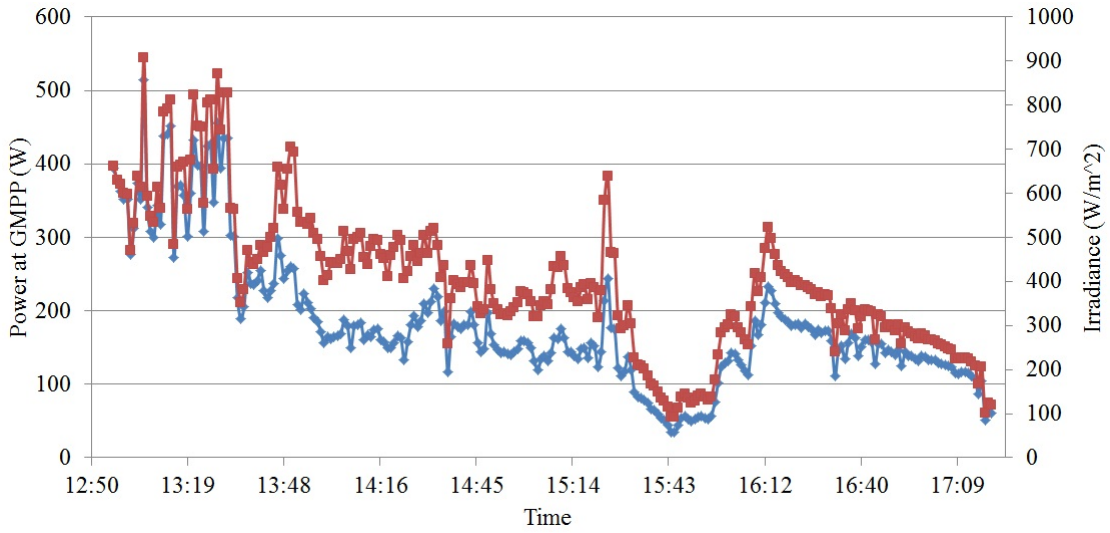

Figure 3.22: Sample of the power (blue) at the GMPP with the irradiance (red) for 20 March 2010 during the 265 minutes of shading.

Table 3.2: Transitions for case 2.

	One MPP transitions	**Two MPP transitions**	**Three MPP transitions**	**Four MPP transitions**	**Five MPP transitions**
Average	12.61	4.30	3.26	0.60	0.01
Minimum	2	0	0	0	0
Maximum	26	11	8	4	1
Standard Deviation	4.67	2.63	2.43	0.92	0.10
Count	3316	1130	858	124	1

Table 3.3: MPP locations for case 2.

	MPP2	**MPP4**	**MPP5**	**MPP6**	**MPP7**	**MPP8**
Average	0.01	4.62	36.30	44.60	72.50	103.37
Minimum	0	0	0	0	1	7
Maximum	1	62	90	87	146	227
Standard Deviation	0.10	9.06	22.49	20.41	23.14	61.00
Count	1	966	9546	11730	19068	27187

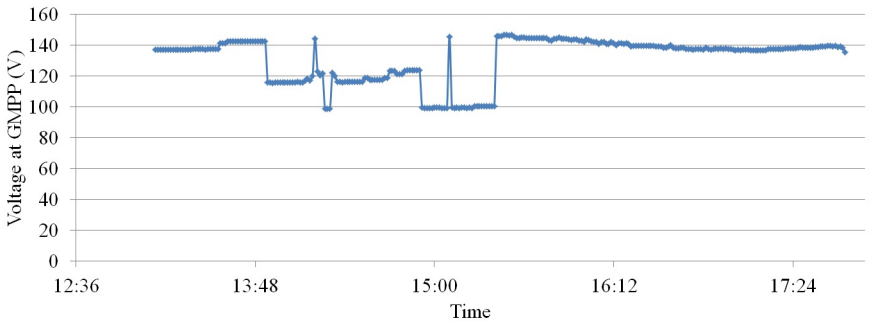

(a) 1 March 2010 GMPP voltage.

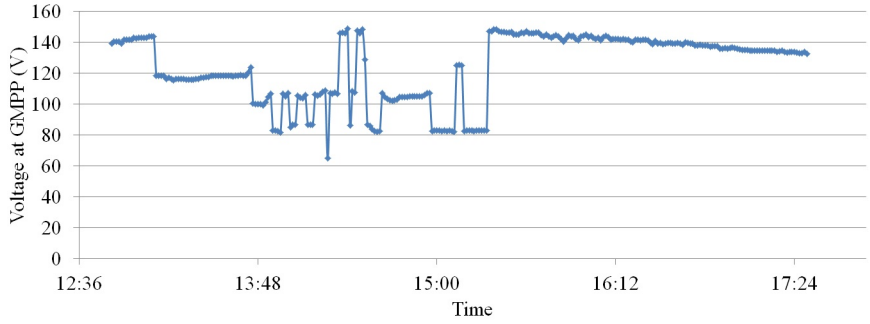

(b) 1 April 2010 GMPP voltage.

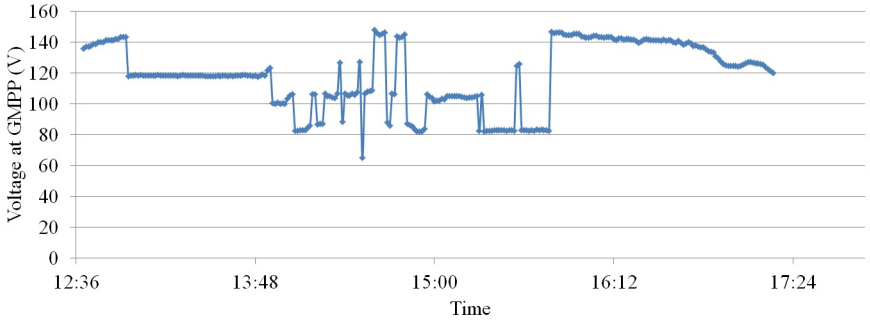

(c) 1 May 2010 GMPP voltage.

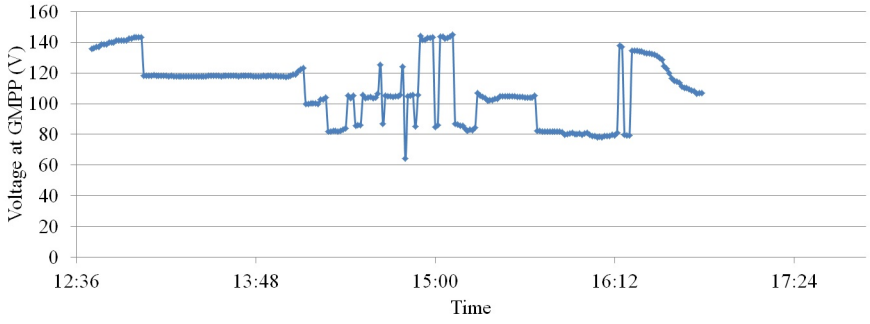

(d) 1 June 2010 GMPP voltage.

Figure 3.23: Variation in the GMPP voltage on the first day of the month for the time of testing.

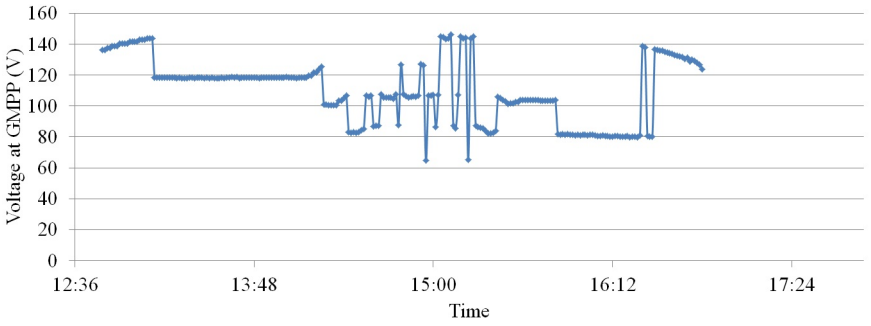

(e) 1 July 2010 GMPP voltage.

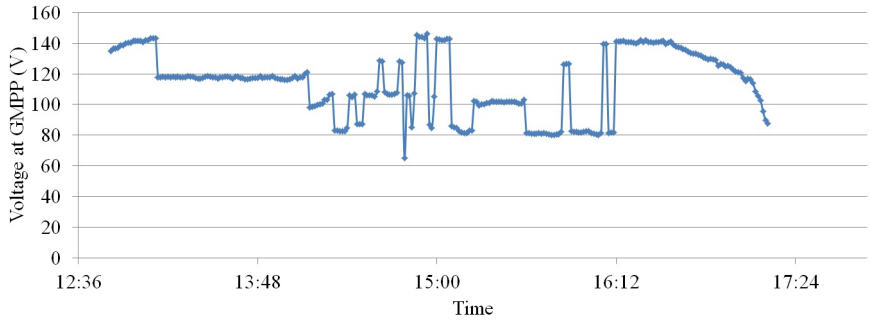

(f) 1 August 2010 GMPP voltage.

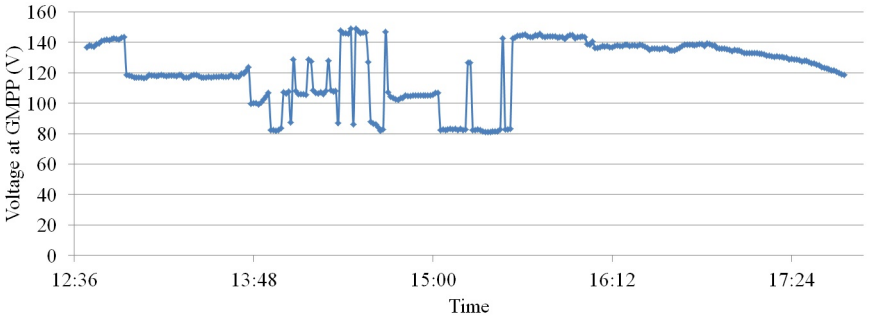

(g) 1 September 2010 GMPP voltage.

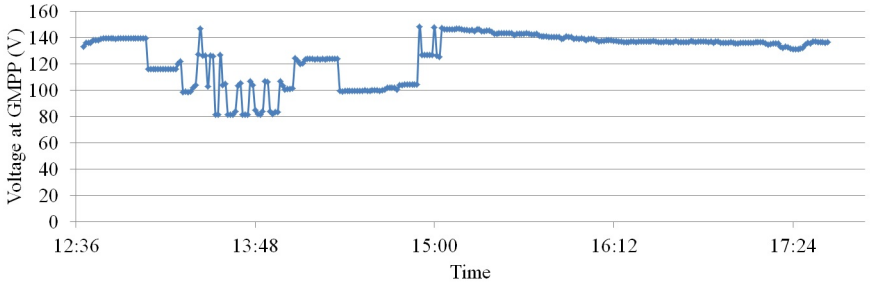

(h) 1 October 2010 GMPP voltage.

Figure 3.23 : Variation in the GMPP voltage on the first day of the month for the time of testing (continued).

the same level (92.08%) or undergo a one MPP transition (4.84%). Two MPP transitions are the next most common (1.65%), followed by three MPP transitions (1.25%) and four MPP transitions (0.18%). Five MPP transitions are very unlikely to occur (0.0015%). During the shading time, the MPP is more likely to be at MPP8 (39.68%), followed by MPP7 (27.83%), MPP6 (17.12%), MPP5 (13.93%) and MPP4 (1.41%). The GMPP is very unlikely to be located at MPP2 (0.0015%).

The results from this test case support the conclusions drawn from case 1. In particular, one MPP transitions are significantly more common than transitions to further away MPPs and a regular pattern of the GMPP movement is exhibited across the year. As the results from case 1 are supported, subsequent case studies in this section will perform the analysis on a smaller subset of the year.

3.6.3 Case 3

Case 1 and case 2 demonstrate that the trends in the movement of the GMPP are fairly independent of the transient irradiance applied, so that in studying the subsequent cases a reduced shaded dataset is used to provide an approximated picture of what happens.

Case 3 involves applying a constant reduction in the irradiance of some modules to represent cell degradation and mismatch. Nine days are used in the study where each day is randomly selected from a month of the year between February and October. The days used in the study are:

- 10 February 2010
- 26 March 2010
- 5 April 2010
- 24 May 2010
- 19 June 2010
- 11 July 2010
- 4 August 2010

- 16 September 2010
- 29 October 2010

For each day, the irradiance between 12:00 and 15:59 is used in the study creating a dataset with 9 days and 21651 minutes where the constant PSC can be assessed.

Each module has a degradation factor applied as its shading factor between 0.90 and 1.00. The degradation factors for each module are:

- Module 1 - 0.90
- Module 2 - 0.95
- Module 3 - 0.93
- Module 4 - 1.00
- Module 5 - 0.95
- Module 6 - 1.00
- Module 7 - 0.96
- Module 8 - 1.00

For 26 March 2010, a 3D representation of the P-V characteristics is given in Fig. 3.24. This shows the P-V curve obtained under each sample condition. It is quite clear that with constant PSC, the GMPP voltage remains at about the same MPP location. The power at the GMPP varies considerably over this time.

The power, voltage and current at the GMPP for each characteristic is also determined to enable the movement of the GMPP to be analysed. The two key points of interest are how the GMPP power and voltage change across the different minutes of the simulation. In each minute, the effects of the changing environmental irradiance or the transient shading, in addition to the constant shading from the cell degradation, influence the irradiance on each module. Figure 3.25, shows the movement of the GMPP power across the 239 test cases for 26 March 2010. Figure 3.26 shows the movement of the GMPP voltage for each of the 239 test cases for 26 March 2010.

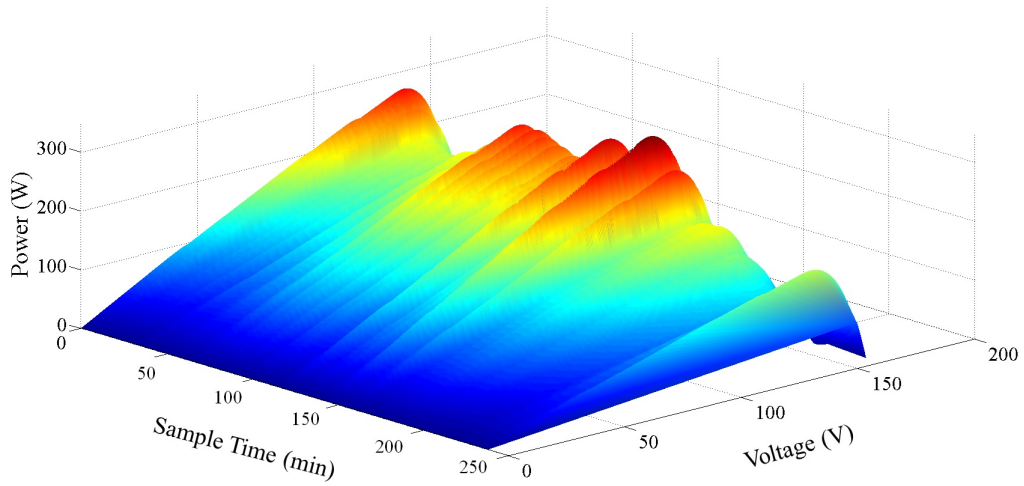

Figure 3.24: Sample 3D representation of P-V characteristics for 26 March 2010 during the 239 minutes of shading with the constant PSC.

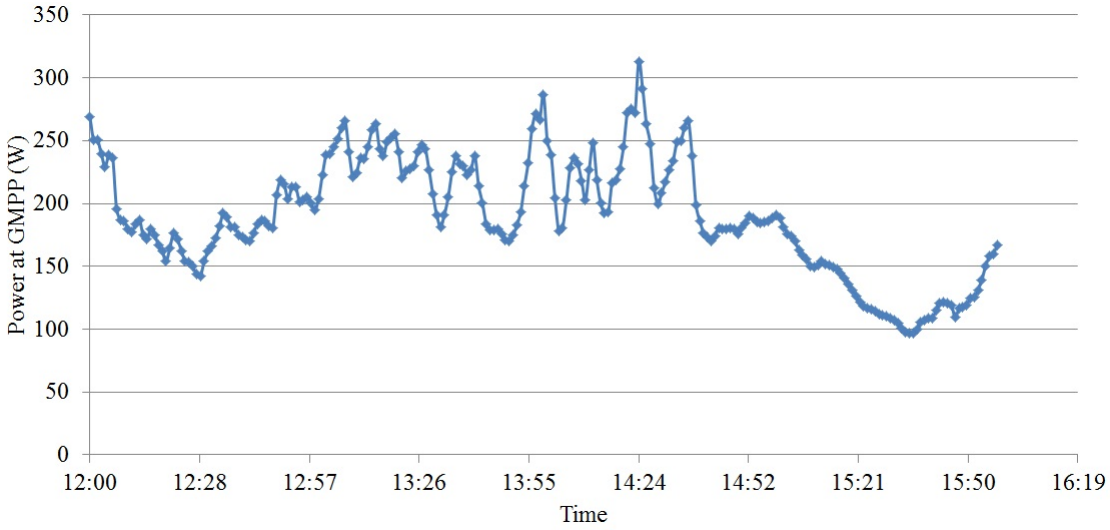

Figure 3.25: Sample of the power at the GMPP for 26 March 2010 during the 239 minutes of shading.

From Fig. 3.25, it can be seen that the power at the GMPP is very variable. When this is graphed with the changing environmental irradiance against time, as shown in Fig. 3.27, it can be seen that the variable power at the GMPP is closely related to the variable environmental irradiance.

From these results it can be seen that the power at the GMPP (the blue series in Fig. 3.27) very closely follows the transient irradiance (red series in Fig. 3.27). The GMPP voltage also remains at MPP8 for the duration of the test and undergoes no transitions to another MPP location. These results suggest that constant PSC alone cannot influence the transitioning of the

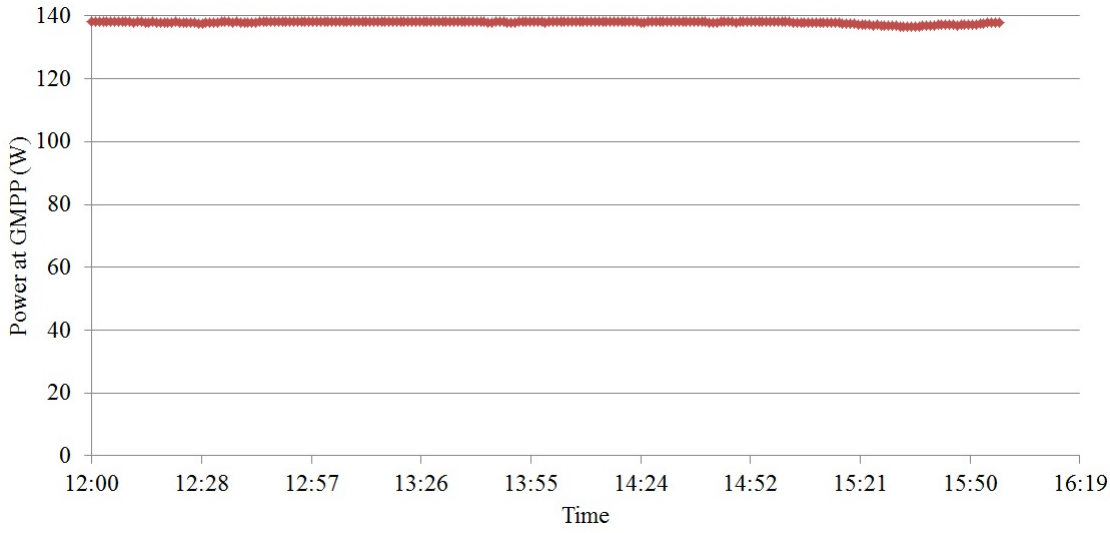

Figure 3.26: Sample of the voltage at the GMPP for 26 March 2010 during the 239 minutes of shading.

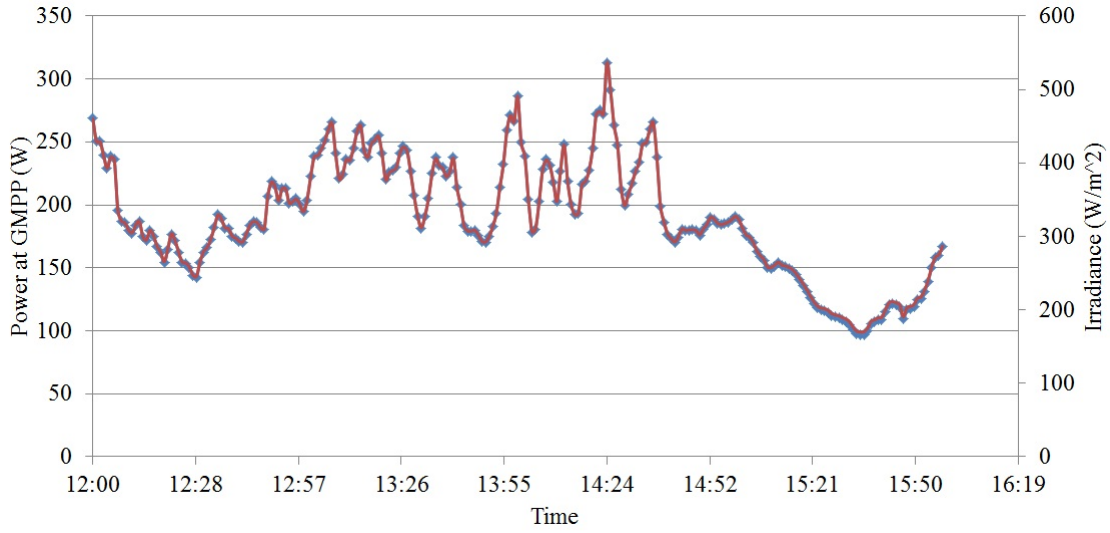

Figure 3.27: Sample of the power (blue) at the GMPP with the irradiance (red) for 26 March 2010 during the 239 minutes of shading.

GMPP to another voltage level. Figures 3.28 and 3.29 show the I-V and P-V characteristics for one minute of the test case for 26 March 2010. This illustrates that constant PSC results in small local peaks appearing on the P-V characteristic, yet does not result in the GMPP transitioning to another voltage level.

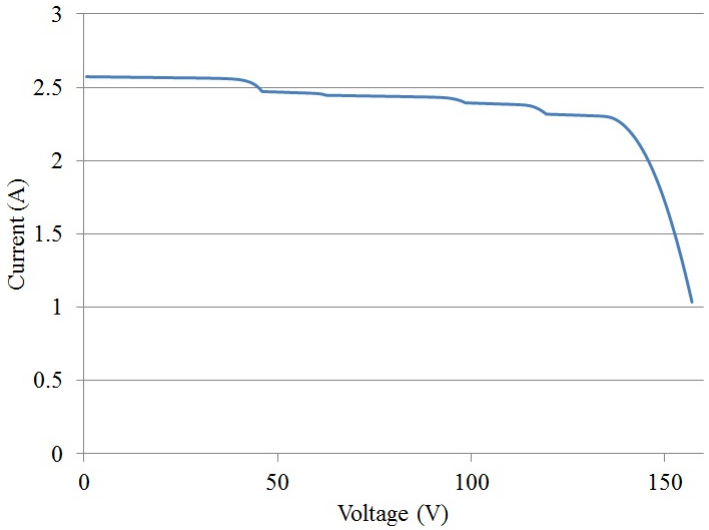

Figure 3.28: Sample of the I-V characteristics for 14:24 on 26 March 2010.

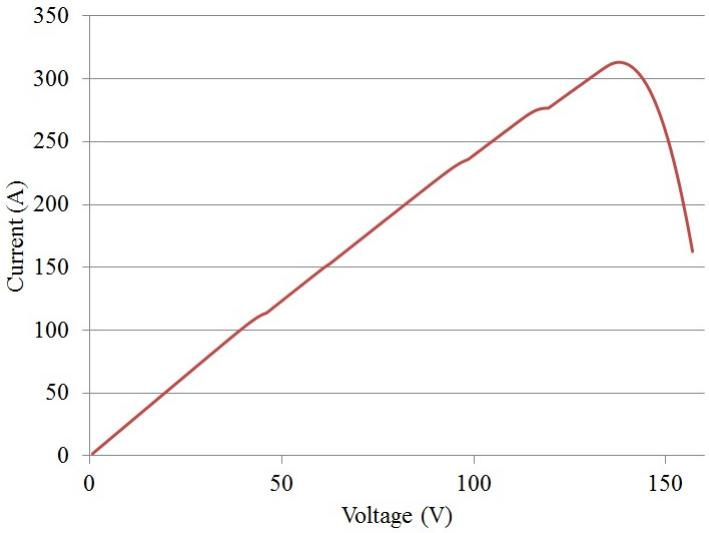

Figure 3.29: Sample of the P-V characteristics for 14:24 on 26 March 2010.

3.6.4 Case 4

Case 4 involves combining the obstacle locations for case 2 with the constant PSC from case 3. This presents a system that will experience all three categorisations of PSC. As with case 3, the same nine sample days between 1 February 2010 and 31 October 2010 are selected. This has produced a dataset with 9 days and 2333 minutes of time where the combined effect of the constant, static and transient partial shading can be assessed.

For 26 March 2010, the P-V characteristics as a 3D representation is given in Fig. 3.30. This shows the P-V curve obtained under each sample condition. Unlike case 3, it can be seen that with constant PSC and static PSC, the GMPP

voltage will move to a different MPP location as the conditions change.

Figure 3.31 compares the power at the GMPP for 26 March 2010 of case 4 with the power from case 2. Case 2 is the blue line and case 4 is the red line. Figure 3.32 compares the voltage at the GMPP for 26 March 2010 of case 4 with the voltage from case 2. As with Fig. 3.31, the blue line represents the voltage for case 2 and the red line represents the voltage for case 4.

From this it can be seen that the power for case 4 is similar although always slightly lower (on average 4.79% lower) than the power from case 2. This is due

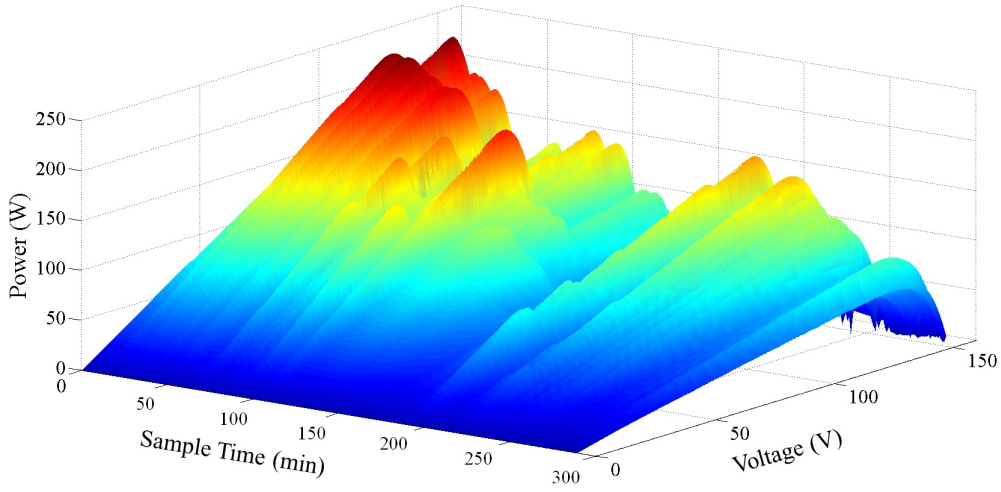

Figure 3.30: Sample 3D representation of P-V characteristics for 26 March 2010 during the 240 minutes of shading with the two obstacles.

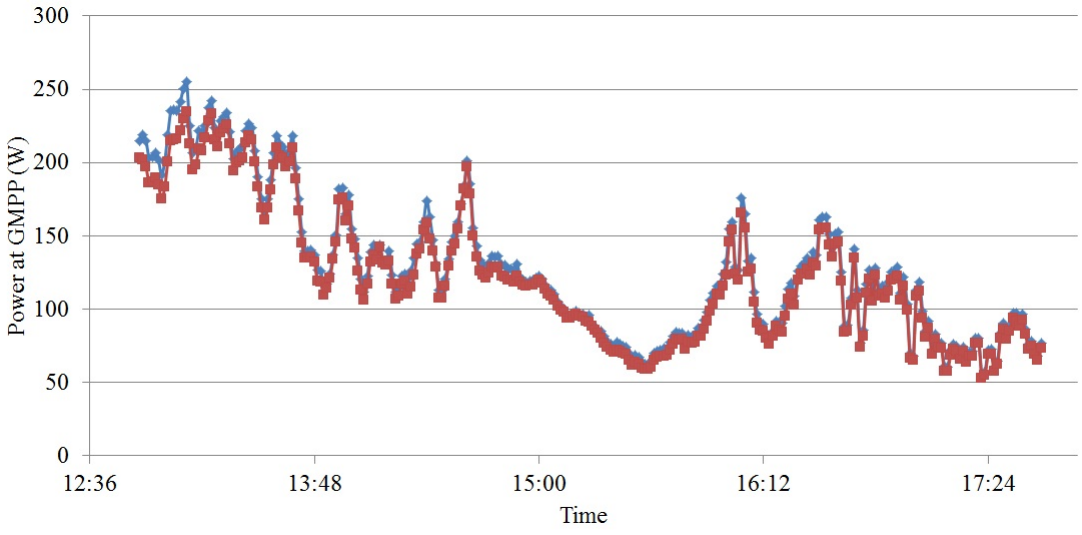

Figure 3.31: Comparison of the power at GMPP for case 2 (blue) and case 4 (red).

to the cell degradation reducing the overall irradiance on most of the modules. The voltage is very similar in both cases, however, there are a 27 minutes in the 289 minutes of the study where the voltage at the GMPP is different between the two cases. As the power at these test cases are not significantly different, these cases may correspond to the situation where there are two MPPs on the P-V characteristic which have similar power and the constant PSC is significant enough to change which MPP is viewed as the preferred GMPP. This is shown in Fig. 3.33, where the characteristics at time 15:04 for case 2 and case 4 are shown. Clearly, the addition of the cell degradation leads to the GMPP being at a different voltage which corresponds to an MPP on the case 2 P-V characteristic with very similar power to the GMPP. However, it is still seen that the trends observed previously regarding transitions between MPPs are still valid for this case study.

The transitions and the MPP locations for case 4 are given in Table 3.4 and Table 3.5, respectively.

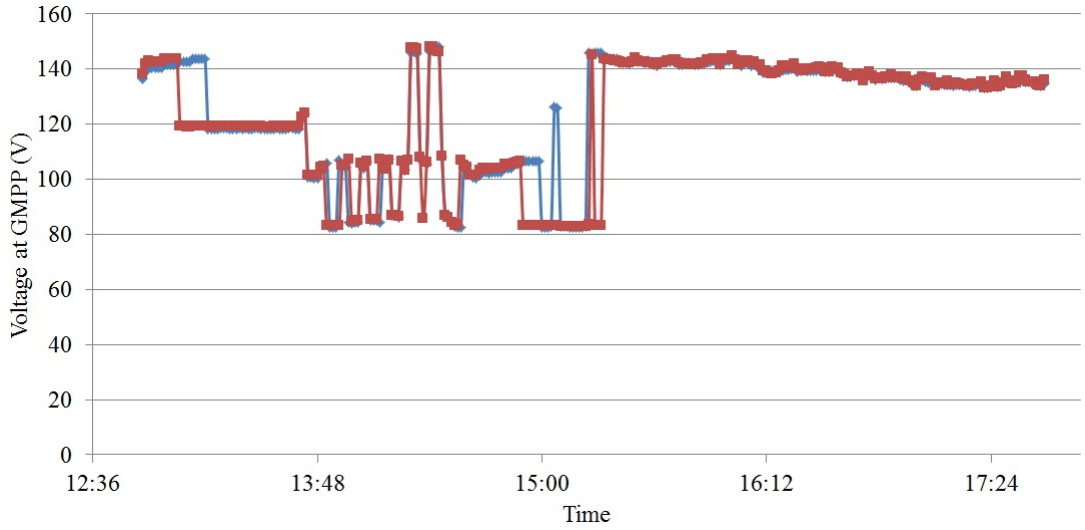

Figure 3.32: Comparison of the voltage at GMPP for case 2 (blue) and case 4 (red).

Table 3.4: Transitions for case 4.

	One MPP transitions	**Two MPP transitions**	**Three MPP transitions**	**Four MPP transitions**
Average	13.33	3.11	3.00	1.56
Minimum	6	0	0	0
Maximum	17	5	7	6
Standard Deviation	4.03	1.91	2.40	1.89
Count	120	28	27	14

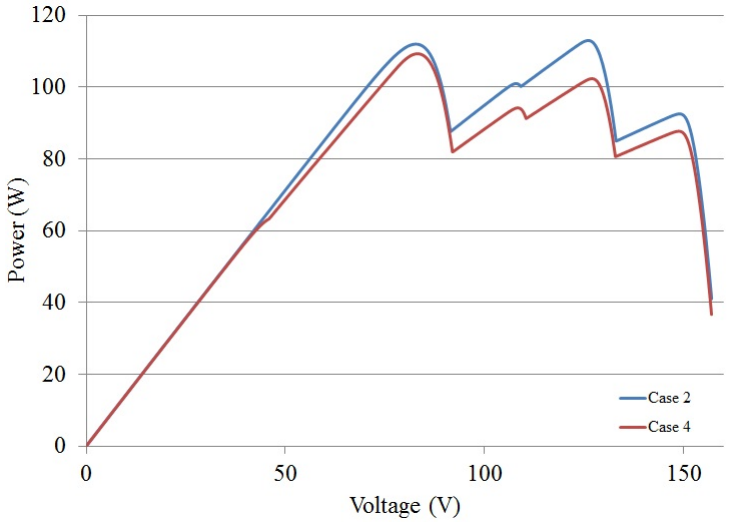

Figure 3.33: Comparison of the P-V characteristics at 15:04 for case 2 (blue) and case 4 (red).

Table 3.5: MPP locations for case 4.

	MPP4	**MPP5**	**MPP6**	**MPP7**	**MPP8**
Average	7	39.44	47.89	78.67	86.22
Minimum	0	0	0	41	21
Maximum	43	62	75	117	161
Standard Deviation	13.24	21.94	20.15	21.72	49.00
Count	63	355	431	708	776

From these results it can be seen that the GMPP will most likely remain at the same level (91.90%), or undergo a one MPP transition (5.14%). Two MPP transitions are the next most common (1.20%), closely followed by three MPP transitions (1.16%), then four MPP transitions (0.60%). During the shading time, the MPP is most likely to be at MPP8 (33.26%), followed by MPP7 (30.35%), MPP6 (18.47%), MPP5 (15.22%), then MPP4 (2.70%). These trends match closely with the results observed for case 2.

3.6.5 Case 5

Case 5 involves extending the model to three obstacles in the environment with constant PSC incorporated to extend the observations of case 4. The nine samples days between 1 February 2010 and 31 October 2010 used with case 3 and case 4 are also used in this analysis. The available data set has 9 days with 2392 minutes of time where the combined effect of the constant, static and transient partial shading can be assessed. The configuration is shown in Fig.

3.34, where the obstacles from case 2 are combined with an additional obstacle of height 6 m and width 1.2 m. The obstacle is located 2 m west and 5 m north of the PV modules.

For 26 March 2010, a 3D representation of the P-V characteristics is given in Fig. 3.35. This shows the P-V curve obtained under each sample condition. Like case 4, it can be seen that with constant PSC and static PSC, the GMPP voltage will move to a different MPP location as the conditions change. A large variation in the GMPP power across the time of interest can also be seen.

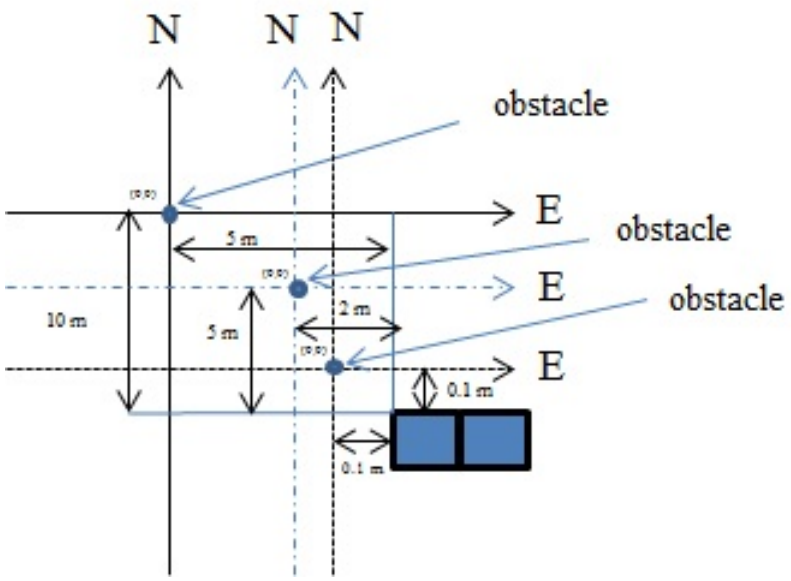

Figure 3.34: XY representation of the three obstacles and PV modules in the environment for case 5.

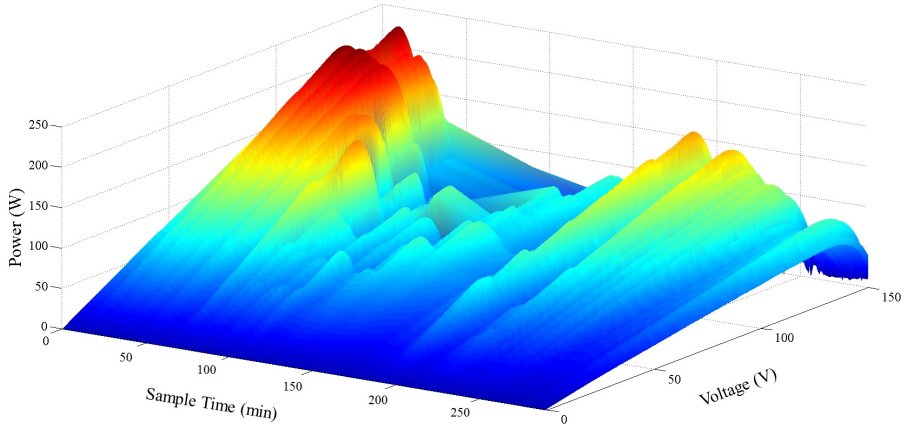

Figure 3.35: Sample 3D representation of P-V characteristics for 26 March 2010 during the 290 minutes of shading with the three obstacles.

The transitions and the MPP locations for case 5 are given in Table 3.6 and Table 3.7, respectively.

From these results, it can be seen that the GMPP will most likely remain at the same level (92.47%), or undergo a one MPP transition (4.85%). Two MPP transitions are the next most common (1.92%), followed by three MPP transitions (0.75%). During the shading time, the MPP is most like to be at MPP8 (35.95%), followed by MPP7 (22.58%), MPP5 (18.85%), MPP4 (12.79%), then MPP6 (9.82%). These trends are similar to those observed in the other cases. The key difference noticed however is the reduced time the MPP is most likely to be at MPP6, which now ranks lower than MPP5 and MPP4 suggesting that this shading configuration leads to the system spending less time around this MPP.

3.7 Analysis of Results

The five case studies presented have shown that the effects that transient, static and constant PSC have on the GMPP are all unique. Conclusions that can be drawn from this analysis include:

- The power at the GMPP is most affected by the transient PSC (the irradiance).
- Constant PSC causes small local peaks to arise in the P-V characteristics however does not influence the GMPP voltage level significantly.

Table 3.6: Transitions for case 5.

	One MPP transitions	**Two MPP transitions**	**Three MPP transitions**
Average	12.9	5.1	2
Minimum	6	0	0
Maximum	19	8	4
Standard Deviation	4.01	2.96	1.49
Count	116	46	18

Table 3.7: MPP locations for case 5.

	MPP4	**MPP5**	**MPP6**	**MPP7**	**MPP8**
Average	34.0	50.1	26.1	60.0	95.6
Minimum	0	0	0	29	16
Maximum	95	81	42	97	172
Standard Deviation	26.5	29.6	15.1	21.1	55.4
Count	306	451	235	540	860

- Constant PSC can influence the voltage at the GMPP when accompanied by static partial shading and the case where there are two peaks on the P-V characteristics with a similar power.
- Static partial shading, caused by the movement of shadow from obstacles in the environment, is the most significant factor in moving the GMPP to a different MPP location.
- The GMPP is more likely to remain at the same MPP location or undergo a transition to an adjacent MPP, than to move to a significantly different voltage.

These conclusions can be used to improve the performance of GMPPT methods as they show the preference for the GMPP to be located at MPP8 under only constant PSC, and to remain at a higher voltage MPP under all other test conditions. Knowing that the GMPP is most likely to only undergo a transition to an adjacent MPP (separated by about $0.8V_{oc}$ [90]), reduces the searching range than can be considered under normal operating conditions. By reducing the searching range, the speed of execution can be improved. While sometimes the GMPP may move outside of this range, it is unlikely to do so.

3.8 Towards a Detailed Model of Partial Shading

The simplified shading model defined in this chapter has been used to approximate the partial shading effects with shorter computational times. In this section, recommendations on how to enhance the simplified model to enable some of its limitations to be addressed are presented. The limitations of the simplified model include that the module is modelled in the horizontal plane while most PV modules have a tilt angle to maximise the available irradiance. Additionally, the simplified model assumes that all shadows lead to each cell being fully shaded, where real shadows have some transmittance, and the effects of direct and diffuse irradiance are considered as a single irradiance parameter.

In this section, possible enhancements to the simplified model are explored by

considering the equations and process required to determine firstly the shading factor and secondly the irradiance on a PV module which is on a tilt angle. The key difference in this analysis is that the PV module and obstacle are modelled in a three dimensional coordinate system. Other future enhancements to the model could include modelling the transmission factor of the shadows and isolating the effects that direct and diffuse irradiance have on the system.

Consider the PV system shown in Fig. 3.36. Here the horizontal irradiance and module irradiance can be written in terms of the elevation angle (α) and the tilt angle β_t [92], as

$$G_{horizontal} = G_{incident} \sin(\alpha) \tag{3.14}$$

$$G_{module} = G_{incident} \sin(\alpha + \beta_t) \tag{3.15}$$

As the horizontal irradiance is given by the Bureau of Meteorology one minute solar data, the module irradiance can be expressed in terms of the horizontal irradiance as given in (3.16).

$$G_{module} = \frac{G_{horizontal} \sin(\alpha + \beta_t)}{\sin \alpha} \tag{3.16}$$

The produces the module irradiance reduction factor to scale the one minute solar data given by

$$\frac{\sin(\alpha + \beta_t)}{\sin \alpha} \tag{3.17}$$

The tilt angle will therefore affect the transient irradiance received by the PV system.

In modelling the PV system with a tilt angle, it becomes necessary to model objects and shadows in the three dimensional coordinate system. Using the system proposed by [84], where the coordinate system is defined by (north, east, zenith), the vector pointing in the direction of the sun can be given by

$$s = \begin{bmatrix} \cos(Azimuth) \cos \alpha \\ \sin(Azimuth) \cos \alpha \\ \sin \alpha \end{bmatrix} \tag{3.18}$$

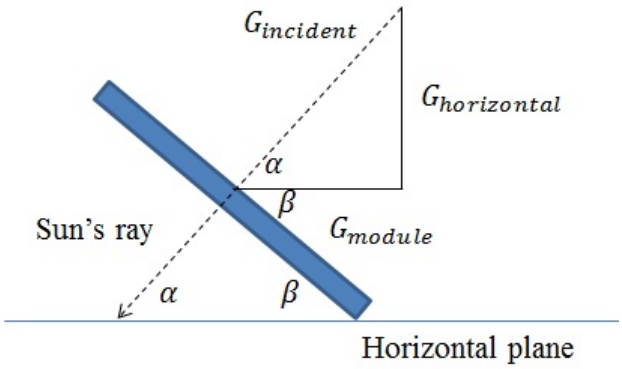

Figure 3.36: PV module at tilt angle β_t.

The intersection of the plane that the PV module is in, where the PV module is defined by $P_1...P_4$, with the shadow ray from the object is given by [84]

$$P_s = P_0 - \frac{a.(P_0 - P_1)}{a.s}s \tag{3.19}$$

where, a is normal to the PV module surface and given by

$$a = (P_2 - P_1) \times (P_4 - P_1) \tag{3.20}$$

Evaluating (3.19), indicates where the ray intersects with the plane that the PV module is in. It is then necessary to see if the shadow projection is actually contained within the module area defined by $P_1...P_4$. This can be found by considering the following.

Let, $V_1 = P_2 - P_1$, $V_2 = P_4 - P_1$, $V_3 = P_4 - P_3$, $V_4 = P_s - P_1$ and $V_5 = P_s - P_3$, where each vector is normalised. If the angle between V_1 and V_4 and the angle between V_3 and V_5 are between 0° and 90°, then the shadow point given by P_s is within the module area. The shadow is contained in the module if the two dot products shown in (3.21) and (3.22) are both greater than zero.

$$criterion_1 = dot(V_1, V_4) \tag{3.21}$$

$$criterion_2 = dot(V_3, V_5) \tag{3.22}$$

The implementation using this technique considers each cell individually for each environmental condition. The value of P_s is computed and then it is determined if it lies within the cell boundaries. If the shadow intersects

the plane within the boundaries of the cell, then the cell is considered to be shaded. As the shadow will be wider than a single point, variations of ± 0.1 m in the x and y directions, corresponding to the point P_0 are considered in steps of 0.01 cm. The combined shaded cells from each iteration of the obstacle point are combined to determine the shading factor of the module.

Each cell is defined by the points $P_1 ... P_4$ in a clockwise direction. As each cell in each module needs to be assessed multiple times for each environmental condition, $20 \times 20 = 400$ times in the implementation described above, this method of finding the shading factor is more computationally demanding and takes much longer to execute than the simple method described earlier in this chapter.

The development of the shading factor of a single module is considered in Fig. 3.37. This occurs with a single obstacle point in the environment located at (5.2685, 10.425, 20). The coordinate P_1 of the module is located at (0.2685, 0.425, 8). The module is on a tilt angle, β_t of 45°.

The shading factor from 10:19 to 10:33 is shown in Fig. 3.38. The irradiance available over this timeframe from the one minute solar data and the irradiance available in the plane of the PV module based on the tilt angle of the module is demonstrated in Fig. 3.39. In Fig. 3.40, the irradiance in the plane of the PV module and the irradiance received by the module based on the shading factor are given.

These preliminary results in developing a more extensive module of PSC show that the simplified model considered earlier in this chapter, which considers that the module is in the horizontal plane, receives far less irradiance than when the module is on an incline. However, due to the extra dimension considered in this analysis, and by considering the shading on a cell by cell basis, the computational burden associated with this method increases considerably when compared with the approximate model used in this chapter. In developing a full model of PV systems under PSC, it would be necessary to model the PV system in the three dimensional coordinate system as described in this section, and also consider the transmission factor of certain objects and the different effects that direct and diffuse irradiance may have on the irradiance received by shaded cells.

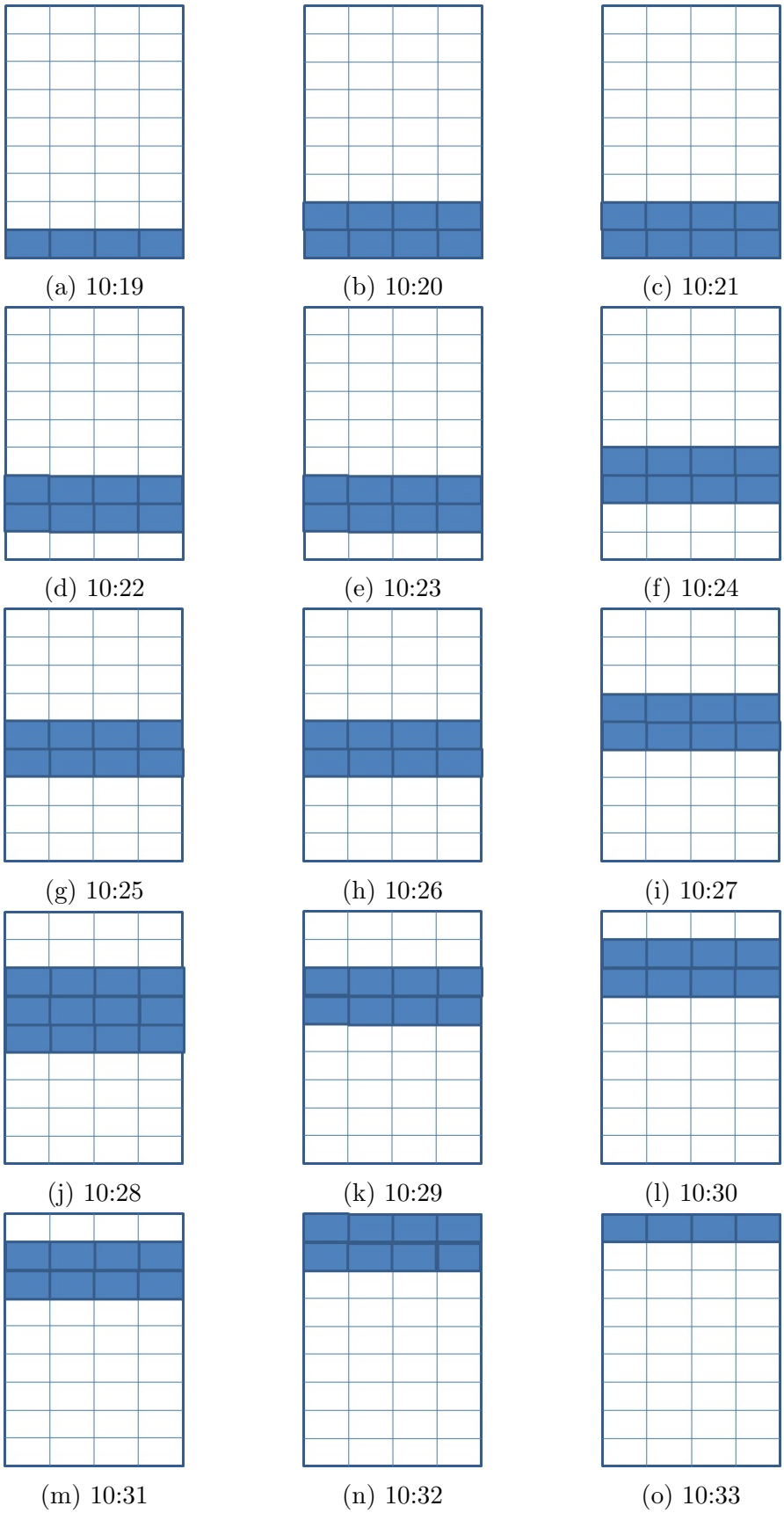

(a) 10:19 (b) 10:20 (c) 10:21

(d) 10:22 (e) 10:23 (f) 10:24

(g) 10:25 (h) 10:26 (i) 10:27

(j) 10:28 (k) 10:29 (l) 10:30

(m) 10:31 (n) 10:32 (o) 10:33

Figure 3.37: Shadow movement over single module between 10:19 and 10:33 on 31 August 2010.

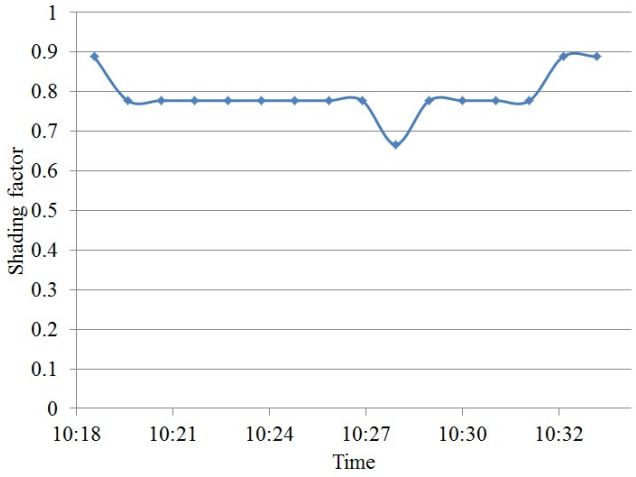

Figure 3.38: Shading factor on a single module between 10:19 and 10:33 on 31 August 2010.

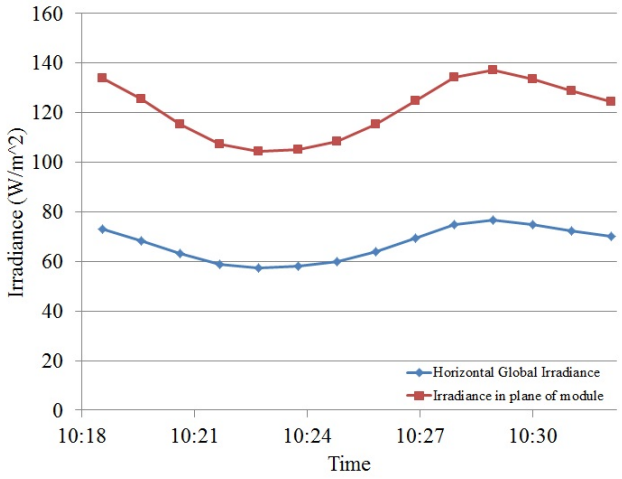

Figure 3.39: One minute irradiance and irradiance in the plane of the PV module between 10:19 and 10:33 on 31 August 2010.

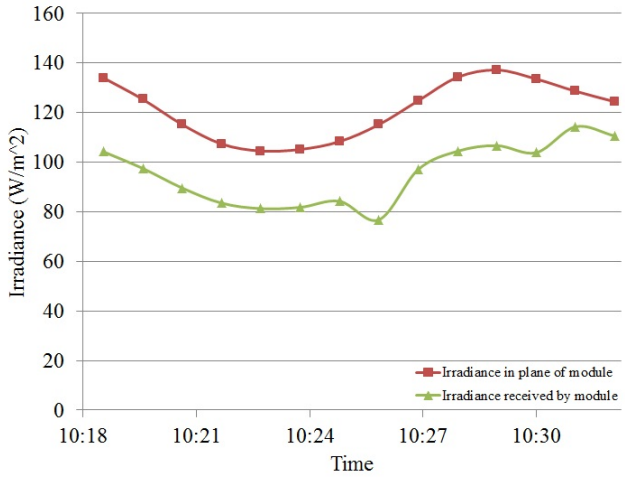

Figure 3.40: One minute irradiance in plane of module and received by the module between 10:19 and 10:33 on 31 August 2010.

3.9 Conclusions

The analysis presented in this chapter has shown that the presence of external obstacles in the environment is the most significant partial shading component which affects the relative location of the GMPP voltage throughout the day. The results indicate that the GMPP will most likely remain around the same MPP in terms of voltage or undergo a transition to an adjacent MPP voltage. In some cases the GMPP moved further than $\pm 0.8V_{oc}$, however this occurred far less frequently than transitions to adjacent MPPs.

Results in this chapter have also shown that the defined constant, static and transient partial shading all affect the power and voltage at the GMPP in different ways. It was identified that the power at the GMPP is most influenced by the transient partial shading, that is, the changing irradiance on the system as the result of cloud cover and the time of day. The static partial shading caused by the shadow of obstacles in the environment has been shown to have a significant effect on the voltage at the GMPP. Constant partial shading, representing cell degradation, has been illustrated to influence the voltage at the GMPP in the case that there are two MPPs with similar power, as cell degradation only represents a small decrease in the irradiance on each module.

The results have identified a preference for the GMPP to remain at the same MPP location with respect to voltage or to undergo a transition to an adjacent MPP (separated by about $0.8V_{oc}$). The implications that this has for MPPT include advising a reduced searching window for GMPPT, enabling a quick check by monitoring the power at adjacent MPPs to ensure the current operating point is most likely the GMPP and to detect changes in the shading conditions and recommending that the starting point of the algorithm should be closer to the open-circuit voltage than at a lower voltage.

In extending the model, it has been identified that utilising a three dimensional coordinate system is necessary to enable the PV module to be oriented with an authentic tilt angle. Future extensions to this model include incorporating a shadow transmission factor and separating the effects of direct and diffuse irradiance.

The observations of this chapter are utilised in Chapter 7 to improve the performance of the proposed simulated annealing (SA) based GMPPT method.

Chapter 4

Review and Comparative Analysis of Maximum Power Point Tracking Techniques for Photovoltaic System

4.1 Introduction

Maximum Power Point Tracking (MPPT) is an important consideration in the operation of Photovoltaic (PV) systems. As has been explored in Chapter 2, PV cells exhibit non-linear power-voltage (P-V) and current-voltage (I-V) characteristics, and there is a unique operating point which corresponds to the maximum power. This maximum power point (MPP) varies with both the temperature and irradiance that the cell experiences.

While uniform conditions are a reasonable assumption when performing indoor testing to validate the performance of modules, these conditions rarely arise in the outdoor environment. In normal operating conditions for PV systems, shadow from surrounding structures, trees and even cell degradation or dirt on the cell surface can result in a non-uniform irradiance and temperature profile across the modules. The non-uniform conditions across a module increase the complexity of the I-V and P-V characteristics leading to multiple local maxima existing in the P-V characteristics. This is primarily due to the fact that bypass diodes are inserted in anti-parallel with modules or sections of a module to avoid hot-spot formation during partial shading conditions (PSC). Hot spot formation can lead to cell damage and limits the available power from the system [49].

Due to the non-linearity in the P-V characteristics, most PV system implemen-

tations require some form of MPPT to move the operating point close to the MPP. A variety of MPPT strategies have been proposed in the literature, and range from simple techniques designed to approximate the MPP to elaborate techniques designed to find the Global MPP (GMPP) under PSC.

In this chapter, criteria for assessing the performance of MPPT methods under PSC will be defined and then the main MPPT methods will be reviewed and their key advantages and limitations will be discussed. Particular focus will be placed on the performance of each technique under the non-uniform environmental conditions that occur in the outdoor environment. There are two key influencing factors which affect the performance of PV systems and these arise due to quickly varying irradiance incident on the panels and the non-uniform irradiance across the panels which is experienced in the case of PSC. The techniques discussed in this chapter are reviewed based on their design to accommodate the second issue identified, that of partial shading, and of locating the global maxima. In some cases for these techniques considerable work has been completed to try to improve the performance of the technique under fast changing irradiance and these implementations are described within the discussion for each technique.

This chapter firstly describes some key criteria for assessing MPPT methods and their performance under PSC and then reviews the MPPT techniques from the literature based on the following four broad classifications:

- Conventional MPPT techniques designed primarily to work for uniform conditions.
- Modification of conventional techniques to improve their performance under PSC.
- Techniques designed specifically for MPPT under PSC.
- Power electronics approaches to improve MPPT performance under non-uniform environmental conditions.

The chapter concludes with a comparison of the approaches and an assessment of their merit in performing MPPT under PSC.

4.2 Criteria for Assessing MPPT Methods and their Performance Under PSC

The *real* environmental conditions in which a PV system is operated may involve rapidly changing irradiance and temperature (primarily due to the passage of clouds) and a non-uniform irradiance profile across the modules (due to shading from objects in the environment). This shading may arise due to other structures and trees in the environment, or from dust or dirt on the cell surface. Additionally, all the modules in a system are unlikely to have identical characteristics and their performance will degrade over time, introducing further non-linearities in the P-V characteristics.

For effective maximum power extraction from PV systems in real environments, a MPPT strategy is needed which can effectively track to the GMPP in these non-uniform and potentially rapidly varying conditions.

The following list of criteria is used in this chapter to assess the performance of each MPPT strategy in performing GMPPT.

- Differentiation between global and local maxima, or ability to locate the global maxima.
- Performance speed, that is, how quickly a MPP is found.
- Speed of response under a change in environmental conditions.
- Oscillations in steady state.
- Dependence on the electrical parameters of the PV panel or system-specific parameters.
- Cost and complexity.

Any suitable technique for application as a GMPPT technique, that can easily be applied to other PV systems, should be able to differentiate between the global and any local maxima, have fast performance and quick response under a change in environmental conditions, minimal oscillations in steady-state, limited dependence on the electrical parameters of the PV panel, and moderate implementation cost and complexity.

4.3 Conventional Maximum Power Point Tracking Methods

In this section, techniques designed to perform MPPT primarily under uniform conditions are described. These range from simple estimation techniques such as the fractional short-circuit current method, to tracking algorithms which are commonly implemented including Perturb and Observe (P&O).

This section firstly considers estimation techniques and then explore the slope based tracking approaches, artificial intelligence approaches, output parameters and single sensor methods, control methods based on sliding mode control, ripple correlation control and extremum seeking control, mechanical tracking and other less common techniques developed to attempt MPPT under uniform conditions.

4.3.1 Maximum Power Point Estimation Techniques

Maximum Power Point Estimation (MPPE) techniques are the simplest maximum power extraction strategy which can be applied to a PV system. These techniques rely on measured values and pre-defined relationships to estimate the likely MPP location under particular environmental conditions. Typically, this pre-defined relationship is designed for uniform operating conditions, which reduces the effectiveness of these techniques under PSC.

The simplest form of MPPE relies on relating the short-circuit current or open-circuit voltage to the MPP current or voltage, respectively, via a linear equation. These techniques are referred to as fractional short-circuit current and fractional open-circuit voltage as they relate the measured quantity to the MPP value using a constant of proportionality, namely k_1 and k_2. In general, k_1 takes a value between 0.71 and 0.78, and k_2 between 0.78 and 0.92 [16]. The fractional open-circuit voltage relationship is given in (4.1) and the fractional short-circuit current relationship is given in (4.2).

$$V_{mpp} \approx k_1 V_{oc} \tag{4.1}$$

$$I_{mpp} \approx k_2 I_{sc} \tag{4.2}$$

The fractional open-circuit voltage and fractional short-circuit current techniques provide a very basic approximation of the MPP location. Over time, as the cells degrade, the constants k_1 and k_2 will no longer represent the MPP location, and under PSC these techniques will have poor performance [93].

In [94], the performance of the fractional open-circuit voltage technique under low power conditions is improved by allowing an adjustable sample time and sample period that depend on the amount of power being produced. Despite these enhancements, the technique will still fail to locate a global maxima under PSC. A MPPT method based on the fractional open-circuit voltage is applied in [95] for High Concentration PV (HCPV) modules. A HCPV system is one where a Fresnel lens, or similar, is used to concentrate the sunlight so that the modules receive between 300 to 2000 suns of equivalent irradiance. An important concern for HCPV systems is tracking the sunlight, so dual axis trackers are implemented and the fractional open-circuit voltage is used in this case to monitor and measure the MPP.

While the fractional short-circuit current and open-circuit voltage techniques rely on a single measurement to estimate the MPP location, other MPPE methods rely on sampling more points on the I-V curve to provide an estimation. In [96], six I-V pairs are sampled to provide an approximation of the I-V characteristic under the relevant uniform conditions. The MPP is then predicted by applying the IVMPPE technique. Other implementations include estimation of the I-V curves based on modelling of the cells under uniform conditions to find the MPP [97] and a single sensor approach relying on an empirical relationship to determine the MPP [98]. The Single Diode Model (SDM) is used to determine a robust analytical relationship using an approximation of the ideal section of the curve to accurately estimate the MPP voltage and current [99] and analytically verified in [100].

Other MPPE techniques include those that rely on the definition of the MPP locus, a relationship linking the locations of the MPPs under different irradiance levels on the I-V characteristics [101–104]. The MPP locus is shown on the uniform I-V characteristics in Fig. 4.1. For simplicity, the MPP locus is often

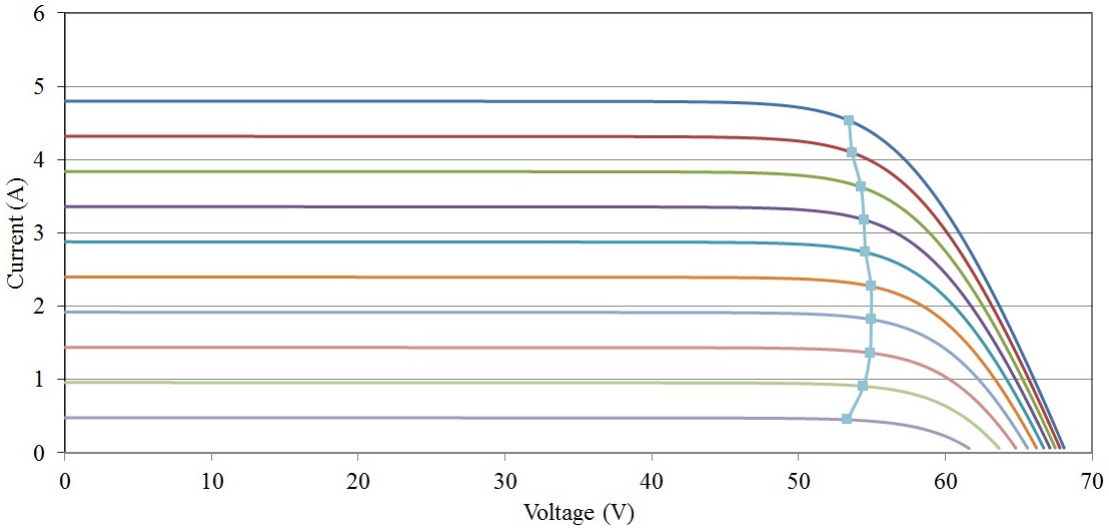

Figure 4.1: MPP locus.

approximated by a linear relationship, or in some cases by a piecewise linear approximation where a different relationship is defined for the low irradiance and high irradiance conditions [103]. In general, to use the MPP locus technique it is necessary to measure some system parameter, be it the short-circuit current or open-circuit voltage, to predict the MPP location. During this measurement, the system will be operating at a lower power than is optimal [101]. The MPP locus is defined based on PV cells experiencing uniform environmental conditions. As such, under PSC the MPP locus will no longer accurately represent the GMPP location.

A MPPE method with increased complexity involves using an Iterated Unscented Kalman Filter with six measured (I,V) points and information of the I-V and P-V curves from the manufacturers datasheet, to firstly approximate the parameters of the SDM and then estimate the MPP location of the characteristic [105]. This technique will only be applicable in the case of uniform environmental conditions as the method will be unable to fit the parameters to the model for non-uniform environmental conditions.

All MPPE techniques require some measurement of a system parameter (such as the short-circuit current or open-circuit voltage) and then use predefined relationships to approximate the MPP. These approximate relationships are developed on the basis of uniform environmental conditions which means that the estimation will most likely fail under PSC. MPPE can be executed quickly

to track to near the MPP, but cannot guarantee operation exactly at the MPP, and power losses occur during the tracking process. As the cells degrade over time and experience non-uniform environmental conditions, the accuracy of the estimation will degrade with time. These approaches exhibit no oscillations in steady-state and can be implemented with low complexity and low cost.

4.3.2 Perturb and Observe/Hill Climbing

The Perturb and Observe (P&O) and Hill Climbing (HC) methods are based on the same premise, that is, a perturbation in some control variable can be used to determine a suitable tracking direction to locate a local maxima. This control variable could be the voltage, current or duty ratio [106].

In general, the HC method uses a perturbation in the duty ratio of the converter [16, 107] while the P&O technique uses a perturbation in the voltage [16,108]. Due to its slow transient response under a change in irradiance and the potential to be affected by noise in the signal, current perturbation is rarely used [106].

These techniques work by comparing the change in power that occurs with a perturbation in the control parameter. This informs whether the algorithm should take a perturbation in the same direction at the next sample time, or in the opposite direction. When operating on the left of the MPP, the PV cell is operating in the current source region which means that a positive step in voltage will lead to a positive change in power. On the right of the MPP, the PV cell is operating in the voltage source region which means that a positive step in voltage will result in a negative change in power. The current source region and voltage source region on the P-V characteristics are shown in Fig. 4.2. When operating at the MPP the derivative of the power with respect to voltage should be zero. These

relationships are given in (4.3).

$$\begin{aligned} \frac{dP}{dV} &> 0 \qquad \text{left of MPP} \\ \frac{dP}{dV} &= 0 \qquad \text{at MPP} \\ \frac{dP}{dV} &< 0 \qquad \text{right of MPP} \end{aligned} \tag{4.3}$$

The flowchart of the P&O algorithm is shown in Fig. 4.3.

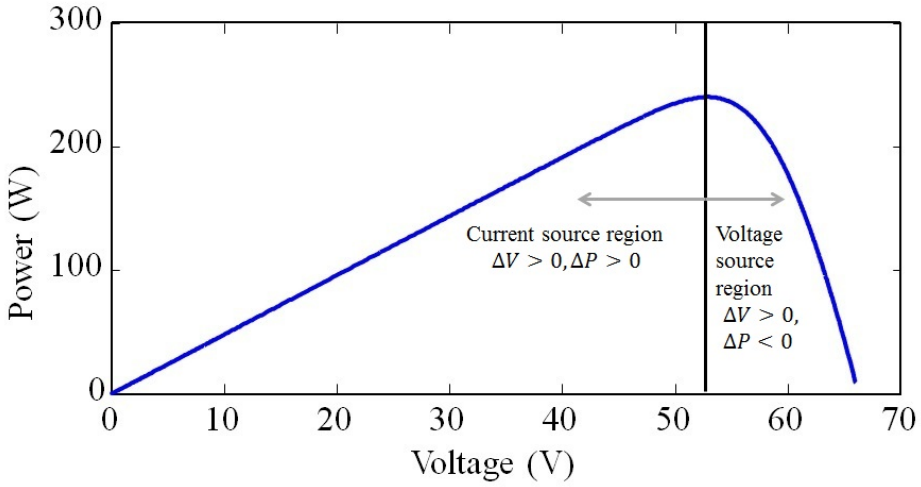

Figure 4.2: P-V characteristics showing the voltage source and current source regions.

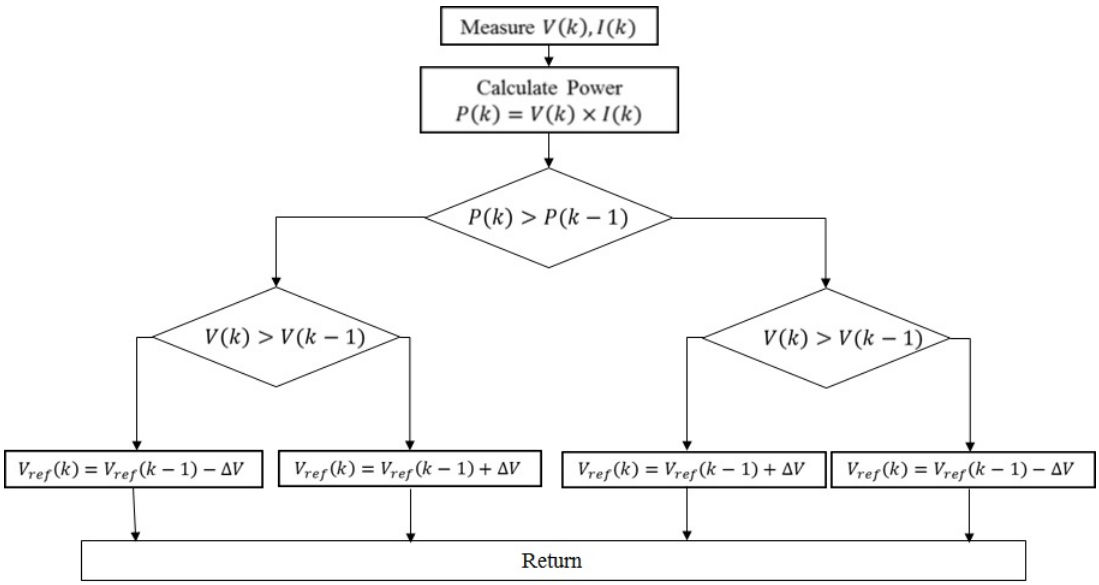

Figure 4.3: Flowchart of P&O technique.

In relatively stable operating conditions the technique has been shown to have good steady-state performance [109, 110], however, when rapid changes in irradiance occur the method may lose the MPP [111–113].

The P&O and HC methods are commonly used for MPPT due to their simplicity and low cost implementations [107, 109, 110, 113]. Their operation does not require knowledge of the PV module characteristics [113, 114], however an appropriate step size does need to be selected. Depending on the step size selected, these techniques may have slow convergence or large oscillations around the MPP [109, 110]. Other disadvantages are that invariably the technique exhibits some oscillations around the MPP resulting in lost energy, the technique has poor performance under rapid changes in irradiance and the technique cannot distinguish between local and global maxima.

During the operation of these techniques, a change in environmental conditions may occur at the same time that a perturbation in the control variable is applied. This means that the change in power observed would be the sum of the change in power due to the perturbation and the change in power due to the change in the environmental conditions. The P&O and HC techniques cannot differentiate if a change in power occurs due to a change in the environmental conditions or due to the applied perturbation and this may lead to tracking in the wrong direction immediately following a change in irradiance [111].

In the literature, several modified versions of the P&O and HC techniques are proposed which address some of the key limitations of the technique. These modified versions address the trade-off between tracking speed and steady-state oscillations, the tendency to track in the wrong direction during changing irradiance and improve the technique for operation under PSC. Techniques proposed to address the trade-off between tracking speed and steady-state oscillations, and the tendency to track in the wrong direction, will be addressed in this section. Modification of the technique to operate under PSC will be described in Section 4.4.

4.3.2.1 Steady-state Oscillation Trade-off

To address the trade-off that exists between tracking speed and steady-state oscillations, variable step size implementations are often proposed [107, 112, 115]. These approaches will apply a large perturbation when the technique is far from the MPP to allow fast tracking, and the perturbation will reduce in size as the technique converges to the MPP resulting in smaller steady-state oscillations. These implementations often rely on system dependent constants, such as a scaling factor which must be tuned for the system and condition [112]. This may limit the effectiveness of the technique. In [109], an approach is proposed to reduce the dependence on system specific constants by developing an adaptive perturbation based on the change in PV system power with PI control. The Ziegler-Nichols tuning process is required to tune the PI controller for this implementation. The perturbation period is optimised using an online procedure based on cross correlation method and implemented using Field Programmable Gate Array (FPGA) in [116]. The Delta P&O method perturbs the duty cycle to locate the optimum operating point, and has a variable step size based on $\frac{dP}{dV}$. The scaling parameter M is automatically tuned in the process [112].

A simple adaptive step size P&O technique is proposed in [117] which initially moves the operating point to approximately 90% of the open-circuit voltage to reduce the tracking time required. As the MPP is approached and the power difference between successive measurements decreases, the perturbation size is also reduced to minimise the oscillations around the MPP.

An adaptive perturbation step size method designed to accelerate tracking performance under a rapid change in irradiance is proposed in [118]. This technique relies on three algorithms being used interchangeably depending on the operating conditions observed. Initially, the technique relies on a current perturbation to perform MPPT tracking in normal conditions. When a sudden change occurs in either the irradiance or PV current, the adaptive control algorithm is initiated which moves closer to the MPP by multiplying the estimated short-circuit current by an optimal proportionality constant. The third algorithm is the variable perturbation algorithm which reduces the perturbation size when the operating point is oscillating around the MPP. Two levels of tuning are used in the implementation, a coarse tuning where the perturbation size is based on the irradiance level which is initiated with the adaptive control algorithm, and

fine tuning where the perturbation size is based on the oscillations around the MPP which is activated when the variable perturbation algorithm is applied. The method implementation assumes uniform environmental conditions and no mismatch across the system.

4.3.2.2 Tracking in the wrong direction

Approaches designed to avoid tracking in the wrong direction when a change in irradiance occurs include the dP-P&O technique [110, 119]. This approach takes an additional power measurement in the middle of the sample period to isolate the effect of the perturbation from the change in environmental conditions. In this case $dP_{0.5}$ contains the change due to the MPPT perturbation and the change due to the irradiance change, while dP_1 only covers the change in irradiance. The change in power due to the perturbation alone can be found by considering (4.4) to (4.6).

$$dP_{0.5} = P(k - 0.5) - P(k - 1) \tag{4.4}$$

$$dP_1 = P(k) - P(k - 0.5) \tag{4.5}$$

$$dP = dP_{0.5} - dP_1 \tag{4.6}$$

The P&O technique can also avoid tracking in the wrong direction by applying the approach described in [120]. In this case, the update frequency is optimised to reduce the likelihood that the technique will track in the wrong direction when a fast change in the environmental conditions occurs.

The Full Curve Estimation (FulCurvE) method is suggested in [112] to avoid tracking in the wrong direction when a change in irradiance occurs. In this approach, the trend of the power-duty cycle (P-D) curve is determined by using three sampled points obtained at a rate faster than atmospheric changes before the step direction is decided. Additionally, to address the steady-state performance trade-off, the FulCurvE method can be integrated with the Delta P&O technique to develop a P&O implementation which has good steady-state and dynamic performance with minimal drift.

4.3.2.3 Other modifications

Strategies designed to address both of the key limitations for the P&O technique include applying an adaptive step size with the dP-P&O technique [121]. This will effectively avoid tracking in the wrong direction under changes in irradiance and will improve the overall tracking speed of the P&O method. Another alternative to enhance the tracking speed involves combining the standard P&O technique with model predictive control [122].

Due to measurement noise and switching transients, power curve traps exist in the P-V curve of a PV cell even when uniform conditions are experienced. The presence of power curve traps when tracking to the MPP may result in the P&O technique becoming trapped on the curve and being unable to locate the maxima. This is overcome in [123] by applying a Generalised P&O (GPO) method which reduces the susceptibility of the technique to become trapped in a local power curve trap. The GPO compares the current measured power with a previous measured power which is multiplied by some value $\alpha_1 < 1$ and does not necessarily compare with the most recent past power measurement. The value α_1 is selected to avoid being trapped in any visible or likely trap in the P-V curve and is calculated based on (4.7).

$$\alpha_1 = \frac{P_{t,min}}{P_{t,max}} \tag{4.7}$$

The GPO method can effectively perform MPPT when the system experiences measurement noise resulting in power curve traps. The implementation however still has the common P&O trade-off between the tracking speed and steady-state oscillations and may still track in the wrong direction when a change in irradiance occurs. Additionally, improving the performance of the system relative to small power curve traps does not help to overcome the presence of local maxima under PSC. Direct duty control techniques are proposed for the P&O technique in [106] which can also reduce the effect of noise on the tracking of the MPP and minimises the oscillations in steady-state.

The HC method has also been modified using a fuzzy systems approach to improve the trade-off between tracking speed and steady-state oscillations in addition to drift under fast changing irradiance [107]. The fuzzy system develops

an adaptive perturbation in the duty cycle based on inputs including the change in power and change in current for the system.

A comparison of three points to determine the perturbation direction is proposed for low power applications in [124]. This technique, the 3-points incremental P&O (3PI-P&O), can detect more states than the standard P&O method which improves its ability to track in the correct direction under changing conditions. The 3PI-P&O technique also integrates a variable duty cycle by halving the step size with each successive step taken.

A variable step-size P&O method has been combined with the Constant Voltage Tracking (CVT) method to improve CVT performance [125]. The CVT technique is first applied to move the operating point to near the MPP, and then the P&O method is used with a step size based on the absolute values of the changing rates of the PV power and voltage as the MPP is approached.

In most variable step-size P&O method implementations the step size is determined based on the derivative of the power with respect to the voltage (i.e. $\frac{dP}{dV}$). As shown in Fig. 4.4 using this relationship results in different step sizes being used when on the left or right of the MPP which could cause issues when defining the maximal step size and the scaling factor. In Fig. 4.4, the blue line shows the P-V characteristic and the red line shows the dP/dV characteristic. These issues are addressed by using the contingence angles of the $\frac{dP}{dV}$ curve to create a more uniform, with respect to mathematical properties, characteristic from which to determine the variable step size [126].

The P&O method is implemented with a single-ended primary-inductor converter (SEPIC) and sliding mode control (SMC) of the input inductor current in [127]. The technique is designed for static PV installations where the atmospheric conditions change slowly and relies on the Power-Current characteristic.

4.3.2.4 Summary

The standard P&O technique is limited by a trade-off between the tracking speed and the steady-state oscillations due to the step size chosen for a particular

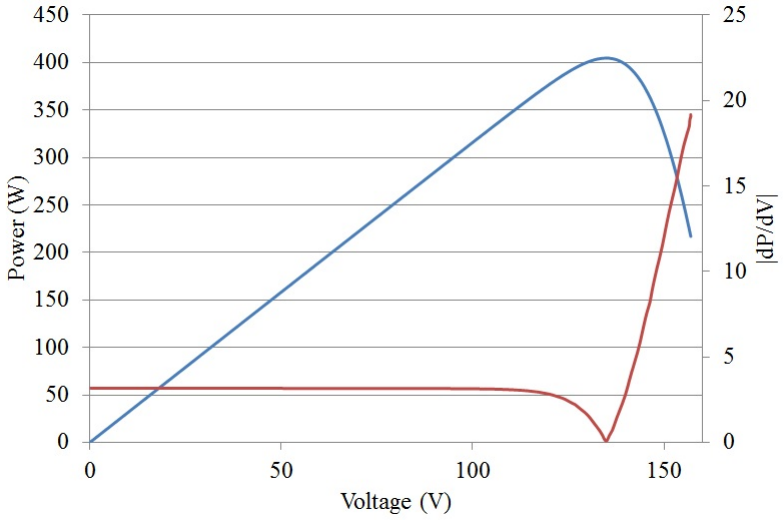

Figure 4.4: dP-dV characteristic.

implementation. Additionally, it cannot distinguish between local and global maxima and may track in the wrong direction under fast changes in irradiance. The technique can be implemented with low complexity and cost. While approaches have been suggested to improve the tracking speed and steady-state oscillation trade-off, the technique will still exhibit some degree of oscillations in steady-state and frequently these implementations either increase the complexity or rely on system dependent constants.

4.3.3 Incremental Conductance Method

The Incremental Conductance (IncCond) MPPT technique is built on the same premise as the HC and P&O techniques as given in (4.3). The only difference is in the implementation. For the IncCond technique, MPPT is achieved by comparing the incremental and instantaneous conductances based on (4.8). Equation (4.8) leads to the IncCond algorithm conditions as given in (4.9). The flowchart of the IncCond method is shown in Fig. 4.5.

$$\frac{dP}{dV} = \frac{d(IV)}{dV} = I + V.\frac{dI}{dV} \approx I + V.\frac{\Delta I}{\Delta V} \tag{4.8}$$

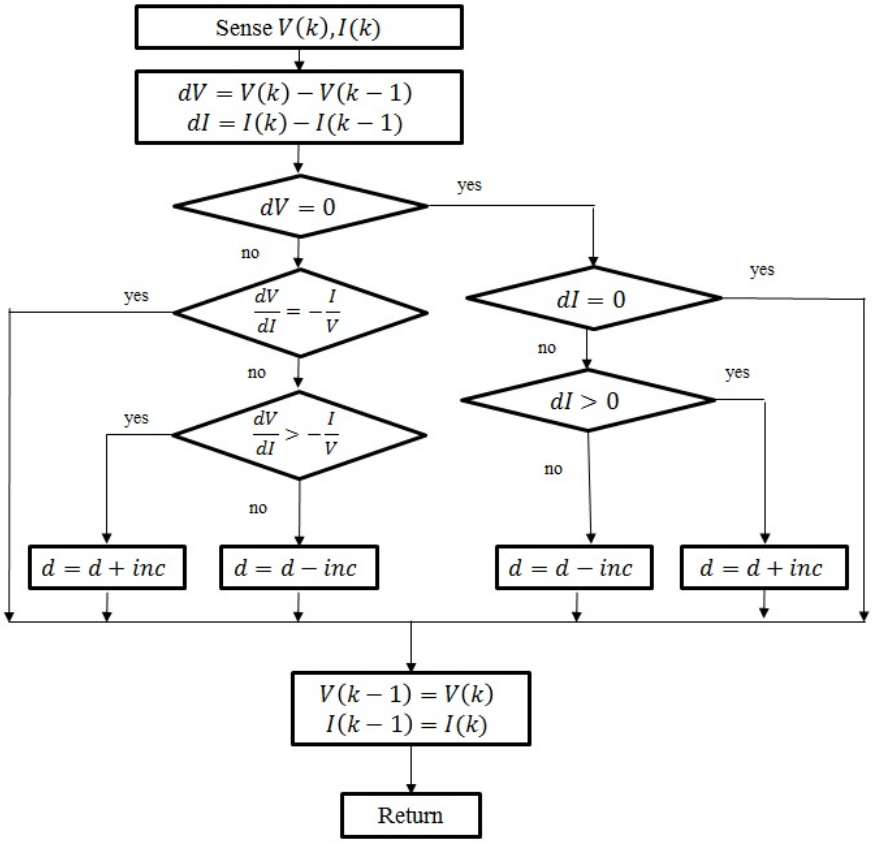

Figure 4.5: Flowchart of the IncCond MPPT method.

$$\begin{aligned} \frac{\Delta I}{\Delta V} &> -\frac{I}{V} && \text{left of MPP} \\ \frac{\Delta I}{\Delta V} &= -\frac{I}{V} && \text{at MPP} \\ \frac{\Delta I}{\Delta V} &< -\frac{I}{V} && \text{right of MPP} \end{aligned} \tag{4.9}$$

In [128], it is suggested that the IncCond technique should be considered as a different implementation of the P&O technique rather than as a technique in its own right. This is because the two techniques are built on the same idea and exhibit very similar performances. However, results in [129] suggest that the IncCond algorithm has a more rapid response to a change in irradiance when compared to the P&O technique and exhibits fewer oscillations in steady-state. Additionally, the IncCond technique has improved robustness to measurement noise due to the control decision being dependent on two distinct variables [130]. The IncCond technique suffers from the same limitations as the P&O technique including a trade-off between tracking speed and steady-state oscillations and an inability to distinguish between local and global maxima.

In some cases, IncCond can be applied using direct control and a single control

loop to simplify the algorithm and avoid tuning the PI controllers [131]. Variable step size approaches to the IncCond technique are proposed to improve the trade-off between tracking speed and steady-state oscillations [132, 133]. When operating on the left-hand side of the MPP there is the potential for a tracking delay to be exhibited due to the sensitivity of the incremental conductance, primarily due to the fact that $\Delta I \approx 0$ as the system is operating in the constant current region. The PI-INC tracking approach, recommended in [134], reduces this tracking delay by using power-increment coarse tracking along the P-V curve until a specific region is entered, called the Threshold Tracking Zone (TTZ). Once inside the TTZ, the algorithm performs IncCond to track to the MPP.

An adaptive variable step-size is defined for the IncCond technique based on a function using the conductance of the PV array [135]. This method also proposes the use of an adaptive tolerance band which is tighter at low irradiance to ensure that the method can be operated with no oscillations in steady-state. The tolerance band overcomes the fact that it is difficult to reach exactly the point where the instantaneous and incremental conductances are equal due to noise and quantisation errors in the measurements.

A FPGA-based IncCond variable step size implementation is presented in [136]. A dynamic model of PV cells is used to compare the operating point to the MPP and select an appropriate step size.

The IncCond technique suffers from the same limitations as the P&O and HC methods. This means that it cannot differentiate between a local and global maxima, and has a trade-off between tracking speed and steady-state oscillations. Additionally, the performance of the algorithm depends on the step size which needs to be optimised for each system considered. The technique can be implemented with relatively low cost and complexity.

4.3.4 Artificial Intelligence Based Approaches

Artificial Intelligence based approaches for MPPT under uniform conditions include approaches using fuzzy systems and neural networks.

Fuzzy logic enables possible outcomes and inputs to be represented on a more natural scale than as simply just true or false. In solving a problem using a fuzzy system, the fuzzy inference process is adopted. This involves, fuzzifying the input variables, evaluating any rules, combining the rule outputs and then defuzzifying the final result [137].

The MPPT implementations using fuzzy systems can be considered in two categories. There are those that use fuzzy systems to determine a variable step size which is then used in another conventional MPPT technique such as P&O [107, 115, 138–140]. The other category relies on a fuzzy model-based approach to MPPT [141–146]. Generally, the Takagi-Sugeno fuzzy system is used in preference to Mamdani, as it requires fewer rules and coefficients and can be implemented with lower complexity and reduced computational time [143–145, 147]. Fuzzy Logic Control (FLC) MPPT approaches are limited in their application as they depend on system specific parameters which must be optimised to ensure effective MPPT.

A fuzzy-based incremental conductance method which uses the error between the instantaneous conductance and incremental conductance is enhanced in [147] to enable tracking under PSC. In particular, this methodology requires three phases. Firstly equations are defined to identify when PSC arise, then a linear function is applied to move the operating point, and finally the conventional MPPT process is applied. The conditions to assess if PSC has occurred, rely on monitoring the change in voltage and the change in current with respect to defined limits.

In [148], FLC is used as an alternative to PI control to control the duty cycle of a SEPIC converter for MPPT operation. The inputs to the FLC are the output voltage error and the change in the error and the output is the required duty cycle.

Artificial Neural Networks (ANN) are modelled on the basis of the structure and interactions of the human brain. Using a configuration of neurons with links, the ANN models the human process of reasoning by passing information between the neurons and is capable of learning by adjusting the weights of the links during training [137]. The ANN is composed of an input and output layer

of neurons, in addition to one or several hidden layers.

Most ANN implementations for PV MPPT under uniform conditions involve generating a non-linear mapping between the environmental conditions and the MPP location [142, 149, 150]. As the cells degrade, this non-linear mapping will no longer represent the MPP location exactly [149]. Weather information can be difficult to measure and may not always be available where the PV system is located [142, 150] limiting the application of ANN-based MPPT. In [142], a two stage approach is implemented which uses the ANN based model to approximate the MPP location and then tracks exactly to the MPP using the P&O technique. By adopting a two stage approach, the reduction of accuracy of the ANN due to the degradation of the cells becomes less significant as the approach can still track to the MPP in two stages. Another two-stage approach involves combining an ANN based model with the IncCond technique [149]. A single stage approach is proposed in [150] which uses 20 nodes in the hidden layer to improve the execution speed. The method has good performance in tracking to the MPP and can react quickly to changes in irradiance, but would require periodic retuning as the cells degrade.

Generally, fuzzy logic and ANN based approaches to PV MPPT provide a good modelling of the non-linear P-V and I-V characteristics, however they require extensive calculations in their implementation [151]. Additionally, the techniques are often trained on uniform I-V and P-V characteristics and cannot provide accurate non-linear modelling as the cells degrade and under PSC. Retraining the algorithms over time adds to the implementation complexity of the techniques and indicates that each implementation is system specific. The techniques can generally track to near the MPP quickly and may exhibit oscillations in steady-state if combined with a technique such as P&O or IncCond in a two-stage approach.

4.3.5 MPPT Based on Output Parameters and Single Sensor Approaches

A variety of different single-sensor implementations for PV MPPT are proposed in the literature as a cost-reducing measure [129]. Many of these implementations rely on optimising the output parameters of the converter such as the load voltage or current to achieve MPPT [129, 152, 153]. The maximised converter output however, may not coincide directly with the MPP of the PV system due to the efficiency of the converter [152].

These techniques, including load current and load voltage maximisation techniques, usually assume that the converter is lossless, such that maximising the load power should maximise the PV system power [16]. Generally, loads can be classified based on their type including voltage-source, current-source, resistive type or a combination. This means that each type of load has an inherent parameter which can be optimised to ensure maximum power. As an example, for the voltage-source type load, to obtain the maximum power it is necessary to maximise the load current. Conversely, for a current-source type load, the load voltage needs to be maximised to achieve maximum power. In [153], three single sensor techniques are mathematically derived which can be applied to current-source and resistive type loads. These implementations use a single voltage sensor to eliminate the cost and complexity involved in using a current sensor.

A single current sensor is used to measure the reference inductor current in [117]. The reference inductor current is correlated with the PV output current and MPPT is implemented based on a method resembling adaptive step size P&O. By reducing the number of sensors required, the implementation cost is reduced without compromising the ability of the system to track to the MPP under uniform conditions.

The P&O technique is implemented with a single current sensor in [154] for the case where multiple PV panels are connected and each has its own MPPT controller. This approach compares the change in current measured with the known change in duty cycle to determine the next perturbation direction.

The gradient ascent algorithm is used to track the MPP by relying on a

measured change in voltage in the single-sensor approach described in [98]. The key objectives of this technique are to minimise the cost of implementation which makes the technique suitable for applications where it is important to minimise cost and complexity.

An empirical current is defined based on the measured voltage and the known duty cycle of the DC-DC converter for a battery charger application [155]. This technique uses the Incremental Resistance (INR) MPPT technique which is simply the dual of the IncCond technique [156].

In [157], a single sensor is used to measure the voltage across a capacitive load. This voltage is then related to a function to determine the direction of tracking. The function is defined based on the derivative of power with respect to time. The technique has been shown to perform well in the presence of noise [157].

A multi-channel system, that is, a system consisting of multiple PV modules which can be controlled independently, is considered in [158]. In this implementation a single current sensor is used resulting in a single Analog to Digital Converter (ADC) being required. The approach works on maximising the load current to achieve MPPT. Two modes are proposed in the implementation, which essentially aim to get each PV panel to supply its maximum current. The technique improves performance under PSC, but adds to the implementation cost. The technique can be considered as a simplified version of the Distributed MPPT approaches considered in Section 4.6.1.

In the cases shown above, for single sensor and output parameter maximisation approaches to PV MPPT, the cost and complexity may be reduced when compared to other techniques. These techniques however, will generally not extract the maximum power from the PV system but rather from the whole system including the conversion stage. Additionally, these techniques do not have the capability to distinguish between local and global maxima. Depending on the actual implementation, such as the P&O implementation in [154], oscillations may be observed in steady-state. The techniques can be operated independently of system specific parameters and are ideally suited to PV systems where cost is the defining factor.

4.3.6 Sliding Mode Control

Sliding Mode Control (SMC) has gained increased attention in recent years due to its good performance and insensitivity to parameter variations [159]. Approaches based on SMC require a suitable switching surface to be designed that represents the required dynamics of the system, and a variable structure control that enables any state that is away from the switching surface to be driven to the switching surface [160].

A number of different implementations utilising SMC for PV MPPT have been proposed [145, 161–164]. Generally, a SMC approach requires an appropriately defined sliding surface [161], which may not be optimal under PSC. Various MPPT techniques are utilised with SMC including a T-S fuzzy based MPPT method [145], a current-based P&O MPPT method [162], and a dynamic optimal voltage estimator to predict the MPP voltage [163]. In [164], a self-optimisation process is included ensuring that the entire system does not need to be modelled, and that the gradient does not need to be measured or evaluated.

In implementing SMC it is essential to first chose an appropriate sliding surface which guarantees that if the state is on the surface it will be driven to zero. Following this it is important to design a controller which will cause the system to reach the sliding surface [165]. The SMC based MPPT of [165] uses a buck converter and a sliding surface which has the error in inductor current and the converter output voltage as sliding states. The IncCond technique is implemented to find the PV voltage desired and then the SMC is used to move towards this operating point.

4.3.7 Ripple Correlation Control

Ripple Correlation Control (RCC) is frequently used in PV MPPT systems as it utilises the switching ripple which is present when switching converters are used [166–168]. This switching ripple acts like an artificial perturbation and, replicating the P&O technique, observation can be achieved by using an integrator to drive the signal error to zero [168]. The RCC approach can therefore perform MPPT like the P&O technique but without having oscillations

around the MPP as it enables absolute convergence to the MPP. The RCC method converges to the GMPP asymptotically without requiring an artificial perturbation and without any knowledge of the system parameters. A discrete implementation of the RCC approach is presented in [166], which is less expensive to implement, and is more flexible and robust.

4.3.8 Extremum Seeking Control

Extremum Seeking Control (ESC) approaches are similar to RCC but require a dither signal to be used. In [169], an Adaptive ESC (AESC) approach is proposed which enhances ESC by using knowledge of the system model. A Lyapunov-based switching scheme is used in [170] to enable the ESC approach to converge to the MPP by reducing the perturbation in the neighbourhood of the MPP rather than converging to the limit cycle. In [74], the ESC approach is also used to perform fault diagnosis.

4.3.9 Parabolic Curve Prediction

A parabolic curve is used in [171] to determine the location of the MPP. This parabolic curve is defined using the previous three duty cycles and the corresponding powers, and is renewed at each sample time. The parabolic curve is used to predict which duty cycle should be sampled next to converge to the MPP. Tracking along the curve will eventually lead to the MPP being located and the performance of the technique under rapidly changing environmental conditions is experimentally verified. As three working points are considered in the technique, it is more robust when compared to techniques, including P&O, which only rely on the comparison of two working points. This ensures that the possibility of tracking in the wrong direction is reduced. The technique can converge quickly and does not exhibit oscillations around the MPP.

The curve is defined by three measured power points P_1, P_2, and P_3. The duty cycles are shifted to ensure that the central measurement P_2 is the largest measurement, and by performing this shifting the technique can converge to the

MPP. An example parabolic curve is shown in Fig. 4.6. Under irradiance change the technique requires a little extra time to shift and rearrange the duty cycles to ensure that the measurement of P_2 is the largest which reduces the efficiency of the technique under these conditions.

4.3.10 Bisection Search Theorem

The Bisection Search Theorem (BST), sometimes referred to as Binary search, is a bracketing approach for finding the roots of equations. It is implemented as a MPPT technique in [172] on a defined function which relates the change in power to the voltage. The BST is applied to find the roots of the function by regulating the voltage of the system. The MPP is tracked by progressively reducing the size of the interval until the MPP is located [172]. The performance under PSC is limited as the existing implementations of the technique have no mechanism to distinguish between local and global maxima.

A binary search approach is combined with RCC to enable fast and accurate searching of the MPP under uniform conditions and irradiance changes [173]. The algorithm has superior performance when compared with P&O and is shown to be able to track a change in environmental conditions by performing a reinitialisation

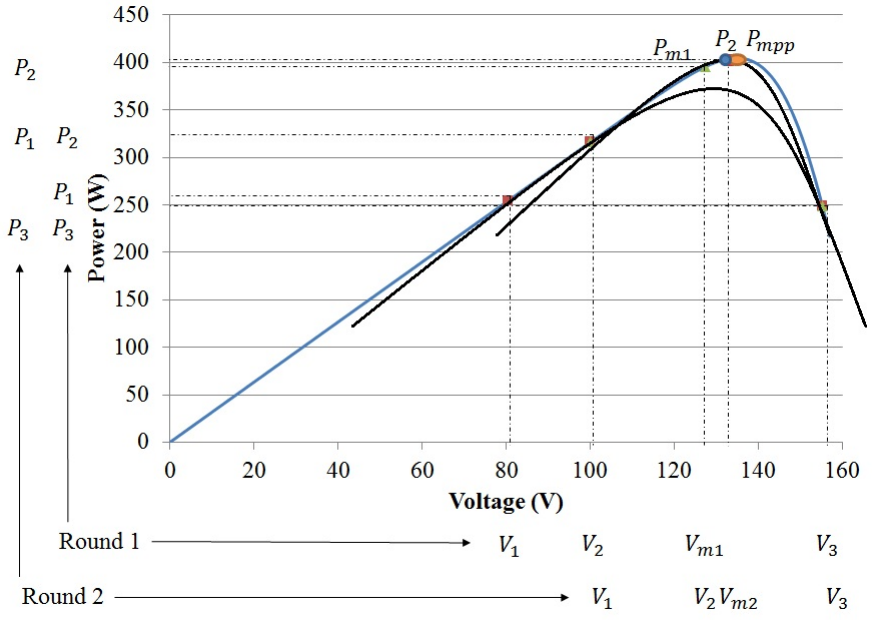

Figure 4.6: Example of parabolic curve prediction MPPT.

when conditions (4.10) and (4.11) are met. The RCC technique is used to help inform the next operating voltage.

$$k_v > |V_{i+1} - V_i| \tag{4.10}$$

$$k_p < |P_{i+1} - P_i| \tag{4.11}$$

where, k_v and k_p are not defined in the paper.

A linear prediction method that extends the Newton Iterative method by using a left and right tangent to improve searching is presented in [174]. This technique enables the MPP to be tracked rapidly without requiring step size reference. The steepest descent and centered differentiation are utilised in [175] to perform MPPT. In this technique, perturbations are stopped once the MPP is reached to avoid oscillations. A change in the environmental conditions must reinitialise the tracking and is detected by measuring either the resistance or conductance to sense a change.

4.3.11 Variable Perturbation Frequency

A variable perturbation frequency is proposed with a variable perturbation step size in [176] for a load current based MPPT. This ensures that when the step size is small the frequency is higher, and when the step size becomes large, the frequency reduces. By adopting the variable frequency of the perturbation, the system has sufficient time to settle before the next perturbation when large steps are taken which will help the technique to avoid tracking in the wrong direction. The implementation requires a single current sensor similar to the approaches in Section 4.3.5 and tracks the MPP by considering the sign of the derivative of output current with respect to duty cycle. This approach can improve the tracking speed and accuracy while maintaining a lower cost. It has no mechanism to distinguish between local and global maxima. Minimal oscillations will be exhibited in steady-state. The technique requires a scaling factor to indicate the perturbation frequency. This scaling factor is calculated based on the current operating point of the system with respect to the maximum change in duty cycle and minimum change in duty cycle permitted in the algorithm.

4.3.12 Variable Inductor

A variable inductor approach is proposed in [177]. The inductance decreases with increasing current (and in turn increasing irradiance) and the technique is implemented using a buck converter. One key advantage of adopting the variable inductor approach is that the inductor size can be reduced by up to 75%. Additionally, the method performs well in low light conditions and has a stable step response.

4.3.13 Beta Method

An intermediate variable β shown in (4.12) forms the basis of the β-method and enables the approach to track to the MPP. At the optimum point, the intermediate variable β should be a constant so the technique tries to drive this parameter to a constant value using a control loop [178, 179].

$$\beta = \ln(\frac{I_{pv}}{V_{pv}}) - c \times V_{pv} \tag{4.12}$$

where, $c = \frac{q}{AKTN_s}$, q is the electron charge ($q = 1.6 \times 10^{-19}C$), A is the diode ideality factor, K is the Boltzmann constant ($1.38 \times 10^{-23}J/K$), T is the temperature on absolute scale (K), and N_s is the number of series connected cells.

Once β is calculated, it is compared with the reference value range given by β_{min} to β_{max} to see if the system has reached steady-state. Once inside this range another conventional MPPT method, such as HC, can be implemented to track directly to the MPP [178, 179]. If outside of this range, the error is calculated and a new duty cycle to test is established. The β-method is not affected considerably by changes in the environmental conditions as these changes do not lead to a significant change in the parameter β.

The β-method can be an effective MPPT solution as it can quickly track to

the MPP and exhibits no steady-state oscillations or tracking issues when a change in irradiance occurs. Additionally, it can be implemented with relatively low complexity and cost. However, due to the definition of β_{min} to β_{max}, the technique will not have the capability to distinguish between local and global maxima as it depends on system specific constants which may no longer represent the system operation under PSC.

4.3.14 Other Approaches

Support Vector Regression (SVR) is used to approximate the irradiance and temperature on a PV module based on the operating voltage and current to then approximate the MPP voltage [180]. In its current form this technique is essentially trained for uniform environmental conditions, as a different mapping function would be required for non-uniform conditions because the irradiance estimated would not reflect the irradiance occurring across the entire PV module. As with neural network techniques, SVR performance will deteriorate with time as the cells degrade and the mapping loses validity. Results in [180] indicate good performance of the technique under load, irradiance and temperature variations.

Adaptive control schemes have been developed for a grid-connected PV system relying on either an adaptive estimator or sliding mode estimator to provide an indication of key parameters [181]. The implementation uses the capacitor and inductor voltage in a full-bridge inverter to give the state of the system. The MPP can be tracked without the need for temperature and irradiance sensors and the current input to the grid has unity power factor.

A MPPT method based on analysis of the Power Plane of the I-V characteristics to achieve MPPT under uniform conditions is proposed in [182]. In this technique, the open-circuit voltage and short-circuit current are sampled to determine the power region of the I-V characteristic. This power region is the curved section of the I-V characteristic which separates the current-source and voltage-source regions. Once the power region is defined, an equation is used internally in the processor to vary the voltage and calculate a corresponding current to give a power rectangle under the I-V curve. Once the voltage and current are found

which corresponds to the power rectangle with the greatest area, the system moves to this point. Processes for detecting fast changing and slow changing irradiance are included in the method, as are approaches for dealing with a change in temperature. To detect a fast change in irradiance and reinitalise tracking in this case, the actual current measured at the voltage corresponding to the MPP is compared with the predicted current. If these currents do not match the tracking is restarted. For slow changing irradiance the current is monitored over time and when the difference in the PV measured current and predicted current rises above some threshold value the tracking is reinitalised. A change in temperature is detected similarly as it will result in a change in the current between the operating point current and the predicted current. In any case, when reinitalising the algorithm it is necessary to sample the open-circuit voltage and short-circuit current to redefine the power region of the I-V characteristic.

4.3.15 Mechanical Tracking

Often MPPT can be combined with a mechanical tracking device to maximise the amount of irradiance on the panel throughout the day and as the seasons change [138, 183]. Mechanical tracking could occur by manually changing the angle of the panels when the seasons change or by using passive, optical or astronomical automatic tracking methods [184]. The MPP is sought by using SMC to determine the azimuth and elevation angles which provide the maximum output power in the system described in [184]. This approach maximises the irradiance on the panel and will maximise the output for a given operating point. Under PSC, the method would be able to track to the angles which provide the most power, however this could still involve operating at a power level below that which is possible for the particular conditions.

4.4 Modified Conventional Techniques for PSC

In this section, approaches to improve the performance of conventional MPPT techniques under PSC will be explored. In particular, periodic reset and curve scanning techniques will be considered, followed by techniques that widen the search range and then two-stage approaches. One common limitation of these approaches is that GMPPT cannot be guaranteed at all times.

4.4.1 Periodic Reset and Periodic Curve Scanning

A very simple enhancement that is often made to conventional MPPT techniques involves a periodic reset of the operating point to improve the probability that the system will locate the GMPP. A periodic reset is used with the 3PI-P&O technique to reduce the likelihood that the algorithm will become trapped at a local maxima [124]. This periodic reset moves the system to a random operating point and occurs every 5-10 minutes, but cannot guarantee GMPPT.

A periodic search is completed every 1-15 minutes in [185] and then the P&O technique is used to achieve exact MPPT tracking. This method works by progressively drawing more power from the DC-DC converter until the GMPP is reached. Once the GMPP is located the algorithm uses the P&O method to remain at this point until the next global search is initiated.

Other techniques perform a periodic sweep of the entire I-V characteristics to identify the GMPP exactly. In [186], a very fast measurement of the I-V characteristics is achieved to locate the GMPP. Due to the speed of the sweep, the power loss during it is minimal. The P-V curve is periodically scanned in [93] leading to GMPPT and a switched impedance circuit is used in [187] to perform an I-V curve trace. One disadvantage of sweeping the entire I-V or P-V curve is that power losses occur during the sweep process and there are some regions of the curve where the MPP is unlikely to be located, as is supported by the analysis in Chapter 3 and the observations of [90]. Additionally, extra circuit components such as switches, capacitors and resistors are often required in these

implementations [187].

A scan of the P-V curve to determine the resistance at the MPP is performed every three minutes to define a suitable resistance for a reconfigurable switched capacitor DC-DC converter to match the converter resistance to the MPP resistance in [188]. The reconfigurable switched capacitor converter has improved efficiency due to the set of capacitors which are connected in series when charging, and then reconfigured to be in parallel, for discharging.

In some cases, a curve sweep can also be performed to enhance the performance of the fractional open-circuit voltage or short-circuit current techniques by defining a more suitable constant of proportionality for use in the current environmental conditions [16]. This approach will improve performance initially, but the changing environmental conditions may quickly lead to this constant no longer being representative of the location of the GMPP and energy losses occur in the measurement process.

Periodic reset and curve scanning techniques generally improve the performance of conventional MPPT techniques with minimal increase in implementation complexity and cost. However, these techniques cannot guarantee GMPPT at all times.

4.4.2 Widen Search Range

Another very simple approach that can improve the tracking of conventional MPPT methods under PSC involves extending the searching range of these techniques [21, 107, 186, 189] or identifying optimal regions within which to search [22, 74]. In [22], ESC is enhanced by defining regions within which the local optimisation strategy can be applied to locate the GMPP. Widening the search range however adds to the time required to search for the GMPP and could lead to considerable power losses during tracking. In [190], it is proposed to search first on the left and then the right of a located optimum in order to locate the GMPP. In some cases, this may still lead to most of the P-V characteristics needing to be swept to ensure GMPPT.

4.4.3 Two-Stage Methods

A variety of two-stage methods are proposed in the literature to improve the performance of conventional MPPT techniques under PSC [132, 187, 190, 191]. These techniques typically use some process in the first stage to move the operating point near to the predicted GMPP and then converge to this point using a conventional MPPT technique (usually P&O or IncCond) in the second stage. In [132], a linear function is defined to move the operating point when PSC are detected and then variable step size IncCond is applied to track the MPP exactly. The technique is simple and can be easily implemented in existing PV installations to enhance MPPT under non-uniform conditions.

An I-V curve trace using a switched impedance circuit, consisting of a capacitor in parallel with a resistor, is adopted in [187] to locate the GMPP when PSC are detected. In the second stage, conventional techniques are used to track the MPP exactly. One disadvantage of this technique is that it requires additional circuit components in its realisation and the power available from the system is reduced during the I-V curve trace.

Several authors define a load line based on an equivalent resistance (proportional to the ratio of the open-circuit voltage to the short-circuit current) to move the operating point in the first stage and then use another MPPT technique in the second stage [187,190–192]. In some operating conditions, the load line may lead to tracking of a local peak, so [190] proposes a global search around the local peak and updating of the load line coefficients based on the GMPP location. The load line method requires online monitoring of both the open-circuit voltage and short-circuit current which means that there will be a periodic loss of power when these measurements are taken.

A variable step size P&O method combined with the fractional open-circuit voltage technique is presented in [193]. When a large change in current is observed, the technique will automatically adjust the operating point to improve the performance under PSC.

A two-stage approach combining P&O in the first stage to locate a local MPP (LMPP) followed by global searching using Particle Swarm Optimisation (PSO) is presented in [194]. By first locating a LMPP, the global searching time required by the PSO method is reduced improving the tracking speed under varying environmental conditions.

Two stage methods improve the performance of conventional MPPT methods with very small increases in implementation complexity and cost. However, the methods are shown to fail in some conditions and may lead to increased tracking time or a reduction in the power available when determining the load line.

4.4.4 Techniques based on observations of the I-V and P-V characteristics under PSC

Some authors have provided a comprehensive study of the I-V and P-V characteristics under PSC and have extended this to observations which can be used to govern a GMPPT technique [90, 195]. The observations of [90] indicate that the separation of MPPs is approximately 80% of the open-circuit voltage of the module and that on either side of the GMPP the MPPs decrease in magnitude. The technique based on the observations of [90] uses conventional MPPT to track the MPP and a global peak search process to search the relevant areas of the P-V curve to locate all MPPs until the GMPP is detected. By performing the search in this way, the entire P-V curve does not need to be considered, reducing the search time required.

The observations from [90] are used in the method proposed in [196] which improves the performance of the IncCond technique under PSC. In this technique, each MPP is tracked by searching at intervals of approximately $0.8V_{oc}$ and then returning to the largest maxima located. A permitted error of 0.06 is applied in the technique to avoid oscillations during steady state. By monitoring the direction of change of the voltage and current it can be identified if a change in irradiance or a change in load has occurred, and the relevant tracking process initiated. The tracking process is either the load variation subroutine to return

to the GMPP under a change in load resistance or the GMPP searching process when a change in irradiance is detected.

In [195], a similar approach of sweeping the P-V curve based on key observations is adopted. By performing a sweep using key characteristics, the portion of the P-V curve that needs to be searched is reduced considerably improving the tracking performance. Auxiliary curves are defined in [195] based on the fact that the change in voltage or current along these curves is much faster than the change occurring along the I-V curve. These curves enable effective MPP searching to occur.

A Voltage Window Search (VWS) algorithm has been proposed based on key characteristics of the spacing between successive MPPs which reduces the amount of the P-V curve which needs to be considered when performing GMPPT [197]. The technique relies upon a global voltage step which has an optimum value approximately equal to the voltage difference between two adjacent power peaks. In the paper, a value between $0.5V_{oc,p}$ and $1.0V_{oc,p}$ is proposed to give optimum results. The technique also relies on a Power Operating Triangle (POT) which is defined by constant current and constant voltage lines and leads to the development of the voltage window (VM). The voltage minimum of the window is determined by the power level and the maximum is fixed at $0.9V_{oc}$. The VWS method is applied periodically unless a large change is detected by monitoring the ratio of the change in power to the change in voltage between successive measurements. After the VWS algorithm is applied, a conventional MPPT technique (in this case P&O) is applied to remain at the GMPP.

The GMPP is predicted based on equations for determining the MPP current and voltage for given meteorological conditions [79]. This prediction technique can accurately predict the GMPP location under PSC and is utilised to compare the performance of the Series-Parallel, Total-Cross-Tied and Bridge-Linked configurations under defined shading scenarios. While the technique shows great accuracy in estimating the location of the GMPP it is not practical to implement as a GMPPT technique as the irradiance on each module or collection of modules needs to be known to estimate the GMPP location.

Techniques based on observations of the I-V and P-V characteristics of PV

systems under PSC can offer improved tracking performance as the searching range is refined. However, these techniques may increase the cost and complexity of conventional MPPT slightly and may involve the temporary tracking of a local MPP.

4.5 Techniques designed to perform MPPT under PSC

This section will address techniques which have been specifically designed to handle GMPPT. The techniques considered include line search methods such as Dividing Rectangles (DIRECT) and Fibonacci search, artificial intelligence approaches and Chaos Search.

4.5.1 Line Search

Several line search MPPT methods have been proposed to deal with PSC including DIRECT [20], and Fibonacci Search [21, 198]. Line search algorithms work by restricting and shifting an interval to locate the optimal interval within which the optimum point lines and then converging to this point [21].

The DIRECT method is based on progressively making the searching interval smaller based on the values of samples within the interval and a condition used to determine which interval is the most promising to hold the optimum value [20]. As the P-V characteristics of the PV module can be verified to be a Lipschitz function, the DIRECT method can be used and in most cases will lead to GMPPT.

For the Fibonacci search method, the length of the interval considered is determined based on the numbers in the Fibonacci sequence [21, 198]. Generally, to make this method suitable for PSC, it is necessary to define a condition to detect when PSC has occurred [21] to enable the method to reinitialise.

Line search methods can enable GMPPT under most conditions with relatively simple test conditions. However, in some cases the techniques will converge to a local MPP and the techniques may depend on the use of special conditions to detect when PSC have occurred. Depending on the initial parameters selected, the method may not converge to the GMPP.

4.5.2 Artificial Intelligence

The main artificial intelligence approach explored in the literature for dealing with PSC is Particle Swarm Optimisation (PSO) [19, 151, 199–202]. PSO approaches are modelled on the basis of birds flocking and fish schooling and use a collection of particles to collectively solve a problem. Each particle's position is updated based on its best position and the best overall position enabling the particles to converge to a global solution. Typically, PSO is applied to time-invariant problems, so mechanisms to detect a change in environmental conditions and reinitialise the global tracking are essential for PV systems [201]. PSO search requires several parameters to be defined including the momentum factor, speed determining constants and the number of agents [19]. In [202], the randomness in the method is reduced by removing the random parameters leading to fewer parameters and improved performance.

The PSO technique is combined with a Gravitational Search Algorithm to minimise oscillations in steady-state for uniform operating conditions where a change in irradiance occurs [203]. This method exhibits superior performance in tracking to the MPP, with the absence of oscillations in steady-state, when compared to each of the algorithms applied independently. While the change in irradiance is considered in the paper and the difference between local and global maxima identified, there is little information to support the PSC simulated for this system.

A technique based on a colony of flashing fireflies has been proposed for GMPPT which exhibits superior performance to PSO [204]. The firefly algorithm is inspired by the behaviour of flashing fireflies when attracting a mate. The algorithm is based on the idea that the fireflies will move towards the brightest firefly where brightness corresponds to the power on the P-V curve corresponding

to that operating point. Performance of the algorithm shows improved capability to track to the GMPP and the PSO technique is simply a special category of the firefly algorithm.

PSO generally has good performance in tracking the GMPP under PSC. However, in some cases if the initial particle positions are not selected appropriately, the method may converge to a local solution [19]. Additionally, the performance is strongly related to the values selected for the system constants.

4.5.3 Chaos Search

A chaotic search approach is defined in [205], which uses dual-carriers to improve the performance. In the search process a logistic mapping is selected and an additional function is used to map the chaos generators. The chaotic search can operate well under PSC and unpredictable environmental conditions. As chaotic behaviour appears random, but can be shown to be deterministic, a chaotic search will have superior performance to a completely random search which makes this technique appropriate for improving MPPT performance under PSC. The implementation requires no extra circuit components, however is more complex than conventional MPPT techniques.

The chaotic search process is combined with PSO for flexible PV modules to develop the Hybrid Chaotic Particle Swarm Optimisation (HCPSO) technique [206]. Flexible PV modules can be applied to curved surfaces which results in the appearance of local MPPs. The HCPSO technique is proposed as an efficient way to track to the GMPP for cells where geometric placement is a significant factor for modifying the P-V characteristics. When the particles (only two used in this implementation) are stuck in a local MPP, the chaotic search will reinitialise their positions. The HCPSO technique is applied every few minutes and then a conventional MPPT method is used to remain at the GMPPT before the next global tracking cycle is initiated.

4.6 Power-Electronics Approaches to MPPT Under PSC

Power Electronics (PE) approaches to MPPT under PSC in PV systems act by using PE circuits to either control the flow of power or enable individual MPPT at cell, string or module level. The key techniques to be discussed in this section include Distributed MPPT (DMPPT) [207–212], monitoring the bypass diode voltages to infer PSC [213], applying differential power processing (DPP) [214], and using the principle of power electronics equaliser [215]. Additionally, changes to the PV system architecture and converter topology can improve performance under PSC such as using the Total-Cross-Tied (TCT) and Bridge-Linked (BL) configurations to improve energy yield [18, 216, 217].

4.6.1 Distributed MPPT

Distributed MPPT (DMPPT) involves each cell, string or module having its own DC-DC converter and MPPT control [211, 212]. This enables the MPPT control to move away from a centralised approach where a single MPP can be tracked, to enable each sub-unit of the system to operate at its own MPP. Centralised and Distributed MPPT architectures are shown in Figs. 4.7 and 4.8, respectively. The level of granularity results in an increase in power, but is also accompanied by an increase in cost [211, 212]. In determining a suitable level of granularity it is essential to determine the power gain for the cost expended.

A case study using Tigo module-level DMPPT PE show an increase in performance accounting for about 30% of the shading losses [218]. These authors also show that module-level DMPPT across 542 systems with the Tigo module level PE have an average annual power loss of 8.3% due to partial shading. In the absence of the module-level PE, this shading loss would increase to about 36% [218].

Usually, simple conventional MPPT techniques are used in the power converters for DMPPT including P&O [207, 208] and IncCond [219], which means that internally to the unit, mismatch and PSC cannot be addressed. For instance, if DMPPT is applied at the module level and there are 36 cells in series with two

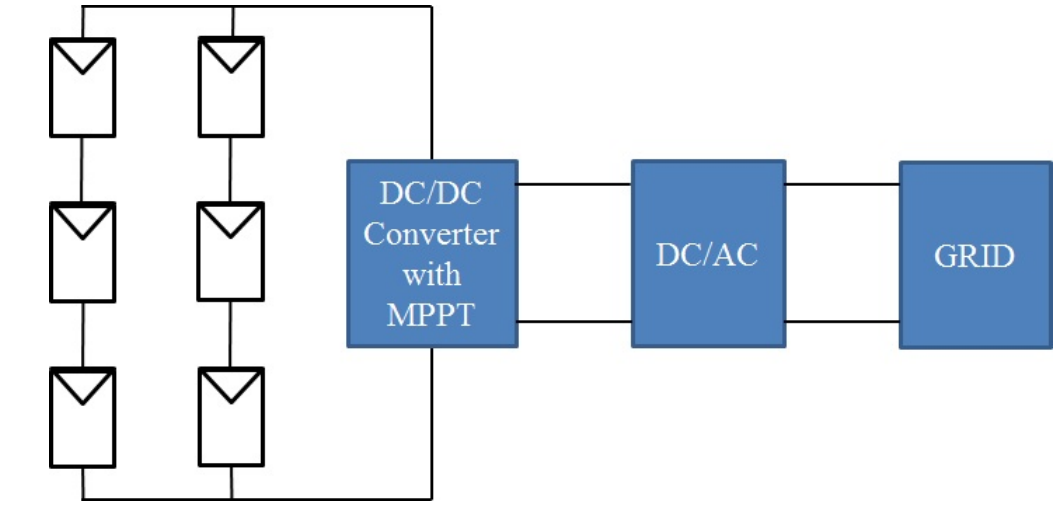

Figure 4.7: Centralised MPPT architecture.

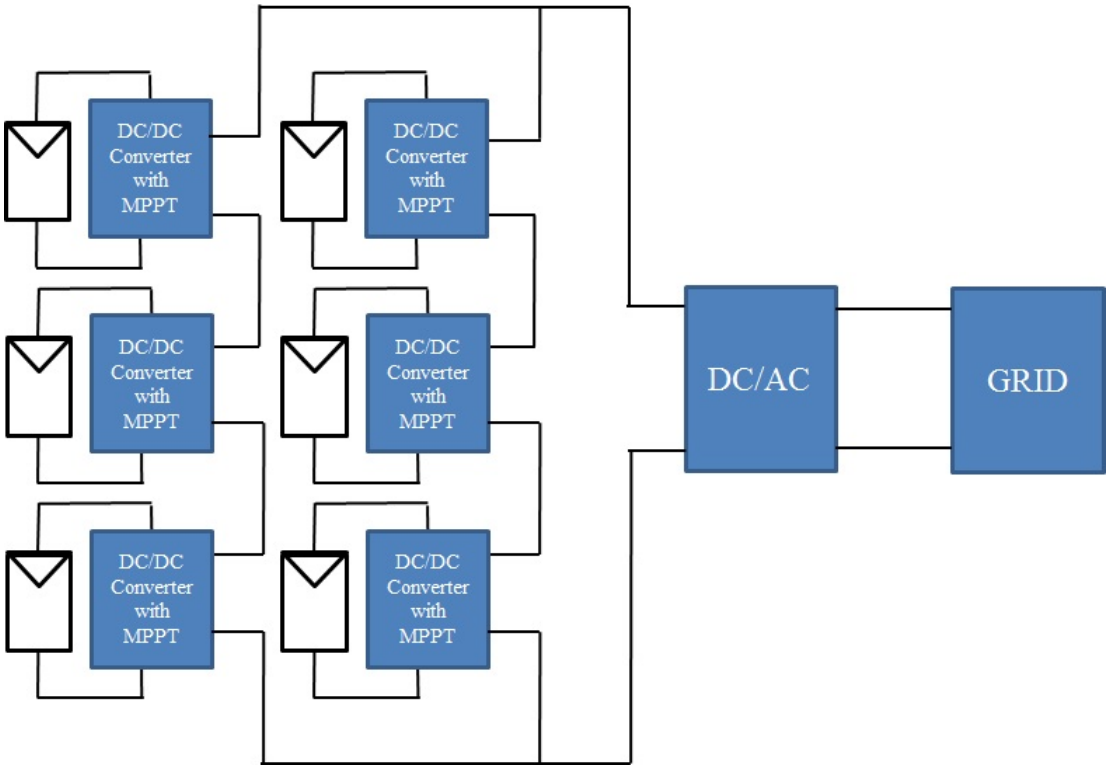

Figure 4.8: Distributed MPPT architecture.

bypass dioes within the module, any shading within the module itself will not be addressed by the implementation [210] (except in the case of a sub-module implementation such as [111]). However, the technique can still substantially improve the power yield from large PV systems exposed to PSC. Another advantage of the technique is that it can increase the reliability, as the failure of a single module or converter will not result in the entire system failing [211].

An analogue technique designed for DMPPT referred to as the Technique

based on the Equalisation of the Output operating points in correspondence of the forced Displacement of the Input operating points of two identical PV systems (TEODI) has been proposed in [220]. This technique relies upon having two identical sub-modules and adjusting either the current drawn for parallel-connected modules, or the voltage for series-connected modules, and using the difference to determine how to shift the duty cycle of each module to move towards the MPP. The limitation of this technique is that it can only be applied to identical sub-modules that experience identical environmental conditions.

A centralised control approach for DMPPT is proposed in [221] which uses vectorial control that perturbs the operating points of all of the DC-DC converters at the same time, and observes the power transferred to the DC-link. The operating point is described in terms of magnitude and angle which enables all PV voltages to be perturbed at the same instant. The method seeks to maximise the power available from the converter so it will not track exactly to the MPP of each PV module comprised in the system.

Another centralised control approach for DMPPT involves using FPGA with the P&O algorithm to control multiple modules [222]. FPGA enables parallel processing to occur and can control multiple PV module converters simultaneously. The approach is limited by the technical specifications of the FPGA in terms of the number of modules which it can provide simultaneous MPPT for.

To minimise the high cost involved in having multiple converters in a DMPPT architecture a multichannel approach with a single sensor, single power inductor and single converter has been proposed in [223]. The key feature of the proposed methodology is that it relies on a multiple-input single inductor converter and has two phases in the MPPT search. In the first stage, the duty cycle of all individual cells, sub-modules or modules (depending on the granularity) are perturbed in the same direction to increase the total power output of the system. In the second stage, the method detects the differences between the duty cycles necessary to enable each sub-section to converge to its own MPP.

Distributed MPPT approaches rely on having multiple DC-DC converters in the system to enable MPPT to be performed at the cell, module or string level. Accompanying any increase in the number of converters there is an increase

in the cost of the system, however the reliability of the whole system will also increase. In choosing to implement a DMPPT system it is important to assess if the energy gains outweigh the increased cost associated with the chosen level of granularity.

4.6.2 Monitoring Bypass Diode Voltages

In [213], it is observed that PSC can, in general, be detected by considering the bypass diode voltages in a system that uses Module Integrated Converters (MIC). When the relevant string of PV cells is not shaded, the bypass diode should be inactive, however when shading occurs it will become active and exhibit a voltage drop. By monitoring the voltages of the bypass diodes it is possible to infer when PSC occurs. When a shading condition is detected, the technique initialises a global search process which scans the entire P-V curve (or sections of the curve which are located at multiples of the rated string voltage) to locate the global maxima. One limitation of the technique is that in some cases local maxima may arise without a change in bypass diode voltage which limits the effectiveness of this technique under all environmental conditions. Additionally, this technique can only be applied to systems where the string voltages are easily accessible and can be measured.

4.6.3 Differential Power Processing

In the Differential Power Processing (DPP) model for achieving maximum power extraction, converters are placed between adjacent PV modules [214]. These converters supply the current difference that exists between the current at the MPP of the two modules and the converter is only active if there is a difference in the power producing capability of the two adjacent modules. Local MPPT between the module is achieved by applying conventional MPPT techniques, in this case P&O. By placing the differential converters between the modules the conversion losses can be minimised and series PV modules can be seen to produce more power under PSC. GMPPT is achieved by allowing each module to operate at its own MPP. The DPP configuration is shown in Fig. 4.9.

A technique designed to overcome the limitations of compensation power-dedicated DC-DC converters (CPDC) for current compensation DMPPT (CPDC-DMPPT) using shunt-connected flyback DC-DC converters is proposed for grid-connected PV systems in [224]. This technique, unlike other CPDC-DMPPT schemes can ensure exact MPPT with relative simplicity. In the flyback converter, the secondary-side diode is replaced by a power MOSFET with an antiparallel diode. When tracking the MPP the module is disconnected from the grid and the converter operates in the special MPPT resonant mode and then operates in the normal flyback mode when connected to the grid.

DPP is applied in a submodule application with communication only between adjacent DPP converters, duty cycle perturbation and voltage measurement in [225] to improve and enable *true* MPPT. The P&O method is applied in each converter and the converters are designed to fit easily into the PV junction box. One key advantage of DPP is that each converter only needs to process the power difference between the two modules, and not the entire power of each module, as is required in other PE approaches to MPPT, leading to using reduced power rating converters which are far less costly than converters which are rated to process the entire module power [225, 226].

One key advantage to using DPP rather than dedicated converters for each module is that at low levels of mismatch conventional approaches may perform better than DMPPT [226]. DPP approaches enable GMPPT to occur with lower power losses in the converters as each DC-DC converter only needs to process the power difference between the two modules. Conventional MPPT methods are applied with DPP approach, so mismatch internal to the module will not be accounted for.

4.6.4 Power Electronics Equaliser

The PE equaliser approach to GMPPT involves a topology in which series-connected cells can be operated with different voltages and currents according to the Power Independence Principle (PIP) [215]. PE equaliser approaches transfer

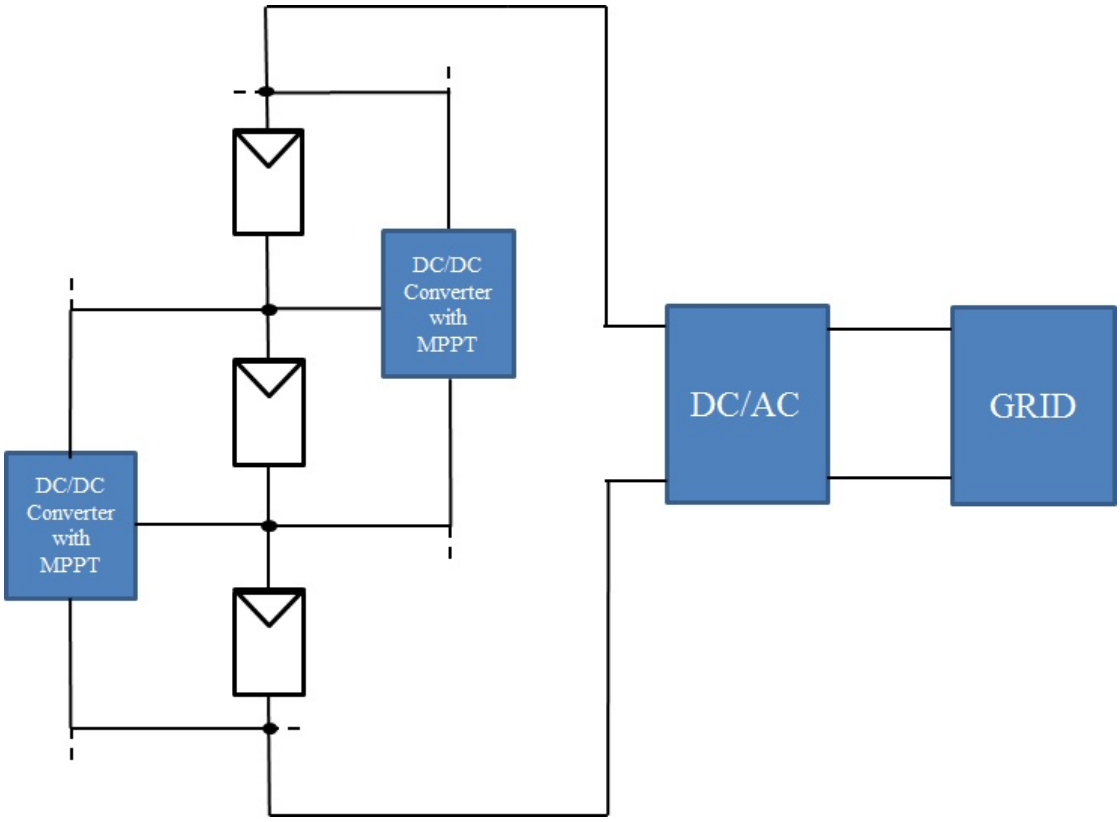

Figure 4.9: Differential Power Processing configuration.

the power from non-shaded modules to shaded modules to enable all modules to act at their MPP and exhibit an equal power level across the system [227]. In [215], an inductive storage element is charged by the non-shaded cells and then connected in parallel to the shaded cells to redistribute the energy between the cells. Implementation of the topology requires a suitably sized inductor, and several switches. Capacitors are used to store the energy from the non-shaded modules in [227].

4.6.5 Topology

The topology of the PV system configuration can also help to improve the power yield in large PV installations. Common configurations include the series-parallel (SP), total-cross-tied (TCT) and bridge-linked (BL) configurations as shown in Fig. 4.10. The configuration used can improve the performance under mismatch due to both cell aging and shading [18, 216, 217]. A study performed by Jazayeri et. al. considers the performance with each of these topologies under PSC [228] and also the effectiveness of bypass diodes. Their results show that the TCT

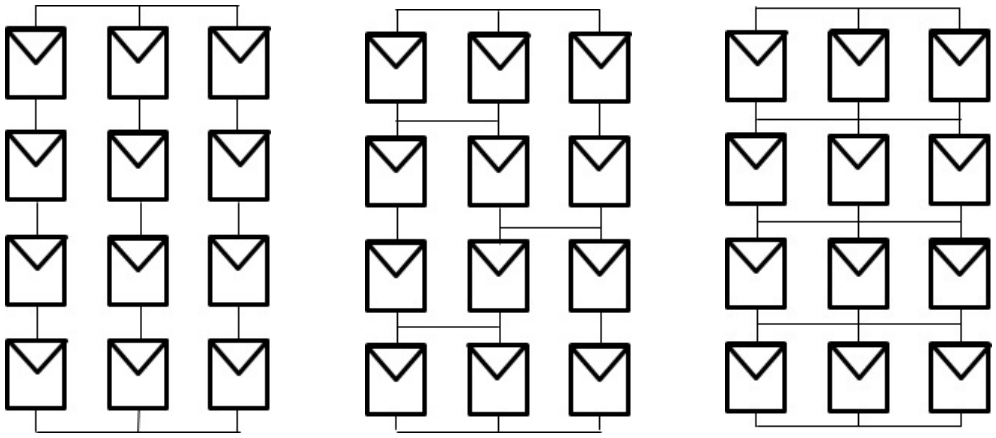

(a) Series-Parallel topology.

(b) Bridge-Linked topology.

(c) Total-Cross-Tied topology.

Figure 4.10: PV system topologies.

configuration, despite its increase complexity, performs much better than the SP and BL topologies. The SP and TCT topologies are considered under PSC to assess the technical and economic implications of selecting one configuration over the other [229]. Results show that while the TCT topology has a higher cost to implement, it is capable of extracting more power under PSC.

4.7 Discussion

Table 4.1 compares the explored MPPT techniques against the criteria established in Section 4.2. For each technique, one or two references are provided. Note that the cost is not included in the table due to the difficulty in estimating the likely cost of each PV system implementation. However, the systems described in the PE based approaches and those that require an increase in circuit complexity, would generally incur additional costs due to the extra power electronics components required.

In Table 4.1, the ability of the technique to reliably identify the GMPP is identified by *no* if it will rarely track to the GMPP, *likely* if the technique may converge to the GMPP, and *usually* if the technique can be considered to be a reliable GMPPT technique. The tracking speed is indicated as *fast*, *slow* or *varies*. Where *varies* is indicated, shows a technique where the tracking speed is directly dependent on the choice of parameters, for instance, the step size in

Table 4.1: Comparison of MPPT techniques.

Technique	**Reliably Identify GMPP**	**Speed**	**Speed under irradiance change**	**Steady-state oscillations**	**Dependence on System Specific Parameters**	**Complexity**
Conventional MPPT techniques						
Perturb and Observe and Hill Climbing [106, 128]	No	Varies	Varies	Common	No	Low
Incremental Conductance [120, 131]	No	Varies	Varies	Common	No	Low
Fractional Short-circuit Current [230]	No	Fast	Fast	No	Yes	Low
Fractional Open-circuit voltage [94, 231]	No	Fast	Fast	No	Yes	Low
Ripple Correlation Control [168]	No	Fast	Fast	No	No	Low
MPP Locus [102, 103]	No	Fast	Fast	No	Yes	Moderate
Extremum Seeking Control [169, 170]	No	Fast	Fast	No	No	Moderate
Sliding Mode Control [161, 162]	No	Fast	Fast	No	Yes	Moderate
Load current/voltage maximisation [152]	No	Fast	Fast	No	No	Low
Fuzzy based [61, 142]	No	Fast	Fast	No	Yes	High
Neural Network based [142, 150]	No	Fast	Fast	No	Yes	High
Bisection Search [172]	No	Varies	Varies	No	No	Low
β-method [179]	No	Fast	Fast	No	No	Moderate
Global MPPT techniques						
Periodic reset [124]	No	Varies	Varies	Sometimes	No	Moderate
Periodic Curve Scanning [185, 186]	No	Varies	Varies	No	No	Moderate
Two stage methods [190, 191]	No	Varies	Varies	Sometimes	Sometimes	Moderate
Two stage methods (equivalent load line) [191, 192]	No	Varies	Varies	Common	Yes	Moderate
Observations of P-V characteristics [90]	Likely	Varies	Varies	No	Yes	Moderate
Refined P-V curve sweeping [22]	Likely	Varies	Varies	Sometimes	Yes	Moderate
Line Search (DIRECT) [20]	Usually	Varies	Varies	No	Yes	Moderate
Line Search (Fibonacci) [21, 198]	Usually	Varies	Varies	No	Yes	Moderate
Particle Swarm Optimisation [201, 202]	Usually	Varies	Varies	No	Yes	Moderate/High
Chaos Search [205]	Usually	Fast	Fast	No	No	Moderate
Power Electronics Based Approaches						
Bypass diodes method [213]	Usually	Slow	Slow	No	No	High
Differential power processing [214]	Usually	Varies	Varies	Sometimes	No	Moderate
PE equaliser [215]	Usually	Fast	Fast	No	Yes	High
Distributed MPPT [211, 212]	Usually	Varies	Varies	Sometimes	No	Moderate
TEODI [220]	Usually	Fast	Fast	No	Yes	Moderate

the P&O method. The presence of steady-state oscillations is characterised by *no*, *sometimes* and *common*. Where *sometimes* is indicated shows a technique which depending on the implementation may exhibit steady-state oscillations. An example of this is applying a periodic reset with the P&O technique. The dependence on system specific parameters is shown by *yes*, *no* or *sometimes*. The case where *sometimes* is indicated relates to the actual implementation for two-stage methods. Finally, the implementation is classified based on its complexity as *low*, *moderate* or *high*. This complexity is based on the characteristics of the technique in terms of the number of components required, potential software complexity and the ease with which the technique could be applied in a new system.

Table 4.1 clearly shows that no single MPPT technique, or approach designed for promoting global maximum power extraction under PSC, is able to meet all of the criteria defined within this chapter. In general, it can be seen that conventional MPPT techniques are usually plagued by a tendency to track a local maxima and may exhibit oscillatory behaviour around the MPP. Additionally, the simplest of these conventional techniques are limited by the definition of system dependent constants which are no longer representative of the system under PSC. Other conventional techniques designed to achieve MPP, including fuzzy and neural network approaches, add to the complexity of the tracking and may still fail under non-uniform conditions. Attempts to improve conventional tracking performance for GMPPT often increases technique complexity and cannot always guarantee GMPPT.

PE based approaches are shown to increase the energy yield under PSC but the cost involved in such systems may outweigh the benefit.

While some techniques are specifically designed to reliably track to the GMPP, these methods often increase the cost and complexity of the system and frequently rely on system dependent parameters which makes it difficult to adapt the technique to use in other systems.

4.8 Conclusion

This chapter has demonstrated that many approaches have been proposed to provide superior operation of PV systems experiencing PSC. In general, conventional MPPT techniques cannot achieve GMPPT without significant modification and techniques designed specifically for this purpose may not always guarantee GMPPT and may involve additional system dependent constants or circuit elements. While an abundance of maximum power extraction strategies have been proposed for PV systems, no single technique can meet all required objectives of a universal global maximum power extraction process.

In anticipation of real environmental conditions it is essential that a GMPPT technique is able to quickly track to the GMPP with minimal implementation complexity. The technique proposed in Chapter 5 is able to perform satisfactorily against the criteria defined in this chapter and is an attempt at creating a universal global maximum power extraction process.

Chapter 5

Proposed Global Maximum Power Point Tracking Technique Based on Simulated Annealing

5.1 Introduction

As presented in Chapter 4, the existing MPPT methods have limitations when tracking the maximum power of a PV system under non-uniform environmental conditions. In particular, conventional methods will often track to a local maxima due to the inherent structure of the technique such as P&O and Hill Climbing (HC) approaches. Techniques designed specifically to achieve GMPPT often increase the cost and complexity of the implementation through the use of additional circuitry and complex algorithms that must be implemented on higher cost processors. Many GMPPT strategies involve optimising the performance for specific conditions such that the method may be unable to track the GMPP under all possible environmental conditions that arise, or may rely on system dependent constants leading to a technique that cannot be easily applied to another PV system without considerable optimisation. PV systems are operated in environments where non-uniform environmental conditions, or *real* environmental conditions become more significant than the uniform operating conditions explored in an indoor laboratory environment. This is due to shadow from objects in the environment, dust or dirt on the module surface, module mismatch due to manufacturing tolerances, module ageing and damage with time, and the rapid changes in irradiance caused by the passage of clouds over the system. As PV systems operate in these real conditions, it is essential that an implemented GMPPT strategy can perform well under these conditions and accurately and reliably track the GMPP. Additionally, it is important that this GMPPT can be achieved without exorbitant costs and complexity to help

minimise the cost of energy associated with PV systems.

This chapter describes the proposed Simulated Annealing (SA) MPPT method. The proposed technique attempts to overcome some of the key limitations of existing MPPT techniques, as described in Chapter 4, for Partial Shading Conditions (PSC). In particular, it has low complexity, can easily be implemented on a low-cost microcontroller and reliably tracks to the GMPP. The performance of the proposed SA method is compared with the common P&O MPPT method and the Particle Swarm Optimisation (PSO) strategy for GMPPT in simulations in this chapter. To verify the effectiveness of the proposed SA method for practical application, an experimental implementation has also been completed.

The modelling and experimental implementation presented in this chapter shows that the SA algorithm, without a considerable amount of optimisation, can effectively converge to the neighbourhood of the GMPP within a small time frame. The technique could then be combined with a local search technique such as P&O when in the vicinity of the GMPP to track it exactly. Alternatively, once SA has located the approximate MPP, the neighbourhood size could be reduced considerably to enable the method to track exactly to the GMPP. Due to the nature of the system considered, in which the passage of clouds does not lead to each module experiencing a different level of irradiance, the main factor influencing the irradiance on each module and the PSC is the shading factor of the module which is based on the number of shaded cells within the module. The shading of the individual cells is a much slower phenomenon than the transitions in irradiance caused by the clouds, so the relative locations of the MPPs should have little variance from each sample time to the next, as has been extensively explored in Chapter 3.

The main features of the proposed SA method are summarised below with respect to the criteria established in Chapter 4:

- SA can reliably locate the neighbourhood of a global maxima.
- The SA implementation has low complexity.
- The method requires no additional circuitry and can be implemented in a low cost microcontroller.

- When optimised, the SA method can achieve GMPPT in a similar time frame or faster than the PSO method, yet with a considerably simpler implementation.
- Tracking with the SA method exhibits no oscillations in steady-state, although may exhibit some apparent oscillations during the searching process due to sampling different voltages.

The key advantages that the SA algorithm has when compared with other methods is that it can achieve reliable GMPPT with a limited increase in complexity beyond the common P&O method. Where the P&O method may become trapped in a local maxima, the SA method incorporates searching capabilities that allow it to escape from a local maxima. Additionally, once the algorithm has converged it remains at a constant operating voltage such that no oscillations are observed in the steady state. Unlike the PSO method, which is frequently implemented in PV systems that experience PSC, the SA method requires fewer parameters to be stored between each iteration. Other methods proposed for GMPPT often require costly processors, additional circuitry, or require knowledge of the PV system parameters or the environmental conditions as has been described in Chapter 4. The SA method is not constrained by these limitations as it can be implemented in a low cost processor, only requires circuitry to read the voltage and current and write the duty cycle (equivalent to what would be required with the P&O method), and can operate successfully without knowledge of the PV system parameters or environmental conditions.

In this chapter, the SA algorithm is firstly described and the key reasons for its good performance in global optimisation are highlighted. The SA and PSO implementations considered for GMPPT in this thesis are then described independently. Simulation results are presented to demonstrate the performance of the SA method on firstly a simple two module system and secondly, the eight module PSC system introduced in Chapter 3. Finally, experimental results are presented showing the performance of the method on the two module experimental setup from Chapter 2.

5.2 The Simulated Annealing Algorithm for Global Optimisation

The SA optimisation technique is based on the physical processes involved in the annealing of metals. In metallurgy, metals are heated up to a high temperature to make them molten and then are cooled in a controlled manner to minimise the energy of the system [232]. During the cooling process, the atoms will start to align to achieve the minimum energy state. However, if the metal is cooled too quickly or 'quenched', then the atoms will not have aligned to achieve the minimum energy state. Depending on the cooling rate, either large or small crystals will be formed.

SA was originally proposed as a global optimisation methodology by Kirkpatrick et. al. [233] and Cerny [234] independently in 1983 and 1985, respectively. Originally, the technique was proposed to perform the travelling salesman problem, and to optimise partitioning, component placement and wiring for electronic circuits [233]. Since the 1980's the technique has found a multitude of applications in very diverse areas including solving the unit commitment problem [235], blind deconvolution [236], image recovery [237] and economic dispatch [238]. Additionally, the technique has been applied in several renewable energy optimisation cases [239–248]. The sizing of components in a Small Autonomous Power System is optimised by a SA algorithm combined with Tabu Search in [239]. The optimum installation angle for fixed-angle PV systems is evaluated using SA in [240]. Optimal expansion of the distribution system is considered in [241], while optimal distributed generation placement and sizing is considered in [242, 243], and energy storage placement in [244]. In [245], the optimal controller parameters for a wind turbine are found using SA. The performance of a genetic algorithm has been enhanced by applying SA to the best individual of each population in the optimisation of an energy generation island based on renewable energy sources [246]. The energy management system in an Electric Vehicle is optimised using the SA algorithm in [248].

In the SA optimisation technique, an initial temperature and cooling schedule control the searching process as the minimum energy state of the system is pursued. At each sample time, a random perturbation in the solution is applied and the corresponding solution energy measured. This energy is then compared with

the current reference energy of the current reference solution and the candidate solution is either accepted or rejected. If the candidate solution has a lower energy than the current reference solution then it will be accepted automatically and the algorithm progresses to the next step. If the candidate solution has a higher energy than the current reference solution, it may still be accepted based on some acceptance probability. This acceptance probability relates the difference in energy between the candidate and current reference solution and the current temperature to decide if the candidate solution should become the reference solution. Initially, the technique starts with a high temperature and is more likely to accept solutions which increase the overall energy of the system slightly. As the cooling schedule progresses and the temperature reduces, the probability that a solution with larger energy will be accepted is also reduced. The probability of accepting a solution with greater energy is given by [234, 249]

$$Pr = \exp\left[-\frac{E(k) - E(k-1)}{T(k)}\right] \tag{5.1}$$

where, $E(k)$ is the energy of the candidate solution, $E(k-1)$ is the energy of the current reference solution and $T(k)$ is the temperature.

The acceptance probability is based on the Boltzmann distribution where at a high temperature all the states have an equal probability. As the temperature reduces, the lowest energy state has non-zero probability. At lower temperatures more time is expended improving the performance of the system in reaching equilibrium [250].

The probability of accepting a worse solution not only depends on the temperature, but also on the difference in energy between the candidate and reference solutions [251]. The higher energy solutions which are accepted by the algorithm at high temperatures generally only result in a small increase in the energy rather than a significant increase [252]. This means that small reductions in solution quality are more likely to be accepted than large reductions [251].

The temperature in the algorithm is reduced by using a cooling schedule. Cooling schedules can be static or adaptive depending on the application [251]. If a constant temperature is used in the algorithm, it becomes the Metropolis algorithm [253], originally proposed by Metropolis et. al. [254] in 1953. Selecting a

suitable cooling schedule is of great importance in ensuring the successful convergence of the algorithm. The geometric cooling schedule is a commonly implemented cooling schedule, which reduces the temperature based on some constant, $\alpha_2 < 1$. The geometric law is given in (5.2), where $T(k)$ is the new temperature and $T(k-1)$ is the previous temperature. While a variety of different ranges for α_2 are suggested in the literature [240,242], typically the constant α_2 takes a value between 0.8 to 0.99 [233, 236–238, 246, 255–257]. An analytical tuning schedule in [258] is defined to determine the initial and final temperatures required on the basis of the maximum and minimum deterioration of the objective function.

$$T(k) = \alpha_2 T(k-1) \tag{5.2}$$

While the geometric cooling schedule is frequently used, a variety of other cooling schedules are also available. These include the logarithmic cooling schedule given in (5.3) which can be shown to enable optimal annealing as long as the constant c is appropriately chosen [259]. The value d^* indicates the maximum depth of all states which are local but not global minima [260].

$$T(k) = \frac{c}{log(k+1)}, c >= d^* \tag{5.3}$$

Other cooling schedules include the linear cooling schedule given by (5.4) [249], and Lundy cooling schedule (5.5) [261].

$$T(k) = T(0) - c_l k \tag{5.4}$$

$$T(k) = \frac{T(k-1)}{1 + \beta_l T(k-1)} \tag{5.5}$$

Another important consideration in the optimisation of the SA algorithm is the stopping criterion. Generally, the algorithm will be stopped once the temperature reaches a pre-defined level, or after a pre-defined number of steps have been completed. Other stopping criteria include stopping when the algorithm has not improved the solution after a certain number of temperature steps [253]. This last criterion can limit the execution time required by the algorithm to converge to the neighbourhood of the global minimum.

Some key advantages of the SA algorithm for global optimisation are described in [235]. These include the independence of the final solution from the initial

solution selected, that the process does not require any knowledge of the system model and that it has been theoretically proven to converge to the global minimum with an appropriately selected cooling schedule [253, 262]. Even if the SA algorithm does not converge directly to the global minimum, it is still very efficient at converging to the neighbourhood of the global minimum [253]. The main limitation of the technique is the trade-off in selecting an appropriate cooling schedule. If the temperature is reduced too quickly, the method may converge to a local minimum, and a slow decrease in temperature may result in the algorithm taking a long time to converge.

Searching within a large neighbourhood can result in a long search time being required [262], yet conversely if the neighbourhood selected is not diverse enough, it may not be possible to locate the global minima [235]. To improve the performance in a large solution space the neighbourhood can also be reduced as the temperature cools, improving the likelihood that the solution will converge to the global maxima [232].

Traditionally, when annealing metals, an equilibrium state is required at each step before the temperature is reduced. For SA this is often not practical as it would lead to the process taking a long time to converge [251]. Most implementations of SA, including those considered in this chapter, are inhomogeneous implementations, as equilibrium is not required before the next temperature step is applied.

SA can be proven to converge to a global minima (or maxima) with a probability of 1 [263]. However, in converging exactly to the global point of interest a substantial amount of time may be required. The analysis of the convergence is done by modelling the process as a sequence of homogeneous Markov chains for each temperature [264, 265]. The transitions in the Markov chain are defined by an accept function and a generate configuration function [265] depending on if the algorithm needs to stay in the current state or generate a new state.

Research has shown that with an appropriately designed cooling function the technique can improve the performance in converging quickly to the optimum point [249, 250, 266, 267].

The first instance of the SA algorithm being applied to PV module MPPT can be found in [247]. The results in [247] are limited to simple uniform environmental conditions and little optimisation of the key parameters of the technique are provided. This chapter fully develops a MPPT algorithm based on the SA optimisation technique which is designed specifically to operate well under both uniform and non-uniform environmental conditions.

The technique is considered in the context of a residential scale PV system and is designed primarily to provide effective GMPPT for slow moving shadow characteristics which arise due to objects in the environment. This slow moving shadow characteristic could also be due to dust or dirt on the surface of the modules.

5.3 Proposed Simulated Annealing Algorithm for GMPPT

The SA optimisation process described in Section 5.2 is designed to locate the global minima of a complex objective function. With a few small modifications the technique can enable the searching of the global maxima. The cost function or energy in the system is represented by the power produced by the PV system and the candidate and reference solutions become the candidate voltage and reference voltage. As the global maxima is sought by the algorithm, cases where a candidate voltage results in a candidate power which is larger than the reference power, this candidate voltage becomes the new reference voltage. When the candidate voltage produces a power less than the reference power the candidate voltage will be accepted based on the acceptance probability given in (5.6), which is similar to the probability given in (5.1).

$$Pr = \exp\left[\frac{P(k) - P(i)}{(k)T}\right] \tag{5.6}$$

where, $P(k)$ is the power at the candidate voltage, $P(i)$ is the power at the reference voltage, and $T(k)$ is the temperature of the system.

The algorithm implemented is inhomogeneous SA, as equilibrium is not required at each temperature level [251]. Rather, approximately four iterations of the search are applied for each temperature in the implementations of the algorithm considered in this chapter.

The proposed SA algorithm for GMPPT performs the following steps:

- Set the initial parameters including the initial temperature (T), parameters of the cooling schedule (α_2), neighbourhood size and final temperature/stopping criterion.
- Select a random voltage $V(i)$ within the neighbourhood.
- Measure the PV current $I(i)$.
- Calculate the power $P(i) = V(i) \times I(i)$.
- While the temperature is greater than the stopping criterion, repeat the following:
  - Select a random voltage $V(k)$ within the neighbourhood.
  - Measure the current $I(k)$.
  - Calculate the power $P(k) = V(k) \times I(k)$.
  - If the power $P(k)$ is greater than the reference power $P(i)$, then voltage $V(k)$ becomes the new reference voltage (i.e. $V(i) = V(k)$).
  - Otherwise, if the power $P(k)$ is less than the reference power $P(i)$, accept the value based on the acceptance probability given in (5.6).
  - If the predefined number of sample points have been considered at this temperature, reduce the temperature by one step using the cooling schedule.

The flowchart of the SA GMPPT algorithm is shown in Fig. 5.1.

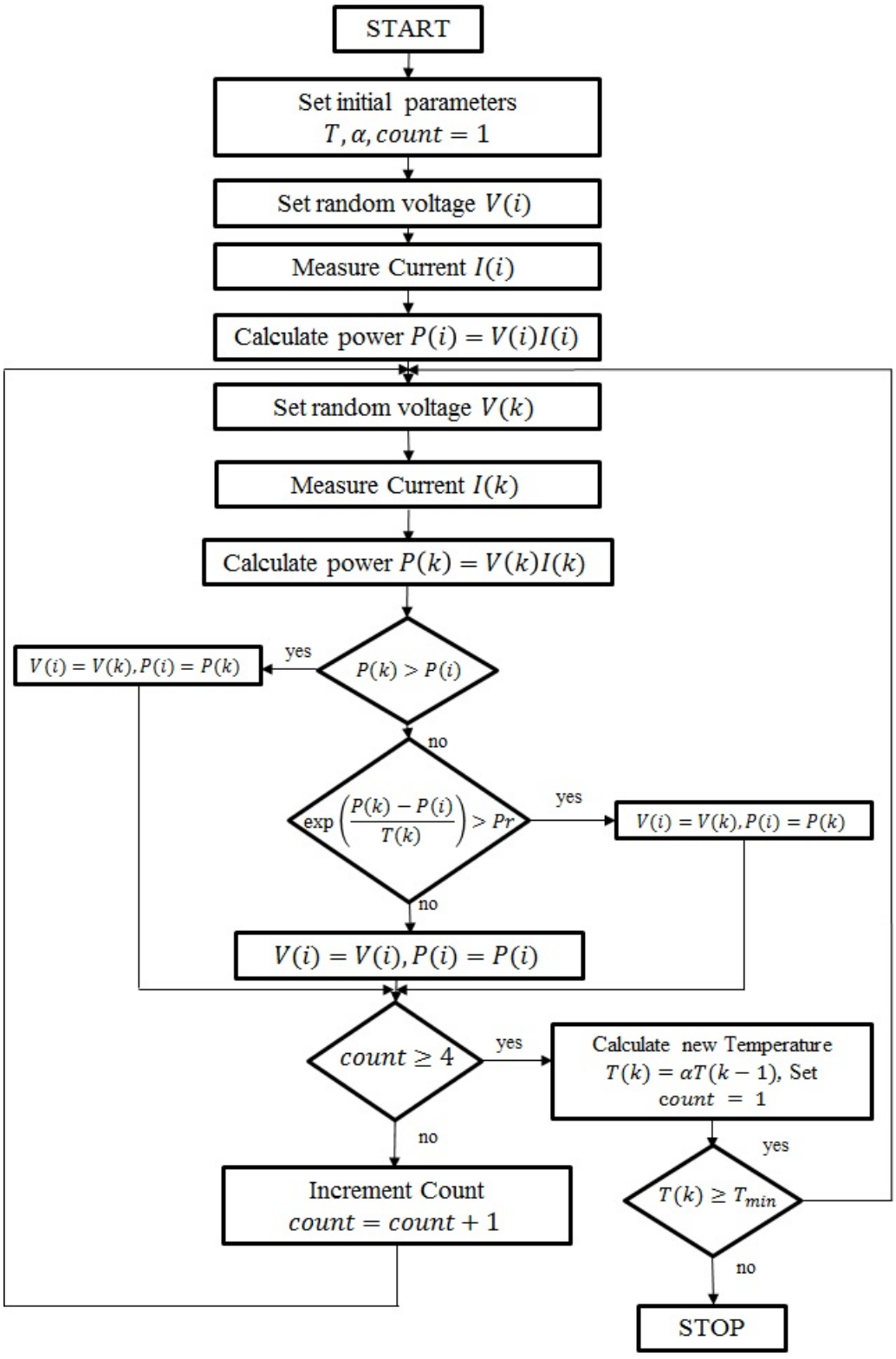

Figure 5.1: Flowchart of the proposed SA GMPPT technique.

5.4 Implementation of Particle Swarm Optimisation Technique for Comparison

The PSO technique implemented in this chapter is considered as a comparison technique for GMPPT. As described in Chapter 4, the PSO method uses a group of particles to collectively solve a problem. The position of each particle is updated based on its own best position and the best global position of all particles. This enables the particles to all converge towards the global solution. The particle position at the next step is given in (5.7).

$$x_i^{k+1} = x_i^k + \Phi_i^{k+1} \tag{5.7}$$

Where, x_i^k is the previous particle position, x_i^{k+1} is the new particle position, and Φ_i^{k+1} is the particle's new velocity.

The particle's velocity is calculated based on the particle's previous velocity, the differences between the particle's current position and its best position, and the difference between the global best position and the particle's current position. The particle velocity is calculated using (5.8).

$$\Phi_i^{k+1} = \omega_i \Phi_i^k + c_1 r_1 (P_{best,i} - x_i^k) + c_2 r_2 (G_{best} - x_i^k) \tag{5.8}$$

Where, ω_i is the inertia weight, c_1, c_2 are the acceleration coefficients, $r_1, r_2 \in U(0,1)$ are random numbers, $P_{best,i}$ is the best position of particle i, and G_{best} is the best position of all particles in the population.

The PSO method is implemented with the following parameters, $\omega_i = 0.4$, $c_1 = 1.2$, $c_2 = 1.6$ obtained from [151]. The method cycles through the particles and the current particle's voltage is applied every 0.05 seconds. In the eight module simulation, described in this chapter, the particles are kept within the range of 15 to 150 V. The flowchart of the PSO method implemented in this chapter is shown in Fig. 5.2.

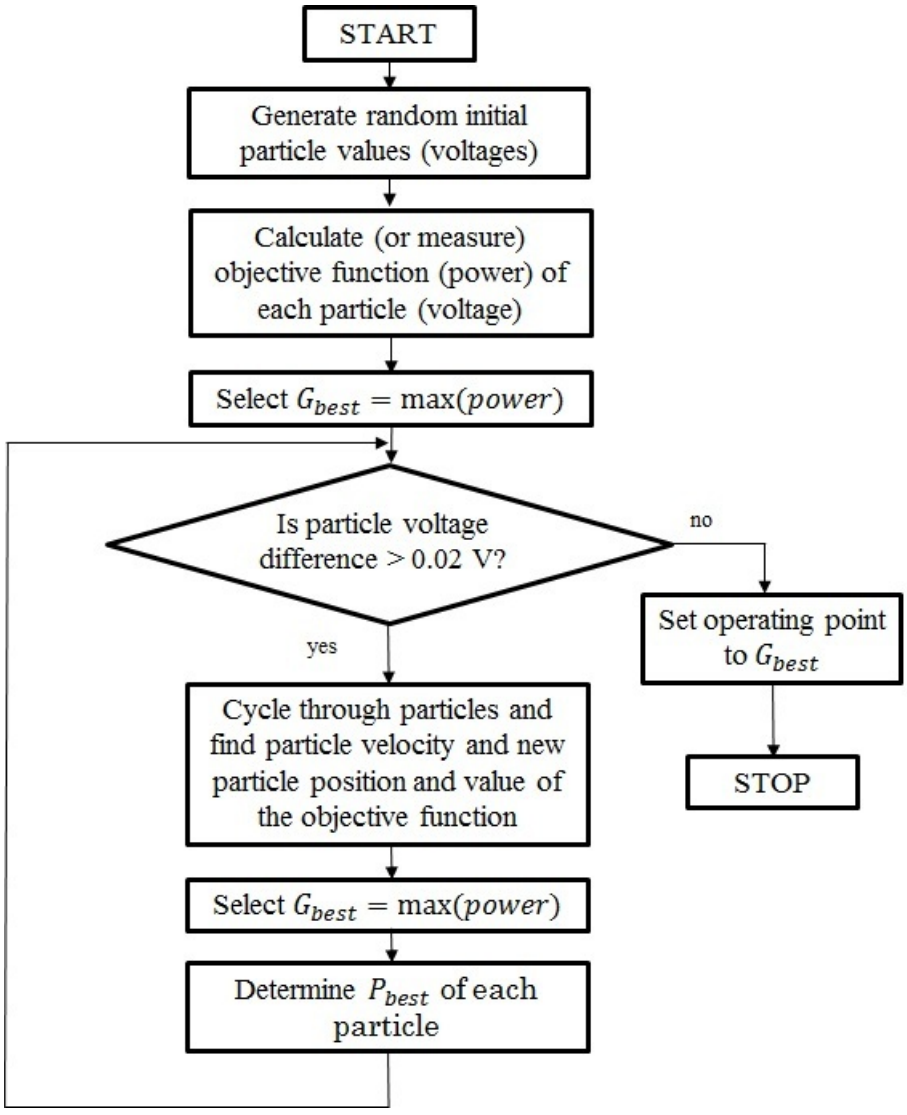

Figure 5.2: Flowchart of the PSO method for GMPPT.

5.5 Implementation of the Proposed Simulated Annealing GMPPT Technique

5.5.1 Simulation of PV system with two module

The P&O, IncCond and SA based MPPT methods are applied on the two module system demonstrated in Chapter 2 for the assessment of the modelling performance. In assessing the MPPT performance, 55 test cases are considered. In these test cases, the irradiance is varied from 100 to 1000 W/m^2 in steps of 100 W/m^2 while the temperature of the modules remains constant at 25°C.

The P&O technique has already been discussed extensively in Chapter 4. The implementation considered in this study is the simplest form of the P&O method where the technique cannot separate whether a change in power is due to a change in the environmental conditions or due to the perturbation and is restricted to a fixed step size. Additionally, for suitable comparison, the method is not enhanced to distinguish between the global and local maxima as part of this study is to show that you can achieve GMPPT with a technique not significantly more complex than the P&O methodology. A 1 V step size is used with a 0.1 second perturbation time.

For comparison the IncCond technique is also implemented with a 1 V step size and 0.1 second perturbation time. The IncCond is also a low cost, simple MPPT method that is frequently utilised in commercial applications.

The geometric cooling schedule is used in this implementation with an initial temperature of 25°C, final temperature 0.2°C, and a temperature update constant of 0.7. This temperature update constant is quicker than the range suggested earlier in this chapter, but shows that satisfactory performance can still be achieved. Temperature update was applied every 0.43 seconds which is approximately every four samples. This means that the algorithm will apply 56 samples in searching for the GMPP. The voltage was perturbed every 0.1 seconds within the range of 13 to 40 V. This range was selected based on the analysis completed in Chapter 3.

The simulation model for the SA implementation is shown in Figs. 5.3 to 5.6.

For each technique and simulation condition, the power deviation from the known GMPP in steady-state, cumulative energy losses in the search, time to MPP and whether the technique located the GMPP were recorded. The average, minimum and maximum for each performance measure for each technique are outlined for the 55 test cases.

Table 5.1 indicates the power deviation in steady-state between the known GMPP power and the measured steady-state power. The percentage value given is the power deviation as a percentage of the target GMPP power. Note that due to the nature of the P&O and IncCond techniques to oscillate around the MPP, the power deviation recorded in these cases is the maximum deviation from the MPP whilst oscillating. Table 5.2 shows the cumulative energy losses and Table 5.3 indicates the time taken for the algorithm to reach the MPP (either local or global depending on which the algorithm successfully locates).

The results show that 100% of the time the SA algorithm converged to the GMPP for this simple two module implementation. For the the P&O and IncCond methods, the convergence to the GMPP was for 55% of the test cases.

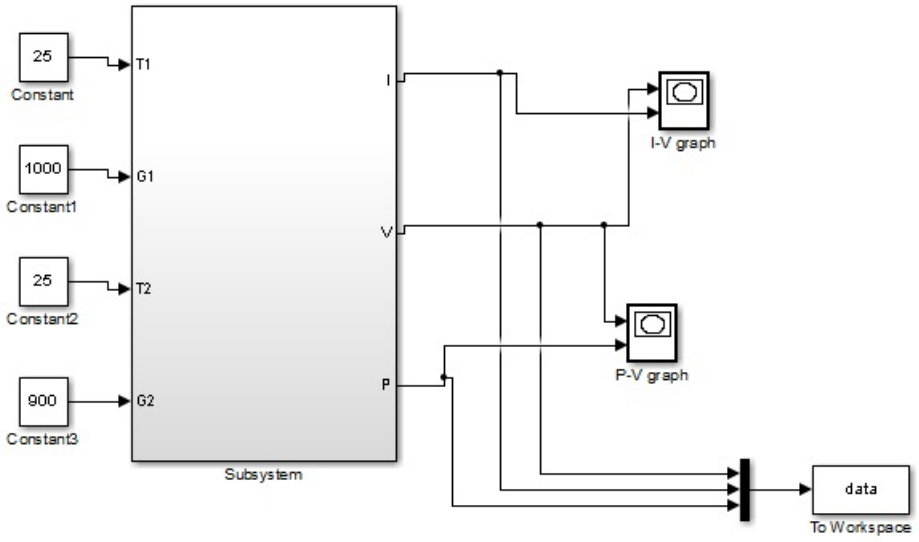

Figure 5.3: Overall two module simulation model.

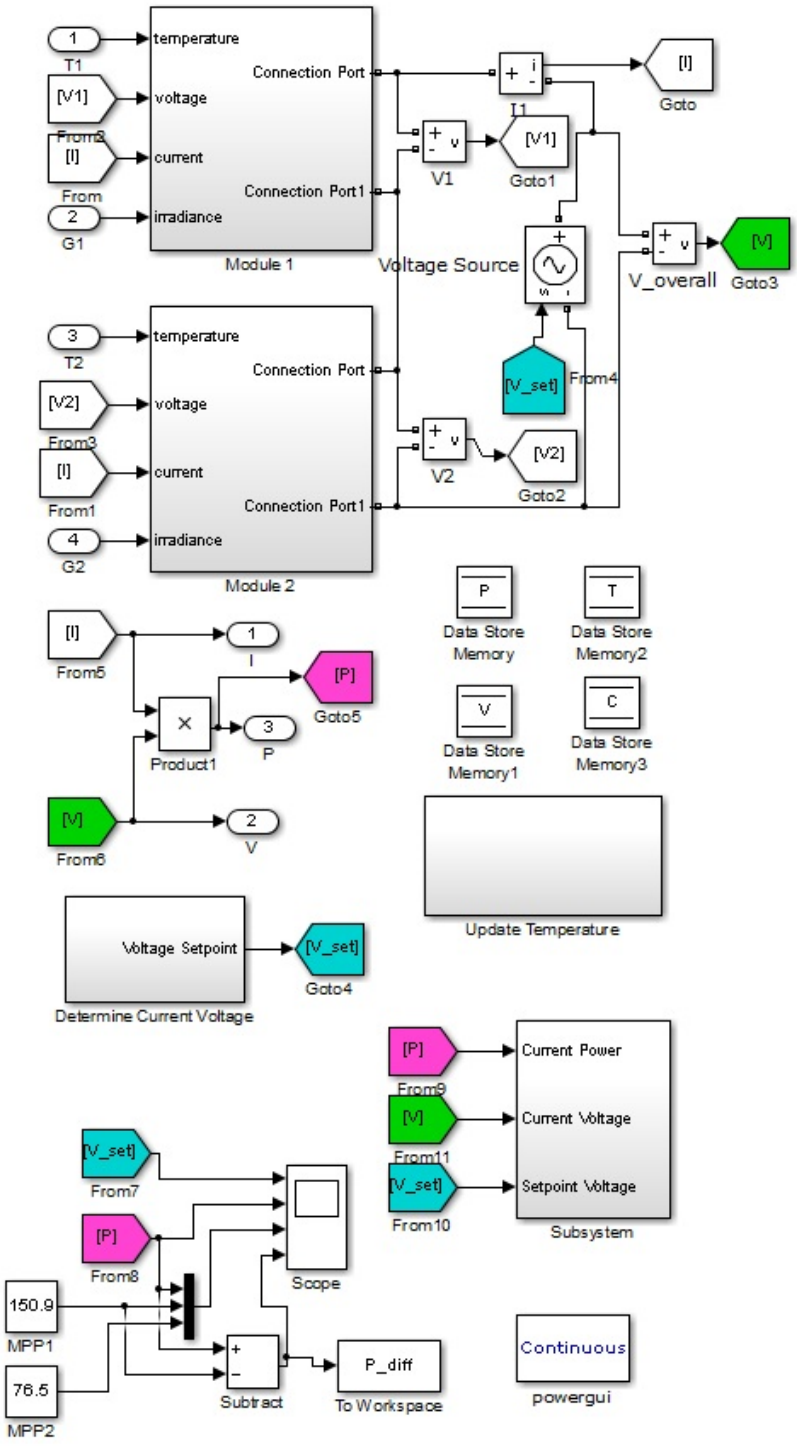

Figure 5.4: Internal model of Fig. 5.3 showing each PV module and temperature update.

Due to the step size used, there was one case where the two modules experienced a similar level of irradiance and both techniques were able to 'step' over the local MPP as it exhibited only a small deviation from the otherwise uniform characteristic. If a smaller step size was used, it is likely that the method would

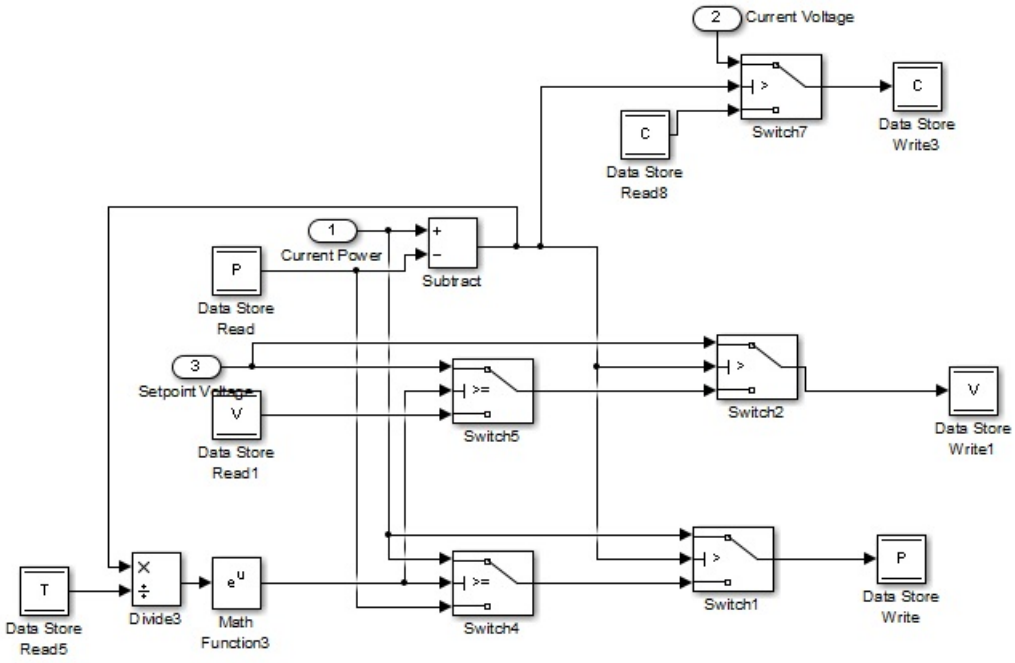

Figure 5.5: SA algorithm.

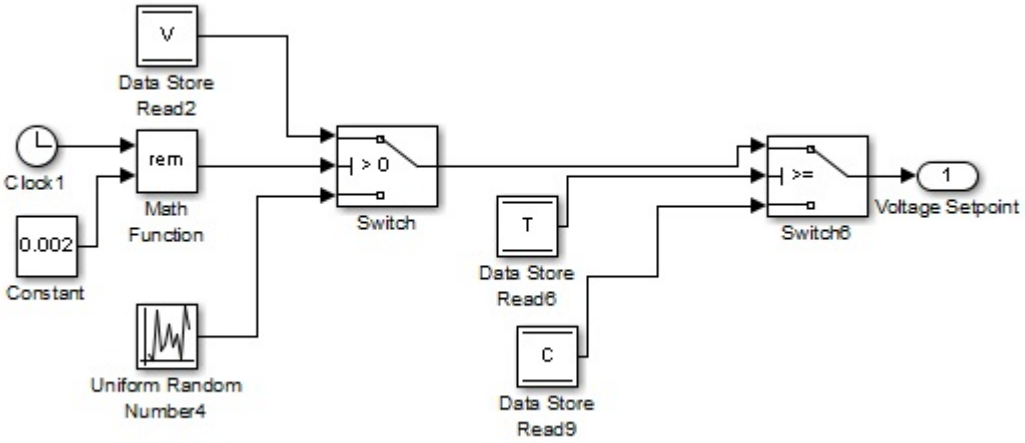

Figure 5.6: Determining the current operating point.

Table 5.1: Power deviation in steady state.

	SA		**P&O**		**IncCond**	
	Error (W)	**%**	**Error (W)**	**%**	**Error (W)**	**%**
Average	-0.385	-0.68	-12.58	-13.74	-12.14	-13.86
Minimum	-0.0001	-0.00	-0.0179	-0.03	-1.2256	-0.10
Maximum	-0.937	-2.07	-64.63	-48.30	-64.38	-48.12

have been trapped in the local MPP. The case demonstrating this is when module one experiences an irradiance of 1000 W/m^2 and module two experiences 900 W/m^2 as shown in Fig. 5.7.

Table 5.2: Cumulative energy loss.

	SA (J)	**P&O (J)**	**IncCond (J)**
Average	-44.05	-149.60	-147.22
Minimum	-14.39	-21.75	-19.68
Maximum	-80.33	-448.58	-447.79

Table 5.3: Time to MPP.

	SA (s)	**P&O (s)**	**IncCond (s)**
Average	3.18	2.08	2.08
Minimum	1.3	1.7	1.7
Maximum	5	3.6	3.6

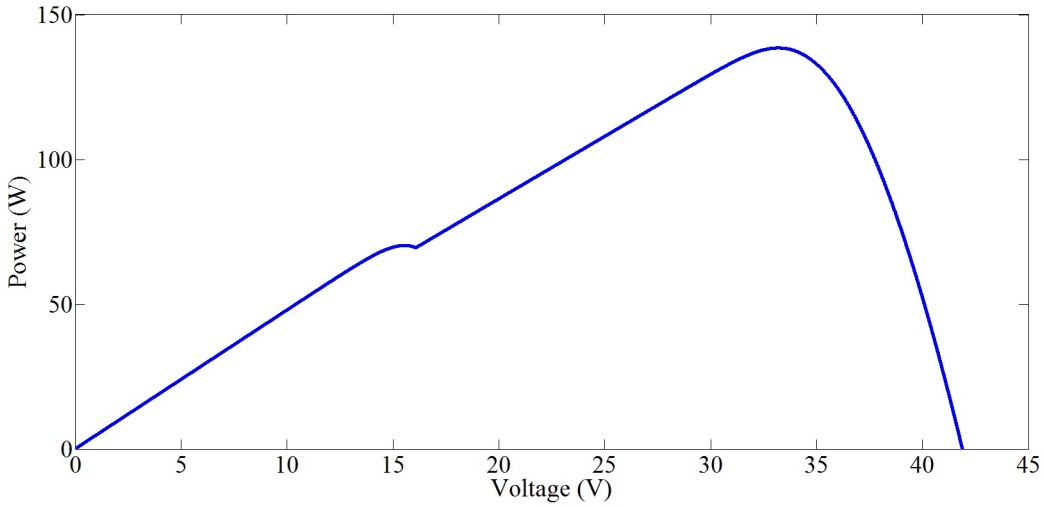

Figure 5.7: P-V characteristics for module one irradiance $1000W/m^2$ and module two irradiance $900W/m^2$.

The results indicate that the SA algorithm outperforms the P&O algorithm with respect to reliably converging to the GMPP, and having a lower power deviation in steady-state and lower cumulative energy losses. While the P&O and IncCond methods with a 1V step size on average converged quicker than the SA algorithm, they frequently converged to the local MPP resulting in considerable energy losses (45% of the test cases).

The performance of the technique on these measures for the two module case indicates that the SA algorithm is capable of converging reliably to the GMPP and that it outperforms the P&O and IncCond methods, particularly under PSC. Figures 5.8, 5.9 and 5.10 demonstrate some sample cases of tracking the MPP us-

ing the P&O, IncCond and SA algorithm, respectively. The solid line represents the power-voltage characteristics, the stars indicate the sample points used by the algorithm and the large circle indicates the final power achieved by the algorithm.

These preliminary results show that the SA method is capable of reliably locating the GMPP on very simple small PV systems. Realistically, PV systems in outdoor environments are composed of more modules in more elaborate configurations that experience much more complex environmental conditions than those considered for the two module system. The purpose of including these two module system simulation results in this thesis is due to the need to validate the algorithm performance experimentally on the available two-module system introduced in Chapter 2. In the next section of this chapter, the SA method is applied to the eight module PV system introduced in Chapter 3 to show its performance under more authentic environmental conditions.

5.5.2 Simulation of PV system with eight series-connected modules

To assess the performance of the proposed method under more complex environmental conditions, the technique is applied to the eight series-connected modules simulation model introduced in Chapter 3 with the same obstacle placement and real one minute irradiance data. The P&O and PSO approaches as described in Chapter 4 and earlier in this chapter are also applied on this model for the same environmental conditions to enable the performance of the method against other common implementations to be assessed.

Two different irradiance data sets are considered in the analysis of the performance of the three techniques. The first data set represents a typical autumn day in Tasmania where the irradiance is highly variable. 58 test cases (from 58 minutes of irradiance data where the modules experience shading due to the obstacle) are considered. These test cases are from 1 April 2010 starting at 1:36 pm AEST. The irradiance from this sample time is shown in Fig. 5.11. This data set will be referred to as the variable irradiance data set. The second data set considered represents a standard Spring day in Tasmania where the irradiance

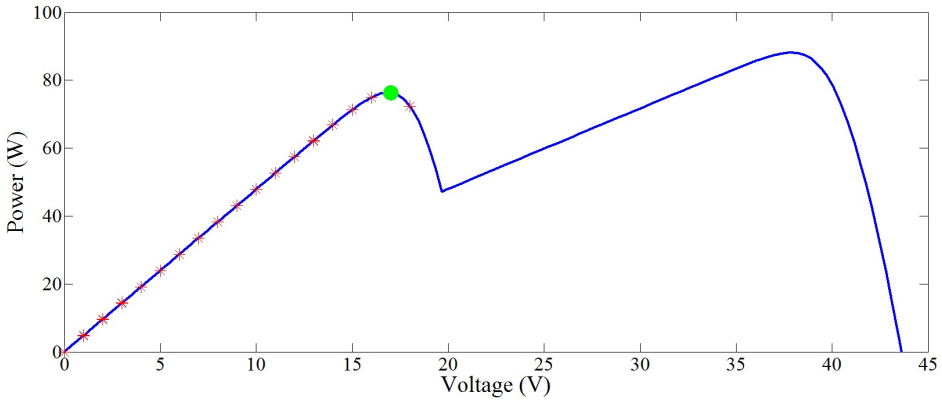

Figure 5.8: Results of MPPT applied to two module system experiencing irradiance of 1000 W/m^2 and 500 W/m^2 on each module using the P&O algorithm.

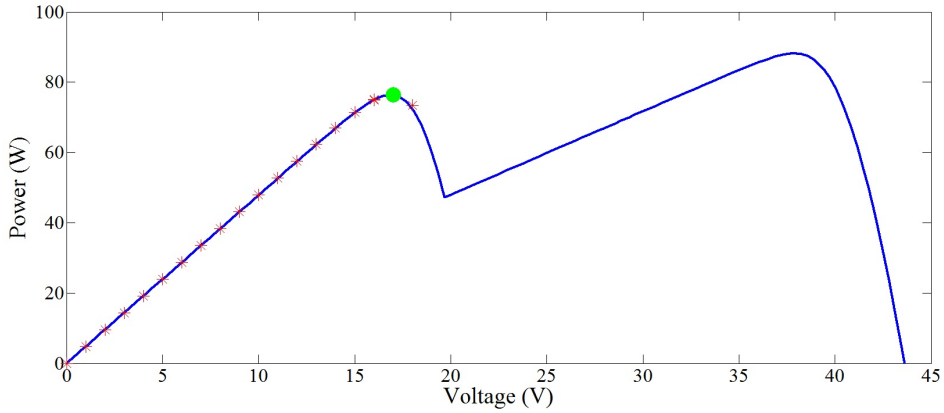

Figure 5.9: Results of MPPT applied to two module system experiencing irradiance of 1000 W/m^2 and 500 W/m^2 on each module using the IncCond algorithm.

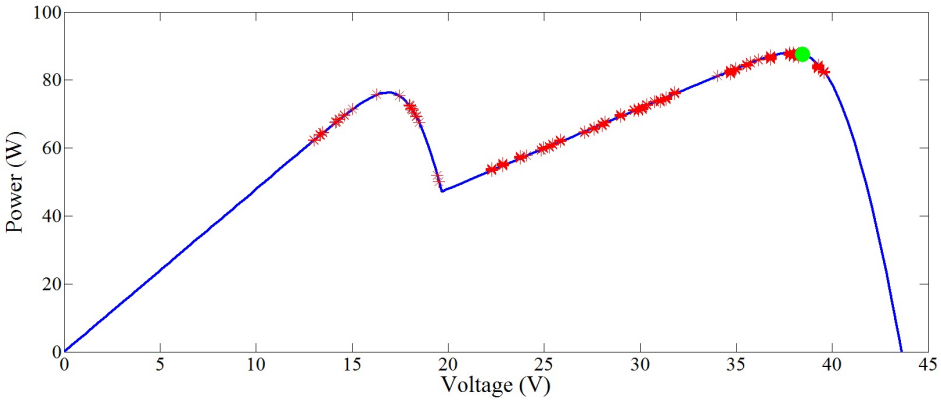

Figure 5.10: Results of MPPT applied to two module system experiencing irradiance of 1000 W/m^2 and 500 W/m^2 on each module using the SA algorithm.

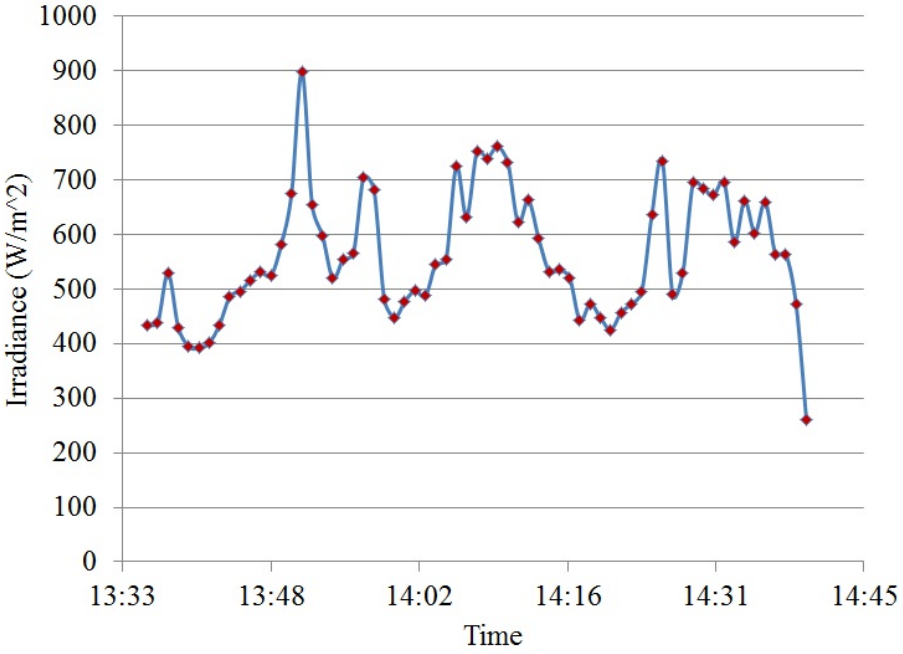

Figure 5.11: Variable day irradiance profile.

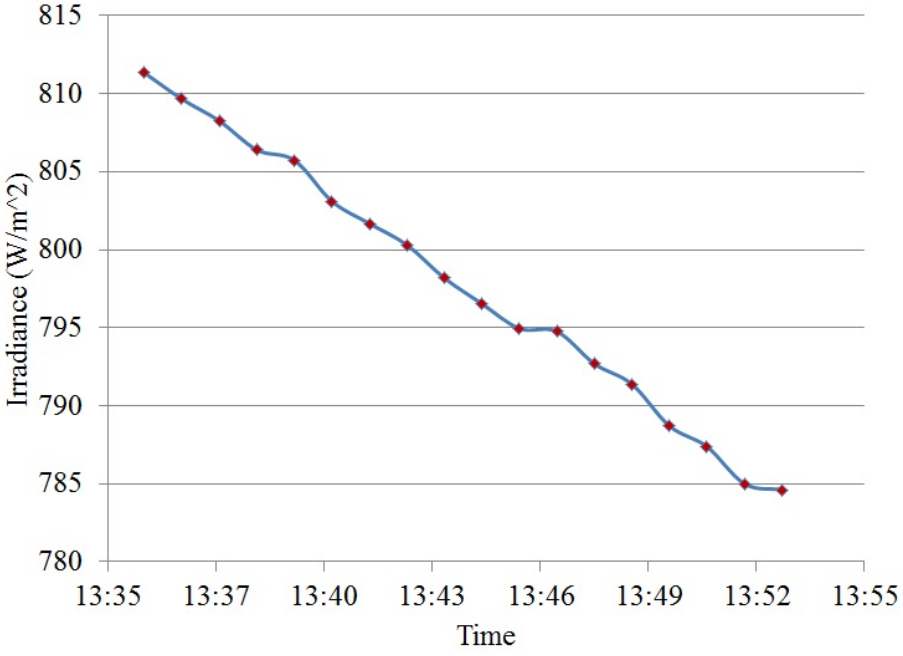

Figure 5.12: Clear day irradiance profile.

varies very slowly. Due to the placement of the obstacle, there are 18 test cases (from the 18 minutes where the modules are shaded). These test cases are from 11 October 2010, starting at 1:36 pm AEST. The irradiance for this Spring day is shown in Fig. 5.12. This will be referred to as the clear irradiance data set.

For the variable and clear irradiance days tested, each algorithm is first performed from a initial starting condition for each test case in the set. This assesses the

capability of each method to converge to the GMPP on startup and shows the performance in converging under different conditions. The performance of each technique is recorded in terms of the time it takes the algorithm to track to near the MPP and the number of cases in which the algorithm converges to within 1% to 5% of the GMPP location in terms of power and voltage. The cases where it converges to a MPP with similar power to the GMPP and the number of cases where it does not converge are also recorded.

For the practical application of the technique to achieve GMPPT in PV systems under PSC, an initialisation condition to detect when PSC has occurred and trigger the global searching process would be necessary, similar to the approaches suggested in [175,201]. In the second implementation of each technique presented in this chapter, a reset condition is applied to allow continuous tracking. For the P&O method, this just means continually tracking rather than resetting to an initial voltage when a change in conditions occurs. As the PSO and SA based methods rely on time-invariant techniques, a special reset condition needs to be established to assess when a change in environmental conditions has occurred and reinitialise a global search. The authors of [201] propose a reintialisation condition based on assessing if the power at the operating point has experienced a change greater than a certain threshold to suggest a new global search should be performed. This condition is given in (5.9), where $P_{pv,new}$ is the new PV power measured at the steady-state operating voltage, $P_{pv,last}$ is the PV power at the operating point when it first becomes the steady-state operating point, and ΔP is some threshold.

$$\frac{|P_{pv,new} - P_{pv,last}|}{P_{pv,last}} >= \Delta P \tag{5.9}$$

An alternative approach involves monitoring the conductance or resistance at the MPP to recommend when a change in environmental conditions has occurred under the uniform environmental conditions case [175]. Extending this idea to the GMPPT of a PV system, by monitoring the resistance or conductance, a substantial change which would indicate potentially moving away from the GMPP would result in the method performing the GMPPT routine again.

In this implementation the PSO and SA approaches are assessed based on the number of times that the reinitalisation condition detects that a change in the

environmental conditions has occurred compared with the known number of times that the environmental conditions change.

The P&O method is implemented with a step size of 0.75 V, and an initial voltage of 10V. A perturbation is applied every 0.05 seconds.

The SA algorithm is applied with an initial temperature of 25°C, final temperature 0.2°C, and temperature update constant of 0.8. Temperature update occurred every 0.4 seconds. These parameters were fairly arbitrarily selected based on observations of the performance with various parameter values and show that satisfactory performance can be achieved with limited optimisation. The voltage was perturbed in the range of 14 to 144 V. The sampling time used was 0.2 seconds. During this sampling time, at t=0 seconds, the algorithm is applied, at t=0.05 seconds the algorithm compares the current operating point with the previous best operating point, and then returns to the best operating point (previous or newly accepted) for the remainder of the sample time.

5.5.2.1 Performance from initial starting condition

The performance of tracking from an initial condition to the MPP for each technique for the variable and clear days are assessed in this section. Figures 5.13 and 5.14 demonstrate the voltage and power tracking with time of the P&O, PSO, and SA methods respectively for one sample case. Clearly, in this case it can be seen that while the P&O and PSO techniques do converge to within 5% of the GMPP power, there is a voltage difference of about 17 V in the final operating point indicating that the technique has converged to a local MPP with similar power to the GMPP. It is noted that there appear to be oscillations in the PSO and SA methods during the searching process, this is due to the methods sampling different voltages the search towards the GMPP. The strategies presented in Chapter 7, provide recommendations on how to reduce the number of samples required by the SA method while still retaining a high GMPP convergence probability.

Several measures for the performance of each technique are considered. First, the time taken by the algorithm to converge is given for the variable irradiance day profile in Table 5.4 and for the clear irradiance day profile in Table 5.5. For the

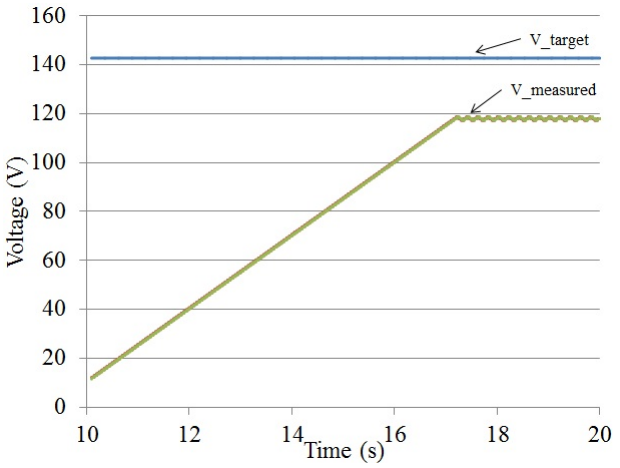

(a) P&O.

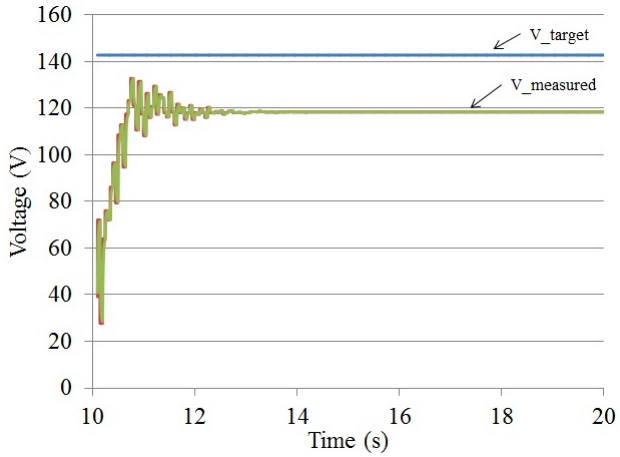

(b) PSO.

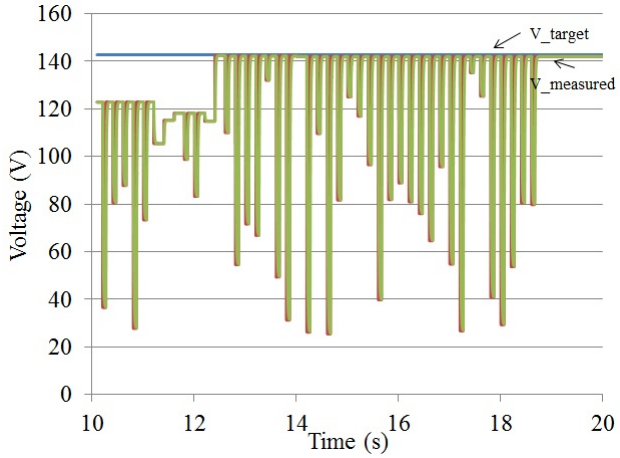

(c) SA.

Figure 5.13: Voltage tracking (a) P&O, (b) PSO, (c) SA.

SA algorithm, this time to converge refers to the time taken for the algorithm to track to near the final operating point without accepting any future operating points which are at a considerably lower power and far from the final operating point. For the P&O method, the convergence time is the time taken to arrive at

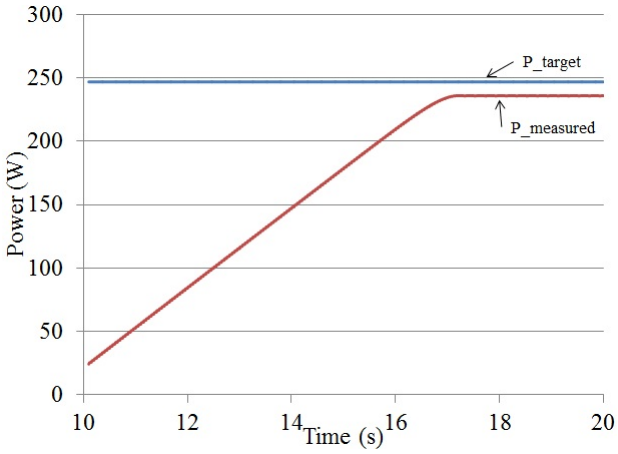

(a) P&O.

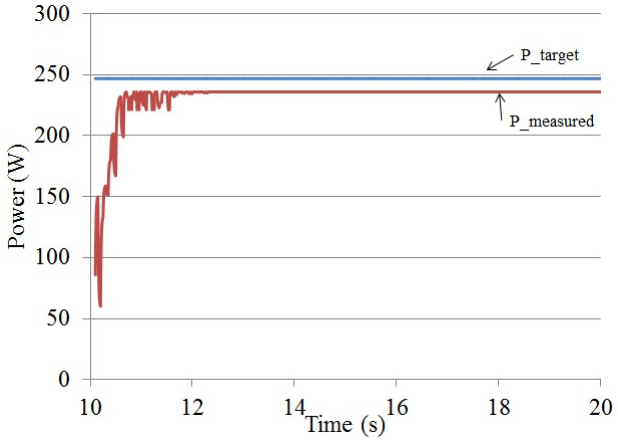

(b) PSO.

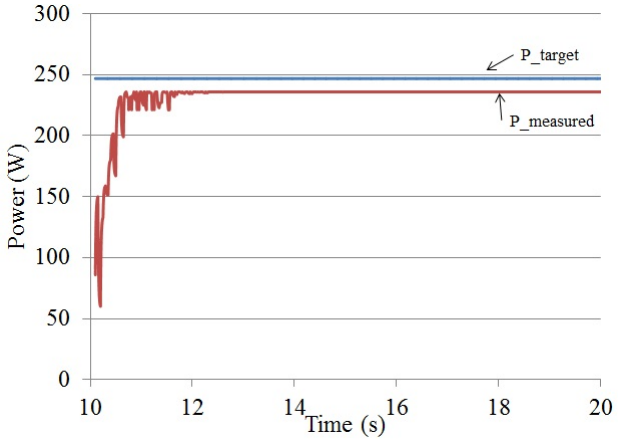

(c) SA.

Figure 5.14: Power tracking (a) P&O, (b) PSO, (c) SA.

the MPP and start oscillating around this point, and for the PSO method it is the time taken for all particles to converge to within 0.02 V of each other.

The convergence of each MPP technique is considered in Table 5.6 and 5.7 for the variable and clear irradiance profiles, respectively. Various convergence measures

Table 5.4: Time to MPP - variable day irradiance profile.

	P&O	**PSO**	**SA**
Average (s)	6.0	3.6	2.9
Standard Deviation (s)	0.9	1.8	1.6
Minimum (s)	4.8	0.35	0.2
Maximum (s)	8.3	10.0	7.4

Table 5.5: Time to MPP - clear day irradiance profile.

	P&O	**PSO**	**SA**
Average (s)	7.24	1.64	2.5
Standard Deviation (s)	0.76	0.51	1.73
Minimum (s)	5.85	0.65	0.2
Maximum (s)	8.35	2.6	7.0

Table 5.6: Performance in converging to GMPP - variable day irradiance profile.

	P&O	**PSO**	**SA**
1% convergence (%)	48.3	58.6	37.9
2% convergence (%)	50.0	60.3	56.9
3% convergence (%)	50.0	63.8	67.2
4% convergence (%)	50.0	63.8	75.9
5% convergence (%)	50.0	67.2	79.3
Converged to other MPP with similar power (%)	6.9	12.1	8.6
Not converged (%)	43.1	20.7	12.1

are considered including a 1% to 5% convergence rating. The convergence rating indicates if the method has converged to within a certain percentage of the known GMPP voltage and power. For instance, the 1% convergence rating gives the number of cases where the method converges to within 1% of the known GMPP voltage and to within 1% of the known GMPP power. The other convergence ratings are defined similarly. Additionally, cases where the method converges to a final operating point with similar power but different voltage to the GMPP are clearly identified. In each case, the performance against each convergence rating is expressed as a percentage of the 58 variable and 18 clear irradiance test cases considered that meet that requirement. The operating point is considered to have not converged if it has an error of more than 5% in the final operating point power when compared to the known GMPP power.

The results show that the SA algorithm performs best in terms of the average, minimum and maximum time to the vicinity of the MPP when compared with the other techniques for the variable day irradiance profile. In particular, the

Table 5.7: Performance in converging to GMPP - clear day irradiance profile.

	P&O	**PSO**	**SA**
1% convergence (%)	52.9	76.5	52.9
2% convergence (%)	58.8	76.5	70.6
3% convergence (%)	58.8	76.5	88.2
4% convergence (%)	58.8	76.5	88.2
5% convergence (%)	58.8	76.5	94.1
Converged to other MPP with similar power (%)	5.9	11.8	5.9
Not converged (%)	35.3	11.8	0.0

PSO technique for the variable day irradiance profile in a few test cases did not converge to a final operating point which is why the time to converge in those cases is 10 seconds. For the clear day irradiance profile, the PSO technique exhibits a better time to find the MPP, showing that the performance of this technique is very dependent on the environmental conditions and starting value.

These results show that when the 1% convergence criterion is applied the performance of the PSO technique is superior to the other techniques. However, as the criterion is relaxed to a 5% convergence, the performance of the SA algorithm becomes considerably better than that of the PSO and P&O methods. This is in line with the goals of the SA GMPPT implementation, which is to converge to near the GMPP such that a local searching process could be initiated to perform fine tracking to the GMPP, similar to the approach suggested in [202], incorporating the PSO method for global searching and the HC method for fine searching. From these results, it is seen that the P&O performance remains the same when the convergence criterion is varied from 2% to 5%. This indicates that due to the step size of the implementation, as the criterion is relaxed the technique has still converged to the local maxima in many cases as it will always locate the maxima at a lower voltage level due to the starting condition of 10 V. It can also be seen in the performance table, that the percentage of cases where the SA algorithm does not converge is far fewer than the percentage of cases where the PSO and P&O methods do not converge. In fact, for the clear day irradiance profile, the SA method converges to either the GMPP or an MPP with similar power (within 5% of the GMPP power) for all test cases.

The performance of the PSO method may be improved by applying the approach described in [19], to select 60-70% of the initial particle positions based on consideration of the anticipated shadow pattern. Taking these

Table 5.8: Performance of reset condition.

	PSO	**SA**
variable weather reset success (%)	70.3	70.3
clear weather reset success (%)	17.6	29.4

steps to improve the performance of the technique would add to the implementation complexity and reduce the universality of the technique as some knowledge of the environment would be required to predict the shadow pattern. The advantage of the SA technique in this case is that it can be applied with a truly random starting point and will still converge in the majority of cases.

The results show that the SA algorithm exhibits better performance in converging to the GMPP when compared to the PSO and P&O methods under the test sets considered. As the SA algorithm has complexity similar to that of the P&O technique and has fewer variables that need to be stored than the PSO technique, it is a simple yet robust approach to achieving GMPPT under PSC.

5.5.2.2 Performance of reset condition

The performance of the implementation with the reset condition is evaluated only for the SA and PSO implementations as the P&O method will continuously track under these conditions and a reset condition is not required. In particular, in this section it is necessary to determine if the reinitialisation condition proposed in [151] is sufficient to enable the PSO and SA methods to detect all changes in the environmental conditions which would require the GMPPT process to be restarted. For the variable and clear day irradiance profiles, the number of times that the reinitialisation condition activates when a change in environmental conditions is known to occur is given as a percentage of the number of changes in irradiance that occur and is presented in Table 5.8.

This shows that in a significant number of cases, a change in the environmental conditions will not trigger a search for the GMPP. In most cases, this is due to the small variation in the optimal operating point which could be easily tracked by implementing the P&O method as a second stage of the process to enable continual tracking. There were however some cases where the power at the current optimal operating point did not change significantly enough to activate

the reinitialisation condition, yet the GMPP moved to another point on the P-V characteristic. In these cases the GMPP usually only moved to the MPP adjacent to the previous optimal operating point in line with the observations presented in Chapter 3. One particular illustration of this is when the technique has located the global maxima on the blue P-V characteristic and then a change in the environmental conditions moves the GMPP to another location the P-V characteristic. The change in power at the current operating point is only small so the method does not detect that a change in the environmental conditions has occurred. This means that the method does not restart the search process and will become stuck at the local maxima. This is shown in Figures 5.15 and 5.16. Realistically, the transitions in real time would be significantly smoother, however this case could still arise when a sudden step in irradiance occurs across some modules in the system such that the GMPP changes significantly while other parts of the system exhibit no change.

5.5.2.3 Transient Performance

The transient performance of the proposed SA method is demonstrated by considering an increasing irradiance and a decreasing irradiance across the entire module while the shading factors remain the same. The results are shown in Figures 5.17 and 5.18, for an increase and decrease in irradiance, respectively. It can be seen that the method continually tracks the power at the operating point and follows the irradiance transient.

5.6 Simulation of the Proposed Simulated Annealing MPPT Method in a Grid Connected PV System

The *Detailed model of a 100 kW Grid Connected PV array* in MATLAB/Simulink (opened by typing 'power_PVarray_grid_det') [268] has been modified to demonstrate the performance of the proposed SA-based method on uniform environmental conditions for a grid connected PV system. The original model utilises the IncCond MPPT method and is used for a comparison of the performance

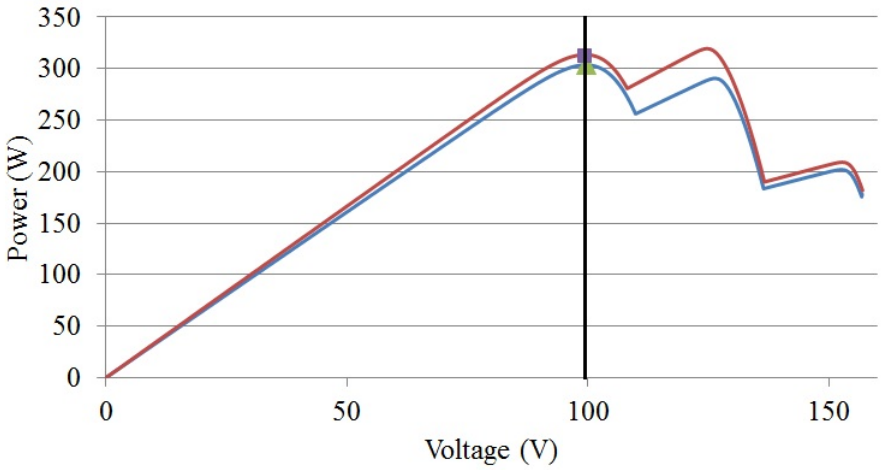

Figure 5.15: P-V characteristics for changing conditions.

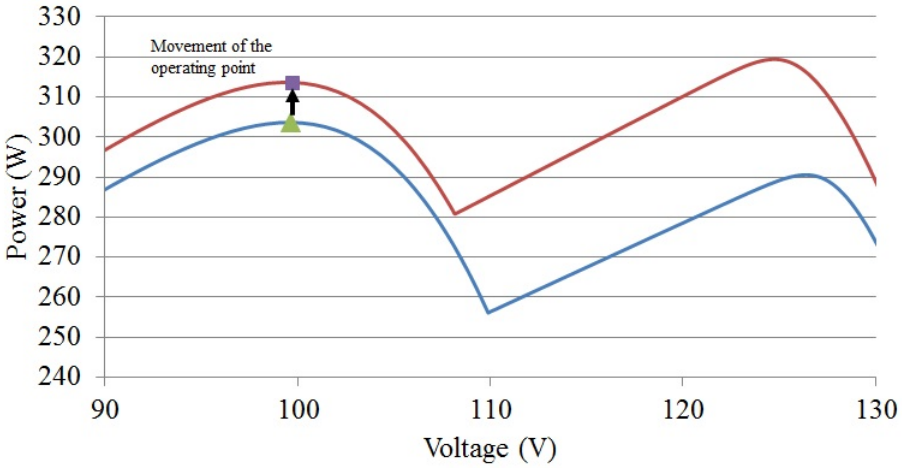

Figure 5.16: P-V characteristics for changing conditions.

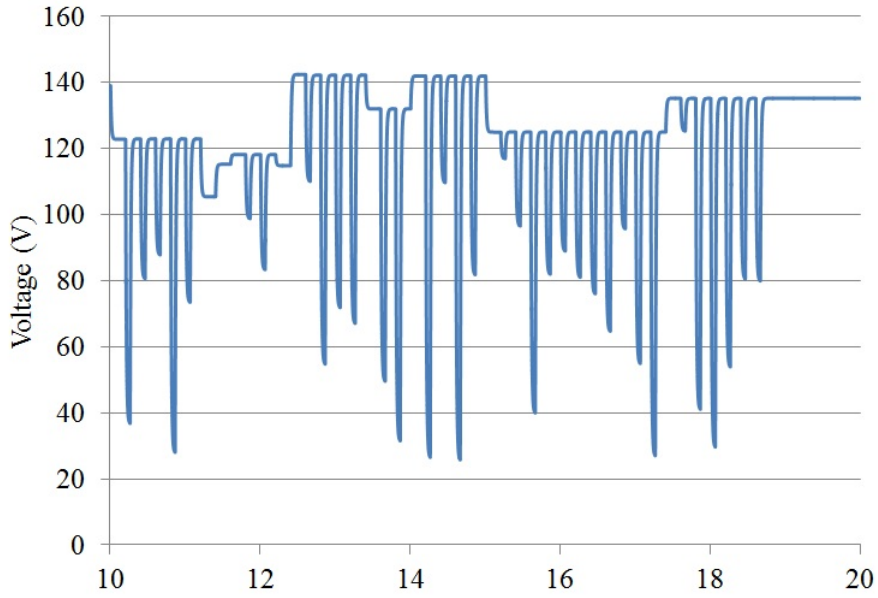

(a) Voltage tracking.

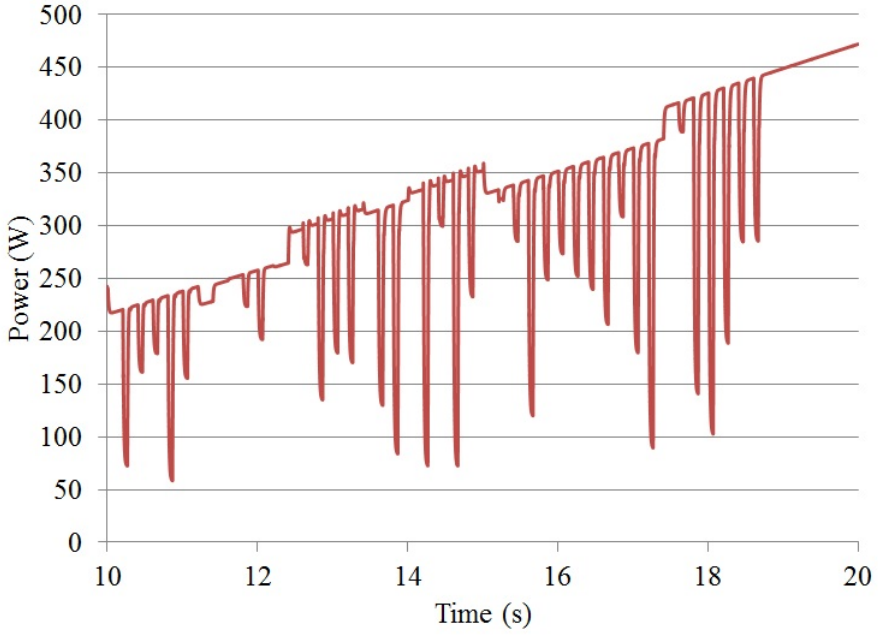

(b) Power tracking.

Figure 5.17: Power and voltage tracking under an irradiance increase from 400 W/m^2 to 800W/m^2.

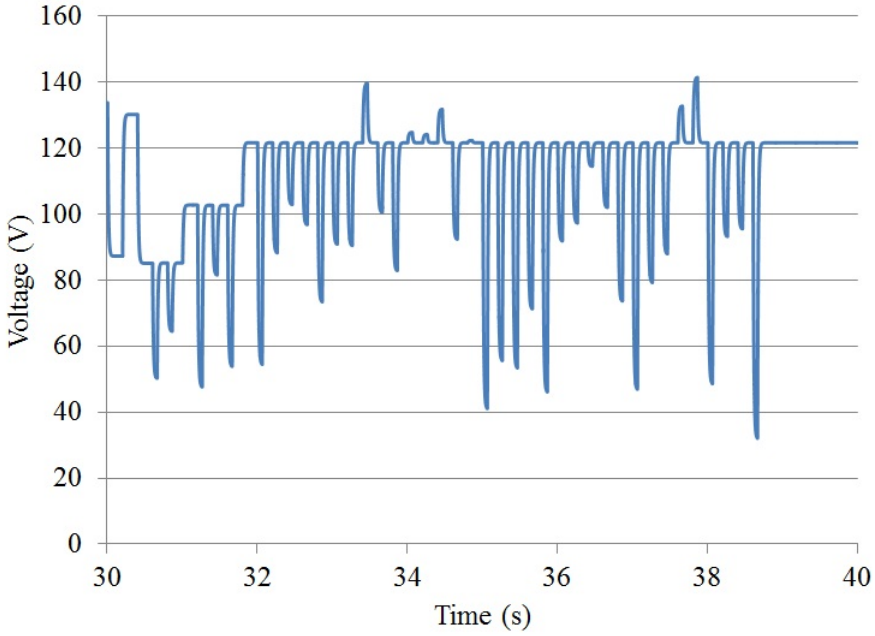

(a) Voltage tracking.

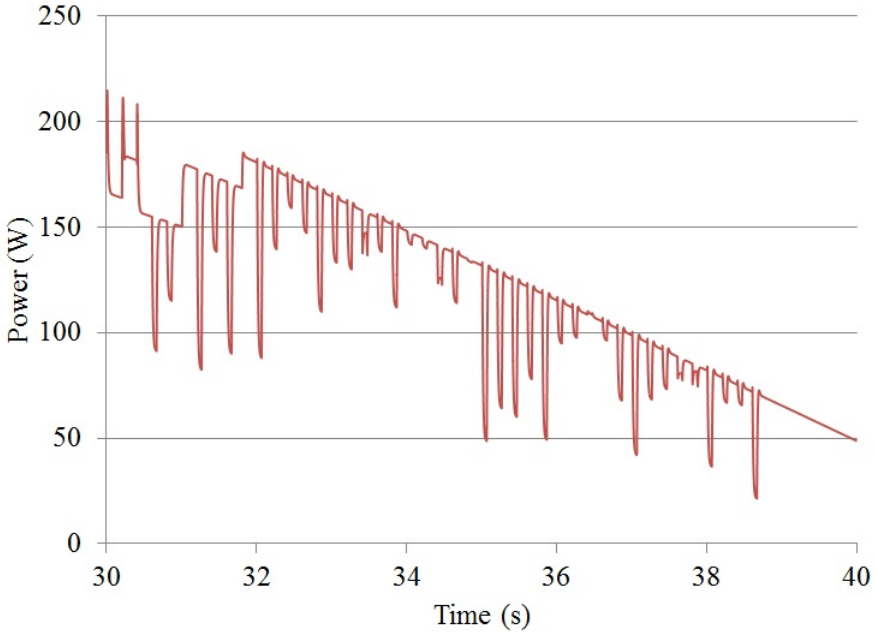

(b) Power tracking.

Figure 5.18: Power and voltage tracking under an irradiance decrease from 1000 W/m^2 to 400W/m^2.

of the proposed technique. The key modification in the program is replacing the MPPT block with the SA method which uses duty cycle as the control parameter. The main intentions for exploring the proposed technique using the existing grid connected model is due to the simplified way that the I-V and P-V characteristics are determined in the model when compared to the more extensive partial shading model developed in this thesis. Additionally, this MATLAB model enables the type of PV panel to be changed very easily so the effect of the key parameters of the MPPT method to be considered in terms of the design of the PV system. However, using the methodology it is only possible to study the performance under uniform environmental conditions.

The block diagram of the system is shown in Fig. 5.19 and a detailed block diagram of the SA MPPT control implemented is shown in Fig. 5.20. The overall MATLAB/Simulink model is shown in Fig. 5.21. The Voltage Source Converter (VSC) control block is shown in Fig. 5.22 and the the IncCond MPPT control block is shown in Fig. 5.23. To implement the SA algorithm, the duty cycle input to the PWM generator in Fig. 5.23 is replaced with the output of the SA algorithm implemented in a MATLAB function. For comparison, for each environmental condition considered in this simulation model, the existing IncCond algorithm is also applied. The IncCond algorithm is executed with an MPPT time window of 200μs, and is incorporated with an Integral Regulator to select the change in duty cycle required. The SA algorithm is implemented with the same temperature parameters as in the eight-module simulation model. Two different cases are considered. In the first case, each method is applied for 10 seconds on constant irradiance and temperature datasets to assess how long each method takes to converge to the MPP, the steady-state power deviation and the energy losses during the tracking process. In the second case, a few samples cases of varying irradiance and temperature during the 10 second test period are considered. The method is assessed based on how well it can follow these changes in the environmental conditions.

The PV array used in the simulation uses 330 SunPower modules (SPR-305). These are connected so that there are 66 parallel strings of five series-connected modules, giving a rated MPP power at STC of 100.7 kW. The key features of each PV module are given in Table 5.9.

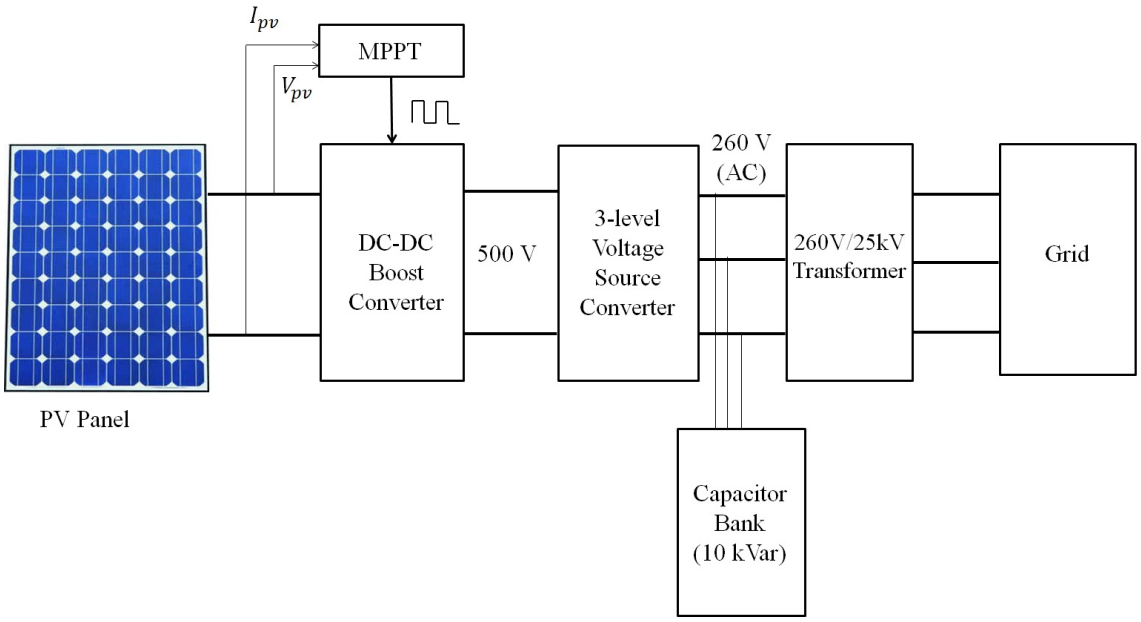

Figure 5.19: Grid connected PV system.

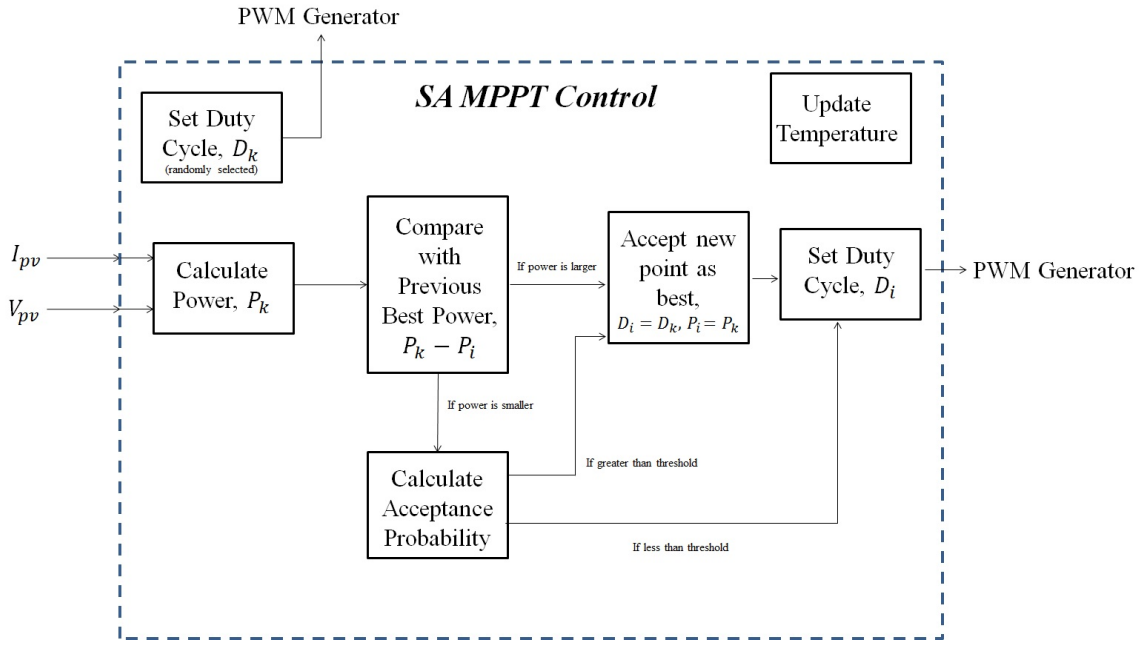

Figure 5.20: SA MPPT for grid connected system.

Table 5.9: Datasheet parameters of SPR-305 modules used in grid connected simulation model.

number of series-connected cells	96
open-circuit voltage (V_{oc})	64.2 V
short-circuit current (I_{sc})	5.96 A
voltage at MPP (V_{mpp})	54.7 V
current at MPP (I_{mpp})	5.58 A

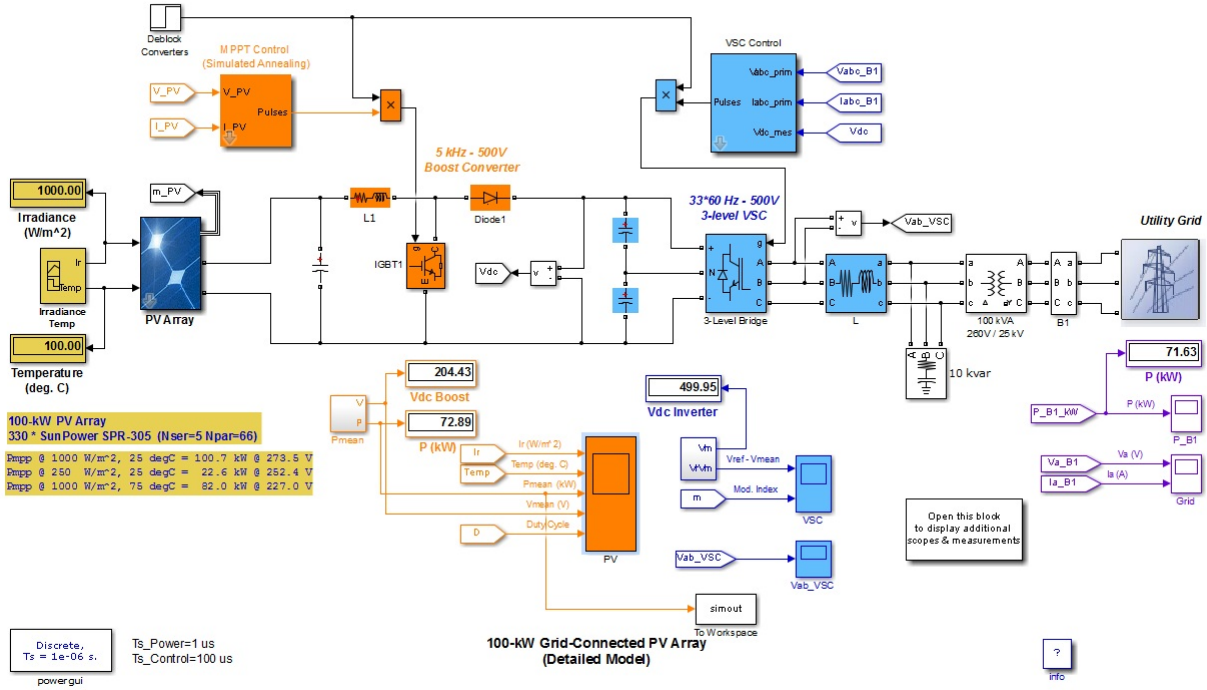

Figure 5.21: Grid connected PV system - MATLAB/Simulink model.

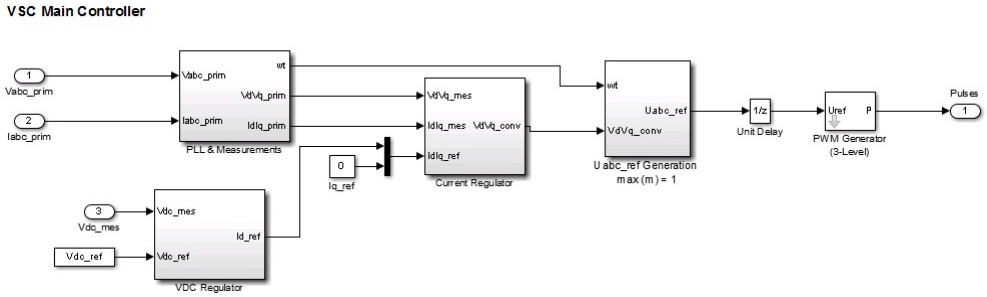

Figure 5.22: Grid connected PV system - VSC main controller from detailed 100 kW PV system model.

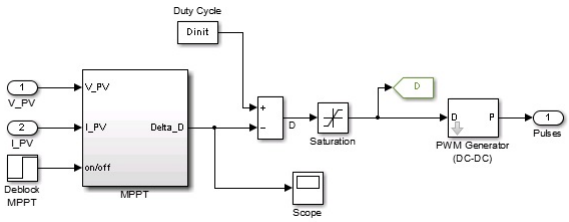

Figure 5.23: Grid connected PV system - IncCond MPPT control from detailed 100 kW PV system model.

5.6.1 Constant temperature and irradiance performance

In this section, the SA and IncCond methods are applied when the PV system experiences constant and uniform irradiance and temperature across all the modules. Ten test cases are considered where the irradiance varies from 250 W/m^2 to 1000 W/m^2 in steps of 250 W/m^2, in line with the P-V curves provided for the array. The temperature remains constant at 25 $°C$. For each test case, the time to find the MPP, the steady-state power deviation from the known MPP, and the energy losses during the tracking process are recorded. The energy losses are found by integrating the power across the 10 second test period and comparing this to the expected system energy if the system was operating at the MPP for the entire test period. The results are shown in Table 5.10. The simulation is also run with constant irradiance of 1000 W/m^2 with varying temperature. The temperatures considered are 50$°C$, 75$°C$ and 100$°C$, in line with the provided P-V curves for the array.

For the varying temperature case the same data is recorded as for the varying irradiance case and is given in Table 5.11.

It can be seen from these results that in general both techniques converge to a similar steady state power deviation around the MPP. From examining the

Table 5.10: Performance of grid connected SA and IncCond on constant environmental conditions.

	IncCond			**SA**		
Irradiance (W/m^2)	Time to MPP (s)	Steady-state power deviation (kW)	Energy lost (kJ)	Time to MPP (s)	Steady-state power deviation (kW)	Energy lost (kJ)
250	0.1	0.1792	2.36	2.2	0.1475	21.21
500	0.4	0.2991	4.49	2.2	0.3730	47.52
750	0.4	0.4499	7.14	0.2	0.4726	71.32
1000	0.4	0.0092	7.48	0.2	0.6546	94.94

Table 5.11: Performance of grid connected SA and IncCond on constant environmental conditions.

	IncCond			**SA**		
Temperature ($°C$)	Time to MPP (s)	Steady-state power deviation (kW)	Energy lost (kJ)	Time to MPP (s)	Steady-state power deviation (kW)	Energy lost (kJ)
50	0.15	0.0409	5.98	0.12	0.0098	76.13
75	0.41	0.0240	8.77	0.8	0.0678	73.34
100	0.43	0.7843	27.84	0.8	0.0059	83.05

results, in about half of the test cases the SA steady-state power deviation is less than the IncCond steady-state power deviation, indicating that on this measure the techniques are quite evenly matched. The IncCond method performed better in terms of the energy lost. This is largely due to the SA method implementation only having a stopping criterion once the temperature gets sufficiently low, which means that it will find the MPP noticeably before the searching process concludes, and will continue returning to this point throughout the testing. By implementing the strategies outlined in Chapter 7 for the stopping criterion, the energy losses of the SA method could be reduced. The IncCond method in general was able to track the MPP in less than one second, while there were two cases of the SA method that took more than two seconds to correctly identify the neighbourhood of the MPP. In most other test cases, the SA method found the MPP in a similar time to the IncCond method.

For comparison, the SA method is also implemented with an additional stopping criterion to see how this influences the effectiveness of the method. The stopping criterion ensures that the SA method will stop searching if it has returned to the best reference voltage four times. In this case, the time to MPP is expressed as the time that it takes for the method to stop searching, and the modified stopping criterion results are compared with the base case implementation of the SA method in Table 5.12 and Table 5.13 for changing irradiance and temperature, respectively.

It can be seen that the modified stopping criterion improves the time taken by the algorithm to stop searching and in most cases results in less energy being lost during the searching process. However, it can be seen that the steady-state power deviation is larger in all test cases indicating that by stopping the search earlier the method is less likely to converge exactly to the GMPP. While the

Table 5.12: Performance of grid connected SA and SA with modified stopping criterion on constant environmental conditions.

	SA			**SA with modified stopping criterion**		
Irradiance (W/m^2)	Time to MPP (s)	Steady-state power deviation (kW)	Energy lost (kJ)	Time to MPP (s)	Steady-state power deviation (kW)	Energy lost (kJ)
250	8.82	0.1475	21.21	1.07	1.4455	17.52
500	8.82	0.3730	47.52	1.07	4.6431	51.311
750	8.82	0.4726	71.32	1.27	5.5470	65.46
1000	8.82	0.6546	94.94	1.27	4.6048	55.14

Table 5.13: Performance of grid connected SA and SA with modified stopping criterion on constant environmental conditions.

	SA			**SA with modified stopping criterion**		
Temperature ($°C$)	Time to MPP (s)	Steady-state power deviation (kW)	Energy lost (kJ)	Time to MPP (s)	Steady-state power deviation (kW)	Energy lost (kJ)
50	8.82	0.0098	76.13	3.07	0.1203	52.76
75	8.82	0.0678	73.34	2.87	2.4650	50.53
100	8.82	0.0059	83.05	1.67	0.3604	32.19

energy lost is small for the simulation time of 10 seconds, if the simulation time was extended, the implementation that tracks to closer to the MPP will result in a lower energy lost during the operation of the system. These results suggest that the stopping criterion must be carefully balanced to ensure that the method can accurately track to the GMPP yet with a faster tracking time. It is worth also noting that in this analysis the IncCond method applied by the technique uses a time window for MPPT of 200μs, which means that the IncCond method applies each tracking step much quicker than the steps applied with the SA implementations. The initial duty cycle for the IncCond method is set to 0.5, which is very close to the duty cycle at the MPP thereby reducing the tracking time required. The SA method starts from a truly random duty cycle.

The sample screen shot of the scope output for the IncCond method when tracking the MPP for a constant irradiance of 1000 W/m^2 is shown in Fig. 5.24.

5.6.2 Varying environmental conditions assessment

The irradiance and temperature are varied across the 10 second test period to show increasing and decreasing transients in the environmental conditions to assess how well each technique is capable of following the MPP under these conditions. The results show that all methods are capable of following the irradiance transient under the simple uniformly varying environmental conditions.

Three implementations are considered for each transient. The IncCond method as implemented in the MATLAB sample model, the SA method from the previous section and the SA method with the modified stopping criterion are all assessed in this section. The simulation runs for 10 seconds and

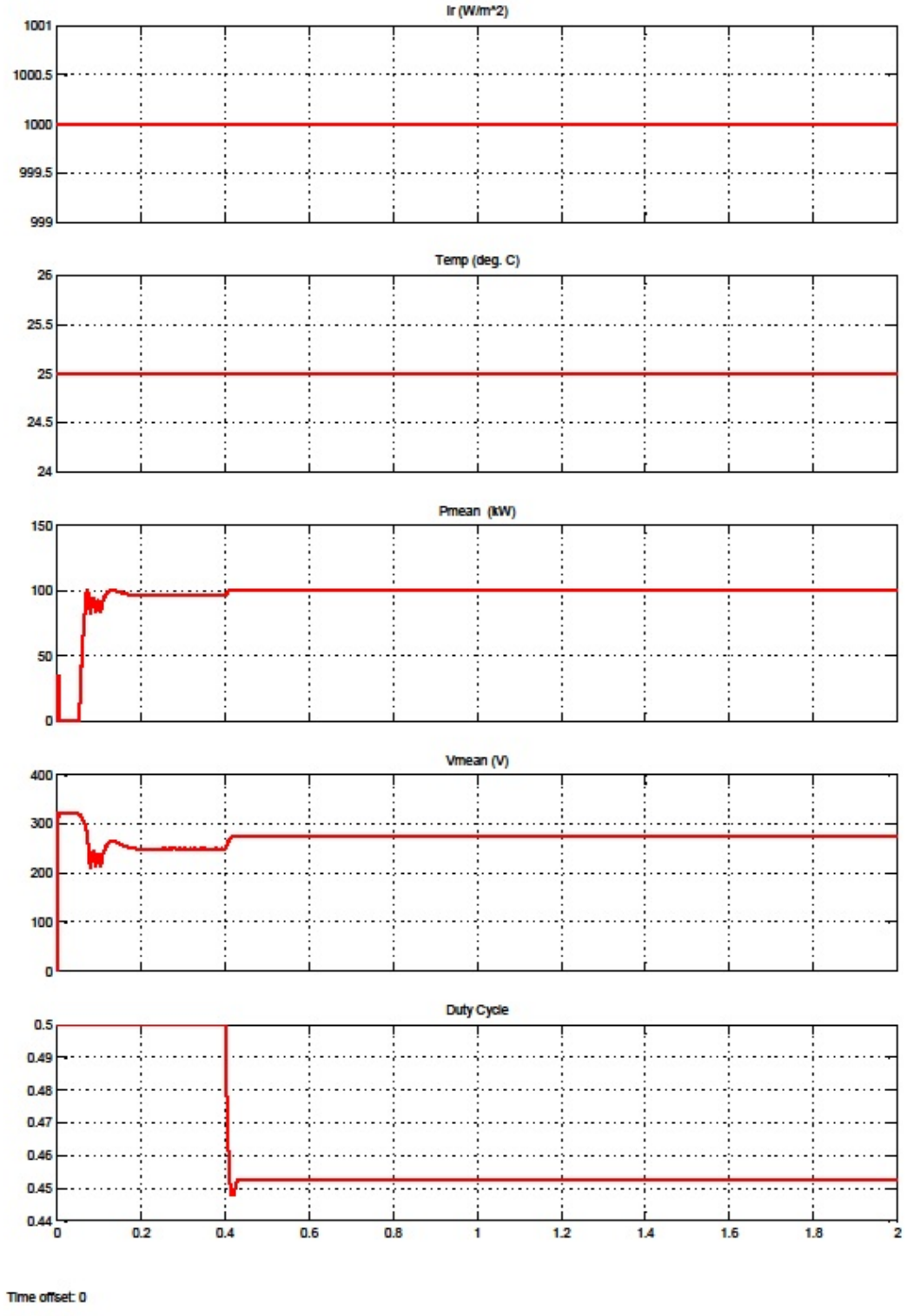

Figure 5.24: MPPT with IncCond for constant irradiance of 1000 W/m^2.

involves the irradiance changing linearly across that time frame. The energy extracted by each technique is considered in the table rather than the energy lost.

Four different irradiance transients are considered and the results are given in Table 5.14 to 5.17. The irradiance transients considered are:

- 1000 W/m^2 to 500 W/m^2
- 500 W/m^2 to 1000 W/m^2
- 500 W/m^2 to 250 W/m^2
- 250 W/m^2 to 500 W/m^2

The output scope for each method is shown for a different irradiance transient in Fig. 5.25 to Fig. 5.27. Figure 5.25 shows the performance of the basic SA implementation for the irradiance transient from 500 to 1000 W/m^2. Figure 5.26 shows the performance of the SA implementation with the modified stopping

Table 5.14: Performance of grid connected SA, SA with modified stopping criterion and IncCond on irradiance transient from 1000 W/m^2 to 500 W/m^2.

	Time to MPP (s)	Steady-state power deviation (kW)	Energy (kJ)
SA	0.7	6.7614	638.67
SA with modified stopping criterion	0.2	6.7615	672.55
IncCond	0.4	0.0190	735.03

Table 5.15: Performance of grid connected SA, SA with modified stopping criterion and IncCond on irradiance transient from 500 W/m^2 to 1000 W/m^2.

	Time to MPP (s)	Steady-state power deviation (kW)	Energy (kJ)
SA	2.25	4.5643	668.14
SA with modified stopping criterion	0.25	12.3666	653.34
IncCond	0.425	0.0086	739.41

Table 5.16: Performance of grid connected SA, SA with modified stopping criterion and IncCond on irradiance transient from 500 W/m^2 to 250 W/m^2.

	Time to MPP (s)	Steady-state power deviation (kW)	Energy (kJ)
SA	2.25	1.1220	316.05
SA with modified stopping criterion	2.05	0.5728	335.14
IncCond	0.45	0.0241	351.18

Table 5.17: Performance of grid connected SA, SA with modified stopping criterion and IncCond on irradiance transient from 250 W/m^2 to 500 W/m^2.

	Time to MPP (s)	Steady-state power deviation (kW)	Energy (kJ)
SA	0.25	1.4473	301.42
SA with modified stopping criterion	0.25	1.4474	6318.02
IncCond	0.428	0.0582	349.30

criterion on the transient from 250 W/m^2 to 500 W/m^2. Finally, Fig. 5.27 shows the performance of the IncCond method on the irradiance transient from 500 to 250 W/m^2.

It can be seen that in each case all methods are able to track the transient MPP. However, the IncCond method consistently tracks the MPP much faster and correspondingly extracts more energy from the system. The SA and modified stopping criterion SA implementations experience a significant steady-state power deviation which occurs due to the operating point continuing to change after the methods have completed the search. With a reinitialisation condition included, as investigated earlier in this chapter and in Chapter 7, this irradiance transient could cause a drop in the power sufficient to restart the SA searching process and leading to improved convergence. However, it can be seen that even without reinitialising the method, the SA implementations converge to the neighbourhood of the MPP and could then be applied with a local search method to accomplish exact MPP tracking. It should be highlighted that one of the key advantages of the SA method is its ability to distinguish between local and global maxima which the IncCond method is incapable of doing. This ability however, is not readily accessible through the uniform conditions grid connected simulation model.

Results show that conventional methods such as the IncCond method, are better than the proposed method in continually tracking the MPP under uniform conditions. However, real PV systems will more frequently experience non-uniform environmental conditions due to shading, cell degradation and mismatch, for which conventional techniques fail to perform adequately. The SA method out performs these conventional techniques and PSO when applied to the systems under PSC studied in this chapter.

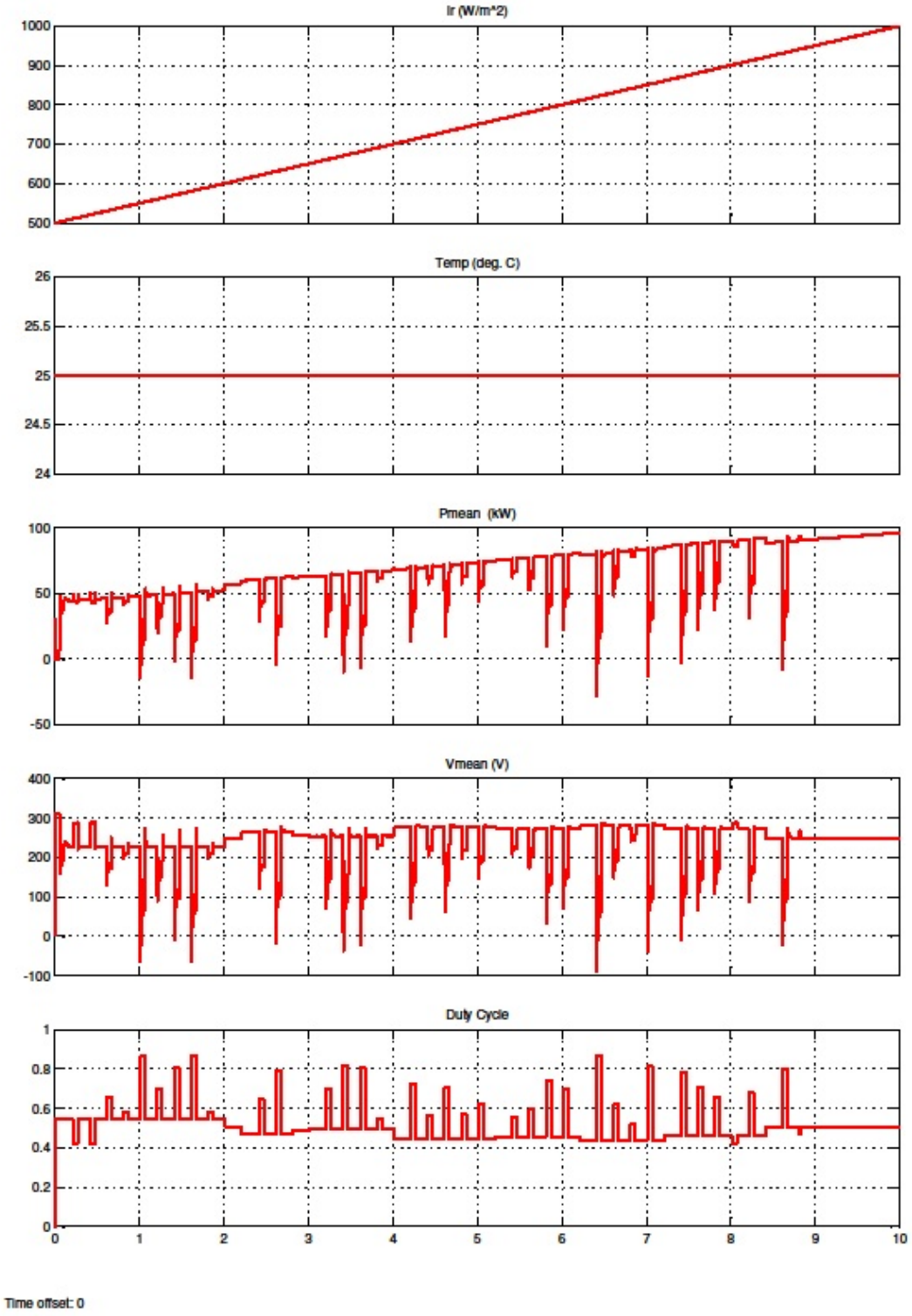

Figure 5.25: MPPT with SA for irradiance transient from 500 W/m^2 to 1000 W/m^2.

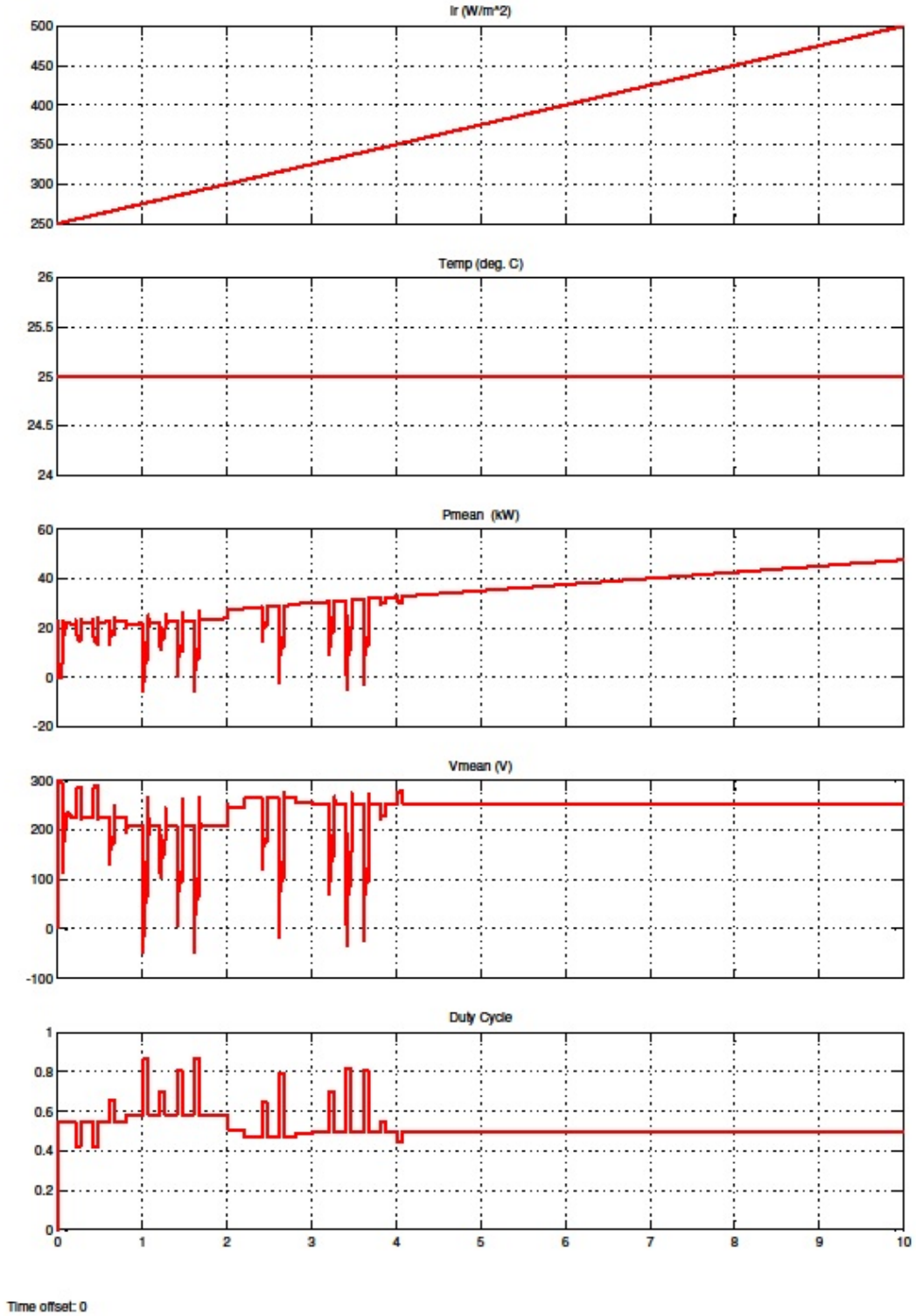

Figure 5.26: MPPT for SA with modified stopping criterion tracking for irradiance transient from 250 W/m^2 to 500 W/m^2.

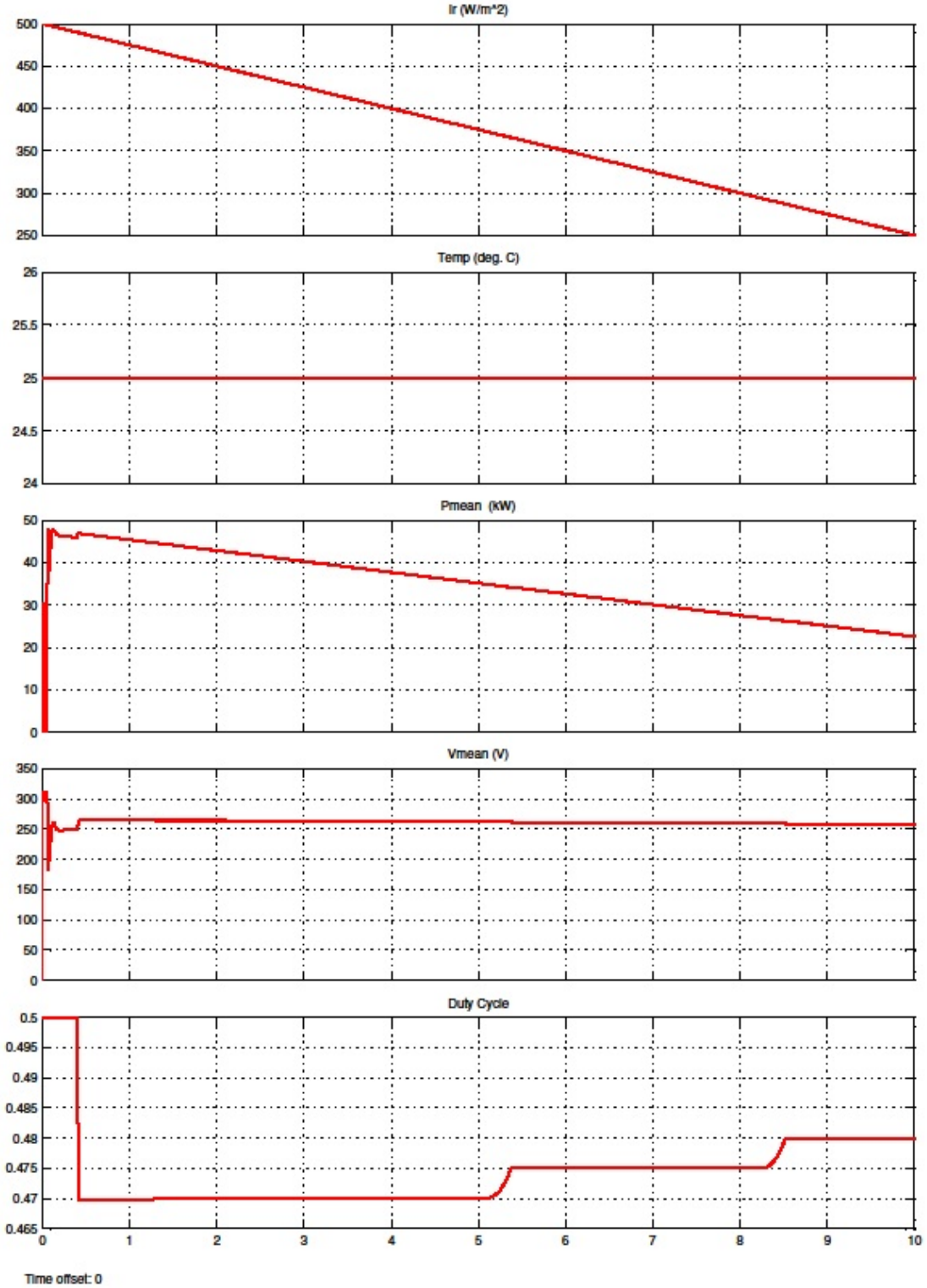

Figure 5.27: MPPT with IncCond for irradiance transient from 500 W/m^2 to 250 W/m^2.

5.7 Experimental Verification

To verify the suitability of the proposed SA-based GMPPT method for application on PV systems, the technique has been applied on the two module system introduced in Chapter 2. MPPT is implemented through a Labview interface which incorporates MATLAB scripts to run the SA MPPT algorithm. Labview is utilised as it provides an effective method for the SA MPPT technique to be easily modified during testing to improve performance. In its current implementation the PV system must be connected to a computer equipped with Labview 2011 and MATLAB 2011b to enable MPPT. Future research into optimising the technique will involve developing a stand-alone prototype which can be implemented on either a low-cost microcontroller or by interfacing with the FPGA on a National Instruments (NI) CompactRIO [269,270].

5.7.1 Experimental setup

The experimental block diagram is shown in Fig. 5.28. The BP380 PV panels are connected to a DC-DC converter, via a Textronix AC622 Current Probe and resistors, and connected to a load of approximately 235 W. Analog Current and voltage measurements are fed into the Labview program via a NI USB-6008 Data Acquisition Device (DAQ) where the control algorithm is executed. The duty cycle, input power, voltage and current to the converter are all monitored on the Labview Interface shown in Fig. 5.29. The Labview interface shows the tracking of the GMPP in four different cases. It can be seen that the duty cycle corresponding to the GMPP has changed slightly between each iteration (it becomes constant once the method has stopped searching), due to changes in the environmental conditions between each test. In the shown tests, an initial temperature of 20°C is used, with a cooling rate of 0.55, final temperature 0.2°C, and with the temperature update occurring every three iterations. These parameters are slightly different to those explored in previous sections of this chapter, and have been selected based on observation of the performance of the method. As there are fewer modules considered in the experimental implementation when compared to the eight module simulation model, there is a smaller voltage range to be considered which is why these parameters can be reduced without significantly affecting the performance. Further studies describing the affects of

each parameter on the performance of the method are presented in Chapter 6. As the MPPT method is implemented as MATLAB scripts in the Labview program it is easy to modify the parameters of the technique and implement other MPPT approaches. The Labview program performs the control algorithm and writes an analog output of between 0 and 5V to a PIC microcontroller which then outputs a PWM signal to control the MOSFETs of the DC-DC converter. The sampling time for the algorithm can be changed in the Labview interface program.

A PIC12F1822 is used in the implementation to output a PWM signal to control the DC-DC converter. The PIC operates with a frequency of approximately 17.5 kHz, and outputs a TTL PWM signal on pin GP2. To control the duty cycle, an analogue input voltage is applied on pin GP4. The input voltage to the PIC is limited to 0 to 5V, where 0 V provides a duty cycle of 0% and 5 V provides a duty cycle of 100%. The HCPL-3180 Integrated Circuits are used to drive the MOSFETs, provide isolation and to boost the logic level of the PWM signal to the required 15 V to switch the MOSFETs.

A schematic diagram showing the DC-DC converter, PIC and measurement is shown in Fig. 5.30. The lines AI0, AI1, AI2, AO0, +5V and 0V all connect to the data acquisition device (DAQ). Line AI0 measures the PV module current, AI1 measures the input voltage to the converter (this is equivalent to the PV module voltage) and AI2 measures the output voltage of the converter (which could be used as the tracking parameter to maximise the output power of the system similar to the approaches considered in [129, 152, 153]). The output, AO0 provides an analog voltage between 0 and 5 V to the PIC to generate the PWM signal.

The control algorithm is executed as embedded MATLAB scripts inside the Labview program. The approach of using Labview to test a MPPT algorithm has previously been explored in [270]. Implementing the algorithm in Labview provides the opportunity to perform rapid prototyping on the algorithm as parameters can be easily adjusted to optimise the technique. The duty cycle is restricted to remain between 0.1 and 0.7.

The block diagram of the Labview interface is shown in Fig. 5.31. The individual frames of the block diagram are shown with a higher resolution in Appendix C.

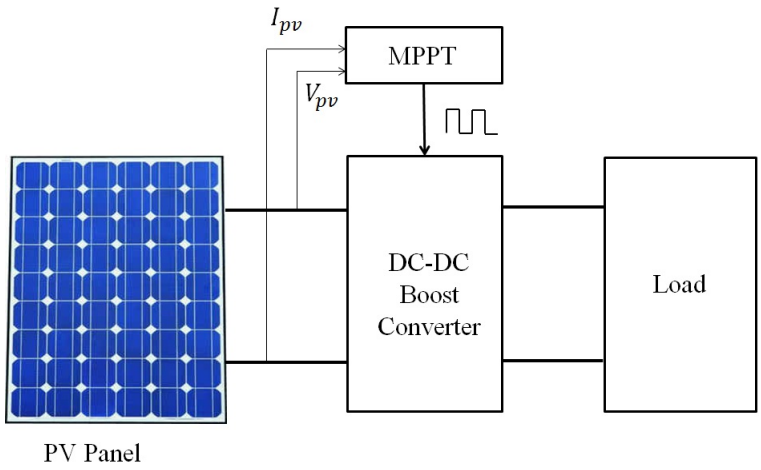

Figure 5.28: Experimental PV system.

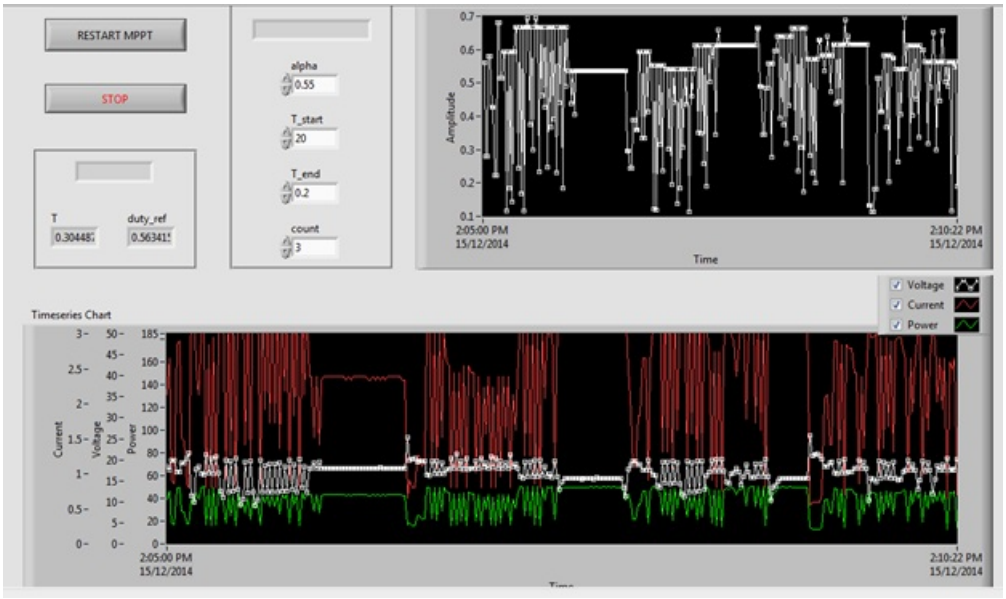

Figure 5.29: Labview interface for MPPT.

The Labview code consists of three main stages. These are initialisation, termination and algorithm execution. The algorithm execution occurs continuously inside a while loop and is contained in a flat structure to control the algorithm execution. In the first frame, the random voltage is selected within the range 0.1 to 0.7 and written to the analog output of the DAQ to be used as the duty cycle input for the PIC microcontroller. In frame 2, a short delay is applied before the voltage and current are read using the input pins on the DAQ. From the voltage and current, the power is calculated and all values are written to the Timeseries Chart. Frame 3 contains the main execution of the SA algorithm and involves comparing the current operating point with the reference point to decide which point should be accepted as the new reference point. This is executed

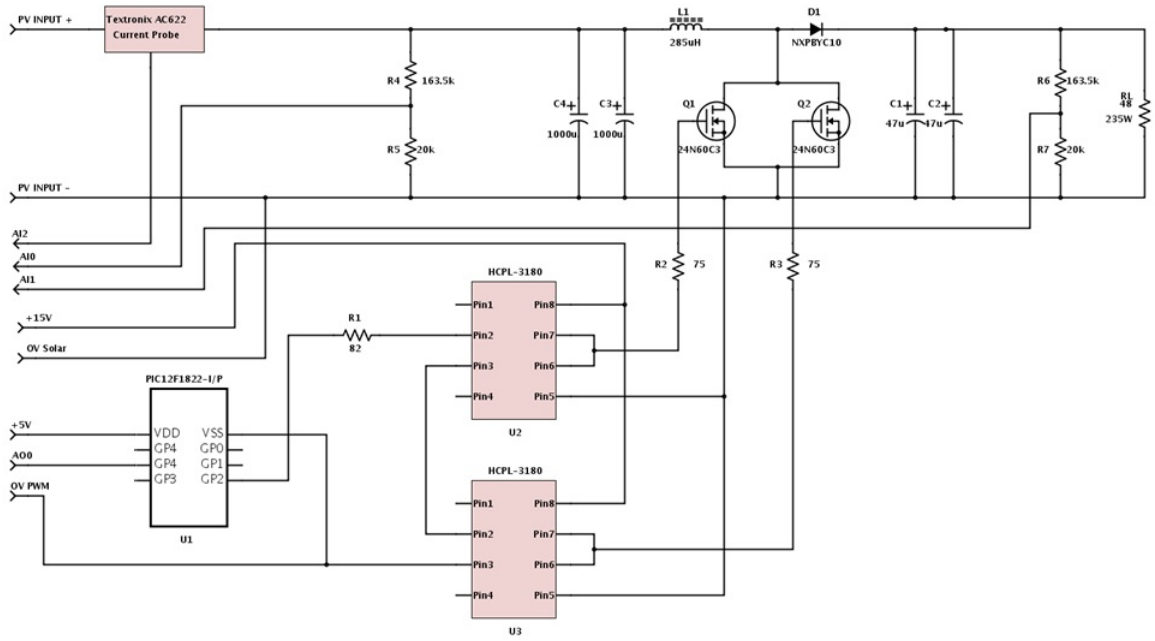

Figure 5.30: DC-DC converter schematic.

within a MATLAB script which also includes a section to update the temperature.

In frame 4, the duty cycle of the best reference operating point chosen in frame 3 is written to the analog output to control the PIC microcontroller. In frame 5, the PV system voltage and are read again after a short delay and the power is calculated. This data is stored in the Timeseries chart. When the stop button is pressed on the front panel, the while loop will exit and the program termination phase will commence.

5.7.2 Experimental results

The performance of the SA GMPPT method is verified experimentally by implementing the system described in the preceding section with the following parameters:

- $T_{start} = 20$
- $T_{stop} = 0.2$
- $\alpha_2 = 0.55$
- $count = 3$

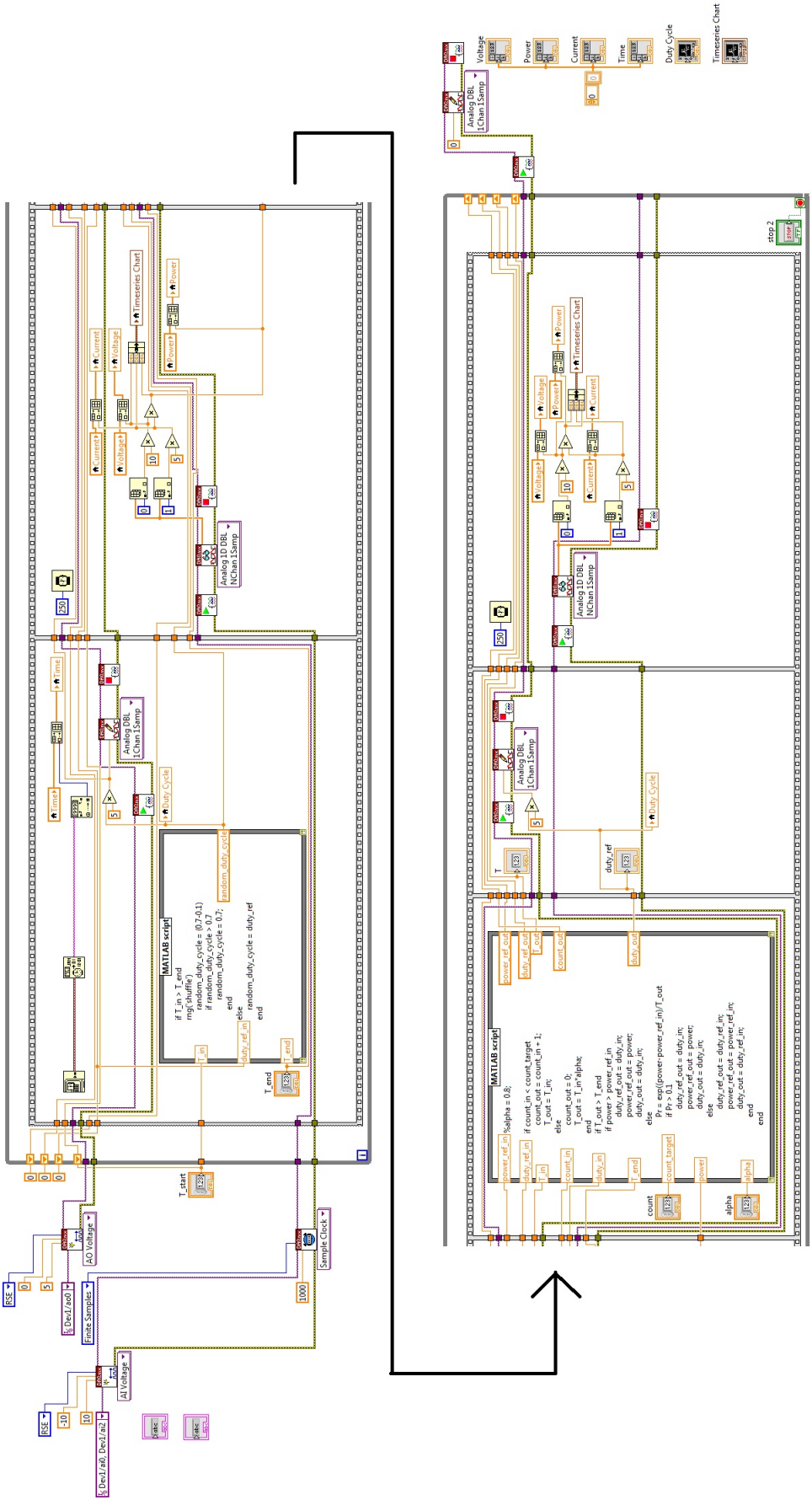

Figure 5.31: Labview block diagram of MPPT control.

Testing was completed on December 15, 2014 for which the temperature in Hobart was approximately 22°C and the sky was predominately clear [271]. PSC were created by using the fabric method described in Chapter 2 and also using natural shadow from the building as shown in Fig. 5.32.

Data is collected when the modules experience uniform irradiance, when module two is covered by one layer of white fabric and when module two is covered by two layers of white fabric. Tests are also conducted with shading from the building. In total, the algorithm has been performed on 64 cases, where 15 cases correspond to uniform irradiance, 24 to shading with one layer of fabric, three to shading with two layers of fabric, six with two layers of fabric and shading from the building and 16 with just shading from the building.

Figure 5.32: Partial shading testing with shadow from building.

Table 5.18: Performance of SA method with experimental implementation under different types of PSC.

	Converged to GMPP	**Near to GMPP**	**Other MPP**	**Converged to other MPP with similar power to GMPP**
uniform conditions	15	0	0	0
one layer of white fabric	7	5	9	3
two layers of white fabric	3	0	0	0
two layers of white fabric and building shade	4	1	1	0
building shade	6	10	0	0

In each case, from the collected data a P-V curve can be drawn to show the GMPP. Due to variations in the weather during the testing it is possible that the GMPP will change slightly from the start of the test to the point where the algorithm converges to an operating point. Because of this, algorithm success is determined by considering if it converges to the vicinity of the correct GMPP in each test case. As has been previously discussed in this chapter, it would be possible to continue to search with a local search algorithm like P&O once in the neighbourhood of the GMPP to improve performance.

For each case, the performance is classified into one of four standards. The first is that the method has converged to the GMPP, which means that the voltage and power must be within about 5% of the GMPP voltage and power found during the search time. The second standard is for cases where the method has clearly converged to near the GMPP yet is just outside of this 5% boundary. The third standard is for cases where the method has resulted in convergence to another MPP with far less power and standard four is for cases where the method has converged to a different MPP yet is still within 5% of the GMPP power.

From these results it can be been that in 79% of the tested cases the method converged to the GMPP and in 4.69% of cases it converged to a MPP with

very similar power to the MPP. This means that in 14% of the tested cases the method converged to an MPP with substantially less power than the GMPP.

The main cases where the method converged to the local MPP was for the case where there was one layer of white fabric on module two. This reduced the irradiance on module two to about 50-60% of the irradiance experienced by module one. Of these cases that converged to the local MPP only two are significant and exhibit a final operating point power that is more than 10 W less than the GMPP power. Due to the level of irradiance reduction, the peaks created for the one layer of fabric case are relatively similar which could account for why the algorithm may converge to the local MPP in some cases.

A sample case showing the convergence for one case where a single layer of white fabric is affixed to module two is described below. In this sample case, the method correctly identifies the GMPP location and then remains at this duty cycle while some transients in the irradiance occur. The duty cycle is given in Fig. 5.33. Small changes in the power and voltage at the operating point after sample 100 can be seen in Figs. 5.34 and 5.35, as a result of the changing environmental conditions after the GMPP has been located. The information obtained during the search can also be combined to form an approximate P-V curve trace, as shown in Fig. 5.36. Note that several points in Fig. 5.36 deviate from the normal smooth P-V curve and that this is due to changes in the ambient environmental conditions. The red line indicates the approximate P-V curve, and the blue dots indicate all sample points considered during the time of interest.

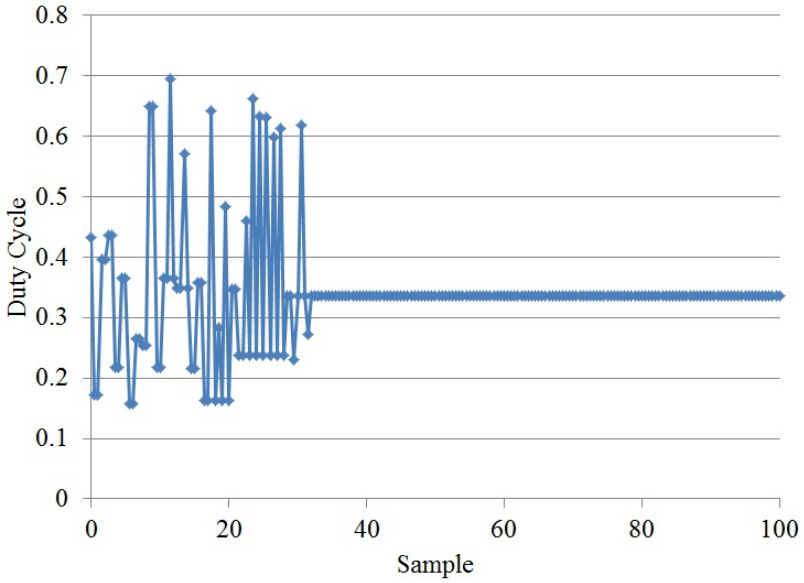

Figure 5.33: Experimental duty cycle for case with irradiance approximately 890 W/m^2 on module one and 530 W/m^2 on module two. Module temperature is approximately 36°C.

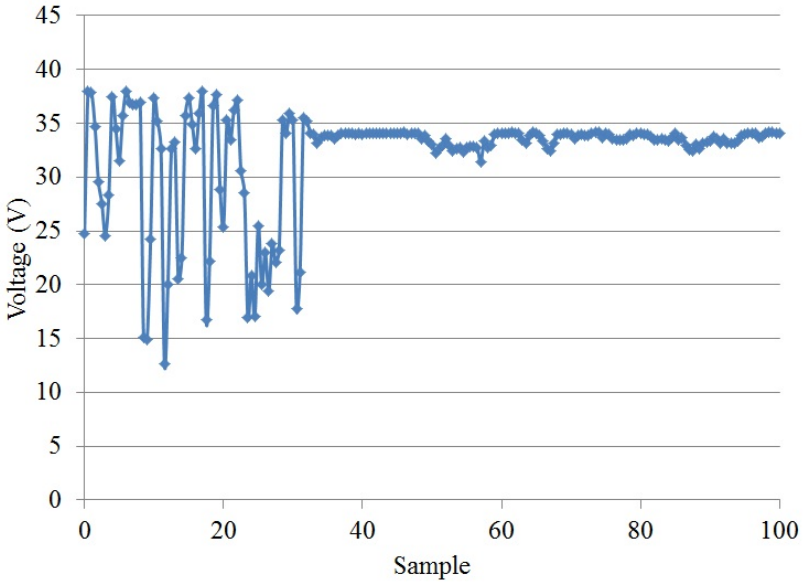

Figure 5.34: Experimental voltage tracking for case with irradiance approximately 890 W/m^2 on module one and 530 W/m^2 on module two. Module temperature is approximately 36°C.

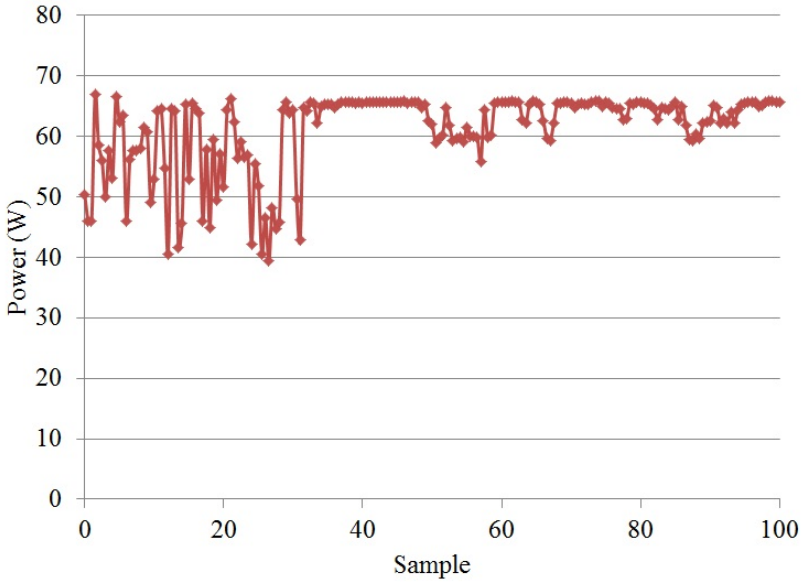

Figure 5.35: Experimental power tracking for case with irradiance approximately 890 W/m^2 on module one and 530 W/m^2 on module two. Module temperature is approximately 36°C.

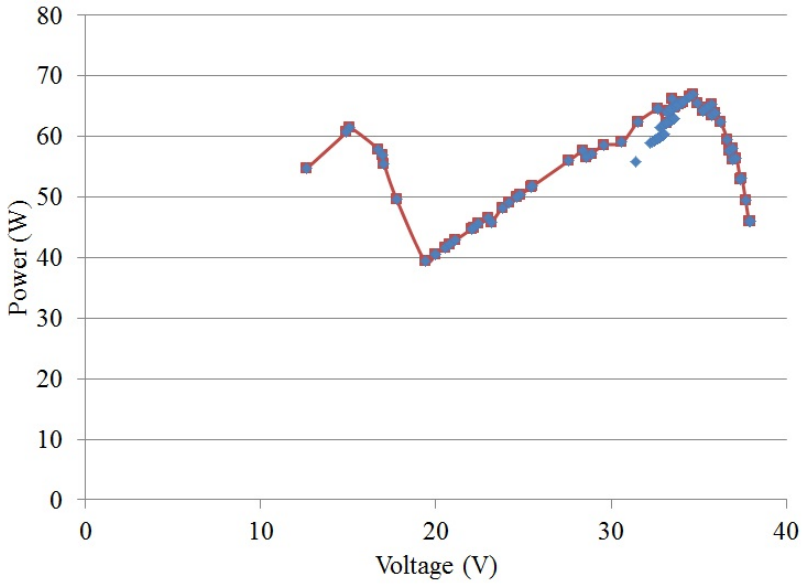

Figure 5.36: Experimental P-V characteristic formed using case with irradiance approximately 890 W/m^2 on module one and 530 W/m^2 on module two. Module temperature is approximately 36°C.

5.8 Conclusion

The key objective of this chapter has been to implement the SA technique for MPPT and highlight the superior performance of the SA method in achieving

GMPPT with very limited optimisation of the parameters. These observations on the performance coupled with other results in this thesis are combined in Chapter 7 to develop an enhanced GMPPT strategy.

The results shown in this chapter demonstrate that the proposed SA based GMPPT method can be suitably applied to small and medium scale PV systems and achieve more reliable GMPPT under PSC than other common techniques. Some key advantages to the proposed approach are its reliability in converging to near the GMPP, its relative simplicity and the fact that the performance is independent of the starting value. When compared with the P&O method, which cannot distinguish between local and global maxima, the proposed technique has clear advantages in enabling GMPPT with only a very small increase in complexity. When compared to the PSO method, for which multiple parameters need to be defined and stored in memory for each iteration, the number of elements requiring storage for the proposed implementation is considerably fewer. Additionally, the proposed method achieves GMPPT independent of the starting condition, while the PSO method may require the initial particle positions to be determined to some degree based on the anticipated environmental conditions.

The results achieved in this chapter have occurred using fairly arbitrary system parameters including the temperature cooling rate, initial and final temperatures. In the form described in this chapter, the technique keeps the same neighbourhood size for each successive random perturbation. Supported by [232], to improve the technique, the neighbourhood size could be reduced as the temperature cools to aid in tracking to the GMPP. In the initial stages, the algorithm is expected to widely search the region, while in the final stages the algorithm needs to converge to the final optimum point [232]. By reducing the neighbourhood size, this becomes more achievable.

Supported by the results in this chapter, the SA algorithm ensures that the operating point moves to within a neighbourhood of the optimum, but may require enhancement with a local search method to ensure direct convergence to the optimum point [239]. The time the algorithm is given to execute within is far less than the worst case time required for convergence, a 'quasi optimal' solution is achieved [263].

Further work on the technique, as described in Chapters 6 and 7, optimises the selection of the key parameters of the technique including neighbourhood size and refines the technique based on observations from the preceding chapters. Utilising the technique as a two-stage methodology combined with P&O for fine searching is also explored.

Chapter 6

Exploring the Key Parameters of the Simulated Annealing Method

In this chapter the key parameters of the SA MPPT method are varied to see how this affects the tracking performance. The influence of these parameters will enable an optimised SA methodology to be established which can quickly and accurately track to the GMPP. Factors which need to be explored include:

- Initial temperature
- Cooling rate
- Cooling frequency
- Acceptance probability threshold
- Neighbourhood size
- Stopping temperature
- Cooling function
- Stopping criterion

These factors are explored with a series of thirty I-V and P-V characteristics obtained using the eight module partial shading simulation model from Chapter 3. The first 10 of these characteristics are from 25 March 2010 for case 1 with one obstacle in the environment. Characteristics 11-20 are from case 2 with two obstacles in the environment and are taken from 23 July 2010. Characteristics 21-25 come from 24 May 2010 in Case 3 with only cell degradation. Characteristics 26-30 are from case 4, where constant partial shading is combined with two obstacles in the environment. These characteristics come from 5 April 2010. Characteristic 1 to Characteristic 30 are shown in Appendix D.

For each characteristic, a software based model is run in MATLAB which will perform the SA GMPPT method with given parameters. For each change in parameter, 100 simulations of the technique is applied on each characteristic to provide a reliable perspective of the effect that each parameter has on the ability of the method to converge to the GMPP quickly and accurately. Prior to each simulation, the random number seed is shuffled to ensure there is no preference for any of the characteristics based on the random number seed.

The parameters representing the base case are those presented in Chapter 5. For reference, the base case uses the geometric cooling schedule with initial temperature of 25°C, final temperature of 0.2°C, temperature update constant of 0.8 and cooling occurred every 4 steps of the algorithm. The neighbourhood size was 14 to 144 V. The implementation considered in this chapter has the same parameters, but the temperature update now occurs every 5 samples. This slightly increases the number of samples required in each iteration of the technique using the base parameters.

In each case the voltage and power at the final operating point is compared with the known GMPP voltage and power and an error value is given for each variable. These provide an indication of how well the method has converged to the GMPP. The number of cases where a worse value has been accepted based on the acceptance probability and the number of samples taken in each case are recorded. The random sample points and the points that the algorithm returns to are recorded for each test case and can be used to identify the point where the technique has converged to the neighbourhood of the GMPP and does not accept any voltages that cause a reduction in the power associated with the reference voltage.

The method is considered to have converged to the neighbourhood of the GMPP if the absolute value of the voltage error is less than 5 V, and the absolute value of the power error is less than 5% of the GMPP power.

6.1 Initial temperature

The initial temperature is varied from 10°C to 25°C in steps of 1°C to assess the effect this has on the performance of the SA GMPPT method.

The average error across the 100 test cases for each temperature and characterstic in the voltage and power at the final operating point compared with the GMPP voltage and power is given in Appendix E Table E.1 and Table E.2 respectively.

The number of cases that converge for each characteristic and for each starting temperature tested is given in Table 6.1. This is shown graphically in Fig. 6.1. From inspection of Fig. 6.1 it can be seen that for each temperature a high number of the cases considered converge. There is no definite improvement in the convergence rate for increasing of the starting temperature. Note that increasing the starting temperature increase the number of samples required by the algorithm, so a smaller starting temperature is desirable.

Fig. 6.2 shows the percentage of case that converge against the starting temperature where the series are grouped based on the number of MPPs observed in each characteristic. It can be seen that for all characteristics the convergence rate with all tested temperatures is greater than 85%. There is also a general trend that shows that the characteristics with fewer MPPs have a higher convergence across all tested starting temperatures.

These results show no obvious trend in improving the convergence to the GMPP by increasing the starting temperature. Figure 6.3 shows the number of samples required at each starting temperature and the average convergence to the GMPP for each starting temperature. It can be clearly seen that as the starting temperature is increased from 10°C to 25°C the number of samples required increases from 90 to 110. The average convergence as the starting temperature is increased from 10°C to 25°C, remains bounded between 94.7 and 96.4. There is no obvious trend suggesting that, on average, the convergence will improve with increasing starting temperature.

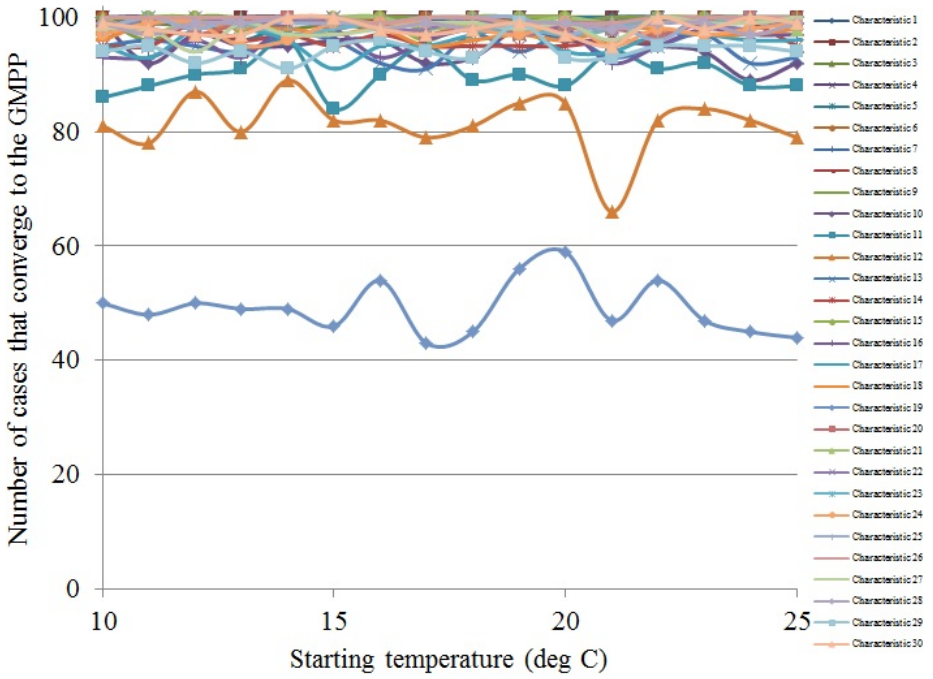

Figure 6.1: Number of cases that converge with increasing starting temperature.

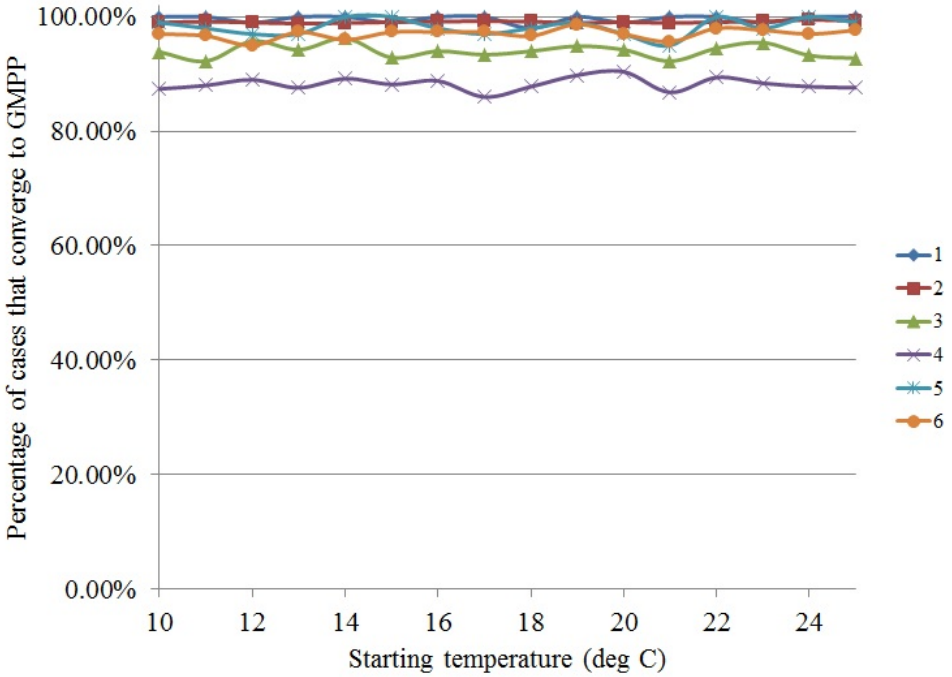

Figure 6.2: Percentage of cases that converge with increasing starting temperature for a particular number of MPPs.

Table 6.1: Number of cases where the final operating point has converged to the GMPP for variations of the starting temperature.

	10	**11**	**12**	**13**	**14**	**15**	**16**	**17**	**18**	**19**	**20**	**21**	**22**	**23**	**24**	**25**
Characteristic 1	100	100	99	100	100	99	100	100	98	100	99	100	100	99	100	100
Characteristic 2	100	99	99	100	100	99	100	100	100	100	100	100	100	100	100	100
Characteristic 3	100	99	99	100	98	99	98	100	99	100	100	100	99	100	99	100
Characteristic 4	100	100	98	100	99	100	99	100	99	100	100	100	100	99	100	98
Characteristic 5	98	99	99	96	99	99	100	100	99	100	100	100	100	99	100	99
Characteristic 6	100	100	100	99	100	98	100	100	100	100	100	99	100	99	100	100
Characteristic 7	100	100	100	100	100	99	99	100	99	99	99	100	99	100	100	99
Characteristic 8	100	100	100	100	100	99	100	100	100	100	100	99	100	100	100	100
Characteristic 9	100	96	100	100	100	100	100	100	100	99	99	100	100	100	100	99
Characteristic 10	99	92	97	95	95	96	96	92	93	98	96	96	95	94	89	92
Characteristic 11	86	88	90	91	96	84	90	95	89	90	88	94	91	92	88	88
Characteristic 12	81	78	87	80	89	82	82	79	81	85	85	66	82	84	82	79
Characteristic 13	95	96	95	94	97	96	92	91	97	94	97	93	95	97	92	93
Characteristic 14	95	95	99	96	97	95	97	95	95	95	95	96	96	100	99	95
Characteristic 15	98	100	100	98	100	100	100	96	100	100	100	98	100	100	100	99
Characteristic 16	93	93	96	93	99	98	93	96	98	97	98	92	95	98	97	97
Characteristic 17	95	93	98	98	96	91	95	95	97	98	94	94	97	97	96	96
Characteristic 18	96	99	99	98	98	97	98	95	96	97	96	98	98	97	97	98
Characteristic 19	50	48	50	49	49	46	54	43	45	56	59	47	54	47	45	44
Characteristic 20	98	98	97	99	100	99	99	97	99	97	98	98	97	99	100	99
Characteristic 21	100	97	100	99	100	100	100	98	99	99	100	99	100	99	100	98
Characteristic 22	99	99	100	99	99	100	98	98	100	97	99	99	100	99	98	100
Characteristic 23	98	100	99	99	97	98	99	99	98	98	97	98	100	99	100	99
Characteristic 24	97	99	99	95	96	99	99	99	98	97	99	95	98	97	98	99
Characteristic 25	98	100	98	100	99	99	99	100	100	100	97	99	96	100	99	100
Characteristic 26	100	100	100	100	100	100	99	100	100	99	99	99	100	100	100	100
Characteristic 27	98	98	94	99	97	97	98	99	99	98	99	96	100	99	99	100
Characteristic 28	99	97	99	99	100	100	98	99	98	99	99	98	99	99	97	99
Characteristic 29	94	95	92	94	91	95	96	94	93	99	93	93	95	95	95	94
Characteristic 30	99	98	97	97	100	100	98	97	98	99	97	95	100	98	100	99

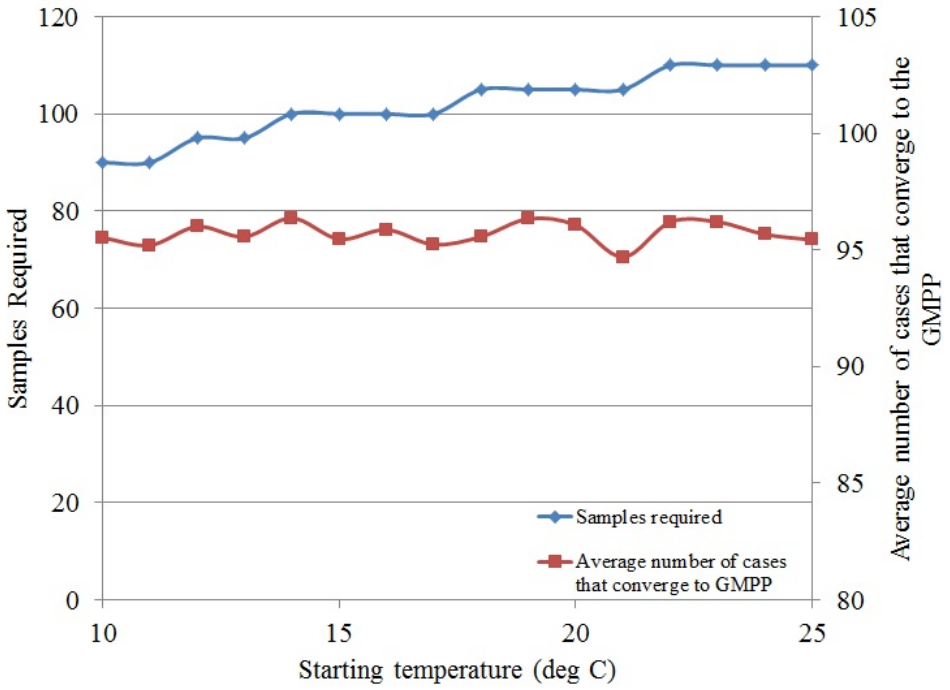

Figure 6.3: Samples required (blue) and average convergence to the GMPP (red) with increasing starting temperature.

The starting temperature, within the bounds considered in this section, has a very limited effect on improving the algorithm performance in converging to the GMPP.

6.2 Cooling rate

The cooling rate (α_2) is varied from 0.45 to 0.95 in steps of 0.05. The average error across the 100 test cases for each cooling rate and characteristic in the voltage and power at the final operating point compared with the GMPP voltage and power is given in Appendix E Table E.3 and Table E.4 respectively. The number of cases where the method converges to the GMPP is for each characteristic and cooling rate is given in Table 6.2.

The number of cases where the final operating points has converged to the GMPP against variations in the cooling rate, α_2 is shown in Fig. 6.4. It can be clearly seen that the number of cases where the algorithm converges to the GMPP for each characteristic increases towards 100% as the cooling rate increases. The only case where the convergence does not approach 100% is for

Table 6.2: Number of cases where the final operating point has converged to the GMPP for variations of the cooling rate.

	0.45	**0.5**	**0.55**	**0.6**	**0.65**	**0.7**	**0.75**	**0.8**	**0.85**	**0.9**	**0.95**
Characteristic 1	91	92	97	95	95	96	100	100	100	100	100
Characteristic 2	93	90	95	98	98	99	100	100	100	100	100
Characteristic 3	80	90	95	91	94	97	97	100	100	100	100
Characteristic 4	84	91	92	94	97	99	99	99	100	100	100
Characteristic 5	87	87	93	91	97	99	100	100	100	100	100
Characteristic 6	87	94	93	99	99	96	98	100	100	100	100
Characteristic 7	89	89	91	93	97	99	99	100	100	100	100
Characteristic 8	93	94	95	96	100	99	100	100	100	100	100
Characteristic 9	85	90	94	96	98	100	99	100	100	100	100
Characteristic 10	67	71	80	76	91	91	91	92	99	100	100
Characteristic 11	77	59	79	78	80	89	85	93	91	100	99
Characteristic 12	72	54	66	63	68	72	77	80	86	94	99
Characteristic 13	80	77	87	86	85	89	95	97	93	100	100
Characteristic 14	73	77	86	82	85	89	92	97	95	99	100
Characteristic 15	89	80	91	95	91	96	94	99	100	100	100
Characteristic 16	76	83	78	88	92	84	93	93	99	100	100
Characteristic 17	75	77	85	89	91	90	93	96	97	98	100
Characteristic 18	78	76	83	86	89	91	95	94	98	99	100
Characteristic 19	37	34	42	46	42	52	47	44	50	54	47
Characteristic 20	80	80	88	86	86	96	94	96	100	100	100
Characteristic 21	88	86	93	92	94	96	97	99	100	100	100
Characteristic 22	88	80	93	92	92	95	96	100	100	100	100
Characteristic 23	89	81	88	92	92	94	96	98	99	99	100
Characteristic 24	80	75	89	92	91	92	94	100	100	99	100
Characteristic 25	84	75	91	93	94	97	96	97	99	100	100
Characteristic 26	86	87	94	92	98	98	99	100	100	100	100
Characteristic 27	80	70	88	90	86	91	93	97	100	100	100
Characteristic 28	80	84	89	86	96	93	97	100	100	100	100
Characteristic 29	63	65	78	79	83	86	87	95	97	100	100
Characteristic 30	86	69	76	88	92	91	94	95	99	100	100

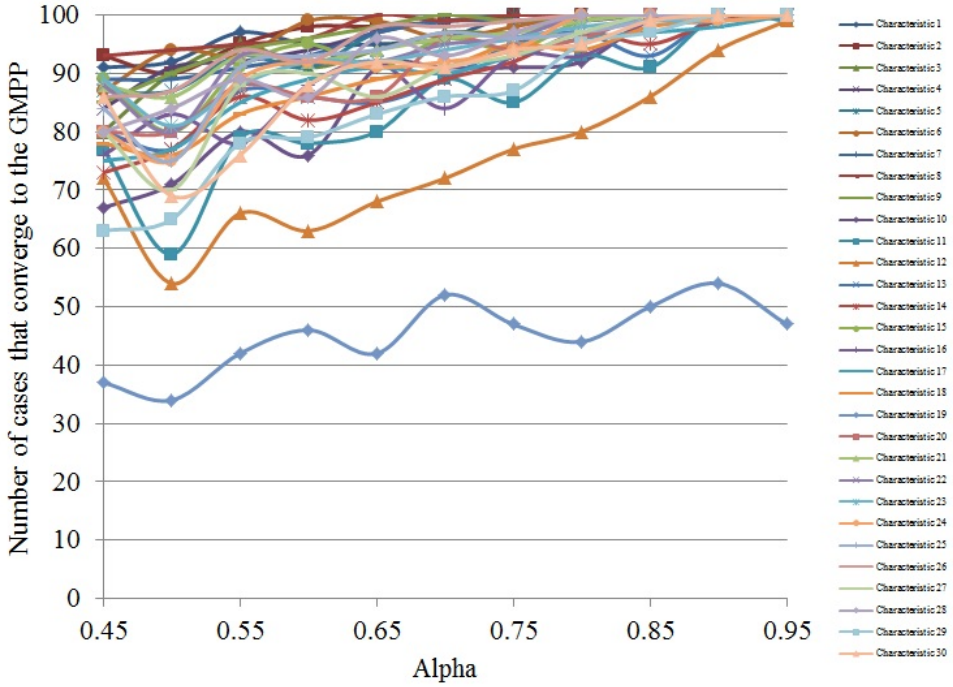

Figure 6.4: Number of cases that converge with increasing cooling rate.

characteristic 19. Characteristic 19 is shown in Fig. 6.5. This clearly shows that for this characteristic there are two MPPs with a similar power which could be the GMPP. The two peaks that resemble the GMPP for characteristic 19 have maximum power 66.25 W and 66.10 W, respectively. This provides a difference of 0.15 W which is small enough to be the result of an error in the resolution of the measurement.

The trends exhibited support the literature in showing that the most appropriate cooling rates, to ensure a sufficient level of convergence, are between 0.8 and 0.99 [233, 236–238, 246, 255–257] as this ensures convergence to the GMPP in over 90% of the cases for 28 of the 30 characteristics. This would require 110 or more samples with the current set of parameters.

When grouped against the number of MPPs observed in the characteristic, Fig. 6.6 shows the percentage of cases for each cooling rate that converge to the GMPP. The general trend that can be observed from this is that for a characteristic with fewer MPPs, a smaller cooling value can be used to still achieve a high percentage of convergence. As the number of MPPs increases, the cooling rate required to ensure a high percentage of convergence also increases. The outlier for four MPPs arises due to characteristic 19, where, as already

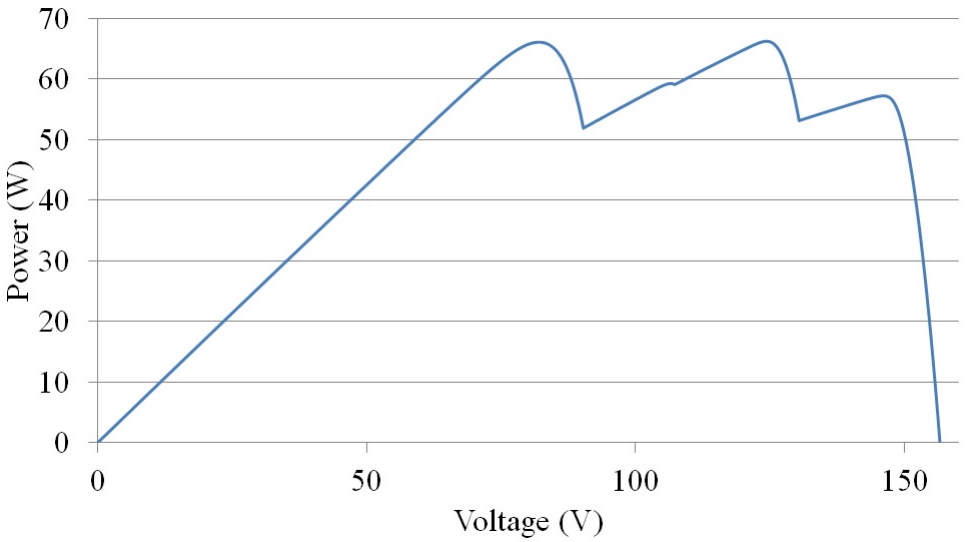

Figure 6.5: P-V curve for characteristic 19.

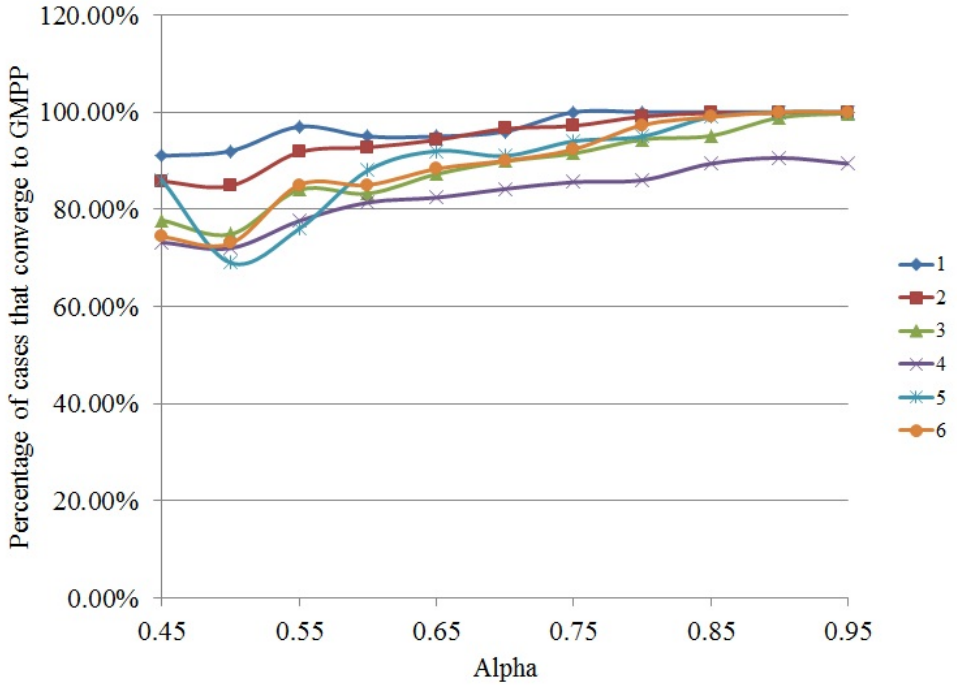

Figure 6.6: Number of cases that converge with increasing cooling rate for a particular number of MPPs.

discussed there are two MPPs with very similar power.

As the cooling rate is increased, the number of samples required by the algorithm also increases. For the lowest cooling rate of 0.45, only 35 samples are required, while for the highest cooling rate of 0.95, 475 samples are required. This suggests that a balance between the number of samples and an acceptable level of convergence needs to be established. Fig. 6.7 shows how the number of samples

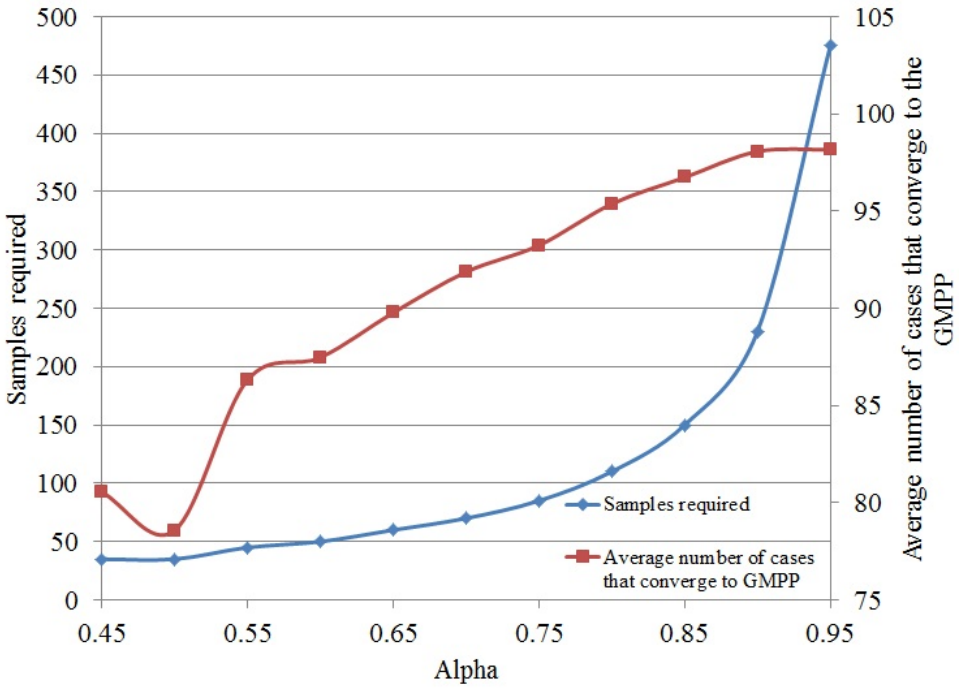

Figure 6.7: Samples required (blue) and average convergence to the GMPP (red) with increasing cooling rate.

varies with the cooling rate and the average number of cases that converged to the GMPP for each cooling rate.

In general, as the cooling rate of the geometric cooling schedule is increased, the convergence of the algorithm improves and the number of iterations required by the technique also increases dramatically. This suggests that this parameter should only be varied slightly so as not to extend the search time required significantly.

6.3 Cooling frequency

The cooling frequency represents the number of iterations that the technique performs at each temperature before the temperature update is applied. To assess the effect this has on the performance of the SA algorithm, the cooling frequency is varied from 2 to 11 in steps of 1. The average error in voltage and in power across the 100 test cases for each cooling frequency and characteristic are given in Appendix E Table E.5 and Table E.6, respectively. The number of cases where the method converges to the GMPP for each characteristic and

cooling frequency is given in Table 6.3.

The number of cases that converge for each characteristic at each cooling frequency is shown in Fig. 6.8. As with variations in the cooling rate, characteristic 19 exhibits poorer convergence across all cooling frequencies. By inspection of Table E.5 and Table E.6, it can be seen that for characteristic 19, a large average voltage error is observed across all cooling frequencies, yet a very small average power error is observed. This suggests that the method will converge to either of the two very similarly valued MPPs and while this appears as though the method has not converged exactly, it is still supplying a considerable amount of power. When grouped against the number of MPPs observed in each characteristic, Fig. 6.9 shows the percentage of cases for each cooling frequency that converge to the GMPP. This shows a convergence of more than 80% for each cooling frequency. The general trend observed is that increasing the cooling frequency increases the percentage of cases that converge to the GMPP. This however is also accompanied by an increase in the number of samples required. The increase in the number of samples needed for each cooling frequency is shown in Fig. 6.10 and exhibits a linear increase. Also shown in Fig. 6.10 is the average number of cases that converge to the GMPP for each cooling frequency. Like variations of the cooling rate, increasing the cooling frequency can improve the convergence to the GMPP, however also leads to a larger number of samples being required.

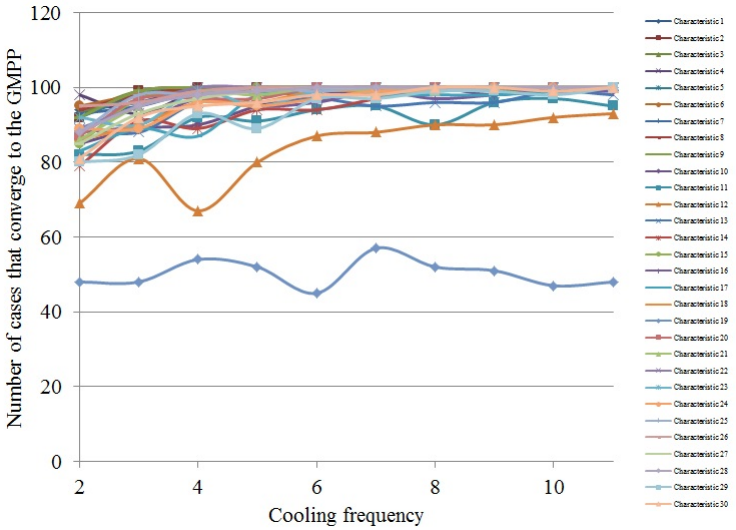

Figure 6.8: Number of cases that converge with increasing cooling frequency for each characteristic.

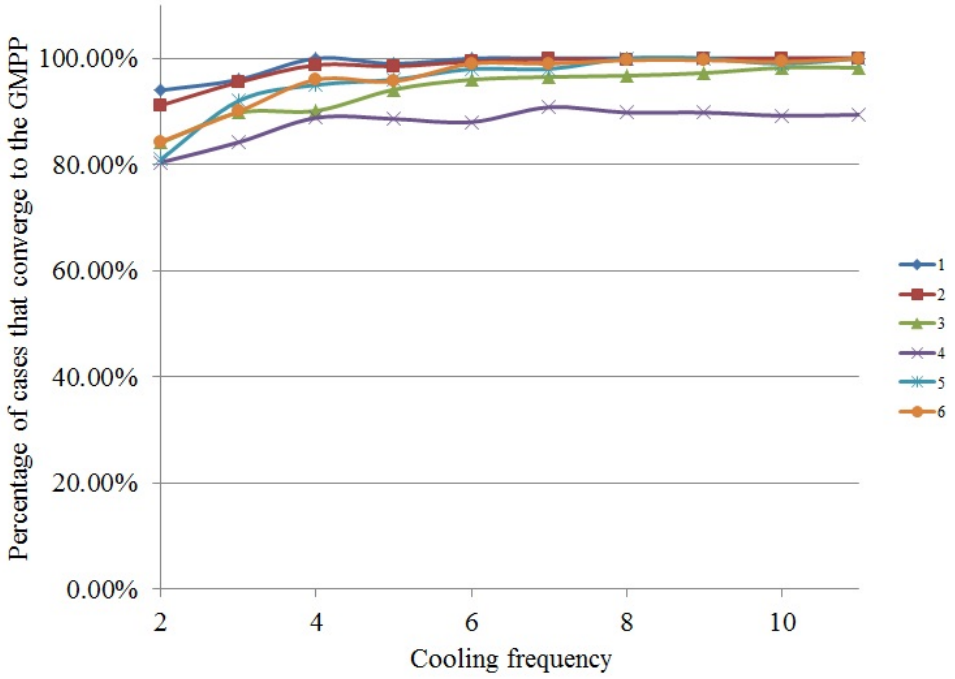

Figure 6.9: Percentage of cases that converge with increasing cooling frequency for a particular number of MPPs.

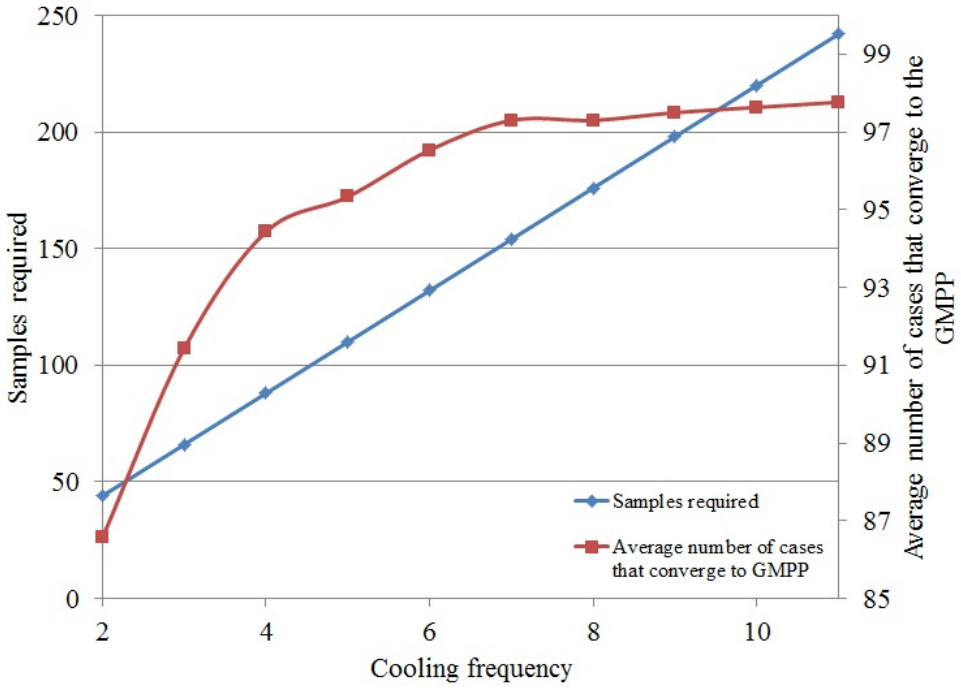

Figure 6.10: Samples required (blue) and average convergence to the GMPP (red) with increasing cooling frequency.

Table 6.3: Number of cases where the final operating point has converged to the GMPP for variations of the cooling frequency.

	2	**3**	**4**	**5**	**6**	**7**	**8**	**9**	**10**	**11**
Characteristic 1	94	96	100	99	100	100	100	100	100	100
Characteristic 2	92	99	100	100	100	100	100	100	100	100
Characteristic 3	93	99	99	100	100	100	100	99	100	100
Characteristic 4	98	93	99	100	100	100	100	100	100	100
Characteristic 5	92	98	100	98	100	100	100	100	100	100
Characteristic 6	95	98	99	99	98	100	100	100	100	100
Characteristic 7	93	95	99	100	100	100	100	100	100	100
Characteristic 8	94	98	100	100	100	100	100	100	100	100
Characteristic 9	92	99	100	100	100	100	100	100	100	100
Characteristic 10	85	89	90	95	98	99	100	98	100	100
Characteristic 11	82	83	92	91	94	95	90	96	97	95
Characteristic 12	69	81	67	80	87	88	90	90	92	93
Characteristic 13	89	88	96	95	97	95	96	96	99	98
Characteristic 14	79	91	89	94	94	97	100	100	99	100
Characteristic 15	85	97	98	100	100	99	100	100	100	100
Characteristic 16	88	90	97	95	96	99	97	98	99	99
Characteristic 17	83	89	87	98	98	98	98	98	99	100
Characteristic 18	86	90	96	96	99	99	100	100	100	100
Characteristic 19	48	48	54	52	45	57	52	51	47	48
Characteristic 20	87	97	97	97	100	100	100	100	100	100
Characteristic 21	86	95	99	98	100	99	99	100	100	100
Characteristic 22	89	95	100	100	100	100	100	100	100	100
Characteristic 23	92	90	99	95	99	100	99	100	100	100
Characteristic 24	89	89	96	95	97	99	99	100	100	100
Characteristic 25	88	98	98	100	99	100	100	100	100	100
Characteristic 26	95	96	99	100	100	100	100	100	100	100
Characteristic 27	85	93	97	99	100	100	100	100	100	100
Characteristic 28	88	95	98	99	100	100	100	100	100	100
Characteristic 29	80	82	93	89	97	97	99	99	98	100
Characteristic 30	81	92	95	96	98	98	100	100	99	100

6.4 Acceptance probability threshold

The acceptance probability threshold is varied from 0.05 to 0.5 in steps of 0.05. The average error in voltage and in power across the 100 test cases for each acceptance probability threshold and characteristic are given in Appendix E Table E.7 and Table E.8, respectively. The percentage of cases where the method converges to the GMPP for each characteristic and each acceptance probability threshold is given in Table 6.4.

The percentage of cases that converge for each characteristic at each acceptance probability threshold is shown in Fig. 6.11. Characteristic 19 again shows a lower convergence than the other cases due to converging to one of the two similar power MPPs. All other characteristics exhibit a convergence of greater than 80% for all acceptance probability thresholds considered. The general trend observed is an increase in the number of cases that converge as the acceptance probability threshold increases.

When grouped against the number of MPPs observed in each characteristic, Fig. 6.12 shows the percentage of cases for each acceptance probability threshold that converge to the GMPP. This shows a general increase in the percentage of cases that converge as the acceptance probability threshold increases. In all cases, the

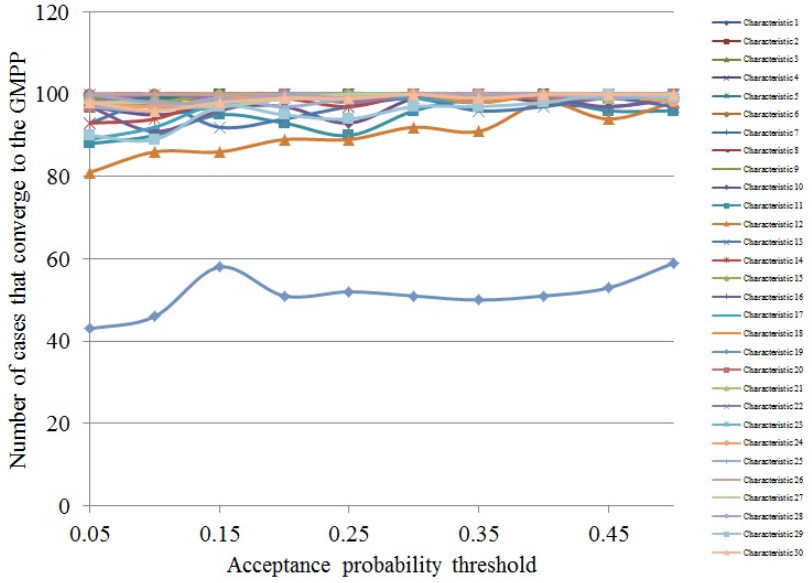

Figure 6.11: Number of cases that converge with increasing acceptance probability threshold for each characteristic.

Table 6.4: Number of cases where the final operating point has converged to the GMPP for variations of the acceptance probability threshold.

	0.05	**0.1**	**0.15**	**0.2**	**0.25**	**0.3**	**0.35**	**0.4**	**0.45**	**0.5**
Characteristic 1	98	100	100	100	100	100	100	100	100	100
Characteristic 2	99	98	100	100	100	100	100	100	100	100
Characteristic 3	97	100	98	100	100	100	100	100	100	100
Characteristic 4	100	99	100	99	100	100	100	99	100	100
Characteristic 5	99	99	100	100	100	100	100	100	100	100
Characteristic 6	100	100	99	100	100	100	100	100	100	100
Characteristic 7	100	100	99	100	100	100	100	100	100	100
Characteristic 8	99	100	100	100	100	100	100	100	100	100
Characteristic 9	99	100	100	100	100	100	100	100	100	100
Characteristic 10	97	95	97	97	93	99	100	98	97	99
Characteristic 11	88	90	95	93	90	96	99	99	96	96
Characteristic 12	81	86	86	89	89	92	91	98	94	98
Characteristic 13	93	98	92	94	97	99	96	97	99	97
Characteristic 14	93	94	99	99	97	100	99	100	100	98
Characteristic 15	98	98	100	100	100	100	100	99	100	100
Characteristic 16	97	91	96	99	99	99	99	99	97	99
Characteristic 17	89	92	98	99	99	99	98	100	100	99
Characteristic 18	98	97	99	100	99	100	98	100	100	100
Characteristic 19	43	46	58	51	52	51	50	51	53	59
Characteristic 20	97	97	97	100	99	100	100	99	99	100
Characteristic 21	100	100	100	99	100	100	100	100	99	100
Characteristic 22	98	100	99	100	98	100	100	100	100	100
Characteristic 23	98	97	97	100	100	100	100	100	100	100
Characteristic 24	98	97	99	99	99	100	100	100	100	98
Characteristic 25	97	96	99	97	99	100	100	100	99	100
Characteristic 26	100	100	100	100	100	100	100	100	100	100
Characteristic 27	98	98	97	99	100	100	99	100	100	100
Characteristic 28	100	98	98	100	99	100	100	100	100	99
Characteristic 29	90	89	97	95	94	97	97	98	100	99
Characteristic 30	98	96	98	99	99	100	99	100	100	100

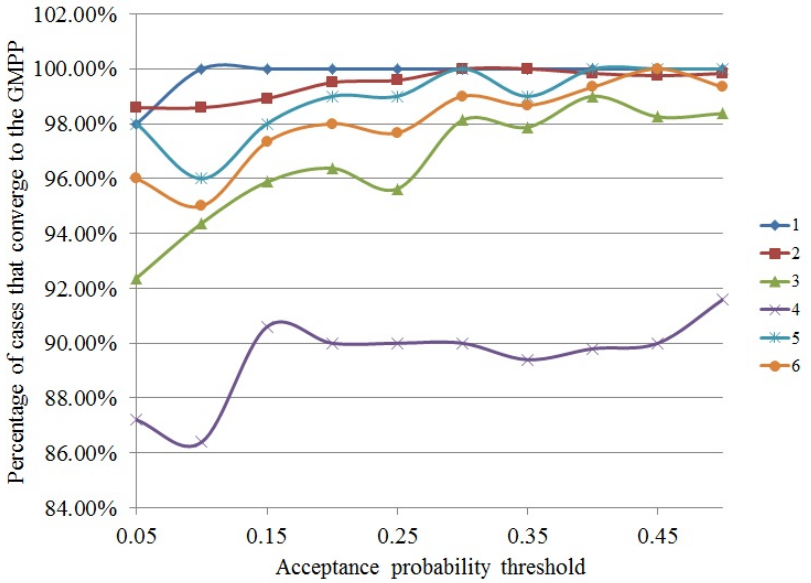

Figure 6.12: Percentage of cases that converge with increasing acceptance probability threshold for a particular number of MPPs.

percentage of cases that converge is greater than 86%.

Figure 6.13 shows how the average number of worse operating points accepted for each acceptance probability threshold and each characteristic varies. This shows that as the acceptance probability threshold increases, the likelihood of a worse operating point being selected as the reference operating point reduces. Interestingly, the characteristic which corresponds to the highest average accepted values across all of the acceptance probability thresholds is the case where there are two MPPs of similar power (Characteristic 19).

The number of samples required remains constant with the increasing acceptance probability threshold. The number of samples required is shown with the average number of cases that converge to the GMPP for the acceptance probability threshold in Fig. 6.14. This shows that, on average, as the acceptance probability threshold increases the convergence improves. This may be because the method accepts fewer worse points as the acceptance probability threshold increases.

Increasing the acceptance probability threshold has a small effect on improving the number of cases that converge without causing a change in the number of samples required.

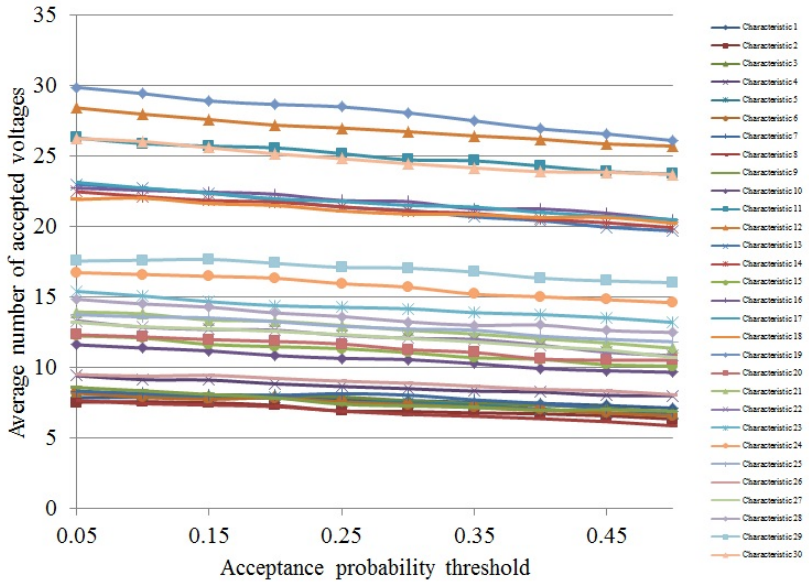

Figure 6.13: Average number of accepted worse operating points against acceptance probability threshold for each characteristic.

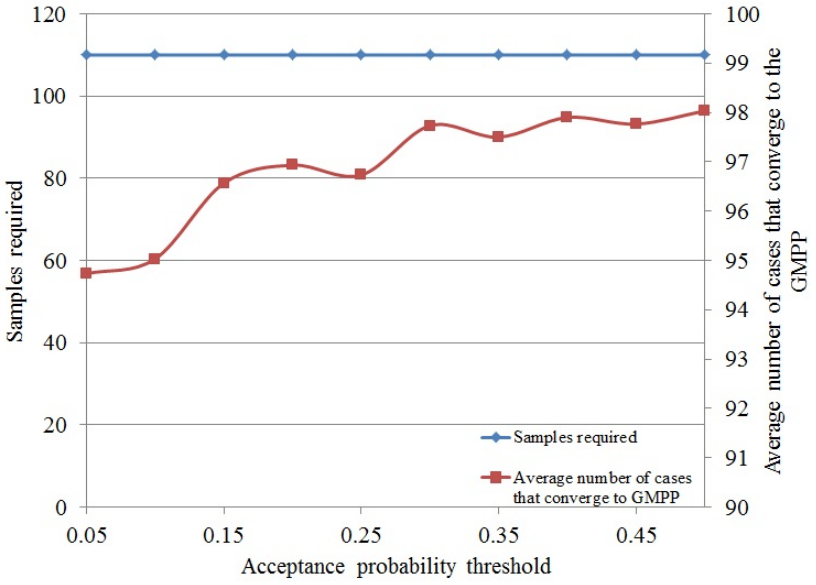

Figure 6.14: Samples required (blue) and average convergence to the GMPP (red) with increasing acceptance probability threshold.

6.5 Neighbourhood size

It is supported in the literature [232, 235, 262], the neighbourhood size can have a significant effect upon the performance of the SA algorithm. To ensure good performance the neighbourhood must be sufficiently small to enable the algorithm to converge in a small time frame, yet it must be large enough to be diverse so that the algorithm can escape from a local maxima. Two studies are considered in this section. In the first study, the neighbourhood size is

kept constant for the entire searching process and neighbourhood sizes ranging from 130 V to 10 V are considered. For the second study, the neighbourhood size is able to be dynamically varied as the temperature reduces. This means that the neighbourhood size can be reduced as the temperature decreases. In both studies, the best operating point is considered to be at the centre of the neighbourhood range, unless this leads to one of the bounds being outside the maximal range. This is shown in Fig. 6.15.

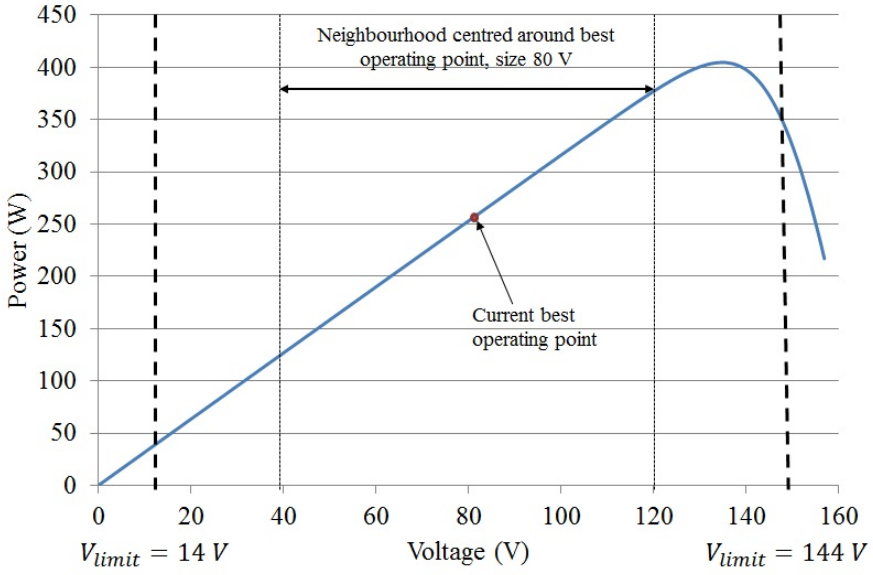

(a) Neighbourhood centred around operating point.

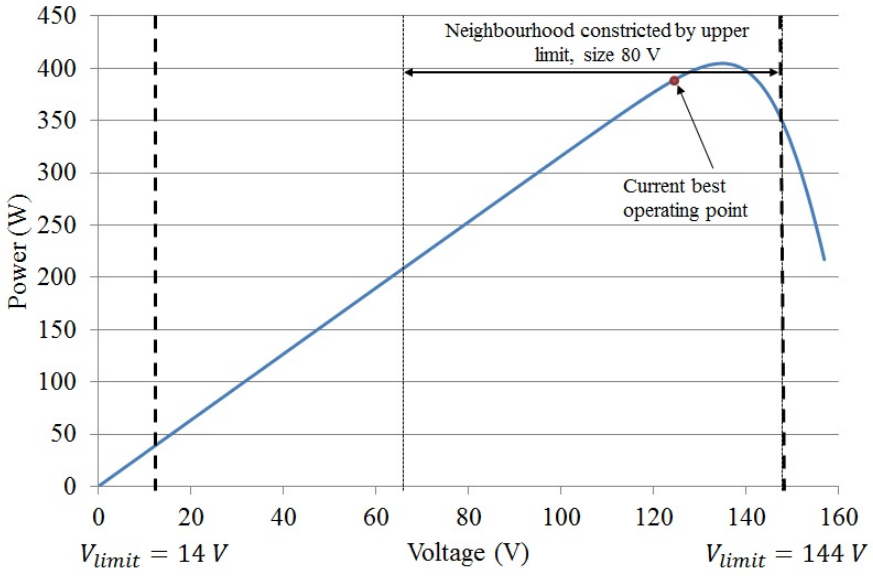

(b) Neighbourhood not centred as limited by upper voltage bound.

Figure 6.15: Neighbourhood configuration for 80 V neighbourhood size on uniform P-V characteristic.

6.5.1 Constant neighbourhood size

The neighbourhood size is held constant for each 100 iterations of the SA method. Each implementation has a different neighbourhood size which varies from 10 to 130 V in steps of 10 V. The average error in voltage and in power across the 100 test cases for each neighbourhood size are given in Appendix E Table E.9 and Table E.10, respectively. The number of cases where the method converges to the GMPP for each characteristic and each neighbourhood size is given in Table 6.5.

The number of cases that converge for each characteristic at each neighbourhood size is shown in Fig. 6.16. At very low neighbourhood sizes such as 10 V, as shown in Fig. 6.16, the number of cases that converge is very poor. As the neighbourhood size increases, the number of cases that converge generally increases. The only cases where this does not occur is for characteristic 19 and characteristic 29. Characteristic 19 has already been discussed and its limitation identified that there are two peaks with very similar MPP power. Characteristic 29 improves its performance once the neighbourhood size increases to over 80 V.

Figure 6.17 shows the average number of cases that converge across all characteristics for each neighbourhood size and the number of samples required. It can be seen that when the performance across all characteristics is averaged, as long as the neighbourhood size is 30 V or greater, the algorithm will successfully converge in more than 90% of the cases. The number of samples required will remain constant.

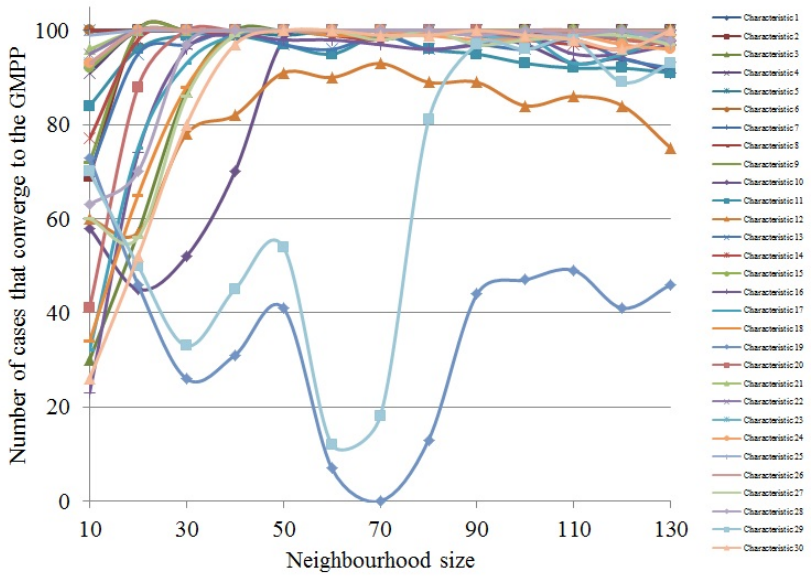

Figure 6.16: Number of cases that converge with increasing neighbourhood size for each characteristic.

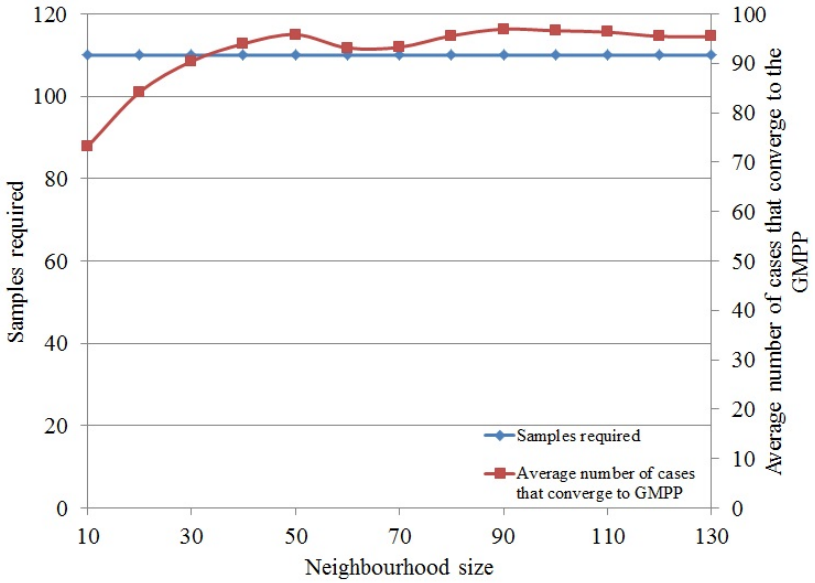

Figure 6.17: Samples required (blue) and average convergence to the GMPP (red) with increasing neighbourhood size.

Table 6.5: Number of cases where the final operating point has converged to the GMPP for variations of the neighbourhood size.

	130	**120**	**110**	**100**	**90**	**80**	**70**	**60**	**50**	**40**	**30**	**20**	**10**
Characteristic 1	100	100	100	100	100	100	100	100	100	100	100	100	100
Characteristic 2	100	100	100	100	100	100	100	100	100	100	100	100	69
Characteristic 3	100	99	99	100	100	100	100	100	100	100	87	57	30
Characteristic 4	99	100	99	100	100	100	100	100	100	100	100	100	91
Characteristic 5	100	100	100	100	100	100	100	100	99	100	100	100	100
Characteristic 6	100	99	99	100	100	100	100	100	100	100	100	100	100
Characteristic 7	100	100	100	100	100	100	100	100	100	100	100	100	100
Characteristic 8	100	100	100	99	100	100	100	100	100	100	100	100	100
Characteristic 9	100	100	100	100	100	100	100	100	100	100	100	100	72
Characteristic 10	91	94	93	97	99	100	98	99	98	70	52	45	58
Characteristic 11	91	92	92	93	95	96	99	95	97	99	99	96	84
Characteristic 12	75	84	86	84	89	89	93	90	91	82	78	57	60
Characteristic 13	92	94	98	96	97	96	99	96	97	100	97	95	70
Characteristic 14	98	96	97	98	99	100	98	99	100	99	100	98	77
Characteristic 15	99	100	100	100	100	100	100	100	100	100	100	100	92
Characteristic 16	97	95	95	99	97	96	97	98	98	99	96	74	23
Characteristic 17	99	95	93	99	100	99	100	99	100	99	93	75	32
Characteristic 18	99	98	100	100	99	100	99	99	100	99	88	65	34
Characteristic 19	46	41	49	47	44	13	0	7	41	31	26	46	73
Characteristic 20	97	98	99	98	100	100	100	100	100	100	100	88	41
Characteristic 21	100	99	100	100	100	100	100	100	100	100	100	100	96
Characteristic 22	99	100	100	100	99	100	100	100	100	100	100	100	95
Characteristic 23	100	99	99	98	99	100	100	100	100	100	100	100	93
Characteristic 24	96	97	99	98	98	99	100	100	100	100	100	100	93
Characteristic 25	97	100	99	99	100	100	100	100	100	100	100	100	99
Characteristic 26	100	100	100	100	100	100	100	100	100	100	100	100	93
Characteristic 27	97	99	99	98	97	100	98	100	100	99	86	56	60
Characteristic 28	98	100	99	100	99	100	100	100	100	100	97	70	63
Characteristic 29	93	89	98	96	97	81	18	12	54	45	33	50	70
Characteristic 30	100	96	98	99	100	99	99	100	100	97	80	52	26

6.5.2 Varying neighbourhood size

To assess the effect of varying the neighbourhood size as the temperature reduces, three different neighbourhood size variation functions are used. The first is a linear function, where the neighbourhood size decreases linearly in size at each temperature update, as shown in Fig. 6.18. This is shown against the temperature in Fig. 6.19, exhibiting a logarithmic relationship with the temperature. The second is a quadratic function related to the temperature update as shown in Fig. 6.20. This is shown against the temperature in Fig. 6.21, where a logarithm relationship of best fit is indicated with coefficient of determination 0.9869. The third is an exponential function as shown in Fig. 6.22. This is shown against the temperature in Fig. 6.23, and exhibits a power relationship against the temperature.

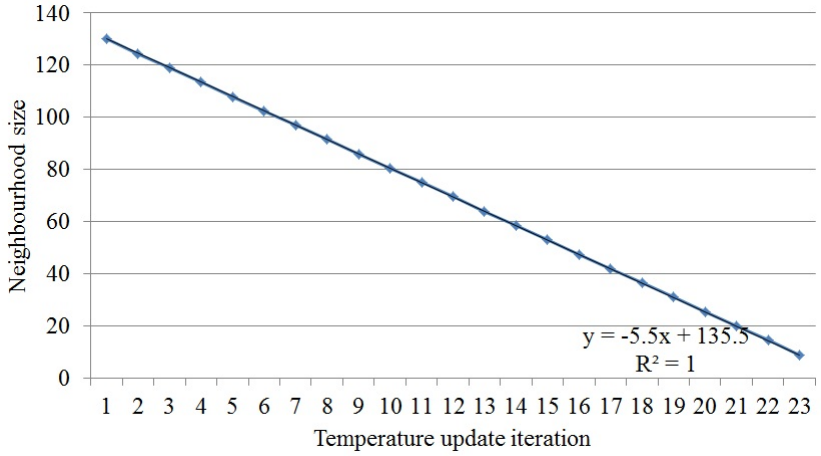

Figure 6.18: Variation of neighbourhood size against temperature iteration for a linear reduction scheme.

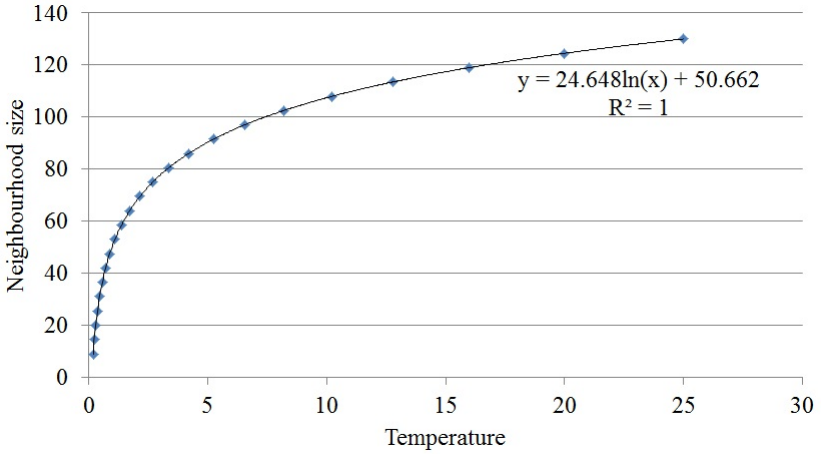

Figure 6.19: Variation of the neighbourhood size against the temperature for a linear reduction scheme.

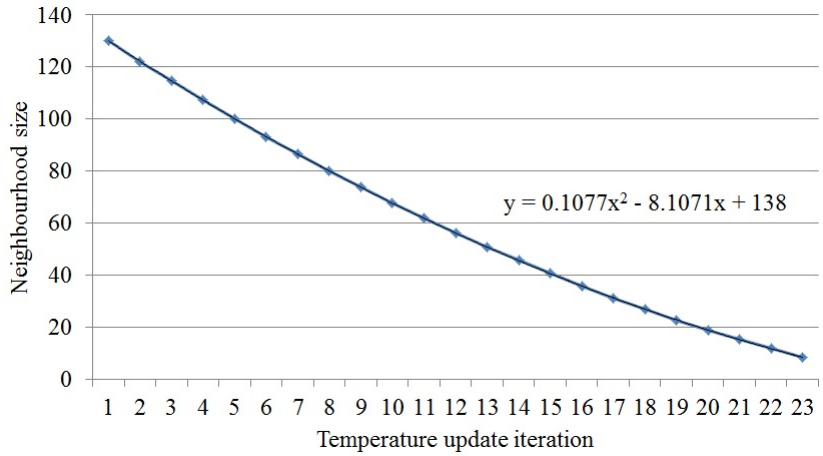

Figure 6.20: Variation of neighbourhood size against temperature iteration for a quadratic reduction scheme.

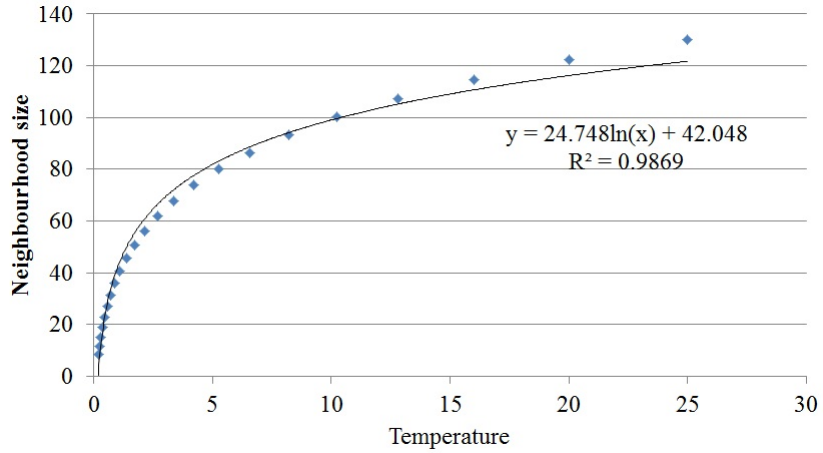

Figure 6.21: Variation of the neighbourhood size against the temperature for a quadratic reduction scheme.

The average error in voltage and in power across the 100 test cases for each neighbourhood reduction function are given in Appendix E Table E.11 and Table E.12, respectively. The number of cases that converge to the GMPP for each characteristic and each neighbourhood size reduction function is given in Table 6.6.

The number of cases that converge for each characteristic and each neighbourhood reduction function are shown in Fig. 6.24. It can be seen that across all characteristics the linear and quadratic cooling schedules exhibits similar performance and the exponential cooling schedule has the worst performance. There are four characteristics where the linear cooling schedule does not achieve a high level of convergence to the GMPP. These are Characteristic 10, Characteristic 12, Characteristic 19 and Characteristic 29. By increasing the neighbourhood

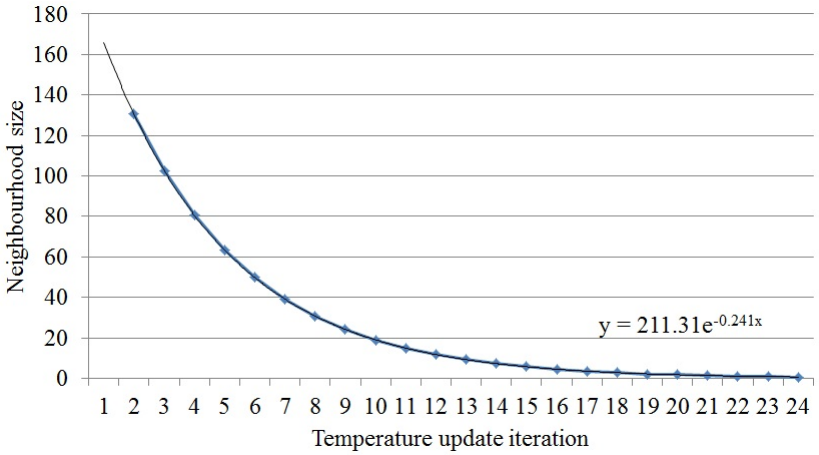

Figure 6.22: Variation of neighbourhood size against temperature iteration for an exponential reduction scheme.

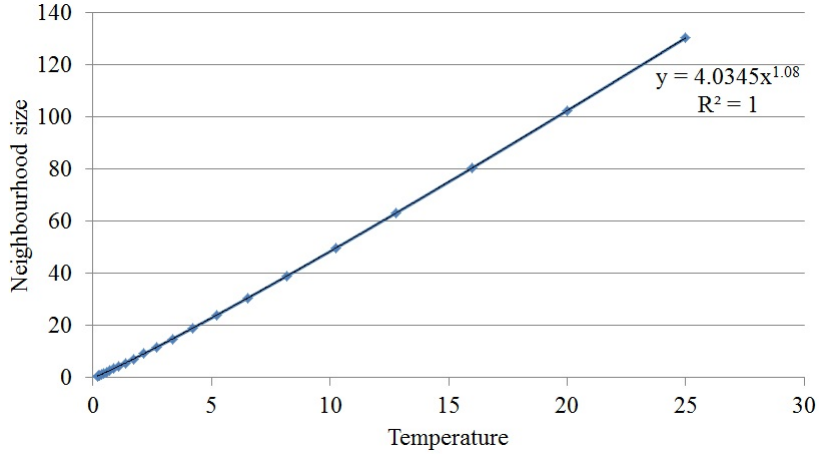

Figure 6.23: Variation of the neighbourhood size against the temperature for an exponential reduction scheme.

size at the final operating point (currently the neighbourhood size is 10 V), the performance may improve on these characteristics.

The number of samples required in each implementation remains at 110. The average number of cases that converge across the 30 characteristics with the linear neighbourhood reduction function is 93.7%, with the quadratic neighbourhood reduction function is 92.9% and with the exponential neighbourhood reduction function is 50.7%. This suggests that using a suitably defined linear neighbourhood reduction function could improve the performance of the SA method.

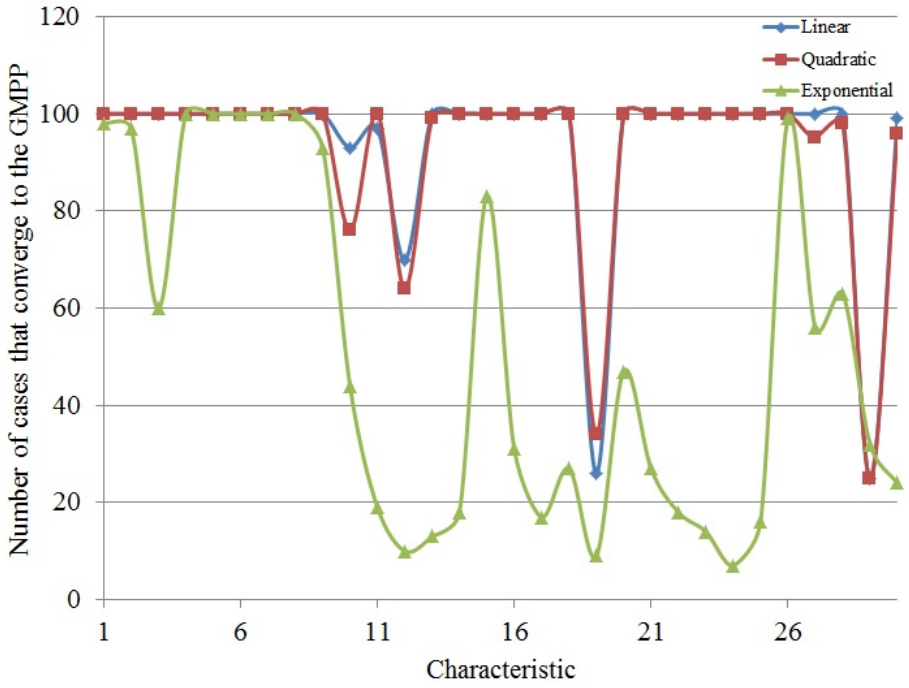

Figure 6.24: Number of cases that converge to the GMPP for different neighbourhood reduction functions for each characteristic.

6.6 Stopping temperature

The stopping temperature is varied from 0.1°C to 1.0°C in steps of 0.1°C while all other parameters are held constant to see how this effects the algorithm performance. The average error in voltage and in power across the 100 test cases for each stopping temperature are given in Appendix E Table E.13 and Table E.14, respectively. The number of cases where the method converges to the GMPP for each characteristic and each stopping temperature is given in Table 6.7.

The number of cases that converge for each characteristic at each stopping temperature is shown in Fig. 6.25. The general trend observed is that when the stopping temperature increases the algorithm converges in fewer cases. This can be related to the number of samples for the changing temperature. When fewer samples are taken the method converges in fewer cases.

The number of samples related to the stopping temperature is given in Fig. 6.26. The average number of cases that converge for each stopping temperature is also shown in Fig. 6.26. This suggests that a small stopping temperature which leads

Table 6.6: Number of cases that converge to the final operating point for different neighbourhood reduction functions.

	Linear	**Quadratic**	**Exponential**
Characteristic 1	100	100	98
Characteristic 2	100	100	97
Characteristic 3	100	100	60
Characteristic 4	100	100	100
Characteristic 5	100	100	100
Characteristic 6	100	100	100
Characteristic 7	100	100	100
Characteristic 8	100	100	100
Characteristic 9	100	100	93
Characteristic 10	93	76	44
Characteristic 11	97	100	19
Characteristic 12	70	64	10
Characteristic 13	100	99	13
Characteristic 14	100	100	18
Characteristic 15	100	100	83
Characteristic 16	100	100	31
Characteristic 17	100	100	17
Characteristic 18	100	100	27
Characteristic 19	26	34	9
Characteristic 20	100	100	47
Characteristic 21	100	100	27
Characteristic 22	100	100	18
Characteristic 23	100	100	14
Characteristic 24	100	100	7
Characteristic 25	100	100	16
Characteristic 26	100	100	99
Characteristic 27	100	95	56
Characteristic 28	100	98	63
Characteristic 29	25	25	32
Characteristic 30	99	96	24

Table 6.7: Number of cases where the final operating point has converged to the GMPP for variations of the stopping temperature.

	0.1	**0.2**	**0.3**	**0.4**	**0.5**	**0.6**	**0.7**	**0.8**	**0.9**	**1**
Characteristic 1	98	100	100	99	96	98	92	98	96	96
Characteristic 2	100	100	100	100	100	100	99	98	98	97
Characteristic 3	100	100	100	99	96	98	97	95	94	97
Characteristic 4	100	100	99	99	97	98	97	94	94	94
Characteristic 5	100	100	100	99	100	98	99	93	92	98
Characteristic 6	99	99	100	99	98	99	100	95	96	88
Characteristic 7	99	100	100	98	97	97	97	95	94	92
Characteristic 8	100	100	99	98	99	100	100	97	92	98
Characteristic 9	99	100	100	98	100	99	99	98	92	92
Characteristic 10	98	91	89	95	81	88	84	81	70	84
Characteristic 11	95	87	77	83	67	57	63	60	68	58
Characteristic 12	96	74	66	59	49	40	34	44	29	26
Characteristic 13	100	94	91	79	84	83	69	69	67	68
Characteristic 14	100	96	93	86	84	83	78	74	69	64
Characteristic 15	99	99	98	98	97	93	94	93	91	83
Characteristic 16	98	97	96	86	84	75	84	81	80	76
Characteristic 17	100	89	92	90	90	91	82	70	70	74
Characteristic 18	99	91	93	92	90	88	78	79	78	74
Characteristic 19	46	47	39	50	46	39	43	34	33	34
Characteristic 20	96	100	99	97	95	90	88	83	85	84
Characteristic 21	100	98	98	95	97	90	93	92	82	85
Characteristic 22	98	99	97	95	96	92	91	88	84	88
Characteristic 23	99	97	97	91	91	91	86	90	80	82
Characteristic 24	100	98	95	93	98	90	84	83	82	81
Characteristic 25	100	100	97	95	96	91	91	95	84	83
Characteristic 26	100	100	99	98	99	95	96	93	95	91
Characteristic 27	98	100	95	92	94	93	86	83	80	83
Characteristic 28	100	100	99	94	100	92	99	89	89	87
Characteristic 29	96	91	91	86	85	80	76	79	78	73
Characteristic 30	100	96	94	89	95	82	87	87	82	71

to an increase in the number of samples required, improves the convergence of the algorithm. The extra samples required as the stopping temperature reduces is much smaller in number than those needed for other parameter variations such as the cooling rate.

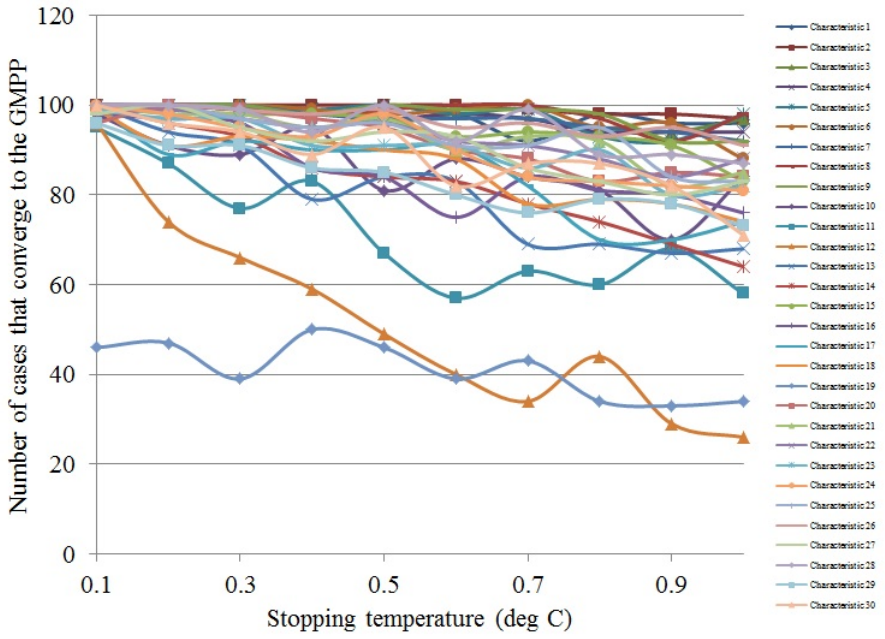

Figure 6.25: Number of cases that converge with increasing stopping temperature for each characteristic.

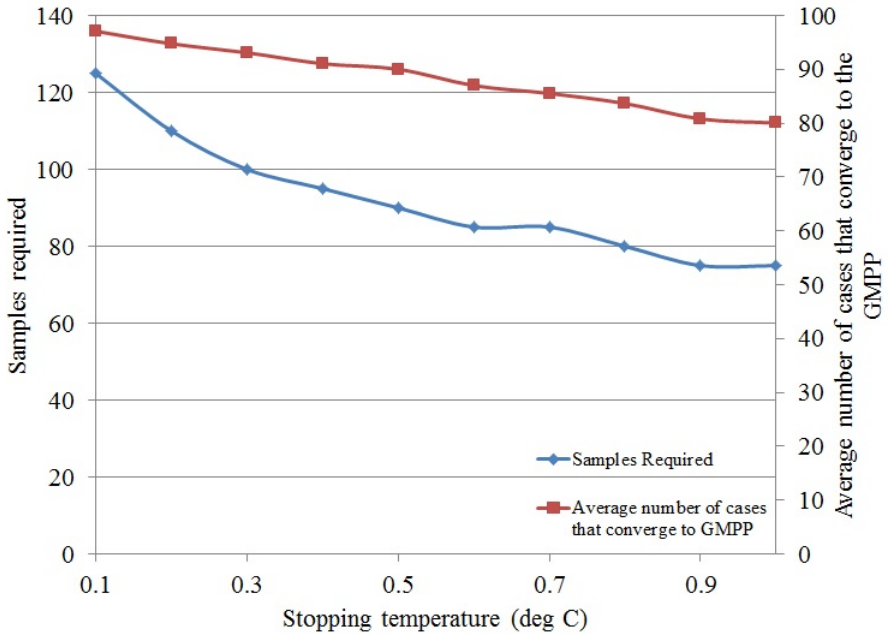

Figure 6.26: Samples required (blue) and average convergence to the GMPP (red) with increasing stopping temperature.

6.7 Cooling function

In this section four different cooling schedules are considered. These are the linear cooling schedule, logarithmic schedule, Lundy cooling schedule and Simulated Quenching (SQ).

6.7.1 Linear cooling schedule

The linear cooling schedule is applied in this section with different values of the cooling constant c_l. Linear cooling is expressed using (6.1), with an initial temperature of 25°C. The temperature is updated after each new sample is considered, and cooling constants of 0.1 to 0.4 in steps of 0.1 are considered.

$$T(k) = T(0) - c_l k \tag{6.1}$$

where, $T(0)$ is the initial temperature (25°C in this implementation), c_l is the cooling constant, and k represents the number of samples considered.

The average error in voltage and in power across the 100 test cases for each linear cooling schedule applied are given in Appendix E Table E.15 and Table E.16, respectively. The number of cases where the method converges to the GMPP for each characteristic and each linear cooling schedule constant is given in Table 6.8.

The number of cases that converge for each characteristic and each linear cooling schedule constant are shown in Fig. 6.27. The number of samples required and the average number of cases that converge to the GMPP for increasing linear cooling schedule constant are shown in Fig. 6.28. It can be seen that as the linear cooling constant increases, the number of samples required rapidly decreases and the average convergence to the GMPP also decreases.

Across the 30 characteristics, the linear cooling schedule has very different results. For instance, with $c_l = 0.1$, convergence to the GMPP ranges from 40% to 100% and remains spread over a large range as c_l increases. This unreliable performance suggests that the linear cooling schedule is not suitable for this application.

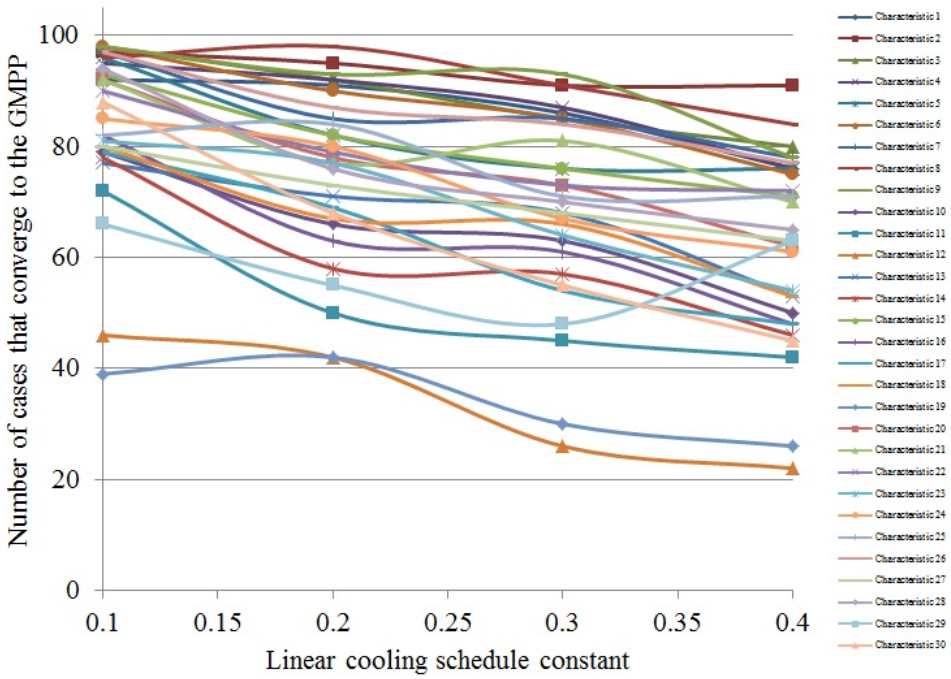

Figure 6.27: Number of cases that converge with increasing linear cooling schedule constant for each characteristic.

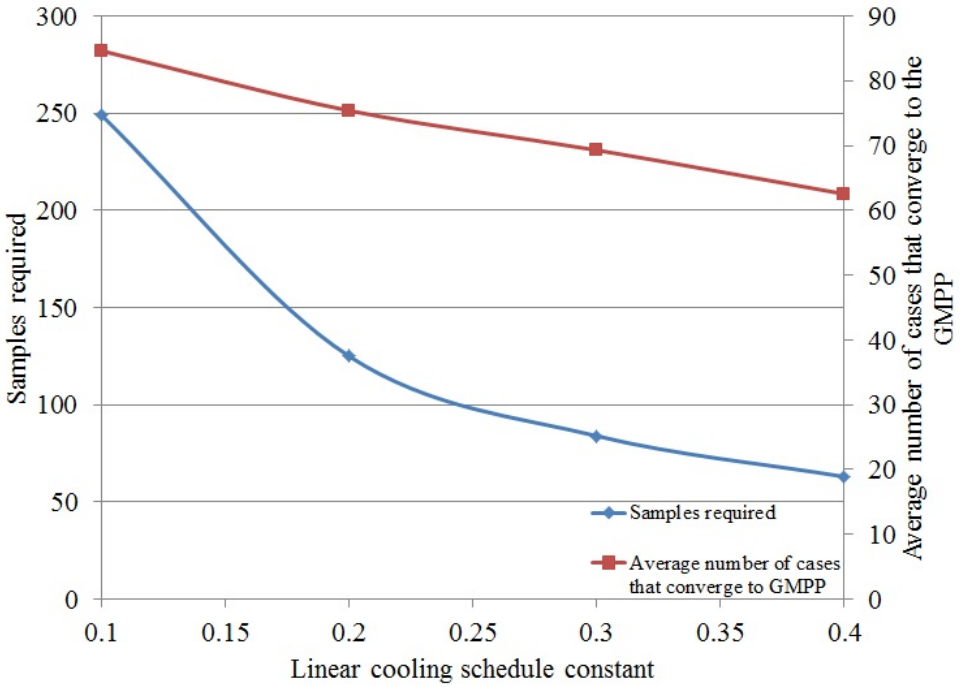

Figure 6.28: Samples required (blue) and average convergence to the GMPP (red) with increasing linear cooling schedule constant.

Table 6.8: Number of cases where the final operating point has converged to the GMPP for variations of the linear cooling schedule constant.

	0.1	**0.2**	**0.3**	**0.4**
Characteristic 1	92	91	86	76
Characteristic 2	97	95	91	91
Characteristic 3	98	92	85	80
Characteristic 4	95	92	87	76
Characteristic 5	96	82	76	76
Characteristic 6	98	90	85	75
Characteristic 7	97	85	85	78
Characteristic 8	96	98	91	84
Characteristic 9	98	93	93	78
Characteristic 10	79	66	63	50
Characteristic 11	72	50	45	42
Characteristic 12	46	42	26	22
Characteristic 13	77	71	68	53
Characteristic 14	78	58	57	46
Characteristic 15	93	82	76	71
Characteristic 16	82	63	61	48
Characteristic 17	79	69	54	48
Characteristic 18	80	67	66	53
Characteristic 19	39	42	30	26
Characteristic 20	92	78	73	62
Characteristic 21	92	77	81	70
Characteristic 22	90	79	73	72
Characteristic 23	81	77	64	54
Characteristic 24	85	80	67	61
Characteristic 25	82	84	71	71
Characteristic 26	97	87	84	77
Characteristic 27	80	73	68	63
Characteristic 28	94	76	70	65
Characteristic 29	66	55	48	63
Characteristic 30	88	68	55	45

6.7.2 Logarithmic cooling schedule

The logarithmic cooling schedule is applied with various values for the constant c to assess how this effects the performance of the SA GMPPT method. Logarithmic cooling is expressed with the relationship

$$T(k) = \frac{c}{\log(k+1)} \tag{6.2}$$

where the constant c should be greater than d^*, that is $c > d^*$ to ensure convergence. The value of d^* indicates the maximum depth of all states which are local but not global minima in the traditional definition of the SA method.

The implementation considered uses a constant c that ranges from 10 to 50 in steps of 10. As the constant is increased, the number of iterations required by the technique to reduce to a low temperature increases, so the method is restricted to only perform 200 iterations for each constant. The logarithmic cooling schedule is shown in Fig. 6.29, where the cooling with 8000 iterations is shown for comparison with the 200 iterations that the method is limited to in this implementation. From Fig. 6.29, it can be seen that by about iteration 100, all temperatures for each cooling constant c exhibit very little change from one iteration to the next.

The average error in voltage and in power across the 100 test cases for each logarithmic cooling schedule constant and characteristic are given in Appendix E Table E.17 and Table E.18, respectively. The number of cases where the method converges to the GMPP for each characteristic and each logarithmic cooling schedule constant is given in Table 6.9. The number of cases that converge for each characteristic at each logarithmic cooling schedule constant is shown in Fig. 6.30. From Fig. 6.30, it can be seen that the algorithm performance for each characteristic reduces as the logarithmic cooling schedule constant is increased. This change in performance is most likely due to the limiting effect of only allowing 200 iterations of the technique for each implementation. As the logarithmic cooling function constant increases, the number of *worse* operating points on average that are accepted in the search process increases as shown in Fig. 6.31. The maximum accepted worse operating points for any single implementation of the algorithm was 79, or 39.5% of the sample points.

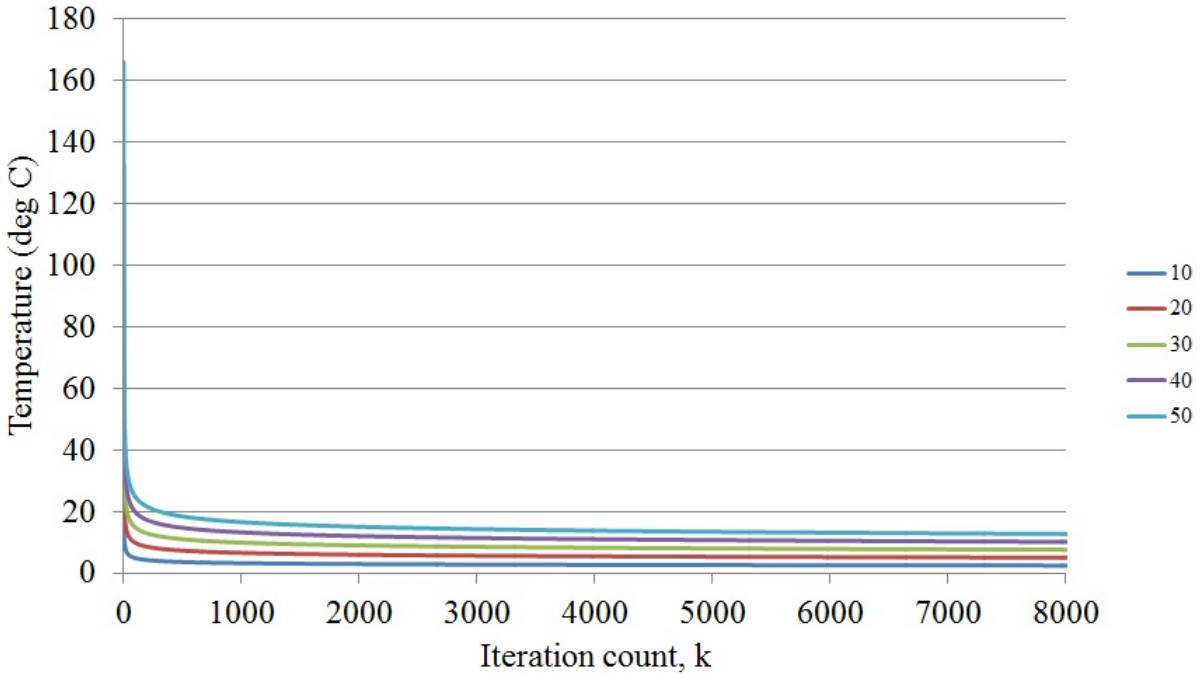

(a) Logarithmic cooling with 8000 iterations.

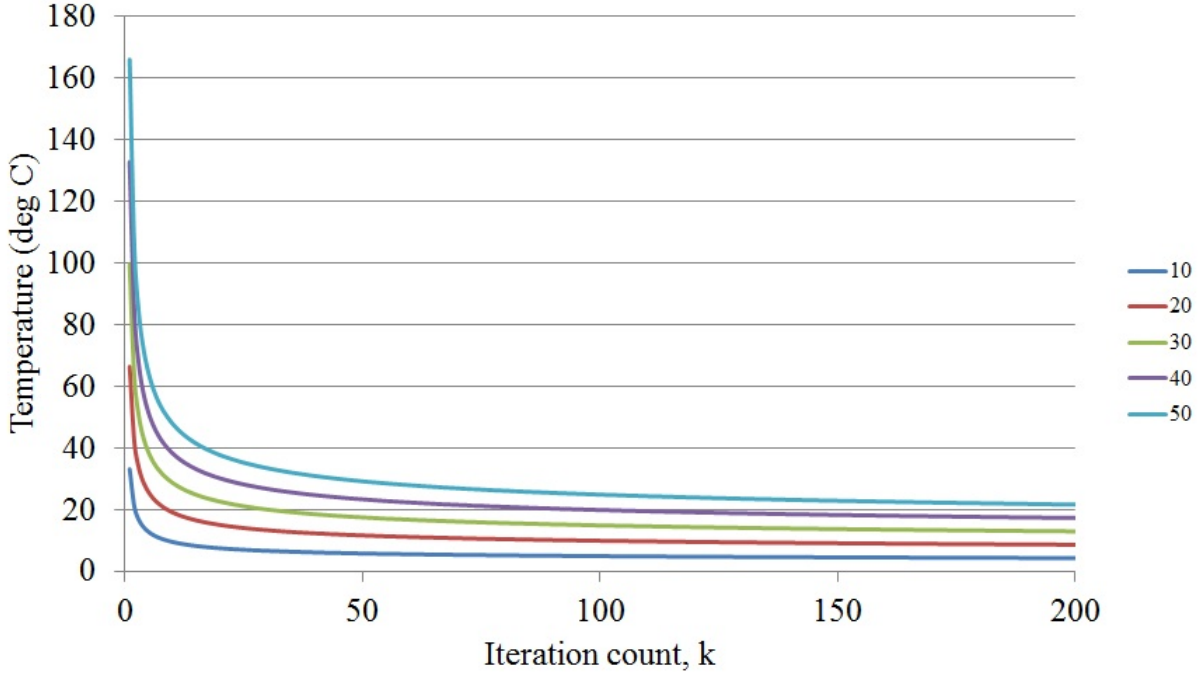

(b) Logarithmic cooling with 200 iterations.

Figure 6.29: Logarithmic cooling schedules for different constants c and different numbers of iterations.

This suggests that with the logarithmic cooling schedule, a much larger number of samples is required to lead to reliable convergence.

As with the linear cooling schedule, the performance across all characteristics is

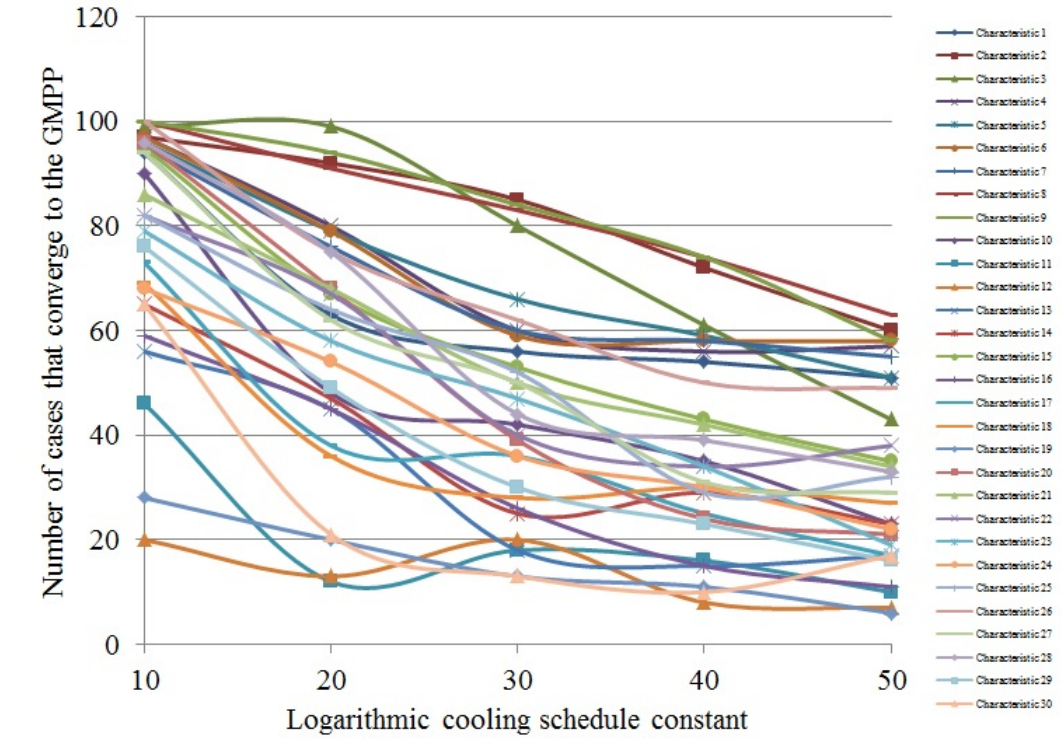

Figure 6.30: Number of cases that converge with increasing logarithmic cooling schedule constant for each characteristic.

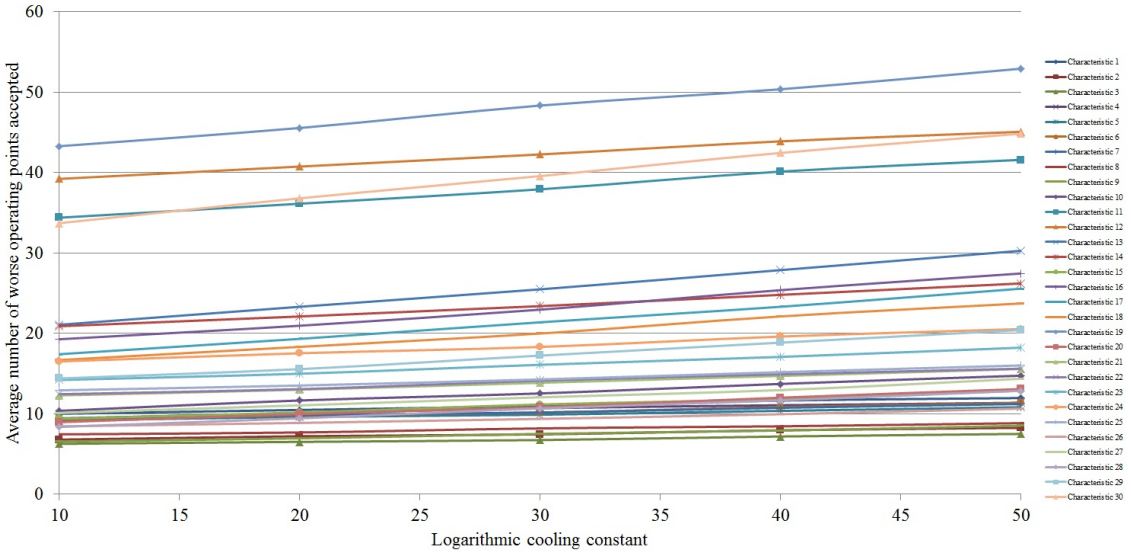

Figure 6.31: Average number of worse operating points accepted for increasing logarithmic cooling constant for each characteristic.

not very consistent. For $c = 10$, the convergence to the GMPP ranges from 20% to 100% and a wide range is observed for all other tested logarithmic cooling constants. This suggests that logarithmic cooling with the number of samples restricted, is not suitable for this application.

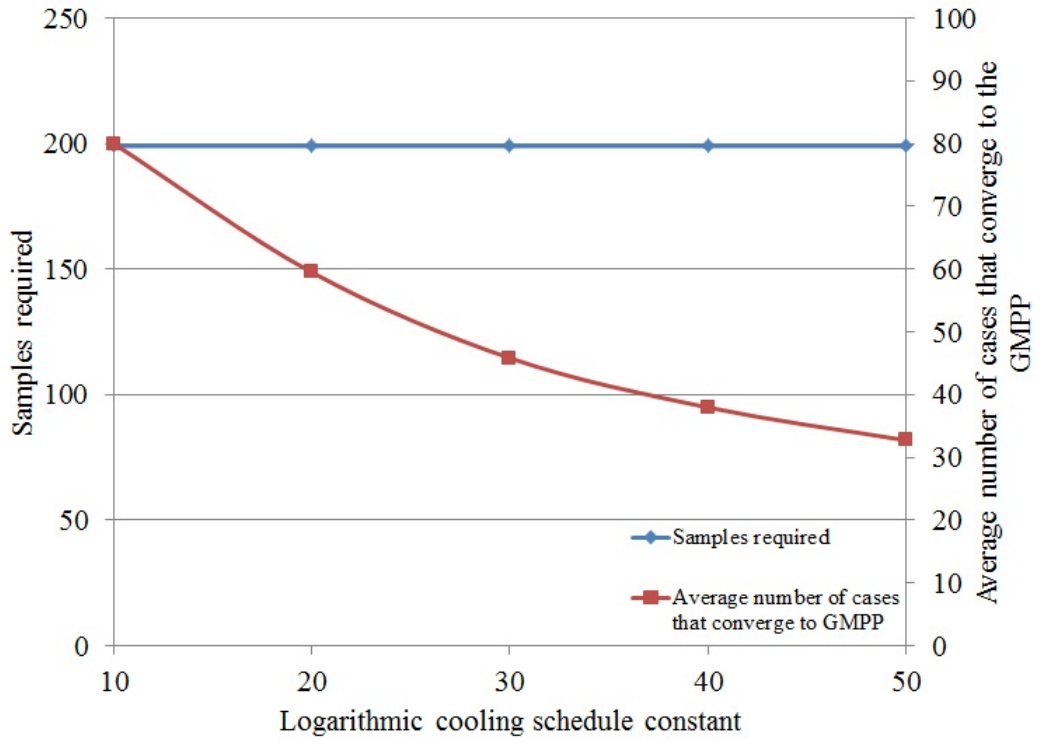

Figure 6.32: Samples required (blue) and average convergence to the GMPP (red) with increasing logarithmic cooling schedule constant.

6.7.3 Lundy cooling schedule

The Lundy cooling schedule is given in (6.3). The constant β_l is varied from 0.01 to 0.05 in steps of 0.01, and the initial temperature is 25°C.

$$T(k) = \frac{T(k-1)}{(1+\beta_l T(k-1))} \tag{6.3}$$

The average error in voltage and in power across the 100 test cases for each Lundy cooling schedule constant are given in Appendix E Table E.19 and Table E.20, respectively. The number of cases where the method converges to the GMPP for each characteristic and each Lundy cooling schedule constant is given in Table 6.10.

The number of cases that converge for each characteristic and each Lundy cooling schedule constant are shown in Fig. 6.33. As with previous cases, the number of cases that converge to the GMPP for characteristic 19 is considerably lower than for the other characteristics due to the similar MPPs in this characterstic. The performance of all other characteristics with the Lundy cooling schedule is very high across all cooling schedule constants considered. The

Table 6.9: Percentage of cases where the final operating point has converged to the GMPP for variations of the logarithmic cooling schedule constant.

	10	**20**	**30**	**40**	**50**
Characteristic 1	94	63	56	54	51
Characteristic 2	97	92	85	72	60
Characteristic 3	99	99	80	61	43
Characteristic 4	97	80	60	56	57
Characteristic 5	96	79	66	59	51
Characteristic 6	97	79	59	58	58
Characteristic 7	95	76	60	58	55
Characteristic 8	100	91	83	74	63
Characteristic 9	100	94	84	74	58
Characteristic 10	90	48	42	35	23
Characteristic 11	46	12	18	16	10
Characteristic 12	20	13	20	8	7
Characteristic 13	56	45	18	15	17
Characteristic 14	65	47	25	29	23
Characteristic 15	95	67	53	43	35
Characteristic 16	59	45	26	15	11
Characteristic 17	73	38	36	25	17
Characteristic 18	69	36	28	30	27
Characteristic 19	28	20	13	11	6
Characteristic 20	96	68	39	24	21
Characteristic 21	86	68	50	42	34
Characteristic 22	82	67	40	34	38
Characteristic 23	79	58	47	34	19
Characteristic 24	68	54	36	30	22
Characteristic 25	82	64	52	29	32
Characteristic 26	100	75	62	50	49
Characteristic 27	94	62	50	31	29
Characteristic 28	96	75	44	39	33
Characteristic 29	76	49	30	23	16
Characteristic 30	65	21	13	10	17

number of samples required and the average number of cases that converge to the GMPP for increasing Lundy cooling schedule constant are shown in Fig. 6.34.

The Lundy cooling schedule exhibits good performance with 98% convergence on average when 100 samples are considered.

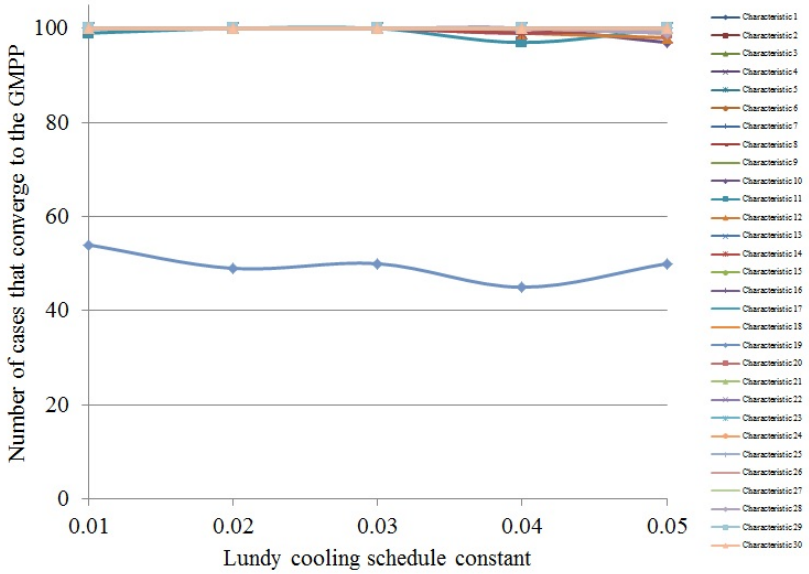

Figure 6.33: Number of cases that converge with increasing Lundy cooling schedule constant for each characteristic.

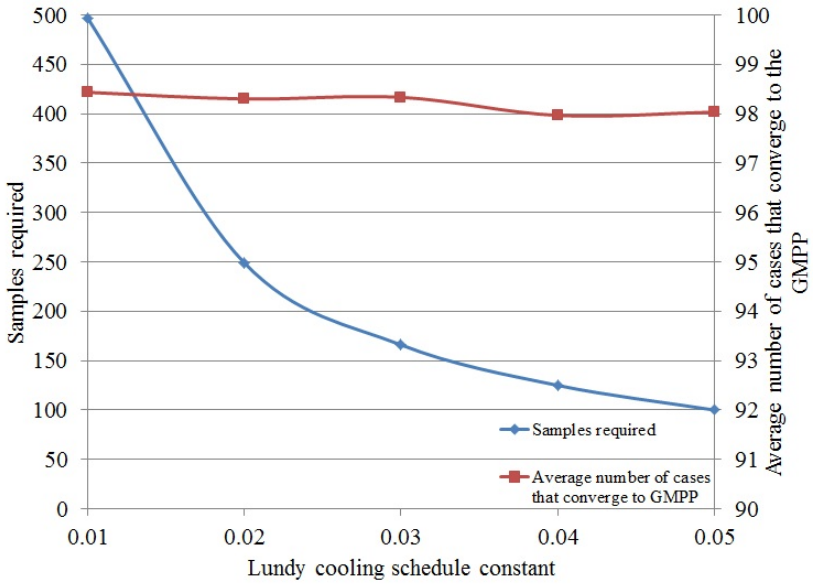

Figure 6.34: Samples required (blue) and average convergence to the GMPP (red) with increasing Lundy cooling schedule constant.

Table 6.10: Percentage of cases where the final operating point has converged to the GMPP for variations of the Lundy cooling schedule constant.

	0.01	**0.02**	**0.03**	**0.04**	**0.05**
Characteristic 1	100	100	100	100	100
Characteristic 2	100	100	100	100	100
Characteristic 3	100	100	100	100	100
Characteristic 4	100	100	100	100	100
Characteristic 5	100	100	100	100	100
Characteristic 6	100	100	100	100	100
Characteristic 7	100	100	100	100	100
Characteristic 8	100	100	100	100	100
Characteristic 9	100	100	100	100	100
Characteristic 10	100	100	100	100	97
Characteristic 11	99	100	100	97	100
Characteristic 12	100	100	100	99	98
Characteristic 13	100	100	100	99	100
Characteristic 14	100	100	100	99	100
Characteristic 15	100	100	100	100	100
Characteristic 16	100	100	100	100	100
Characteristic 17	100	100	100	100	100
Characteristic 18	100	100	100	100	100
Characteristic 19	54	49	50	45	50
Characteristic 20	100	100	100	100	99
Characteristic 21	100	100	100	100	100
Characteristic 22	100	100	100	100	100
Characteristic 23	100	100	100	100	100
Characteristic 24	100	100	100	100	100
Characteristic 25	100	100	100	100	100
Characteristic 26	100	100	100	100	99
Characteristic 27	100	100	100	100	99
Characteristic 28	100	100	100	100	99
Characteristic 29	100	100	100	100	100
Characteristic 30	100	100	100	100	100

6.7.4 Simulated Quenching

Simulated Quenching (SQ) is assessed with a rate between 0.2 and 0.8 in steps of 0.2. This uses the exponential cooling schedule given in (6.4). The temperature is updated every four iterations, where k is a count of the number of samples used by the method. The initial temperature is 25°C.

$$T(k) = \frac{T(0)}{\exp(1 - c_q)k} \tag{6.4}$$

The average error in voltage and in power across the 100 test cases for each SQ cooling constant are given in Appendix E Table E.21 and Table E.22, respectively. The number of cases where the method converges to the GMPP for each characteristic and each SQ cooling constant is given in Table 6.11.

The number of cases that converge for each characteristic and each SQ cooling constant are shown in Fig. 6.35. The number of samples required and the average number of cases that converge to the GMPP for increasing SQ cooling constant are shown in Fig. 6.36.

As the cooling constant increases, it can be seen that the number of cases that converge for each characteristic (except characteristic 19) increases. It can also be seen that as the cooling constant increases, the range of the number of cases that converge across all characteristics becomes smaller. SQ has very good performance with a small number of samples. From Fig. 6.36 an average convergence of greater than 80% is achieved with only 40 samples. As the quenching constant is increased, the average number of cases that converge approaches 100% as the number of samples increases to 90.

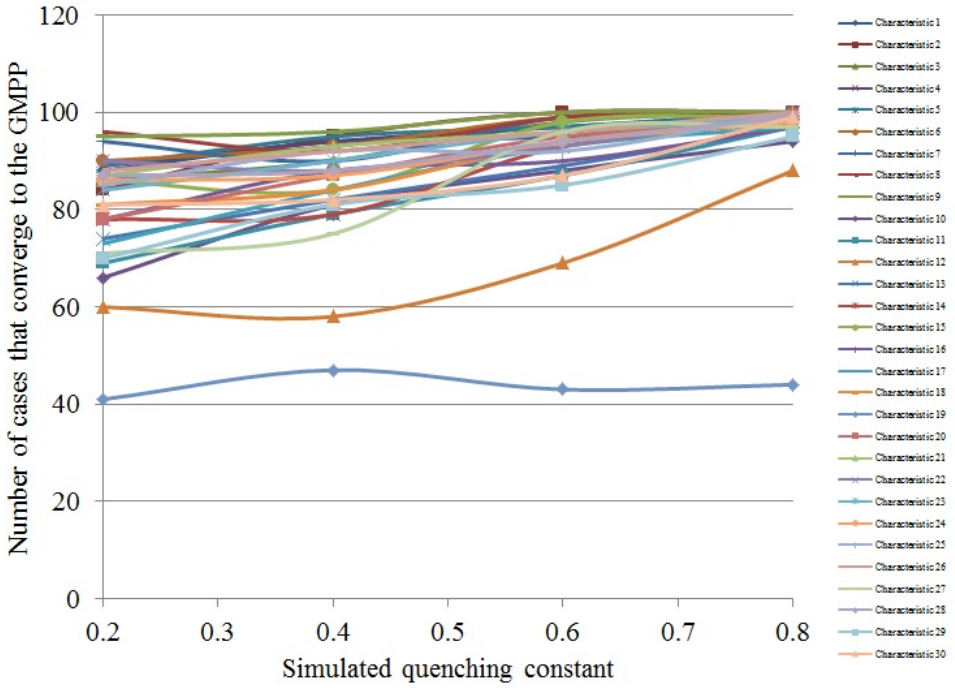

Figure 6.35: Number of cases that converge with increasing SQ schedule constant for each characteristic.

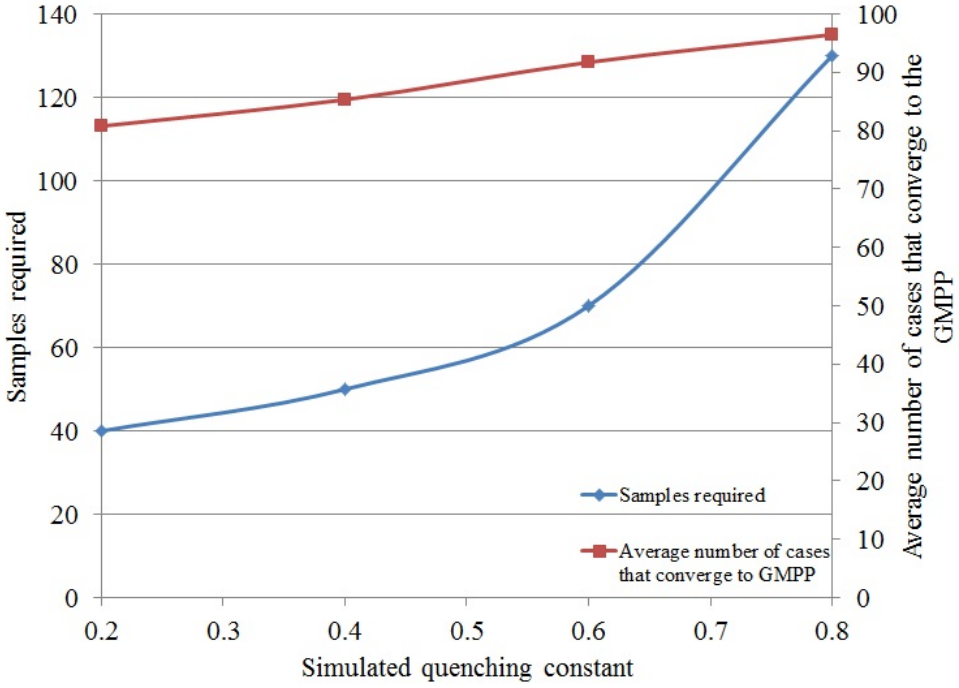

Figure 6.36: Samples required (blue) and average convergence to the GMPP (red) with increasing SQ cooling schedule constant.

Table 6.11: Percentage of cases where the final operating point has converged to the GMPP for variations of the SQ cooling schedule constant.

	0.2	**0.4**	**0.6**	**0.8**
Characteristic 1	88	94	95	99
Characteristic 2	84	95	100	100
Characteristic 3	86	90	98	100
Characteristic 4	89	94	97	100
Characteristic 5	89	95	97	100
Characteristic 6	90	93	99	100
Characteristic 7	94	90	99	100
Characteristic 8	96	92	99	100
Characteristic 9	95	96	100	100
Characteristic 10	66	81	88	94
Characteristic 11	69	79	87	97
Characteristic 12	60	58	69	88
Characteristic 13	74	82	89	97
Characteristic 14	78	79	93	98
Characteristic 15	86	84	98	99
Characteristic 16	78	88	90	97
Characteristic 17	73	84	93	97
Characteristic 18	81	84	94	99
Characteristic 19	41	47	43	44
Characteristic 20	78	87	95	99
Characteristic 21	87	93	96	99
Characteristic 22	90	88	93	100
Characteristic 23	84	90	96	99
Characteristic 24	86	87	94	98
Characteristic 25	85	92	92	100
Characteristic 26	88	92	96	100
Characteristic 27	71	75	96	97
Characteristic 28	87	88	94	99
Characteristic 29	70	81	85	95
Characteristic 30	81	82	87	99

6.8 Stopping criterion

The stopping criterion implemented involves stopping the searching process once the solution has not improved for a certain number of samples. The range used is between 2 samples with no improvement to 10 samples with no improvement. This is the stopping criterion limit.

The average error in voltage and in power across the 100 test cases for each stopping criterion are given in Appendix E Table E.23 and Table E.24, respectively. The number of cases where the method converges to the GMPP for each characteristic and each stopping criterion is given in Table 6.12.

The number of cases that converge for each characteristic and each stopping criterion limit are shown in Fig. 6.37. The average number of samples required before the search is stopped for each characteristic is shown in Fig. 6.38. The average number of samples required and the average number of cases that converge to the GMPP for increasing stopping criterion limit are shown in Fig. 6.39.

As the stopping criterion limit is increased, the number of cases that converge to the GMPP also increases as does the number of samples required before the

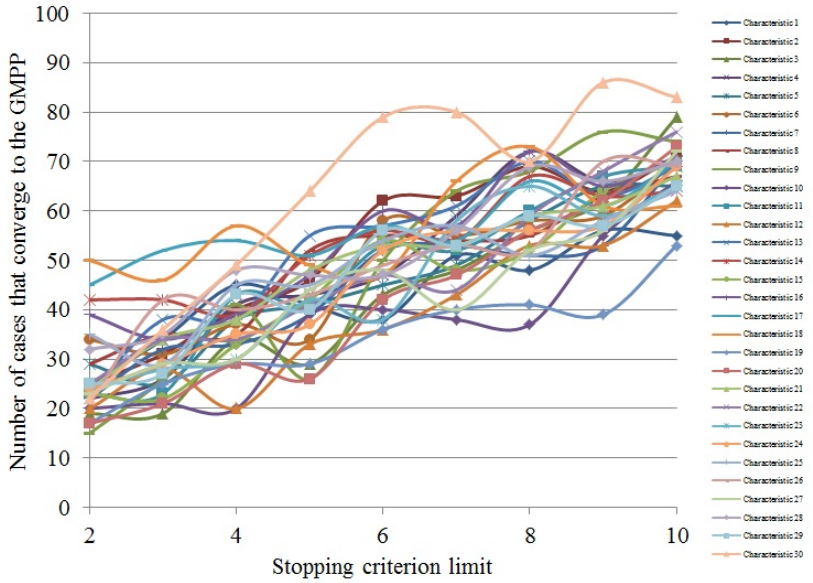

Figure 6.37: Number of cases that converge with increasing stopping criterion for each characteristic.

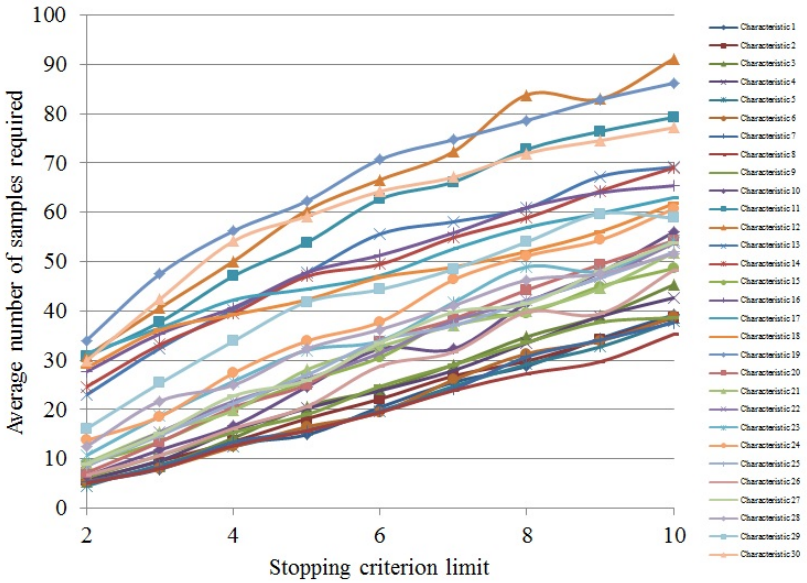

Figure 6.38: Average number of samples required for each characteristic and each stopping criterion limit.

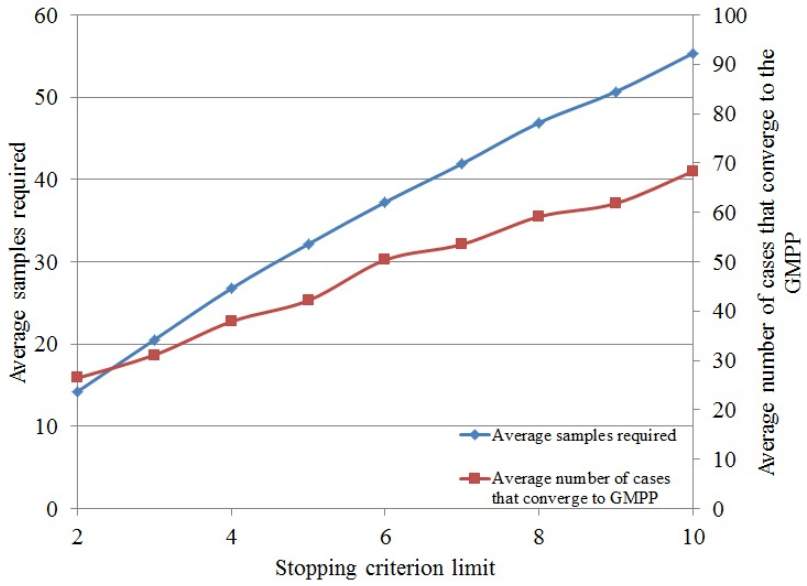

Figure 6.39: Samples required (blue) and average convergence to the GMPP (red) with increasing stopping criterion.

method converges. Even when a limit of 10 is used, which corresponds to an average number of samples of 55 required, the convergence is less than 70%. Applying a stopping criterion may be a suitable step to take later in the search process than from the outset as is explored in this section. If the stopping criterion is applied once the temperature has reduced to below a certain level, the algorithm is more likely to have converged to the neighbourhood of the GMPP before this stopping criterion ceases the search process.

Table 6.12: Percentage of cases where the final operating point has converged to the GMPP for variations of the stopping criterion.

	2	**3**	**4**	**5**	**6**	**7**	**8**	**9**	**10**
Characteristic 1	25	34	45	41	38	51	48	56	55
Characteristic 2	25	31	40	46	62	63	69	64	71
Characteristic 3	19	19	34	29	43	48	56	62	79
Characteristic 4	22	26	41	43	47	59	72	66	70
Characteristic 5	29	25	38	41	45	49	58	65	65
Characteristic 6	34	31	37	34	58	55	58	59	70
Characteristic 7	22	32	33	39	52	53	51	53	70
Characteristic 8	29	35	35	52	55	54	55	63	67
Characteristic 9	15	26	41	26	50	64	68	76	74
Characteristic 10	20	21	20	39	40	38	37	55	66
Characteristic 11	23	23	43	41	53	52	60	67	69
Characteristic 12	20	28	20	33	36	43	53	53	62
Characteristic 13	23	38	38	55	57	61	70	63	69
Characteristic 14	42	42	39	51	56	54	67	63	64
Characteristic 15	23	22	33	42	54	48	52	64	70
Characteristic 16	39	34	39	47	60	57	72	65	71
Characteristic 17	45	52	54	51	57	54	66	61	70
Characteristic 18	50	46	57	49	47	66	73	61	61
Characteristic 19	17	25	29	29	36	40	41	39	53
Characteristic 20	17	21	29	26	42	47	56	62	73
Characteristic 21	24	34	38	48	53	53	59	61	67
Characteristic 22	25	34	34	41	47	44	59	68	76
Characteristic 23	24	28	30	42	38	58	65	59	65
Characteristic 24	24	29	35	37	52	56	56	57	69
Characteristic 25	35	29	45	45	54	57	51	58	64
Characteristic 26	21	42	40	43	49	53	52	70	69
Characteristic 27	23	29	30	44	48	40	52	56	72
Characteristic 28	32	35	48	47	47	56	69	66	70
Characteristic 29	25	27	43	40	56	53	59	57	65
Characteristic 30	22	36	49	64	79	80	70	86	83

6.9 Conclusions

The studies presented in this chapter have explored many different implementations of the SA methodology for PV GMPPT to assess which implementation has the most potential for practical applications. Key observations from the studies conducted are given below and recommendations on approaches to investigate to develop a more robust SA based GMPPT method are suggested.

The key observations from the studies are:

- Initial temperature - varying the initial temperature within the bounds considered in this chapter has no definite effect on improving the algorithm performance.
- Cooling rate - as the cooling rate is increased the number of cases that converge also increases however this is accompanied by a steep increase in the number of samples required.
- Cooling frequency - as the cooling frequency is increase the number of cases that converge also increases, however this is accompanied by an increase in the number of samples required. The number of samples required increased linearly and is not as significant as the increase in samples for the cooling rate.
- Acceptance probability threshold - as the acceptance probability threshold increases the number of cases that converge slightly increases. There is no increase in the number of samples required.
- Neighbourhood size
  - Constant neighbourhood size - for all neighbourhood sizes greater than 30 V, the method converged in 90% of cases on average with no increase in samples. This suggests that the lower bound for the neighbourhood size should perhaps be $2 \times 0.8V_{oc}$ (approx 35 V) to enable the method to explore fully.
  - Neighbourhood reduction function - the linear reduction function exhibited superior results to the quadratic and exponential functions with no increase in the number of samples required.
- Stopping temperature - as the stopping temperature is reduced slightly

more samples are required and the method converges in more cases.

- Cooling function
  - Linear cooling function - the number of cases that converge with the linear cooling schedule implementations considered is not consistent across all characteristics.
  - Logarithmic cooling function - the number of cases that converge with the logarithmic cooling schedule (limited to 200 samples) is not consistent across all characteristics.
  - Lundy cooling function - the number of cases that converge with the Lundy cooling schedule is large. By modifying the cooling constant the number of samples increase, but the convergence on average is not affected significantly.
  - Simulated Quenching - the number of cases that converge with SQ is large and requires far fewer samples than other implementations.
- Stopping criterion - as the stopping criterion limit is increased there is a slight improvement in the number of cases that converge to the GMPP. It may be better to apply the stopping criterion later in the search process to enable the SA method to search fully before it converges.

These observations lead to the merged and improved SA based implementations considered in the Chapter 7. In particular, the following parameters warrant further investigation:

- Variable acceptance probability threshold
- Linear neighbourhood reduction function
- Lundy cooling schedule
- Simulated quenching
- Stopping criterion applied after a certain temperature threshold

Chapter 7

Towards a Generalised Simulated Annealing Based Global Maximum Power Point Tracking Technique

7.1 Introduction

The results described in Chapter 3, Chapter 5 and Chapter 6 of this thesis explore PSC that PV systems experience and the development of a GMPPT method based on the technique of Simulated Annealing (SA). In this chapter, the results from these studies and from other studies in the literature [90] are incorporated to design an optimised GMPPT strategy based on the SA method.

In this chapter, possible enhancements to the technique are first described based on the identified limitations of the GMPPT method proposed in Chapter 5. These enhancements are explored in the context of the results presented in Chapter 6, leading to multiple different improved SA GMPPT implementations.

7.2 Developing a Generalised GMPPT Method Based on Simulated Annealing

In Chapter 5, the SA GMPPT method is applied with fairly arbitrarily selected parameters for the cooling rate, initial and final temperatures. Additionally, this technique is applied across a wide search range from 14 V to 144 V for

the eight module system. Despite these wide parameters the technique still exhibits good performance in tracking to the GMPPT in all the test conditions, particularly when compared to the performance of common techniques such as the P&O and PSO methods under the same conditions. A few limitations however are noticed. The first is that the reset condition applied (for SA and PSO implementations) is insufficient to detect all changes in environmental conditions that would require the algorithm to commence a global search. The second is that the technique frequently will locate the vicinity of the GMPP early in the search and then continually return to this point until the stopping criterion of the final temperature is reached. Thirdly, the search space used is very wide and a large percentage of this search space may represent conditions where the GMPP is unlikely to lie. Finally, the method is good at locating the GMPP neighbourhood, however it will not necessarily converge directly to the exact GMPP. This chapter seeks to reduce the effects that these limitations have on the performance of the SA method based on observations from the study in Chapter 3 and Chapter 6, and from other studies to develop a GMPPT technique that is truly able to be universally applied and achieve GMPPT in a reliable manner.

The first limitation relates to the reset conditions. While in many cases the power at the global maxima will not vary significantly from one sample to the next indicating that this remains the GMPP, there are some cases where this phenomena will not be observed. The sample case in Chapter 5, Section 5.5.2.2, characterising a case where the environmental conditions change, resulting in a new GMPP but without a significant change in the current operating power so that a new global search is not initiated, represents this situation. A sudden step change in irradiance on some modules in the system could cause this situation to arise. In this case the reset condition is insufficient to restart the global searching. One way that this could be overcome involves integrating some key observations from Chapter 3 and from [90]. The partial shading studies in Chapter 3 indicate that the GMPP between successive environmental conditions will usually only move to an adjacent MPP. The results from [90], show that the spacing of the MPPs is about 80% of the open-circuit voltage. These observations can be combined to create a test condition to assess if a change in environmental conditions has occurred using only two samples. Simply, if no change in environmental conditions has been detected for a suitable period of time, the method can simply take a sample at about $0.8V_{oc}$ less than the current

operating point and $0.8V_{oc}$ more than the current operating point and compare these samples with the current best operating point. If one or both of these samples are larger than the current best operating point power this indicates that a new global search is required. If they are both less than the current best operating point power it indicates that a new global search is most likely not required. While this strategy will not guarantee GMPPT under all changes in environmental conditions, it will improve the likelihood that the algorithm will reinitialise a global search when most changes in the environmental conditions occur.

By restricting the algorithm to only end when the final temperature is reached, the technique may locate the global maxima early in the search and continue to sample away from this point and then return to it without improving the solution quality for a considerable period of the search time. An example of this is shown in Fig. 7.1 which demonstrates that the method may waste a lot of energy in searching points that are unlikely to improve the solution quality. Figure 7.1 illustrates how the method has converged to and retains the approximate GMPP as the best operating point from sample 56 onwards. This leaves 165 samples (or 75%) of the searching time where the solution quality does not significantly improve. To overcome this an alternative stopping criterion, like that proposed in [253] could be used to allow the technique to stop searching once it has not found a better solution for 2-10 successive samples. Instead of limiting the stopping criterion to a set number of samples which, as shown in Chapter 6, will often not improve the solution quality despite the reduction in searching time, it is proposed to link the number of samples to the temperature of the search to ensure that at the start of the search the algorithm must remain around the GMPP without accepting a lower point for longer than a larger number of samples than when the temperature reduces and the time progresses. This ensures that the algorithm still has the opportunity to search widely initially, but then when a reduction in temperature occurs can stop the searching process much quicker.

The SA GMPPT implementations considered previously in this thesis require a large searching range of 130 V. Using the observations from [90], that the successive MPPs lie at around 80% of the open-circuit voltage, it is possible to refine the searching range of the method to be within narrow bands around each

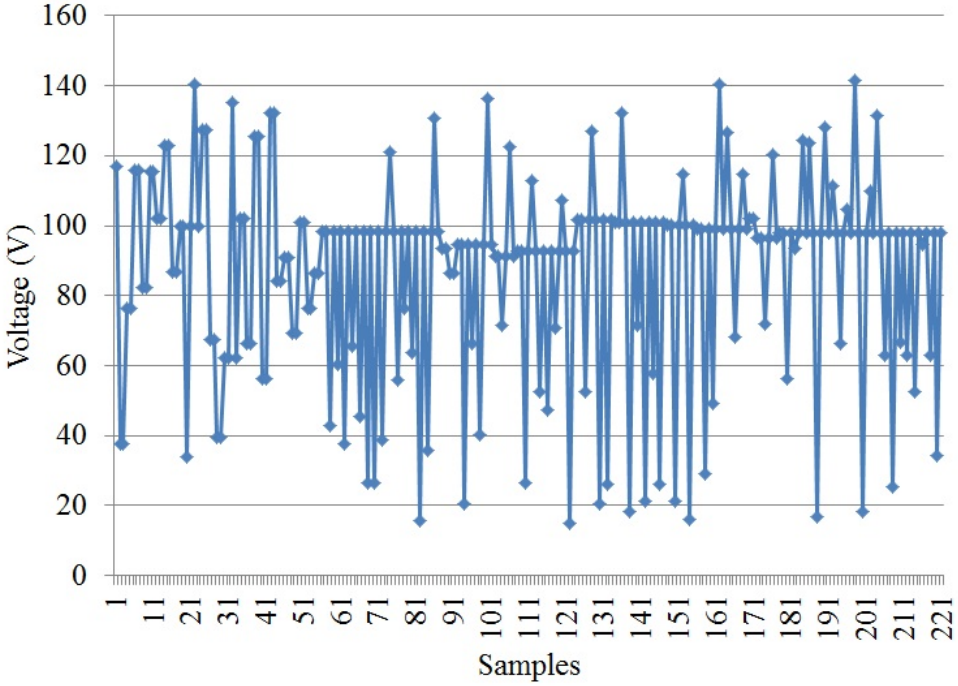

(a) Voltage tracking sample.

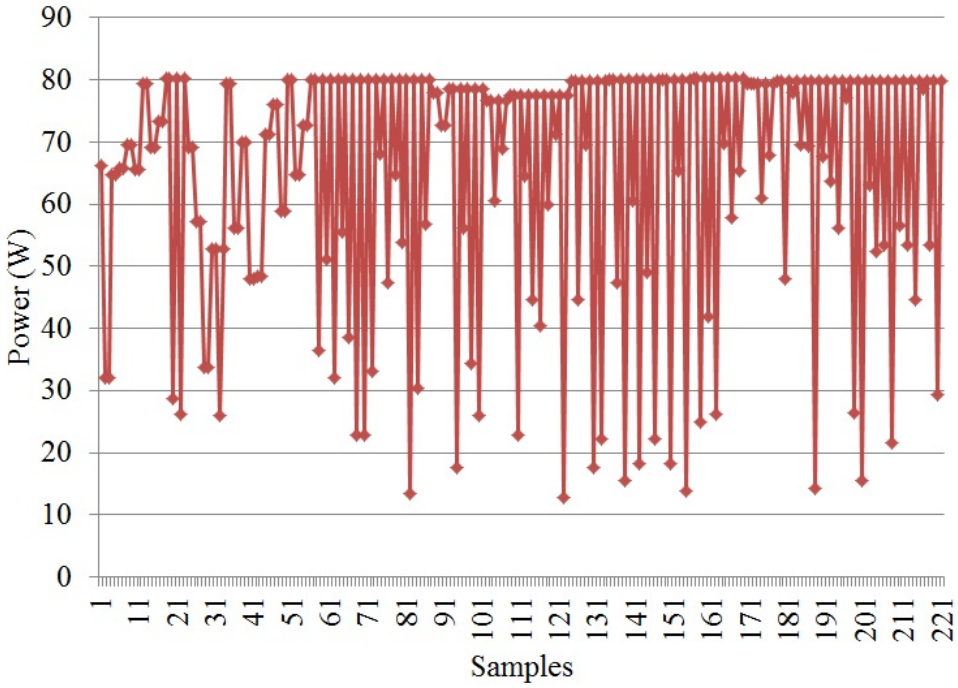

(b) Power tracking sample.

Figure 7.1: Sample case for tracking the GMPP of characteristic 13 with base parameters showing that the algorithm has located the GMPP neighbourhood well before the search is concluded.

MPP. By limiting each searching band, to 10 V centred around each prospective MPP, the search space considerably reduces and the probability of quickly

locating the GMPP increases dramatically. Based on the original searching range of 14 V to 144 V, by adopting the neighbourhood bands the complete search range reduces to 80 V (or 61.5% of the original searching range). This could also be incorporated with the observations from Chapter 3 that the GMPP moves by usually no more than one MPP away in terms of voltage to reduce the searching space under most conditions to a fraction of what it was before.

The SA method is shown to frequently converge well to the neighbourhood of the GMPP but has a weaker performance in converging directly to the GMPP. This is evidenced by the change in the performance of the method when a 1% convergence criterion was applied compared with a 5% convergence rating in Chapter 5. By combining the method with a local search methodology, similar to the approach used in [202] for combining the PSO method with a local search method based on P&O, the performance in converging directly to the GMPP can be improved. As the SA method will reliably locate the neighbourhood of the GMPP, P&O could be applied as a local search method with a small step size to minimise oscillations in steady state.

Combining these efforts to improve the GMPPT performance this chapter develops several implementations of the SA based GMPPT method that perform much more effectively than the method demonstrated in Chapter 5. The methods could be easily generalised to perform effectively on any other PV system, even when using fairly arbitrarily selected temperature parameters. The key enhancements to this method are:

- Reduced searching window to 61.5% of the original searching window used in Chapter 5 for the eight module system. This will potentially reduce the oscillations in the output power slightly.
- Stopping criterion based upon the acceptance of the best operating point that reduces the number of samples without change required before stopping as the temperature reduces.
- Reset condition enhanced to check the power at the two closest MPP locations if a change in environmental conditions has not been detected for a set period of time.
- Combining SA GMPPT with a local searching process based on the P&O method to improve the fine tracking to the GMPP.

7.3 Improved SA GMPPT Implementation

In this section, several SA based GMPPT implementations are considered which combine the results from Chapter 6 with the key suggestions above to improve the performance of the method.

The results from Chapter 6 have shown the superior performance of the Lundy cooling schedule when compared to the geometric cooling schedule used in Chapter 5. In this section, enhancements to the technique are applied on an implementation with the geometric cooling schedule as well as an implementation with the Lundy cooling schedule.

7.3.1 Geometric cooling schedule with restricted searching bands

The neighbourhood available for searching is reduced to be defined by 10 V bands centred around the approximate MPP locations. The center of these locations is defined as $0.8V_{oc}$ where V_{oc} is multiples of the open-circuit voltage for a single module at STC. These centred neighbourhood bands are then centred at 17.7 V, 35.4 V, 53.0 V, 70.7 V, 88.4 V, 106.1 V, 123.8 V, and 141.4 V. Voltages within all bands have the same probability to be selected. The same parameters as the base implementation are applied. That is, initial temperature 25°C, final temperature 0.2°C, acceptance probability threshold 0.1 and with five samples at each temperature. The method is applied on the same 30 characteristics from Chapter 6.

This implementation leads to an average convergence across the 30 characteristics of 95.57%, which is only slightly higher (0.38%) than the average convergence with these parameters in previous tests. This is based on the average convergence to the GMPP for all cases in Chapter 6 that use the same geometric cooling schedule parameters as this implementation.

The observations of Chapter 3 indicate that the GMPP is more frequently located at the higher voltage MPP locations than the lower voltage GMPP

locations for the case studies considered. In all subsequent studies on restricted neighbourhoods, each searching band is given a weighting based on how probable it is that the GMPP voltage will lie within that particular band. This improves the likelihood that a higher voltage will be selected as a sample point than a lower voltage, but still allows the method to search fully.

7.3.2 Geometric cooling schedule with restricted weighted searching bands

The neighbourhood searching bands defined in Section 7.3.1 are utilised in this section with the same parameters for the SA implementation. The MPP neighbourhood searching bands are now weighted so that there is a preference to select sample points that are at a higher voltage.

This implementation leads to an average convergence across the 30 characteristics of 97.8%. When compared to the previous implementation of the geometric cooling schedule with the same parameters and restricted neighbourhoods, this leads to an average performance improvement of 2.23%. The performance improvement with the weighted restricted neighbourhoods is much more significant that the improvement that comes with just restricting the searching space.

7.3.3 Lundy cooling schedule with restricted weighted searching bands

Like Section 7.3.2, the neighbourhood is restricted to 10 V bands around the likely MPP locations. These bands are weighted so that selecting a higher voltage is more probable than selecting a lower voltage. To reduce the number of samples used, the Lundy cooling schedule is applied with a constant of 0.05. In the implementation considered in Chapter 6, this set of parameters lead to an average convergence of 98%. With the restricted neighbourhoods, this average convergence across the 30 sample characteristics increases to 99.1%, an increase of 1.1%.

7.3.4 Geometric cooling schedule with restricted searching bands and local search

The implementation of Section 7.3.2 is combined with a local search P&O methodology of varying perturbation sizes to assess how this improves the performance. In each case, the percentage of cases that converge before and after the P&O method is applied can be considered. The P&O method should improve the fine tracking of the method to the exact GMPP and should lead to improved performance when irradiance transients occur.

The perturbation step size is varied from 0.1 V to 1 V, in steps of 0.1 V. The number of cases that converge for each characteristic with each P&O step size before P&O is applied and after P&O is applied are shown in Table 7.1 and Table 7.2, respectively. From inspection of Table 7.1 and Table 7.2, it can be seen that after the P&O method is applied the number of cases that converge increases. In fact, 530 extra test cases in total converge across the different step size implementations and the 30 characteristics. Before the P&O method is applied, the average convergence was in 97.5% of cases. After the P&O method was applied, this increased by 1.77% to 99.3%.

The highest average convergence is observed with the two stage SA implementation that utilises P&O as the local search stage with the smallest step size.

7.3.5 Lundy cooling schedule with restricted searching bands and local search

The Lundy cooling schedule implementation of Section 7.3.3 is enhanced in this section with a local search P&O implementation like that considered in Section 7.3.4. The number of cases that converge for each characteristic with each P&O step size both before and after the P&O process is applied are shown in Table 7.3 and Table 7.4, respectively.

By comparing the differences between Table 7.3 and Table 7.4, it is possible to see that the P&O method improves the performance by leading to a total of 106

Table 7.1: Number of cases where the final operating point has converged to the GMPP for variations of the P&O step size after the first stage where the SA algorithm is applied.

	0.1	**0.2**	**0.3**	**0.4**	**0.5**	**0.6**	**0.7**	**0.8**	**0.9**	**1**
Characteristic 1	98	99	99	99	99	100	100	100	99	99
Characteristic 2	100	100	100	100	100	100	100	100	100	100
Characteristic 3	100	100	100	100	100	100	100	100	100	100
Characteristic 4	100	100	100	99	99	100	100	99	99	100
Characteristic 5	98	100	98	100	100	99	98	98	100	100
Characteristic 6	99	100	99	100	100	99	100	99	100	99
Characteristic 7	100	100	100	100	99	100	97	100	100	99
Characteristic 8	100	100	100	100	100	100	100	100	100	100
Characteristic 9	100	100	100	100	100	100	100	100	100	100
Characteristic 10	100	100	100	100	100	100	100	100	100	100
Characteristic 11	97	98	100	98	99	97	96	97	98	97
Characteristic 12	99	100	100	99	100	99	100	99	100	100
Characteristic 13	96	98	97	96	98	97	100	97	97	95
Characteristic 14	88	94	98	91	96	93	94	90	91	97
Characteristic 15	100	100	100	100	100	100	100	100	100	100
Characteristic 16	96	90	91	92	91	92	94	86	87	85
Characteristic 17	87	90	82	90	89	86	90	89	91	86
Characteristic 18	89	86	90	92	89	85	82	89	91	89
Characteristic 19	95	88	84	85	86	88	92	91	91	88
Characteristic 20	100	100	100	100	100	100	100	100	100	100
Characteristic 21	100	100	100	100	100	100	100	100	100	100
Characteristic 22	100	100	100	100	100	100	100	100	100	100
Characteristic 23	100	100	100	100	100	100	100	100	100	100
Characteristic 24	100	100	99	100	100	100	100	100	100	100
Characteristic 25	100	99	100	100	100	100	100	100	100	100
Characteristic 26	99	100	100	100	100	100	99	100	100	100
Characteristic 27	100	100	100	100	100	100	100	100	100	100
Characteristic 28	100	100	100	100	100	100	100	100	100	100
Characteristic 29	100	100	100	100	100	100	100	100	99	98
Characteristic 30	88	93	85	90	88	79	85	84	86	81

Table 7.2: Number of cases where the final operating point has converged to the GMPP for variations of the P&O step size after the second stage where the P&O algorithm is applied.

	0.1	**0.2**	**0.3**	**0.4**	**0.5**	**0.6**	**0.7**	**0.8**	**0.9**	**1**
Characteristic 1	100	100	100	100	100	100	100	100	100	100
Characteristic 2	100	100	100	100	100	100	100	100	100	100
Characteristic 3	100	100	100	100	100	100	100	100	100	100
Characteristic 4	100	100	100	100	100	100	100	100	100	100
Characteristic 5	100	100	100	100	100	100	100	100	100	100
Characteristic 6	100	100	100	100	100	100	100	100	100	100
Characteristic 7	100	100	100	100	100	100	100	100	100	100
Characteristic 8	100	100	100	100	100	100	100	100	100	100
Characteristic 9	100	100	100	100	100	100	100	100	100	100
Characteristic 10	100	100	100	100	100	100	100	100	100	100
Characteristic 11	100	100	100	100	100	100	100	100	100	100
Characteristic 12	99	100	100	100	100	100	100	100	100	100
Characteristic 13	100	100	100	100	100	100	100	100	100	100
Characteristic 14	100	100	100	100	100	100	100	100	100	100
Characteristic 15	100	100	100	100	100	100	100	100	100	100
Characteristic 16	100	100	100	100	100	100	100	100	100	100
Characteristic 17	100	100	100	100	100	100	100	100	100	100
Characteristic 18	100	100	100	100	100	100	100	100	100	100
Characteristic 19	95	90	85	87	87	89	92	91	91	88
Characteristic 20	100	100	100	100	100	100	100	100	100	100
Characteristic 21	100	100	100	100	100	100	100	100	100	100
Characteristic 22	100	100	100	100	100	100	100	100	100	100
Characteristic 23	100	100	100	100	100	100	100	100	100	100
Characteristic 24	100	100	100	100	100	100	100	100	100	100
Characteristic 25	100	100	100	100	100	100	100	100	100	100
Characteristic 26	99	100	100	100	100	100	99	100	100	100
Characteristic 27	100	100	100	100	100	100	100	100	100	100
Characteristic 28	100	100	100	100	100	100	100	100	100	100
Characteristic 29	100	100	100	100	100	100	100	100	99	98
Characteristic 30	93	94	89	92	89	84	88	87	90	86

more cases that are considered to have converged. Before the P&O method was applied, the average convergence was in 99.28% of cases. After the P&O method was applied, this increased slightly to 99.63%.

The highest average convergence is observed with the two stage SA implementation that utilises P&O as the local search stage with the smallest step size.

7.3.6 Geometric cooling schedule with restricted searching bands and modified stopping criterion

As described in Chapter 6, using the same stopping criterion across the entire search time resulting in poorer results. For this reason, the stopping criterion constant is defined by a linear function in this section. The linear function ensures that at high temperature that algorithm requires a large number of samples to not be accepted, while at a lower temperature fewer samples not being accepted could be indicative of convergence. The linear function proposed, has a stopping criterion constant of 40 at 25°C, and of 10 at approximately 0.2°C. This function is shown in Fig. 7.2.

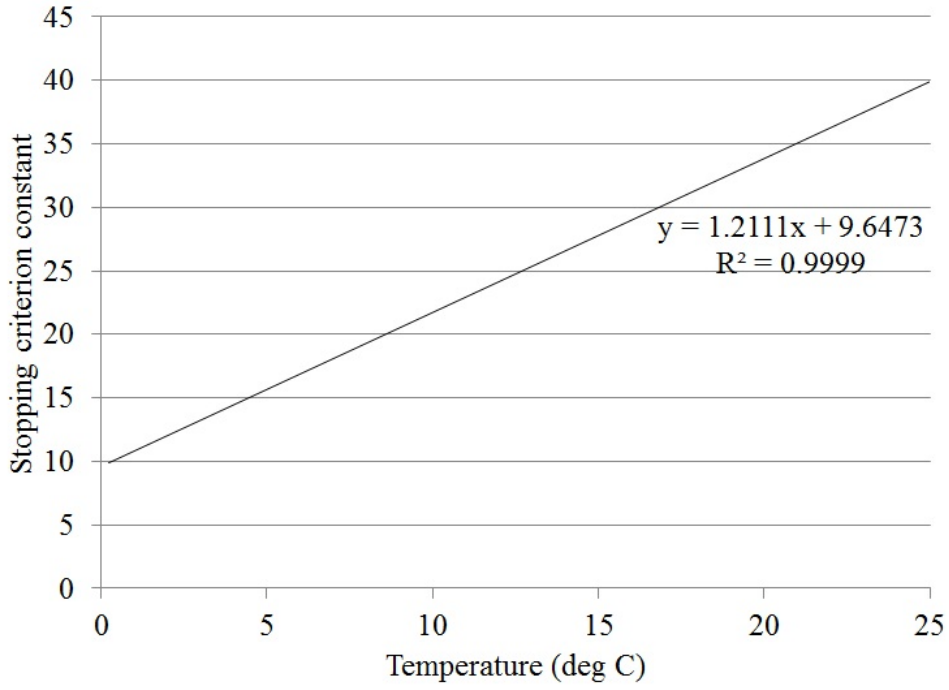

Figure 7.2: Linear function to describe the variation of the stopping criterion constant with the temperature.

Table 7.3: Number of cases where the final operating point has converged to the GMPP for variations of the P&O step size after the first stage where the SA algorithm with Lundy cooling schedule is applied.

	0.1	**0.2**	**0.3**	**0.4**	**0.5**	**0.6**	**0.7**	**0.8**	**0.9**	**1**
Characteristic 1	99	100	100	100	100	100	100	100	98	100
Characteristic 2	100	100	100	100	100	100	100	100	100	100
Characteristic 3	100	100	100	100	100	100	100	100	100	100
Characteristic 4	100	100	100	100	100	100	100	100	100	100
Characteristic 5	100	100	100	100	100	99	100	100	100	100
Characteristic 6	100	100	100	100	100	100	100	100	100	100
Characteristic 7	100	100	100	100	100	100	100	100	100	100
Characteristic 8	100	100	100	100	100	100	100	100	99	100
Characteristic 9	100	100	100	100	100	100	100	100	100	100
Characteristic 10	100	100	100	100	100	100	100	100	100	100
Characteristic 11	100	100	100	100	100	100	100	100	100	100
Characteristic 12	100	100	100	100	100	100	100	100	100	100
Characteristic 13	100	100	100	100	100	100	100	100	99	100
Characteristic 14	100	100	100	99	100	99	100	100	100	99
Characteristic 15	100	100	100	100	100	100	100	100	100	100
Characteristic 16	97	96	97	96	96	96	96	97	99	96
Characteristic 17	99	96	98	96	97	99	99	97	96	97
Characteristic 18	94	98	99	96	96	98	98	100	96	100
Characteristic 19	93	90	91	89	89	89	93	86	95	92
Characteristic 20	100	100	100	100	100	100	100	100	100	100
Characteristic 21	100	100	100	100	100	100	100	100	100	100
Characteristic 22	100	100	100	100	100	100	100	100	100	100
Characteristic 23	100	100	100	100	100	100	100	100	100	100
Characteristic 24	100	100	100	100	100	100	100	100	100	100
Characteristic 25	100	100	100	100	100	100	100	100	100	100
Characteristic 26	100	100	100	100	100	100	100	100	100	100
Characteristic 27	100	100	100	100	100	100	100	100	100	100
Characteristic 28	100	100	100	100	100	100	100	100	100	100
Characteristic 29	100	100	100	100	100	100	100	100	100	100
Characteristic 30	97	96	97	97	96	98	97	98	99	96

Table 7.4: Number of cases where the final operating point has converged to the GMPP for variations of the P&O step size after the second stage where the P&O algorithm is applied. The SA method in the first stage is applied with Lundy cooling schedule.

	0.1	**0.2**	**0.3**	**0.4**	**0.5**	**0.6**	**0.7**	**0.8**	**0.9**	**1**
Characteristic 1	100	100	100	100	100	100	100	100	100	100
Characteristic 2	100	100	100	100	100	100	100	100	100	100
Characteristic 3	100	100	100	100	100	100	100	100	100	100
Characteristic 4	100	100	100	100	100	100	100	100	100	100
Characteristic 5	100	100	100	100	100	100	100	100	100	100
Characteristic 6	100	100	100	100	100	100	100	100	100	100
Characteristic 7	100	100	100	100	100	100	100	100	100	100
Characteristic 8	100	100	100	100	100	100	100	100	100	100
Characteristic 9	100	100	100	100	100	100	100	100	100	100
Characteristic 10	100	100	100	100	100	100	100	100	100	100
Characteristic 11	100	100	100	100	100	100	100	100	100	100
Characteristic 12	100	100	100	100	100	100	100	100	100	100
Characteristic 13	100	100	100	100	100	100	100	100	100	100
Characteristic 14	100	100	100	100	100	100	100	100	100	100
Characteristic 15	100	100	100	100	100	100	100	100	100	100
Characteristic 16	100	100	100	100	100	100	100	100	100	100
Characteristic 17	100	100	100	100	100	100	100	100	100	100
Characteristic 18	100	100	100	100	100	100	100	100	100	100
Characteristic 19	93	91	91	89	89	89	93	86	95	92
Characteristic 20	100	100	100	100	100	100	100	100	100	100
Characteristic 21	100	100	100	100	100	100	100	100	100	100
Characteristic 22	100	100	100	100	100	100	100	100	100	100
Characteristic 23	100	100	100	100	100	100	100	100	100	100
Characteristic 24	100	100	100	100	100	100	100	100	100	100
Characteristic 25	100	100	100	100	100	100	100	100	100	100
Characteristic 26	100	100	100	100	100	100	100	100	100	100
Characteristic 27	100	100	100	100	100	100	100	100	100	100
Characteristic 28	100	100	100	100	100	100	100	100	100	100
Characteristic 29	100	100	100	100	100	100	100	100	100	100
Characteristic 30	99	97	98	98	98	99	99	98	99	97

With this modified stopping criterion and the restricted neighbourhoods, the average convergence across the 30 characteristics is 88.9%. This is considerably lower than what is seen when the restricted neighbourhoods alone is used to enhance the technique. The key advantage however to using the modified stopping criterion is that it significantly reduces the number of samples required. The average number of samples required and the number of cases that converge is shown for each characteristic in Fig. 7.3.

7.3.7 Lundy cooling schedule with restricted searching bands and modified stopping criterion

The modified stopping criterion constant linear function from Section 7.3.6 is utilised with the Lundy cooling function and restricted neighbourhood searching bands. This leads to an average convergence of 88.1% across the 30 characteristics. As with Section 7.3.6, the number of samples required by the implementation is considerably reduced. The average number of samples required and the number of cases that converge is shown for each characteristic in Fig. 7.4.

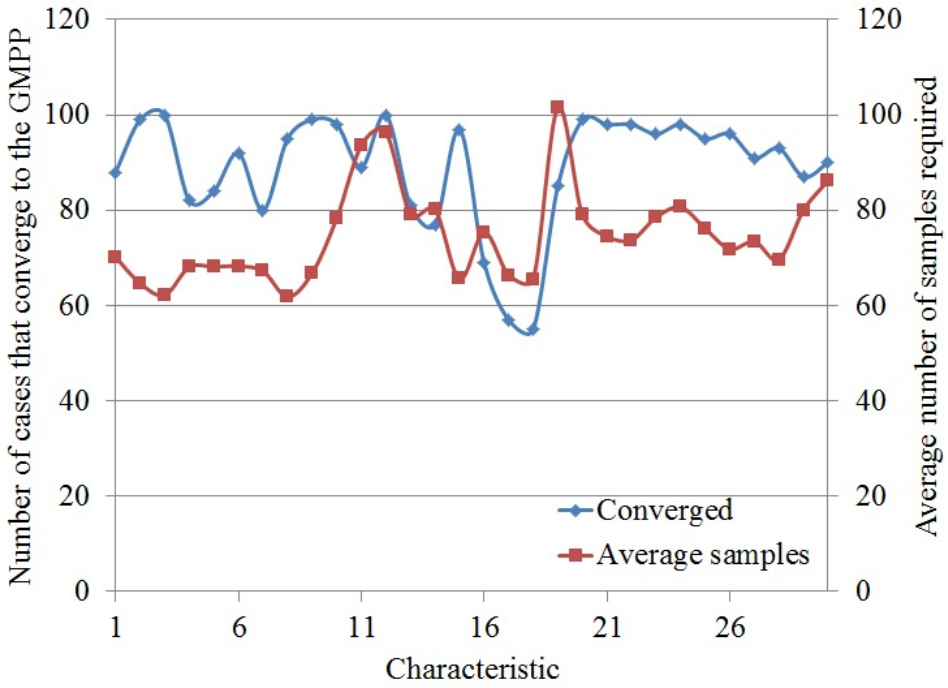

Figure 7.3: Average number of samples required and number of cases that converge for each characteristic with the geometric cooling schedule enhanced with restricted neighbourhood searching bands and linear function modified stopping criterion.

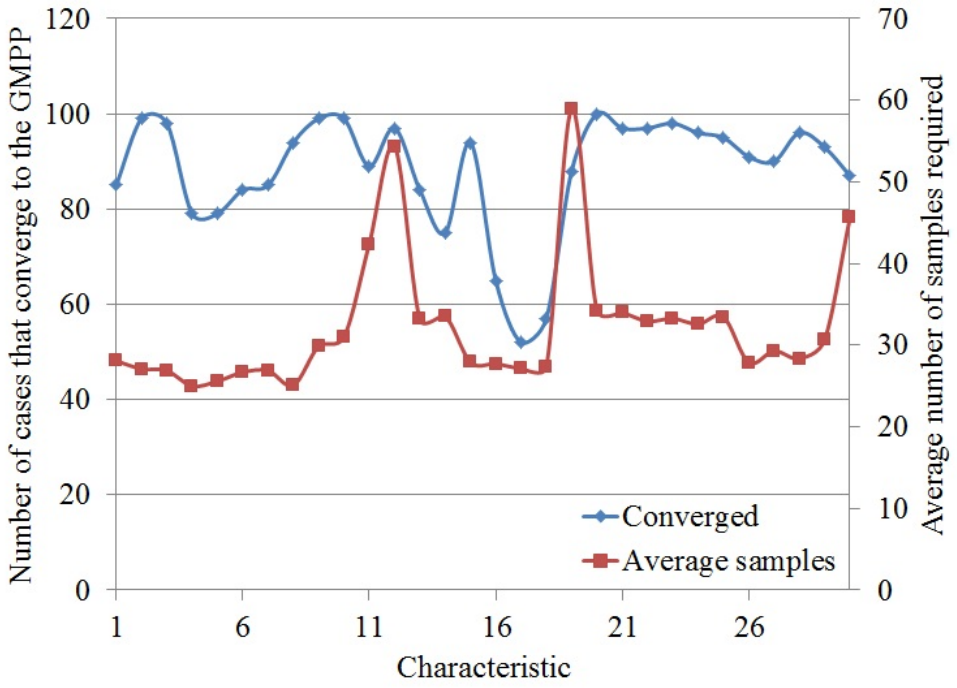

Figure 7.4: Average number of samples required and number of cases that converge for each characteristic with the Lundy cooling schedule enhanced with restricted neighbourhood searching bands and linear function modified stopping criterion.

7.3.8 Geometric cooling schedule with restricted searching bands, modified stopping criterion and local search

The performance from Section 7.3.6 demonstrates that the modified stopping criterion can reduce the average number of samples required by the algorithm, but leads to a smaller number of cases that converge to the GMPP. In this section, the modified stopping criterion implementation is combined with a local search. P&O is used as the local search method with a step size of 0.1 V. The error during the local search is monitored to give an indication of how many samples are required to converge to the GMPP. Before local search is applied, the SA method results in convergence in 88.8% of cases. After the local search, the method has converged in 98.7% of cases. This is a significant improvement after the local search is applied, however is less than what is observed when the local search was used with the implementation prior to the modified stopping criterion being applied. The key advantage that this technique presents is a significantly

reduced number of samples being required to deliver good convergence. The average number of samples required and the number of cases that converge after the first stage SA and second stage P&O methods are applied is shown for each characteristic in Fig. 7.5. From Fig. 7.5, it is shown that the number of cases that converge to the GMPP increases after the P&O method is applied. When compared to Fig. 7.3, the average number of samples required is not significantly more in the current implementation, yet a greatly improved performance is exhibited.

7.3.9 Lundy cooling schedule with restricted searching bands, modified stopping criterion and local search

The Lundy cooling schedule combined with restricted searching bands, a modified stopping criterion and a local search is detailed in this section. The stopping criterion constant is defined by the linear relationship $0.6055 * T + 4.8236$. After the SA algorithm is applied in the first case the average percentage of cases that

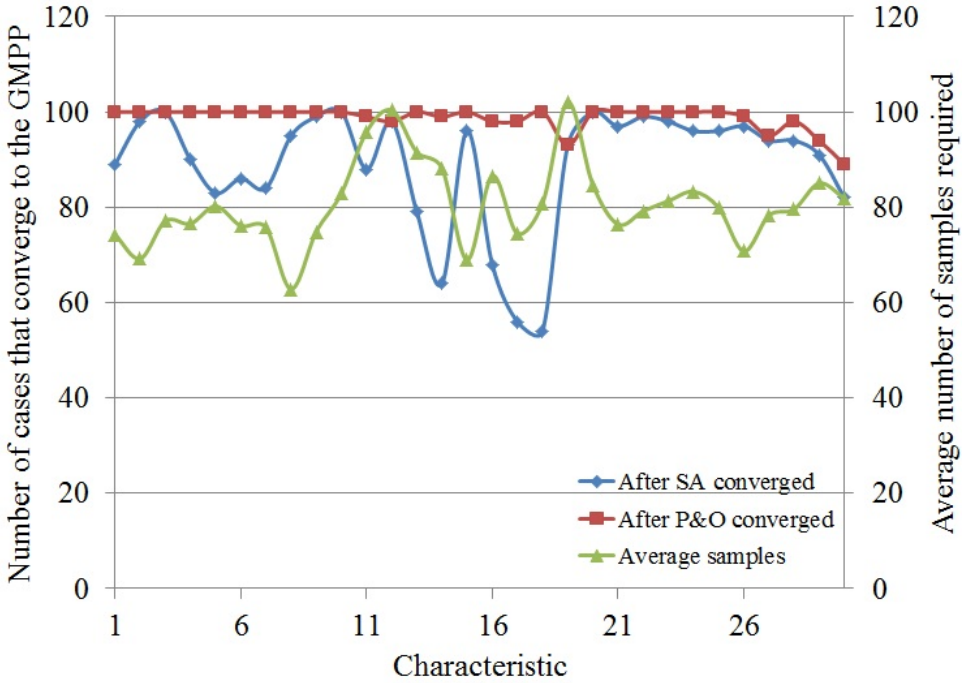

Figure 7.5: Average number of samples required and number of cases that converge for each characteristic with the geometric cooling schedule enhanced with restricted neighbourhood searching bands, linear function modified stopping criterion and local search based on P&O.

converge across the 30 characteristics is 99.23%. Once the second stage of the algorithm is applied, the average percentage of cases that converge increases to 99.53%. This is a small increase in the performance. The number of samples required for each of these implementations is, on average, 101.9. Having a larger number of samples has lead to the improved performance of this implementation of the technique. The average number of samples required and the number of cases that converge after the first stage SA and second stage P&O methods are applied is shown for each characteristic in Fig. 7.6. The modified stopping criterion constant function used in this case leads to a greater number of cases that converge after the SA portion of the method with more samples being required in this implementation. The modified stopping criterion is unlikely to operate with the parameters of the modified stopping criterion constant equation given above.

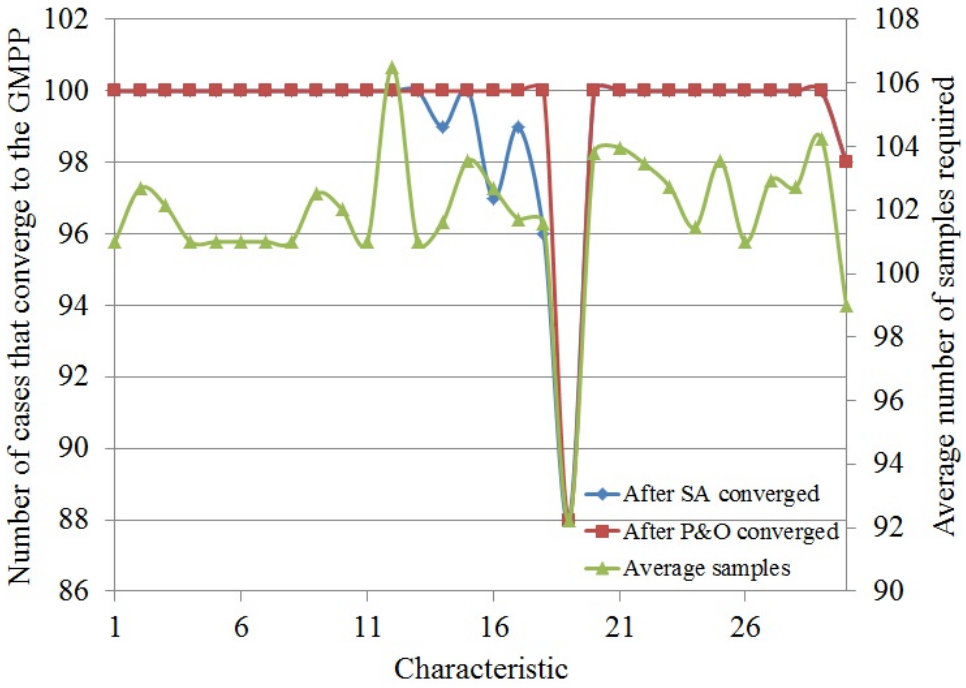

Figure 7.6: Average number of samples required and number of cases that converge for each characteristic with the Lundy cooling schedule enhanced with restricted neighbourhood searching bands, linear function modified stopping criterion and local search based on P&O.

7.3.10 Geometric cooling schedule with restricted searching bands, local search and reset condition

The analysis completed in this chapter has shown that the performance of the SA method with the geometric cooling schedule is improved by restricting the neighbourhood searching bands and performing a local search once the SA algorithm has converged. In this section, two reset conditions are assessed to determine their performance in detecting a change in environmental conditions. The first condition, has been explored in Chapter 5 and relies on monitoring the power at the operating point to detect when a large change occurs. In this implementation if the change in power at the operating point is greater than 5 W, a global search will be initiated. The second condition involves periodically taking a sample approximately one MPP (about 17.7 V) below and above the current best operating point to assess if a change in conditions has possibly occurred. This is aligned with the observations from Chapter 3 which suggest that the GMPP is likely to remain at the same MPP or transition to an adjacent MPP.

If no change in the environmental conditions is detected, the method will continue to apply the P&O method. The variable and clear day irradiance profiles, with a single obstacle placed in the environment, from Chapter 5 are used in this analysis.

For the clear day irradiance profile, neither condition restarts the global search, even when a change in the GMPP voltage has occured. Of the 17 cases in the clear irradiance profile, the method failed to locate the GMPP in 6 cases.

For the variable day irradiance profile in 38 of the 58 cases, the method correctly tracked the GMPP. Only condition two to initiate a global search was successful in this implementation. Condition one did not detect any cases where a global search should be initiated. In only one case where the reset condition triggered a global search did the method end up tracking a local maxima. These results suggest that the sampling points chosen for the second reset condition need further tuning to improve the performance of the method.

7.3.11 Lundy cooling schedule with restricted searching bands, local search and reset condition

The two reset conditions from Section 7.3.10 are utilised with the Lundy cooling schedule implementation of the SA method with restricted searching bands and the P&O method as a local search mechanism. The clear and variable irradiance profiles with obstacle placement from Chapter 5 are used in this analysis.

Like in Section 7.3.10, neither condition leads to the global search being restarted for the clear day irradiance profile, even when a change in the conditions occurs. Of the 17 cases, the method has failed to locate the GMPP in 6 cases.

For the variable day irradiance profile, the method correctly identifies the GMPP in 38 of the 58 cases. Only reset condition two was successful in detecting when to initiate a global search. There were no cases where a global search was initiated that lead to a local MPP.

7.4 Conclusions and Future Enhancements

Conclusions that can be drawn from the analysis in this chapter suggest that:

- Neighbourhood searching bands around each MPP improve the performance.
- Weighted neighbourhood searching bands around each MPP have a more significant effect on improving the performance than non-weighted bands.
- Lundy cooling schedule implementations typically converge in more cases that implementations that use the geometric cooling schedule.
- A local search with small step size can improve the accuracy of the method.
- A modified stopping criterion can be a beneficial enhancement to the SA method, but is best applied in an implementation that also includes a local search method.

- Reset conditions for time-invariant approaches such as SA and PSO need further investigation.

These enhancements have lead to several implementations of the SA method that have superior performance to the method presented in Chapter 5. Further development on the method will reduce the number of samples required in the searching process and establish a more robust reset condition for time-invariant methods such as SA and PSO to improve their usefulness in PV systems operating under changing non-uniform conditions.

Chapter 8

Conclusions and Suggestions for Future Research

This thesis has presented a comprehensive analysis of the key issues that are involved in operating PV systems in a residential environment from the perspective of the consumer. In particular, the effects of Partial Shading Conditions (PSC) have been extensively explored and three key types of PSC defined to assess the effect each has on the relative location of the Global Maximum Power Point (GMPP) voltage. As consumers are driven by a need to extract maximum possible power from their PV system to ensure a good return on their investment, Maximum Power Point Tracking (MPPT) methods have been reviewed to assess their performance in locating the GMPP under the non-uniform environmental conditions that frequently arise in the residential environment. A Simulated Annealing (SA) based GMPPT method has been proposed and studied extensively to assess the effect of each parameter of the method and to combine key observations to enhance the capabilities of the proposed technique. The SA method has been selected as the focus for this research as it achieves reliable global peak identification without requiring extensive parameters, memory of multiple previous points, and has complexity not significantly greater than the Perturb and Observe (P&O) method.

8.1 Conclusions

In this thesis several conclusions have been reached. These conclusions are summarised below:

- Under PSC, the GMPP will most likely remain at the same MPP or undergo a transition to an adjacent MPP rather than moving to a significantly different voltage level.

- There is no single MPPT method that can perform GMPPT reliably and accurately and be easily adapted to other PV systems, without potentially having significant cost or complexity.
- The SA GMPPT method proposed, can perform GMPPT well with arbitarily selected parameters.
- The most significant parameters to improve the performance of the SA based GMPPT method with respect to the percentage of cases that converge and limiting the number of samples required, are the cooling schedule, stopping criterion, and neighbourhood size.
- Combining the SA based GMPPT method with a local search improves the performance in converging exactly to the GMPP and in providing continuous tracking.
- An improved reset condition for time-invariant MPPT methods is needed.

The main outcomes and contribution of the thesis are summarised as follows.

8.1.1 Modelling and Parameter Estimation of PV cells

In Chapter 2, the key concerns involved in modelling PV cells under both uniform and non-uniform conditions have been explored. Analytical parameter estimation methods designed to extract the five key parameters of the Single Diode Model (SDM) have been compared with respect to their modelling performance. MATLAB/Simulink based models of an individual BP380 PV module, and of two series-connected BP380 PV modules, have been developed and validated using experimentally measured I-V and P-V curves. The models show a good accuracy at modelling the I-V and P-V characteristics, however they have a maximum error of about 5% around the MPP. The SDM is selected due to a need to balance computational time with accuracy.

8.1.2 Assessment of Partial Shading Conditions

Partial Shading Conditions are defined as either constant, static or transient, depending on the time scale of their influence on the PV system, in Chapter 3. A methodology for exploring the influence of each type of shading has been presented, including projecting shadows from objects in the environment onto the PV modules to establish a shading factor for the static PSC. Five case studies have been described considering the three types of PSC. Key observations include that the GMPP voltage is most likely to remain at the same MPP or undergo a transition to an adjacent MPP location. Under the case studies it was also observed that the GMPP was typically in the higher voltage range than in the lower voltage range. These observations have been shown to be useful in guiding the development of GMPPT techniques.

8.1.3 Review and Comparative Analysis of MPPT Methods

Chapter 4 has extensively reviewed and compared all major maximum power extraction strategies identified in the literature with consideration of the performance of these techniques against key criteria. The key criteria assess how well each method is capable of performing GMPPT under non-uniform environmental conditions. Other key factors include the cost and complexity of the implementation. Of all the techniques considered, very few are shown to perform satisfactorily on all key criteria, suggesting that there is still a need for a low complexity and low cost, reliable GMPPT technique.

8.1.4 Development of a GMPPT Method Based on Simulated Annealing

The proposed SA based GMPPT method has been introduced in Chapter 5. Simulation results have been presented comparing the performance of the SA method against the P&O and IncCond methods in a two module system, and comparing the SA method with the P&O and Particle Swarm Optimisation

(PSO) methods in the eight module simulation model from Chapter 3. Experimental validation using the two series-connected BP380 PV modules under non-uniform environmental conditions has also been demonstrated. All implementations of the SA algorithm in this chapter showed satisfactory performance with arbitrarily selected parameters.

8.1.5 Towards an Improved SA Based GMPPT Method

To improve the suitability of the SA based GMPPT technique, Chapter 6 explored the key parameters of the SA method in simulation to assess which parameters had the greatest influence on improving the performance. Results from this chapter suggest that reducing the neighbourhood size and using the Lundy cooling schedule or Simulated Quenching, can improve the performance of the SA method and reduce the number of samples required in searching for the GMPP.

Chapter 7 combined observations from Chapters 3, 5, and 6 to develop several improved SA based GMPPT implementations. Key enhancements included using weighted neighbourhood searching bands around each MPP, utilising the Lundy cooling schedule, and combining the SA based method with a second stage local search method to improve the exact convergence to the GMPP. The usefulness of reset conditions to determine when a change in environmental conditions occurs was also explored and warrants further investigation.

8.2 Suggestions for Future Research

The focus of this thesis has been on the issues involved in PV generation from the perspective of the consumer who has rooftop PV installed at their home or business. For this reason, the goal is to maximise the power available under all environmental conditions. The other key factor involved in PV installations in a residential environment is the connection of these systems to battery storage

systems or to the distribution network.

The Australian electricity grid, similar to others around the world, was initially designed on the basis of centralised generation providing power through distribution networks to residential and industrial loads [6]. As such, the progression of power through the network traditionally was from generation to transmission to distribution to loads [272]. With increased incentives and increased uptake of PV systems in the form of residential PV (as shown in Chapter 1), the electricity network is modified significantly by the presence of distributed generation in the distribution phase of the network. By increasing the penetration of distributed generation in the electricity network, the system now relies on the transaction of power generation and consumption [273]. Installing PV systems into the distribution grid can have an impact on the operation of the grid. A single PV installation is shown to have a negligible effect on the distribution system, but when more PV systems are included in the grid, the impacts can become significant [274]. The key issues relate to the fluctuating nature of the PV power, harmonics that the PV system can introduce in the electricity grid, and the effects of PV on protection systems. These issues can affect residential and large scale PV systems with different levels of severity [7–13]. Another issue for PV systems is detecting when the system has become islanded and changing the operation mode accordingly [275].

The focus of this research so far has considered the operation of a PV system with the SA based GMPPT method largely independently of the grid. The next stages involve exploring the effects that the SA method may introduce into the grid and developing strategies to mitigate any unfavourable effects. In its searching process, the SA algorithm needs to sample a wide range of voltages (or duty cycles) which could potentially lead to stress on the components of the converter. Quantifying the stress on the converter and providing options to mitigate this is a key step for future research.

For small scale residential PV systems, geographical dispersion is not possible to mitigate the voltage unbalance, caused by fluctuating power, at a single point of connection to the network, and any modifications to the network would incur significant costs. Forecasting, energy storage and reactive support are all possible options to mitigate voltage unbalance at points in the system [7, 10].

By integrating appropriately sized energy storage system with a PV system, constant power production can be achieved which would allow the system to be scheduled like a conventional generator [276].

PSC analysis presented in this thesis has focused on a simplified mapping of obstacles onto the PV modules. Future research to build on the proposed PSC assessment strategy would involve modelling complex obstacle shapes, isolating direct and diffuse irradiance and their effects, and modelling the tilt plane of the PV system. Incorporating the transmittance of each type of object could also form a useful enhancement to the assessment strategy. The PSC assessment strategy could also be extended to explore the PSC effects of large-scale PV systems. For a large scale system, the transient irradiance will become more significant as it is not possible to assume that there is uniform irradiance across all modules. This could be combined with a study of forecasting cloud cover and modelling the passage of clouds over a PV system.

Approaches such as Nested Annealing (NA) have been proposed to further reduce the time required by the SA algorithm, by breaking the sample space into sections and annealing each of these with a different temperature and cooling schedule to lead to the overall global optimal solution [265]. NA may be a possible future extension to the GMPPT problem for PV systems under partial shading as it would enable the key areas of interest of the search space to be searched more efficiently. In particular, combining the idea of NA with the results from [90] which shows the relative spacing of the MPPs is approximately 80% of the open-circuit voltage of each module, the search space considered by the technique could be considerably reduced. As each section can be annealed independently with a different temperature and cooling schedule, the sections where the GMPP is more likely to lie could be searched more exhaustively while sections where the GMPP is less likely to be located could undergo a cursory search. This would enable the results from Chapter 3 indicating the likely locations and movement of the relative GMPP to further guide the search.

As shown in Chapter 7, there is a need for a reset condition which can reliably determine when the environmental conditions have changed. This is an important area of future research, as the development of a suitable reset condition is not just important for PV systems with the SA algorithm, but also for other

time-invariant MPPT approaches such as PSO.

While the SA algorithm has been shown to perform well with arbitrarily selected parameters, future studies could generalise these parameters in terms of the key information on the manufacturer datasheets, to enable a robust and reliable GMPPT method based on SA, to be easily applied to any PV system.

Bibliography

[1] Hydro Tasmania, "Hydro Tasmania - our power stations," 2015. [Online]. Available: http://www.hydro.com.au/energy/our-power-stations

[2] Hydro Tasmania, "Hydro Tasmania - wind power," 2015. [Online]. Available: http://www.hydro.com.au/energy/our-power-stations/wind-power

[3] Australian Government Clean Energy Regulator, "RET - Small-scale installations by postcode," 2015. [Online]. Available: http://ret.cleanenergyregulator.gov.au/REC-Registry/Data-reports#SGU–Solar-Deemed

[4] L. Reid, K. Ellsworth-Krebs, and D. McCauley, "Conceptualising prosumption: exploring energy production and consumption in Scotland," in *Third European conference on behaviour and energy efficiency (BEHAVE) 2014*, 2014, pp. 1–15.

[5] Clean Energy Council, "Clean energy Australia report 2013," Tech. Rep., 2013.

[6] N. Hadjsaid, M. Alvarez-Herault, R. Caire, B. Raison, J. Descloux, and W. Bienia, "Novel architectures and operation modes of distribution network to increase DG integration," in *IEEE PES General Meeting*. IEEE, Jul. 2010, pp. 1–6.

[7] R. Yan and T. K. Saha, "Investigation of voltage stability for residential customers due to high photovoltaic penetrations," *IEEE Transactions on Power Systems*, vol. 27, no. 2, pp. 651–662, May 2012.

[8] I. T. Papaioannou, M. C. Alexiadis, C. S. Demoulias, D. P. Labridis, and P. S. Dokopoulos, "Modeling and field measurements of photovoltaic units connected to LV grid. study of penetration scenarios," *IEEE Transactions on Power Delivery*, vol. 26, no. 2, pp. 979–987, Apr. 2011.

[9] M. E. Baran, H. Hooshyar, Z. Shen, and A. Huang, "Accommodating high PV penetration on distribution feeders," *IEEE Transactions on Smart Grid*, vol. 3, no. 2, pp. 1039–1046, Jun. 2012.

[10] R. Passey, T. Spooner, I. MacGill, M. Watt, and K. Syngellakis, "The potential impacts of grid-connected distributed generation and how to address them: a review of technical and non-technical factors," *Energy Policy*, vol. 39, no. 10, pp. 6280–6290, Oct. 2011.

[11] P. D. F. Ferreira, P. M. S. Carvalho, L. A. F. M. Ferreira, and M. D. Ilic, "Distributed energy resources integration challenges in low-voltage networks: voltage control limitations and risk of cascading," *IEEE Transactions on Sustainable Energy*, vol. 4, no. 1, pp. 82–88, Jan. 2013.

[12] P.-C. Chen, R. Salcedo, Q. Zhu, F. de Leon, D. Czarkowski, Z.-P. Jiang, V. Spitsa, Z. Zabar, and R. E. Uosef, "Analysis of voltage profile problems due to the penetration of distributed generation in low-voltage secondary distribution networks," *IEEE Transactions on Power Delivery*, vol. 27, no. 4, pp. 2020–2028, Oct. 2012.

[13] W. A. Omran, M. Kazerani, and M. M. A. Salama, "Investigation of methods for reduction of power fluctuations generated from large grid-connected photovoltaic systems," *IEEE Transactions on Energy Conversion*, vol. 26, no. 1, pp. 318–327, Mar. 2011.

[14] W. Xiao, A. Elnosh, V. Khadkikar, and H. Zeineldin, "Overview of maximum power point tracking technologies for photovoltaic power systems," in *IEEE Industrial Electronics Society Conference (IECON)*, 2011, pp. 3900–3905.

[15] B. Subudhi and R. Pradhan, "A comparative study on maximum power point tracking techniques for photovoltaic power systems," *IEEE Transactions on Sustainable Energy*, vol. 4, no. 1, pp. 89–98, 2013.

[16] T. Esram and P. L. Chapman, "Comparison of photovoltaic array maximum power point tracking Techniques," *IEEE Transactions on Energy Conversion*, vol. 22, no. 2, pp. 439–449, 2007.

[17] M. A. G. de Brito, L. Galotto, L. P. Sampaio, G. de Azevedo e Melo, and C. A. Canesin, "Evaluation of the main MPPT techniques for photovoltaic applications," *IEEE Transactions on Industrial Electronics*, vol. 60, no. 3, pp. 1156–1167, 2013.

[18] A. Bidram, A. Davoudi, and R. S. Balog, "Control and circuit techniques to mitigate partial shading effects in photovoltaic arrays," *IEEE Journal of Photovoltaics*, vol. 2, no. 4, pp. 532–546, Oct. 2012.

[19] M. Miyatake, M. Veerachary, F. Toriumi, N. Fujii, and H. Ko, "Maximum power point tracking of multiple photovoltaic arrays: a PSO approach," *IEEE Transactions on Aerospace and Electronic Systems*, vol. 47, no. 1, pp. 367–380, 2011.

[20] T. L. Nguyen and K. S. Low, "A global maximum power point tracking scheme employing DIRECT search algorithm for photovoltaic systems," *IEEE Transactions on Industrial Electronics*, vol. 57, no. 10, pp. 3456–3467, 2010.

[21] M. Miyatake, T. Inada, I. Hiratsuka, Z. Hongyan, H. Otsuka, and M. Nakano, "Control characteristics of a fibonacci-search-based maximum power point tracker when a photovoltaic array is partially shaded," in *International Power Electronics and Motion Control Conference (IPEMC)*, vol. 2, 2004, pp. 816–821 Vol.2.

[22] P. Lei, Y. Li, and J. Seem, "Sequential ESC based global MPPT control for photovoltaic array with variable shading," *IEEE Transactions on Sustainable Energy*, vol. 2, no. 3, pp. 348–358, 2011.

[23] "BP 380 80 W photovoltaic module datasheet." [Online]. Available: http://www.solarcharge.com.au/docs/off-grid-solar-panel-BP-80-Watt.pdf

[24] H. Patel and V. Agarwal, "MATLAB-based modeling to study the effects of partial shading on PV array characteristics," *IEEE Transactions on Energy Conversion*, vol. 23, no. 1, pp. 302–310, Mar. 2008.

[25] F. Adamo, F. Attivissimo, A. Di Nisio, and M. Spadavecchia, "Analysis of the uncertainty of the double-diode model of a photovoltaic panel," in *IEEE Instrumentation and Measurement Technology Conference (I2MTC)*, 2011, pp. 1–5.

[26] M. E. Ropp and S. Gonzalez, "Development of a MATLAB/simulink model of a single-phase grid-connected photovoltaic system," *IEEE Transactions on Energy Conversion*, vol. 24, no. 1, pp. 195–202, 2009.

[27] L. Bun, B. Raison, G. Rostaing, S. Bacha, A. Rumeau, and A. Labonne, "Development of a real time photovoltaic simulator in normal and abnormal operations," in *IECON 2011 - 37th Annual Conference of the IEEE Industrial Electronics Society*, Nov. 2011, pp. 867–872.

[28] M. G. Villalva, J. R. Gazoli, and E. R. Filho, "Comprehensive approach to modeling and simulation of photovoltaic arrays," *IEEE Transactions on Power Electronics*, vol. 24, no. 5, pp. 1198–1208, 2009.

[29] J. A. Mazer, *Solar cells: an introduction to crystalline photovoltaic technology.* Kluwer Academic Publishers, 1997.

[30] M. R. Patel, *Wind and solar power systems: design, analysis, and operation.* CRC Press, 2006.

[31] M. A. Green, *Solar cells: operating principles, technology, and system applications.* Prentice-Hall, 1982.

[32] A. Keyhani, *Design of smart power grid renewable energy systems.* John Wiley & Sons, 2011.

[33] J. Yuncong, J. A. A. Qahouq, and M. Orabi, "Matlab/Pspice hybrid simulation modeling of solar PV cell/module," in *IEEE Applied Power Electronics Conference and Exposition (APEC)*, 2011, pp. 1244–1250.

[34] R. Hassan, G. Radman, and D. Gao, "User-friendly LabView tool to study effects of partial shading on PV characteristics," in *2011 Proceedings of IEEE Southeastcon*, Mar. 2011, pp. 64–67.

[35] A. Chatterjee and A. Keyhani, "Thevenin's equivalent of photovoltaic source models for MPPT and power grid studies," in *IEEE Power and Energy Society General Meeting*, 2011, pp. 1–7.

[36] D. M. Riley and G. K. Venayagamoorthy, "Characterization and modeling of a grid-connected photovoltaic system using a recurrent neural network," in *The 2011 International Joint Conference on Neural Networks*, Jul. 2011, pp. 1761–1766.

[37] A. Keyhani, "Modeling of photovoltaic microgrids for bulk power grid studies," in *IEEE Power and Energy Society General Meeting*, 2011, pp. 1–6.

[38] Y. Jiang, J. A. A. Qahouq, and I. Batarseh, "Improved solar PV cell Matlab simulation model and comparison," in *Proceedings of 2010 IEEE International Symposium on Circuits and Systems*, May 2010, pp. 2770–2773.

[39] M. K. Alam, F. Khan, and A. M. Imtiaz, "Optimization of subcell interconnection for multijunction solar cells using switching power converters," *IEEE Transactions on Sustainable Energy*, vol. 4, no. 2, pp. 340–349, Apr. 2013.

[40] V. Ganapati, C.-S. Ho, and E. Yablonovitch, "Air gaps as intermediate selective reflectors to reach theoretical efficiency limits of multibandgap solar cells," *IEEE Journal of Photovoltaics*, vol. 5, no. 1, pp. 410–417, Jan. 2015.

[41] A. McEvoy, L. Castaner, and T. Markvart, *Solar cells: materials, manufacture and operation*. Newnes, 2005.

[42] M. A. Green, K. Emery, Y. Hishikawa, W. Warta, and E. D. Dunlop, "Solar cell efficiency tables (Version 45)," *Progress in Photovoltaics: Research and Applications*, vol. 23, no. 1, pp. 1–9, Jan. 2015.

[43] K. Green, M. A. Emery, Y. Hishikawa, W. Warta, and E. D. Dunlop, "Solar cell efficiency tables (version 43)," *Progress in Photovoltaics: Research and Applications*, vol. 22, no. 1, pp. 1–9, Jan. 2014.

[44] G. Farivar and B. Asaei, "A new approach for solar module temperature estimation using the simple diode model," *IEEE Transactions on Energy Conversion*, vol. 26, no. 4, pp. 1118–1126, 2011.

[45] A. Chatterjee, A. Keyhani, and D. Kapoor, "Identification of photovoltaic source models," *IEEE Transactions on Energy Conversion*, vol. 26, no. 3, pp. 883–889, Sep. 2011.

[46] Solar3D, "Solar3D - breakthrough 3-dimensional solar cell technology," 2010. [Online]. Available: http://www.solar3d.com/

[47] CSIRO, "CTRL+P: printing Australia's largest solar cells," 2013. [Online]. Available: http://www.csiro.au/Portals/Media/Printing-Australias-largest-solar-cells.aspx

[48] M. Hammonds, "Printed solar cells as easy to produce as t-shirts!" Jun. 2013. [Online]. Available: http://www.australianscience.com.au/environmental-science/printed-solar-cells-as-easy-to-produce-as-t-shirts/

[49] S. Moballegh and J. Jiang, "Partial shading modeling of photovoltaic system with experimental validations," in *2011 IEEE Power and Energy Society General Meeting*, Jul. 2011, pp. 1–9.

[50] Y. Mahmoud, W. Xiao, and H. H. Zeineldin, "A simple approach to modeling and simulation of photovoltaic modules," *IEEE Transactions on Sustainable Energy*, vol. 3, no. 1, pp. 185–186, 2012.

[51] M. C. Di Piazza, M. Pucci, A. Ragusa, and G. Vitale, "Analytical versus neural real-time simulation of a photovoltaic generator based on a DC-DC converter," *IEEE Transactions on Industry Applications*, vol. 46, no. 6, pp. 2501–2510, 2010.

[52] J. A. Dolan, R. Lee, Y.-H. Yeh, C. Yeh, D. Y. Nguyen, S. Ben-Menahem, and A. K. Ishihara, "Neural network estimation of photovoltaic I–V curves under partially shaded conditions," in *The 2011 International Joint Conference on Neural Networks*, Jul. 2011, pp. 1358–1365.

[53] H. Andrei, T. Ivanovici, G. Predusca, E. Diaconu, and P. Andrei, "Curve fitting method for modeling and analysis of photovoltaic cells characteristics," in *Proceedings of 2012 IEEE International Conference on Automation, Quality and Testing, Robotics*, May 2012, pp. 307–312.

[54] E. I. Ortiz-Rivera, "Approximation of a photovoltaic module model using fractional and integral polynomials," in *2012 38th IEEE Photovoltaic Specialists Conference*, Jun. 2012, pp. 002 927–002 931.

[55] F. Adamo, F. Attivissimo, A. Di Nisio, and M. Spadavecchia, "Characterization and testing of a tool for photovoltaic panel modeling," *IEEE Transactions on Instrumentation and Measurement*, vol. 60, no. 5, pp. 1613–1622, May 2011.

[56] A. Yazdani, A. R. Di Fazio, H. Ghoddami, M. Russo, M. Kazerani, J. Jatskevich, K. Strunz, S. Leva, and J. A. Martinez, "Modeling guidelines and a benchmark for power system simulation studies of three-phase single-stage photovoltaic systems," *IEEE Transactions on Power Delivery*, vol. 26, no. 2, pp. 1247–1264, Apr. 2011.

[57] M. Jensen, R. Louie, M. Etezadi-Amoli, and M. Sami Fadali, "Model and simulation of a 75kW PV solar array," in *IEEE PES Transmission and Distribution Conference and Exposition*, 2010, pp. 1–5.

[58] F. Caracciolo, E. Dallago, D. G. Finarelli, A. Liberale, and P. Merhej, "Single-variable optimization method for evaluating solar cell and solar module parameters," *IEEE Journal of Photovoltaics*, vol. 2, no. 2, pp. 173–180, Apr. 2012.

[59] F. Attivissimo, A. Di Nisio, M. Savino, and M. Spadavecchia, "Uncertainty analysis in photovoltaic cell parameter estimation," *IEEE Transactions on Instrumentation and Measurement*, vol. 61, no. 5, pp. 1334–1342, May 2012.

[60] B. K. Nayak, A. Mohapatra, and K. B. Mohanty, "Parameters estimation of photovoltaic module using nonlinear least square algorithm: a comparative study," in *2013 Annual IEEE India Conference (INDICON)*, Dec. 2013, pp. 1–6.

[61] B. N. Alajmi, K. H. Ahmed, S. J. Finney, and B. W. Williams, "A maximum power point tracking technique for partially shaded photovoltaic systems in microgrids," *IEEE Transactions on Industrial Electronics*, vol. 60, no. 4, pp. 1596–1606, Apr. 2013.

[62] S. M. MacAlpine, R. W. Erickson, and M. J. Brandemuehl, "Characterization of power optimizer potential to increase energy capture in photovoltaic systems operating under nonuniform conditions," *IEEE Transactions on Power Electronics*, vol. 28, no. 6, pp. 2936–2945, Jun. 2013.

[63] E. Meyer and E. van Dyk, "Assessing the reliability and degradation of photovoltaic module performance parameters," *IEEE Transactions on Reliability*, vol. 53, no. 1, pp. 83–92, Mar. 2004.

[64] P. Junsangsri and F. Lombardi, "Double diode modeling of time/temperature induced degradation of solar cells," in *2010 53rd IEEE International Midwest Symposium on Circuits and Systems*, Aug. 2010, pp. 1005–1008.

[65] S. Guo, T. M. Walsh, A. G. Aberle, and M. Peters, "Analysing partial shading of PV modules by circuit modelling," in *2012 38th IEEE Photovoltaic Specialists Conference*, Jun. 2012, pp. 002 957–002 960.

[66] R. Ramaprabha and B. L. Mathur, "MATLAB based modelling to study the influence of shading on series connected SPVA," in *2009 Second International Conference on Emerging Trends in Engineering & Technology*, 2009, pp. 30–34.

[67] Y.-H. Ji, J.-G. Kim, S.-H. Park, J.-H. Kim, and C.-Y. Won, "C-language based PV array simulation technique considering effects of partial shading," in *2009 IEEE International Conference on Industrial Technology*, Feb. 2009, pp. 1–6.

[68] E. V. Paraskevadaki and S. A. Papathanassiou, "Evaluation of MPP voltage and power of mc-Si PV modules in partial shading conditions," *IEEE Transactions on Energy Conversion*, vol. 26, no. 3, pp. 923–932, Sep. 2011.

[69] O. G. Garcia, J. C. Hernandez, and F. Jurado, "Assessment of shading effects in photovoltaic modules," in *2011 Asia-Pacific Power and Energy Engineering Conference*, Mar. 2011, pp. 1–4.

[70] G. Liu and S. K. Nguang, "A general modeling method that simulates photovoltaic arrays for environmental and electrical variability," in *The 2010 IEEE International Conference on Information and Automation*, Jun. 2010, pp. 195–200.

[71] Y.-J. Wang and P.-C. Hsu, "Analytical modelling of partial shading and different orientation of photovoltaic modules," *IET Renewable Power Generation*, vol. 4, no. 3, p. 272, 2010.

[72] A. Mäki, S. Valkealahti, and J. Leppäaho, "Operation of series-connected silicon-based photovoltaic modules under partial shading conditions," *Progress in Photovoltaics: Research and Applications*, vol. 20, no. 3, pp. 298–309, May 2012.

[73] Y. Wang and P. Hsu, "Analysis of partially shaded PV modules using piecewise linear parallel branches model," *World Academy of Science, Engineering and Technology*, vol. 60, pp. 783–789, 2009.

[74] P. Lei, Y. Li, Q. Chen, and J. E. Seem, "Extremum seeking control based integration of MPPT and degradation detection for photovoltaic arrays," in *American Control Conference (ACC)*, 2010, pp. 3536–3541.

[75] J. S. Stein, S. McCaslin, C. W. Hansen, W. E. Boyson, and C. D. Robinson, "Measuring PV system series resistance without full IV curves," in *2014 IEEE 40th Photovoltaic Specialist Conference (PVSC)*, Jun. 2014, pp. 2032–2036.

[76] D. Sera, "Series resistance monitoring for photovoltaic modules in the vicinity of MPP," 2010, pp. 4506–4510.

[77] R. M. Smith, D. C. Jordan, and S. R. Kurtz, "Outdoor PV module degradation of current-voltage parameters," in *2012 World Renewable Energy Forum*, 2012, pp. 1–7.

[78] Kimo Instruments, "KIMO — SL 200 - solarimeter," 2014. [Online]. Available: http://www.kimo.fr/produits/276/sl_200.html?lang=en

[79] S. Moballegh and J. Jiang, "Modeling, prediction, and experimental validations of power peaks of PV arrays under partial shading conditions," *IEEE Transactions on Sustainable Energy*, vol. 5, no. 1, pp. 293–300, Jan. 2014.

[80] K. Ding, X. Bian, H. Liu, and T. Peng, "A MATLAB-simulink-based PV module model and its application under conditions of nonuniform irradiance," *IEEE Transactions on Energy Conversion*, vol. 27, no. 4, pp. 864–872, Dec. 2012.

[81] Bureau of Meteoroloy, "One minute solar data," 2012. [Online]. Available: http://www.bom.gov.au/climate/data/oneminsolar/about-IDCJAC0022.shtml

[82] Bureau of Meteoroloy, "Basic climatological station metadata," 2014. [Online]. Available: http://www.bom.gov.au/clim_data/cdio/metadata/pdf/siteinfo/IDCJMD0040.091148.SiteInfo.pdf

[83] National Renewable Energy Laboratory, "Oahu archive instrument descriptions and histories." [Online]. Available: http://www.nrel.gov/midc/oahu_archive/

[84] V. Quaschning and R. Hanitsch, "Shade calculations in photovoltaic systems," in *ISES Solar World Conference*, 1995, pp. 1–5.

[85] K. Jazayeri, S. Uysal, and M. Jazayeri, "MATLAB/simulink based simulation of solar incidence angle and the sun's position in the sky with respect to observation points on the Earth," in *2013 International Conference on Renewable Energy Research and Applications (ICRERA)*, Oct. 2013, pp. 173–177.

[86] M. Drif, P. Pérez, J. Aguilera, and J. Aguilar, "A new estimation method of irradiance on a partially shaded PV generator in grid-connected photovoltaic systems," *Renewable Energy*, vol. 33, no. 9, pp. 2048–2056, Sep. 2008.

[87] Deutsche Gesellschaft für Sonnenenergie, *Planning and Installing Photovoltaic Systems: A Guide for Installers, Architects and Engineers*. Routledge, 2013. [Online]. Available: http://books.google.com/books?id=AWIqAAAAQBAJ&pgis=1

[88] C. Honsberg and S. Bowden, "The sun's position— PVEducation." [Online]. Available: http://pveducation.org/pvcdrom/properties-of-sunlight/suns-position

[89] M. Iqbal, *An introduction to solar radiation.* Elsevier, 2012.

[90] H. Patel and V. Agarwal, "Maximum power point tracking scheme for PV systems operating under partially shaded conditions," *IEEE Transactions on Industrial Electronics*, vol. 55, no. 4, pp. 1689–1698, 2008.

[91] National Renewable Energy Laboratory, "Oahu solar measurement grid - 1-second global horizontal irradiance." [Online]. Available: http://www.nrel.gov/midc/oahu_archive/

[92] C. Honsberg and S. Bowden, "PV education - solar radiation on a tilted surface," 2015. [Online]. Available: http://www.pveducation.org/pvcdrom/properties-of-sunlight/solar-radiation-on-tilted-surface

[93] B. Bekker and H. J. Beukes, "Finding an optimal PV panel maximum power point tracking method," in *AFRICON Conference in Africa (AFRICON)*, vol. 2, 2004, pp. 1125–1129 Vol.2.

[94] O. Lopez-Lapena and M. Penella, "Low-power FOCV MPPT controller with automatic adjustment of the sample&hold," *Electronics Letters*, vol. 48, no. 20, p. 1301, 2012.

[95] Yu-Pei Huang, "A rapid maximum power measurement system for high-concentration photovoltaic modules using the fractional open-circuit voltage technique and controllable electronic load," *IEEE Journal of Photovoltaics*, vol. 4, no. 6, pp. 1610–1617, Nov. 2014.

[96] J. M. Blanes, F. J. Toledo, S. Montero, and A. Garrigós, "In-site real-time photovoltaic I–V curves and maximum power point estimator," *IEEE Transactions on Power Electronics*, vol. 28, no. 3, pp. 1234–1240, Mar. 2013.

[97] W. Xiao, M. Lind, W. Dunford, and A. Capel, "Real-time identification of optimal operating points in photovoltaic power systems," *IEEE Transactions on Industrial Electronics*, vol. 53, no. 4, pp. 1017–1026, Jun. 2006.

[98] A. Pandey, N. Dasgupta, and A. K. Mukerjee, "A simple single-sensor MPPT solution," *IEEE Transactions on Power Electronics*, vol. 22, no. 2, pp. 698–700, Mar. 2007.

[99] G. Farivar, B. Asaei, and S. Mehrnami, "An analytical solution for tracking photovoltaic module MPP," *IEEE Journal of Photovoltaics*, vol. 3, no. 3, pp. 1053–1061, Jul. 2013.

[100] A. Kuperman, "Comments on "an analytical solution for tracking photovoltaic module MPP"," *IEEE Journal of Photovoltaics*, vol. 4, no. 2, pp. 734–735, Mar. 2014.

[101] S. Patel and W. Shireen, "Fast converging digital MPPT control for photovoltaic (PV) applications," in *2011 IEEE Power and Energy Society General Meeting*, Jul. 2011, pp. 1–6.

[102] V. Scarpa, S. Buso, and G. Spiazzi, "Low-complexity MPPT technique exploiting the PV module MPP locus characterization," *IEEE Transactions on Industrial Electronics*, vol. 56, no. 5, pp. 1531–1538, 2009.

[103] Yi-Hua Liu, Zong-Zhen Yang, Shun-Chung Wang, and Jia-Wei Huang, "A novel analog MPPT technique for low power photovoltaic systems," in *IEEE Region 10 Conference*, Nov. 2011, pp. 833–837.

[104] L. V. Hartmann, M. A. Vitorino, M. B. a. d. R. Correa, and A. M. N. Lima, "Combining model-based and heuristic techniques for fast tracking the maximum-power point of photovoltaic systems," *IEEE Transactions on Power Electronics*, vol. 28, no. 6, pp. 2875–2885, Jun. 2013.

[105] A. K. Abdelsalam, S. Goh, O. Abdelkhalik, S. Ahmed, and A. Massoud, "Iterated unscented Kalman filter-based maximum power point tracking for photovoltaic applications," in *IECON 2013 - 39th Annual Conference of the IEEE Industrial Electronics Society*, Nov. 2013, pp. 1685–1693.

[106] M. A. Elgendy, B. Zahawi, and D. J. Atkinson, "Assessment of perturb and observe MPPT algorithm implementation techniques for PV pumping applications," *IEEE Transactions on Sustainable Energy*, vol. 3, no. 1, pp. 21–33, Jan. 2012.

[107] B. Alajmi, K. Ahmed, S. Finney, and B. Williams, "Fuzzy logic controlled approach of a modified hill climbing method for maximum power point in microgrid stand-alone photovoltaic system," *IEEE Transactions on Power Electronics*, vol. 26, no. 4, pp. 1022–1030, 2011.

[108] G. Carannante, C. Fraddanno, M. Pagano, and L. Piegari, "Experimental performance of MPPT algorithm for photovoltaic sources subject to inhomogeneous insolation," *IEEE Transactions on Industrial Electronics*, vol. 56, no. 11, pp. 4374–4380, Nov. 2009.

[109] A. K. Abdelsalam, A. M. Massoud, S. Ahmed, and P. N. Enjeti, "High-performance adaptive perturb and observe MPPT technique for photovoltaic-based microgrids," *IEEE Transactions on Power Electronics*, vol. 26, no. 4, pp. 1010–1021, Apr. 2011.

[110] D. Sera, R. Teodorescu, J. Hantschel, and M. Knoll, "Optimized maximum power point tracker for fast-changing environmental conditions," *IEEE Transactions on Industrial Electronics*, vol. 55, no. 7, pp. 2629–2637, Jul. 2008.

[111] A. Chikh and A. Chandra, "An optimum method for maximum power point tracking in photovoltaic systems," in *IEEE Power and Energy Society General Meeting*, 2011, pp. 1–6.

[112] A. Pandey, N. Dasgupta, and A. Mukerjee, "High-performance algorithms for drift avoidance and fast tracking in solar MPPT system," *IEEE Transactions on Energy Conversion*, vol. 23, no. 2, pp. 681–689, Jun. 2008.

[113] R. A. Mastromauro, M. Liserre, and A. Dell'Aquila, "Control issues in single-stage photovoltaic systems: MPPT, current and voltage control," *IEEE Transactions on Industrial Informatics.*, vol. 8, no. 2, pp. 241–254, May 2012.

[114] H. Al-Atrash, I. Batarseh, and K. Rustom, "Effect of measurement noise and bias on hill-climbing MPPT algorithms," *IEEE Transactions on Aerospace and Electronic Systems*, vol. 46, no. 2, pp. 745–760, Apr. 2010.

[115] Jia-Wei Huang, Chun-Liang Liu, Rong-Ceng Leou, and Yi-Hua Liu, "Design and implementation of a FLC-based MPPT technique for photovoltaic systems," in *IEEE Region 10 Conference*, Nov. 2011, pp. 903–907.

[116] P. Manganiello, M. Ricco, G. Petrone, E. Monmasson, and G. Spagnuolo, "Optimization of perturbative PV MPPT methods through on line system identification," *IEEE Transactions on Industrial Electronics*, vol. 61, no. 12, pp. 1–1, 2014.

[117] H. Patel and V. Agarwal, "MPPT scheme for a PV-fed single-phase single-stage grid-connected inverter operating in CCM with only one current sen-

sor," *IEEE Transactions on Energy Conversion*, vol. 24, no. 1, pp. 256–263, Mar. 2009.

[118] S. K. Kollimalla and M. K. Mishra, "Variable perturbation size adaptive P&O MPPT algorithm for sudden changes in irradiance," *IEEE Transactions on Sustainable Energy*, vol. 5, no. 3, pp. 1–1, 2014.

[119] Byunggyu Yu, Gwonjong Yu, and Youngroc Kim, "Design and experimental results of improved dynamic MPPT performance by EN50530," in *IEEE 33rd International Telecommunications Energy Conference (INTELEC)*, Oct. 2011, pp. 1–4.

[120] S. B. Kjaer, "Evaluation of the "hill climbing" and the "incremental conductance" maximum power point trackers for photovoltaic power systems," *IEEE Transactions on Energy Conversion*, vol. 27, no. 4, pp. 922–929, 2012.

[121] F. Scarpetta, M. Liserre, and R. A. Mastromauro, "Adaptive distributed MPPT algorithm for photovoltaic systems," in *38th Annual Conference on IEEE Industrial Electronics Society*, Oct. 2012, pp. 5708–5713.

[122] M. Mosa, H. Abu Rub, M. E. Ahmed, and J. Rodriguez, "Modified MPPT with using model predictive control for multilevel boost converter," in *38th Annual Conference on IEEE Industrial Electronics Society*, Oct. 2012, pp. 5080–5085.

[123] D. C. Jones and R. W. Erickson, "Probabilistic analysis of a generalized perturb and observe algorithm featuring robust operation in the presence of power curve traps," *IEEE Transactions on Power Electronics*, vol. 28, no. 6, pp. 2912–2926, Jun. 2013.

[124] A. Ingegnoli and A. Iannopollo, "A maximum power point tracking algorithm for stand-alone photovoltaic systems controlled by low computational power devices," in *IEEE Mediterranean Electrotechnical Conference*, 2010, pp. 1522–1527.

[125] Q. Yang and Q. Wang, "An improving control method of CTV +P&O on photovoltaic power generation maximum power point tracking," in *2013 5th International Conference on Intelligent Human-Machine Systems and Cybernetics*, vol. 1, Aug. 2013, pp. 285–288.

[126] L. Tang, Y. Zhang, W. Xu, and C. Zeng, "Novel variable step-size maximum power point tracking control strategy for PV systems based on contingence

angles," in *2013 IEEE Energy Conversion Congress and Exposition*, Sep. 2013, pp. 3904–3911.

[127] F. Guinjoan, C. Alonso, L. Martnez-Salamero, L. Sguier, and C. Cabal, "Maximum power point tracking based on sliding-mode control for output-series connected converters in photovoltaic systems," *IET Power Electronics*, vol. 7, no. 4, pp. 914–923, Apr. 2014.

[128] D. Sera, L. Mathe, T. Kerekes, S. V. Spataru, and R. Teodorescu, "On the perturb-and-observe and incremental conductance MPPT methods for PV systems," *IEEE Journal of Photovoltaics*, vol. 3, no. 3, pp. 1070–1078, Jul. 2013.

[129] Phan Quoc Dzung, Nguyen Truong Dan Vu, Nguyen Bao Anh, Le Minh Phuong, Le Chi Hiep, and Hong-Hee Lee, "The low-cost single-stage grid connected photovoltaic system with a modified MPPT method," in *IEEE International Conference on Power System Technology (POWERCON)*, Oct. 2012, pp. 1–6.

[130] M. A. Elgendy, B. Zahawi, and D. J. Atkinson, "Assessment of the incremental conductance maximum power point tracking algorithm," *IEEE Transactions on Sustainable Energy*, vol. 4, no. 1, pp. 108–117, Jan. 2013.

[131] A. Safari and S. Mekhilef, "Simulation and hardware implementation of incremental conductance MPPT with direct control method using cuk converter," *IEEE Transactions on Industrial Electronics*, vol. 58, no. 4, pp. 1154–1161, 2011.

[132] Y. H. Ji, D. Y. Jung, J. G. Kim, J. H. Kim, T. Lee, and C. Y. Won, "A real maximum power point tracking method for mismatching compensation in PV array under partially shaded conditions," *IEEE Transactions on Power Electronics*, vol. 26, no. 4, pp. 1001–1009, 2011.

[133] Fangrui Liu, Shanxu Duan, Fei Liu, Bangyin Liu, and Yong Kang, "A variable step size INC MPPT method for PV systems," *IEEE Transactions on Industrial Electronics*, vol. 55, no. 7, pp. 2622–2628, Jul. 2008.

[134] G.-C. Hsieh, H.-I. Hsieh, C.-Y. Tsai, and C.-H. Wang, "Photovoltaic power-increment-aided incremental-conductance MPPT with two-phased tracking," *IEEE Transactions on Power Electronics*, vol. 28, no. 6, pp. 2895–2911, Jun. 2013.

[135] S. Dwari, L. Arnedo, S. Oggianu, and V. Blasko, "An advanced high performance maximum power point tracking technique for photovoltaic systems," in *2013 Twenty-Eighth Annual IEEE Applied Power Electronics Conference and Exposition (APEC)*, Mar. 2013, pp. 3011–3015.

[136] M. R. Chavoshian, A. Rouholamini, H. R. Naji, R. Fadaeinedjad, and R. Faraji, "FPGA-based real time incremental conductance maximum power point tracking controller for photovoltaic systems," *IET Power Electronics*, vol. 7, no. 5, pp. 1294–1304, May 2014.

[137] M. Negnevitsky, *Artificial intelligence: a guide to intelligent systems*, 2nd ed. Pearson Education Limited, 2002.

[138] A. Al Nabulsi and R. Dhaouadi, "Efficiency optimization of a DSP-based standalone PV system using fuzzy logic and dual-MPPT control," *IEEE Transactions on Industrial Informatics.*, vol. 8, no. 3, pp. 573–584, Aug. 2012.

[139] R. Garraoui, L. Sbita, and M. Ben Hamed, "MPPT controller for a photovoltaic power system based on fuzzy logic," in *10th International Multi-Conferences on Systems, Signals & Devices 2013 (SSD13)*, Mar. 2013, pp. 1–6.

[140] N. A. Rahim, A. Che Soh, M. A. M. Radzi, and M. A. A. M. Zainuri, "Development of adaptive perturb and observe-fuzzy control maximum power point tracking for photovoltaic boost dc–dc converter," *IET Renewable Power Generation*, vol. 8, no. 2, pp. 183–194, Mar. 2014.

[141] I. Purnama, Y.-K. Lo, and H.-J. Chiu, "A fuzzy control maximum power point tracking photovoltaic system," in *IEEE International Conference on Fuzzy Systems (FUZZ-IEEE)*, Jun. 2011, pp. 2432–2439.

[142] A. M. Z. Alabedin, E. F. El-Saadany, and M. M. A. Salama, "Maximum power point tracking for photovoltaic systems using fuzzy logic and artificial neural networks," in *IEEE Power and Energy Society General Meeting*, Jul. 2011, pp. 1–9.

[143] C.-S. Chiu, "T-S fuzzy maximum power point tracking control of solar power generation systems," *IEEE Transactions on Energy Conversion*, vol. 25, no. 4, pp. 1123–1132, Dec. 2010.

[144] C.-S. Chiu and Y.-L. Ouyang, "Robust maximum power tracking control of uncertain photovoltaic systems: a unified T-S fuzzy model-based ap-

proach," *IEEE Transactions on Control Systems Technology*, vol. 19, no. 6, pp. 1516–1526, Nov. 2011.

[145] S. Mishra and P. C. Sekhar, "Ts fuzzy based adaptive perturb algorithm for MPPT of a grid connected single stage three phase VSC interfaced PV generating system," in *IEEE Power and Energy Society General Meeting*, Jul. 2012, pp. 1–7.

[146] A. M. Noman, K. E. Addoweesh, and H. M. Mashaly, "A fuzzy logic control method for MPPT of PV systems," in *38th Annual Conference on IEEE Industrial Electronics Society*, Oct. 2012, pp. 874–880.

[147] S. Mishra and P. C. Sekhar, "Takagi–Sugeno fuzzy-based incremental conductance algorithm for maximum power point tracking of a photovoltaic generating system," *IET Renewable Power Generation*, vol. 8, no. 8, pp. 900–914, Nov. 2014.

[148] A. El Khateb, N. A. Rahim, J. Selvaraj, and M. N. Uddin, "Fuzzy logic controller based SEPIC converter for maximum power point tracking," *IEEE Transactions on Industry Applications*, vol. 50, no. 4, pp. 1–1, 2014.

[149] Hong-Hee Lee, Le Minh Phuong, Phan Quoc Dzung, Nguyen Truong Dan Vu, and Le Dinh Khoa, "The new maximum power point tracking algorithm using ANN-based solar PV systems," in *IEEE Region 10 Conference*, Nov. 2010, pp. 2179–2184.

[150] M. Asiful Islam and M. Ashfanoor Kabir, "Neural network based maximum power point tracking of photovoltaic arrays," in *IEEE Region 10 Conference*, Nov. 2011, pp. 79–82.

[151] K. Ishaque, Z. Salam, M. Amjad, and S. Mekhilef, "An improved particle swarm optimization (PSO)- based MPPT for PV with reduced steady state oscillation," *IEEE Transactions on Power Electronics*, vol. 27, no. 8, pp. 3627–3638, 2012.

[152] D. Shmilovitz, "On the control of photovoltaic maximum power point tracker via output parameters," *IEE Proceedings - Electric Power Applications*, vol. 152, no. 2, p. 239, 2005.

[153] G. A. Amaratunga and C. Urayai, "Single-sensor maximum power point tracking algorithms," *IET Renewable Power Generation*, vol. 7, no. 1, pp. 82–88, Jan. 2013.

[154] J. A. Abu Qahouq, "Multiple solar panels maximum power point tracking using the output current," in *2011 IEEE 33rd International Telecommunications Energy Conference (INTELEC)*, Oct. 2011, pp. 1–5.

[155] G. M. Dousoky, E. M. Ahmed, and M. Shoyama, "Current-sensorless MPPT with DC-DC boost converter for photovoltaic battery chargers," in *2012 IEEE Energy Conversion Congress and Exposition (ECCE)*, Sep. 2012, pp. 1607–1614.

[156] Q. Mei, M. Shan, L. Liu, and J. M. Guerrero, "A novel improved variable step-size incremental-resistance MPPT method for PV systems," *IEEE Transactions on Industrial Electronics*, vol. 58, no. 6, pp. 2427–2434, Jun. 2011.

[157] E. Dallago, D. G. Finarelli, U. P. Gianazza, A. L. Barnabei, and A. Liberale, "Theoretical and experimental analysis of an MPP detection algorithm employing a single-voltage sensor only and a noisy signal," *IEEE Transactions on Power Electronics*, vol. 28, no. 11, pp. 5088–5097, Nov. 2013.

[158] Y. Jiang and J. Abu Qahouq, "Single-sensor multi-channel maximum power point tracking controller for photovoltaic solar systems," *IET Power Electronics*, vol. 5, no. 8, p. 1581, 2012.

[159] K. Young, V. Utkin, and U. Ozguner, "A control engineer's guide to sliding mode control," *IEEE Transactions on Control Systems Technology*, vol. 7, no. 3, pp. 328–342, May 1999.

[160] J. Hung, W. Gao, and J. Hung, "Variable structure control: a survey," *IEEE Transactions on Industrial Electronics*, vol. 40, no. 1, pp. 2–22, 1993.

[161] Y. Levron and D. Shmilovitz, "Maximum power point tracking employing sliding mode control," *IEEE Transactions on Circuits and Systems I: Regular Papers*, vol. 60, no. 3, pp. 724–732, Mar. 2013.

[162] E. Bianconi, J. Calvente, R. Giral, E. Mamarelis, G. Petrone, C. A. Ramos-Paja, G. Spagnuolo, and M. Vitelli, "A fast current-based MPPT technique employing sliding mode control," *IEEE Transactions on Industrial Electronics*, vol. 60, no. 3, pp. 1168–1178, Mar. 2013.

[163] E. Jimenez-Brea, A. Salazar-Llinas, E. Ortiz-Rivera, and J. Gonzalez-Llorente, "A maximum power point tracker implementation for photovoltaic cells using dynamic optimal voltage tracking," in *25th Annual IEEE Ap-*

plied Power Electronics Conference and Exposition (APEC), Feb. 2010, pp. 2161–2165.

[164] A. H. Alqahtani and V. I. Utkin, "Self-optimization of photovoltaic system power generation based on sliding mode control," in *38th Annual Conference on IEEE Industrial Electronics Society*, Oct. 2012, pp. 3468–3474.

[165] A. Hussain, A. Kumar, and L. Behera, "Sliding mode control of a buck converter for maximum power point tracking of a solar panel," in *2013 IEEE International Conference on Control Applications (CCA)*, Aug. 2013, pp. 661–666.

[166] J. W. Kimball and P. T. Krein, "Discrete-time ripple correlation control for maximum power point tracking," *IEEE Transactions on Power Electronics*, vol. 23, no. 5, pp. 2353–2362, Sep. 2008.

[167] A. M. Bazzi and P. T. Krein, "Concerning "maximum power point tracking for photovoltaic optimization using ripple-based extremum seeking control"," *IEEE Transactions on Power Electronics*, vol. 26, no. 6, pp. 1611–1612, Jun. 2011.

[168] T. Esram, J. W. Kimball, P. T. Krein, P. L. Chapman, and P. Midya, "Dynamic maximum power point tracking of photovoltaic arrays using ripple correlation control," *IEEE Transactions on Power Electronics*, vol. 21, no. 5, pp. 1282–1291, 2006.

[169] X. Li, Y. Li, J. E. Seem, and P. Lei, "Maximum power point tracking for photovoltaic systems using adaptive extremum seeking control," in *IEEE Conference on Decision and Control and European Control Conference*, Dec. 2011, pp. 1503–1508.

[170] S. Moura and Y. Chang, "Asymptotic convergence through Lyapunov-based switching in extremum seeking with application to photovoltaic systems," in *American Control Conference*, 2010, pp. 3542–3548.

[171] F.-S. Pai, R.-M. Chao, S. H. Ko, and T.-S. Lee, "Performance evaluation of parabolic prediction to maximum power point tracking for PV array," *IEEE Transactions on Sustainable Energy*, vol. 2, no. 1, pp. 60–68, Jan. 2010.

[172] P. Wang, H. Zhu, W. Shen, F. H. Choo, P. C. Loh, and K. K. Tan, "A novel approach of maximizing energy harvesting in photovoltaic systems based on

bisection search theorem," in *IEEE Applied Power Electronics Conference and Exposition (APEC)*, 2010, pp. 2143–2148.

[173] N. Shiota, V. Phimmasone, T. Abe, and M. Miyatake, "A MPPT algorithm based on the binary-search technique with ripples from a converter," in *2013 International Conference on Electrical Machines and Systems (ICEMS)*, Oct. 2013, pp. 1718–1721.

[174] L. Tang, W. Xu, C. Zeng, D. Dorrell, and X. Yu, "A linear-prediction maximum power point tracking algorithm for photovoltaic power generation," in *38th Annual Conference on IEEE Industrial Electronics Society*, Oct. 2012, pp. 3334–3339.

[175] W. Dunford, P. Palmer, and A. Capel, "Application of centered differentiation and steepest descent to maximum power point tracking," *IEEE Transactions on Industrial Electronics*, vol. 54, no. 5, pp. 2539–2549, Oct. 2007.

[176] Y. Jiang, J. A. Abu Qahouq, and T. A. Haskew, "Adaptive step size with adaptive-perturbation-frequency digital MPPT controller for a single-sensor photovoltaic solar system," *IEEE Transactions on Power Electronics*, vol. 28, no. 7, pp. 3195–3205, Jul. 2013.

[177] L. Zhang, W. G. Hurley, and W. Wolfle, "A new approach to achieve maximum power point tracking for PV system with a variable inductor," in *The 2nd International Symposium on Power Electronics for Distributed Generation Systems*, Jun. 2010, pp. 948–952.

[178] S. Jain and V. Agarwal, "Comparison of the performance of maximum power point tracking schemes applied to single-stage grid-connected photovoltaic systems," *IET Electric Power Applications*, vol. 1, no. 5, p. 753, 2007.

[179] T. Dineshkumar and M. Subramani, "Design and implementation maximum power point tracking in photovoltaic cells," in *International Conference on Energy Efficient Technologies for Sustainability*, Apr. 2013, pp. 792–795.

[180] A. O. Ibrahim and O. Basir, "A novel sensorless support vector regression based multi-stage algorithm to track the maximum power point for photovoltaic systems," in *2013 IEEE Power & Energy Society General Meeting*, Jul. 2013, pp. 1–5.

[181] F. Jaramillo-Lopez, G. Damm, G. Kenne, and F. Lamnabhi-Lagarrigue, "Adaptive control scheme for maximum power point tracking of a photovoltaic system connected to the grid." in *2013 European Control Conference (ECC)*, 2013, pp. 3053–3058.

[182] J. S. C. M. Raj and A. E. Jeyakumar, "A novel maximum power point tracking technique for photovoltaic module based on power plane analysis of I-V characteristics," *IEEE Transactions on Industrial Electronics*, vol. 61, no. 9, pp. 4734–4745, Sep. 2014.

[183] P. S. Pai and S. Beevi, "Dual maximization of solar power for medium power application," in *2013 International Conference on Renewable Energy Research and Applications (ICRERA)*, Oct. 2013, pp. 269–273.

[184] A. H. ALQahtani, M. S. Abuhamdeh, Y. M. Alsmadi, and V. I. Utkin, "Photovoltaic power optimization using sliding mode control with a two-axis tracking system," in *2013 IEEE Energytech*, Jul. 2013, pp. 1–6.

[185] E. Koutroulis and F. Blaabjerg, "A new technique for tracking the global maximum power point of PV arrays operating under partial-shading conditions," *IEEE Journal of Photovoltaics*, vol. 2, no. 2, pp. 184–190, 2012.

[186] D. Wang, "A method for instantaneous measurement of PV VI characteristics and its application for MPPT control," in *IEEE Photovoltaic Specialists Conference*, 2010, pp. 2904–2907.

[187] S. Bifaretti, V. Iacovone, L. Cina, and E. Buffone, "Global MPPT method for partially shaded photovoltaic modules," in *IEEE Energy Conversion Congress and Exposition (ECCE)*, 2012, pp. 4768–4775.

[188] P. K. Peter and V. Agarwal, "On the input resistance of a reconfigurable switched capacitor DC–DC converter-based maximum power point tracker of a photovoltaic source," *IEEE Transactions on Power Electronics*, vol. 27, no. 12, pp. 4880–4893, Dec. 2012.

[189] C. Y. Yang, C. Y. Hsieh, F. K. Feng, and K. H. Chen, "Highly efficient analog maximum power point tracking (AMPPT) in a photovoltaic system," *IEEE Transactions on Circuits and Systems I: Regular Papers*, vol. 59, no. 7, pp. 1546–1556, 2012.

[190] S. Kazmi, H. Goto, O. Ichinokura, and G. Hai-Jiao, "An improved and very efficient MPPT controller for PV systems subjected to rapidly varying

atmospheric conditions and partial shading," in *Australasian Universities Power Engineering Conference (AUPEC)*, 2009, pp. 1–6.

[191] K. Kobayashi, I. Takano, and Y. Sawada, "A study on a two stage maximum power point tracking control of a photovoltaic system under partially shaded insolation conditions," in *IEEE Power Engineering Society General Meeting*, vol. 4, 2003, p. 2617 Vol. 4.

[192] M. Sokolov and D. Shmilovitz, "A modified MPPT scheme for accelerated convergence," *IEEE Transactions on Energy Conversion*, vol. 23, no. 4, pp. 1105–1107, Dec. 2008.

[193] S. Kabir, R. Bansal, and M. Nadarajah, "Effects of partial shading on photovoltaic with advanced MPPT scheme," in *IEEE International Conference on Power and Energy (PECon)*, Dec. 2012, pp. 354–359.

[194] K. L. Lian, J. H. Jhang, and I. S. Tian, "A maximum power point tracking method based on perturb-and-observe combined with particle swarm optimization," *IEEE Journal of Photovoltaics*, vol. 4, no. 2, pp. 626–633, Mar. 2014.

[195] G. Escobar, C. N. M. Ho, and S. Pettersson, "Maximum power point searching method for partial shaded PV strings," in *IEEE Industrial Electronics Society Conference (IECON)*, 2012, pp. 5726–5731.

[196] Kok Soon Tey and S. Mekhilef, "Modified incremental conductance algorithm for photovoltaic system under partial shading conditions and load variation," *IEEE Transactions on Industrial Electronics*, vol. 61, no. 10, pp. 5384–5392, Oct. 2014.

[197] M. Boztepe, F. Guinjoan, G. Velasco-Quesada, S. Silvestre, A. Chouder, and E. Karatepe, "Global MPPT scheme for photovoltaic string inverters based on restricted voltage window search algorithm," *IEEE Transactions on Industrial Electronics*, vol. 61, no. 7, pp. 3302–3312, Jul. 2014.

[198] R. Ramaprabha, B. Mathur, A. Ravi, and S. Aventhika, "Modified fibonacci search based MPPT scheme for SPVA under partial shaded conditions," in *International Conference on Emerging Trends in Engineering and Technology (ICETET)*, 2010, pp. 379–384.

[199] K. Ishaque, Z. Salam, and A. Shamsudin, "Application of particle swarm optimization for maximum power point tracking of PV system with di-

rect control method," in *IEEE Industrial Electronics Society Conference (IECON)*, 2011, pp. 1214–1219.

[200] L. R. Chen, C. H. Tsai, Y. L. Lin, and Y. S. Lai, "A biological swarm chasing algorithm for tracking the PV maximum power point," *IEEE Transactions on Energy Conversion*, vol. 25, no. 2, pp. 484–493, 2010.

[201] L. Yi-Hwa, H. Shyh-Ching, H. Jia-Wei, and L. Wen-Cheng, "A particle swarm optimization-based maximum power point tracking algorithm for PV systems operating under partially shaded conditions," *IEEE Transactions on Energy Conversion*, vol. 27, no. 4, pp. 1027–1035, 2012.

[202] K. Ishaque and Z. Salam, "A deterministic particle swarm optimization maximum power point tracker for photovoltaic system under partial shading condition," *IEEE Transactions on Industrial Electronics*, vol. 60, no. 8, pp. 3195–3206, 2013.

[203] B. G. S. Dhas and S. N. Deepa, "A hybrid PSO and GSA-based maximum power point tracking algorithm for PV systems," in *2013 IEEE International Conference on Computational Intelligence and Computing Research*, Dec. 2013, pp. 1–4.

[204] K. Sundareswaran, S. Peddapati, and S. Palani, "MPPT of PV systems under partial shaded conditions through a colony of flashing fireflies," *IEEE Transactions on Energy Conversion*, vol. 29, no. 2, pp. 463–472, Jun. 2014.

[205] L. Zhou, Y. Chen, K. Guo, and F. Jia, "New approach for MPPT control of photovoltaic system with mutative scale dual carrier chaotic search," *IEEE Transactions on Power Electronics*, vol. 26, no. 4, pp. 1038–1048, 2011.

[206] C. Konstantopoulos and E. Koutroulis, "Global maximum power point tracking of flexible photovoltaic modules," *IEEE Transactions on Power Electronics*, vol. 29, no. 6, pp. 2817–2828, Jun. 2014.

[207] J. Yuncong, J. A. A. Qahouq, A. Hassan, M. E. Ahmed, and M. Orabi, "Energy efficient fine-grained approach for solar photovoltaic management system," in *IEEE International Telecommunications Energy Conference (INTELEC)*, 2011, pp. 1–4.

[208] R. C. N. Pilawa-Podgurski and D. J. Perreault, "Sub-module integrated distributed maximum power point tracking for solar photovoltaic applications," in *IEEE Energy Conversion Congress and Exposition (ECCE)*, 2012, pp. 4776–4783.

[209] N. Femia, G. Lisi, G. Petrone, G. Spagnuolo, and M. Vitelli, "Distributed maximum power point tracking of photovoltaic arrays: novel approach and system analysis," *IEEE Transactions on Industrial Electronics*, vol. 55, no. 7, pp. 2610–2621, 2008.

[210] R. Alonso, E. Roman, A. Sanz, V. E. M. Santos, and P. Ibanez, "Analysis of inverter-voltage influence on distributed MPPT architecture performance," *IEEE Transactions on Industrial Electronics*, vol. 59, no. 10, pp. 3900–3907, 2012.

[211] A. Elasser, M. Agamy, J. Sabate, R. Steigerwald, R. Fisher, and M. Harfman-Todorovic, "A comparative study of central and distributed MPPT architectures for megawatt utility and large scale commercial photovoltaic plants," in *IEEE Industrial Electronics Society Conference (IECON)*, 2010, pp. 2753–2758.

[212] S. Poshtkouhi, V. Palaniappan, M. Fard, and O. Trescases, "A general approach for quantifying the benefit of distributed power electronics for fine grained MPPT in photovoltaic applications using 3D modeling," *IEEE Transactions on Power Electronics*, vol. 27, no. 11, pp. 4656–4666, 2012.

[213] S. V. Dhople, R. Bell, J. Ehlmann, A. Davoudi, P. L. Chapman, and A. D. Domínguez-García, "A global maximum power point tracking method for PV module integrated converters," in *IEEE Energy Conversion Congress and Exposition (ECCE)*, 2012, pp. 4762–4767.

[214] P. S. Shenoy, K. A. Kim, B. B. Johnson, and P. T. Krein, "Differential power processing for increased energy production and reliability of photovoltaic systems," *IEEE Transactions on Power Electronics*, vol. 28, no. 6, pp. 2968–2979, 2013.

[215] L. F. L. Villa, H. Tien-Phu, J. C. Crebier, and B. Raison, "A power electronics equalizer application for partially shaded photovoltaic modules," *IEEE Transactions on Industrial Electronics*, vol. 60, no. 3, pp. 1179–1190, 2013.

[216] H. Ghoddami and A. Yazdani, "A single-stage three-phase photovoltaic system with enhanced maximum power point tracking capability and increased power rating," *IEEE Transactions on Power Delivery*, vol. 26, no. 2, pp. 1017–1029, Apr. 2011.

[217] W. Xiao, N. Ozog, and W. G. Dunford, "Topology study of photovoltaic interface for maximum power point tracking," *IEEE Transactions on Industrial Electronics*, vol. 54, no. 3, pp. 1696–1704, Jun. 2007.

[218] A. J. Hanson, C. A. Deline, S. M. MacAlpine, J. T. Stauth, and C. R. Sullivan, "Partial-shading assessment of photovoltaic installations via module-level monitoring," *IEEE Journal of Photovoltaics*, vol. 4, no. 6, pp. 1618–1624, Nov. 2014.

[219] S.-M. Chen, T.-J. Liang, and K.-R. Hu, "Design, analysis, and implementation of solar power optimizer for DC distribution system," *IEEE Transactions on Power Electronics*, vol. 28, no. 4, pp. 1764–1772, Apr. 2013.

[220] G. Petrone, G. Spagnuolo, and M. Vitelli, "An analog technique for distributed MPPT PV applications," *IEEE Transactions on Industrial Electronics*, vol. 59, no. 12, pp. 4713–4722, 2012.

[221] C. A. Ramos-Paja, G. Spagnuolo, G. Petrone, S. Serna, and A. Trejos, "A vectorial MPPT algorithm for distributed photovoltaic applications," in *2013 International Conference on Clean Electrical Power (ICCEP)*, Jun. 2013, pp. 48–51.

[222] P. Ganeshkumar and A. Ahmed, "FPGA based multi-module converter controller for photovoltaic maximum power point tracking," in *2013 International Conference on Electrical Machines and Systems (ICEMS)*, Oct. 2013, pp. 148–151.

[223] J. A. Abu Qahouq and Y. Jiang, "Distributed photovoltaic solar system architecture with single-power inductor single-power converter and single-sensor single maximum power point tracking controller," *IET Power Electronics*, vol. 7, no. 10, pp. 2600–2609, Oct. 2014.

[224] P. Sharma and V. Agarwal, "Exact maximum power point tracking of grid-connected partially shaded PV source using current compensation concept," *IEEE Transactions on Power Electronics*, vol. 29, no. 9, pp. 4684–4692, Sep. 2014.

[225] S. Qin, S. T. Cady, A. D. Dominguez-Garcia, and R. C. N. Pilawa-Podgurski, "A distributed approach to maximum power point tracking for photovoltaic submodule differential power processing," *IEEE Transactions on Power Electronics*, vol. 30, no. 4, pp. 2024–2040, Apr. 2015.

[226] C. Olalla, C. Deline, D. Clement, Y. Levron, M. Rodriguez, and D. Maksimovic, "Performance of power-limited differential power processing architectures in mismatched PV systems," *IEEE Transactions on Power Electronics*, vol. 30, no. 2, pp. 618–631, Feb. 2015.

[227] Z. Salam and M. Z. Ramli, "A simple circuit to improve the power yield of PV array during partial shading," in *IEEE Energy Conversion Congress and Exposition (ECCE)*, Sep. 2012, pp. 1622–1626.

[228] M. Jazayeri, S. Uysal, and K. Jazayeri, "A comparative study on different photovoltaic array topologies under partial shading conditions," in *2014 IEEE PES Transmission and Distribution Conference and Exposition*, Apr. 2014, pp. 1–5.

[229] G. Cipriani, V. Di Dio, D. La Manna, R. Miceli, and G. Ricco Galluzzo, "Technical and economical comparison between different topologies of PV plant under mismatch effect," in *2014 Ninth International Conference on Ecological Vehicles and Renewable Energies (EVER)*, Mar. 2014, pp. 1–6.

[230] M. Masoum, H. Dehbonei, and E. Fuchs, "Theoretical and experimental analyses of photovoltaic systems with voltage and current-based maximum power-point tracking," *IEEE Transactions on Energy Conversion*, vol. 17, no. 4, pp. 514–522, Dec. 2002.

[231] M. Adly, H. El-Sherif, and M. Ibrahim, "Maximum power point tracker for a PV cell using a fuzzy agent adapted by the fractional open circuit voltage technique," in *IEEE International Conference on Fuzzy Systems (FUZZ-IEEE)*, Jun. 2011, pp. 1918–1922.

[232] S.-I. Ao and L. Gelman, *Electrical engineering and intelligent systems.* Dordrecht: Springer, 2012.

[233] S. Kirkpatrick, D. J. Gelatt, and M. P. Vecchi, "Optimization by simulated annealing," *Science*, vol. 220, no. 4598, pp. 671–680, 1983.

[234] V. Černý, "Thermodynamical approach to the traveling salesman problem: An efficient simulation algorithm," *Journal of Optimization Theory and Applications*, vol. 45, no. 1, pp. 41–51, Jan. 1985.

[235] S. A.-H. Soliman and A.-A. H. Mantawy, *Modern optimization techniques with applications in electric power systems.* Dordrecht: Springer, 2011.

[236] B. McCallum, "Blind deconvolution by simulated annealing," *Optics Communications*, vol. 75, no. 2, pp. 101–105, 1990.

[237] J. Ohtsubo and K. Nakajima, "Image recovery by simulated annealing with known Fourier modulus," *Optics Communications*, vol. 86, no. 3, pp. 265–270, 1991.

[238] K. Wong and C. Fung, "Simulated annealing based economic dispatch algorithm," *IEE Proceedings - Generation, Transmission and Distribution*, vol. 140, no. 6, pp. 509–515, 1993.

[239] Y. A. Katsigiannis, P. S. Georgilakis, and E. S. Karapidakis, "Hybrid simulated annealing–tabu search method for optimal sizing of autonomous power systems with renewables," *IEEE Transactions on Sustainable Energy*, vol. 3, no. 3, pp. 330–338, Jul. 2012.

[240] Y.-M. Chen, C.-H. Lee, and H.-C. Wu, "Calculation of the optimum installation angle for fixed solar-cell panels based on the genetic algorithm and the simulated-annealing method," *IEEE Transactions on Energy Conversion*, vol. 20, no. 2, pp. 467–473, Jun. 2005.

[241] J. Mitra, "Application of computational intelligence in optimal expansion of distribution systems," in *IEEE Power and Energy Society General Meeting*, Jul. 2008, pp. 1–8.

[242] Yanhong Yang, Wei Pei, and Zhiping Qi, "Optimal sizing of renewable energy and CHP hybrid energy microgrid system," in *IEEE PES Innovative Smart Grid Technologies*, May 2012, pp. 1–5.

[243] T. Sutthibun and P. Bhasaputra, "Multi-objective optimal distributed generation placement using simulated annealing," in *International Conference on Electrical Engineering/Electronics Computer Telecommunications and Information Technology (ECTI-CON)*, 2010, pp. 810–813.

[244] A. K. Barnes, J. C. Balda, A. Escobar-Mejia, and S. O. Geurin, "Placement of energy storage coordinated with smart PV inverters," in *IEEE PES Innovative Smart Grid Technologies (ISGT)*, Jan. 2012, pp. 1–7.

[245] V. Evangelin Jeba, S. Ravichandran, and R. Kumudini Devi, "Optimal control of grid connected variable speed wind energy conversion system," in *International Conference on Energy Efficient Technologies for Sustainability*, Apr. 2013, pp. 393–399.

[246] D. L. Anton, S. L. Garrison, M. Gorensek, S. R. Sherman, R. Carapellucci, and L. Giordano, "Modeling and optimization of an energy generation island based on renewable technologies and hydrogen storage systems," *International Journal of Hydrogen Energy*, vol. 37, no. 3, pp. 2081–2093, 2012.

[247] M. A. Azam, S. Abdullah-Al-Nahid, M. A. Kabir, and S. M. H. Chowdhury, "Microcontroller based maximum power tracking of PV using stimulated annealing algorithm," in *International Conference on Informatics, Electronics & Vision (ICIEV)*, May 2012, pp. 298–303.

[248] J. P. F. Trovao, V. D. N. Santos, P. G. Pereirinha, H. M. Jorge, and C. H. Antunes, "A simulated annealing approach for optimal power source management in a small EV," *IEEE Transactions on Sustainable Energy*, vol. 4, no. 4, pp. 867–876, Oct. 2013.

[249] Y. Nourani and B. Andresen, "A comparison of simulated annealing cooling strategies," *Journal of Physics A: Mathematical and General*, vol. 31, no. 41, pp. 8373–8385, Oct. 1998.

[250] B. Moses, "Convergence of annealing algorithms for co-operative UAVs," *Recent Advances in Applied and Theoretical Mathematics*, pp. 109–116, 2013.

[251] G. Zäpfel, R. Braune, and M. Bögl, *Metaheuristic search concepts: a tutorial with applications to production and logistics*. Dordrecht: Springer, 2010.

[252] D. L. Poole and A. K. Mackworth, *Artificial intelligence: foundations of computational agents*. Cambridge: Cambridge University Press, 2010.

[253] B. Doerr and A. Auger, *Theory of randomized search heuristics: foundations and recent developments*. Singapore: World Scientific Publishing Company, 2011.

[254] N. Metropolis, A. W. Rosenbluth, M. N. Rosenbluth, A. H. Teller, and E. Teller, "Equation of state calculations by fast computing machines," *The Journal of Chemical Physics*, vol. 21, no. 6, p. 1087, Dec. 1953.

[255] K. Ishaque, Z. Salam, S. Mekhilef, and A. Shamsudin, "Parameter extraction of solar photovoltaic modules using penalty-based differential evolution," *Applied Energy*, vol. 99, pp. 297–308, 2012.

[256] M. Sadeghzadeh and M. Taherbaghal, "A new method for decoding an encrypted text by genetic algorithms and its comparison with tabu search and simulated annealing," *Management Science Letters*, vol. 4, no. 2, pp. 213–220, 2014.

[257] H. Ihlayyel and S. Abdullah, "Hybridization of simulated annealing with principle axis search and k-nearest neighbor for attribute reduction on financial time series forecasting," in *International Conference on Engineering Education*, 2013, pp. 100–108.

[258] J. Frausto-Solis, M. Sanchez-Perez, E. Linan-Garcia, J. P. Sanchez-Hernandez, and M. Ramachandran, "Cluster perturbation simulated annealing for protein folding problem," *Journal of Universal Computer Science*, vol. 19, no. 15, pp. 2207–2223, 2013.

[259] B. Hajek, "Cooling schedules for optimal annealing," *Mathematics of Operations Research*, vol. 13, no. 2, pp. 311–329, May 1988.

[260] B. Hajek, "A tutorial survey of theory and applications of simulated annealing," in *1985 24th IEEE Conference on Decision and Control*, vol. 24, 1985, pp. 755–760.

[261] H. Cohn and M. J. Fielding, "Simulated annealing: searching for an optimal temperature schedule," *SIAM Journal on Optimization*, vol. 9, no. 3, pp. 779–802, 1999.

[262] E. K. P. Chong and S. H. Zak, *An introduction to optimization*. Hoboken: Wiley, 2011.

[263] S. Rajasekaran, "On the convergence time of simulated annealing," *Technical Reports (CIS)*, 1990.

[264] V. Granville, M. Krivanek, and J.-P. Rasson, "Simulated annealing: a proof of convergence," *IEEE Transactions on Pattern Analysis and Machine Intelligence*, vol. 16, no. 6, pp. 652–656, Jun. 1994.

[265] S. Rajasekaran and J. H. Reif, "Nested annealing: a provable improvement to simulated annealing," *Theoretical Computer Science*, vol. 99, no. 1, pp. 157–176, Jun. 1992.

[266] F. Glover and G. A. Kochenberger, Eds., *Handbook of metaheuristics*, ser. International Series in Operations Research & Management Science. Boston: Kluwer Academic Publishers, 2003, vol. 57.

[267] D. Mitra, F. Romeo, and A. Sangiovanni-Vincentelli, "Convergence and finite-time behavior of simulated annealing," in *1985 24th IEEE Conference on Decision and Control*, Dec. 1985, pp. 761–767.

[268] The MathWorks Inc, "Detailed model of a 100-kW grid-connected PV array - MATLAB & Simulink Example - MathWorks Australia," 2014. [Online]. Available: http://au.mathworks.com/help/physmod/sps/examples/detailed-model-of-a-100-kw-grid-connected-pv-array.html

[269] National Instruments Corporation, "NI CompactRIO - rugged, high-performance reconfigurable control and monitoring system - National Instruments," 2014. [Online]. Available: http://www.ni.com/compactrio/

[270] J. P. Shankarrao, "FPGA implementation of maximum power point tracking algorithm for PV systems," Ph.D. dissertation, National Institute of Technology Rourkela, 2013.

[271] AccuWeather, "Hobart December weather 2014 - AccuWeather forecast for Tasmania Australia," 2015. [Online]. Available: http://www.accuweather.com/en/au/hobart/15390/december-weather/15390?monyr=12/1/2014&view=table

[272] S. J. Chapman, *Electric machinery and power system fundamentals*. McGraw-Hill, 2002.

[273] Guohui Yuan, "Improving grid reliability through integration of distributed PV and energy storage," in *2012 IEEE PES Innovative Smart Grid Technologies (ISGT)*. IEEE, Jan. 2012, pp. 1–2.

[274] K. Fekete, Z. Klaic, and L. Majdandzic, "Expansion of the residential photovoltaic systems and its harmonic impact on the distribution grid," *Renewable Energy*, vol. 43, pp. 140–148, Jul. 2012.

[275] C. L. Trujillo, D. Velasco, G. Garcera, E. Figueres, and R. Ortega, "Reconfigurable control scheme for a microinverter working in both grid connected and island mode," in *2011 IEEE International Symposium on Industrial Electronics*. IEEE, Jun. 2011, pp. 1477–1481.

[276] H. Beltran, E. Bilbao, E. Belenguer, I. Etxeberria-Otadui, and P. Rodriguez, "Evaluation of storage energy requirements for constant production in PV power plants," *IEEE Transactions on Industrial Electronics*, vol. 60, no. 3, pp. 1225–1234, Mar. 2013.

Appendix A

Single Module PV Model

This appendix contains further figures of the single PV module model used for model validation. Fig. A.1 shows the calculation of the light generated current using (2.13). Fig. A.2 shows the calculation of the shunt resistance current. Fig. A.3 shows the calculation of the junction thermal voltage. Fig. A.4 shows the calculation of the diode current using (2.14).

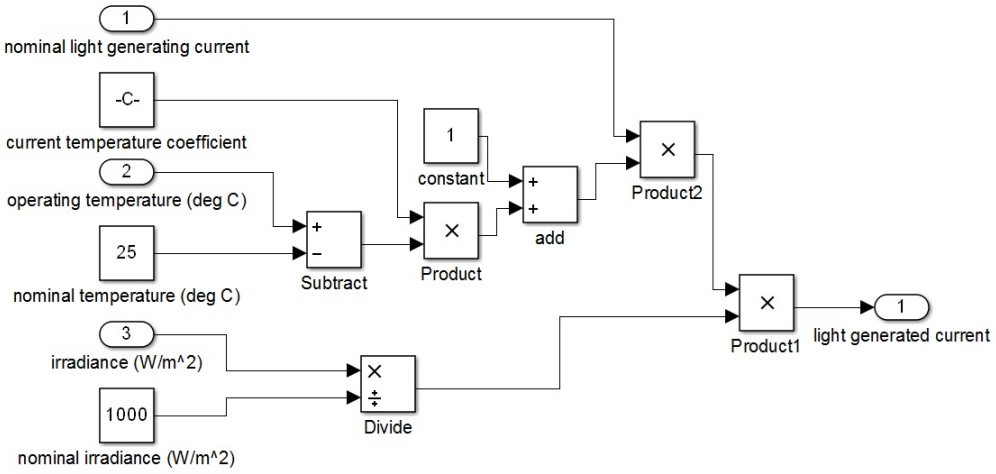

Figure A.1: Light generated current calculation.

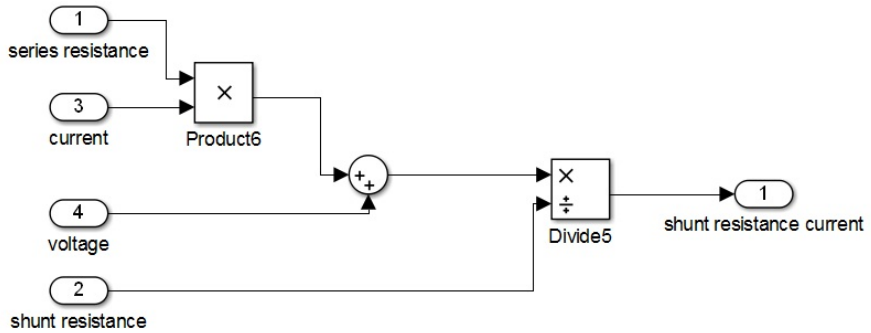

Figure A.2: Shunt resistance current calculation.

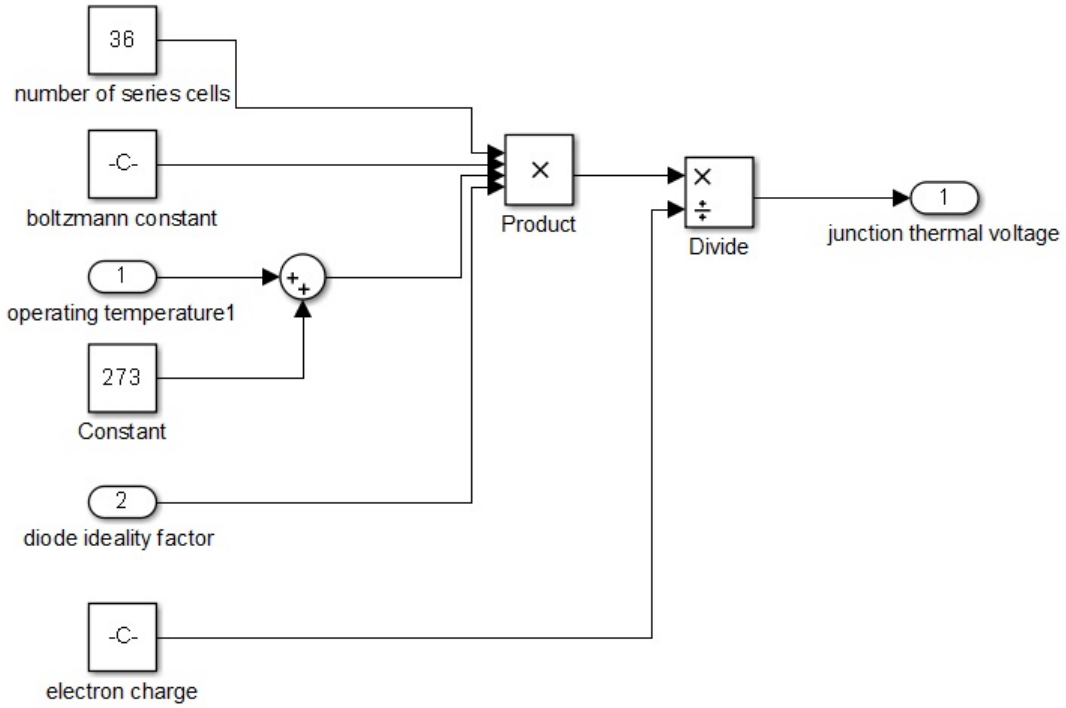

Figure A.3: Junction thermal voltage calculation.

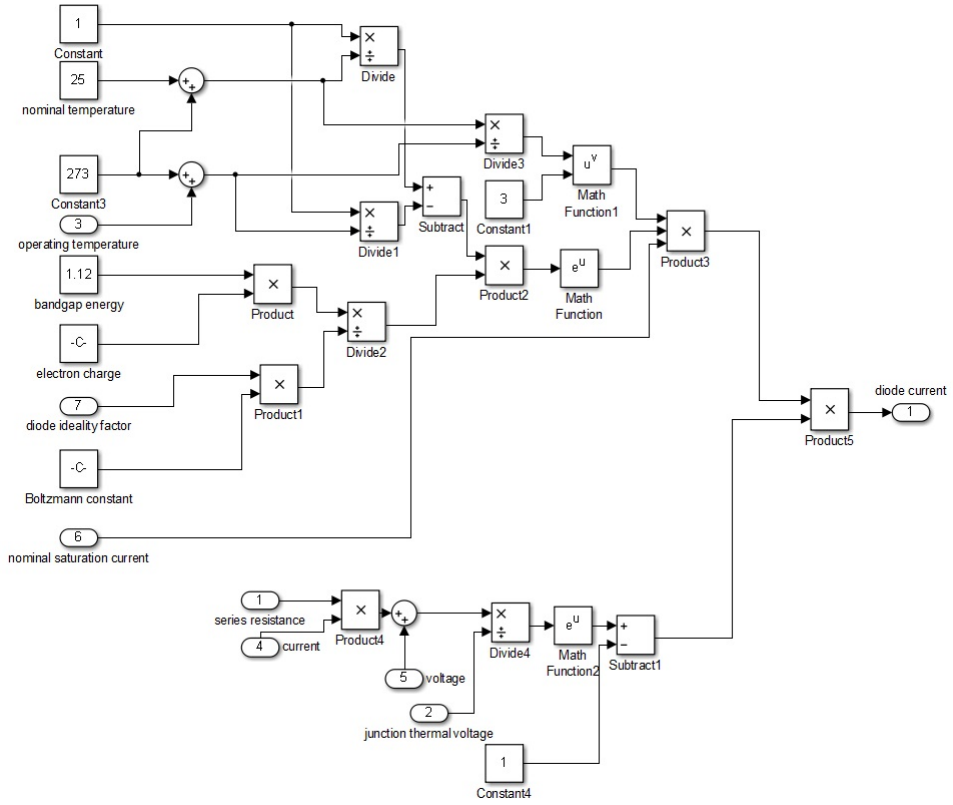

Figure A.4: Diode current calculation.

Appendix B

Sample Output Files for Partial Shading Conditions Assessment

This appendix contains sample extracts from the output files generated for one day of data processed using the Partial Shading Conditions Assessment process outlined in Chapter 3. The day of interest is April 1, 2010. Fig. B.1 represents an extract from the file *2010_april_day_1.xlsx*, showing how the voltage, current and power vary across the sample time. This data file can be used to reproduce the I-V and P-V characteristics for each sample condition.

Fig. B.2 provides an extract of the file *2010_april_mpps.xlsx*. This file takes all the information of the P-V characteristics and combines it to determine the GMPP. This file is important for studying how the GMPP moves when the transient, static and constant partial shading affect the system.

Fig. B.3 demonstrates an extract of a shaded patterns file. There is a corresponding file for each module in the system. The cells are referenced in 9 cell groups such at column C refers to cell (1,1), while column D refers to cell (1,2).

Fig. B.4 shows an extract from the *2010_april_shadow_location.xlsx* file for which there is one obstacle in the environment from Case 1 detailed in Chapter 3.

Fig. B.5 gives an extract of the file *2010_april_irradiance_on_all_modules.xlsx*. In each case, the transient irradiance from the one minute solar data is combined with the shading factor to provide the irradiance on each module that would be fed into the eight module simulation model.

	A	B	C	D	E
1	2.4	2.400085	0.13968	2.311134	0.322818
2	2.4	2.400099	0.164094	2.31112	0.37924
3	2.4	2.400099	0.164094	2.31112	0.37924
4	2.4	2.4001	0.164834	2.311286	0.380978
5	2.4	2.4001	0.165574	2.309945	0.382467
6	2.4	2.400101	0.166337	2.308113	0.383926
7	2.4	2.400102	0.168581	2.302728	0.388197
8	2.4	2.400105	0.173069	2.291957	0.396668
9	2.4	2.40011	0.182045	2.270415	0.413318
10	2.4	2.400121	0.199997	2.227331	0.445459
11	2.4	2.400143	0.2359	2.143709	0.505702
12	2.4	2.400186	0.307707	2.143685	0.659627
13	2.4	2.400241	0.397609	2.143661	0.852339
14	2.4	2.400299	0.493239	2.143638	1.057327
15	2.4	2.400362	0.597147	2.143617	1.280055
16	2.4	2.400431	0.710479	2.143597	1.522981
17	2.4	2.400506	0.834867	2.143576	1.7896
18	2.4	2.400589	0.97227	2.143553	2.084112
19	2.4	2.400682	1.125054	2.143529	2.411586
20	2.4	2.400785	1.295994	2.143503	2.777967
21	2.4	2.400902	1.48816	2.143473	3.189831
22	2.4	2.401022	1.686046	2.143442	3.613942

Figure B.1: Extract from file *2010_april_day_1.xlsx*, where the columns correspond to A - sample reference, B - sample time, C - voltage, D - current, E = power.

	A	B	C	D	E
1	0	100	58.69816	132.5607	0.442802
2	0.1	439.07	246.8353	142.7192	1.729518
3	0.2	529.15	283.3811	118.0797	2.399913
4	0.3	429.73	230.69	118.4174	1.948108
5	0.4	394.66	211.8638	118.6248	1.785999
6	0.5	391.79	210.3399	118.4933	1.775121
7	0.6	401.24	215.3982	118.1436	1.823189
8	0.7	434.83	226.5154	120.6458	1.877524
9	0.8	486.06	236.873	123.8658	1.912336
10	0.9	495.84	225.787	100.1015	2.255582
11	1	516.86	235.1968	100.5611	2.338845
12	1.1	531.05	241.5602	100.297	2.408449
13	1.2	525.14	238.9067	100.4091	2.379334
14	1.3	581.87	283.1935	123.5132	2.292819
15	1.4	675.64	332.6043	121.1677	2.744991
16	1.5	899.04	437.1816	119.5405	3.657184
17	1.6	653.67	316.5702	122.8116	2.577691
18	1.7	598.69	271.5257	99.93015	2.717155
19	1.8	520.25	236.7079	100.5784	2.353465
20	1.9	553.81	251.6652	99.86803	2.519978
21	2	565.1	256.6727	100.3154	2.558658
22	2.1	706.03	318.2176	99.59846	3.195005
23	2.2	682.63	328.8746	122.2461	2.690267
24	2.3	481.81	227.462	124.0995	1.8329

Figure B.2: Extract from file *2010_april_mpps.xlsx*, where the columns correspond to A - sample reference, B - irradiance, C - power at GMPP, D - voltage at GMPP, E = current at GMPP.

	A	B	C	D	E	F	G	H	I	J	K	L	M	N	O	P	Q	R	S	T	U	V	W	X	Y	Z	AA	AB	AC	AD	AE	AF	AG	AH	AI	AJ	AK	AL
1	0	1	0	0	0	0	0	0	0	0	0	0	0	0	0	0	0	0	0	0	0	0	0	0	0	0	0	0	0	0	0	0	0	0	0	0	0	0
2	0.1	0.833	0	0	0	0	0	1	1	1	1	0	0	0	0	0	0	0	1	1	0	0	0	0	0	0	0	0	0	0	0	0	0	0	0	0	0	0
3	0.2	0.75	0	0	0	0	1	1	1	1	1	0	0	0	0	0	0	1	1	1	0	0	0	0	0	0	0	0	1	0	0	0	0	0	0	0	0	0
4	0.3	0.667	0	0	0	1	1	1	1	1	1	0	0	0	0	0	1	1	1	1	0	0	0	0	0	0	0	1	1	0	0	0	0	0	0	0	0	0
5	0.4	0.583	0	0	1	1	1	1	1	1	0	0	0	0	0	1	1	1	1	1	0	0	0	0	0	0	1	1	1	0	0	0	0	0	0	0	0	1
6	0.5	0.472	0	1	1	1	1	1	1	0	0	0	0	0	1	1	1	1	1	1	0	0	0	0	1	1	1	1	1	0	0	0	0	0	0	0	1	1
7	0.6	0.389	1	1	1	1	1	1	0	0	0	0	1	1	1	1	1	1	1	0	0	0	0	1	1	1	1	1	1	0	0	0	0	0	0	1	1	1
8	0.7	0.361	1	1	1	1	1	0	0	0	0	1	1	1	1	1	1	0	0	0	0	0	1	1	1	1	1	1	1	0	0	0	0	1	1	1	1	1
9	0.8	0.417	1	1	1	0	0	0	0	0	0	1	1	1	1	1	0	0	0	0	0	1	1	1	1	1	1	1	0	0	0	0	1	1	1	1	1	1
10	0.9	0.472	1	1	0	0	0	0	0	0	0	1	1	1	1	1	0	0	0	0	1	1	1	1	1	1	0	0	0	0	0	1	1	1	1	1	1	0
11	1	0.556	1	1	0	0	0	0	0	0	0	1	1	1	0	0	0	0	0	0	1	1	1	1	1	0	0	0	0	0	1	1	1	1	1	1	0	0
12	1.1	0.667	0	0	0	0	0	0	0	0	0	1	1	0	0	0	0	0	0	0	1	1	1	1	0	0	0	0	0	1	1	1	1	1	1	0	0	0
13	1.2	0.722	0	0	0	0	0	0	0	0	0	1	1	0	0	0	0	0	0	0	1	1	1	0	0	0	0	0	0	1	1	1	1	1	0	0	0	0
14	1.3	0.833	0	0	0	0	0	0	0	0	0	0	0	0	0	0	0	0	0	0	1	1	0	0	0	0	0	0	0	1	1	1	1	0	0	0	0	0
15	1.4	0.861	0	0	0	0	0	0	0	0	0	0	0	0	0	0	0	0	0	0	1	1	0	0	0	0	0	0	0	1	1	1	0	0	0	0	0	0
16	1.5	0.861	0	0	0	0	0	0	0	0	0	0	0	0	0	0	0	0	0	0	1	1	0	0	0	0	0	0	0	1	1	1	0	0	0	0	0	0
17	1.6	0.944	0	0	0	0	0	0	0	0	0	0	0	0	0	0	0	0	0	0	0	0	0	0	0	0	0	0	0	1	1	0	0	0	0	0	0	0
18	1.7	1	0	0	0	0	0	0	0	0	0	0	0	0	0	0	0	0	0	0	0	0	0	0	0	0	0	0	0	0	0	0	0	0	0	0	0	0
19	1.8	1	0	0	0	0	0	0	0	0	0	0	0	0	0	0	0	0	0	0	0	0	0	0	0	0	0	0	0	0	0	0	0	0	0	0	0	0
20	1.9	1	0	0	0	0	0	0	0	0	0	0	0	0	0	0	0	0	0	0	0	0	0	0	0	0	0	0	0	0	0	0	0	0	0	0	0	0
21	2	1	0	0	0	0	0	0	0	0	0	0	0	0	0	0	0	0	0	0	0	0	0	0	0	0	0	0	0	0	0	0	0	0	0	0	0	0
22	2.1	1	0	0	0	0	0	0	0	0	0	0	0	0	0	0	0	0	0	0	0	0	0	0	0	0	0	0	0	0	0	0	0	0	0	0	0	0
23	2.2	1	0	0	0	0	0	0	0	0	0	0	0	0	0	0	0	0	0	0	0	0	0	0	0	0	0	0	0	0	0	0	0	0	0	0	0	0
24	2.3	1	0	0	0	0	0	0	0	0	0	0	0	0	0	0	0	0	0	0	0	0	0	0	0	0	0	0	0	0	0	0	0	0	0	0	0	0
25	2.4	1	0	0	0	0	0	0	0	0	0	0	0	0	0	0	0	0	0	0	0	0	0	0	0	0	0	0	0	0	0	0	0	0	0	0	0	0
26	2.5	1	0	0	0	0	0	0	0	0	0	0	0	0	0	0	0	0	0	0	0	0	0	0	0	0	0	0	0	0	0	0	0	0	0	0	0	0
27	2.6	1	0	0	0	0	0	0	0	0	0	0	0	0	0	0	0	0	0	0	0	0	0	0	0	0	0	0	0	0	0	0	0	0	0	0	0	0

Figure B.3: Extract from file *2010_april_shaded_patterns_1.xlsx*, where the columns correspond to A - sample reference, B - shading factor, C - cell(1,1), D - cell (1,2)... AL - cell (4,9).

	A	B	C
60477	23.79974	-2.38564	-19.5991
60478	23.8	-2.38564	-19.5991
60479	23.80004	-2.26148	-19.5828
60480	23.80008	-2.26148	-19.5828
60481	23.80013	-2.26148	-19.5828
60482	23.80018	-2.26148	-19.5828
60483	23.80024	-2.26148	-19.5828
60484	23.8003	-2.26148	-19.5828
60485	23.80037	-2.26148	-19.5828
60486	23.80044	-2.26148	-19.5828
60487	23.80052	-2.26148	-19.5828
60488	23.80062	-2.26148	-19.5828
60489	23.80072	-2.26148	-19.5828
60490	23.80084	-2.26148	-19.5828
60491	23.80098	-2.26148	-19.5828
60492	23.80115	-2.26148	-19.5828
60493	23.80136	-2.26148	-19.5828
60494	23.80163	-2.26148	-19.5828
60495	23.80198	-2.26148	-19.5828
60496	23.80247	-2.26148	-19.5828
60497	23.8029	-2.26148	-19.5828
60498	23.80334	-2.26148	-19.5828
60499	23.80377	-2.26148	-19.5828
60500	23.80417	-2.26148	-19.5828
60501	23.80456	-2.26148	-19.5828
60502	23.80496	-2.26148	-19.5828
60503	23.8054	-2.26148	-19.5828

Figure B.4: Extract from file *2010_april_shadow_location.xlsx*, where the columns correspond to A - sample reference, B - x coordinate of tip of shadow, C - y coordinate of tip of shadow.

	A	B	C	D	E	F	G	H	I
94495	35.5179	545.98	545.98	409.485	242.6578	500.4817	545.98	545.98	545.98
94496	35.51799	545.98	545.98	409.485	242.6578	500.4817	545.98	545.98	545.98
94497	35.51807	545.98	545.98	409.485	242.6578	500.4817	545.98	545.98	545.98
94498	35.51815	545.98	545.98	409.485	242.6578	500.4817	545.98	545.98	545.98
94499	35.51823	545.98	545.98	409.485	242.6578	500.4817	545.98	545.98	545.98
94500	35.51831	545.98	545.98	409.485	242.6578	500.4817	545.98	545.98	545.98
94501	35.51838	545.98	545.98	409.485	242.6578	500.4817	545.98	545.98	545.98
94502	35.51846	545.98	545.98	409.485	242.6578	500.4817	545.98	545.98	545.98
94503	35.51854	545.98	545.98	409.485	242.6578	500.4817	545.98	545.98	545.98
94504	35.51861	545.98	545.98	409.485	242.6578	500.4817	545.98	545.98	545.98
94505	35.51869	545.98	545.98	409.485	242.6578	500.4817	545.98	545.98	545.98
94506	35.51876	545.98	545.98	409.485	242.6578	500.4817	545.98	545.98	545.98
94507	35.51884	545.98	545.98	409.485	242.6578	500.4817	545.98	545.98	545.98
94508	35.51891	545.98	545.98	409.485	242.6578	500.4817	545.98	545.98	545.98
94509	35.51898	545.98	545.98	409.485	242.6578	500.4817	545.98	545.98	545.98
94510	35.51906	545.98	545.98	409.485	242.6578	500.4817	545.98	545.98	545.98
94511	35.51913	545.98	545.98	409.485	242.6578	500.4817	545.98	545.98	545.98
94512	35.5192	545.98	545.98	409.485	242.6578	500.4817	545.98	545.98	545.98
94513	35.51927	545.98	545.98	409.485	242.6578	500.4817	545.98	545.98	545.98
94514	35.51934	545.98	545.98	409.485	242.6578	500.4817	545.98	545.98	545.98
94515	35.51941	545.98	545.98	409.485	242.6578	500.4817	545.98	545.98	545.98
94516	35.51949	545.98	545.98	409.485	242.6578	500.4817	545.98	545.98	545.98
94517	35.51956	545.98	545.98	409.485	242.6578	500.4817	545.98	545.98	545.98
94518	35.51963	545.98	545.98	409.485	242.6578	500.4817	545.98	545.98	545.98
94519	35.5197	545.98	545.98	409.485	242.6578	500.4817	545.98	545.98	545.98
94520	35.51977	545.98	545.98	409.485	242.6578	500.4817	545.98	545.98	545.98

Figure B.5: Extract from file *2010_april_irradiance_on_all_modules.xlsx*, where the columns correspond to A - time, B - module 1 irradiance, C - module 2 irradiance, D - module 3 irradiance, E - module 4 irradiance, F - module 5 irradiance, G - module 6 irradiance, H - module 7 irradiance, I - module 8 irradiance.

Appendix C

Experimental Implementation Labview Code

The five frames of the Labview Interface for experimental implementation of the SA method as described in Chapter 5 are shown in Fig. C.1 to Fig. C.5, respectively. Fig. C.1, shows the initialisation of the program and also demonstrates the selection of the random duty cycle using a Matlab script. This frame also shows the duty cycle as an analog output being written to port AO0 to provide the duty cycle to the PIC microcontroller. Figure C.2, incorporates a short delay to enable the duty cycle from the previous frame to be established and then takes a measurement of the PV system current and voltage using channel AI0 and AI1 of the DAQ. The time delay can be easily modified here to improve the execution speed of the algorithm. Power, voltage and current data obtained during this frame are then written to the Timeseries chart. Frame 3, as shown in Fig. C.3, demonstrates the main component of the SA algorithm, implemented as a MATLAB script, where the current operating point is compared with the reference operating point to decide whether the new point is to be accepted or not. The starting temperature, ending temperature, count reference and cooling rate (α_2) are all used in this frame. Additionally, this frame contains temperature update code. In frame 4, as shown in Fig. C.4, the duty cycle of the best reference operating point is sent to the PIC to enable the system to return to the best operating point. Fig. C.5 contains the program termination phase in addition to frame 5 of the structure. In frame 5, after a short delay the voltage and current of the PV panel are read and stored in the Timeseries chart.

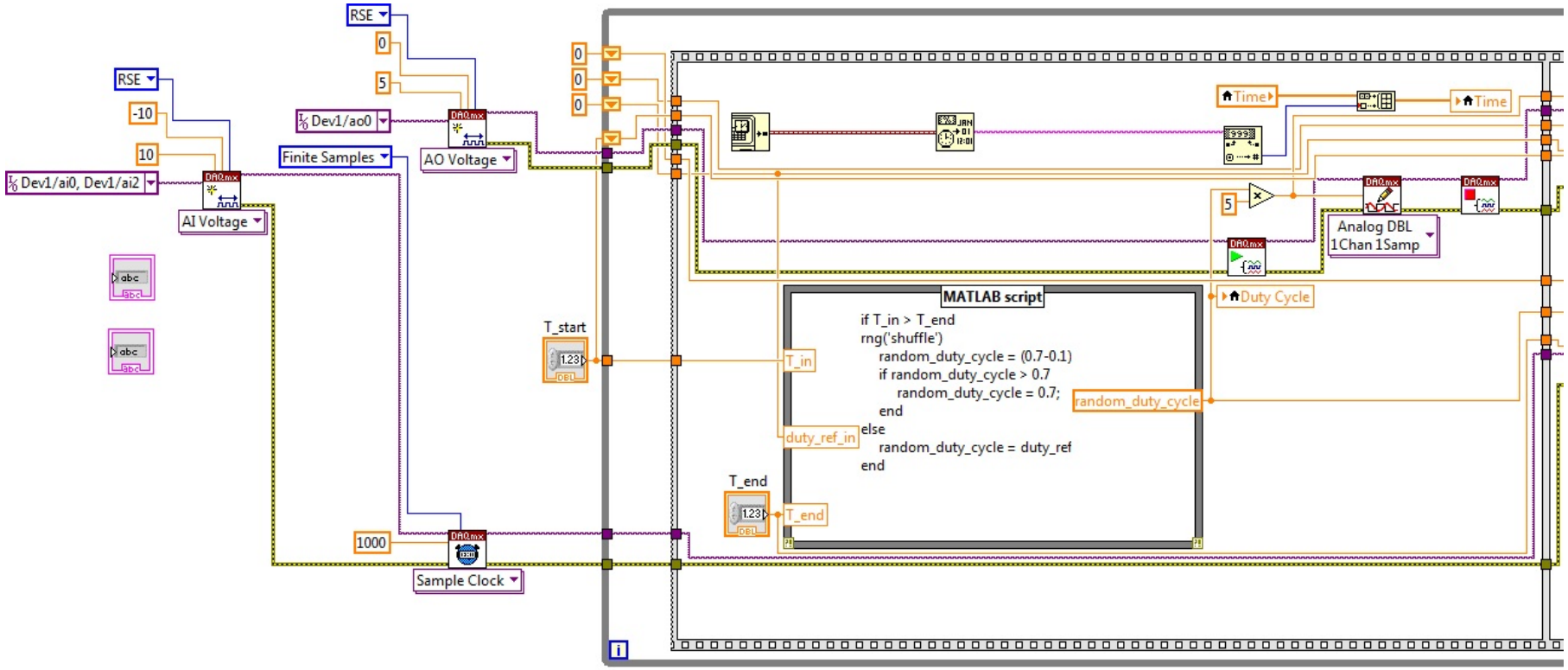

Figure C.1: First frame of Labview MPPT flat structure.

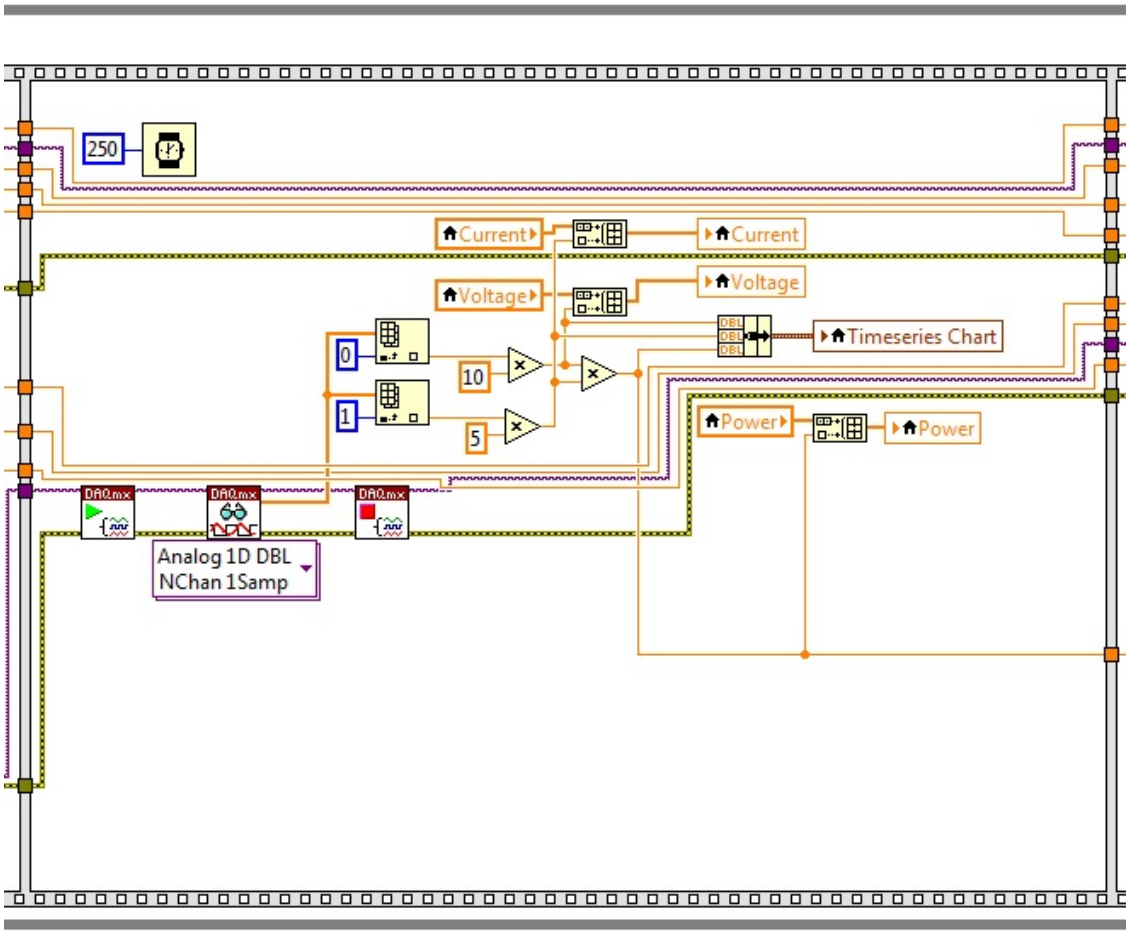

Figure C.2: Frame 2 of Labview MPPT flat structure.

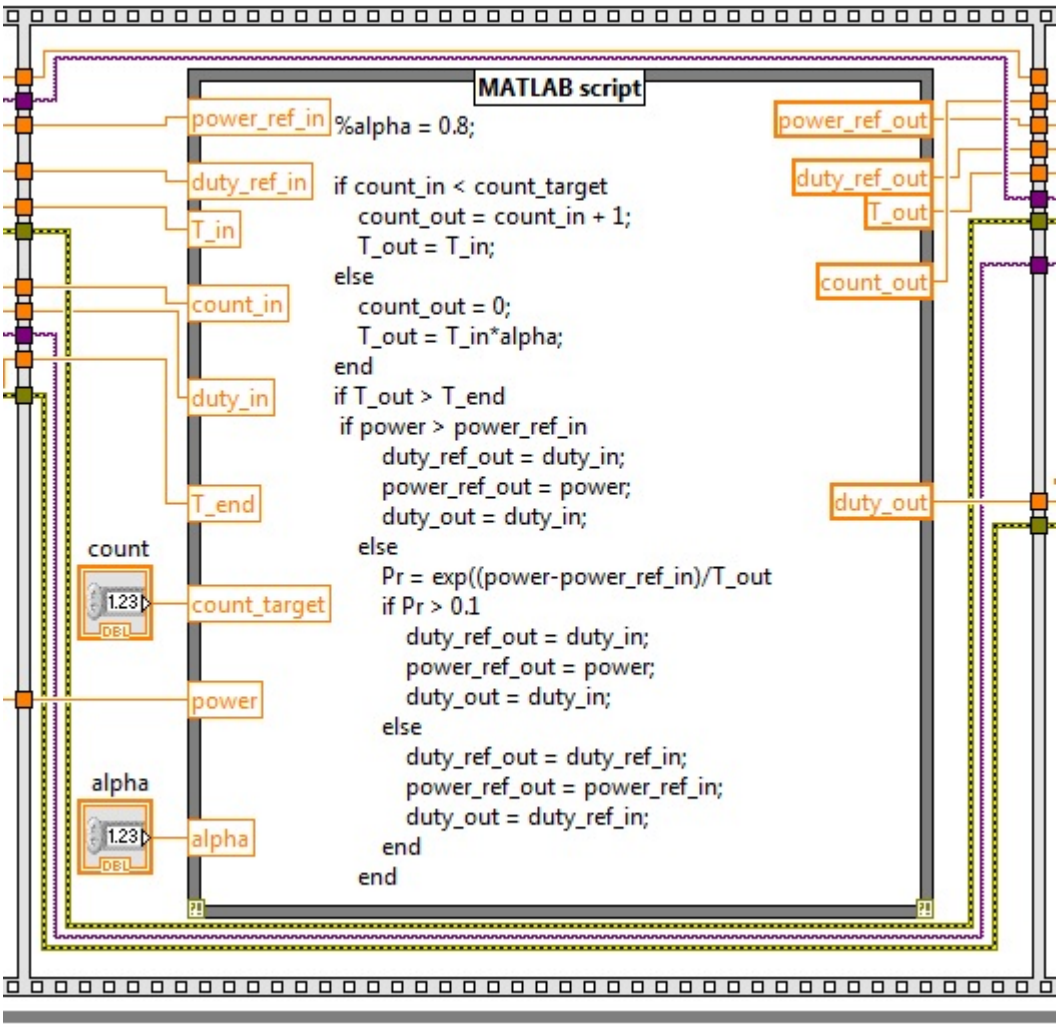

Figure C.3: Frame 3 of Labview MPPT flat structure.

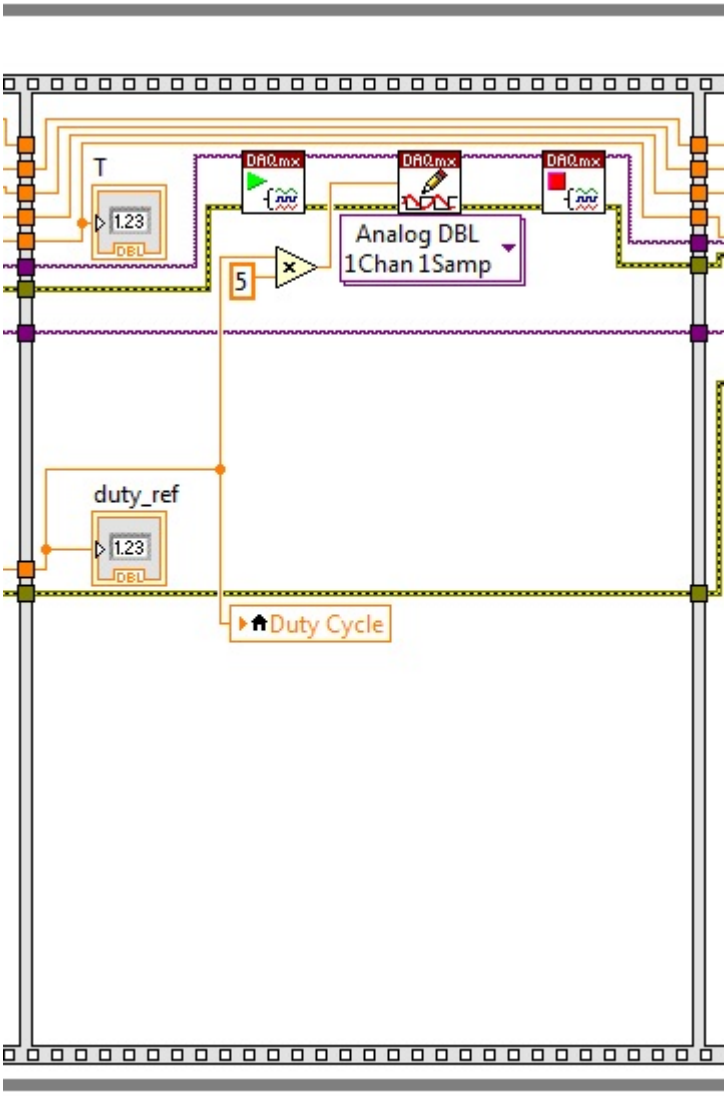

Figure C.4: Frame 4 of Labview MPPT flat structure.

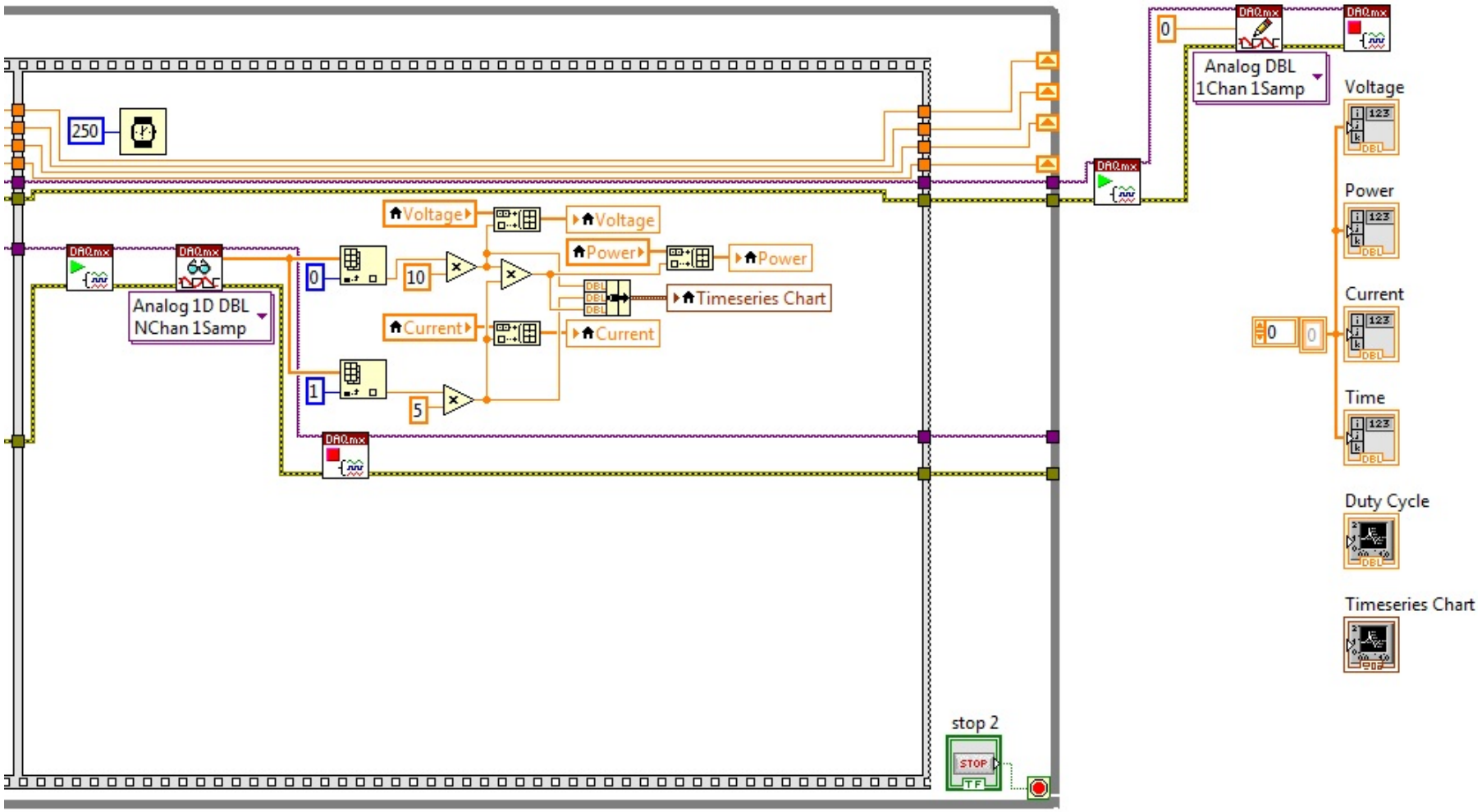

Figure C.5: Final frame of Labview MPPT flat structure.

Appendix D

P-V characteristics to Assess Performance of SA Method Under Different Parameter Values

Characteristic 1 to Characteristic 30 are shown in Fig. D.1 to D.30.

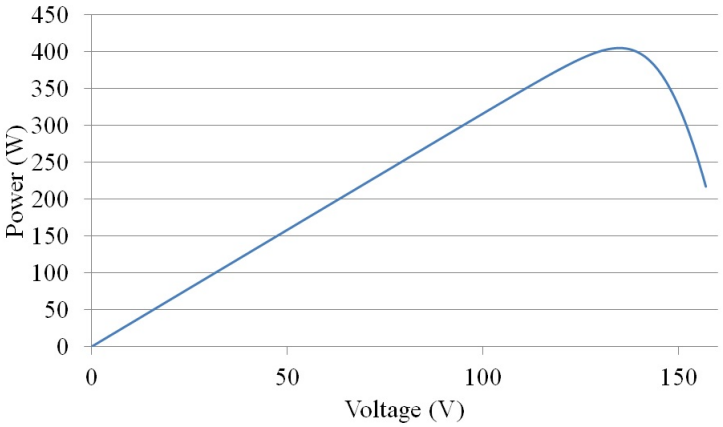

Figure D.1: P-V curve for characteristic 1.

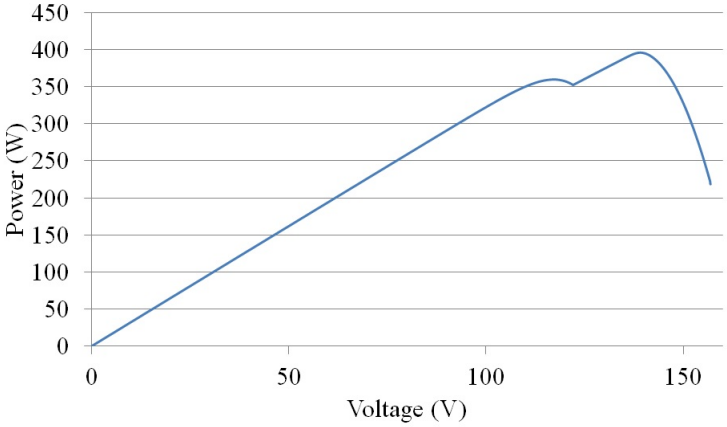

Figure D.2: P-V curve for characteristic 2.

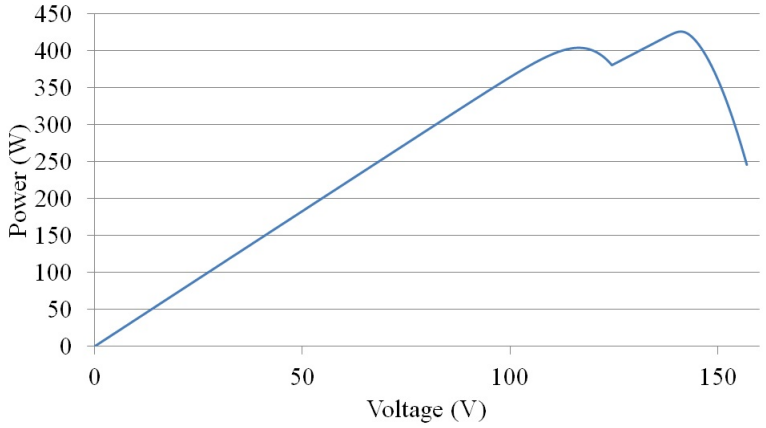

Figure D.3: P-V curve for characteristic 3.

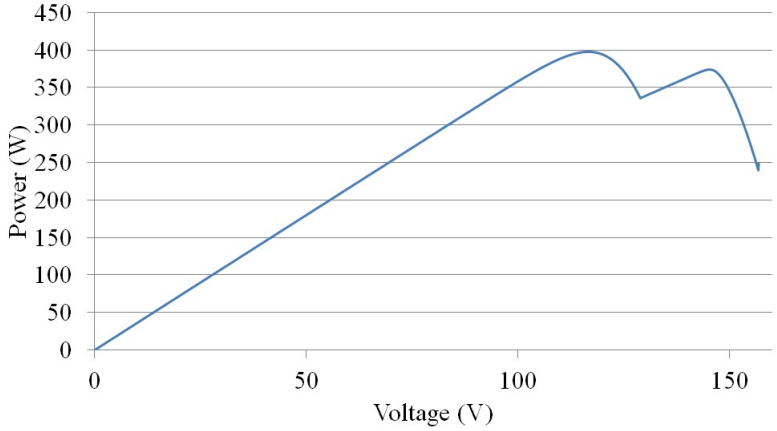

Figure D.4: P-V curve for characteristic 4.

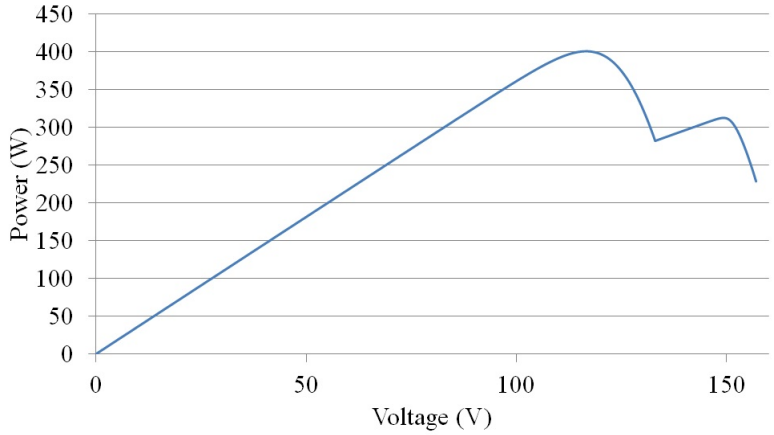

Figure D.5: P-V curve for characteristic 5.

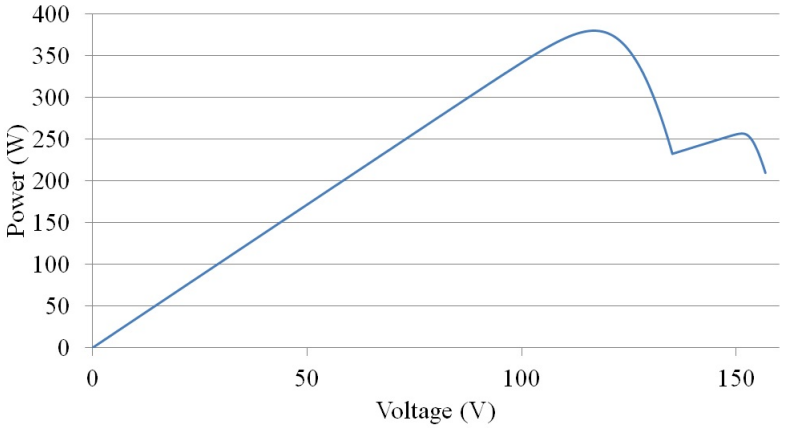

Figure D.6: P-V curve for characteristic 6.

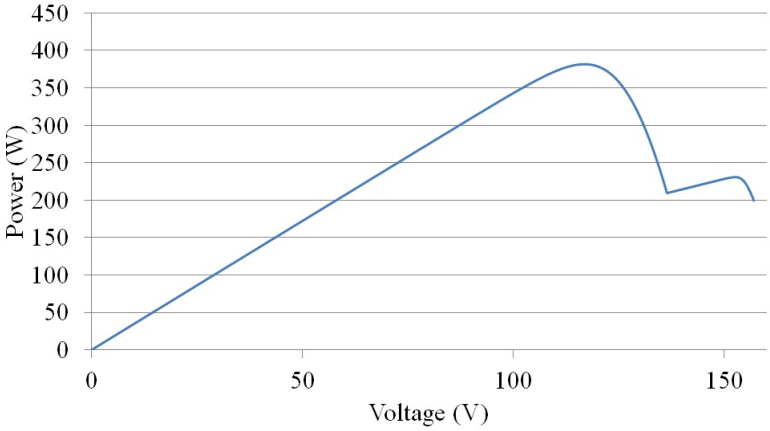

Figure D.7: P-V curve for characteristic 7.

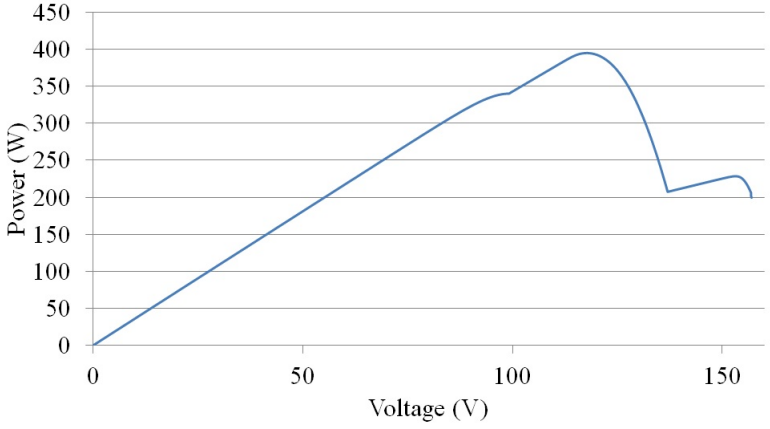

Figure D.8: P-V curve for characteristic 8.

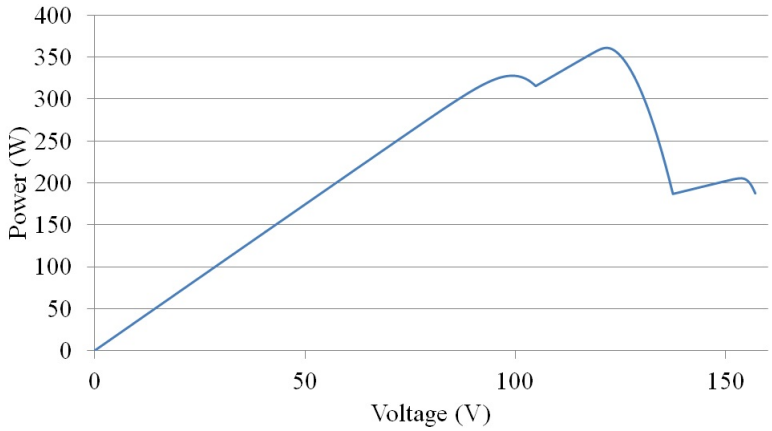

Figure D.9: P-V curve for characteristic 9.

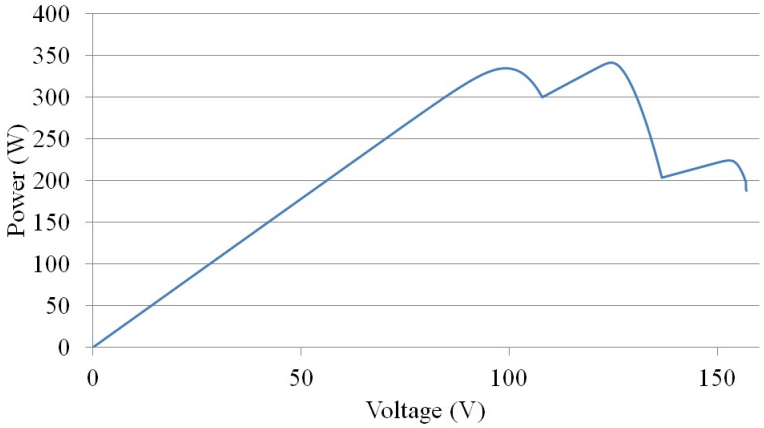

Figure D.10: P-V curve for characteristic 10.

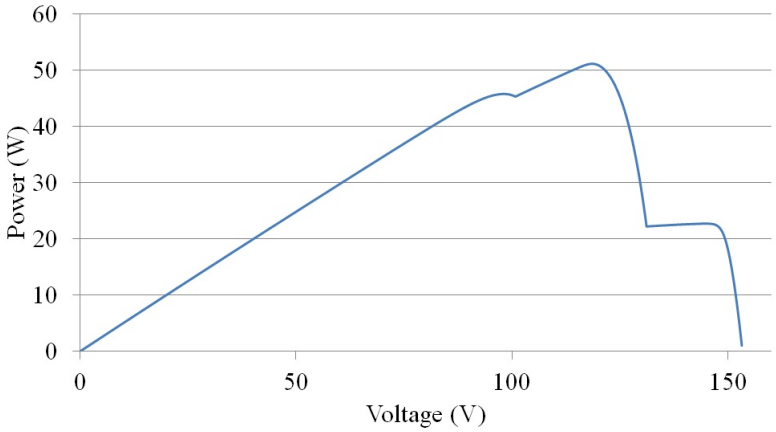

Figure D.11: P-V curve for characteristic 11.

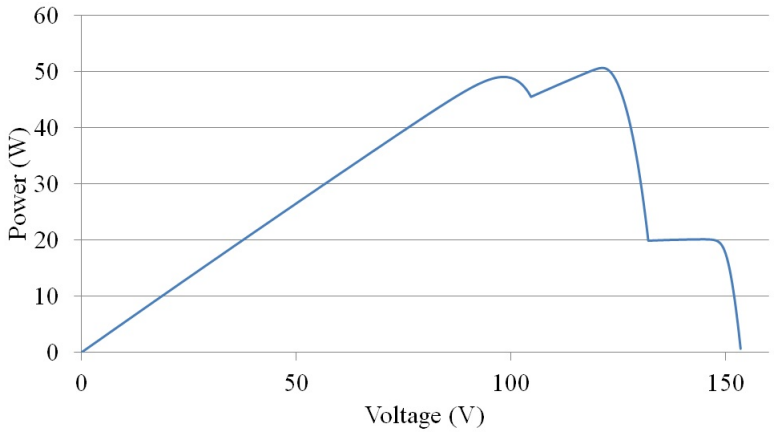

Figure D.12: P-V curve for characteristic 12.

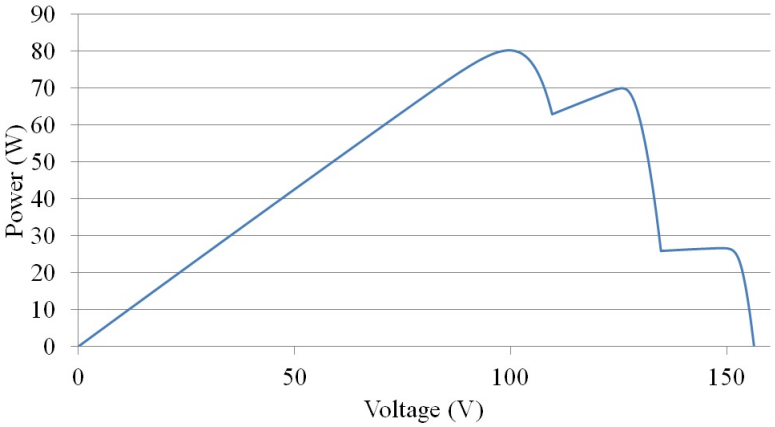

Figure D.13: P-V curve for characteristic 13.

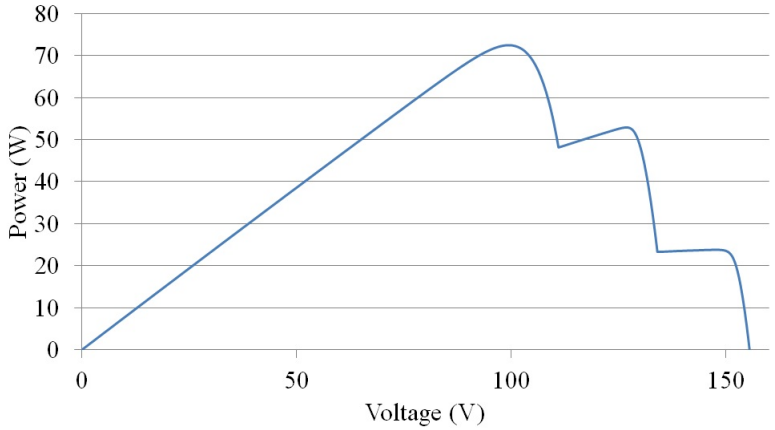

Figure D.14: P-V curve for characteristic 14.

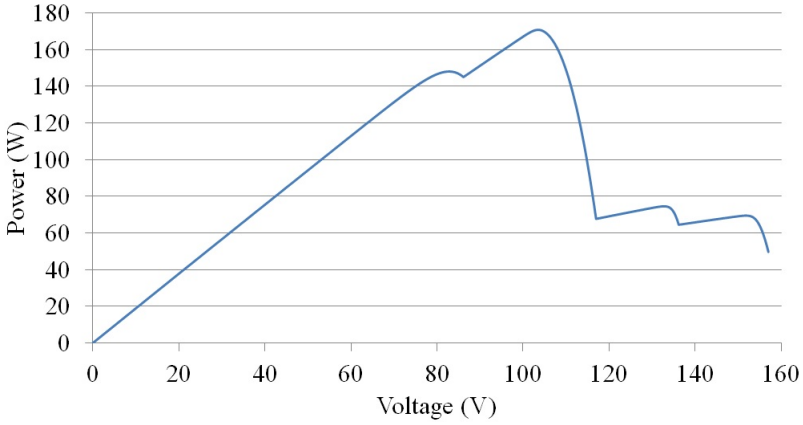

Figure D.15: P-V curve for characteristic 15.

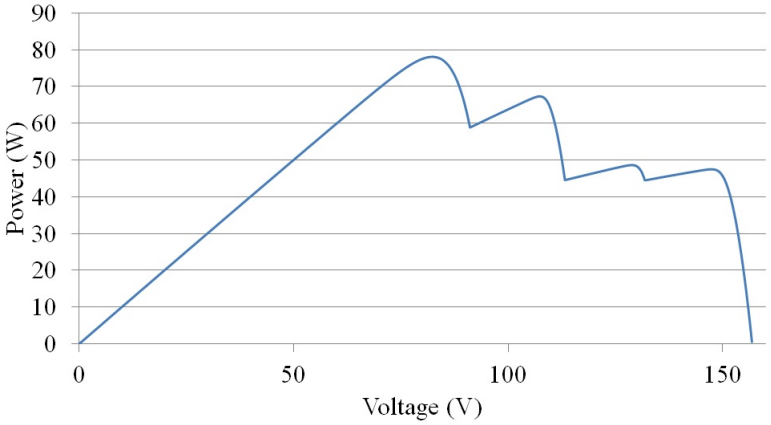

Figure D.16: P-V curve for characteristic 16.

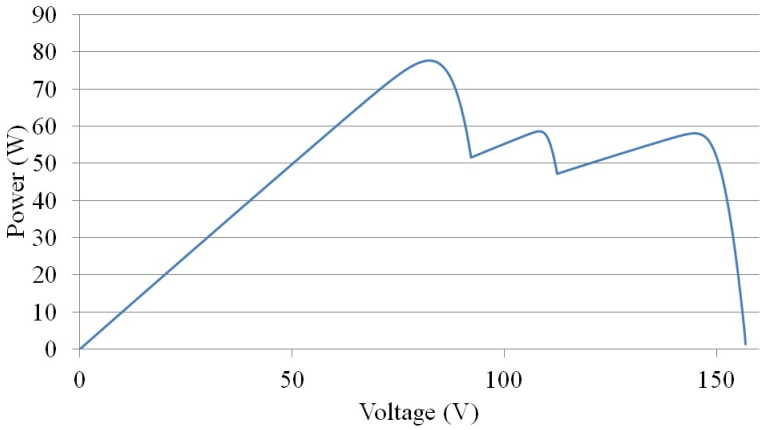

Figure D.17: P-V curve for characteristic 17.

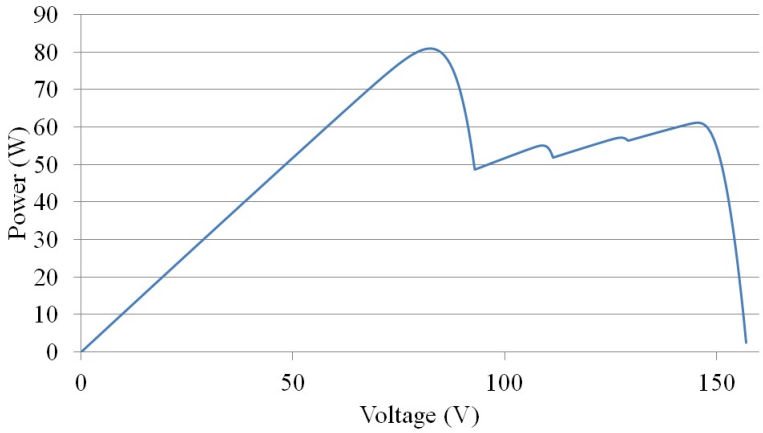

Figure D.18: P-V curve for characteristic 18.

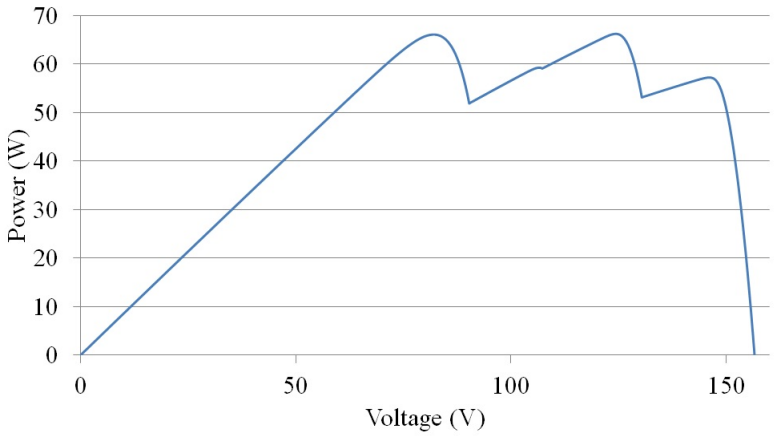

Figure D.19: P-V curve for characteristic 19.

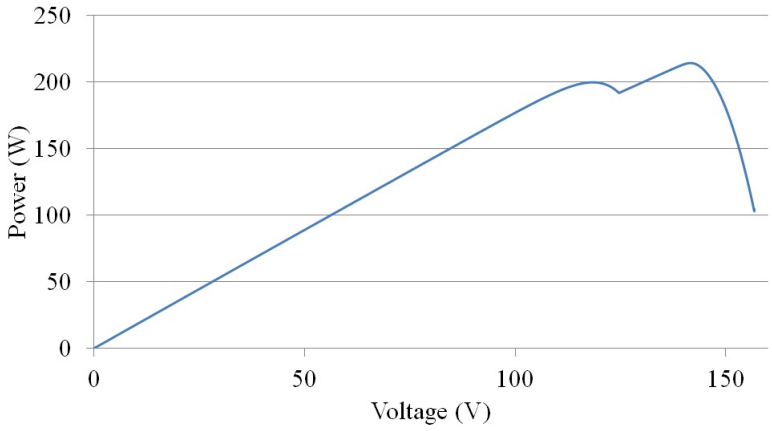

Figure D.20: P-V curve for characteristic 20.

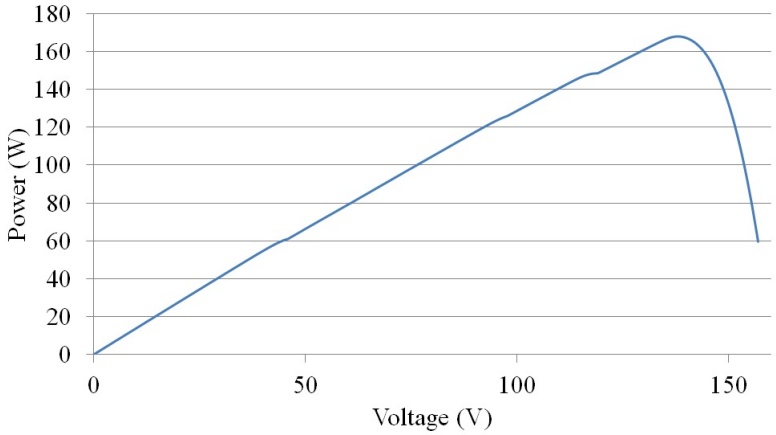

Figure D.21: P-V curve for characteristic 21.

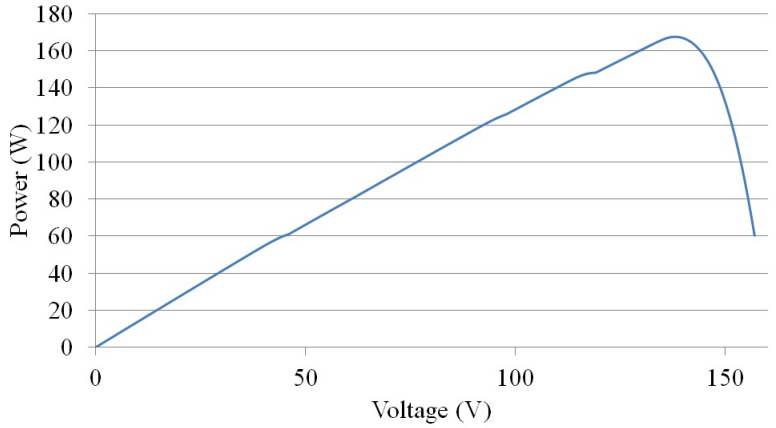

Figure D.22: P-V curve for characteristic 22.

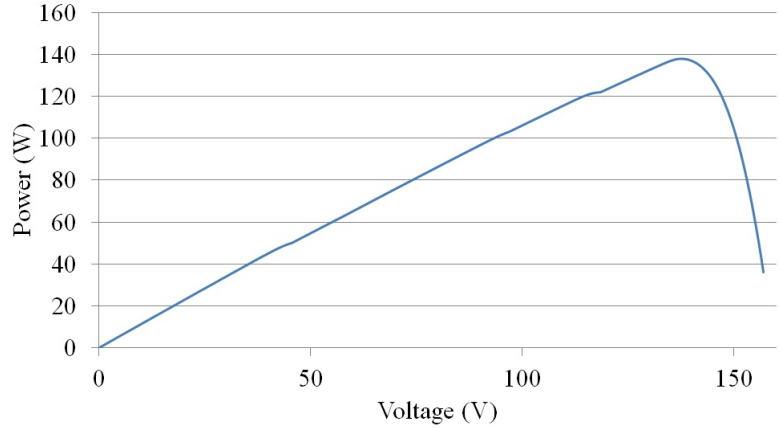

Figure D.23: P-V curve for characteristic 23.

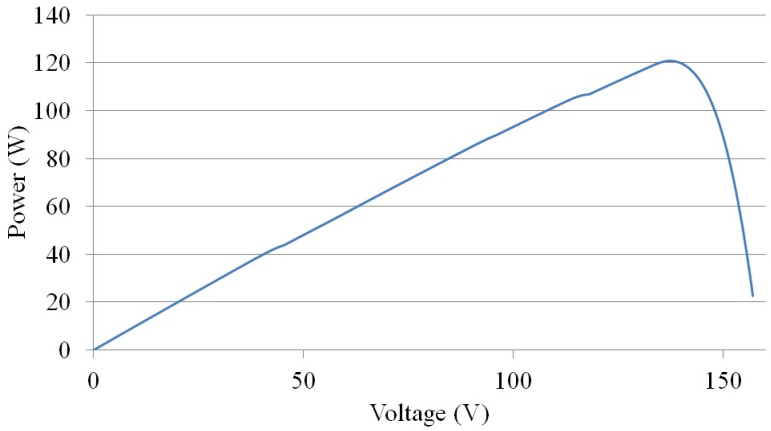

Figure D.24: P-V curve for characteristic 24.

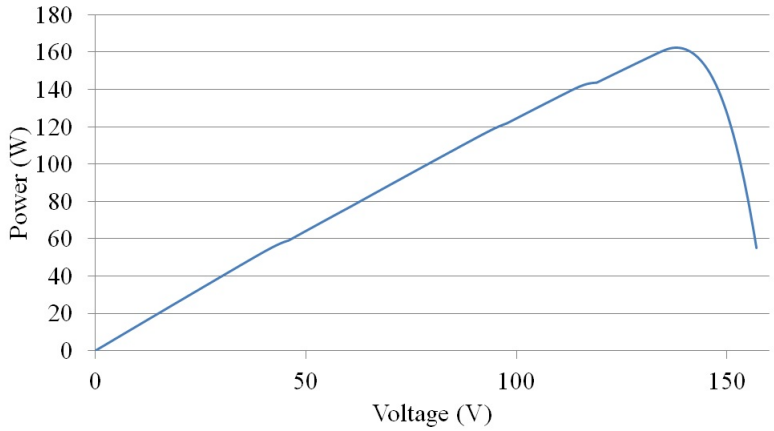

Figure D.25: P-V curve for characteristic 25.

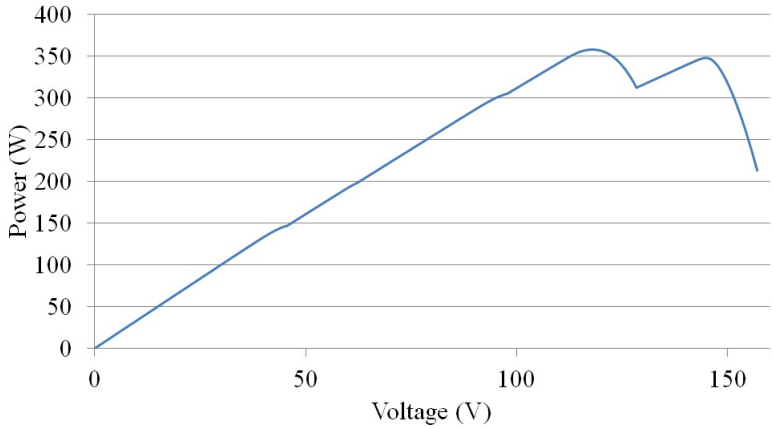

Figure D.26: P-V curve for characteristic 26.

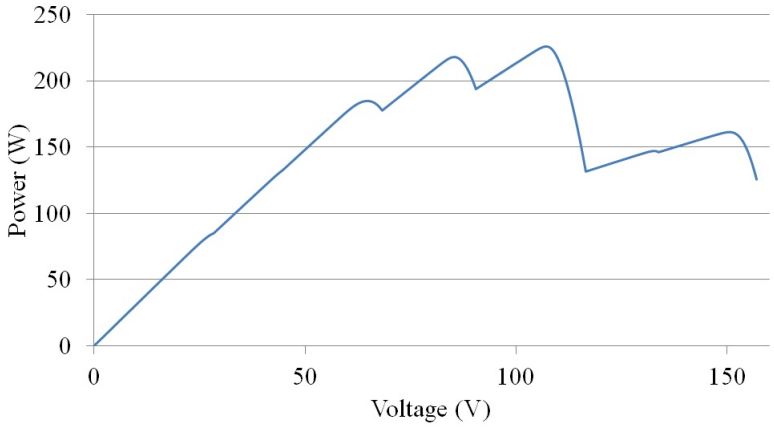

Figure D.27: P-V curve for characteristic 27.

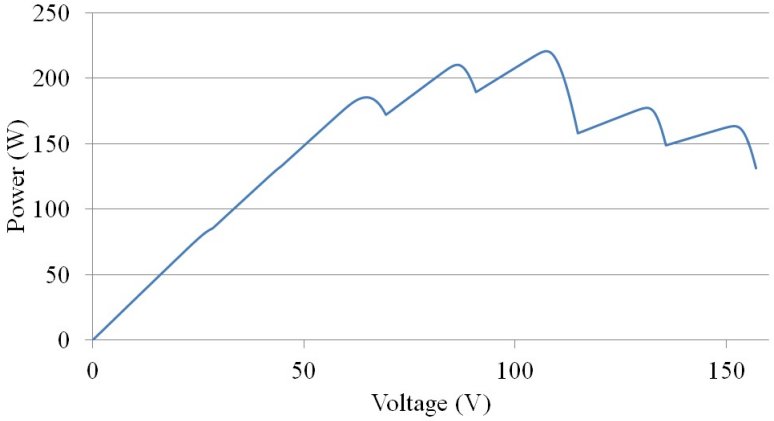

Figure D.28: P-V curve for characteristic 28.

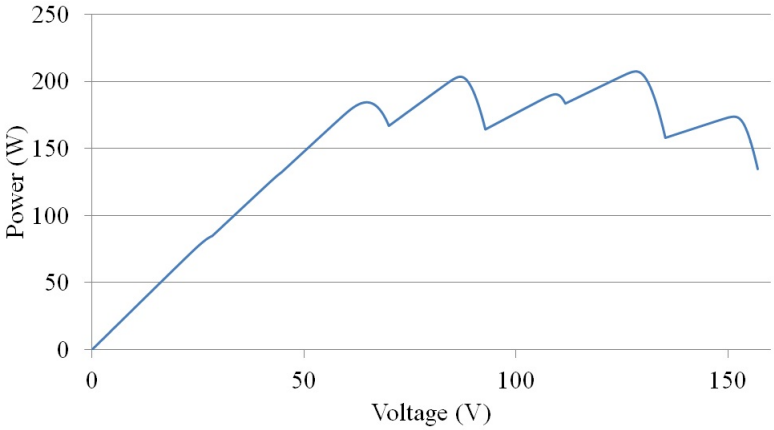

Figure D.29: P-V curve for characteristic 29.

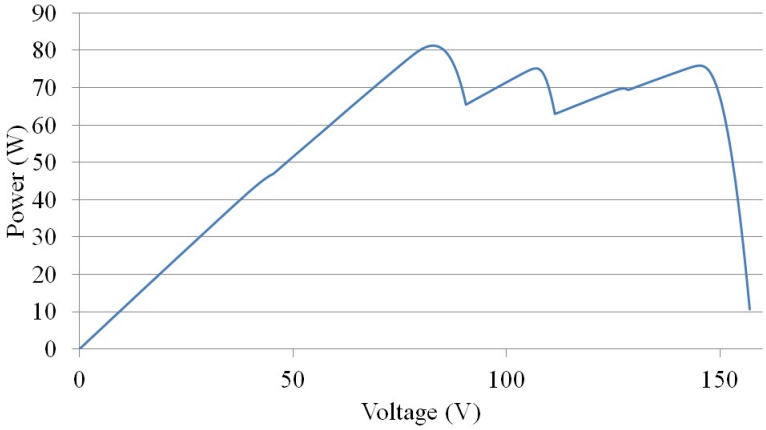

Figure D.30: P-V curve for characteristic 30.

Appendix E

Average Voltage and Power Errors at the Final Operating Point to Assess Performance of SA Algorithm with Parameter Variations

The average voltage and power error at the final operating point for variations in the starting temperature of the SA algorithm are given in Table E.1 and Table E.2, respectively.

The average voltage and power error at the final operating point for variations in the cooling rate of the SA algorithm are given in Table E.3 and Table E.4, respectively.

The average voltage and power error at the final operating point for variations in the cooling frequency of the SA algorithm are given in Table E.5 and Table E.6, respectively.

The average voltage and power error at the final operating point for variations in the acceptance probability threshold of the SA algorithm are given in Table E.7 and Table E.8, respectively.

The average voltage and power error at the final operating point for variations in the neighbourhood size of the SA algorithm are given in Table E.9 and Table E.10, respectively.

The average voltage and power error at the final operating point for variations in the neighbourhood size reduction function of the SA algorithm are given in Table E.11 and Table E.12, respectively.

The average voltage and power error at the final operating point for variations in the stopping temperature of the SA algorithm are given in Table E.13 and Table E.14, respectively.

The average voltage and power error at the final operating point for variations in the linear cooling schedule of the SA algorithm are given in Table E.15 and Table E.16, respectively.

The average voltage and power error at the final operating point for variations in the logarithmic cooling schedule of the SA algorithm are given in Table E.17 and Table E.18, respectively.

The average voltage and power error at the final operating point for variations in the Lundy cooling schedule of the SA algorithm are given in Table E.19 and Table E.20, respectively.

The average voltage and power error at the final operating point for variations in the Simulated Quenching algorithm are given in Table E.21 and Table E.22, respectively.

The average voltage and power error at the final operating point for variations in the stopping criterion of the SA algorithm are given in Table E.23 and Table E.24, respectively.

Table E.1: Average voltage error for the final operating point for variations of the initial temperature.

	10 ° C	**11 ° C**	**12 ° C**	**13 ° C**	**14 ° C**	**15 ° C**	**16 ° C**	**17 ° C**	**18 ° C**	**19 ° C**	**20 ° C**	**21 ° C**	**22 ° C**	**23 ° C**	**24 ° C**	**25 ° C**
Characteristic 1	0.3474	0.7064	0.3050	0.2587	-0.0343	0.2278	0.4644	0.3292	0.2746	0.1218	0.5434	0.0958	0.2942	0.4740	0.1074	0.4495
Characteristic 2	0.3467	0.0109	0.0872	-0.1466	-0.1445	-0.0621	0.0740	0.1440	0.0308	0.1289	0.2894	-0.0863	0.0515	0.1252	0.0920	-0.0059
Characteristic 3	0.2498	0.5746	0.2448	0.1732	0.3300	0.2765	0.2516	0.2478	0.2253	0.0577	0.2209	0.2338	0.5026	0.1479	0.3007	0.0404
Characteristic 4	0.3659	0.3486	0.0883	0.1712	0.2703	0.1967	0.3850	-0.0008	-0.0651	0.3114	0.1645	0.0741	0.4640	0.6574	0.4803	0.6170
Characteristic 5	0.3881	0.6633	0.4123	0.0805	0.4546	0.4991	0.2439	0.2565	0.2203	0.2197	0.3703	0.0752	0.3891	0.5242	0.2203	0.3334
Characteristic 6	0.4459	0.2930	0.2205	0.1114	0.2186	0.3836	0.3194	0.8413	0.2620	0.2447	0.2082	0.4271	0.0252	0.2470	0.2918	0.1416
Characteristic 7	-0.2241	0.1024	-0.0897	0.0159	0.0769	0.1704	0.2604	0.0266	0.1359	-0.2452	-0.1881	0.1013	0.2087	0.0465	-0.1328	0.2081
Characteristic 8	0.0139	0.1287	-0.2314	-0.0160	-0.0137	-0.1552	0.1103	-0.0943	-0.1031	0.0734	-0.2606	-0.0150	-0.0857	0.0321	-0.0336	0.1299
Characteristic 9	0.0459	0.5066	0.2901	0.1378	0.1538	0.2975	0.0255	0.2027	0.2193	0.2943	0.0180	0.1870	0.1484	0.1193	0.4716	0.3348
Characteristic 10	0.6701	2.2359	0.9486	1.3492	1.5813	1.1953	1.2541	2.3539	1.9435	0.8770	1.3958	1.2567	1.5517	1.8519	3.0581	2.2199
Characteristic 11	1.4205	1.5019	1.0991	1.0153	0.7489	1.3712	1.2302	0.6730	1.3016	1.4197	0.7444	0.7769	1.0020	0.7439	1.7786	1.4642
Characteristic 12	4.0824	4.1502	3.6640	4.1354	2.5507	3.8017	4.3147	4.2967	3.4995	3.1672	2.9473	5.7711	3.5148	3.0228	3.7921	3.4649
Characteristic 13	0.4558	0.8190	0.6745	0.8720	0.4404	0.8286	1.1489	0.8270	0.3094	0.6015	0.5793	0.8002	0.9625	0.4227	0.7534	0.8532
Characteristic 14	0.5507	0.6759	0.4791	0.4929	0.3757	0.4222	0.5547	0.3956	0.7299	0.5806	0.7717	0.6353	0.4399	0.7675	0.5359	0.7201
Characteristic 15	0.5288	0.0528	0.3712	0.4583	0.1970	0.3138	0.2146	0.4895	0.3473	0.2060	0.0219	0.1885	0.3009	0.1688	0.3152	0.2014
Characteristic 16	0.7657	1.0766	0.8480	0.4132	0.5240	0.2490	0.8044	0.3134	0.5574	0.5262	0.4962	0.6542	0.5587	0.7433	0.4855	0.7588
Characteristic 17	0.6599	1.0185	0.5328	0.1399	0.6641	1.2477	0.5011	0.7305	0.2466	0.6950	0.8403	0.4768	0.6581	0.6411	0.9762	0.6857
Characteristic 18	0.1882	0.2162	0.0638	0.2741	-0.0310	0.4997	0.1554	0.8181	0.5286	0.2541	0.0991	0.2055	0.1585	0.3654	0.3819	0.6431
Characteristic 19	21.7370	22.3806	21.5627	21.3127	22.4304	22.1608	19.2661	24.0407	23.6833	18.8420	17.8051	22.4955	19.6769	22.7977	23.3397	22.6259
Characteristic 20	0.2571	0.6657	0.4719	0.3764	0.2069	0.7082	0.5143	0.8021	0.5491	0.4364	0.4762	0.6891	0.5186	0.7548	0.3504	0.7078
Characteristic 21	0.0337	0.2974	0.4512	0.1574	0.0664	-0.1435	0.3071	-0.0635	0.1337	0.1726	0.4328	0.1189	0.2044	0.1428	0.3685	0.3593
Characteristic 22	0.2244	-0.0150	-0.0893	0.3508	0.1740	-0.1579	0.0490	0.3315	0.0754	0.2831	0.0253	0.0301	-0.0039	-0.0211	-0.0140	0.3060
Characteristic 23	0.2250	0.1320	0.2998	0.2477	0.1993	0.2109	0.1039	0.3485	0.1283	-0.0656	0.0114	0.3200	0.0914	0.4484	0.5069	-0.1023
Characteristic 24	0.0667	0.3194	0.1227	-0.0416	-0.0718	0.3296	-0.0636	0.0397	0.4201	0.2559	0.0972	0.3464	0.1448	0.8831	0.1517	-0.1669
Characteristic 25	0.2215	-0.0968	-0.1272	0.4562	0.1058	-0.0884	0.1325	0.0317	0.2185	-0.3082	0.2304	0.1792	-0.1691	0.1666	0.1181	-0.1787
Characteristic 26	0.1640	0.0137	-0.1116	0.3314	0.1343	0.0599	0.2388	0.0873	0.1361	0.0807	0.1949	-0.2604	0.2056	0.2969	0.1304	-0.0766
Characteristic 27	0.7785	0.7900	1.8274	0.5608	0.9612	1.0792	0.9343	0.5052	0.7085	0.8282	0.5472	1.0283	0.3994	0.3524	0.6870	0.6946
Characteristic 28	0.3979	1.0558	0.6265	0.2076	0.0692	0.2036	0.7175	0.5603	0.8758	0.5732	0.4661	0.9730	0.5912	0.5011	0.8253	0.7585
Characteristic 29	2.8656	2.1611	3.4885	2.9979	4.0112	2.4622	2.1241	2.9183	2.9216	1.0414	2.9683	3.7364	2.5817	2.4901	2.1258	3.1051
Characteristic 30	0.0898	0.5933	0.2452	-0.1482	0.1873	0.3887	-0.0746	-0.5908	0.3842	-0.4427	0.1281	0.1039	-0.0023	0.8624	0.2732	0.1960

Table E.2: Average power error for the final operating point for variations of the initial temperature.

	10 ° C	**11 ° C**	**12 ° C**	**13 ° C**	**14 ° C**	**15 ° C**	**16 ° C**	**17 ° C**	**18 ° C**	**19 ° C**	**20 ° C**	**21 ° C**	**22 ° C**	**23 ° C**	**24 ° C**	**25 ° C**
Characteristic 1	0.7083	0.6678	0.6618	0.8496	0.4814	0.6005	0.6357	0.6602	0.7287	0.6458	0.7106	0.7723	0.6809	0.6371	0.6012	0.6003
Characteristic 2	1.0856	1.3039	1.2714	1.0908	1.1259	1.3272	1.0421	1.5474	1.1693	1.0140	1.2720	1.1557	1.3779	0.8830	1.1990	0.8129
Characteristic 3	1.3015	1.7630	1.1955	1.3296	1.4089	1.4078	1.5865	1.1866	1.5727	1.0272	1.6148	1.3406	1.7926	1.3863	1.7490	1.0420
Characteristic 4	0.7174	0.7647	0.8030	0.6351	0.7986	0.7398	0.7756	0.9361	0.6347	0.7261	0.5775	0.6076	0.8032	0.7678	0.6572	0.9492
Characteristic 5	0.8696	0.8931	0.7549	0.9906	0.7757	0.7806	0.8009	1.0030	0.8092	0.7652	0.5599	0.5857	0.5868	0.8988	0.8621	0.8371
Characteristic 6	0.7788	0.6803	0.7003	0.7006	0.5508	0.6282	0.8467	0.8520	0.6137	0.7006	0.6974	0.7191	0.6323	0.8873	0.5722	0.7054
Characteristic 7	0.8099	0.6543	0.6814	0.5777	0.7147	0.8353	0.8071	0.9038	0.7252	0.6774	0.7719	0.7435	0.7469	0.6992	0.5370	0.6925
Characteristic 8	0.8793	0.6656	0.7499	0.9436	0.8340	1.1192	0.8330	1.0824	0.9070	0.7479	1.0609	1.1308	0.9711	0.7837	0.7911	1.0803
Characteristic 9	1.2027	1.8486	1.4166	1.2984	0.9330	1.4551	1.3439	1.4965	1.1713	1.7303	1.3600	1.5196	1.5472	1.5432	1.4957	1.5283
Characteristic 10	1.4226	1.7023	1.5027	1.5286	1.6745	1.7506	1.5942	1.6836	1.5946	1.6713	1.5681	1.4691	1.6471	1.6519	1.9456	1.5365
Characteristic 11	0.6137	0.6650	0.5267	0.5508	0.4365	0.5899	0.5548	0.4426	0.5671	0.5860	0.5051	0.4759	0.5355	0.4846	0.5937	0.5423
Characteristic 12	0.6395	0.7810	0.5772	0.6909	0.4939	0.6569	0.6772	0.6682	0.6068	0.6115	0.5905	0.8575	0.5937	0.5159	0.5652	0.7040
Characteristic 13	0.4929	0.4891	0.4596	0.5039	0.3900	0.5118	0.5854	0.5574	0.4510	0.5546	0.4540	0.5985	0.4162	0.4464	0.5652	0.5445
Characteristic 14	0.5407	0.4669	0.3621	0.5557	0.3672	0.4581	0.4279	0.5299	0.4361	0.5383	0.5185	0.4546	0.4409	0.4016	0.4591	0.5549
Characteristic 15	0.8492	0.7744	0.7084	1.1865	0.6269	1.0211	0.9243	1.1651	0.8888	1.0731	0.7461	0.9655	0.8404	0.7245	0.9629	0.9630
Characteristic 16	0.7421	0.6359	0.4933	0.5507	0.4222	0.4485	0.5907	0.5062	0.4476	0.4540	0.5273	0.6251	0.4381	0.5140	0.5698	0.5424
Characteristic 17	0.5585	0.5684	0.4838	0.5659	0.5172	0.5944	0.6166	0.6310	0.6031	0.5244	0.6086	0.6271	0.5116	0.5550	0.6025	0.4519
Characteristic 18	0.5307	0.5740	0.5010	0.5440	0.4252	0.4968	0.4946	0.7069	0.5965	0.5144	0.6013	0.4239	0.5957	0.5423	0.4892	0.4954
Characteristic 19	0.4381	0.3996	0.4682	0.4364	0.4591	0.5193	0.5244	0.4903	0.4524	0.4120	0.4169	0.4420	0.4211	0.4179	0.3499	0.5275
Characteristic 20	0.9345	1.1140	0.9873	0.8556	0.7580	0.8153	0.8317	1.1064	0.8844	0.9194	0.9540	1.0550	0.9748	0.8841	0.7563	0.9526
Characteristic 21	0.5766	0.8237	0.5890	0.6844	0.5675	0.6065	0.6838	0.7658	0.8450	0.6169	0.6092	0.6914	0.5213	0.6485	0.6909	0.5976
Characteristic 22	0.7181	0.7526	0.5966	0.6841	0.5765	0.6925	0.6626	0.7215	0.6059	0.7157	0.6627	0.6530	0.4891	0.6810	0.7876	0.5852
Characteristic 23	0.6745	0.5256	0.4925	0.5940	0.6544	0.6118	0.6834	0.4624	0.5569	0.7863	0.6164	0.6963	0.4859	0.5575	0.6433	0.7092
Characteristic 24	0.5962	0.6146	0.5164	0.7675	0.5975	0.4829	0.6227	0.5125	0.5818	0.7223	0.5036	0.7428	0.5253	0.6832	0.5675	0.4584
Characteristic 25	0.8539	0.5894	0.6477	0.6343	0.6513	0.5520	0.6317	0.5670	0.5186	0.5949	0.7244	0.7443	0.8224	0.6612	0.5718	0.6550
Characteristic 26	0.7270	0.7828	0.7804	0.7558	0.7768	0.7568	0.8936	0.7508	0.8134	0.8756	0.9554	1.0055	0.7469	0.8099	0.6455	0.7706
Characteristic 27	1.2728	1.3831	1.8344	1.0476	1.4129	1.6470	1.2570	1.2488	1.2579	1.4344	1.4348	1.4610	0.9361	1.2122	1.1848	1.6103
Characteristic 28	1.2694	1.7172	1.1693	1.2197	0.9386	1.2153	1.1779	1.3656	1.6579	1.2743	1.3849	1.5765	1.2870	1.4506	1.5262	1.3891
Characteristic 29	1.1625	1.2302	1.1184	1.1336	1.0992	1.0227	1.0422	1.5168	1.2887	1.1315	1.3183	1.2560	1.1049	1.2121	1.1429	1.2792
Characteristic 30	0.5985	0.6408	0.6440	0.7970	0.4959	0.3883	0.6538	0.8868	0.4718	0.4246	0.6252	0.7194	0.5070	0.6233	0.4620	0.5600

Table E.3: Average voltage error for the final operating point for variations of the cooling rate.

	0.45	0.50	0.55	0.60	0.65	0.70	0.75	0.80	0.85	0.90	0.95
Characteristic 1	0.4408	0.3176	-0.1907	0.8546	0.3156	0.3849	0.1897	-0.0104	0.3959	0.2505	-0.0243
Characteristic 2	0.2718	0.8156	0.6459	0.1848	0.2079	0.0793	0.2130	0.2288	-0.1391	0.1827	-0.0084
Characteristic 3	3.2830	1.6402	0.8953	1.4590	0.8201	0.9168	0.4251	0.1828	0.0469	0.0707	0.0437
Characteristic 4	0.7975	0.6832	1.1338	0.1764	0.5131	0.3393	0.5165	0.3851	0.4006	0.0298	0.3063
Characteristic 5	0.7443	0.3196	0.2213	0.3736	0.2461	-0.1321	0.3676	-0.0412	0.3446	0.3199	0.1369
Characteristic 6	1.1228	0.2184	0.4639	0.4818	0.4430	0.3612	0.8551	0.3906	0.4920	0.2106	0.2155
Characteristic 7	-0.0600	0.3466	0.0685	-0.2495	0.1331	0.0366	0.1212	-0.1126	-0.0723	-0.0732	0.0449
Characteristic 8	0.4449	0.0935	-0.0240	-0.3184	-0.0976	-0.1940	-0.2144	-0.0970	-0.2613	0.1692	0.0468
Characteristic 9	1.4092	0.9348	1.0884	0.5964	0.4424	-0.0290	0.4149	0.1311	0.0977	0.1903	0.0900
Characteristic 10	8.6268	7.3000	5.6342	6.2307	2.7155	2.7946	2.5405	2.0940	0.3081	0.0798	-0.0243
Characteristic 11	2.3670	4.3891	2.1301	2.0711	2.3045	1.1974	1.2120	0.8541	1.1821	0.9422	0.3504
Characteristic 12	5.6848	8.0998	6.1702	6.3485	6.0009	6.1212	4.8893	4.3630	3.5222	1.8482	0.6394
Characteristics 13	1.1207	1.3841	0.8290	1.4821	1.1272	0.8951	0.8778	0.5222	1.1041	0.3110	0.3534
Characteristics 14	1.7001	1.8303	0.3581	1.4627	0.9421	0.8133	0.9357	0.5475	0.4569	0.2774	0.3012
Characteristics 15	0.8773	1.7318	1.4418	0.7599	0.4944	0.1312	0.5872	0.3421	0.0971	-0.0105	0.0492
Characteristic 16	0.9987	0.9178	1.5994	0.6947	0.5820	0.9037	0.7456	0.5911	0.4603	0.5286	0.3065
Characteristic 17	0.9712	1.5625	1.4904	0.8101	0.7013	0.9798	0.7970	0.6412	0.5768	0.3847	0.3589
Characteristic 18	1.1593	0.5289	0.8582	1.1027	0.2599	0.6178	0.2713	0.4450	-0.2043	0.0560	-0.0776
Characteristic 19	23.4772	24.7285	23.8595	21.3799	24.3485	20.0065	22.8648	23.2971	21.5250	19.8920	22.7068
Characteristic 20	2.9073	3.1483	2.5978	2.0584	1.7841	0.7190	0.8991	0.5537	0.2339	0.1582	0.0808
Characteristic 21	0.6973	1.6600	1.0229	0.4557	0.6284	0.2051	0.5162	-0.2849	-0.1225	0.1229	0.0258
Characteristic 22	0.3290	1.2048	0.1302	0.2041	0.7163	0.4523	0.1144	0.0452	0.2519	0.0093	0.0324
Characteristic 23	0.7937	1.3129	1.1173	0.6245	0.7678	0.7466	0.1777	0.4519	0.1996	-0.0207	0.0481
Characteristic 24	1.3072	1.2935	1.0779	1.0787	0.1112	0.1693	-0.0073	0.3619	-0.2837	0.0448	0.0193
Characteristic 25	1.3237	2.1900	0.7740	0.5468	0.4716	-0.1192	0.4443	0.1789	0.0793	-0.0053	0.0194
Characteristic 26	-0.8700	-0.6319	0.1235	-0.2016	0.4560	0.3451	-0.0929	0.5527	0.0438	-0.3075	-0.0467
Characteristic 27	4.2005	6.0943	2.7483	2.0322	3.3903	2.4128	1.8433	0.9182	0.3130	0.1734	0.1259
Characteristic 28	3.6828	2.7867	2.2074	2.5524	1.6781	1.0542	1.0426	0.4462	0.2839	0.4119	0.2214
Characteristic 29	13.1625	12.1125	8.3600	9.1360	6.7229	5.4162	5.4943	2.6582	1.6369	0.1829	0.0804
Characteristic 30	-2.7718	-4.2806	-4.5471	-0.1373	-0.7042	-0.3820	-0.8876	-0.3381	0.0770	0.0795	0.2229

Table E.4: Average power error for the final operating point for variations of the cooling rate.

	0.45	0.50	0.55	0.60	0.65	0.70	0.75	0.80	0.85	0.90	0.95
Characteristic 1	1.9554	1.7580	1.0750	1.3264	1.2814	1.2386	0.9793	0.7115	0.3808	0.3474	0.3190
Characteristic 2	3.6162	4.5783	2.7442	2.7005	2.3664	1.7337	1.4021	1.3622	0.8960	0.6737	0.3581
Characteristic 3	6.4210	4.6044	3.4847	3.8801	2.7685	2.3039	2.0906	1.3950	1.1325	0.6959	0.3439
Characteristic 4	3.3277	2.4639	2.5314	1.6436	1.4413	0.9991	1.2131	0.7956	0.5616	0.4342	0.2737
Characteristic 5	2.5916	2.9763	2.0545	2.2021	0.9762	1.0110	0.9653	0.9927	0.5678	0.4368	0.2976
Characteristic 6	2.4121	2.1808	1.8208	1.2548	1.0624	1.2616	1.0472	0.7193	0.6031	0.3879	0.2837
Characteristic 7	2.8636	2.4420	2.3589	1.9236	1.3005	0.9268	1.0075	0.5532	0.6174	0.4769	0.2948
Characteristic 8	3.6483	2.9462	2.7580	2.1591	1.1805	1.4845	1.0942	0.8815	0.6599	0.4830	0.2669
Characteristic 9	6.4372	4.7607	4.1520	3.1723	2.3759	1.8669	1.6580	1.3388	0.8461	0.6384	0.4594
Characteristic 10	4.1416	4.0408	3.7147	3.5390	2.0137	2.4270	2.0600	1.6641	0.8871	0.6972	0.3778
Characteristic 11	1.0541	1.6963	0.9837	0.9411	1.0100	0.5940	0.6820	0.5084	0.5507	0.3529	0.2681
Characteristic 12	0.9111	1.3201	0.9290	1.0571	1.0444	0.9026	0.7458	0.6952	0.5987	0.4364	0.2577
Characteristic 13	1.1851	1.1146	0.8403	0.9372	0.7859	0.6485	0.5730	0.4323	0.4668	0.2645	0.2411
Characteristic 14	1.3853	1.2410	1.0121	0.9283	0.7344	0.6710	0.6442	0.3999	0.5083	0.2900	0.2451
Characteristic 15	2.5898	4.0490	2.7088	2.1549	2.1910	1.4133	1.4666	0.9636	0.7827	0.4071	0.3464
Characteristic 16	1.5433	1.2295	1.4070	1.1075	0.7780	1.0284	0.6669	0.7275	0.3524	0.3100	0.2526
Characteristic 17	1.6347	1.6133	1.0601	0.9046	0.8205	0.8295	0.7820	0.5810	0.5016	0.3301	0.3037
Characteristic 18	1.7252	2.0615	1.3363	1.0757	0.8934	0.9037	0.6787	0.6478	0.3805	0.3843	0.2908
Characteristic 19	0.8328	1.1561	0.6353	0.6945	0.5580	0.5908	0.5080	0.4431	0.4203	0.3821	0.2995
Characteristic 20	3.2277	3.4139	2.4186	2.4256	2.2279	1.2026	1.5573	0.9298	0.5600	0.6129	0.2748
Characteristic 21	1.9349	2.1885	1.4270	1.5595	1.3748	1.0531	0.7727	0.6341	0.5809	0.3619	0.3241
Characteristic 22	1.8815	2.2241	1.5233	1.2591	1.2297	1.1019	0.9496	0.7280	0.4241	0.3485	0.3529
Characteristic 23	1.5276	2.0851	1.4781	1.2451	1.0533	0.9936	0.6542	0.6444	0.5576	0.4110	0.2488
Characteristic 24	1.5643	1.8436	1.2447	1.0087	1.0082	0.9348	0.7647	0.5443	0.4720	0.4626	0.2935
Characteristic 25	1.9441	2.7158	1.6129	1.2740	1.1212	0.8416	0.9605	0.6999	0.5224	0.3527	0.2854
Characteristic 26	3.1659	3.1872	2.1119	1.7965	1.8234	1.3091	0.9765	0.9165	0.5883	0.4527	0.2788
Characteristic 27	4.4093	4.7135	3.0614	2.8179	2.7682	2.1373	2.1073	1.7709	0.9550	0.5469	0.3654
Characteristic 28	3.9934	4.1060	2.8912	3.1547	2.6505	2.3426	1.8303	1.2342	0.9463	0.7556	0.4636
Characteristic 29	3.5569	3.8145	2.5856	2.5794	2.1062	2.0492	1.4739	1.1858	0.8504	0.6743	0.3299
Characteristic 30	1.4255	2.4168	2.0630	1.3885	1.0000	1.0476	0.8422	0.7014	0.4901	0.3629	0.3021

Table E.5: Average voltage error for the final operating point for variations of the cooling frequency.

	2	**3**	**4**	**5**	**6**	**7**	**8**	**9**	**10**	**11**
Characteristic 1	0.5386	0.5579	0.2976	0.1769	0.5477	0.0765	0.1675	0.3036	0.1147	0.1764
Characteristic 2	0.8562	0.3198	0.1583	-0.0007	0.2420	0.1524	-0.0384	-0.2723	0.0400	-0.1422
Characteristic 3	1.4845	0.6323	0.2209	0.1704	0.1024	0.0880	-0.0032	0.0600	0.0103	-0.0538
Characteristic 4	0.4977	0.7646	0.3621	0.3323	0.2689	0.0865	0.1952	0.0969	0.2356	0.1088
Characteristic 5	1.1855	0.1099	0.0829	0.2992	0.4605	0.1574	0.2838	0.1712	0.1782	0.1194
Characteristic 6	0.6285	0.4009	0.4781	0.0396	0.3807	0.4976	0.4420	0.2708	0.2122	0.3697
Characteristic 7	0.4375	0.1911	0.3386	-0.0290	0.1652	0.1815	-0.0818	0.0894	0.1332	0.1625
Characteristic 8	0.1112	-0.4942	-0.1010	0.1041	0.0751	-0.1237	0.0383	-0.1382	-0.0135	0.1801
Characteristic 9	1.0267	0.1244	0.2047	0.1397	0.0998	0.0489	-0.0453	0.2606	0.1871	-0.0474
Characteristic 10	4.1406	3.0221	2.6546	1.4006	0.5561	0.2663	0.0566	0.4781	-0.0211	0.0637
Characteristic 11	2.0897	1.7244	0.9618	1.3363	1.3050	0.8232	1.0215	0.5852	0.6361	0.8976
Characteristic 12	6.7309	3.7249	6.5366	3.8040	3.3188	2.3333	2.1334	2.9071	1.9128	1.3527
Characteristic 13	0.4402	1.0757	0.8333	0.5941	0.6827	0.8617	0.5828	0.6816	0.1659	0.6764
Characteristic 14	1.6648	0.7794	0.6680	1.0313	1.0715	0.5173	0.4688	0.4498	0.2334	0.2698
Characteristic 15	0.9181	0.8151	0.4492	0.4867	0.2056	0.3496	0.3048	0.1104	0.2244	0.1321
Characteristic 16	1.0504	0.3464	0.8079	0.8469	0.5611	0.4201	0.8783	0.1649	0.2241	0.2887
Characteristic 17	1.5793	0.3704	1.5323	0.7012	0.3012	0.7797	0.8036	0.3386	0.5036	0.4028
Characteristic 18	0.9246	0.8996	0.6688	0.7360	0.0579	0.2229	0.0529	-0.0778	0.3251	0.1977
Characteristic 19	22.0671	22.3944	19.9292	20.6738	24.1849	18.2942	20.5262	21.4144	22.9438	22.3328
Characteristic 20	2.2392	0.9468	1.0609	0.6594	0.3120	0.5206	0.1644	0.3736	0.0587	0.1866
Characteristic 21	1.3317	0.4029	0.0076	0.1143	0.0328	0.0515	0.0384	0.1877	-0.0365	-0.1558
Characteristic 22	1.2847	0.2033	-0.0571	0.4159	0.1830	0.2488	-0.0545	0.0870	0.1669	0.1569
Characteristic 23	0.5658	0.5872	0.2166	0.3394	0.4188	0.0380	0.0314	0.1342	0.0925	0.2261
Characteristic 24	0.8839	0.2113	0.2621	0.3137	0.2803	0.0054	0.0823	0.2486	0.2269	-0.1633
Characteristic 25	1.0169	-0.0781	0.0161	0.1547	0.0484	-0.3799	0.0344	0.2702	-0.0909	-0.0603
Characteristic 26	-0.5552	0.3596	-0.1312	0.0154	0.1007	0.2837	-0.1630	0.2522	0.0111	-0.0715
Characteristic 27	3.5242	1.7166	1.2849	0.7411	0.2697	0.4676	0.1653	0.0197	0.3253	0.2724
Characteristic 28	2.0904	1.5947	0.8527	0.5203	0.3990	0.3410	0.4585	0.2261	0.1433	0.2991
Characteristic 29	8.4377	7.7712	3.1292	4.7927	1.7541	1.6723	0.6517	0.5021	1.1433	0.2946
Characteristic 30	-0.2494	-1.7672	0.3343	0.3612	0.5557	0.2387	0.2045	0.2475	-0.1575	-0.0903

Table E.6: Average power error for the final operating point for variations of the cooling frequency.

	2	**3**	**4**	**5**	**6**	**7**	**8**	**9**	**10**	**11**
Characteristic 1	1.7270	1.1480	0.8132	0.7159	0.6816	0.5126	0.5441	0.3698	0.4758	0.3049
Characteristic 2	3.9185	1.4670	1.5422	1.4496	1.1483	0.8783	0.8390	0.6970	0.6325	0.5642
Characteristic 3	4.0036	2.0449	1.7204	1.4048	1.0400	0.9875	0.7783	1.0637	0.7631	0.6908
Characteristic 4	1.6691	1.6377	0.8979	0.9355	0.6822	0.6180	0.5899	0.4697	0.4294	0.4822
Characteristic 5	2.2285	1.2051	0.7904	0.8429	0.6126	0.6151	0.5611	0.4404	0.3296	0.5069
Characteristic 6	1.3070	1.0956	0.9442	0.8073	0.8926	0.5457	0.4568	0.3455	0.5084	0.5083
Characteristic 7	2.0599	1.4231	0.8895	0.7292	0.6735	0.5434	0.4200	0.4452	0.4481	0.4908
Characteristic 8	2.5136	1.6038	1.1518	1.0117	0.8627	0.7476	0.5413	0.4635	0.5199	0.4508
Characteristic 9	4.1140	2.1180	1.4780	1.2833	1.1482	0.8218	0.8247	0.8370	0.7604	0.4618
Characteristic 10	3.0726	2.4156	1.6985	1.3502	0.9543	1.0224	1.0185	0.8911	0.7487	0.5525
Characteristic 11	0.9737	0.7261	0.5249	0.5055	0.5129	0.4252	0.4819	0.3394	0.3269	0.4093
Characteristic 12	0.9399	0.8550	0.8519	0.6930	0.5828	0.5748	0.4955	0.4854	0.4548	0.4152
Characteristic 13	0.9262	0.7840	0.4689	0.4676	0.3304	0.5925	0.4068	0.4348	0.3170	0.2886
Characteristic 14	1.0840	0.6606	0.7156	0.5393	0.5480	0.4061	0.2874	0.3480	0.3445	0.3154
Characteristic 15	2.5906	1.6085	1.2389	0.9410	0.6147	0.8498	0.7242	0.5609	0.7517	0.5326
Characteristic 16	1.0334	0.8087	0.5499	0.6039	0.5405	0.3665	0.4924	0.4371	0.3571	0.3060
Characteristic 17	1.2680	0.7583	0.8727	0.5295	0.4220	0.4673	0.4620	0.2631	0.3667	0.3224
Characteristic 18	1.1716	0.7431	0.5258	0.5731	0.4904	0.4506	0.3940	0.3103	0.3495	0.3290
Characteristic 19	0.5668	0.5220	0.4010	0.5029	0.4860	0.3546	0.3357	0.3688	0.3621	0.2966
Characteristic 20	2.4654	1.2874	1.3609	1.1522	0.6294	0.6748	0.5875	0.6684	0.4381	0.5634
Characteristic 21	1.9392	1.1033	0.7478	0.6894	0.4039	0.6869	0.5720	0.4401	0.3384	0.3553
Characteristic 22	1.5418	0.9123	0.6602	0.5266	0.5303	0.4780	0.4559	0.4731	0.4492	0.2753
Characteristic 23	1.1811	1.1282	0.6398	0.7302	0.5131	0.4428	0.4871	0.3776	0.4017	0.3891
Characteristic 24	1.2008	1.0671	0.7034	0.6929	0.5501	0.4877	0.4425	0.3792	0.3993	0.4439
Characteristic 25	1.5724	0.9242	0.7836	0.6085	0.6654	0.5200	0.4705	0.4960	0.3670	0.3370
Characteristic 26	1.9879	1.3879	0.9699	0.8944	0.6744	0.7180	0.4650	0.5827	0.6030	0.4542
Characteristic 27	3.3194	2.1244	1.7889	1.2702	0.9440	1.0752	0.6893	0.8009	0.8320	0.7294
Characteristic 28	3.1466	1.9193	1.5094	1.3262	1.1998	1.0162	0.9964	0.7508	0.7023	0.8286
Characteristic 29	2.2756	1.9919	1.2295	1.1465	0.9563	0.9415	0.7027	0.7081	0.5721	0.5398
Characteristic 30	1.4622	1.0605	0.8640	0.6946	0.5205	0.5097	0.4716	0.4383	0.3856	0.3837

Table E.7: Average voltage error for the final operating point for variations of the acceptance probability threshold.

	0.05	**0.1**	**0.15**	**0.2**	**0.25**	**0.3**	**0.35**	**0.4**	**0.45**	**0.5**
Characteristic 1	0.2434	0.1419	0.3862	0.3021	0.1333	0.2222	0.2708	0.1914	0.2690	0.1320
Characteristic 2	-0.1784	-0.1947	-0.2090	-0.1545	0.0322	0.1179	-0.0816	0.1757	0.2180	0.0569
Characteristic 3	0.1580	0.3736	0.2809	0.3169	0.1799	0.2673	0.2777	0.1094	0.1225	-0.0144
Characteristic 4	0.4037	0.1004	0.4194	0.1664	0.2865	0.2004	0.2068	0.1946	0.1802	0.3504
Characteristic 5	0.2558	0.1410	0.1757	0.2407	0.2597	0.3602	0.1683	0.2358	0.1756	0.2345
Characteristic 6	-0.0452	0.2888	0.3435	0.5696	0.3708	0.3261	0.1883	0.0655	0.2659	0.5019
Characteristic 7	0.1692	0.1422	-0.1226	-0.0806	0.1191	0.1204	0.0479	0.0477	0.3020	-0.0026
Characteristic 8	-0.1565	-0.1135	-0.2432	0.0319	-0.2603	0.0551	-0.0674	-0.1054	-0.0963	-0.0846
Characteristic 9	0.3703	0.1289	-0.0720	0.0372	0.0631	0.1431	0.1504	-0.0240	0.0176	0.2180
Characteristic 10	1.2012	1.3511	0.9509	0.9519	2.0214	0.4792	0.1534	0.5280	0.9978	0.2450
Characteristic 11	1.2001	1.0811	0.9482	1.0803	0.7980	0.9456	0.6473	0.4486	0.3934	0.5478
Characteristic 12	3.7380	2.8093	2.7647	2.7915	2.5270	2.4220	2.1275	0.7435	1.6188	1.0043
Characteristic 13	0.5927	0.8611	0.5184	0.9414	0.6221	0.3402	0.6046	0.5988	0.2594	0.3727
Characteristic 14	0.5197	0.5732	1.0095	0.6564	0.1975	0.0987	0.2633	0.3682	0.5317	0.4353
Characteristic 15	0.2563	0.3525	0.2066	0.3766	0.0381	0.2816	0.2049	0.2369	0.2757	0.1452
Characteristic 16	0.7258	0.7659	0.7241	0.5848	0.2746	0.6741	0.6679	0.2158	0.5522	0.4840
Characteristic 17	1.2387	0.7057	0.4535	0.7489	0.4792	0.1743	0.6015	0.1719	0.2647	0.2602
Characteristic 18	0.0265	0.2760	-0.1590	-0.2098	0.1608	0.3622	0.0334	-0.0240	-0.1451	0.0561
Characteristic 19	24.2216	22.9886	18.3916	21.4453	20.1942	20.9214	20.5877	21.2532	20.2450	17.6941
Characteristic 20	0.7318	0.9027	0.5628	0.2872	0.4370	0.1744	0.0854	0.4857	0.2072	0.2487
Characteristic 21	0.2211	0.0413	-0.1913	0.1300	0.0968	0.1330	0.1884	-0.1576	-0.0922	-0.0899
Characteristic 22	-0.1220	-0.1477	0.3927	0.2993	0.1373	0.3911	0.2024	-0.0097	-0.2031	-0.1036
Characteristic 23	0.5628	0.6336	-0.2636	-0.1218	0.0351	-0.1827	-0.0567	-0.0074	-0.0383	0.0838
Characteristic 24	0.2646	0.4022	0.0598	-0.0616	0.3011	0.0139	0.2845	0.0347	0.1150	-0.1298
Characteristic 25	-0.0325	0.1416	-0.1606	0.2694	0.2458	-0.0729	0.0981	-0.0255	-0.0217	0.0209
Characteristic 26	-0.1120	0.3142	0.2055	-0.0085	-0.0458	0.0471	0.0092	-0.0296	-0.0514	0.0549
Characteristic 27	1.0179	0.9945	0.8832	0.5695	0.3678	0.3363	0.5749	0.4954	0.4635	0.2007
Characteristic 28	0.3537	0.8211	0.6898	0.4467	0.5141	0.3092	0.3681	0.1859	0.2281	0.3112
Characteristic 29	3.6202	5.1043	1.7820	2.4862	2.8620	1.4222	1.7472	1.2805	0.4543	0.7803
Characteristic 30	0.7668	0.6270	-0.3123	0.5251	0.2548	0.0899	-0.5320	0.0036	-0.1886	0.1685

Table E.8: Average power error for the final operating point for variations of the acceptance probability threshold.

	0.05	**0.1**	**0.15**	**0.2**	**0.25**	**0.3**	**0.35**	**0.4**	**0.45**	**0.5**
Characteristic 1	0.8446	0.6975	0.6335	0.7160	0.5767	0.3860	0.4347	0.3790	0.4502	0.3101
Characteristic 2	1.2095	1.2780	1.1809	0.8762	1.1058	0.9309	0.7705	0.8601	0.7308	0.7334
Characteristic 3	1.8928	1.2375	1.4336	1.2040	1.5029	1.1912	1.0406	0.9798	0.8277	0.8839
Characteristic 4	0.8244	0.7677	0.6453	0.7151	0.6385	0.5369	0.5590	0.5323	0.3541	0.4127
Characteristic 5	0.8476	0.8388	0.6553	0.6785	0.4200	0.4725	0.4554	0.4325	0.4557	0.3495
Characteristic 6	0.8370	0.8383	0.8705	0.4661	0.5995	0.4029	0.5530	0.4262	0.4546	0.3920
Characteristic 7	0.8359	0.6719	0.8139	0.4598	0.6356	0.5713	0.4168	0.4069	0.5280	0.4178
Characteristic 8	1.0731	0.7350	0.6917	0.7810	0.7518	0.6725	0.5879	0.5737	0.7297	0.3283
Characteristic 9	1.5954	1.2843	1.4873	1.0424	0.9639	1.0028	0.9967	0.7942	0.7670	0.8443
Characteristic 10	1.7121	1.3699	1.2760	1.4511	1.3769	1.1185	1.1545	0.9796	1.1903	0.9152
Characteristic 11	0.6318	0.5018	0.4095	0.4489	0.5014	0.3832	0.3722	0.3171	0.2924	0.2864
Characteristic 12	0.6360	0.5744	0.5929	0.4552	0.4568	0.4060	0.4051	0.2942	0.3360	0.3053
Characteristic 13	0.4991	0.3516	0.4917	0.5178	0.3485	0.2661	0.3766	0.2759	0.2511	0.2489
Characteristic 14	0.6385	0.5717	0.4082	0.4149	0.4228	0.3022	0.3491	0.2162	0.2648	0.3487
Characteristic 15	1.0523	1.1906	0.8082	0.7142	0.7618	0.7521	0.6042	0.7073	0.5719	0.4969
Characteristic 16	0.6296	0.7027	0.5017	0.4198	0.4491	0.3402	0.3013	0.3225	0.3347	0.3302
Characteristic 17	0.6620	0.6364	0.5080	0.4938	0.3822	0.3304	0.3540	0.2697	0.2785	0.3248
Characteristic 18	0.5046	0.6063	0.5042	0.3605	0.3887	0.3853	0.3276	0.2867	0.2795	0.2849
Characteristic 19	0.5387	0.4075	0.4173	0.3380	0.3707	0.3325	0.3157	0.2733	0.2456	0.2207
Characteristic 20	1.1189	1.3623	0.9504	0.6620	0.7185	0.5803	0.5901	0.7081	0.6296	0.6579
Characteristic 21	0.6770	0.5453	0.5118	0.4723	0.4746	0.4736	0.4190	0.3578	0.3912	0.3250
Characteristic 22	0.7324	0.6165	0.6320	0.4503	0.5317	0.4252	0.4038	0.3609	0.4170	0.2860
Characteristic 23	0.7487	0.7153	0.5483	0.4610	0.3789	0.3774	0.3976	0.3798	0.3858	0.3550
Characteristic 24	0.8561	0.7404	0.6507	0.4915	0.4649	0.4369	0.4646	0.2260	0.2212	0.3935
Characteristic 25	0.8657	0.9290	0.6908	0.6264	0.6106	0.3987	0.3626	0.3663	0.4462	0.3721
Characteristic 26	1.0679	1.0867	0.6705	0.5602	0.6432	0.6287	0.7575	0.4199	0.4623	0.3261
Characteristic 27	1.5726	1.6050	1.2550	1.1158	1.1200	1.0372	1.0677	1.0234	0.9010	0.7395
Characteristic 28	1.0874	1.3136	1.3408	0.9717	1.1457	1.0496	1.0030	0.7088	0.7758	0.8931
Characteristic 29	1.5766	1.4031	1.0151	0.8959	0.9364	1.0098	1.0127	0.8274	0.6137	0.6597
Characteristic 30	0.6752	0.7237	0.5829	0.5765	0.5623	0.4092	0.4835	0.3309	0.3790	0.2971

Table E.9: Average voltage error for the final operating point for variations of the neighbourhood size.

	130	**120**	**110**	**100**	**90**	**80**	**70**	**60**	**50**	**40**	**30**	**20**	**10**
Characteristic 1	0.4731	0.3571	0.3080	0.2217	0.3632	0.2110	0.2607	0.4814	0.0614	0.2733	0.2716	0.1562	0.2607
Characteristic 2	-0.1033	-0.0066	0.0633	-0.1760	0.2098	-0.0548	0.1092	-0.0580	0.0023	-0.0450	-0.1121	-0.0190	6.7302
Characteristic 3	0.0930	0.3306	0.2128	-0.0210	-0.0276	-0.0028	0.0774	0.1247	0.0178	0.0203	3.1682	10.4164	17.1580
Characteristic 4	0.3067	0.4688	0.4271	-0.1313	0.3027	0.2725	0.1338	0.0663	0.3680	0.0591	0.2283	0.0819	-2.1655
Characteristic 5	0.3460	0.3031	0.2271	0.1922	0.2990	0.2087	0.2893	0.0938	0.2937	0.1714	0.2209	0.1671	0.1667
Characteristic 6	0.3006	0.0739	0.5255	0.4137	0.1155	0.3333	0.4186	0.1316	0.0900	0.3015	0.3015	0.1423	0.3544
Characteristic 7	0.1071	0.2534	0.1554	-0.0224	-0.0325	0.0591	0.2611	0.0588	0.0602	-0.1030	0.0268	-0.0948	-0.0828
Characteristic 8	-0.2713	-0.0617	-0.0313	0.0134	0.0735	0.1944	0.1915	0.0629	-0.2768	0.0594	0.0592	-0.0484	-0.1075
Characteristic 9	0.4250	0.2371	0.2552	-0.0370	0.0513	0.1170	-0.0151	0.0519	0.0661	0.0085	0.0582	-0.0687	6.2481
Characteristic 10	2.4764	1.6918	1.8961	1.0051	0.4223	0.2229	0.6002	0.3907	0.7998	7.6705	12.1966	14.0028	10.7588
Characteristic 11	0.5954	1.6140	0.7706	1.1036	0.7446	0.6675	0.6252	0.7676	0.9894	0.7028	0.4717	1.1181	3.5743
Characteristic 12	5.1134	3.8492	3.2627	2.7167	2.3531	2.9259	1.5697	2.6638	1.8575	3.6132	5.5819	10.5272	9.4877
Characteristic 13	0.7961	0.7074	0.2116	0.7609	0.4502	1.0117	0.6388	0.5832	0.3571	0.6523	-0.3812	-0.9651	-7.1806
Characteristic 14	0.6982	0.3762	0.7689	0.5364	0.5340	-0.1812	0.5769	0.6619	0.1121	0.3852	0.7837	0.2062	-5.7308
Characteristic 15	0.1510	0.4248	0.2108	0.4623	0.4857	0.0876	0.1637	0.4022	0.2222	0.0204	0.0523	0.1395	-2.0125
Characteristic 16	0.4867	0.4265	0.6515	0.5960	0.9434	0.8509	0.3228	0.8070	0.4477	0.4240	-0.4475	-6.8609	-22.9514
Characteristic 17	0.3713	1.2925	0.8130	0.6788	0.3785	0.6350	0.2833	0.3340	0.3657	0.4526	-2.9639	-8.3813	-29.0532
Characteristic 18	0.2844	0.0436	0.4633	0.0512	-0.2345	0.2192	0.3082	0.3085	0.0896	-0.5666	-7.0731	-20.1901	-31.8105
Characteristic 19	23.7415	26.0604	21.5697	23.2108	24.7476	37.3113	42.9039	39.7838	25.4381	29.6163	31.7041	23.2005	9.5280
Characteristic 20	0.8325	0.3923	0.1466	0.5644	0.2813	0.3458	0.2979	0.2908	0.1125	0.2006	0.1291	2.8455	13.8384
Characteristic 21	0.1970	0.3436	-0.0687	0.2859	0.1701	-0.0225	0.1149	-0.2305	-0.0975	0.0264	-0.1531	0.1455	1.0913
Characteristic 22	0.2638	0.3534	0.1669	-0.1460	0.4937	0.0006	0.0168	0.1502	0.2384	0.3040	-0.0404	-0.0129	0.8158
Characteristic 23	0.2701	0.3487	0.2241	0.0929	0.2766	0.1964	0.1180	-0.1084	0.0403	-0.0051	-0.1539	-0.1800	1.5139
Characteristic 24	0.5355	0.3520	0.3677	0.0359	0.1580	0.0871	0.1259	0.1375	0.0131	0.0732	0.1881	-0.0138	0.8123
Characteristic 25	-0.0866	0.1815	0.2254	0.1582	-0.1830	-0.1933	-0.2476	-0.0786	0.0814	-0.1173	0.0569	-0.2149	0.2571
Characteristic 26	0.0239	0.0159	0.0096	-0.0555	0.0161	-0.2499	0.1807	-0.0066	0.0490	-0.1436	0.1152	-0.1110	-1.7414
Characteristic 27	0.9875	0.4094	0.6593	0.6705	0.8607	0.5242	0.6056	0.1904	0.2284	0.4070	3.1065	7.2667	-5.1231
Characteristic 28	0.7058	0.1976	0.3860	0.1682	0.2839	0.1380	0.1165	0.2602	0.0191	0.0747	0.8026	4.7305	-4.3132
Characteristic 29	3.0697	4.8271	1.4208	2.0018	1.6656	8.1773	34.2737	36.7258	19.3286	22.9032	27.9996	21.7402	10.7631
Characteristic 30	0.4666	0.8554	0.4029	0.1896	0.0950	0.2435	0.1697	0.1225	0.1680	-0.2087	-9.1374	-18.5384	-30.3564

Table E.10: Average power error for the final operating point for variations of the neighbourhood size.

	130	**120**	**110**	**100**	**90**	**80**	**70**	**60**	**50**	**40**	**30**	**20**	**10**
Characteristic 1	0.6386	0.5974	0.6264	0.4526	0.4030	0.3856	0.3803	0.3487	0.3509	0.3467	0.2439	0.2618	0.2392
Characteristic 2	1.2818	1.2026	0.8241	0.9010	1.0161	0.6959	0.6172	0.4866	0.5205	0.5843	0.3540	0.3042	11.4388
Characteristic 3	1.2845	1.3813	1.3898	0.9865	1.0949	0.8393	0.7965	0.7299	0.6328	0.5022	3.3247	9.7531	15.5680
Characteristic 4	0.8771	0.7267	0.7545	0.6559	0.4778	0.4728	0.5150	0.4324	0.3699	0.3393	0.3234	0.2311	2.5927
Characteristic 5	0.6413	0.6968	0.5650	0.6220	0.6409	0.5163	0.5224	0.3916	0.5022	0.3480	0.3255	0.2757	0.2236
Characteristic 6	0.8211	0.6256	0.8184	0.6367	0.5328	0.4999	0.5274	0.3698	0.4380	0.3688	0.3761	0.2480	0.2335
Characteristic 7	0.8960	0.5243	0.6474	0.5241	0.5247	0.4758	0.4834	0.5401	0.4439	0.3588	0.3262	0.2432	0.2259
Characteristic 8	0.9276	0.6385	0.7466	0.7873	0.7714	0.6159	0.4078	0.4654	0.3916	0.4296	0.2739	0.2957	0.2257
Characteristic 9	1.1536	1.1434	1.0089	1.0634	1.0913	0.8667	0.6520	0.6737	0.5359	0.5795	0.3905	0.3792	9.5425
Characteristic 10	1.6759	1.5935	1.7118	1.6094	1.0406	0.8424	0.8433	0.8900	0.9582	2.5239	3.5314	4.0556	3.1198
Characteristic 11	0.5327	0.5465	0.5016	0.4882	0.4606	0.3620	0.3707	0.4227	0.4031	0.2976	0.2811	0.3968	0.9999
Characteristic 12	0.7765	0.5571	0.6271	0.5742	0.5130	0.5042	0.4394	0.5180	0.4350	0.5551	0.6605	0.9333	0.9000
Characteristic 13	0.4899	0.5064	0.3158	0.3946	0.3507	0.3967	0.3059	0.3937	0.3215	0.3071	0.5686	0.7771	3.3250
Characteristic 14	0.3937	0.5813	0.4296	0.3593	0.3601	0.3404	0.2911	0.3615	0.2943	0.2975	0.3080	0.5162	4.7526
Characteristic 15	1.1218	1.0910	0.7035	0.6162	0.6804	0.6617	0.5249	0.6189	0.4738	0.3159	0.3713	0.3588	7.9739
Characteristic 16	0.4969	0.6455	0.5725	0.4843	0.4464	0.4940	0.5091	0.4693	0.4008	0.3114	0.6887	3.7899	12.3443
Characteristic 17	0.4607	0.6233	0.5239	0.4262	0.3357	0.4228	0.2812	0.2967	0.3233	0.3434	1.6592	5.0888	13.5870
Characteristic 18	0.5390	0.4641	0.3915	0.4683	0.3840	0.3512	0.3397	0.3641	0.2635	0.5387	2.6933	7.4406	14.9781
Characteristic 19	0.4366	0.4646	0.4844	0.4459	0.4842	0.4821	0.4584	0.4204	0.4046	0.3498	0.3911	0.3851	0.5393
Characteristic 20	1.1642	0.9093	0.7958	0.9473	0.6754	0.7037	0.5344	0.6119	0.4463	0.5165	0.3009	2.0576	8.8260
Characteristic 21	0.7020	0.5581	0.4517	0.5761	0.5033	0.4336	0.4182	0.4032	0.3146	0.3229	0.2621	0.3192	1.0737
Characteristic 22	0.6553	0.5597	0.5216	0.5789	0.6493	0.4704	0.3688	0.4488	0.3450	0.3308	0.2516	0.2610	0.9046
Characteristic 23	0.6327	0.4970	0.5001	0.6115	0.4349	0.4536	0.3883	0.4114	0.3141	0.3564	0.2687	0.3228	1.2611
Characteristic 24	0.5724	0.5990	0.5708	0.5291	0.4825	0.4473	0.3425	0.4162	0.4240	0.3643	0.2588	0.2313	0.8254
Characteristic 25	0.6440	0.6517	0.5648	0.5629	0.5181	0.4474	0.5157	0.4089	0.3616	0.2957	0.2762	0.2644	0.5299
Characteristic 26	0.8285	0.6274	0.7263	0.6195	0.6325	0.4627	0.4625	0.4649	0.4315	0.3693	0.2298	0.3039	0.9681
Characteristic 27	1.7329	1.2302	1.3916	1.1078	1.0510	1.0894	0.8995	0.8137	0.5185	0.5642	1.6162	6.3251	18.4044
Characteristic 28	1.4102	1.2733	1.2867	1.2573	0.9232	0.7150	0.7574	0.6761	0.5644	0.4677	0.9082	4.8413	12.9633
Characteristic 29	1.2149	1.2078	1.1091	0.9959	0.9046	1.7276	3.8519	4.1628	2.4575	2.6015	3.1026	3.0023	3.1204
Characteristic 30	0.5543	0.6439	0.5875	0.4381	0.3918	0.4154	0.4055	0.2935	0.3123	0.4828	1.4897	3.1408	4.7904

Table E.11: Average voltage error for the final operating point for different neighbourhood reduction functions.

	Linear	**Quadratic**	**Exponential**
Characteristic 1	0.4277	0.4400	0.7537
Characteristic 2	0.1430	0.0485	0.6129
Characteristic 3	-0.0721	0.0615	9.9821
Characteristic 4	-0.0446	0.2519	0.4366
Characteristic 5	0.0373	-0.2016	0.7625
Characteristic 6	0.2756	0.0998	0.4689
Characteristic 7	-0.0034	0.0774	0.4966
Characteristic 8	-0.0310	-0.0741	-0.0295
Characteristic 9	0.0484	0.0376	1.8240
Characteristic 10	1.8765	6.1448	14.5442
Characteristic 11	0.6799	0.6451	45.3385
Characteristic 12	7.2392	8.4860	45.4494
Characteristic 13	0.2094	0.2240	26.5153
Characteristic 14	0.5641	0.1921	28.8201
Characteristic 15	0.0400	0.1122	3.7859
Characteristic 16	0.2971	0.0811	9.7548
Characteristic 17	0.2716	0.3800	20.8567
Characteristic 18	0.0535	-0.0243	10.3239
Characteristic 19	31.5498	28.3877	47.3571
Characteristic 20	0.0564	0.1739	14.0182
Characteristic 21	0.1842	0.1437	18.8481
Characteristic 22	0.0973	0.2220	21.9738
Characteristic 23	0.0296	-0.1624	41.4715
Characteristic 24	-0.0217	0.1934	50.9842
Characteristic 25	-0.0390	0.1517	22.5669
Characteristic 26	0.0331	-0.0333	0.0486
Characteristic 27	0.1064	1.0824	9.9094
Characteristic 28	0.0454	0.4896	8.3034
Characteristic 29	31.3440	31.2075	29.1960
Characteristic 30	-0.6317	-1.1529	4.4836

Table E.12: Average power error for the final operating point for different neighbourhood reduction functions.

	Linear	**Quadratic**	**Exponential**
Characteristic 1	0.2025	0.2900	0.9680
Characteristic 2	0.4167	0.2895	1.5335
Characteristic 3	0.3443	0.3421	9.2790
Characteristic 4	0.2770	0.2750	0.5317
Characteristic 5	0.2834	0.2310	0.8179
Characteristic 6	0.2373	0.2406	0.6631
Characteristic 7	0.2775	0.2422	0.7435
Characteristic 8	0.2469	0.2912	0.5947
Characteristic 9	0.4533	0.2977	2.8621
Characteristic 10	0.8616	1.8429	4.3105
Characteristic 11	0.3034	0.2496	17.1237
Characteristic 12	0.7123	0.8307	14.0037
Characteristic 13	0.2530	0.3374	22.1958
Characteristic 14	0.2312	0.1840	19.7819
Characteristic 15	0.2577	0.2957	4.5573
Characteristic 16	0.2662	0.2053	12.3070
Characteristic 17	0.2941	0.2268	22.3125
Characteristic 18	0.2480	0.2336	16.5833
Characteristic 19	0.3323	0.3175	13.1941
Characteristic 20	0.2631	0.3089	9.7211
Characteristic 21	0.2611	0.2497	19.1379
Characteristic 22	0.2831	0.2792	22.3394
Characteristic 23	0.2485	0.1989	37.3750
Characteristic 24	0.2381	0.2931	40.7825
Characteristic 25	0.2460	0.2455	22.4269
Characteristic 26	0.3123	0.2720	0.9562
Characteristic 27	0.4174	0.7003	4.1750
Characteristic 28	0.3305	0.5315	5.5119
Characteristic 29	3.3319	3.3182	5.8890
Characteristic 30	0.2958	0.4763	14.2906

Table E.13: Average voltage error for the final operating point for variations of the stopping temperature.

	0.1	**0.2**	**0.3**	**0.4**	**0.5**	**0.6**	**0.7**	**0.8**	**0.9**	**1**
Characteristic 1	0.2928	0.4341	0.2566	0.5551	0.7307	0.8336	0.7242	0.7124	0.6987	0.6149
Characteristic 2	0.1253	-0.0581	-0.1597	-0.1915	0.2503	0.3362	0.0276	0.1143	0.2855	0.4429
Characteristic 3	-0.0672	0.2155	0.2206	0.4188	0.5302	0.2789	0.5320	0.8346	1.0935	1.1600
Characteristic 4	0.1274	0.4551	0.0615	0.1292	0.6682	0.1692	0.7265	0.6578	0.0542	0.3429
Characteristic 5	0.3331	0.1932	0.4474	0.5876	0.5862	0.2235	0.9982	0.8159	0.6021	0.5995
Characteristic 6	0.4485	0.3300	0.3764	0.1352	0.4129	0.0283	0.3617	0.4026	0.7192	1.0423
Characteristic 7	0.1607	0.0049	0.1710	-0.0596	0.1915	-0.0093	0.3401	0.3673	0.1674	0.8088
Characteristic 8	-0.1366	0.0639	-0.2226	0.1896	-0.1676	0.0186	0.1219	-0.1012	0.1565	0.0585
Characteristic 9	0.3495	0.3448	0.2129	0.2575	0.3265	0.3171	0.2402	0.5680	0.5816	0.7730
Characteristic 10	0.7387	2.4221	3.1153	1.7627	4.8603	3.1210	4.1257	4.7244	7.4226	4.2485
Characteristic 11	0.4764	1.6856	1.9123	1.6633	2.6712	3.6882	3.5749	4.1053	4.2901	5.3409
Characteristic 12	1.4122	5.5082	6.1660	8.1163	8.9718	10.1858	12.7034	9.4589	14.9307	15.2974
Characteristic 13	0.3640	0.8452	0.9076	1.6450	0.7839	1.1928	1.9808	2.4595	1.7523	2.0478
Characteristic 14	0.3114	0.1179	0.6713	1.3729	1.2445	1.0545	2.2053	1.0644	1.4586	1.8229
Characteristic 15	0.0807	0.1819	0.3579	0.2840	0.1154	0.6154	0.8894	0.8550	1.2553	1.3897
Characteristic 16	0.2579	0.5250	0.2700	1.3753	1.2879	1.7104	0.9198	1.2070	1.2175	1.8517
Characteristic 17	0.3046	1.1446	0.9206	1.2317	1.1945	1.1360	1.0416	2.3582	2.2358	1.4098
Characteristic 18	0.1125	0.2953	0.4486	0.4502	0.4446	0.4359	0.9506	1.3663	1.4318	1.4463
Characteristic 19	23.3549	22.5898	24.8126	19.4794	21.1847	22.7954	20.1379	24.4597	21.1439	25.8321
Characteristic 20	0.3317	0.4850	0.4651	0.9593	1.0701	1.5559	2.0079	2.2458	2.5919	2.0849
Characteristic 21	0.1306	-0.0751	0.3970	0.0668	0.1309	0.5968	0.2945	0.6176	1.0129	0.8529
Characteristic 22	0.3306	0.1982	0.4844	0.3437	0.0838	0.7641	0.6293	0.5144	1.4220	1.0917
Characteristic 23	-0.2341	0.1209	0.1951	0.8016	0.4404	0.7596	0.7253	0.4376	2.0846	1.5978
Characteristic 24	0.0483	0.3163	0.1390	-0.1489	0.1374	0.5600	0.5955	0.6303	0.5364	1.3392
Characteristic 25	-0.0264	0.1183	0.2321	0.4925	0.0564	0.5225	0.7717	0.3236	1.1185	0.7917
Characteristic 26	0.2523	-0.2777	0.0530	0.2195	0.0490	-0.0866	0.1742	-0.1786	-0.0998	-0.6909
Characteristic 27	0.7546	0.2919	1.0310	1.9925	1.8291	1.9865	2.7541	3.7070	4.0441	3.3229
Characteristic 28	0.2708	0.4506	0.6252	1.1859	0.6052	1.5921	0.6274	1.6869	1.5813	2.8528
Characteristic 29	1.9435	4.4069	4.1174	5.4816	6.0697	7.2701	9.4281	8.3120	7.3525	8.8857
Characteristic 30	0.1538	0.5392	-0.7118	-1.3857	0.7233	-2.3362	-1.6762	-1.8356	-4.3233	-4.8875

Table E.14: Average power error for the final operating point for variations of the stopping temperature.

	0.1	**0.2**	**0.3**	**0.4**	**0.5**	**0.6**	**0.7**	**0.8**	**0.9**	**1**
Characteristic 1	0.6077	0.5029	0.7079	0.8333	1.4766	1.0953	1.5198	1.5714	1.4045	1.3808
Characteristic 2	1.1259	1.1739	1.5324	1.6498	1.8321	2.1017	1.8019	2.2467	2.6150	2.3104
Characteristic 3	1.0928	1.4188	1.5737	1.7555	2.3446	2.0488	2.6579	2.5947	3.3676	3.2153
Characteristic 4	0.5090	0.5723	1.0655	1.1713	1.1601	1.5567	1.4848	1.8639	2.1136	1.8457
Characteristic 5	0.4719	0.5453	1.0462	1.0826	1.1414	1.7079	1.2692	1.8393	2.0387	2.1663
Characteristic 6	0.4859	0.7151	1.0880	1.1872	1.0326	1.3819	1.3715	2.2890	1.7926	2.4102
Characteristic 7	0.6509	0.5585	1.0144	1.2893	1.2736	1.6990	1.5460	1.8990	2.0399	2.2445
Characteristic 8	0.6046	0.9797	1.4669	1.6413	1.5531	1.6816	2.2316	2.0787	3.0031	2.6705
Characteristic 9	1.3656	1.3444	1.3725	1.6180	2.1528	2.6779	2.7194	2.8875	4.0971	3.4949
Characteristic 10	1.1192	2.0319	1.8673	1.8413	2.6641	2.9133	2.3395	3.1809	4.1593	3.1506
Characteristic 11	0.3308	0.6867	0.8121	0.7071	1.2298	1.5211	1.6325	1.5547	1.7683	1.8610
Characteristic 12	0.3886	0.7798	0.9819	1.2317	1.4317	1.6216	1.7486	1.7191	2.0766	2.1966
Characteristic 13	0.2775	0.5042	0.6335	0.8412	0.9786	1.0014	1.3208	1.8298	1.7153	1.4983
Characteristic 14	0.3126	0.5173	0.6200	0.8359	0.9249	1.0144	1.0744	1.2849	1.4125	1.7083
Characteristic 15	0.8347	0.8402	1.1141	1.1742	1.5706	2.0689	2.0180	2.1110	2.1953	2.9261
Characteristic 16	0.3377	0.4143	0.6492	0.8723	1.0414	1.3031	1.0426	1.5281	1.5154	1.4866
Characteristic 17	0.3325	0.7852	0.7682	0.7912	0.9607	0.8930	1.1506	1.5745	1.7409	1.6948
Characteristic 18	0.3994	0.6263	0.7470	0.7508	1.0507	1.1734	1.5389	1.3931	1.6077	1.6449
Characteristic 19	0.2964	0.4673	0.6670	0.6158	0.9525	0.9093	1.0622	1.1811	1.6536	1.5902
Characteristic 20	0.8839	0.8732	1.1786	1.5291	1.6040	1.9795	2.3741	2.7447	2.9038	2.7013
Characteristic 21	0.3721	0.5745	0.9800	1.0932	0.8929	1.4645	1.5352	1.3757	2.2956	2.1854
Characteristic 22	0.5298	0.6176	0.9134	1.0212	1.0372	1.4466	1.4126	1.4761	1.9146	1.8363
Characteristic 23	0.4839	0.7260	0.8283	1.1389	1.2023	1.3983	1.4165	1.3431	2.1340	1.9985
Characteristic 24	0.4510	0.6178	0.8696	1.0516	0.9849	1.2698	1.3109	1.7291	1.5382	1.7065
Characteristic 25	0.4549	0.5593	0.8854	0.9581	1.1433	1.3766	1.3393	1.2468	1.6585	1.8269
Characteristic 26	0.6722	0.8657	1.2899	1.2618	1.3182	1.8169	1.7957	2.3394	2.2900	2.6006
Characteristic 27	1.3438	1.2463	1.8448	2.6360	2.5479	2.2383	2.9603	3.1501	3.2656	3.6716
Characteristic 28	0.9876	1.2215	1.8209	2.1153	1.4407	2.4732	1.8248	2.9359	2.9591	3.1359
Characteristic 29	0.8918	1.2873	1.5400	1.9513	2.0748	2.5389	2.3219	2.4879	2.7014	3.2846
Characteristic 30	0.4014	0.6828	0.9685	1.2315	0.9523	1.6566	1.4923	1.6622	1.8818	2.4033

Table E.15: Average voltage error for the final operating point for variations of the linear cooling schedule constant.

	0.1	**0.2**	**0.3**	**0.4**
Characteristic 1	0.3701	0.9482	0.8149	0.7953
Characteristic 2	0.4770	0.6569	0.7253	1.1666
Characteristic 3	0.4172	1.4926	3.0274	3.4220
Characteristic 4	0.7337	0.2729	1.0210	0.8905
Characteristic 5	0.3740	0.6369	1.1914	0.7838
Characteristic 6	0.7374	0.6059	0.7257	1.3058
Characteristic 7	0.3594	0.5940	0.3438	1.2395
Characteristic 8	-0.3709	0.3333	-0.0256	0.4146
Characteristic 9	0.2400	0.7195	1.2209	1.6163
Characteristic 10	5.7014	8.6998	8.9998	11.5171
Characteristic 11	3.3220	6.3330	6.9387	8.1652
Characteristic 12	8.9557	11.2639	13.8701	16.8519
Characteristic 13	0.9754	0.6650	0.5638	1.1028
Characteristic 14	1.9470	1.9636	2.8784	3.6109
Characteristic 15	1.0024	1.7637	1.9160	2.3246
Characteristic 16	1.2775	1.2216	0.9032	1.5490
Characteristic 17	1.4072	2.6111	2.6017	3.4614
Characteristic 18	1.5258	1.4441	1.8648	2.8036
Characteristic 19	23.0575	23.6288	25.2440	25.2217
Characteristic 20	1.3950	3.2596	5.4177	6.8382
Characteristic 21	0.6797	1.5436	1.6581	2.2529
Characteristic 22	0.5406	1.2348	2.8162	1.7105
Characteristic 23	0.9428	2.0629	2.4069	4.3176
Characteristic 24	0.1204	1.4741	2.7910	2.6154
Characteristic 25	1.1258	0.4234	2.3791	2.8234
Characteristic 26	-0.4161	-1.4778	-0.9405	-1.1267
Characteristic 27	3.7589	4.2060	5.9949	6.2595
Characteristic 28	1.4368	4.1451	5.4080	5.2318
Characteristic 29	12.5808	14.7885	16.5916	12.6967
Characteristic 30	-2.6041	-3.3134	-8.3671	-14.5363

Table E.16: Average power error for the final operating point for variations of the linear cooling schedule constant.

	0.1	**0.2**	**0.3**	**0.4**
Characteristic 1	1.7769	2.1209	2.7797	3.7520
Characteristic 2	2.6824	3.3358	4.9081	4.6169
Characteristic 3	2.5261	4.1957	5.9574	7.3784
Characteristic 4	1.6120	2.1661	3.2337	4.4735
Characteristic 5	1.5583	3.4221	4.5146	4.4094
Characteristic 6	1.8385	2.4454	3.4221	4.4998
Characteristic 7	1.5815	2.8752	3.0698	3.8738
Characteristic 8	2.3248	2.8591	3.3518	4.7385
Characteristic 9	2.1415	4.4318	5.1052	7.4817
Characteristic 10	3.3621	5.0759	5.6820	6.8693
Characteristic 11	1.2512	2.3207	2.4030	2.8067
Characteristic 12	1.4629	1.7245	2.2127	2.9143
Characteristic 13	1.3553	1.6637	2.7883	3.5167
Characteristic 14	1.2833	1.8877	2.5680	3.4172
Characteristic 15	2.6015	3.6204	4.6377	4.5061
Characteristic 16	1.3180	2.5428	3.0205	4.0159
Characteristic 17	1.4720	1.9464	2.9464	4.4487
Characteristic 18	1.4708	1.9504	2.6480	3.3352
Characteristic 19	0.9969	1.4016	1.9102	2.1646
Characteristic 20	1.7845	3.3199	4.7471	5.8851
Characteristic 21	1.6073	2.5896	2.9955	3.3759
Characteristic 22	1.3981	2.2589	3.0644	3.1926
Characteristic 23	1.7117	2.3853	2.8202	4.5259
Characteristic 24	1.2568	1.8865	3.1457	3.4735
Characteristic 25	2.0179	1.8770	3.0288	3.3784
Characteristic 26	1.4076	3.2309	4.0439	4.9080
Characteristic 27	3.6404	5.0438	6.4869	6.4385
Characteristic 28	2.4600	5.3445	6.6594	6.6331
Characteristic 29	3.1588	3.6501	4.7692	4.3013
Characteristic 30	1.4573	2.8034	3.3700	4.2541

Table E.17: Average voltage error for the final operating point for variations of the logarithmic cooling schedule constant.

	10	**20**	**30**	**40**	**50**
Characteristic 1	0.3764	1.7624	1.2357	3.0902	3.4448
Characteristic 2	0.2397	1.0319	1.5604	3.7376	4.7632
Characteristic 3	0.3870	0.6588	3.8728	7.8971	12.0435
Characteristic 4	0.7263	0.6759	0.2994	0.2725	0.9025
Characteristic 5	0.6466	0.8144	1.7205	1.3160	2.3777
Characteristic 6	0.4655	1.0030	2.3451	1.2053	0.9443
Characteristic 7	0.6481	1.0556	1.9575	2.0189	1.8817
Characteristic 8	-0.3815	0.0155	0.7355	0.6049	1.1564
Characteristic 9	0.2322	0.5040	1.6221	2.9466	5.3917
Characteristic 10	2.9342	12.5097	11.7566	15.5539	16.9760
Characteristic 11	7.2284	18.4821	19.1798	21.5774	28.8208
Characteristic 12	16.0235	21.0970	21.8647	33.9912	36.1704
Characteristic 13	1.9016	1.7890	2.7838	1.7725	5.7577
Characteristic 14	1.7460	5.3562	5.4747	5.0864	7.9657
Characteristic 15	0.4435	2.2952	5.2600	5.8774	11.0254
Characteristic 16	2.0112	1.1105	-3.8650	0.0732	-6.8073
Characteristic 17	1.4152	2.9191	-3.2621	0.1486	-7.3177
Characteristic 18	1.7132	1.3370	-2.8285	-2.2199	-5.4428
Characteristic 19	21.9583	22.2708	23.3272	30.4778	35.7239
Characteristic 20	1.2089	5.4187	10.9736	16.1945	17.8628
Characteristic 21	1.2310	2.1163	6.3896	9.1076	11.4095
Characteristic 22	0.7846	2.8094	6.1453	10.0983	10.2317
Characteristic 23	1.2611	4.6000	6.3464	10.9779	16.5427
Characteristic 24	1.7566	4.3823	9.1121	14.9017	18.2624
Characteristic 25	0.8788	2.7875	5.3908	10.3740	12.3482
Characteristic 26	-0.1958	-2.1046	-2.0250	-1.9594	-2.9313
Characteristic 27	1.7785	7.1807	8.5094	12.4500	13.2055
Characteristic 28	0.9121	3.2611	10.2467	10.9415	11.1970
Characteristic 29	10.0461	15.5298	19.6607	25.7810	30.9126
Characteristic 30	-5.7506	-16.1484	-18.0144	-14.3533	-16.2198

Table E.18: Average power error for the final operating point for variations of the logarithmic cooling schedule constant.

	10	**20**	**30**	**40**	**50**
Characteristic 1	2.0553	4.5621	6.1464	8.2031	9.2021
Characteristic 2	2.2943	4.3823	6.2013	9.5863	12.7308
Characteristic 3	2.1168	2.8770	7.4051	11.2991	16.5317
Characteristic 4	2.0656	3.9370	7.0415	8.6817	10.4511
Characteristic 5	1.9703	3.9443	6.0128	8.5664	10.2653
Characteristic 6	1.9252	4.2167	7.1653	8.9623	9.0453
Characteristic 7	1.8710	4.1921	7.2325	7.9220	9.2747
Characteristic 8	2.0866	4.0479	5.7320	7.3864	9.7166
Characteristic 9	2.2452	4.5635	6.4094	9.9801	14.0721
Characteristic 10	2.6381	7.0869	9.8041	12.9912	15.4659
Characteristic 11	2.7189	6.3095	7.5321	9.0287	12.1667
Characteristic 12	2.6950	4.3929	5.0957	9.8632	10.7157
Characteristic 13	2.3424	4.8799	10.2633	12.1796	13.3169
Characteristic 14	1.8072	4.3323	8.1551	11.4193	15.6473
Characteristic 15	2.1110	5.2207	8.0677	10.9869	15.4606
Characteristic 16	2.3029	5.6127	8.3372	13.4298	15.5770
Characteristic 17	1.6718	5.9354	8.6068	14.0113	17.3279
Characteristic 18	1.7208	5.6864	9.1880	14.6322	15.4180
Characteristic 19	2.8452	5.4283	6.9153	9.0304	11.5312
Characteristic 20	1.8950	5.2111	9.6454	13.1593	15.4308
Characteristic 21	1.9084	3.2681	7.0390	9.5738	12.1826
Characteristic 22	2.1851	3.5714	7.0412	10.4814	11.0409
Characteristic 23	1.8677	4.6515	6.2697	9.6025	13.7783
Characteristic 24	2.4038	4.0697	6.8517	11.1398	13.3168
Characteristic 25	2.1226	4.0747	6.5737	10.4894	12.7652
Characteristic 26	1.6324	5.2588	8.0233	11.0057	12.2949
Characteristic 27	2.3193	6.0921	8.4810	13.2552	14.6801
Characteristic 28	2.1499	4.9675	11.0212	13.6865	16.8601
Characteristic 29	2.8871	6.7017	10.5110	13.8271	17.8360
Characteristic 30	3.0963	7.9710	10.8263	12.6776	11.3216

Table E.19: Average voltage error for the final operating point for variations of the Lundy cooling schedule constant.

	0.01	**0.02**	**0.03**	**0.04**	**0.05**
Characteristic 1	0.2217	0.3781	0.3400	0.2759	0.0352
Characteristic 2	-0.0201	-0.1412	-0.0197	0.0309	-0.0273
Characteristic 3	-0.0747	-0.0740	0.1642	-0.0544	0.1380
Characteristic 4	0.0875	0.2518	0.2283	0.1130	-0.0556
Characteristic 5	-0.0116	0.2098	-0.0594	0.1905	-0.0152
Characteristic 6	-0.0154	0.1181	0.1604	0.1612	0.3631
Characteristic 7	-0.1124	0.0022	-0.1504	-0.0209	0.2917
Characteristic 8	0.0624	0.0720	0.0577	-0.0765	-0.0025
Characteristic 9	0.0722	0.0938	0.2334	0.0293	0.1096
Characteristic 10	-0.0249	0.0525	0.0430	0.1305	0.7024
Characteristic 11	0.5676	0.2049	0.6173	0.7144	0.3783
Characteristic 12	0.5970	0.7757	0.7951	0.8949	0.7307
Characteristic 13	0.0943	0.5785	0.3217	0.3055	0.3812
Characteristic 14	0.2823	0.4085	0.2890	0.1243	0.6828
Characteristic 15	0.0365	0.1776	0.2721	0.2801	0.2188
Characteristic 16	0.2325	0.3269	0.1622	0.5055	0.5342
Characteristic 17	0.2976	0.2020	0.6040	0.1113	0.4894
Characteristic 18	0.0365	-0.1170	0.1094	0.1844	0.1628
Characteristic 19	19.7510	22.0366	21.3982	23.6206	21.6120
Characteristic 20	0.0303	0.0861	0.1110	0.1974	0.3119
Characteristic 21	-0.1169	0.0970	-0.1216	-0.1349	0.0848
Characteristic 22	-0.1498	-0.1842	0.1169	-0.1491	0.0287
Characteristic 23	-0.0156	-0.0444	-0.1254	0.1246	0.0778
Characteristic 24	0.1128	-0.1195	0.1020	0.0232	-0.0179
Characteristic 25	-0.0005	0.1240	-0.0483	0.1095	-0.0611
Characteristic 26	-0.0007	-0.0291	-0.0359	0.1250	0.0167
Characteristic 27	0.1263	0.1079	0.1956	0.1052	0.4532
Characteristic 28	0.0861	0.0458	-0.0157	0.1818	0.3672
Characteristic 29	0.2070	0.1109	0.1264	0.1694	0.4800
Characteristic 30	0.1681	0.2159	-0.0412	0.3723	0.1614

Table E.20: Average power error for the final operating point for variations of the Lundy cooling schedule constant.

	0.01	**0.02**	**0.03**	**0.04**	**0.05**
Characteristic 1	0.2148	0.2434	0.2745	0.2938	0.3912
Characteristic 2	0.2219	0.2930	0.4518	0.4404	0.6935
Characteristic 3	0.1907	0.2974	0.4660	0.6118	0.6678
Characteristic 4	0.1942	0.2652	0.3297	0.2982	0.3857
Characteristic 5	0.2684	0.2673	0.2750	0.4195	0.3493
Characteristic 6	0.2453	0.2461	0.2367	0.3038	0.4467
Characteristic 7	0.2653	0.2682	0.2782	0.3794	0.3935
Characteristic 8	0.2229	0.2480	0.2758	0.4115	0.5301
Characteristic 9	0.2207	0.2642	0.5309	0.6980	0.8446
Characteristic 10	0.2696	0.3312	0.4689	0.6038	1.0323
Characteristic 11	0.2366	0.2265	0.2926	0.3079	0.2696
Characteristic 12	0.2618	0.3122	0.2558	0.2841	0.2767
Characteristic 13	0.2215	0.2112	0.2336	0.2846	0.2856
Characteristic 14	0.2036	0.2349	0.2341	0.2294	0.2742
Characteristic 15	0.2426	0.2442	0.3300	0.4240	0.4598
Characteristic 16	0.1590	0.2439	0.2008	0.2818	0.2868
Characteristic 17	0.1776	0.2520	0.2656	0.2956	0.3276
Characteristic 18	0.2184	0.2624	0.2534	0.2897	0.3282
Characteristic 19	0.2451	0.2665	0.2504	0.3122	0.3575
Characteristic 20	0.2174	0.3202	0.3085	0.4135	0.5173
Characteristic 21	0.2396	0.2045	0.2790	0.2955	0.2959
Characteristic 22	0.2299	0.2553	0.2898	0.2821	0.3207
Characteristic 23	0.2334	0.2457	0.2753	0.2684	0.3075
Characteristic 24	0.2051	0.2266	0.2842	0.2360	0.3122
Characteristic 25	0.2103	0.2663	0.2872	0.2575	0.4183
Characteristic 26	0.2406	0.2490	0.3304	0.3927	0.4055
Characteristic 27	0.2721	0.3024	0.5080	0.5750	0.9149
Characteristic 28	0.2726	0.2727	0.3563	0.5281	0.7419
Characteristic 29	0.2910	0.2595	0.3090	0.3726	0.6304
Characteristic 30	0.2075	0.2186	0.3171	0.2812	0.3375

Table E.21: Average voltage error for the final operating point for variations of the SQ cooling schedule constant.

	0.2	**0.4**	**0.6**	**0.8**
Characteristic 1	1.2691	0.2586	0.5940	0.2361
Characteristic 2	1.4465	0.7976	-0.0117	0.0584
Characteristic 3	3.0754	1.4260	0.7039	0.3084
Characteristic 4	0.8828	0.1052	0.2936	0.3468
Characteristic 5	0.6079	0.5053	0.3007	0.5040
Characteristic 6	0.4742	0.5925	0.5337	0.5109
Characteristic 7	0.3300	0.4525	0.4667	0.1182
Characteristic 8	0.2322	0.1734	0.1446	-0.0309
Characteristic 9	0.4714	0.1336	0.3672	0.1628
Characteristic 10	8.6537	5.2221	3.0605	1.7603
Characteristic 11	2.5165	1.3660	0.2494	0.5956
Characteristic 12	6.4450	7.8911	6.1461	2.7292
Characteristic 13	1.9954	1.4288	1.0904	0.6747
Characteristic 14	1.6202	1.8079	0.5017	0.4666
Characteristic 15	1.3933	0.7098	0.5524	0.4605
Characteristic 16	0.7763	0.9177	0.7263	0.7653
Characteristic 17	2.0176	1.2500	0.4980	0.5812
Characteristic 18	1.6491	1.1089	0.5922	0.2226
Characteristic 19	24.2133	22.3871	24.0478	23.6102
Characteristic 20	3.0997	2.5747	0.9770	0.5401
Characteristic 21	0.7157	0.9075	0.5680	-0.1124
Characteristic 22	0.7428	1.2414	0.2881	0.0063
Characteristic 23	1.1564	0.2348	0.1331	0.1096
Characteristic 24	1.5342	0.6573	0.1880	-0.0315
Characteristic 25	0.7455	0.3062	0.5374	0.0334
Characteristic 26	-0.5207	-0.2559	-0.3094	0.3384
Characteristic 27	5.2390	5.5072	1.1779	0.9139
Characteristic 28	2.2866	2.4910	1.0084	0.4961
Characteristic 29	11.9564	6.7095	5.5969	2.5641
Characteristic 30	-3.6881	-3.2489	-1.9407	0.4112

Table E.22: Average power error for the final operating point for variations of the SQ cooling schedule constant.

	0.2	**0.4**	**0.6**	**0.8**
Characteristic 1	2.6407	1.4186	1.3118	0.7294
Characteristic 2	4.8920	3.2455	1.3121	1.0705
Characteristic 3	5.4462	4.1616	2.1876	1.3404
Characteristic 4	2.3897	1.9600	1.2817	0.6181
Characteristic 5	2.4841	2.0911	1.5557	0.6430
Characteristic 6	2.2023	1.8997	1.0611	0.6391
Characteristic 7	2.3749	2.0163	1.1821	0.9097
Characteristic 8	2.4762	2.4881	1.6120	0.7224
Characteristic 9	3.3552	3.1663	1.7214	0.9167
Characteristic 10	4.5524	3.4750	2.0615	1.5964
Characteristic 11	1.2492	0.9189	0.6583	0.4311
Characteristic 12	1.0166	1.2001	0.9165	0.5471
Characteristic 13	1.3879	1.1164	0.6614	0.4211
Characteristic 14	1.2797	1.1813	0.6251	0.4332
Characteristic 15	3.1885	2.8232	1.4013	0.9831
Characteristic 16	1.8069	0.9281	0.8773	0.4396
Characteristic 17	1.8288	1.2333	0.8500	0.4642
Characteristic 18	1.2773	1.1370	0.6244	0.4436
Characteristic 19	0.8083	0.5900	0.5118	0.4287
Characteristic 20	3.3610	2.5470	1.3097	0.8266
Characteristic 21	2.0201	1.1249	0.8471	0.6181
Characteristic 22	1.7515	1.5538	1.2310	0.5459
Characteristic 23	1.7212	1.2558	0.8461	0.5598
Characteristic 24	1.6016	1.2219	0.9168	0.4821
Characteristic 25	1.9398	1.1085	1.3365	0.4773
Characteristic 26	2.9699	1.9226	1.5504	0.6491
Characteristic 27	5.0186	4.3337	2.2262	1.1619
Characteristic 28	3.4975	3.2133	2.2311	1.1581
Characteristic 29	2.8720	2.3712	1.9316	1.0605
Characteristic 30	1.8530	1.6888	1.2363	0.6423

Table E.23: Average voltage error for the final operating point for variations of the stopping criterion.

	2	**3**	**4**	**5**	**6**	**7**	**8**	**9**	**10**
Characteristic 1	18.2505	8.4333	6.5909	7.5942	6.2198	4.2136	5.2210	3.5488	2.7470
Characteristic 2	20.8726	16.1328	14.2276	8.9960	7.9179	6.2775	4.5050	4.8485	3.0151
Characteristic 3	23.5415	20.7097	17.0731	16.6593	12.1692	10.0592	9.5363	6.9551	3.8381
Characteristic 4	3.9886	1.4324	1.5903	1.2196	2.9840	-0.8029	0.8969	0.7490	-0.1461
Characteristic 5	6.6241	7.4453	3.3353	3.5279	3.3886	2.7999	2.5719	2.3513	2.4439
Characteristic 6	7.8662	5.6002	4.2540	5.4190	3.0390	1.9131	2.7878	2.3137	0.9320
Characteristic 7	8.5545	8.3562	5.2147	4.1017	2.5084	2.4585	2.6178	1.7302	1.3911
Characteristic 8	10.9046	6.7665	5.3541	4.5931	1.9756	3.7448	2.0017	1.4885	1.6402
Characteristic 9	16.7452	12.0710	12.4908	10.8307	7.7622	5.5254	4.6689	2.3440	3.0695
Characteristic 10	17.4343	17.5429	17.7985	16.2833	12.5541	14.1409	14.8110	11.0334	8.6043
Characteristic 11	13.7183	13.9151	10.2487	9.0671	6.1740	6.6301	5.4815	3.5073	3.0948
Characteristic 12	17.4638	16.8244	16.9384	14.6058	14.5251	11.4862	10.0240	9.0403	7.1000
Characteristic 13	4.4052	-1.1539	0.5407	0.5494	0.8225	2.4751	2.4285	1.2354	1.6655
Characteristic 14	5.1811	4.2802	4.9094	4.9948	3.8324	3.1068	2.7669	3.4429	2.2701
Characteristic 15	13.3902	12.4807	11.1796	8.9098	5.9173	5.2916	5.0331	4.0473	2.7638
Characteristic 16	-0.3856	-1.2395	1.3450	1.4057	1.5073	1.4460	1.5670	2.7004	0.7336
Characteristic 17	-1.5406	3.4072	3.0105	2.5213	2.5301	2.8607	2.1501	2.5939	1.7412
Characteristic 18	-2.6547	2.5656	2.1053	2.2326	3.6836	2.7158	1.2773	2.4712	2.7191
Characteristic 19	24.0945	20.6785	22.0129	24.8054	20.5187	21.9272	22.8772	21.7511	18.5839
Characteristic 20	24.2883	21.6607	15.8205	15.9206	11.6299	10.1608	8.5124	6.5304	4.9850
Characteristic 21	17.6143	12.5755	10.4810	7.9786	5.0717	6.7272	3.4181	5.0354	3.8916
Characteristic 22	16.8844	11.9222	12.3227	8.1533	6.9765	7.2707	4.5328	3.0889	2.5734
Characteristic 23	18.0406	16.0818	12.4863	8.5640	8.4818	5.3476	2.9258	4.1785	3.6229
Characteristic 24	16.2587	14.1441	11.4094	9.3961	7.3980	4.2824	4.4341	4.1632	1.6297
Characteristic 25	15.0840	14.5839	8.9265	10.1195	6.7176	5.2106	5.2061	4.6164	3.0220
Characteristic 26	0.5645	0.2689	0.3886	-2.4350	-2.7199	-2.1931	-3.2898	-0.9793	-2.0776
Characteristic 27	14.4780	12.7447	13.0556	12.3083	8.5906	9.6101	7.1199	8.0347	5.6254
Characteristic 28	9.8181	9.8999	8.5322	8.8782	9.5671	6.3457	5.3290	6.1910	4.9357
Characteristic 29	25.3597	25.2221	19.3598	17.7375	13.7404	14.4766	12.7004	12.3732	13.4526
Characteristic 30	-16.0886	-13.4404	-10.5565	-6.7243	-1.6724	-1.8942	-6.0362	-0.6551	-2.5192

Table E.24: Average power error for the final operating point for variations of the stopping criterion.

	2	**3**	**4**	**5**	**6**	**7**	**8**	**9**	**10**
Characteristic 1	47.1134	21.3538	18.1008	17.4014	13.5133	9.5906	11.3458	8.2197	8.5235
Characteristic 2	42.6686	31.6600	28.6582	20.1244	17.2093	14.4497	11.8143	12.1020	8.9954
Characteristic 3	38.9987	30.7663	27.3764	26.0776	17.8715	17.1270	14.0217	11.2615	8.0373
Characteristic 4	35.5976	33.3713	21.6726	17.0522	13.1071	10.3424	6.2010	8.0963	7.0299
Characteristic 5	36.4516	31.0561	19.4100	16.6787	17.0040	11.6216	10.2375	8.2030	7.6097
Characteristic 6	35.2352	24.6720	21.0911	18.2946	10.9797	10.6452	9.2894	8.5415	6.3825
Characteristic 7	36.1066	32.4243	21.5209	19.2566	10.7812	11.4466	10.6673	8.8450	7.1543
Characteristic 8	43.8657	26.1023	23.5076	18.4598	15.6352	16.0040	11.8088	11.5159	9.6058
Characteristic 9	41.5988	30.1559	26.3234	26.8217	19.2266	13.4507	12.0600	8.4824	10.2042
Characteristic 10	24.8364	20.4785	19.3103	13.0669	10.9407	11.0451	8.7351	7.0142	5.6852
Characteristic 11	4.8186	4.5986	3.5858	3.1588	2.1421	2.4100	2.0750	1.4072	1.3620
Characteristic 12	3.5123	3.8124	3.1521	2.4831	2.2074	2.1320	1.4764	1.4369	1.1034
Characteristic 13	9.3326	6.3608	5.4894	3.5093	2.6393	2.0586	2.0814	1.9766	1.6854
Characteristic 14	6.5316	4.9242	4.6344	3.6965	2.4060	2.6548	2.4916	2.1165	2.0291
Characteristic 15	20.3412	18.5226	15.8596	13.5378	9.6023	8.6067	8.0577	7.0365	5.2350
Characteristic 16	6.2505	7.0764	5.7665	4.2790	3.7120	3.0931	2.4000	2.3993	2.1936
Characteristic 17	6.5814	3.8625	3.2204	3.7175	3.2439	2.9459	2.2707	2.3609	1.9419
Characteristic 18	5.9929	4.8030	3.4398	3.3843	3.3583	2.7827	2.2194	2.6091	2.2231
Characteristic 19	5.6432	4.3291	2.5354	1.5183	1.5673	1.1745	1.1020	0.8989	0.6971
Characteristic 20	22.2539	19.7838	14.0899	13.2884	10.2113	9.1358	7.5849	6.0968	4.9734
Characteristic 21	18.1833	12.7632	11.1852	9.4421	6.3494	6.9184	4.6173	5.8851	4.8201
Characteristic 22	17.6035	12.6366	12.9524	8.9884	7.3768	8.3345	5.3221	4.2107	3.3603
Characteristic 23	15.5334	13.5537	11.2983	7.7274	7.6104	5.0080	3.6839	4.5131	3.5744
Characteristic 24	12.5816	10.7471	8.3229	7.5164	6.1757	3.8419	3.8466	3.9615	2.6526
Characteristic 25	15.6261	14.5534	9.9624	10.5157	7.1698	6.0694	5.7516	5.7493	4.4266
Characteristic 26	29.1808	22.6508	17.9190	15.1956	12.4978	11.7048	10.5556	7.9744	7.1695
Characteristic 27	19.9055	17.0205	15.0013	12.5292	9.9528	10.8001	8.7898	7.5406	5.5054
Characteristic 28	21.1403	15.9514	11.3185	10.5107	11.0711	8.7673	6.3025	7.0962	6.0123
Characteristic 29	16.3712	12.3095	8.2811	6.6980	5.0058	5.3987	4.7087	4.6926	3.7502
Characteristic 30	8.5513	6.3093	4.4556	3.0728	1.9269	1.7542	2.4168	1.2837	1.6447